55th HIGHWAY GEOLOGY SYMPOSIUM

KANSAS CITY, MISSOURI, SEPTEMBER 7-10, 2004

PROCEEDINGS

SPONSORED BY

KANSAS DEPARTMENT OF TRANSPORTATION
MISSOUIRI DEPARTMENT OF TRANSPORTATION
KANSAS GEOLOGICAL SURVEY
MISSOURI GEOLOGICAL SURVEY AND RESOURCE ASSESSMENT DIVISION
UNIVERSITY OF MISSOURI – KANSAS CITY

TABLE OF CONTENTS

Proceedings Papers

HIGHWAY GEOLOGY SYMPOSIUM
55th ANNUAL

Kansas City, Missouri
SEPTEMBER 7th– 10th, 2004

The Kansas Department of Transportation along with the Missouri Department of Transportation, Kansas Geological Survey, Missouri Geologic Survey and Resource Assessment Division, and University of Missouri – Kansas City Departments of Geosciences welcomes you to the 55th Annual Highway Geology Symposium.

The Local State Steering Committee has strived to put together what we hope is an interesting, educational and enjoyable Symposium. Authors will be presenting some very interesting topics such as geophysical methods, laboratory studies, design considerations and case studies of geo-engineering projects.

Again, welcome, and enjoy the Symposium, we hope your experience in the Heart of America is enjoyable.

Host Committee
Co-Chairmen
55th Annual Highway Geology Symposium

Bob Henthorne, P.G.   John F. Szturo P.G
Kansas Department of Transportation   HNTB Corporation

I

55th HIGHWAY GEOLOGY SYMPOSIUM
SPONSORS

The following companies have graciously contributed toward sponsorship of the Symposium. The HGS relies on sponsor contributions for events such as refreshment breaks, field trip lunches and other activities and want these sponsors to know that their contributions are very much appreciated.

Janod Inc.
555 VT, Suite 122,
Route 78
Swanton, VT, 05488
Phone (802) 868-5058 / Fax (450) 424-2614
www.janod.biz/
info@janod.biz

Janod has specialized in rock stabilization and rock remediation since 1968. Janod was founded in 1968 by Douglas Journeaux, and at that time, soft earth tunneling was the principle part of our operations. In 1970 Janod was introduced to rock slope stabilization when called in by Quebec Cartier Mining to perform some emergency work along the railway. Janod has since become a specialist in rock stabilization, and employs a combination of innovative mechanized equipment and highly trained rock remediation technicians who have an intimate knowledge of geology and influence of climatic conditions on exposed rock structures.

Geobrugg North America, LLC.
Geobrugg Protection Systems
551 W. Cordova Road, PMB 730
Santa Fe, New Mexico 87505
Phone (505) 438 6161 / Fax (505) 438 6166
www.us.geobrugg.com
info@us.geobrugg.com

Geobrugg helps protect people and infrastructures from the forces of nature. The technologically mature protection systems of steel wire nets developed and produced by us are now used all over the world. Our dynamic and static barrier systems offer proven protection against rock falls, avalanches, mud flows and slope failures.

HI-TECH Rockfall Construction, Inc.
2328 Hawthorne Street
P.O. Box 674
Forest Grove, OR 97116-0674
Phone (503) 357-6508
Fax (503) 357-7323
HTRockfall@aol.com
www.HI-TECHRockfall.com

"The Rockfall Specialists"

HI-TECH Rockfall is a General Contractor who, since 1996, has specialized in rockfall mitigation and is considered to be the industry leader in designing and installing rockfall protection systems throughout the United States. HI-TECH constructs a vast array of rockfall mitigation systems in a variety of locations such as highways, railroads, dams, quarries, mines, construction sites, commercial and residential properties. HI-TECH has installed over 6,877,00 sf of wire mesh drapery, 927,000 sf of cable net drapery, 74,597 sf of Tecco mesh, 57,038 lf of rock bolts, dowels and anchors, 31,295 lf of rockfall and debris flow barriers and 7,178 crew hours of scaling.

wyllie
norrish
ROCK ENGINEERS

Wyllie & Norrish Rock Engineers

17918 NE 27th Street	**Suite 200, 1311 Howe Street**
Redmond, WA 98052	**Vancouver, BC V6Z 2P3**
(425) 861-7327	**(604) 691-1717**

Wyllie & Norrish Rock Engineers provides consulting engineering services throughout North America in the specialty areas of rock slopes, foundations, tunnels, and blasting. The company has operating offices in Seattle, WA and in Vancouver, B.C. Drawing on their combined 65 years of professional experience emphasizing practical solutions, the founding partners provide consulting services for investigations, design, contract specifications, construction monitoring and claim resolution.

Baker
ChallengeUs.

Michael Baker Jr., Inc.
4301 Dutch Ridge Road
Beaver, PA 15009
(724) 495-7711 or (800) 642-2537
FAX (724) 495-4017

http://www.mbakercorp.com/
mailto:Civil@mbakercorp.com

Michael Baker Corporation has evolved into one of the leading engineering and energy management firms by consistently solving complex problems for its clients. We view challenges as invitations to innovate.

Baker has been providing geotechnical services since the mid-1950's. Professional geotechnical engineers and geologists are supported by a staff of highly trained assistants. Expertise covers most major facets of geotechnical investigation and design, including geologic reconnaissance, subsurface investigations, geotechnical analysis and design, and geotechnical construction phase services.

55th HIGHWAY GEOLOGY SYMPOSIUM EXHIBITORS

The host committee for the 55th Annual Highway Geology Symposium would like to express it's appreciation to the following exhibitors and sponsors. You are invited to visit their displays and please be sure to express your appreciation.

AIS Construction Co
797 Rincon Hill Rd.
Carpenteria, CA 93013
Phone (805) 684-4334
Fax (805) 566-0109
www.aisconstruction.com
andy@aisconstruction.com

American Mountain Management Inc.
Financial Plaza Building
1135 Terminal Way, Suite 106
Reno, Nevada, 89502-2145
Phone (866) 466-7223 (toll free US & Canada)
Fax (450) 455-8762
andre@mountainmanagement.biz

ASP Enterprises
109 NW Victoria Dr.
Lees Summit, MO 64086
Phone (816) 554-1191
Fax (816) 554-2262
www.aspent.com
henryf@aspent.com

Blackhawk Geoservices, Inc
301 Commercial Road, Suite B
Golden, CO 80401
Phone (303) 278-8700
Fax (303) 278-0789
www.blackhawkgeo.com
info@blackhawkgeo.com

Bowser – Morner
4518 Taylorsville Rd
Dayton, OH
Phone (937) 236-8805
Fax (937) 233-2016
www.bowser-morner.com
taugustine@bowser-morner.com

Central Mine Equipment Co.
4215 Rider Trail North
Earth City, MO 63045
Phone (800) 325-8827
Fax (314) 291-4880
www.cmeco.com
flint@cmeco.com

Contour Products
4001 Kaw Drive
Kansas City, KS 66102
Phone (913) 321-4114
Fax (913) 321-8063
www.contourfoam.com
jonb@contourfoam.com

Crux Subsurface Inc.
16707 E. Euclid Ave
Spokane Valley, WA 99216
Phone (509) 892-9409
Fax (509) 892-9408
www.cruxsub.com
scott@cruxsub.com

Durham Slope Indicator
902 A Scorchie Rd
Marion, IL 62959
Phone (618) 998-0011
Fax (618) 923-7427
www.durhamgeo.com
lmiller@durhamgeo.com

Geobrugg North America, LLC.
Geobrugg Protection Systems
551 W. Cordova Road, PMB 730
Santa Fe, New Mexico 87505
Phone (505) 438 6161
Fax (505) 438 6166
www.us.geobrugg.com
info@us.geobrugg.com

Geomation, Inc.
14828 W. 6th Ave, Suite 1-B
Golden, CO 80401
Phone (720) 746-0100
Fax (720) 746-1100
www.geomation.com
choquet@geomation.com

Geopier Foundation Co.
807 W. 48th St, Suite 501
Kansas City, MO 64112
Phone (816) 531-6026
Fax (816) 531-4574
www.geopiers.com
geopier@kc.rr.com

GeoSystems/Kleinfelder
2812 Hunter Drive
Blue Springs, MO 64015
Phone (816) 228-2555
Fax (816) 228-1024
www.Kleinfelder.com
osmith@geosystemseng.com

Geotechnology, Inc.
9136 Cody
Overland Park, KS 66214
Phone (913) 438-1900
Fax (913) 438-1923
www.geotechnology.com
c_jones@geotechnology.com

gINT Software
7710 Bell Road
Windsor, CA 95492
Phone (707) 838-1271
Fax (707) 838-1274
www.gcagint.com
LLOVE@gcagint.com

Golder Associates
540 North Commercial Street, Suite 250
Manchester, New Hampshire 03101-1146
Phone (603) 668 0880
Fax (603) 668 1199
www.golder.com/
amacdonald@golder.com

Hayward Baker Inc.
1130 Annapolis Road, Suite 202
Odenton, Maryland 21113
Phone (410) 551-8200
Fax (410) 551-1900
www.keller-ge.co.uk
jksidhu@kellerfoundations.com

Hi-Tech Rockfall Construction, Inc.
P.O. Box 674
Forest Grove, OR 97116
Phone (503) 357-6508
Fax (503) 357-7323
www.hi-techrockfall.com
HTRockfall@aol.com

Janod Inc.
555 VT, Suite 122,
Route 78
Swanton, VT, 05488
Phone (802) 868-5058
Fax (450) 424-2614
www.janod.biz/
info@janod.biz

The Judy Company
9133 Woodend Rd
Kansas City. KS 66111
Phone (913) 422-5088
Fax (913) 422-5307
www.judycompany.com
kabud@judycompany.com

LaFarge North America
Lafarge North America
600 SW Jefferson St, Suite 204
Lees Summit, MO 64063
Phone (816) 225-2789
www.lafarge.com

P.E. LaMoreaux & Associates, Inc. (PELA)
106 Administration Road, Suite 4
Oak Ridge, Tennessee 37830
Phone (865) 483-7483
Fax (865) 483-7639
www.pela-tenn.com
info@pela-tenn.com

Layne Geoconstruction
60 Fireworks Circle
Bridgewater, MA 02324
Phone (508) 588-8889
Fax (508) 588-8989
www.laynegeo.com
kahurley@laynechristensen.com

Loadtest Inc.
2631-D NW 41st St.
Gainesville, FL 32606
Phone (352) 378-3717
Fax (352) 378-3934
www.Loadtest.com
Info@Loadtest.com

Maccaferri, Inc.
10303 Governor Lane Blvd
Williamsport, MD 21795
Phone (301) 223-6910
Fax (301) 223-4356
www.maccaferri-usa.com
gbrunet@maccaferri-usa.com

Michael Baker Jr. Inc
4301 Dutch Ridge Road
Beaver, PA
Phone (724) 495-7711
Fax (724) 495-4001
www.mbakercorp.com
cruppen@mbakercorp.com

Mirafi Construction Products
365 South Holland Drive
Pendergrass, GA 30567
Phone (888) 795-0808
Fax (706) 693-1780
www.tcmirafi.com
brett_odgers@rtcusa.com

Monir/Isherwood/Soldata
3100 Ridgeway Drive, Unit 3
Mississauga, ON, Canada L5L5M5
Phone (905) 820-3480
Fax (905) 820-3492
marcelo@monir.ca

Qore Inc
422 Codell Drive
Lexington, KY 40509
Phone (859) 293-5518
Fax (859) 299-2481
www.qore.net
rwilson@qore.com

Rotec International, LLC.
PO Box 31536
Sante Fe, NM 87594
Phone (505) 984-8868
www.rotecinternational-usa.com
thommen@swcp.com

RST Instruments Ltd.
200-2050 Hartley Ave.
Coquitlam, BC
V3K 6W5, Canada
Phone (604) 540-1100, (800) 665-5599
Fax (604) 540-1005
www.rstinstruments.com/
info@rstinstruments.com

Ruen Drilling, Inc
PO Box 267
Clark Fork, ID 83811
Phone (208) 266-1151
Fax (208) 266-1379
www.ruendrilling.com
office@ruendrilling.com

SIMCO Drilling Equipment, Inc
802 S. Furnas Drive
Osceola, LA 50213
Phone (800) 338-9925
Fax (641) 342-6764
www.simcodrill.com
info@simcodrill.com

Technos, Inc
10430 NW 31 Terrace
Miami, FL 33172
Phone (305) 718-9594
Fax (305) 718-9621
www.technoc-inc.com
info@technos-inc.com

Tensar Earth Technologies
715 Christ Lane
Belleville, IL 62221
Phone (618) 234-4510
Fax (618) 234-8797
www.tensarcorp.com
lsimonton@tensarcorp.com

Terracon, Inc
13910 W. 96th Terr
Lenexa, KS 66215
Phone (913) 492-7777
Fax (913) 492-7443
www.terracon.com
cwvalenta@terracon.com

URS Corporation
10975 El Monte
Overland Park, KS 66211
Phone (913) 344-1000
Fax (913) 344-1011
www.urscorp.com
thomas_merker@urscorp.com

Vertec Contractors Inc.
555 VT, Route 78, Suite 252
Swanton, VT, 05488
Tel (450) 455-9690
Fax (450) 424-2614
www.verteccontractors.biz/
info@verteccontractors.biz

Wyllie and Norrish Rock Engineers
17918 NE 27th St
Redmond, WA 98052
Phone (425) 861-7327
Fax (425) 861-7327
nnorrish@msn.com

Highway Geology Symposium

Future Symposia Schedule and Contact List

Year	State	Host Coordinator	Telephone Number	Email
2005	North Carolina	Russell Glass	(828) 298-3874	frgeol@aol.com
2006	Colorado	Jon White	(303) 866-3551	jonathan.white@state.co.us
2007	Pennsylvania	Chris Ruppen	(724) 495-4079	cruppen@mbakercorp.com
2008	New Mexico	Erik Rorem	(505) 438-6161	erik.rorem@geobrugg.com
2009	New York	Mike Vierling	(518) 471-4378	michael_vierling@thruway.state.ny.us

55th Annual Highway Geology Symposium
September 7 - 10, 2004
Fairmont Plaza Hotel, Kansas City, MO

GENERAL INFORMATION

On behalf of the Kansas Department of Transportation, Missouri Department of Transportation, HNTB, Missouri Geologic Survey, Kansas Geologic Survey and the University of Missouri, Kansas City, we would like to welcome you to the 55th Annual Highway Geology Symposium. The symposium is scheduled for September 7th through the 10th at the Fairmont Plaza Hotel on World Famous Country Club Plaza in Kansas City Missouri.

The 55th Annual HGS, beginning on Wednesday, September 8, consists of a full day of technical presentations, a full day field trip, and concludes with a final half day of technical presentations on Friday, September 10.

TRB WORKSHOP:

The Symposium will be preceded on Tuesday, September 7th by a 1/2 day Transportation Research Board (TRB) workshop. The workshop will consist of a morning technical session on Geotechnical Methods Revisited. This workshop is sponsored by TRB Committees AFP10 andAFP20. The registration fee for the TRB workshop is $25.00 (Please see registration form).

Guest Tour:

A full-day tour begins by a trip to Andre's Confiserie Suisse for Coffee and Pastries, than to the Nelson-Atkins Art Museum for a guided tour. Lunch will be at the Daniel Webster School. Following lunch there will be a driving tour of Kansas City. The cost for this tour is $40. Please see Registration Form.

55th Annual
Highway Geology Symposium
Kansas City, Missouri

Tuesday, September 7, 2004

11:00 am-7:00 pm   TRB and HGS Registration

TRB Mid-Year Meeting Agenda

Moderator: Bob Henthorne, KDOT

1:00 pm-2:00 pm   *Geotechnical Investigations and Testing in Soils*
        Ben Rivers, FHWA

2:00 pm-3:00 pm   *Coring Methods and Testing*
        Scott Tunison, Crux Subsurface, Inc.

3:00 pm-3:30 pm   Break

3:30 pm-4:00 pm   *Coring Methods and Testing,* Continued

4:00 pm-4:30 pm   *Optical and Acoustical Televiewer Borehole Logging-Improved Oriented Core Logging Techniques.*
        Peter Ingraham, Golder Assoc.

4:30 pm-5:00 pm   *Sonic Drilling*
        Tom Ruda, Deidrich Drill Inc.

5:30 pm-7:00 pm   Welcome reception – Sponsor introductions – Visit with Exhibitors
Poster Session

Wednesday, September 8th 2004

7:00 am-12:00 pm   HGS Registration

8:00 am-8:10 am   *Welcome*
Bob Henthorne, KSDOT and John Szturo, HNTB
55th Annual HGS Co-Chairmen

8:10 am-9:00 am   *Geologic Settings of Missouri and Kansas*
        Mimi Garstang – Missouri State Geologist
        Lee Allison – Kansas State Geologist

Technical Session I - Moderator: Andrea Prince – URS Corporation

9:00 am-9:20 am   *Legal Issues for Geotechnical Investigations*
                          Carmen Bakarich, KDOT

9:20 am-9:40 am   *Geotechnical Challenges of Design/Build Transportation Projects*
                          Clint Harris, P.E., Terracon

9:40 am-10:00 am   *You Want It Where?Design Challenges Associated With*
                         Constructing the New Dolwick Connector Into the Existing I-275
                         Embankment
                          Darrin Beckett, P.E., QORE, Inc.
                          Craig Lee, P.E., QORE, Inc.

10:00 am-10:20 am   Break

Technical Session II - Moderator: Casey Jones – Geotechnology Inc.

10:20 am-10:40 am   *Identifying Areas with Subsidence Potential beneath U.S. 50*
                          Highway in Eastern Reno County, Kansas, using High-Resolution
                          Seismic Reflection
                           Richard D. Miller, Kansas Geological Survey

10:40 am-11:00 am   *A 2-D MASW Shear-Wave Velocity Profile Along A Test*
                          Segment of I-70, St. Louis, Missouri
                           T. Thitimakorn, University of Missouri-Rolla
                           N. Anderson, University of Missouri-Rolla
                           T. Fennessey, Missouri DOT
                           R. Lauer, Missouri DOT

11:00 am-11:20 am   *Remote Sensing Studies, Carroll and Tippecanoe Counties,*
                          Indiana, With Engineering Geology Applications
                           Yinghui Sui, Purdue University
                           Huagen Liu, Purdue University
                           Terry R. West, Purdue University

11:20 am-11:40 am   *Layne talk*
                           Thomas Hurley, Layne GeoConstruction

11:40 am-12:00 pm   *Case History of the South Street Sinkhole*
                          Frederick, Maryland
                           A. David Martin, Maryland State Highway Administration

12:00 pm-1:30 pm   **Lunch – On your own**

Technical Session III - Moderator: Mike Fritz – MoDot

1:30 pmam-1:50 pm   *The Expectations and Realities of Geophysical Investigations*
In Karst
         Joseph A. Fischer, Geoscience Services
         Donald L. Jagel, Advanced Geophysical
         Joseph J. Fischer, Geoscience Services
         Richard S. Ottoson, Geoscience Services

1:50 pm-2:10 pm   *Debris Flow Remediation*
         Erik Rorem, Geobrugg Protection Systems

2:10 pm-2:30 pm   *A Detailed Study of The New Baltimore Landslide*
Along Pennsylvania Turnpike
         Ryan S. Tinsley, Michael Baker Jr., Inc.
         Abdul Shakoor, Kent State University

2:30 pm-2:50 pm   *Washington SR-20 Rock Avalanche – Characterization,*
Analysis and Monitoring
         R. Burk, URS
         N. Norrish, Wyllie & Norrish Rock Engineers
         S. Lowell, WSDOT
         M. Molinari, URS
         R. LaHusen, USGS
         J. Schick, URS
         B. Strickler, URS

2:50 pm-3:10 pm   *The Russell I-70 Sinkhole Saga Continues*
         Neil Croxton, Kansas Department of Transportation

3:10 pm-3:30 pm   Break

Note: Technical Sessions IV and V are Concurrent Sessions
Concurrent Session IV

Technical Session IV- Moderator: Wayne Duryee – HNTB Corporation

3:30 pm-3:50 pm   *Slope Stabilization Using Recycled Plastic Pins*
         J. Erik Loehr, University of Missouri-Columbia
         John J. Bowders, University of Missouri-Columbia
         Cheng-Wei Chen, University of Missouri-Columbia
         Katy S. Chandler, University of Missouri-Columbia
         Patrick H. Carr, The Judy Company, Inc.

3:50 pm-4:10 pm   *A Masonry Wall and Slide Repair Using Soil Nails*
and Rock Dowels
         Drew Gelfenbein,
         Christopher Benda, P.E.,
         Peter Ingraham, P.E.

4:10 pm-4:30 pm	*US 35/I 64 Interchange, Embankment and MSE Wall* *Design and Construction Using Lightweight Backfill* James C. Fisher, West Virginia DOT

4:30 pm-4:50 pm   *Soil Nailing: DOT's Warming Up to New Technology*
                   Patrick Carr, The Judy Company.

4:50 pm-5:10 pm   *Monitoring Shallow Slope Failures in the Ozark Plateau*
                   Using Time Domain Reflectometery
                           Norman D. Dennis, Ph.D., P.E., University of Alabama
                           Voon Wong, McClelland Engineers
                           Chong Wei OoiDept. Of Engineering, University of
                           Arkansas

5:10 pm-5:30 pm   *Design Considerations for Hybrid MSE/Shoring Retaining Walls*
                           Frank Harrison, P.E. Golder Associates Inc.
                           Kimberly Morrison, P.E., R.G., Golder Associates Inc.
                           Jim Collin, P.E., Ph.D., The Collin Group
                           Scott Anderson, P.E., Ph.D., FHWA

5:30 pm-5:45 pm   Field Trip Overview

Concurrent Session V

Technical Session V - Moderator: Bruce Harvel – MoDOT
:

3:30 pm-3:50 pm   *Observations on Drainage and Strength Characteristics of*
                   Missouri Roadway Base
                           Awilda M. Blanco, University of Missouri-Columbia
                           John J. Deeken, University of Missouri-Columbia
                           John J. Bowders, University of Missouri-Columbia
                           William J. Likos, University of Missouri-Columbia
                           John P. Donahue, MODOT

3:50 pm-4:10 pm   *Use of Lime Kiln Dust for Stabilization of Fine-Grained*
                   Subgrade Soils
                           Timothy D. Shevlin, Civil & Environmental Consultants,
                           Abdul Shakoor, Kent State University

4:10 pm-4:30 pm   *Exploding Roads in Texas: an Ounce of Prevention is Worth*
                   a Pound of Cure
                           Pat Harris, Texas Transportation Institute

4:30 pm-4:50 pm   *Subsurface Surprizes in a Fast-Track Design/Build Project*
                           Patrick Poepsel and James Sheahan, HDR Inc.

4:50 pm-5:10 pm   *Geological and Geochemical Aspects of Sulfate Heaves Along the*
                   US-550 Corridor in Northern New Mexico
                           Frank Harrison and Nancy Dessenberger,
                           Golder Associates Inc.

| 5:10 pm-5:30 pm | *Granites of the United States and Relationships Pertaining to their Use as Aggregate*
George H. Davis, MODOT |
| 5:30 pm-5:45 pm | Field Trip Overview |

Thursday, September 9, 2004

8:30 am-3:30 pm	Geology Field Trip of Kansas City
8:30 am-3:30 pm	Guest Trip
3:45 pm-5:00 pm	Steering Committee Meeting
6:00 pm-7:00 pm	Social Hour and Exhibits - Cash Bar
7:00 pm-10:00 pm	Annual Banquet and Program Guest Speaker – Karin Jacoby – City of Kansas City, Missouri Brush Creek Flood Control Project

Friday, September 10th 2004
Technical Session VI - Moderator: Syed Hasan – U. of Missouri, Kansas City

8:00 am-8:20 am	*Grout Stabilization of Compressible Embankment Fills Beneath Bridge Approach Slabs, SR51 HOV Lanes Design-Build Project, Phoenix, Arizona* Daniel N. Frechette, Ph. D., P.E. AMEC Earth & Environmental, Inc. Nicholas J. LaFrontz, P.E., AMEC Earth & Envir., Inc.
8:20 am-8:40 am	*Mine Paste-Soil Backfills-A new Application of Paste Technology* Michael Thompson, Golder Associates
8:40 am-9:00 am	*Recent Development of Geosynthetic-Reinforced Column Supported Embankments* Jie Han, University of Kansas James G. Collin, The Colin Group Jie Huang, University of Kansas
9:00 am-9:20 am	*Investigating the Potential Impacts of Past Mining Activities, on the Widening of SR 68, Mohave County, Arizona* Nick Priznar, AZDOT Robert Cummings, Saguaro GeoServices, Inc.
9:20 am-9:40 am	*Philosophy of Evaluating Surface-Fault-Rupture Hazards in the Puget Sound Region, Washington* Jeffery Keaton, AMEC David H. McCormack, Aspect Consulting

9:40 am-10:00 am   *Geological and Design Considerations for Replacement of*
                     Suspension Cable Anchorages, Bear Mountain Bridge, Hudson
                     River, New York
                             Danny J. Van Roosendaal, Haley & Aldrich, Inc.
                             Andrew F. McKown, Haley & Aldrich, Inc.

10:00 am-10:20 am   Break

Technical Session VII - Moderator: Jim Brennan – KSDOT

10:20 am-10:40 am   *Rockfall Closure Impact and Economic Assessment for*
                     Rockfall Sites in Tennessee
                             Vanessa Bateman, Tennessee Department of Transportation

10:40 am-11:00 am   *Soil Survey Use of GPS GIS with GPS and Automation*
                     Applications for Soils Design
                             Matthew Trainum, Iowa Dept. of Transportation

11:00 am-11:20 am   *Evaluation of Some Geologic Factors Affecting the Quality of*
                     Limestone Construction Aggregate
                             Evan Franseen, Kansas Geological Survey
                             Jason McKirahan, Marathon Oil Company
                             Robert H. Goldstein, University of Kansas

11:20 am-11:40 am   *MORFH RS: A Rockcut Rating System for Missouri*
                     Highways
                             Norbert H. Maerz, University of Missouri – Rolla
                             Ahmed Youssef, University of Missouri – Rolla
                             Robert Lauer, MODOT

11:40 am-12:00 pm   *Drilled Shaft Design, Construction, and Inspection*
                     Challenges on the Kentucky Lock Project
                             Charles "Tony" Hunley, P.E., S.E., American Consulting
                             Engineers, PLC
                             Kurt Schaefer, P.E., FMSM Engineers

Concluding Remarks – Adjournment

Poster Session: *Analysis and Assessment of the Slope Stability in a Copper Mine*
                     Lijun Zhang, Morgan State University
                     Duowen Ding, Morgan State University

HIGHWAY GEOLOGY SYMPOSIUM

HISTORY, ORGANIZATION AND FUNCTION

Established to foster a better understanding and closer cooperation between geologists and civil engineers in the highway industry, the Highway Geology Symposium (HGS) was organized and held its first meeting on March 14, 1950, in Richmond, Virginia. Attending the inaugural meeting were representatives from state highway departments (as referred to at the time) from Georgia, South Carolina, North Carolina, Virginia, Kentucky, West Virginia, Maryland and Pennsylvania. In addition, a number of federal agencies and universities were represented. A total of nine technical papers were presented.

W.T. Parrott, an engineering geologist with the Virginia Department of Highways, chaired the first meeting. It was Mr. Parrott who originated the Highway Geology Symposium.

It was at the 1956 meeting that future HGS leader, A.C. Dodson, began his active role in participating in the Symposium. Mr. Dodson was the Chief Geologist for the North Carolina State Highway and Public Works Commission, which sponsored the 7th HGS meeting.

Since the initial meeting, 52 consecutive annual meetings have been held in 32 different states. Between 1950 and 1962, the meetings were held east of the Mississippi River, with Virginia, West Virginia, Ohio, Maryland, North Carolina, Pennsylvania, Georgia, Florida and Tennessee serving as host state.

In 1962, the Symposium moved west for the first time to Phoenix, Arizona where the 13th annual HGS meeting was held. Since then it has alternated, for the most part, back and forth for the east to the west. The Annual Symposium has moved to different locations as follows:

List of Highway Geology Symposium Meetings

No.	Year	HGS Location	No.	Year	HGS Location
1st	1950	Richmond, VA	2nd	1951	Richmond, VA
3rd	1952	Lexington, VA	4th	1953	Charleston, W VA
5th	1954	Columbus, OH	6th	1955	Baltimore, MD
7th	1956	Raleigh, NC	8th	1957	State College, PA
9th	1958	Charlottesville, VA	10th	1959	Atlanta, GA
11th	1960	Tallahassee, FL	12th	1961	Knoxville, TN
13th	1962	Phoenix, AZ	14th	1963	College Station, TX
15th	1964	Rolla, MO	16th	1965	Lexington, KY
17th	1966	Ames, IA	18th	1967	Lafayette, IN
19th	1968	Morgantown, WV	20th	1969	Urbana, IL
21st	1970	Lawrence, KS	22nd	1971	Norman, OK
23rd	1972	Old Point Comfort, VA	24th	1973	Sheridan, WY

25th	1974	Raleigh, NC		26th	1975	Coeur d'Alene, ID
27th	1976	Orlando, FL		28th	1977	Rapid City, SD
29th	1978	Annapolis, MD		30th	1979	Portland, OR
31st	1980	Austin, TX		32nd	1981	Gatlinburg, TN
33rd	1982	Vail, CO		34th	1983	Stone Mountain, GA
35th	1984	San Jose, CA		36th	1985	Clarksville, IN
37th	1986	Helena, MT		38th	1987	Pittsburgh, PA
39th	1988	Park City, UT		40th	1989	Birmingham, AL
41st	1990	Albuquerque, NM		42nd	1991	Albany, NY
43rd	1992	Fayetteville, AR		44th	1993	Tampa, FL
45th	1994	Portland, OR		46th	1995	Charleston, WV
47th	1996	Cody, WY		48th	1997	Knoxville, TN
49th	1998	Prescott, AZ		50th	1999	Roanoke, VA
51st	2000	Seattle, WA		52nd	2001	Cumberland, MD
53rd	2002	San Luis Obispo, CA		54th	2003	Burlington, VT
55th	2004	Kansas City, MO				

Unlike most groups and organizations that meet on a regular basis, the Highway Geology Symposium has no central headquarters, no annual dues, and no formal membership requirements. The governing body of the Symposium is a steering committee composed of approximately 20-25 engineering geologist and geotechnical engineers from state and federal agencies, colleges and universities, as well as private service companies and consulting firms throughout the country. Steering committee members are elected for three-year terms, with their elections and re-elections being determined principally by their interests and participation in and contribution to the Symposium. The officers include a chairman, vice chairman, secretary, and treasurer, all of whom are elected for a two-year term. Officers, except for the treasurer, may only succeed themselves for one additional term.

A number of three-member standing committees conduct the affairs of the organization. The lack of rigid requirements, routing, and relatively relaxed overall functioning of the organization is what attracts many of the participants.

Meeting sites are chosen two or four years in advance and are selected by the Steering Committee following presentations made by representatives of potential host states. These presentations are usually made at the steering committee meeting, which is held during the Annual Symposium. Upon selection, the state representative becomes the state chairman and a member protem of the Steering Committee.

The symposia are generally for two and one-half days, with a day-and-a-half for technical papers and a full day field trip. The Symposium usually begins on Wednesday morning. The field trip is usually Thursday, followed by the annual banquet that evening. The final technical session generally ends by noon on Friday. In recent years this schedule has been modified to better accommodate climate conditions and tourism benefits.

The field trip is the focus of the meeting. In most cases, the trips cover approximately from 150 to 200 miles, provide for six to eight scheduled stops, and require about eight hours.

Occasionally, cultural stops are scheduled around geological and geotechnical points of interest. To cite a few examples: in Wyoming (1973), the group viewed landslides in the Big Horn Mountains; Florida's trip (1976) included a tour of Cape Canaveral and the NASA space installation; the Idaho and South Dakota trips dealt principally with mining activities; North Carolina provided stops at a quarry site, a dam construction site, and a nuclear generation site; in Maryland, the group visited the Chesapeake Bay hydraulic model and the Goddard Space Center; The Oregon trip included visits to the Columbia River Gorge and Mount Hood; the Central Mineral Region was visited in Texas; and the Tennessee meeting in 1981 provided stops at several repaired landslides in Appalachia regions of East Tennessee.

In Utah (1988) the field trip visited sites in Provo Canyon and stopped at the famous Thistle Landslide, while in New Mexico in 1990 the emphasis was on rockfall treatment in the Rio Grande River canyon and included a stop at the Brugg Wire Rope headquarters in Santa Fe.

Mount St. Helens was visited by the field trip in 1994 when the meeting was in Portland, Oregon, while in 1995 the West Virginia meeting took us to the New River Gorge bridge that has a deck elevation 876 feet above the water.

In Cody, Wyoming the 1996 field trip visited the Chief Joseph Scenic Highway and the Beartooth uplift in northwestern Wyoming. In 1997 the meeting in Tennessee visited the newly constructed future I-26 highway in the Blue Ridge of East Tennessee. The Arizona meeting in 1998 visited Oak Creek Canyon near Sedona and a mining ghost town at Jerrome, Arizona.

At the technical sessions, case histories and state-of-the-art papers are most common; with highly theoretical papers the exception. The papers presented at the technical sessions are published in the annual proceedings. Some of the more recent proceedings my be obtained from the Treasurer of the Symposium.

Banquet speakers are also a highlight and have been varied through the years.

A Medallion Award was initiated in 1970 to honor those persons who have made significant contributions to the Highway Geology Symposium. The selection was and is currently made from the members of the national steering committee of the HGS.

A number of past members of the national steering committee have been granted Emeritus status. These individuals, usually retired, resigned from the HGS Steering Committee, or are deceased, have made significant contributions to the Highway Geology Symposium. A total of 20 persons have been granted the Emeritus status. Ten are now deceased.

Several Proceedings volumes have been dedicated to past HGS Steering Committee members who have passed away. The 36th HGS Proceedings were dedicated to David L. Royster (1931-1985, Tennessee) at the Clarksville, Indiana Meeting in 1985. In 1991 the Proceedings of the 42nd HGS meeting held in Albany, New York was dedicated to Burrell S. Whitlow (1929-1990, Virginia).

HIGHWAY GEOLOGY SYMPOSIUM
55th ANNUAL

KANSAS CITY, MISSOURI
SEPTEMBER 7-10, 2004

LOCAL ORGANIZING COMMITTEE

Bob Henthorne – Kansas Department of Transportation
Mike Fritz – Missouri Department of Transportation
John Szturo – HNTB Corporation
Jamie Szturo – Volunteer
Andrea Prince – URS Corporation
Bruce Harvel – Missouri Department of Transportation
Bruce Wilkinson – Haley and Aldrich
Casey Jones – Geotechnology Inc.
Clay Rathbun – The Judy Company
James Mehnert – HNTB Corporation
Wayne Duryee – HNTB Corporation
Syed Hasan – University of Missouri – Kansas City

SPONSORED BY:

Kansas Department of Transportation
Missouri Department of Transportation
Kansas Geological Survey
Missouri Department of Natural Resources
University of Missouri – Kansas City

HIGHWAY GEOLOGY SYMPOSIUM

EMERITUS MEMBERS OF THE STEERING COMMITTEE

Emeritus Status is granted by the Steering Committee

R.F. Baker*
David Bingham
Virgil E. Burgat*
Robert G. Charboneau*
Hugh Chase*
A.C. Dodson*
Walter F. Fredericksen
Brandy Gilmore
Joseph Gutierrez
Charles T. Janik
John Lemish
Bill Lovell
George S. Meadors, Jr.*
Willard McCasland
David Mitchell
W.T. Parrot*
Paul Price*
David L. Royster*
Bill Sherman
Mitchell Smith
Sam Thornton
Berke Thompson*
Burrell Whitlow*
Earl Wright
Ed J. Zeigler
Steve Sweeney

*Deceased

HIGHWAY GEOLOGY SYMPOSIUM

MEDALLION AWARD WINNERS

The Medallion Award is presented to individuals who have made significant contributions to the Highway Geology Symposium over many years. The award, instituted in 1969, is a 3.5-inch medallion mounted on a walnut shield and appropriately inscribed. The award is presented during the banquet at the annual Symposium.

Hugh Chase*	-	**1970**
Tom Parrott*	-	**1970**
Paul Price*	-	**1970**
K.B. Woods*	-	**1971**
R.J. Edmonson*	-	**1972**
C.S. Mullin*	-	**1974**
A.C. Dodson*	-	**1975**
Burrell Whitlow*	-	**1978**
Bill Sherman	-	**1980**
Virgil Burgat*	-	**1981**
Henry Mathis	-	**1982**
David Royster*	-	**1982**
Terry West	-	**1983**
Dave Bingham	-	**1984**
Vernon Bump	-	**1986**
C.W. "Bill" Lovell	-	**1989**
Joseph A. Gutierrez	-	**1990**
Willard McCasland	-	**1990**
W.A. "Bill" Wisner	-	**1991**
David Mitchell	-	**1993**
Harry Moore	-	**1996**
Earl Wright	-	**1997**
Russell Glass	-	**1998**
Harry Ludowise	-	**2000**
Sam Thornton	-	**2000**

*Deceased

GEOTECHICAL CHALLENGES OF DESIGN/BUILD TRANSPORTATION PROJECTS

By Clint J. Harris, P.E. [1] M. ASCE

ABSTRACT

Design/Build transportation projects involve a great deal of complex issues on a limited budget and fast-paced schedule. Rarely seen are the geotechnical impacts/contributions to the project. However, having a geotechnical consultant that is committed to innovative ideas and working closely with the design-build team can be a significant benefit and lead to overall increased savings. Savings to the project can be both from a financial as well as time and effort standpoint. The paper will go over the role of the geotechnical consultant on design/build projects and how value engineering can save in the overall construction costs. Specific case studies of successful and failed value engineering programs from the I-15 Reconstruction Project in Salt Lake City, Utah and the Southeast Corridor Multi-modal Transportation Project (TREX) in Denver, Colorado will be discussed. The geotechnical challenges included building large embankments on soft, highly compressible, low strength soils, and the construction of traditional retaining walls on expansive soils with limited right-of-way.

Case Studies include the use of innovative geotechnical concepts and earned value engineering programs.

INTRODUCTION

The case studies presented herein are based on the two largest design/build transportation projects within the United States, the I-15 Reconstruction Project in Salt Lake City, Utah and the Southeast Corridor Multi-modal Transportation Project also known as "TREX" in Denver, Colorado. The construction costs for these projects are in excess of $1.6 billion.

1st Project

The I-15 Reconstruction Project involved total reconstruction of 17 miles of Interstate 15 and Interstate 80 within Salt Lake City, Utah. This project included the construction of over 140 bridge structures and several miles of mechanically stabilized earth (MSE) retaining walls.

2nd Project

The TREX project involved the construction of 19 miles new light rail transit and 17 miles of highway widening of Interstate 25 and Interstate 225 throughout Denver, Colorado. This project

---

[1] Clint J. Harris, P.E. is a Geotechnical Project Manager for Terracon Consultant, Inc. in Wheat Ridge, Colorado.

included the construction of over 61 bridge structures, over 3 million square feet of retaining walls, three light rail transit park-n-ride structures, and two underground drainage tunnels.

SITE CONDITIONS

I-15 Reconstruction Project

The subsurface soil conditions can be generalized as very soft to medium stiff normally consolidated lake bed sediments consisting primarily of lean to fat clays with minor interbedded silt and sand lenses to depths of about 75 to 80 feet. At many locations, a substantial sand deposit was encountered below the clay deposits. The lakebed sediments continue to an estimated depth of about 1,000 feet.

The laboratory test results and settlement/consolidation monitoring results from the original construction of Interstate 15 during the 1960's confirmed that the normally consolidated very soft to medium stiff clay soil would have a settlement/consolidation duration on the order of 1½ to 3 years. The laboratory tests and piezo cone soundings also indicated that the clay materials had very low shear strengths and would most likely needed specialized attention during embankment and retaining wall construction to maintain slope stability.

The project is located near side the Wasatch Fault which has a probabilistic Maximum Credible Earthquake (MCE) of 7.5 on the Richter Scale. Horizontal ground accelerations on the order of 0.6 to 0.72g were anticipated with this MCE. A large seismic criterion coupled with poor subgrade soil conditions also attributed to specialized lateral structural foundation designs and the need for mitigation for possible liquefiable sand soil throughout the project.

Settlement/consolidation calculations indicated that primary consolidation on the order of about 10 to 15 % of the embankment heights may occur. It was anticipated that secondary or post construction settlement/consolidation would be on the order of about 6 to 10 inches over a 10-year period. The design/build team proposed that a post construction settlement/consolidation on the order of 3 inches or less during the 10 year warranty period would lead to better ride performance, so this became the settlement/consolidation criteria for the project.

TREX Project

The subsurface conditions along the TREX alignment primarily consists of approximately 10 feet of wind blown clays with some silt and sands overlying the claystone and sandstone bedrock. The clay soils and claystone bedrock are generally considered to be expansive material. These materials typically expand 2 to 4 percent. Claystone bedrock in some areas may expand as much as 8 percent. In another segment of the project, there are up to 75 feet of alluvial sands and gravels overlying very hard Denver Blue claystone bedrock. This area is typically called the "Narrows" a name given to this stretch of highway because of its narrowly excavated/depressed passageway.

The design challenges of the TREX Project primarily consisted of construction in saturated alluvial materials and expansive soil/bedrock conditions, a limited right-of-way for highway widening, having to accommodate multiple municipalities, and having to provide design recommendations on a fast paced design schedule.

VALUE ENGINEERING PROGRAMS

I-15 Reconstruction Project

Due to the highly compressible and low strength subsurface clay soils throughout the project, the geotechnical design that reduced the time for construction of embankments was paramount to the success or failure of the project. Value engineering (VE) concepts that made the most impact on the construction schedule included the use of wick drains with differing wick spacing and patterns, the use of lightweight materials, the use of geotechnical instrumentation, and subsurface improvement techniques. This paper will primarily focus on the state of the practice techniques.

Also due to the highly compressible soils, the bridge foundations were supported on closed end steel pipe piles extending to depths of about 100 feet. Extremely high horizontal ground acceleration values associated with the Maximum Credible Earthquake (MCE) caused most of the bridge foundations to be governed by lateral capacity of the subsurface soils. This meant that up to 25 piles were used at each bent foundation. VE concepts that also aided in reducing geotechnical conservatism in the design process and therefore saving on the number or length of piles could equate to enormous savings to the project. These VE concepts included full scale vertical and lateral pile load test programs and pressuremeter tests to better predict lateral response and capacity of the subgrade soils.

I-15 Value Engineering Programs

Geofoam Embankments - In areas where either the construction schedule demanded immediate construction and time for consolidation of the subgrade soils was not possible, or where impact of the settlement/consolidation of the subgrade soils would cause damage to adjacent structures.

Geofoam blocks are high-density polystyrene blocks weighing approximately 1 pound per cubic foot, (pcf). These blocks are placed and clipped together and encapsulated in hydrocarbon resistant sheeting and used as embankment fill. After a desired height has been achieved, a distribution slab consisting of 12 inches of concrete is placed over the top of the geofoam mass in order to distribute the traffic loads more evenly over the surface of the blocks.

Figure 1. Geofoam Blocks

Figure 2.   Distribution Slab

The use of geofoam for embankments for the I-15 Reconstruction Project, although about twice the cost of Mechanically Stabilized Earth (MSE) retaining walls, allowed the contractor to immediately construct the roadway above the geofoam wall without having to wait for consolidation of the subgrade soils to occur. Some of the geofoam wall costs were recouped by not having to install costly wick drains. Most importantly, the use of geofoam on the project reduced potential claims against the Design/Build contractor by eliminating the possible future long-term consolidation of the subgrade soils and potential damage to the nearby structures.

Figure 3. Geofoam Along Widening of Interstate 80

Lime Cement Columns – During the technical proposal phase of the bid process, the geotechnical design team had produced a technical proposal to use lime cement columns throughout the project in order to reduce actual settlement/consolidation and increase global stability of embankments. The lime cement column design and construction procedures are discussed in great detail by Saye et al. Lime cement columns, although a theoretical marvel, was not practical from a fast paced design/build point of view. This was one EV concept that proved not to be "valuable" due to the extensive construction period required for installation. The installation of one field of lime cement columns along Interstate 80 and State Street in Salt Lake City took approximately 6 months, twice the allotted time period. This delay in construction almost cost the contractor liquidated damages in the amount of $35,000/day, the fee that Utah Department of Transportation would have charged the DB contractor for not meeting a road opening deadline. Lime cement columns appeared not to be a practical solution on fast paced design/build projects.

Figure 4. Wall SS-01 over Lime Cement Column area. Note, proximity of Nearby Building

Another valuable lesson learned from the installation of lime cement columns is that they should not be installed next to existing buildings. The building seen on the right on Figure 4 underwent several inches of heave caused by high injection pressures during the installation process.

High Strength Geotextile Reinforcement- Low strength soils existed throughout most of the project alignment. In these soft soil areas, roadway embankments up to 45 feet in height were proposed to be constructed. Due to the low strength soils and using the SHANSEP methodology (Ladd, 2), this would require as much as four stages of embankment construction. The use of high strength geotextile fabric was proposed by the geotechnical engineering team as a method of reducing the construction stages and ultimately reducing the construction duration for each embankment. High strength, bi-directional, weaved fabric having a shear strength of 375 kPa (54 psi) was utilized for this project. The geotextile fabric was installed at the base of the embankment being extended enough to provide sufficient "bonding" lengths. In some cases, as much as three layers of the geotextile fabric was utilized to meet "during construction", "end of construction" and long term factors of safety. A safety factor of 1.3 was utilized for "during and end of construction" condition and a factor of safety of 1.5 was utilized for the long-term condition. Embankment stage heights were determined by global slope stability calculations. Typical embankment heights of up to 16 feet were generally permissible without the use of geotextile fabric. However, with the use of geotextile fabric, an embankment could be constructed to a first stage height of approximately 26 feet. In most cases, several stages of embankment construction was "skipped" by using geotextile fabric.   The main value of this concept was in saving time, which allowed the contractor to collect valuable "milestone bonus awards".

Figure 5. High Strength Geotextile

Instrumentation Program – In order to possibly increase the embankment construction schedule, increase the overall safety of the construction, and reduce the typical conservatism in the geotechnical design, an instrumentation program was proposed and adopted by the Design/Build team. The instrumentation program consisted of settlement/consolidation measuring devices, which included magnet reed switches, monometers, and settlement/consolidation plates. Other instruments included both horizontal and vertical inclinometers, strain gauges on high strength geotextile fabric, and both open and closed-hole piezometers.

Magnet reed switches were installed as deep as 100 feet below the existing grade prior to embankment construction. As embankments were being placed measurements of settlement/consolidation at several depths were being collected. This data allowed the geotechnical engineer to determine the probable neutral plane of the pile foundations. The determination of the neutral plane was critical in the design phase of this project due to "down-drag" or negative skin friction effects of consolidating soil around the pile foundations. This information allowed the piles to be much shorter than originally determined.

Of all the settlement/consolidation measuring devices, the plain settlement/consolidation plates were the more reliable. Other settlement monitoring devices were not reliable because of error during the installation process or other human errors during the instrument reading process.
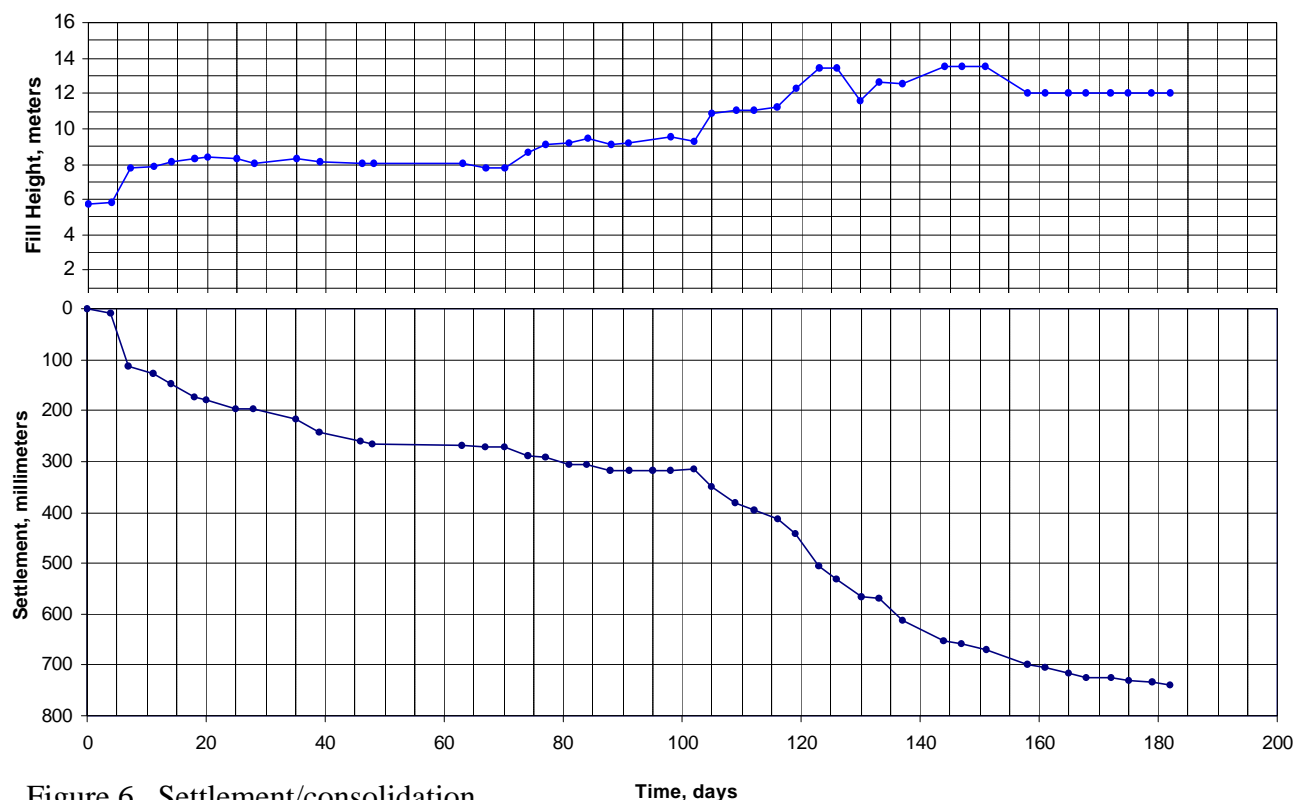
Figure 6. Settlement/consolidation

However settlement/consolidation and/or rods would also tend to be damaged during the embanking process. To account for this, redundant settlement/consolidation we used. The data collected from the settlement/consolidation plates allowed the contractor to pave much earlier than anticipated in the geotechnical reports. Settlement plate data indicated that most fill areas where wick drains were installed were reaching the end of primary consolidation approximately 30 to 60 days ahead of the anticipated schedule. The Aasaoka method of predicting the end of primary consolidation, first introduced in 1978, was utilized on this project. This figure above is an actual settlement/consolidation curve as embankment was being placed. Note that the primary settlement/consolidation is approximately 2.5 feet and was essentially completed 60 days after the final lift date.

Figure 7. Inclinometer

Inclinometers – As discussed previously, there was a need for rapid embankment construction throughout the corridor, however, safety concerns were paramount. Slope instability or failure was not acceptable from both a design and construction view point. The irreversible affects of a massive slope failure would have delayed the entire project and possibly cost the project millions of dollars in missed "milestone bonuses". To make sure that the embankments were being constructed at a safe rate as well as reducing the conservative nature of the geotechnical engineers, several hundred slope inclinometers were installed throughout the project. Slope inclinometers are a great tool to determine the soil deformation under a loaded situation. The rate of fill placement is directed by the daily reading of the inclinometers. "Threshold" levels were determined by the rate of soil movement and a rate of fill placement or a stop notice was then given to the contractor. This cautious process allowed the safe placement of embankments at the safest rate of fill placement. Consequently, this observational approach allowed the contractor to "ramp load" the embankments, which saved the contractor several months of waiting for consolidation to occur and strength to build up before proceeding to the next stage of embankment construction. The inclinometer became a vital and indispensable to the contractor instrument because it reduced the construction time by as much as half.

The total cost of the instrumentation program was approximately slightly over 3 million dollars and saved the contractor approximately 1 to 1.5 years of potential construction delays. This by far was the best value engineering program on the project.

Pile Load Tests and Pressuremeter Testing - With approximately 140 bridge structures on the project it was determined that site specific full scale pile load tests would save the project

possible millions of dollars. Nine pile load tests were completed throughout the project for differing soil conditions. Actual pile load tests, as required by the contract, allowed the design engineers to reduce the factors of safety from 2.5 to 2, therefore, reducing the overall number of piles for the entire project. Lateral load tests were also performed to determine the lateral capacity of the soil.

Figure 8. Pile Load Testing

This allowed for slight modifications to the LPILE parameters in order to give a more realistic result. The lateral load test allowed the design engineers to increase the capacity by as much as 10 percent.

Pressuremeter testing was also performed at the beginning of the project to better determine the lateral load characteristics of the subgrade soils. Pressuremeter testing indicated that a increase in lateral load capacity of 10 percent was probable by using developed P-Y curves. However, from a design/build viewpoint this would have slowed down the lateral load analyses of all 140-bridge structures. To save time, it was decided that the Pressuremeter information would not be utilized, however, the LPILE parameters would be later adjusted when the full-scale lateral load tests were completed.

TREX Project

Due to the saturated alluvial soils in the "Narrows" and limited right-of-way throughout the project, several VE concepts were utilized on this project. All of these VE concepts did not necessarily increase profits for the project, however, they did limit liability from a construction point of view. VE concepts that were utilized on the project primarily consisted of:

1. Additional Borings for Tunneling,
2. O-Cell Load Testing,
3. Well Point Pump Testing,
4. Pressuremeter Testing,
5. Instrumentation of Drilled Shaft Retaining Walls / Tunnels, and
6. Falling Weight Deflectometer Testing

For simplicity, only the more interesting VE concepts will be discussed herein.

Additional Borings and Analyses for Tunnels - As discussed previously, the TREX project is divided into two distinct geologic areas. The "Narrows" predominately consists of saturated alluvial sandy soil. The "Narrows" is sometimes referred to as "Lake Logan" by local residence because it tends to flood with several feet of water every so often due to the poor drainage in the area and under-designed and antiquated storm sewer systems. When this flooding occurs, the entire Interstate is shut down and traffic is diverted along local streets. As part of this project an elaborate storm water drainage system was constructed to collect surface water from the Interstate and divert it into a 13-foot diameter tunnel which eventually out-falls into the South Platte River about a mile from the site. The construction of the 13-foot diameter tunnel was one of the most complicated challenges for this project.

The tunnel extends underneath Mississippi Avenue from just south of Broadway Boulevard to the southbound lanes of the proposed LRT corridor. From just south of Broadway the drainage system is converted from a segmental tunnel system to a series of drainage boxes which was constructed with a cut and cover method.

The tunnel portion underneath Mississippi Avenue was constructed with a earth balance tunneling machine. The theory was that the saturated alluvial material would be less affected by a controlled tunneling process. Even with extreme care in both the design and preparatory process, there were several sinkholes that developed underneath Mississippi Avenue due to the accelerated tunneling process.

Figure 9. Sink Hole at Mississippi Avenue

Also as part of this drainage system another smaller diameter tunnel was constructed underneath the Interstate. The fear was that sink-holes would develop underneath the Interstate and possibly

cause some accidents. Another more experienced tunneling contractor was brought in for this segment of tunnel. Also as a safety measure, several more soil borings and de-watering pump tests were performed to better define the soil stratigraphy, profile and characteristics.

The benefits of this VE program was that sinkholes did not develop under the Interstate, however, they did develop where the geotechnical engineers had predicted they would.

Drilled Shaft Pile Load Test – Pile load tests are often performed to reduce the conservatism in the geotechnical design and/or confirm the actual load capacities of the soil/bedrock. For the TREX Project, the design team chose to use an Osterberg Load Cell (O-Cell) pile load testing device to perform three drilled shaft pile load tests along the corridor.

O-Cells were chosen by the design team because this type of load test can measure both side friction and end bearing components of vertical capacity separately. This was important because it determined if the "Denver Method" was appropriate. The "Denver Method" calculates the drilled shaft end-bearing component by dividing the standard penetration (N-value) by half and multiplying by 1000. The result is the end bearing value in

Figure 11. O-Cell Load Test Devices

pounds per square foot. The side friction component is typically 10% of the end-bearing component. These results are published in the proceeding of the ASCE Geotrans 2004 Conference held in Los Angeles, California.

The O-Cell Load tests provided valuable information as to the appropriateness of the "Denver Method" of calculating drilled shaft capacities. The actual results did not differ much from the predicted values, however, the savings to the contractor was in a reduction of the required safety factor from a factor-of-safety of 2.5 to 2.0.

Instrumentation of Drilled Shaft Retaining Walls – Another geotechnical challenge along the entire project consisted of limited access and right-of-way. Because of the limited access and right-of-way, typical MSE and cast-in-place retaining wall systems could not be constructed along several miles of alignment. Drilled shaft cantilever retaining walls were constructed.

The VE concept of instrumenting the drilled shaft retaining walls was to possibly reduce the conservatism in the geotechnical designs and therefore reduce the overall lengths of the drilled

shafts. The drilled shafts typically ranged from 2 to 4 feet in diameter and the construction costs grew exponentially with increases to diameters. Therefore, small shortening on the lengths would result in large savings to the contractor.

Some of the drilled shaft retaining walls were located within close proximity to critical utilities or structures. Therefore, monitoring of wall movement could better determine the safe rate of soil removal in front of the retaining walls. If too much movement was observed then the excavation process would be stopped until a new design was implemented. Below is a picture of two drilled shaft retaining walls that were monitored prior to the bridge deck being placed over the top. The geotechnical engineer determined that the building adjacent to the retaining walls could only deflect ½ inch prior to damage being observed in the building.

Figure 12: Adjacent Structure Next to Drilled Shaft Retaining Walls

The lateral displacement of the drilled shaft retaining walls as the material was being excavated proved to be of little value except in the case where there were critical structures nearby. For the most part, the excavation process for these retaining walls took place after most of the retaining walls were designed and constructed. Therefore, there was not an opportunity to reduce the drilled shaft lengths. There were also too many variables that could have been the difference between the predicted deflections and the actual deflections. These variables can range from the actual versus the design strength of the concrete, using the crack section moduli of the concrete, the lateral earth pressures were too high in the design versus what was seen in the field. Some of the drilled shafts did deflect as predicted as in the adjacent structures areas as seen in Figure 12. However, most deflected about ½ of the predicted. An in-depth analyses is given in the ASCE Geotrans2004 proceedings.

Conclusion

Value Engineering concepts for large design/build projects can be very beneficial to the design/build team as well as to the engineering profession. Value Engineering projects have been tracked by the Federal Highway Administration (FHWA) in large transportation projects from the year 2000 to 2003. The results indicate that VE programs are very beneficial by reducing project expenditures. In most cases, VE programs have a published return on investment ratio of 116:1 to 145:1.

As shown in the above case studies, there should be good communication between the contractor and the engineer wishing to perform the VE program. The contractor should be aware of the possible failures and the benefits from performing such tests.

References

Aasaoka, A. (1978). "Observational Procedure of Settlement/consolidation Prediction", *Soils and Foundations, Japan*. 18 (4), 87-101.

Attwooll, W. J., Turner, W. G., "Measured Pile Setup During Load Testing and Production Piling: I-15 Reconstruction Project in Salt Lake City, Utah," *Transportation Research Record No. 1663, Transportation Research Board (TRB)*, 1999.

Attwooll, et al., "Selection of Driven Pile Design Parameters for the I-15 Reconstruction Project," *Deep Foundations Congress, Geotechnical Special Publication No. 116, ASCE*, 2002.

Attwooll, W. J., "Analysis of T-REX O-Cell Tests and Drilled Shaft Design Recommendations", Presented to Colorado Association of Geotechnical Engineers (CAGE), 2002.

FHWA, "Value Engineering and the Federal Highway Administration", FHWA web site http://www.fhwa.dot.gov/ve/.

Ladd, C.C. "Stability evaluation during staged construction" *Journal of Geotechnical Engineering Division*, ASCE, 117 (4), 537-613, 1991.

Ladd, C.C. " THE TWENTY-SECOND TERZAGHI LECTURE" *1986 Annual Convention*, ASCE, 540-614, 1986.

Sisson, R.C., Harris, C.J., Mokwa, R.L., "Design of Cantilever Soldier Pile Retaining Walls in Stiff Clays and Claystones", "GeoSupport 2004 Drilled shafts, Micropiling, Deep Mixing, Remedial Methods, and Specialty Foundation Systems", *ASCE Geotechnical Special Publication No. 124*, 309-321, 2004.

Saye, S. R., Esrig, M. I., Williams, J. L., Pilz J., Bartlett S.F., "Lime Cement Columns for the Reconstruction of Interstate 15 in Salt Lake City, Utah." *ASCE Geo-Odessey, Blacksburg, VA.* , June 10 - 13th, 2001.

YOU WANT IT WHERE?:

DESIGN CHALLENGES ASSOCIATED WITH CONSTRUCTING THE NEW

DOLWICK CONNECTOR INTO THE EXISTING I-275 EMBANKMENT

By Darrin Beckett, P.E.[1] and Craig Lee, P.E.[2]

The Kentucky Transportation Cabinet (KYTC) is currently coordinating the design of a new section of roadway (the Dolwick Connector) in the northwest corner of Kenton County, Kentucky, between Erlanger and Crescent Springs. One section of the proposed alignment, approximately 1000 ft. long, crosses an embankment that supports the ramp from southbound I-75/71 to westbound I-275. The embankment was constructed in the early 1970's; is approximately 150 feet high; has an approximate 2H:1V slope; and consists of a heterogeneous mixture of limestone, shale, and clay. Due to design constraints, the proposed roadway must be placed within the limits of the existing embankment. Furthermore, the embankment slope cannot be flattened due to environmental concerns associated with the creek at the toe. As a result, the proposed roadway grade will be achieved by excavating into the existing embankment. KYTC is concerned about the overall stability of the embankment. Although there is no current evidence of instability in this embankment, numerous slope failures in embankment fills have occurred in the Northern Kentucky area. Because of the history of slope instability in the area and the proximity of the major interstate interchange, the KYTC Geotechnical Branch is approaching the design of this section of roadway very cautiously. Earth retaining systems consisting of permanent rock anchor (tiedback) retaining walls with soldier beams drilled into rock were selected as the means to support the proposed slope configuration. One wall is proposed just above the Dolwick Connector to support the roadway excavation and a second wall is proposed below the Dolwick Connector to improve the global stability of the entire embankment. The paper focuses on the challenges associated with site characterization and geotechnical design of the retaining walls. QORE and KYTC selected soil design parameters and geotechnical design criteria for the wall using engineering judgement and indirect correlations. QORE used the selected parameters to evaluate retaining wall loads at selected locations using both conventional earth pressure and limit equilibrium methods and then developed relationships to determine design loads along the walls. The project is currently scheduled to be let to contract in April, 2002. The results of the geotechnical investigation, including all subsurface data, retaining wall design loads, and other geotechnical design criteria, will be included in the contract documents. The retaining walls will be bid using design-build contracting.

LOCATION AND DESCRIPTION

The project site is located in the northwest corner of Kenton County, Kentucky, between Erlanger, Kentucky and Crescent Springs, Kentucky. The project is an extension of Dolwick Road from Turfway Road East to Crescent Springs Road. The horizontal alignment of the extension follows I-275, I-71/75, and ramp H that conveys southbound I-71/75 to westbound I-275. As such, several hundred feet of earth retaining systems will be used to establish the finished grade for the new roadway extension near the existing I-275 embankment. **The Project is currently under construction. There have been a whole set of challenges associated with construction that we will update in the near future.**

The Kentucky Transportation Cabinet (KTC) is concerned about the overall stability of the existing embankment in its current configuration and its modified configuration with the proposed retaining structures. Numerous landslides have occurred in the Northern Kentucky area in embankments constructed with material derived from the Kope formation. These are well documented and relatively well understood. We are unaware of any evidence of instability associated with this embankment.

Between Station 37+00 to Station 55+50 an earth retention system is required to create the horizontal space necessary for the 2-lane template and to stabilize the existing I-275 ramp. In this section the alignment will be excavated into the existing I-275 ramp embankment as it parallels the existing roadway. The earth retention system through this area will consist of drilled-in soldier pile tiedback walls.

From Station 43+00 to Station 49+50, a right (upper) and left (lower) wall is required. The purpose of the walls is to stabilize the existing I-275 ramp and to stabilize the slope below the planned connector road.

TOPOGRAPHY AND DRAINAGE

Kenton County is located in the Outer Blue Grass region in Northern Kentucky. The north boundary of the county is the Ohio River with the Licking River making up the east boundary. Kenton County and northern Kentucky is well dissected with numerous small streams, rivers and minor drainage features. The topography is characterized as "hilly". Flat areas occur mainly along broad ridges and along major streams. In the vicinity of the project, elevations range from about 850 feet MSL along I-275 to about 650 feet MSL in Dry Creek that runs along the toe of the existing I-275 ramp embankment.

GEOLOGY
The project site is mapped on the Covington quadrangle of the United States Geologic Survey (USGS) Geologic Map. According to the geologic map, the project following rock formations arranged from highest to lowest elevation.

Table No. 1: Generalized Geologic Section

Bull Fork Formation	Above 830 feet Mean Sea Level (MSL)
Bellevue Tongue of the Grant Lake Limestone	820 - 830 feet MSL
Fairview Formation	700 – 820 feet MSL
Kope Formation	Below 700 feet MSL

These formations consist of thin, horizontally bedded limestone with interbedded non-durable shale. The percentage of limestone and the integrity of the shale vary between the formations and help identify the formation. The Bull Fork Formation is at least 85 feet thick and consists of interbedded limestone and shale with the limestone making up more than 50 percent of the unit. The limestone beds are typically less than four inches thick but can be as thick as 12 inches.

The Bellevue Tongue of the Grant Lake Limestone is reportedly 7 to 20 feet thick and consists of rubbly, fossiliferous limestone with thin shale partings.

Underlying the Bellevue Tongue of the Grant Lake Limestone, the Fairview extends to the top of the Kope Formation. According to the geologic map, the Fairview is 90 to 120 feet thick and consists of interbedded limestone and shale. The horizontal beds are typically six inches or less but can be up to 15 inches thick. Our experience is that the shale makes up about one-half to two-thirds of the formation, with the shale content increasing at the bottom of the formation.

The Kope Formation underlies the Fairview Formation. The geologic map suggests the Kope is 205 to 240 feet thick. It consists of interbedded limestone and shale with the shale making up more than 85 percent of the formation. The limestone is very thinly bedded and the shale is less resistant to weathering than the other formations.

The Bull Fork and The Bellevue Tongue of the Grant Lake Limestone make up a large portion of the cut material generated from the surrounding roadways and was likely used to construct the existing I-275 ramp embankment. We also anticipate that deeper cuts that extended below elevation 820 feet will include the Fairview Formation. The formations used in constructing the existing embankment will affect interpretation of the existing embankment properties.

DRILLING AND SAMPLING

Field drilling and sampling was performed by the Kentucky Transportation Cabinet (KTC) forces and Horn and Associates in June and July of 2000. The recovered soil and rock samples were sealed, labeled and transported back to the KTC laboratory for logging and subsequent laboratory testing. The exploration included:

- § 40 auger soundings to rock then rock core
- § 24 soil test (standard penetration test and shelby tube) borings to rock then rock core
- § 10 auger soundings to rock with observation well

Borings were advanced at 50-foot intervals along the centerline of both the right and left walls. These borings are referred to as "wall borings". Each of the wall borings were advanced into rock and core samples obtained for subsequent logging and testing. Seven of the borings along the right wall were drilled as soil test borings with standard penetration tests performed at 5-foot vertical intervals to auger refusal. Typically, the wall borings for the right wall were located 22 feet right of roadway centerline. Eleven of the borings along the left wall were drilled as soil test borings with standard penetration tests performed at 5-foot vertical intervals to auger refusal. Typically, the wall borings for the left wall were located 75 feet left of roadway centerline. Soil test borings and rock coring were also advanced uphill of the proposed retaining walls to determine the conditions in the anticipated anchor bond zone. These borings were spaced at 200-foot intervals. For the right wall, six anchor borings were drilled approximately 75 feet right of centerline. For the left wall four anchor borings were drilled located 20 to 45 feet left of centerline.

INSTRUMENTATION

Open standpipe observation wells were installed at six locations as part of this exploration phase. Three observation wells were previously installed by KTC as part of a preliminary exploration. The majority of the observation wells are dry. Where water was noted, it usually occurs within a few feet of the top of rock.

In addition to the groundwater observation wells, slope inclinometers were installed at five boring locations. The inclinometers were seated into rock and the annulus around the inclinometer pipe backfilled with small crushed limestone (#9) aggregate. As of this date, the slope inclinometers how no movement. KTC personnel are currently responsible for reading the instrumentation.

EXISTING EMBANKMENT

The existing I-275 embankment was constructed in the 1970s. The embankment was constructed to a vertical height of 150 feet using an approximate 2H:1V slope. Reportedly, the existing I-275 ramp embankment was constructed of material generated during construction of the adjacent roadway projects. As mentioned previously, this material consists largely of rock from the Bull Fork, Bellevue Tongue of the Grant Lake Limestone, and Fairview formations. The borings indicate the embankment fill consists primarily of degraded clay-shale and limestone.

The samples were classified under both the Unified Soil Classification System (USCS) and AASHTO system. The majority of the samples (75) classified as CL under the USCS system with GC and SC each making up about one-fifth of the remaining samples. The gravel and sand sized pieces are likely limestone and shale pieces broken during SPT sampling. AASHTO classification ranges from A-2 to A-7-6, with the majority of the samples classifying as A-6 and A-7-6. Table No. 4 summarizes the test data for all the samples.

Table No. 2: Summary of Embankment Soil Properties

	Moisture Content, %	Liquid Limit	Plasticity Index	Percent Passing #4 Sieve, %	Percent Passing #200 Sieve, %
Average Value	29	39	20	76	57
Range of Values	3 - 30	28 – 57	12 – 35	46 - 100	20 – 100

Packer testing was performed in the embankment fill material at four locations. The purpose of the packer testing was to measure the permeability of the embankment material to evaluate if the fill could be classified as open graded rock fill or a soil fill. The Packer testing was performed using a double packer system under a low differential pressure of 20 psi. The testing was performed at 5-foot intervals as the boring progressed through the fill. The water flow was measured and recorded at one minute intervals for five minutes and then averaged. The hydraulic conductivity of the fill ranged from $6x10^{-4}$ cm/sec to $2x10^{-3}$ cm/sec.

To evaluate if the embankment fill materials could be characterized as a soil or rock fill, the permeability measured in the field was compared to "typical" permeability values for known particle size distributions. NAVFAC DM 7.2 provides typical values for the coefficient of permeability for compacted materials based on USCS groups. These are presented in Table 6. The permeability observed during the packer testing were typically in the range of 10^{-3} cm/sec, the embankment fill materials are more typical of a well graded gravel or well or poorly graded sands (GW, SW/SP) as opposed to a soil fill.

ROCK CONDITION

The rock cores recovered from the upper elevations throughout the project area were consistent with the Fairview Formation. The retrieved samples consisted of interbedded limestone and shale. The percent limestone for each core run was determined by the KTC geologist and is noted on the subsurface data sheets. The percent limestone for the right side wall and anchor borings averages 34 percent limestone. Below elevation 700 feet MSL, the percent limestone drops to 16 percent. This is strong indication that the Kope Formation begins in the project area at about elevation 700 feet MSL. Slake

Durability Index (SDI) testing was performed by KTC. The SDI values ranged from 9 to 95 with an average SDI value of 69.

The percent limestone for the left side wall and anchor borings averages 16 percent limestone with most of the sampled core occurring below 700 feet MSL. As a comparison, the percent limestone for the right wall averaged 34 percent. This is strong indication that the contact between the Fairview Formation and the Kope Formation begins in the project area at about elevation 700 feet MSL. Slake Durability Index (SDI) testing was performed by KTC. For the left wall, the SDI values ranged from 9 to 84 with an average SDI value of 54.

The top of rock (TOR) depth and the Base of Weathered Rock (BWR) were determined at each core location. The TOR is somewhat subjective and is based on a visual observation of the cores by the KTC geologist. TOR represents the depth where the material, visually, has the bedding structure of the parent rock. The BWR represents the KTC geologist interpretation of the lowest elevation of significant weathering. Evidence of weathering includes clay-like shale seams, water stains, mud seams, and broken and stained rock. Below the BWR, the rock is slightly weathered to not weathered.

ANALYSES

To complete our assessment of the Dolwick Connector retaining walls, several key tasks were identified. In general, these tasks included:

- § Determination of shear strength parameters for the I-275 embankment
- § Computation of wall loads and pressures
- § Evaluation of the stability of the designed slope below the left wall
- § Evaluation of the global stability of the proposed slope configuration
- § Modifications to increase the global stability

EMBANKMENT SHEAR STRENGTH PARAMETERS

Our understanding is that the I-275 ramp embankment has not exhibited any signs of slope instability since construction. We did not observe any evidence of slope instability in our site visits. Many embankments of similar geometric configuration in the northern Kentucky area have experienced slope instability. The majority of those are constructed of rock derived from the Kope Formation and lower Fairview formations. These materials are much less resistant to weathering and the Kope contains an appreciable increase in the shale content.

It is our opinion that the embankment consists of higher quality material than those that have experienced recurring slope failures. This is evidenced by the formations that makeup the "cut" materials in the surrounding roadway cuts and the long-term performance of the embankment, even after benches were cut into the embankment for

drilling purposes. It is clear from the data that the embankment is not constructed of clean, durable limestone shot rock and should not be modeled as a rock embankment.

We decided to first model the embankment as a shale embankment using the Shale Rating System developed by J. A. Franklin. The shale rating system groups rock materials according to slake durability index and plasticity index. The Shale Rating system yielded a range for the angle of internal friction of 12 to 17 degrees with cohesion ranging from 120 to 170 psf. Mid-range values were input into our slope stability model of the existing slope and the factors of safety computed. Most of the factors of safety were below 1.0, with many in the 0.7 to 0.8 range. These results did not correspond with the observed long-term performance of the embankment. We concluded that the embankment should not be modeled purely as a shale embankment.

In our opinion, the embankment should be modeled as a hybrid embankment, recognizing that the limestone pieces will contribute to the overall stability of the embankment. Numerous researchers have discussed the shear strength parameters of such embankments including Hopkins, Santi, Franklin and others. We reviewed the literature and decided that for Kentucky shales, the effective stress shear strength parameters are framed by the following values: angle of internal friction (24 to 28 degrees) and cohesion (100 to 300 psf). The final design parameters are 24 degrees and 100 psf.

TIEDBACK WALL LOADS

A variety of analysis procedures and design assumptions were used to determine the range of possible earth pressures acting on the retaining wall. The Rankine method, Rankine-Bell method, apparent earth pressure method, and the limit equilibrium analysis method were used to assess possible wall loads at four representative (critical) cross-sections. The limit equilibrium analysis included a traffic live load surcharge of 600 psf applied on roadway surfaces and a construction live load surcharge of 260 psf on the slope above the walls. The surcharges were not considered for the other analyses as they included an infinite slope above the wall instead of the actual geometry of the constructed slope. In our opinion, the infinite slope along with the surcharges, is conservative and the inclusion of the surcharges is unwarranted.

The Rankine, Rankine-Bell and apparent earth pressure methods determine the wall loads based on statically determinate conditions. For these three analysis methods, the lateral earth pressure coefficient is determined from the Mueller-Breslau (1906) equation such that:

$$K_a := \frac{(\cos(\phi - \theta))^2}{(\cos(\theta))^2 \cdot \cos(\delta + \theta) \cdot \left(1 + \sqrt{\frac{\sin(\phi + \delta) \cdot \sin(\phi - \beta)}{\cos(\delta + \theta) \cdot \cos(\beta - \theta)}}\right)^2}$$

where:

β	= backfill slope
δ	= wall friction
ϕ	= soil friction angle
θ	= wall inclination from vertical.

While the Rankine analysis method assumes that the backfill behind the wall is horizontal, incorporating the Mueller-Breslau lateral earth pressure coefficient into the analysis accounts for a sloping backfill condition.

APPARENT EARTH PRESSURE METHOD

The apparent earth pressure analysis method was developed to approximate the loads and stresses actually observed in braced excavations. It is intended to approximate maximum load conditions and thus provide an upper-bound solution to analysis problems. The apparent earth pressure analysis method for sands is based on the equation:

$$p = 0.65 \cdot k_a \cdot \gamma \cdot H$$

FACTORS OF SAFETY

The wall loads were computed under the most probable physical conditions by the limit equilibrium method using a design factor of safety of 1.4. The design factor of safety, however, is less than the 1.6 to 1.8 recommended by the KTC Geotechnical Manual for slopes adjacent to highway structures. We believe the 1.4 factor of safety value is reasonable because:

- § It is greater than the typical factor of safety (1.3) for tiedback walls reported in the FHWA manuals

- § All the tiedback anchors will be proof tested during actual construction

It is important to understand how the concept of factor of safety was used in our analyses. The Kentucky Transportation Cabinet, Geotechnical Manual 1997, presents a range of recommended factors of safety for roadway embankments, structures, soil cut slopes, and landslide corrections. These recommendations were used as a guide for our analyses. We also took into account the amount and integrity of the data along with construction considerations such as proof testing of all tiedback anchors.

LIMIT EQUILIBRIUM METHOD

Slope stability programs (such as PC Stabl) that incorporate the limit equilibrium method can be used to compute the forces required to stabilize a slope. The advantage to this method is that the actual slope configuration, subsurface conditions, and water level can be input and evaluated. The other methods assume an infinite beta slope above the wall and are somewhat conservative for this project. FHWA IF-99-015 cautions that the limit equilibrium method should be checked with a "hand calculation method" such as the apparent earth pressure method. This is because of the various ways that commercial slope stability programs distribute anchor forces to slices.

The limit equilibrium analysis method can be used to assess the reasonableness of design assumptions by selective use of soil conditions and input parameters. By performing limit equilibrium analyses with varying soil conditions and parameters, the sensitivity to possible adverse conditions or estimated parameters can be determined. Under similar conditions, the limit equilibrium model and the Rankine analysis produced similar wall loads.

LIMIT EQUILIBRIUM – APPARENT EARTH PRESSURE CORRELATION
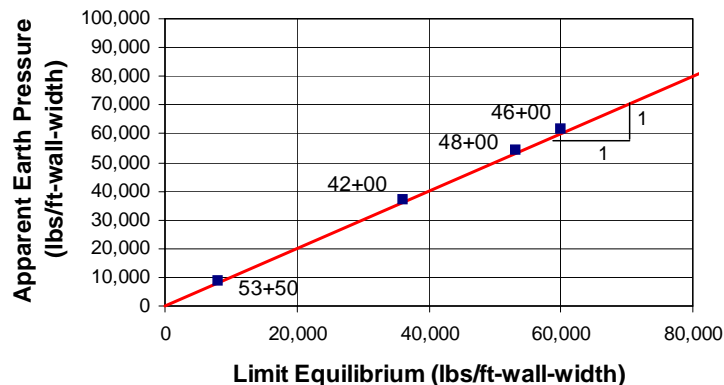
Figure 1 Relationship Between Limit Equilibrium and Apparent Earth Pressure (lbs)

From previous discussion, the apparent earth pressure method is an approximation of the actual wall loads based on observed, upper bound conditions. Additionally, current research has confirmed that the apparent earth method is conservative due to its design assumptions. The extent of the conservatism can be determined by comparing the apparent earth method with the limit equilibrium analysis method. By balancing the limit equilibrium method with various factors of safety equivalent wall loads can be determined. Figure 1 shows an approximate 1:1 correlation between the apparent earth method and the limit equilibrium analysis based on a 1.4 factor of safety.
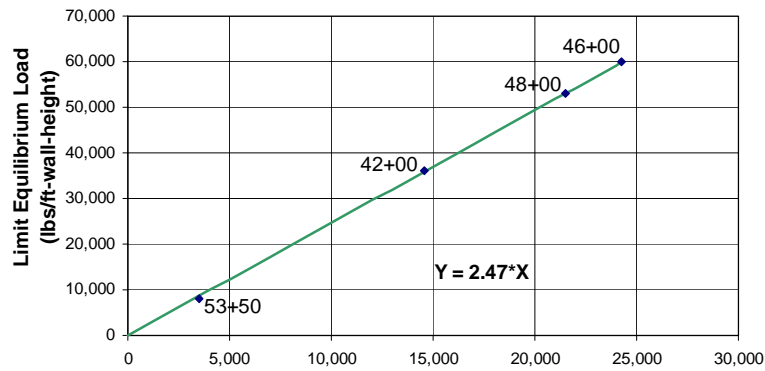
Based on Figure 1, the limit equilibrium method with a 1.4 factor of safety and a 100-psf cohesion value is roughly equivalent to the apparent earth pressure method.

DERIVATION OF WALL LOAD EQUATION

The limit equilibrium method is a relatively labor intensive analysis method to perform and it would be difficult to perform the analysis for each pile location. Thus, it is beneficial to find a model that reasonably approximates the limit equilibrium method but does not require the extensive calculations. Once an approximating equation is determined, the basic wall geometry can be assessed from the design drawings, and the design loads can quickly be determined.

Based on the previous discussions, the limit equilibrium method can be approximated by the apparent earth method. Thus, it is reasonable to assume that an equation of similar form to the apparent earth method could accurately predict the limit equilibrium results. This also satisfies the "hand calculation" check of the limit equilibrium method.

The wall loads are dependent on the soil strength parameters and the slope geometry. For the Dolwick Connector analysis, the soil strength is constant with a 24-degree internal friction angle and 100 psf cohesion and the soil-wall interface inclination is assumed constant at 0 (vertical). <u>The remaining variables that control wall load are the backslope (Beta value) and the wall height</u>.

Thus, a general equation to calculate the limit equilibrium load based on observed physical parameters could be determined. By combining various contributing factors and plotting them against the limit equilibrium wall load, a simplified relationship could be determined. A regression analysis was then used to assess the "accuracy" of the simplified equation. Figure 4 shows the relationship between the limit equilibrium wall load and Height^2 x Beta where wall height is in feet and Beta is in degrees.

Figure 2. Design Wall Load (pounds) and Design Wall Height^2 x Beta

A linear regression was used to establish a best-fit line between the data values to develop a simplifying equation that approximates total wall load per unit width of wall. We determined that the simplified equation reasonably described the relationship indicated by the data points and would become the design load equation.

$$P = 2.47 \cdot \beta \cdot H^2$$

where:

P = design soil load per unit wall width (lbs/ft)
b = backfill slope (degrees)
H = design wall height (feet)

GLOBAL STABILITY

The overall stability of the post-construction embankment was checked using the design shear strength parameters for the embankment material. The embankment was modeled with both tiedback walls in-place. Between stations 43+00 to 49+50, both left and right tiedback walls are proposed. Elsewhere, only one tiedback wall is proposed. The tiedback walls were modeled by distributing the horizontal pressure over the height of the wall. A high water elevation of 685 feet MSL was assumed in the creek. A minimum factor of safety of 1.4 was established as the acceptance criteria where two walls are used and 1.5 where only a single wall is used.

The wall loads computed by the relationship described in Figure 2 satisfies the factor of safety of 1.4 for local stability. However, when both the left and right wall are in place, the design does not yield a factor of safety of 1.4 against global failure of the embankment. In those instances, the left wall loads were increased to achieve the target factor of safety of 1.4 for global stability. We recognize that these are less than the KTC target factor of safety of 1.6 for embankments associated with structures. The lower factors of safety are reasonable for this project for the following reasons:

- The embankment is an existing embankment that has been stable for more than 25 years. We know of no evidence of slope movements.
- The post-construction embankment includes two tiedback walls constructed under a comprehensive Quality Assurance/Quality Control program. This program includes proof testing of all anchors and performance testing of representative anchors
- The soldier piles for the walls are socketed into rock.
- Compared to the existing slope configuration, the post-construction embankment geometry actually unloads the slope and improves surface drainage.

EARTH PRESSURE DISTRIBUTION

FHWA Publication IF-99-015 "Geotechnical Engineering Circular No. 4: Ground Anchors and Anchored Systems" and FHWA Publication RD-97-130 "Design Manual for Permanent Ground Anchor Walls" were used as reference documents in assigning the pressure distributions. Tiedback walls (permanent ground anchor walls) use a trapezoidal distribution of the earth pressure along the wall from the top of the soldier pile to the bottom of lagging.

SOIL PASSIVE RESISTANCE

FHWA Publications RD-97-130 and IF-99-015 were used in evaluating the use of soil passive pressures in designing the wall system. Some soil passive resistance is allowed along the length of the pile in designing the wall from stations 43+50 to 49+00. From stations 43+00 to 49+50, the left wall is present and stabilizes the embankment against sliding away from the right wall. The soil passive resistance was determined by assuming a cohesionless material and using an angle of internal friction of 24 degrees. The soil passive resistance value is a net value that subtracts out the active pressure on the backside of the pile.

At a depth of 20 feet below the ground surface, we calculated a passive soil pressure value of 4 ksf. In accordance with the recommendations presented in the FHWA manuals, we applied a factor of safety of 1.5 to that value to arrive at the recommended design maximum value of 2.5 ksf. The soil passive resistance is shown on Figure 3, Geotechnical Detail (typical).

RECOMMENDATIONS

The Report of Geotechnical Engineering Evaluation, dated April, 2001 contains a complete set of recommendations. The following recommendations are abbreviated from that report.

TIEDBACK WALLS

7.1.1   Use a tiedback wall designed, constructed, and instrumented in accordance with the **Special Note for Tiedback Walls**. The wall should be designed, constructed, and instrumented in accordance with the **Special Note for Tiedback Walls**. Payment will be by the square foot of facing.

7.1.2   Design wall loads and design wall heights are shown on the geotechnical wall profile sheets. Consider these loads to be working loads for Service Load or Load Factor Design. Wall loads include all applicable traffic and construction live load surcharges and hydrostatic pressures. A trapezoidal earth pressure distribution is specified for tiedback walls.

7.1.3   The Highest Allowable Pile Tip Elevation for soldier piles is the highest elevation that provides rock conditions to provide sufficient bearing resistance. The Highest Allowable Pile Tip Elevations are presented on the geotechnical wall profile sheets for each 50-foot station. Use linear interpolation to determine the Highest Allowable Pile Tip Elevations at intermediate stations.

7.1.4 Allowable axial end bearing pressure for soldier piles is 40 ksf at or below the Highest Allowable Pile Tip Elevation. No axial side resistance on rock socket is allowed.

7.1.5 Allowable lateral rock socket resistance pressure for soldier piles is 20 ksf and can be applied below the Highest Allowable Pile Tip Elevation over one socket diameter.

7.1.6 Passive soil resistance is permitted from Stations 43+50 to 49+00 only beginning at 10 feet below bottom of lagging. The allowable passive pressure distribution is shown on the detail. Apply passive soil resistance over a width of three times the diameter of the backfill around the soldier beam. The width may not exceed the center to center pile spacing.

7.1.7 Install and lock-off all right wall anchors between Stations 40+50 to 50+00 prior to beginning the excavation for the left wall. The left wall soldier pile installation may begin at the contractor's discretion.

7.1.10 Controlled Low Strength Material (CLSM) is permitted as backfill around the piles in lieu of concrete. The CLSM minimum strength is 1000 pounds per square inch.

INSTRUMENTATION AND MONITORING

7.5.1 Install instrumentation to monitor the performance of the right wall after construction. The instrumentation program should include inclinometers, load cells, and survey monuments.

7.5.2 7.5.2   Monitor the inclinometers four times a year the first year and then at least twice a year thereafter.

7.5.3 Monitor the lock-off load weekly during construction, at least four times the first year, and then at least twice a year thereafter.

7.5.4 At 200-foot intervals along the top of the wall, establish surface survey monuments. This will allow a visual confirmation of the alignment of the wall. This can be checked once a year.

STATION 46+00

I-275 RAMP

TOP OF LAGGING AND
SOLDIER BEAM

TIMBER LAGGING

CONCRETE FACING

0.2 H_D

P_D

0.6 H_D

PERMANENT
ROCK
ANCHOR(S)

H_D

DOLWICK CONNECTOR FINAL
GRADE PER ROADWAY PLANS

2' MIN

0.2 H_D

BOTTOM OF LAGGING
AND CONCRETE FACING

10'

20'

$P_D = \dfrac{L_D}{0.8 H_D} = 2.3$ ksf

SOLDIER BEAM

$P_P = 2.5$ ksf

TOP OF ROCK (TOR)

$P_P = 2.5$ ksf

3' MIN.

HIGHEST ALLOWABLE
PILE TIP ELEVATION

$P_{RS} = 20$ ksf

$D_{RS} \geq 0$

DESIGN PILE
TIP ELEVATION

$q_A = 40$ ksf

Figure 3 Geotechnical Detail (typical)

Figure 4 Cross-Section at Station 46+00

HIGH-RESOLUTION SEISMIC REFLECTION
TO IDENTIFY AREAS WITH SUBSIDENCE POTENTIAL
BENEATH U.S. 50 HIGHWAY IN EASTERN RENO COUNTY, KANSAS

Richard D. Miller, Kansas Geological Survey,
1930 Constant Avenue, Lawrence, Kansas 66047-3726, (785) 864-2091, rmiller@kgs.ku.edu
Robert Henthorne, Kansas Dept of Transportation,
2300 Van Buren, Topeka, Kansas 66611, (785) 291-3860, roberth@ksdot.org

Abstract

High-resolution seismic reflections were used to map the upper 200 m along an approximately 22 km stretch of U.S. 50 highway in Reno County, Kansas, where natural and anthropogenic salt dissolution is known to threaten ground stability. Surface subsidence in this part of Kansas can range from gradual (an inch per year) to catastrophic (tens of feet per second), representing a significant risk to public safety. Primary objectives of this study were to delineate the Permian Hutchinson Salt layer beneath the proposed alignment of the new U.S. 50 bypass around the City of Hutchinson. Of secondary interest were any features with subsidence potential beneath U.S. 50 east of the City of Hutchinson in Reno County, a distance of around 15 km crossing the dissolution front of the salt beds. The high signal-to-noise ratio and resolution of these seismic reflection data allowed detection, delineation, and evaluation of several abnormalities in the rock salt layer and overlying Permian sediments. Locations were identified where failure and associated episodes of material collapse into voids left after periodic and localized leaching of the 125 m deep, 40 m thick Permian Hutchinson Salt member were evident. Anomalies were identified within the salt and overlying rock layers with seismic characteristics consistent with collapse structures. Of particular interest were features with the potential to migrate to the surface in areas where no subsidence has been previously observed. Anhydrite and shale layers several meters thick within the salt are uniquely distinguishable and appear continuous for distances of several kilometers. High noise levels from the heavy traffic load carried on U.S. 50 and maintaining continuous subsurface coverage beneath the Arkansas River presented significant challenges to both the acquisition and processing of these data. Over a dozen unique features potentially related to subsidence risk were identified.

Introduction

Sinkholes are common hazards to property and human safety the world over (Beck et al., 1999). Their formation is generally associated with subsurface subsidence that occurs when overburden loads exceed the strength of the roof rock bridging voids or rubble zones formed as a result of dissolution or mining. Understanding sinkhole processes and what controls their formation rate is key to reducing their impact on human activities, and in the case of anthropogenic, potentially avoiding their formation altogether. Sinkholes can form naturally or anthropogenically from the dissolution of limestone (karst), gypsum, or rock salt, or from mine/tunnel collapse. With the worldwide abundance of limestone, karst-related sinkholes are by far the most commonly encountered and studied. Both simple and complex sinkholes have formed catastrophically and/or gradually, as the result of dissolution of limestone or rock salt, and by natural and man-induced dissolution processes in many parts of Kansas (Merriam and Mann, 1957).

In central Kansas most sinkholes are the result of leached out volumes of the Permian

Hutchinson Salt member of the Wellington Formation (Watney et al., 1988) (Figure 1). Sink-holes forming above salt layers have been studied throughout Kansas (Frye, 1950; Walters, 1978) and the United States (Ege, 1984). Studies of subsidence related to mining of the salt around Hutchinson, Kansas (Walters, 1980), disposal of oil field brine near Russell, Kansas (Walters, 1991), and natural dissolution through fault/fracture-induced permeability (Frye and Schoff, 1942) have drawn conclusions about the mechanism responsible for subsidence geome-tries and rates based on surface and/or borehole observations. Using only surface observations and borehole data, a great number of assumptions and a good deal of geologic/mechanical sense must be drawn on to define and explain these features and their impact. High-resolution seismic reflection profiling has proven an effective tool in 3-D mapping the subsurface expression and predicting future surface deformation associated with dissolution of the Hutchinson Salt in Kansas (Steeples et al., 1986; Miller et al., 1993; Anderson et al., 1995a; Miller et al., 1995; Miller et al., 1997).

Salt dissolution sinkholes are found in all areas of Kansas where the Hutchinson Salt is present in the subsurface. Sinkholes have been definitely correlated to failed containment of disposal wells injecting oil field brine wastewater using stem pressure tests and/or seismic reflec-tion investigations at a variety of sites throughout central Kansas (Steeples et al., 1986; Knapp et al., 1989; Miller et al., 1995; Miller et al., 1997). Sinkholes that have formed by natural dissolution and subsidence processes are most commonly documented at the depositional edges on the west and north and erosional boundary on the east of the Hutchinson Salt (Frye and Schoff, 1942; Frye, 1950; Merriam and Mann, 1957; Anderson et al., 1995a). The vast majority of published works studying the source of localized leaching of salt in Kansas directly contradict suggestions that recent land subsidence in Kansas is mostly natural in origin (Anderson et al., 1995a).

Natural dissolution of the Hutchinson Salt is not uncommon in Kansas and has been occurring for millions of years (Ege, 1984). Faults extending up to Pleistocene sediments con-taining fresh water under hydrostatic pressure are postulated as the conduits instigating salt dissolution and subsidence along the western boundary of the salt in Kansas (Frye and Schoff, 1942). Paleosinkholes resulting from dissolution of the salt before Pleistocene deposition have been discovered previously with high-resolution seismic surveys (Anderson et al., 1998).

Subsidence can occur at rates ranging from gradual to catastrophic. Subsidence rates are to some extent related to the type of deformation in the salt (ductile or brittle) and the strength of rocks immediately above the salt layer. As salt is leached, the resulting pore space provides the differential pressure necessary to support creep (Carter and Hansen, 1983). If this pore space gets large enough to exceed the strength of the roof rock, the unsupported span will fail and subsidence occurs (Figure 2). Depending on the strength of the roof rock and therefore the size of the void, characteristics of the failure within and just above the salt will dictate how the void progresses upward until it eventually reaches the ground surface. In general, gradual surface subsidence is associated with ductile deformation that—besides vertically sinking—progresses outward, forming an ever-growing bowl-shaped depression with bed geometries and offsets con-strained by normal fault geometries (Steeples et al., 1986; Anderson et al., 1995b). When rapid to catastrophic subsidence rates are observed, failure within the salt is usually brittle with void area migrating to surface as an ever-narrowing cone with bed offsets and rock failure controlled by reverse-type fault planes (Davies, 1951; Walters, 1980; Rokar and Staudtmeister, 1985).

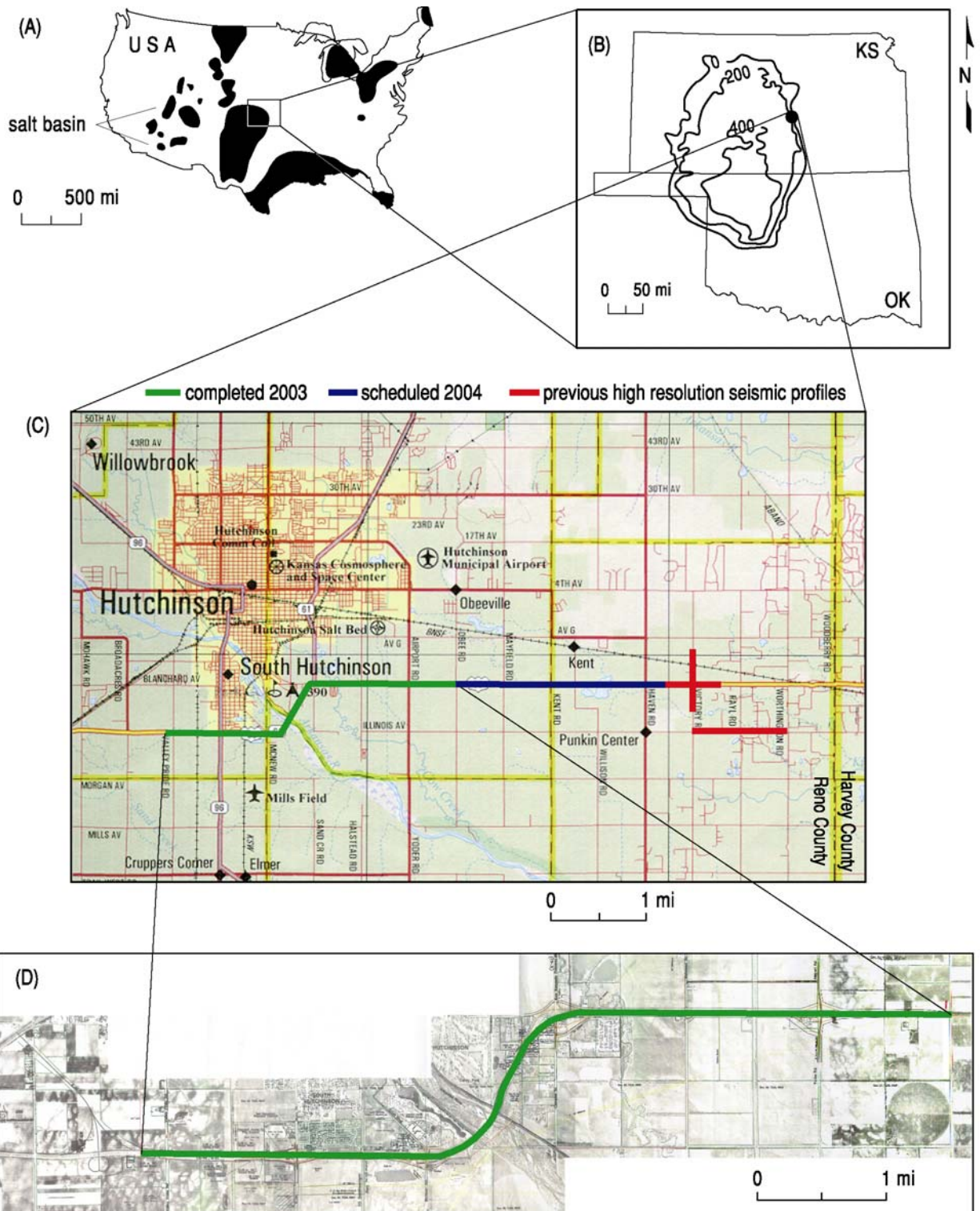Figure 1. Site map for seismic reflection study along proposed new U.S. 50 bypass around Hutchinson, Kansas. Major salt basins of North America (A). Areas extent and thickness of the Permian Hutchinson Salt member in Kansas and Oklahoma (B). Seismic profiles acquired and planned along and near Highway U.S. 50 and the dissolution front (C). Seismic profile map along the proposed U.S. 50 bypass around Hutchinson (D).

brine disposal

CRET
weathered shale — bedrock
shale
+ + + + + + + + + + + + SALT +
+ + + + + + + + + + + + + +
- - - - - - - - - - - -
PERM

weathered shale — bedrock
shale
+ + + + + + + + SALT
+ + + + + + + +
- - - - - - - - - - -

weathered shale — bedrock
shale
+ + + + + + + + SALT
+ + + + + + + +
- - - - - - - - - - -
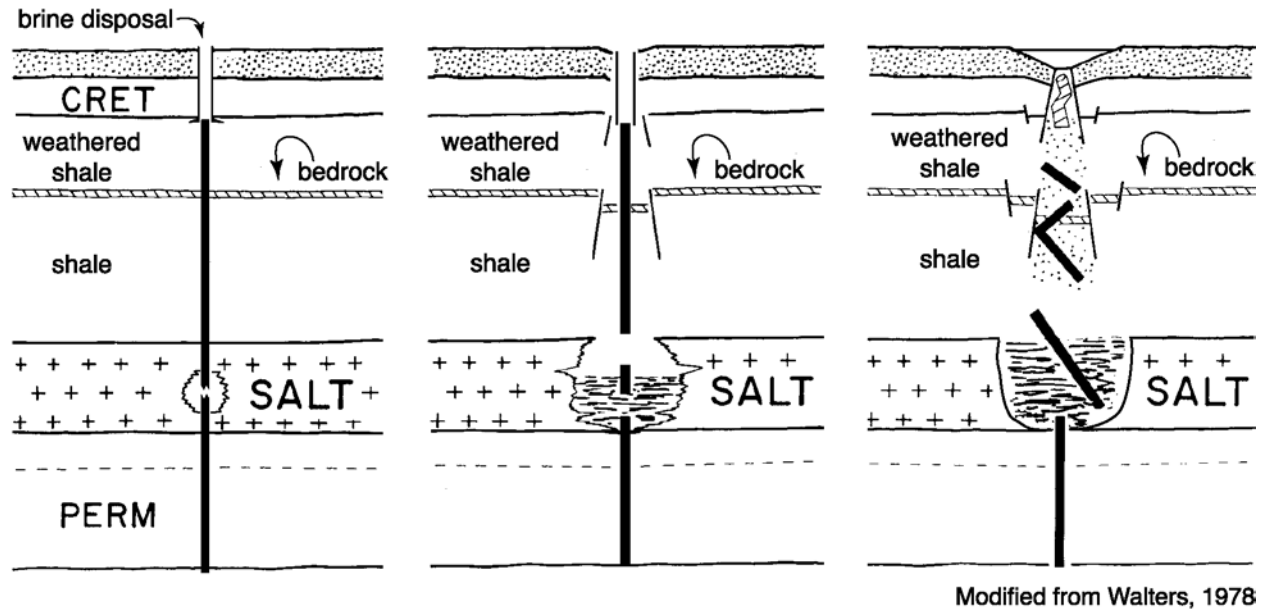
Modified from Walters, 1978

Figure 2. Cartoon of the dissolution and subsidence process across time when instigated by fluids introduced by lost containment in a disposal well.

Seismic reflection data targeting beds altered by dissolution and subsidence in this area have ranged in quality and interpretability from poor (Miller et al., 1995) to outstanding (Miller et al., 1997). Interpretations when data quality is poor have unfortunately been relegated to in-direct inference of structural processes and subsurface expression (mainly from interpretations of structural deformation in layers above the salt) due to low signal-to-noise ratios. However, data with excellent signal-to-noise ratios and resolution have allowed direct detection of structures and geometries that appear characteristic of complex sinkholes. Resolution potential and signal-to-noise ratio of seismic data from this study are superior to any previously published that have targeted the salt interval. These data provide conclusive images of important structural features and unique characteristics that control sinkhole development.

Concerns for public safety and elevated maintenance costs associated with potential future surface subsidence along a newly proposed four-lane bypass around the city of Hutchin-son, Kansas, are justified considering the tendency for sinkholes to form in eastern Reno County, Kansas, associated with the natural dissolution front, aging oil field wells, and voids (jugs) remaining from salt dissolution mining practices. As an example, the formation of a sinkhole just 15 km east of the proposed bypass on U.S. 50 has become a nuisance for maintenance crews, vehicle traffic, and public officials trying to calm the concerns of local residence. Subsidence of U.S. 50 below construction grade at its intersection with Victory Road totaled 30 cm when first measured during a 1998 elevation survey. Routine elevation surveys conducted since that time have monitored the pattern and rate of subsidence. At an average subsidence rate of around 20 cm/yr, the highway surface at its centerline has sunk about 1 m since its construction. The current sinkhole is symmetric, with a very regular bowl-shaped geometry around 100 m in diameter that retains water most of the year.

Geologic Setting

Several major salt basins exist throughout North America (Ege, 1984). The Hutchinson Salt Member occurs in central Kansas, northwestern Oklahoma, and the northeastern portion of the Texas panhandle, and is prone to and has an extensive history of dissolution and formation of sinkholes (Figure 1). In Kansas, the Hutchinson Salt possesses an average net thickness of 76 m and reaches a maximum of over 152 m in the southern part of the basin. Deposition occurring during fluctuating sea levels caused numerous halite beds, 0.15 to 3 m thick, to be formed inter-bedded with shale, minor anhydrite, and dolomite/magnesite. Individual salt beds may be continuous for only a few miles despite the remarkable lateral continuity of the salt as a whole (Walters, 1978).

Rock salt under a depositional load is almost incompressible, highly ductile, and easily deformed by creep (Baar, 1977). Plastic deformation of the salt associated with creep is expected naturally to occur in these salts (Anderson et al., 1995b). Thin anhydrite beds within the halite succession have a strong acoustic response. Considering the extreme range of possible strain rates the salt can experience during creep deformation, these thin interbeds can possess quite dramatic, high frequency folds within relatively short distances.

Redbed evaporites overlaying the Hutchinson Salt Member are a primary target of any study in Kansas looking at salt dissolution sinkhole development and associated risks to the environment and human activity. Failure and subsidence of these evaporite units are responsible for the eventual formation of sinkholes and provide a pathway for groundwater to gain access to the salt. In proximity to the dissolution front fractures, faults, and collapse structures compromise the confining properties of the Permian shale bedrock and put the major fresh water aquifer (Plio-Pleistocene Equus Beds) in this part of southern Kansas at risk. Along the eastern boundary (dissolution front), the salt, which ranges from 0 to over 100 m thick, is buried beneath about 120 m of Permian redbed evaporites.

The eastern margin of the salt was exposed during late Tertiary where erosion and leaching began the 30 km westward progression of the front to its present day location (Bayne, 1956). The ability of the front to migrate while under as much as 100 m of sediments was a direct consequence of ready access to an abundant supply of groundwater (Watney et al., 1988). Subsidence of Permian, Cretaceous, and Tertiary rocks has progressed along the migration front as the salt has been leached away. While this subsidence was going on, Quaternary alluvium was being deposited in volumes consistent with the salt that was being removed. This processes resulted in today's moderate to low surface relief that masks the extremely distorted (faulted and folded—non-tectonic) rock layers within the upper Wellington and Ninnescah shales (Anderson et al., 1998).

Seismically, all Permian and younger reflectors are important to accurate interpretation of the stacked sections. Model studies show significant time delays (static) and geometric distortions that are to be expected below recent subsidence (Anderson et al., 1995b). "Pull downs" in time result from the localized decreases in material velocities within a sinkhole. The velocity structure and small radius of curvature of the synforms, characteristic of salt dissolution and subsidence in this area, can produce diffractions and distort reflections on vertically incident reflection sections. Reflections from beneath the salt will have a subdued expression of the post-salt subsidence. Estimations of subsidence and therefore volume of rock salt removed based on time section estimations alone (without compensation for velocity variability) may exceed actual by

as much as 25 to 50 percent in this area. Considering this geologic setting, it is reasonable to compensate for compaction-related static causing this lateral decrease in velocity by "flattening" on the top of the Chase Group.

Most of the upper 700 m of rock at this site is Permian shales (Merriam, 1963). The currently disputed Permian/Pennsylvanian boundary is about 700 m deep and seismically marked by a strong sequence of cyclic reflecting events. The Chase Group (top at 250 m deep), Lower Wellington Shales (top at 175 m deep), Hutchinson Salt (top at 125 m deep), Upper Wellington Shales (top at 70 m deep), and Ninnescah Shale (top at 25 m deep) make up the packets of reflecting events easily identifiable and segregated within the Permian portion of the section. Bedrock is defined as the top of the Ninnescah Shale with the unconsolidated Plio-Pleistocene Equus Beds making up the majority of the upper 30 m of sediment. Thickness of Quaternary alluvium that fills the stream valleys and paleosubsidence features goes from 0 to as much as 100 m depending on the dimensions of the features.

Seismic Reflection Fundamentals

Seismic reflection is a powerful geophysical tool, in use since the 1920s that uses sound energy for underground exploration (Waters, 1987; Dobrin, 1976; Coffeen, 1978; Telford et al., 1976; Sheriff, 1978). For most of the first sixty years seismic reflection, surveys targeted rock layers of petroleum interest at depth generally exceeding 1 km. Using seismic reflection techniques to image targets less than 100 m has only been attempted with published success since the 1980s. Key to using seismic reflection to image shallow targets is the production and recording of high frequency signal. Most recently the technique is finding new applications characterizing geologic and hydrologic settings at depths between 3 and 30 m below the ground surface.

Seismic reflection techniques depend on the existence of discrete seismic velocities and/or mass density changes in the subsurface known as acoustic impedance contrasts. Mathematically, acoustic impedance is simply the product of the mass density and acoustic wave velocity. Acoustic impedance contrasts occur at natural boundaries between geologic layers, although manmade boundaries, such as tunnels and mines, also represent contrasts. The classic use of seismic reflection is to identify the boundaries of layered geologic units. However, the technique can also be used to search for localized anomalies such as sand/clay lenses and cavities.

For the purposes of this paper we will focus on compressional waves (P-waves), which propagate through the earth behaving similar to sound waves propagating through the air. When sound waves (voices, explosions, horns, etc.) come in contact with a wall cliff, or building (all representing acoustic contrasts between air and a solid material) it is common to hear an echo. When a P-wave comes in contact with an acoustical contrast underground, echoes (reflections) are also generated. P-waves reflections can be thought of as sound wave echoes from underground acoustic impedance contrasts. In the underground environment, the situation is more complex than in the air because some P-wave energy impinging on a solid acoustical interface can also be transmitted across the interface, refracted at the interface and/or converted to other types of seismic waves at the interface.

Seismic methods are sensitive to the physical properties of earth materials and relatively insensitive to the chemical makeup of contained fluids in earth materials. Electrical methods are sensitive to contained fluids and the presence of magnetic or electrically conductive materials.
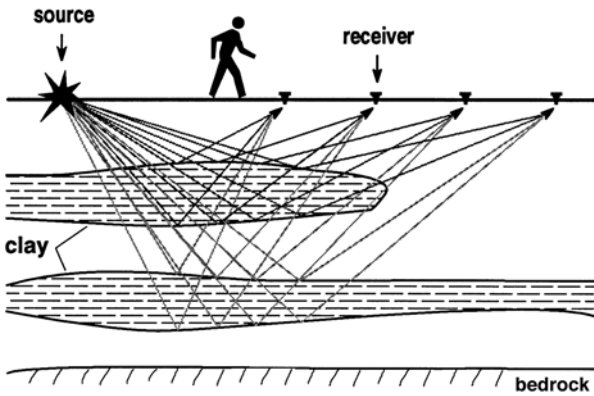
Figure 3. Simple layered earth model with clay layers above bedrock. A seismic source imparts sound energy to the ground. The seismic waves (ray as drawn here) propagate through the material, reflecting uniquely from each boundary between different material types. Seismic energy is recorded at the ground surface using a regular grid of receivers.
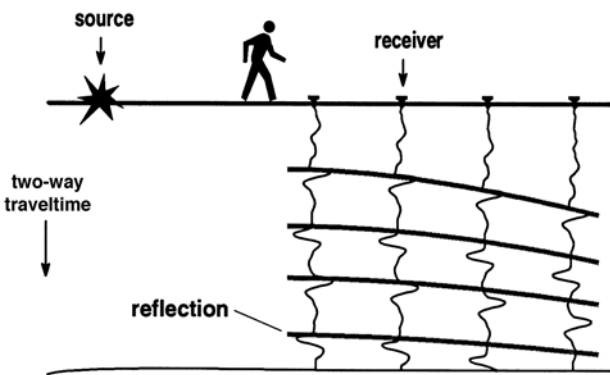

Figure 4. Seismic representation of layered earth. Two-way travel time from the start of energy moving through the ground until recorded by receivers at ground surface. The hyperbolic or curved nature of the reflections is related to the non-linear increase in travel path of reflected energy with linear increase in offset of receiver.

The measurable physical properties upon which seismic methods depend are quite different from the important physical properties for electrical and magnetic methods. Methods such as seismic reflection, refraction, crosshole tomography, and vertical seismic profiling all rely on similar physical properties of the earth. Ground penetrating radar (GPR) is a reflected wave technique that also relies on contrasts in earth materials, but rather than acoustic property changes, GPR is sensitive to changes in electrical conductivity.

Understanding seismic reflection is best accomplished using models of a simple layered earth (Figure 3). Seismic energy introduced into the ground from a point is radiated spherically away from that point at the velocity of the earth material. This process can best be visualized by recalling how waves generated from a pebble in a still pond move outward across the water's surface. A water wave like that just described propagates in two dimensions, whereas seismic energy moves through the earth as a three-dimensional phenomenon. An arbitrarily large number of rays can be traced outward from the source, but one will follow Fermat's principle of least time and will travel the shortest distance between the source, reflecting point, and receiver. The reflecting point will be represented as a pulse or wavelet on time measurements of ground motion. This echo from underground rock layers is referred to as a reflection. In the case of a single, flat-lying layer and a flat topographic surface (Figure 3), the path of least time will be from the energy source to a reflecting point midway between the source and receiver, and then straight to the receiver. The incident angle of the down-going ray will be equal to the angle of the up-going reflected ray.

Seismic energy is measured in time. Reflections returning from acoustic contrasts (reflectors) arrive some time after the energy was released from the source. The time required for a seismic pulse or wavelet to travel from the source to the reflector and then to the receiver is referred to as the two-way travel time. The two-way travel time of a reflection arrival increases hyperbolically as the offset between the source and receiver increases linearly (Figure 4). A
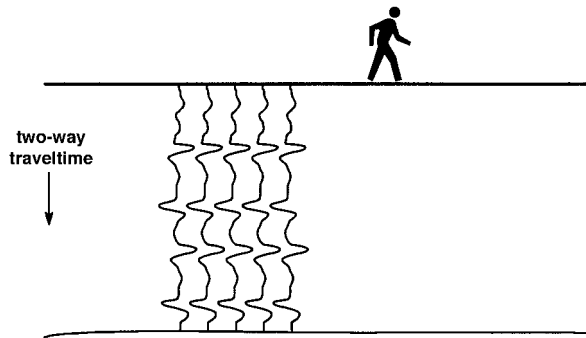
Figure 5. Seismic section with reflection arrivals corrected for offset and therefore different length travel paths.
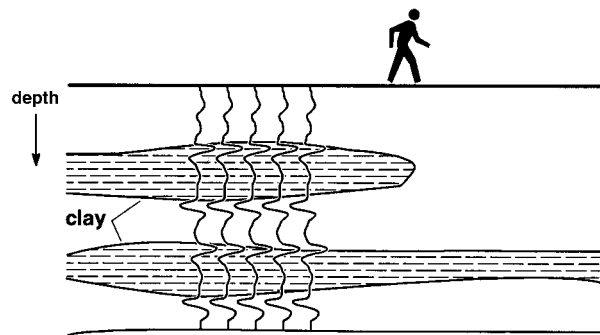

Figure 6. Time-to-depth converted seismic traces with reflections matched with reflectors. Geology can be inferred by trace-to-trace coherency of reflection wavelets.

discriminating characteristic of reflection events on shot gathers is their hyperbolic arrival pattern referred to as "moveout." The curvature of the reflection event as mapped from trace to trace is directly related to the average velocity of earth materials between the source/receiver and reflector.

Mapping reflectors requires the variability in reflection arrival times be removed or at least minimized so the seismic section approaches equivalence with a geologic cross-section, many times compared to a highway road cut. Adjusting for variable travel paths requires some knowledge of the average material velocity the seismic energy traveled through. Using coherency of the reflection arrivals from trace to trace a unique hyperbolic curve can be extracted which, based on arrival time of the reflections, distance between traces, and distance from source, can be used to estimate the overall velocity along the travel path. This velocity calculated in this fashion is referred to as the normal moveout velocity (NMO) and for most cases and applications can be used interchangeably with the average velocity. Using this NMO velocity, reflections can be adjusted to simulate vertically incident seismic wave travel paths (Figure 5).

Matching reflections with reflectors requires time-to-depth corrections and correlation of reflection wavelets from the same interface between adjacent traces. This process is generally accomplished using the NMO velocity function, defined in time and spatially relative to stations or receivers on the ground surface, to determine the time adjustment necessary to simulate a vertical travel path. Once adjustments are made wavelet characteristics can be used to infer reflector characteristics (Figure 6). For example, changes in polarity along a trace generally represents dramatic changes in material properties or acoustic impedance across a layer such as harder material to softer material and then back to a harder material; also, changes in wavelet characteristics from trace to trace can be indications of lateral changes in layer thickness or lithology. Considering the resolution of the seismic method (related to the finite bandwidth of reflected wavelets) and the non-infinite signal-to-noise ratio, a significant amount of ambiguity is always associated with geologic interpretations of seismic data.

Seismic reflection data is normally complicated by noise and interference of one reflection with another as a result of resolution limits associated with a narrower reflection bandwidth, lower reflection upper corner frequency, and relatively thin beds. Each "wiggle" does not have a unique meaning that can or should be extracted from the data. A cross-section of earth will have an acoustic impedance contrast at each change between layers (Figure 7). This sequence of

acoustic impedance contrasts can be represented by a series of spikes with a length related to the reflectivity or difference between the acoustic impedance of the material above relative to the material below the interface. This "spike" trace is also known as the reflectivity series for this earth model (Figure 7b). Each source generates a source wavelet with different characteristics controlled by the source itself and the earth materials the source is coupled to. Starting with an earth model, generating a reflectivity series, and then convolving with a source wavelet is the process used to produce a synthetic seismic trace. Starting with the seismic trace and then working to a geologic model is the most commonly used approach for interpreting real seismic data.

Figure 7. Depth and materials (a) represented as a time series of spikes with length indicative of reflection strength (b) and model reflection trace with finite bandwidth reflection wavelets as would be expected from zero offset seismic traces (c).

Seismic Acquisition

A continuous profile, a little over 10 km in length was acquired along the existing U.S. 50 highway right-of-way around Hutchinson, Kansas (Figure 1). In moving to meet the ever-growing vehicle load on the current highway, engineers proposed several possible transects skirting the southern edge of Hutchinson intended to accommodate a new four-lane limited access highway generally consistent with the current two-lane road that is there. With the known threat sinkholes in this area represents—both naturally occurring and as a result of dissolution mining—the subsurface between the base of the salt and bedrock beneath the proposed highway transect was examined using high resolution seismic reflection. The objective of this survey was to expose any feature lurking below ground that might someday threaten the stability of the road surface. These data were acquired using a rolling fixed-spread design that eliminated the need for a roll-along switch and extended the range of far offsets available during processing. This survey design provided the wide range of source offsets necessary for detailed velocity analysis, close receiver spacing for improved confidence in event identification, and maximized the range of imageable depths.

Even though no sinkholes were visible at the ground surface, evidence for historical dissolution and subsidence not visible at the ground surface has been observed in several locations around eastern Reno County, Kansas. This historical dissolution and subsidence, referred to as "paleosinkholes," is an indication that fresh water has had access to the salt in this area previously and has found a pathway to carry the dissolved salt away from the dissolution front. Several naturally forming sinkholes in this area have seen resent reactivation and formation of a surface depression. Therefore, looking for paleosinkholes and old salt mine dissolution jugs will be critical to final placement of this proposed bypass around Hutchinson.
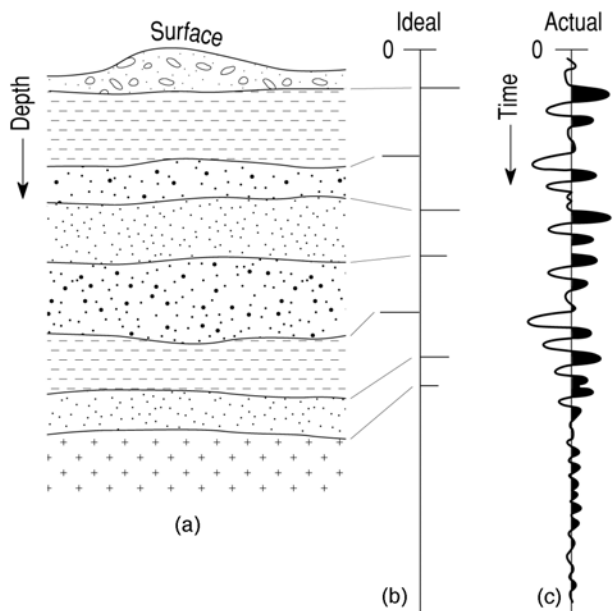
Acquisition parameters were defined based on experience and walkaway tests near the start of the profile on the western end of the survey. Twin Mark Products L28E 40Hz geophones were planted at 2.5 m intervals in approximate 1 m arrays. Geophones were planted into firm to hard soil at the base of the road ditch in small divots left after the top few inches of loose material were removed to insure good coupling. Four 60-channel Geometrics StrataView seismographs were networked to simultaneously record 240 channels of data. An IVI Minivib1 using a prototype Atlas valve delivered three 10 second, 25-250 Hz up-sweeps at each 5 m spaced shot location. Experiments at this site were consistent with bench tests, which suggested this new rotary valve design will produce up to four times the peak force of conventional valves at 250 Hz. The pilot was telemetried from the vibrator to the seismograph and recorded as the first trace of each shot record. Each of the three sweeps generated per shot station was individually recorded and stored in an uncorrelated format with the ground force pilot-occupying channel 1.

All sweeps were recorded into the fixed 240-channel spread with the source incrementally moving from shot station to shot station through the middle half of the spread. Once the center 120 receiver stations (60 shot stations) were shot through, the back 120 receiver stations were moved to the front and the process repeated. Since all shot records were recorded uncorrelated, QC involved visual inspection of the recorded pilot trace, audio monitoring of the pilot trace on an RF scanner, inspection of the vibrator power spectra after each shot, and review of a correlated shot record after every 5 to 10 shot stations. With the exception of receiver stations not instrumented due to excess or thick gravel or asphalt or stations taken off-line when their offset exceeded 300 m, the survey was recorded with 98 percent live receivers within the optimum recording window (Hunter et al., 1984).

Seismic Processing

A basic common midpoint (CMP) processing flow was used in a fashion consistent with well-established 2-D high-resolution seismic reflection methodologies (Steeples and Miller, 1990). All lines were processed using WinSeis2, beta seismic data processing software (next generation of WinSeis Turbo) from the Kansas Geological Survey. Any reflection data acquired in this highly disturbed subsurface setting will be plagued with static problems and subject to dramatic swings in NMO velocity over relatively short distances; this data set was no exception.

Data were recorded and stored uncorrelated to allow precorrelation processing in hopes of increasing the signal-to-noise ratio and resolution potential (Doll and Çoruh, 1995). Removal of noisy traces and amplitude scaling were precorrelation processing steps that significantly enhanced signal-to-noise and resolution potential. Attempts to improve the data quality precorrelation through frequency filtering, spectral whitening, and frequency-wave number (F-k) filtering were unsuccessful. Storing data uncorrelated also allowed tests to be run with different methods of correlation and correlating with different pilot traces. These data were optimally correlated using the synthetic drive signal. Storing data uncorrelated and unstacked required 30 times more storage space, about 50 percent more acquisition time, and 5 times more data transfer time. Improvements in signal-to-noise ratio and resolution made these increases cost effective.

Emphasis was placed on noise suppression, maintaining true amplitude, and compensating for velocity irregularities. Noise suppression focused on vehicle noise from the highway, livestock along the lines, powerline noise, surface waves, first arrivals, and air-coupled waves. Muting and hum filtering (Xia and Miller, 2000) improved signal-to-noise appreciably. The

three individual shot gathers acquired at each shotpoint were vertically stacked after all the noise suppression operations were complete. With the exception of the 1 sec AGC used precorrelation and display gains, only spherical divergence was used to adjust trace amplitudes. With the large depth window of interest, a relatively wide optimum offset window was maintained, which after noise mutes resulted in true trace folds ranging from 1 to a maximum of 30 (Liberty and Knoll, 1998). Velocity was defined in groups of 20 CMPs with at least one control point for each 100 ms time window and a minimum of five points selected in the first 200 ms. Each line is defined by a velocity function with over 400 time/velocity pairs determined with the aid of several iterations of correlation static corrections and velocity analysis.

Even when reflections were interpretable within the noise cone an inside mute was applied after the air-coupled wave to avoid signal degradation of reflection wavelets on CMP stacked sections. Inside mutes are a common practice for shallow (upper 1 km) seismic reflection processing (Baker et al., 1998). It is however, uncommon and counterintuitive to remove confidently identifiable reflection events regardless of where they are relative to other energy arrivals. The likelihood of wavelet distortion sufficient to reduce the resolution potential or lose the trace-to-trace coherency of reflections is significantly increased when surgically muting noise immersed in signal. Analogous to inoperable tumors, attempts to precisely remove just noise—especially air-wave noise—at tolerances of a millisecond or two run the risk of cutting too severely and/or defining mute tapers that are too steep, thereby irreparably altering the reflection waveform. Stacking waveforms into the fold that have been distorted by overly aggressive mutes will compromise the accuracy of the information contained in the waveform, and in some cases produce artifacts that can be misinterpreted as true earth response.

Powerline noise was pronounced on shot gathers where power lines were located along the south side of the road. A complex combination of 60 Hz, 120 Hz, and 180 Hz noise bleeding from overhead power lines masked most of the seismic energy even after correlation along portions of the road. A hum filter was very effective in eliminating powerline noise without affecting the amplitude or phase of the seismic data (Xia and Miller, 2000). This predictive filter produced a noticeable increase in signal-to-noise without loss of resolving potential.

Interpretation

Confidently interpretable reflections on shot gathers are essential to optimizing the acquisition, processing, and interpretation of high-resolution seismic reflection data. Reflections can be interpreted on raw, correlated shot records (scaled for display purposes) from around 50 ms to two-way time depths in excess of 500 ms (Figure 8). Considering the optimum window for these data, it was imperative to keep a wide range of offsets to insure the entire target zone was imaged. Reflections with dominant frequencies of around 200 Hz can be interpreted as deep as 200 ms, while the dominant frequency of reflections at 500 ms have dropped to around 100 Hz. With dominant frequencies of some reflections exceeding 200 Hz, a 2.5 ms static between adjacent traces represents a 180º phase shift and complete cancellation. Therefore, it is critical that static irregularities be compensated for before the data are CMP stacked. Reflection events can be traced through the air-coupled wave and just into the ground roll wedge. To avoid any contamination by air-coupled wave, all energy after the airwave was removed during processing.

For quality control reasons it is important that reflections interpreted at two-way times less than 50 ms on CMP stacks can be correlated with equivalent 50 ms reflection hyperbolae on
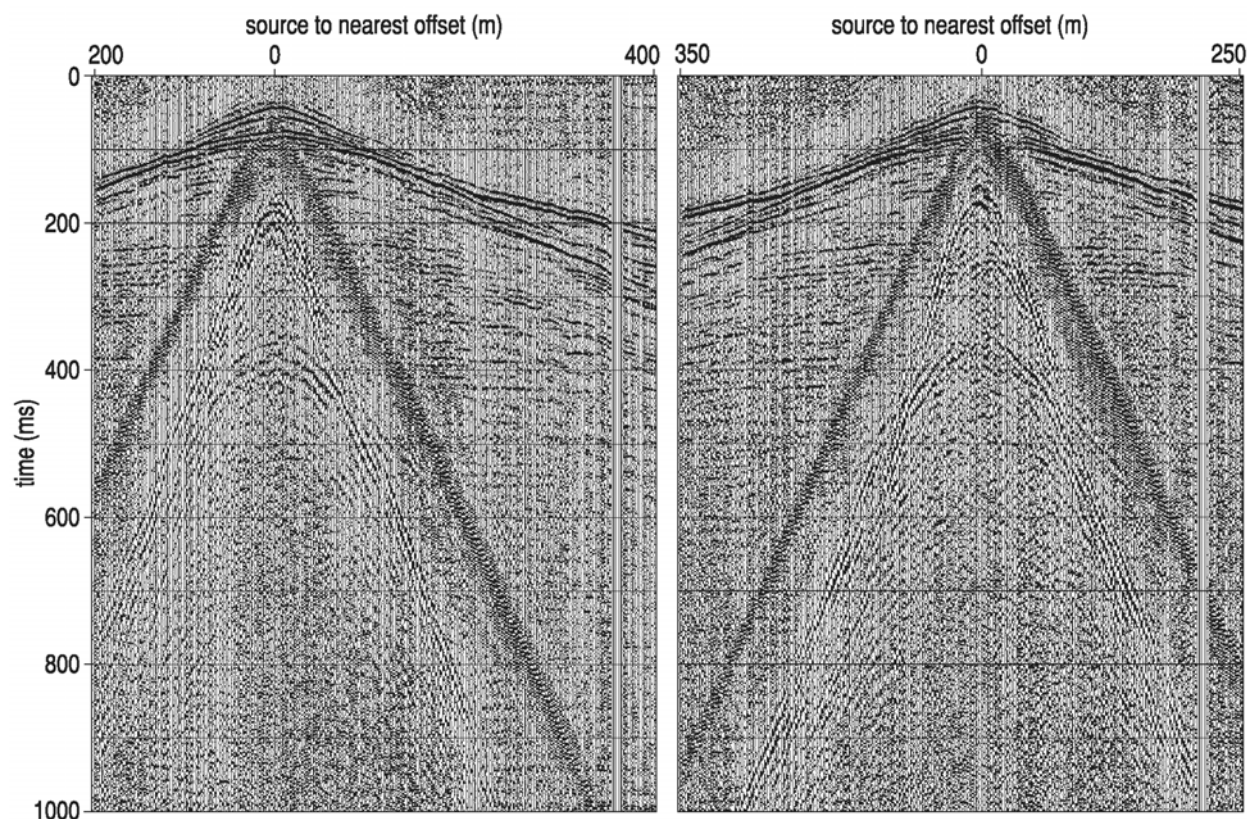
Figure 8. Correlated shot gathers from along profile. Reflection events have diagnostic curvature and high fre-quency wavelets.

shot gathers. Identification of these reflections on field files and tracking of them throughout the processing flow was necessary to ensure CMP sections were correctly stacked and interpreted. Ultra shallow reflections (< 50 ms) were a critical aspect in discerning the periods since Permian that these sediment-filled sinkholes may have been active.

From interpretations of reflection from raw shot gathers it can be estimated that reflectors from 15 m to over 1 km were imaged by these data (Figure 8). Even under these extremely noisy conditions, contending with wind, vehicles, and power lines along with an extremely variable near surface at overpasses, access road fill, the Arkansas River, and railroad grade, the data are of exceptional quality. Bed resolution using the half-wavelength criteria is around 2 m at the top of the salt unit. Reflections identified on the shot gather extend from the Permian through the upper Pennsylvanian.

CMP stacked section from this 10+ km survey are all of excellent quality (Figure 9). Data from the western extreme of the profile provide an excellent look at the seismic character of a segment of Permian rocks not disturbed by dissolution-induced subsidence. The salt interval has been identified using a combination of nearby well logs and depth estimates from NMO velocity conversions. Two-way travel time to the top of the salt is around 170 ms with a salt interval that is clearly distinguishable on seismic data from the surrounding Permian rocks.
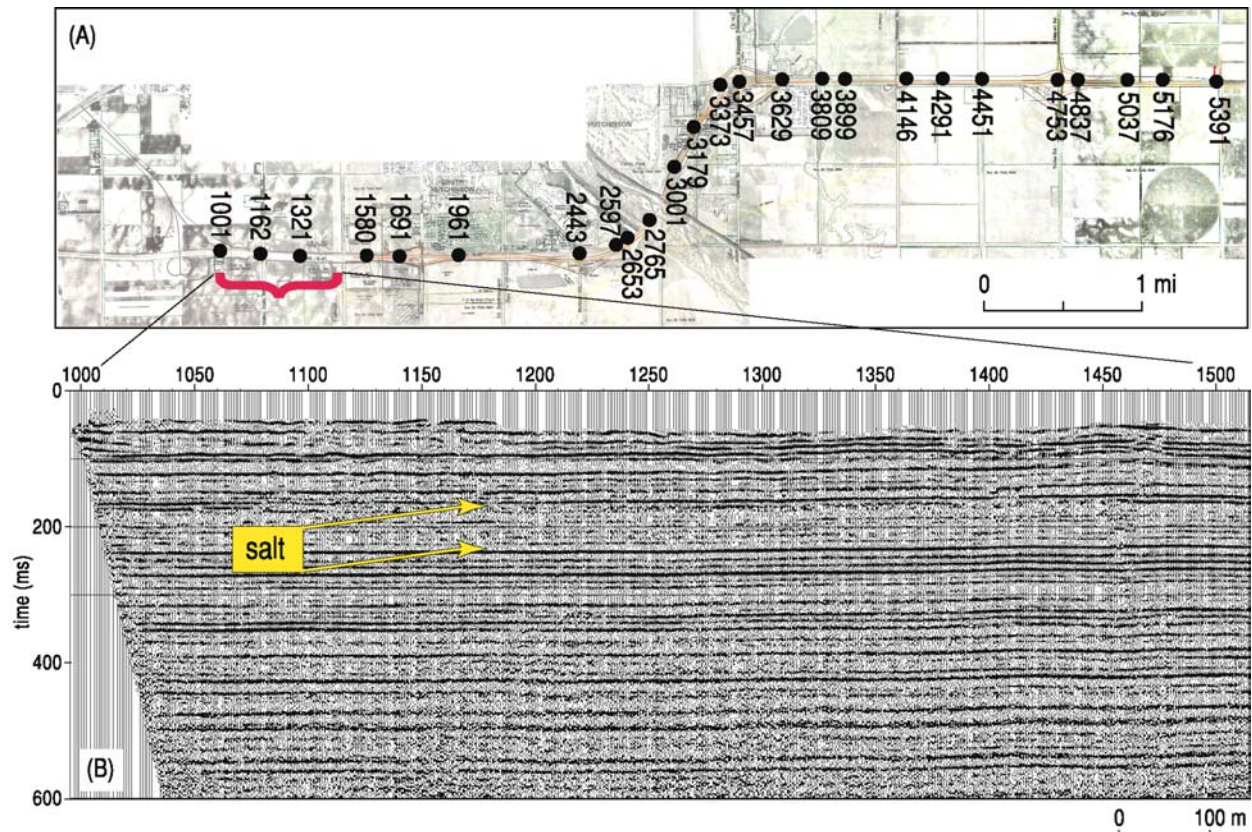
Figure 9. Seismic stations were DGPS located to within ±2 cm (x, y, z) (A). Seismic section from first 1.25 km clearly demonstrates the data quality and signature of undisturbed salt (B).
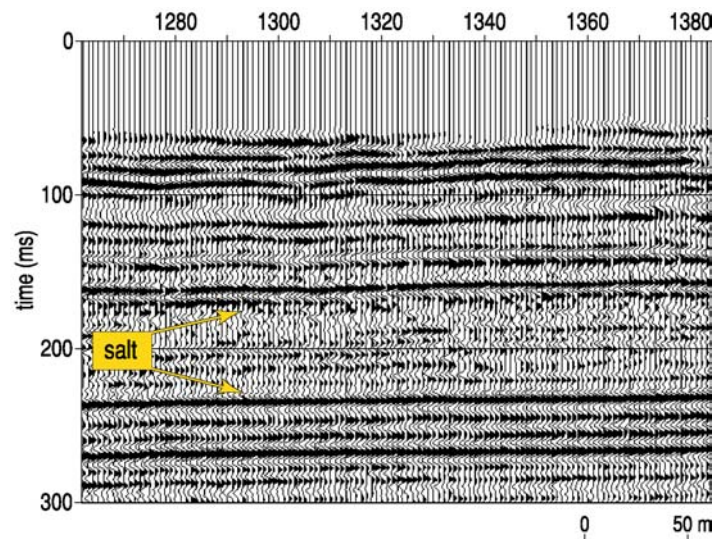
Figure 10. Expanded view of salt interval and layers above and immediately below. Reflections from within the salt are unique in comparison to those from surrounding Permian layers.

Critical to identifying areas of disturbed salt and any overburden that might be susceptible to collapse due to irregularities within the salt is a clear understanding of how native, undisturbed salt and overburden appear on CMP stacked seismic sections. A strong reflection at about 170 ms interpreted to be the Milan Limestone marks the top of the salt, followed by a subdued set of relatively discontinuous reflections to about 230 ms where another high amplitude reflection, likely the Carlton Limestone, is interpreted to be the basal contact between the salt and surrounding rocks of the Sumner Group (Figure 10). Reflections
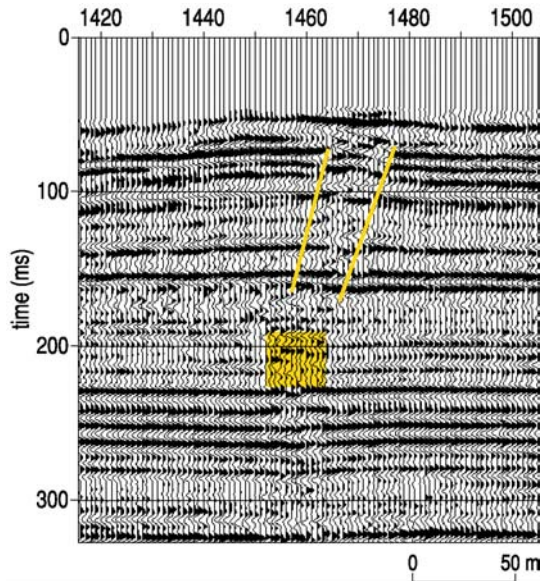
Figure 11. Disturbed area within the salt and associated chimney where rocks between the salt and bedrock appear altered.

from within the salt layer possess geometries consistent with channel-cut-and-fill deposition. These intra-salt beds are likely shales and anhydrites.

A somewhat unusual feature interpreted on these seismic data is a small area of disturbed salt with a volume of rock extending upward from the salt to near the bedrock surface that appears to be disturbed and possibly offset with some related subsidence (Figure 11). The disturbed area within the salt can be identified by the loss of continuity of the intra-salt reflections. Immediately below the basal salt contact at about 230 ms is a slightly disturbed zone that increases in area with depth that is likely the shadow effect (scatter and decreased overburden velocity) related to the disturbed reflections within the salt and is an artifact. A chimney feature extending toward the bedrock surface appears to be a fracture zone associated with the anomaly in the salt. Localized layers above the salt and this anomaly appear to form a very subdued syncline. This fracture zone could well be related to salt creep and not dissolution. With the many zones where water is confined in the Permian redbeds between the salt and bedrock surface, this fracture zone could well have allowed water access to the salt, but without an exit point for the saturated brine solution to leave the salt. The leaching process started but was halted before sufficient salt was dissolved to create a void of sufficient size for large-scale subsidence to occur.

The only clearly identifiable paleosinkhole across the 10 km profile was identified near the intersection of U.S. Highway 50 and Kansas state Highway 96 (Figure 12). Reflection
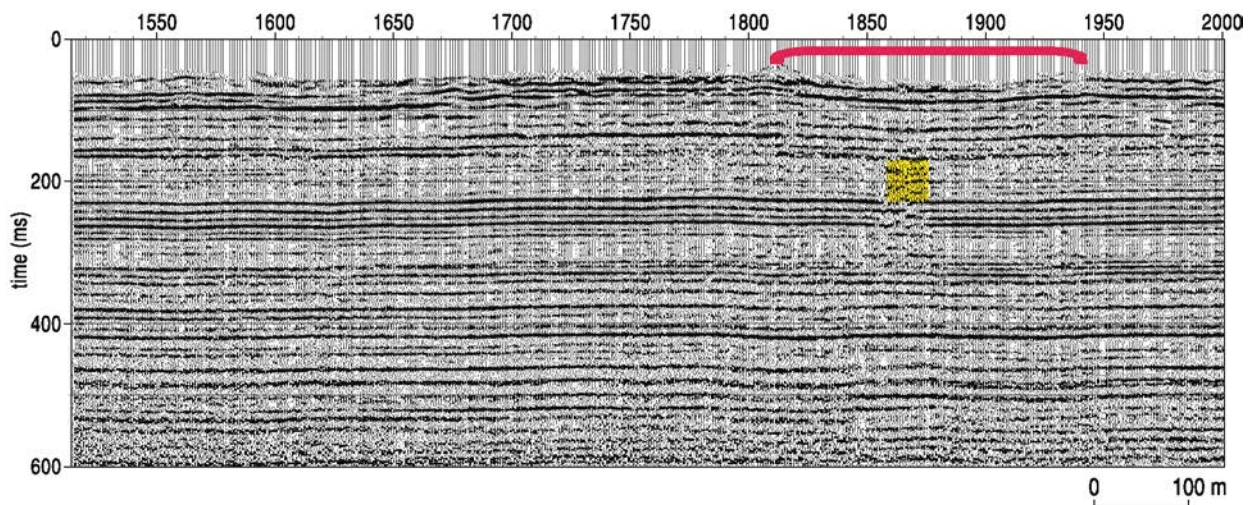
Figure 12. Paleosinkhole evident about 2 km from the beginning of profile and approximately beneath the stretch of highway that includes the overpass of Highway 96.

characteristics of the salt and overlying sediments across the almost 1 km between the anomaly identified beneath station 1470 and 1800 appear very undisturbed with "normal" depositional features interpretable in reflections within the upper 300 m. Between stations 1800 and 1950 a very pronounced depression in the shallower sediments is evident. In general, this anomaly possesses the classical reflection drape above the salt indicative of plastic deformation that occurs as salt gradually dissolves and overlying sediments subside into the void. The only significant faulting evident in this feature is at the edges of the bowl-shaped structure indicative of more brittle deformation.

A close-up of the paleosinkhole beneath station 1870 provides a very intriguing view of this ancient, yet potentially dangerous feature (Figure 13). Clearly all the leached salt responsible for this more than 300 m wide feature at the bedrock surface came from little more than a 50 m wide stretch of salt. Key to this discovery is what appear to be competent layers within the salt that are beneath the bedrock expression of the sinkhole. This implies dissolution occurred within a relatively small volume, then due to salt creep this 50 m wide zone of dissolution reduced the pressure regime and affected salt more than 100 m away. As salt creeped toward this low-pressure area, wide expanses of unsupported roof rock began forming until subsidence occurred, with the edges of salt creep defined by faults that extended to the bedrock surface.

Immediately south of an area known to have been dissolution mined in the past are scatter features which could be related to old mining activities (Figures 14 and 15). Scattering of seismic energy is generally related to bed terminations or other point source features. Considering the scatter points (apex of seismic energy) are within the salt, at the contact between the salt and cap rock, within the Ninnescah shale, and most strongly at the bedrock surface, it is difficult to say with confidence these features are a remnant of dissolution mining. With scatters coming from what appears to be the bedrock surface or very near the bedrock surface, this area should already be experiencing surface subsidence if these scatters were from an old salt jug. More
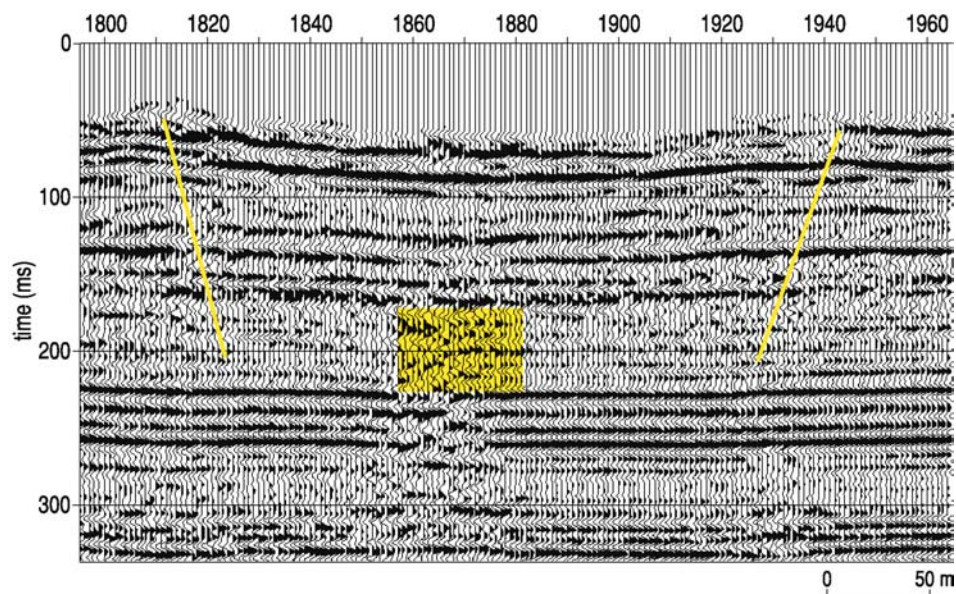
Figure 13. An area of active dissolution from where the salt was previously dissolved, allowing creep and the formation of a much larger surface depression than salt void volume.
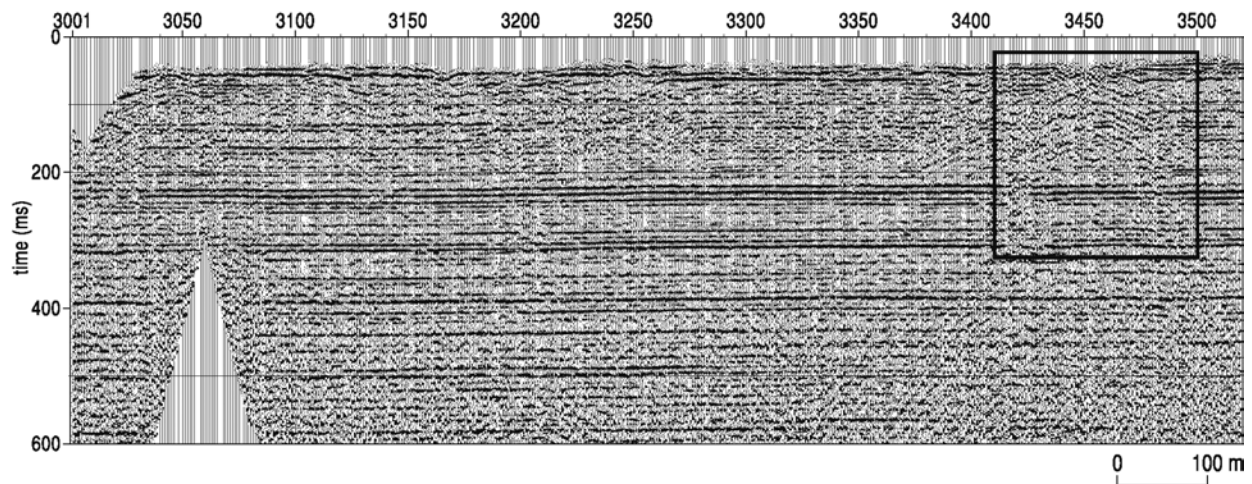
Figure 14. Scatter seismic energy related to bed termination. These highly developed scatter patterns are areas for more concentrated study. The most likely scenario involves uncompensated surface noise, out-of-the-plane features, or bedrock abnormalities. However, this type of seismic signature could be indicative of a void or anomaly such as an abandoned salt jug.
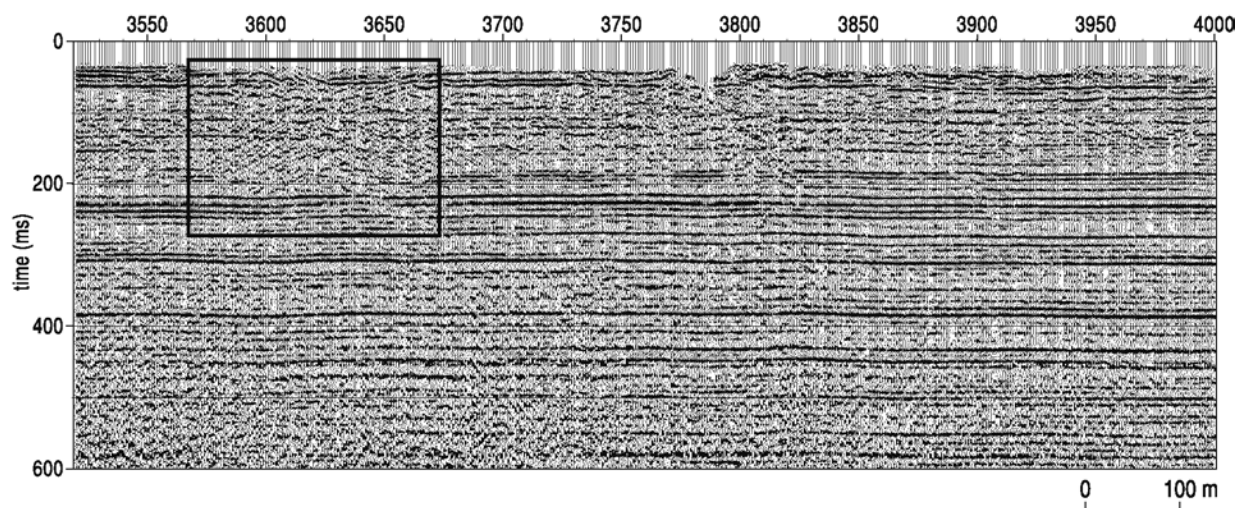
Figure 15. As observed on Figure 14, this scatter pattern of seismic energy could be an indication of bed terminations into void associated with old salt jugs.

likely explanations include out-of-the-plane features, uncompensated surface noise, or bedrock abnormalities. Since it is still possible that these features are related to old salt jugs, they need to be studied further to determine if previous mining activities or unrelated dissolution of the salt is involved in any way.

Probably one of the most intriguing, yet least significant feature for highway planners, is what appears to be a large fault zone beneath station 4430 (Figure 16). This fault zone appears to have minimal vertical offset, but possesses a marked change in character of reflections across this zone. The reflection identified as from the top of the salt changes in both frequency and amplitude, as well most events above about 250 ms appear to have changes in character across
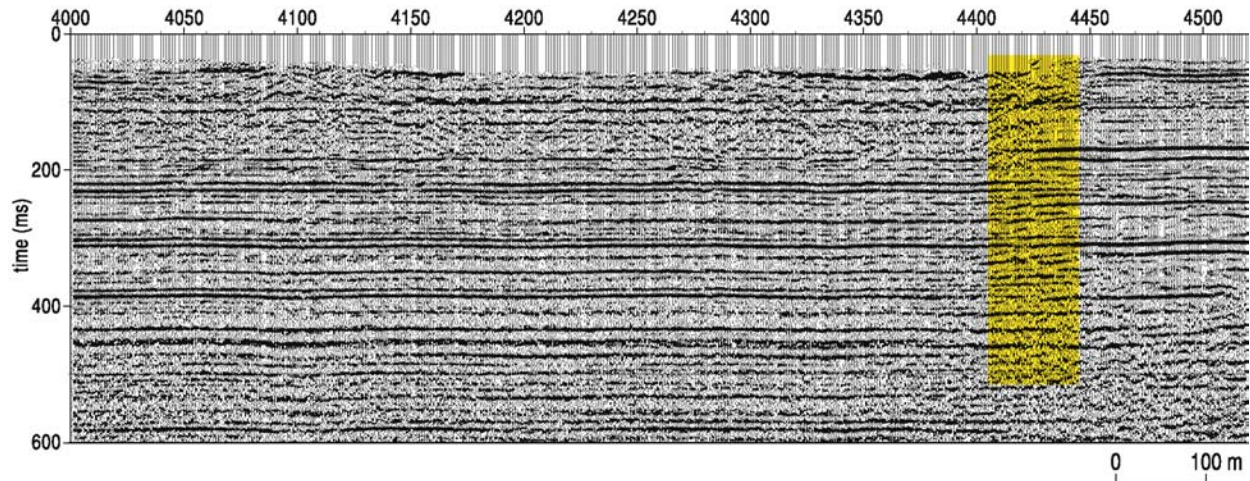
Figure 16. A fault is clearly evident on these data beneath station 4430. An abrupt change in reflection characteristic, diffraction, and apparent bed offset are all key indicators of faulting.

this fault that range from dramatic to subtle. Below 250 ms the fault zone is still evident but lacks as much change in seismic wavelet characteristics as shallower in the section. From a purely speculative perspective this fault has all the characteristics expected from a predominantly strike-slip fault. Correlations with local geology are not yet complete, but will likely provide key insights into this feature.

Near the end of this 10+ km seismic profile is what appears to be a change in the basal salt contact (Figure 17). Around station 4630 the reflections from near the base of the salt layer at about 230 ms change gradually across about a kilometer from a relatively distinctive higher amplitude single-wavelet event to what appears to be a very cyclic lower resolution wavelet. This change appears to be consistent with an apparent thinning in the salt layer. However, from
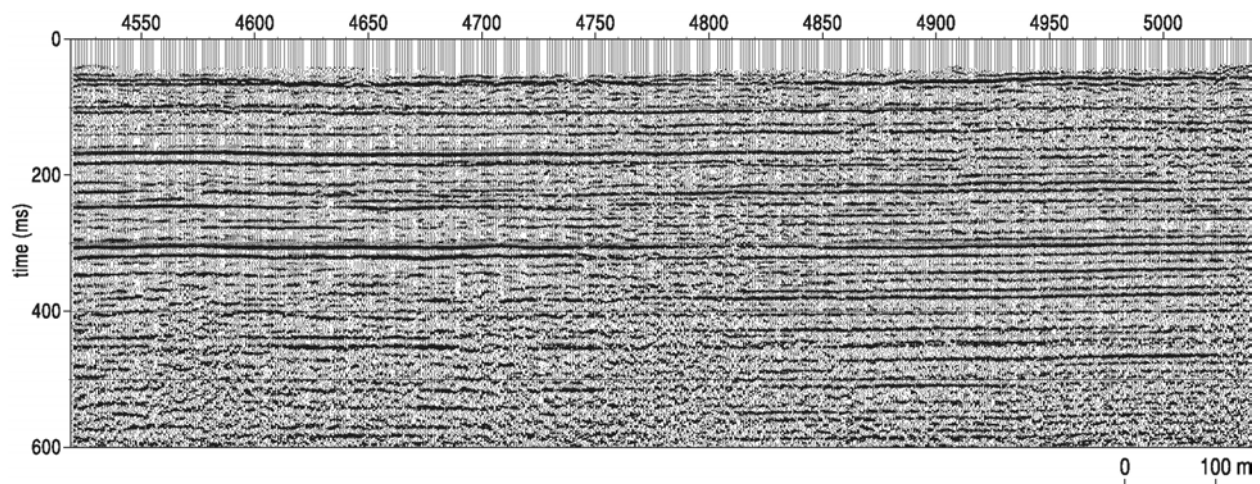
Figure 17. Near the eastern end of this 10+ km survey the seismic signature of the salt layer appears to change, thinning some with reflection frequencies within the salt layer dropping notably.

a highway stability perspective this change is not significant. Throughout the last 1.5 km of the profile the salt layer changes seismically, indicative of a change in geology, but it does not appear to possess abnormalities associated with missing salt or with clear subsidence potential.

Conclusions

High-resolution seismic reflection provided a relatively continuous view of key rock layers above the base of the Hutchinson Salt beneath the proposed new alignment of the U.S. 50 bypass south of the city of Hutchinson, Kansas. Several features with the potential to affect the ground surface along or beneath the future highway were discovered. A paleosinkhole with indications of reactivation since it originally formed represents a risk of gradual subsidence in the highway surface at some point in time. Also, chimney features associated with salt creep are areas for monitoring. A fault intersecting the highway alignment cannot be avoided by the new highway and it has not provided a conduit for fresh water to gain access to the salt at this time. The area above the fault will also require monitoring for any indication of ground subsidence, but does not represent a significant threat to highway stability. Diffraction or scatter associated with bed terminations or point source re-radiation was identified in two locations adjacent to known areas where dissolution salt mining has been active previously. It is not unreasonable to suggest these features might be related to that mining activity. If they are related to dissolution mining activity, they represent the most significant risk of accelerated failure and subsidence in this area. More study of these diffraction/scatter features is needed to better define their source.

Acknowledgments

References

Anderson, N.L., W.L. Watney, P.A. Macfarlane, and R.W. Knapp, 1995a, Seismic signature of the Hutchinson Salt and associated dissolution features: Kansas Geol. Survey Bulletin 237, p. 57-65.

Anderson, N.L., R.W. Knapp, D.W. Steeples, and R.D. Miller, 1995b, Plastic deformation and dissolution of the Hutchinson Salt Member in Kansas: Kansas Geol. Survey Bulletin 237, p. 66-70.

Anderson, N.L., A. Martinez, and J.F. Hopkins, 1998, Salt dissolution and surface subsidence in central Kansas: A seismic investigation of the anthropogenic and natural origin models: Geophysics, v. 63, p. 366-378.

Baar, C.A., 1977, Applied salt-rock mechanics 1: Elsevier Scientific Publishing Company, 294 p.

Baker, G.S., D.W. Steeples, and M. Drake, 1998, Muting the noise cone in near-surface reflection data: An example from southeastern Kansas: Geophysics, v. 63, p. 1332-1338.

Bayne, C.K., 1956, Geology and ground-water resources of Reno County, Kansas: Kansas Geological Survey Bulletin 120.

Beck, B.F., A.J. Pettit, and J.G. Herring, eds., 1999, Hydrogeology and engineering geology of sinkholes and Karst–1999: A.A. Balkema.

Carter, N.L., and F.D. Hansen, 1983, Creep of rock salt: Tectonophysics, v. 92, p. 275-333.

Coffeen, J.A., 1978, Seismic exploration fundamentals: PennWell Publishing Company, Tulsa, OK, 277 p.

Dobrin, M.B., 1976, Introduction to geophysical prospecting: McGraw-Hill Book Company, New York.

Doll, W.E., and C. Çoruh, 1995, Spectral whitening of impulsive and swept-source shallow seismic data [Exp. Abs.]: Soc. Explor. Geophys., p. 398-401.

Davies, W.E., 1951, Mechanics of cavern breakdown: National Speleological Society, v. 13, p. 6-43.

Ege, J.R., 1984, Formation of solution-subsidence sinkholes above salt beds: U.S. Geological Survey Circular 897, 11 p.

Frye, J.C., 1950, Origin of Kansas Great Plains depressions: Kansas Geological Survey Bulletin 86, pt. 1, p. 1-20.

Frye, J.C., and S.L. Schoff, 1942, Deep-seated solution in the Meade Basin and vicinity, Kansas and Oklahoma: American Geophysical Union Transactions, v. 23, pt. 1, p. 35-39.

Hunter, J.A., S.E. Pullan, R.A. Burns, R.M. Gagne, and R.S. Good, 1984, Shallow seismic-reflection mapping of the overburden-bedrock interface with the engineering seismograph–Some simple techniques: Geophysics, v. 49, p. 1381-1385.

Knapp, R.W., D.W. Steeples, R.D. Miller, and C.D. McElwee, 1989, Seismic reflection surveys at sinkholes in central Kansas: Geophysics in Kansas, D.W Steeples, ed.: Kansas Geological Survey Bulletin 226, p. 95-116.

Liberty, L.M., and M. Knoll, 1998, Time varying fold in high-resolution seismic reflection data: a recipe for optimized acquisition and quality control processing and interpretation: Proceedings of the Symposium on the Application of Geophysics to Engineering and Environmental Problems (SAGEEP 98), March 22-26, Chicago, p. 745-751.

Merriam, D.F., and C.J. Mann, 1957, Sinkholes and related geologic features in Kansas: Transactions Kansas Academy of Science, v. 60, p. 207-243.

Merriam, D.F., 1963, The geologic history of Kansas: Kansas Geol. Survey Bulletin 162, 317 p.

Miller, R.D., D.W. Steeples, L. Schulte, and J. Davenport, 1993, Shallow seismic reflection study of a salt dissolution well field near Hutchinson, Kansas: Mining Engineering, October, p. 1291-1296.

Miller, R.D., D.W. Steeples, and T.V. Weis, 1995, Shallow seismic-reflection study of a salt-dissolution subsidence feature in Stafford County, Kansas: in N.L. Anderson and D.E. Hedke, eds., Geophysical Atlas of Selected Oil and Gas Fields in Kansas: Kansas Geological Survey Bulletin 237, p. 71-76.

Miller, R.D., A.C. Villella, J. Xia, 1997, Shallow high-resolution seismic reflection to delineate upper 400 m around a collapse feature in central Kansas: Environmental Geosciences, v. 4, n. 3, p. 119-126.

Rokar, R.B., and K. Staudtmeister, 1985, Creep rupture criteria for rock salt: Sixth International Symposium on Salt, B.C. Schreiber and H.L. Harner, eds., Salt Institute Inc., Virginia, v. 1, p. 455-462.

Sheriff, R.E., 1978, A first course in geophysical exploration and interpretation: International Human Resources Development Corp., Boston, 313 p.

Steeples, D.W., R.W. Knapp, and C.D. McElwee, 1986, Seismic reflection investigation of sink-holes beneath interstate highway 70 in Kansas: Geophysics, v. 51, p. 295-301.

Steeples, D.W., and Miller, R.D., 1990, Seismic reflection methods applied to engineering, environmental, and groundwater problems: Soc. Explor. Geophys., Geotechnical and Environmental Geophysics, Stan Ward, ed., Vol. 1: Review and tutorial, p. 1-30.

Telford, W.M., et al., 1976, Applied geophysics: Cambridge University Press, New York, 860 p.

Walters, R.F., 1978, Land subsidence in central Kansas related to salt dissolution: Kansas Geological Survey Bulletin 214, p. 1-32.

Walters, R.F., 1980, Solution and collapse features in the salt near Hutchinson, Kansas: South-central Section, Geological Society of America, Field Trip Notes, 10 p.

Walters, R.F., 1991, Gorham Oil Field: Kansas Geological Survey Bulletin 228, p. 1-112.

Waters, K.H., 1987, Reflection seismology—A tool for energy resource exploration, 3rd ed., John Wiley and Sons, New York, 538 p.

Watney, W.L., J.A. Berg, and S. Paul, 1988, Origin and distribution of the Hutchinson Salt (lower Leonardian) in Kansas: Midcontinent SEPM Special Publication No. 1., p. 113-135.

Xia, J., and R.D. Miller, 2000, Design of a hum filter for suppressing power-line noise in seismic data: Journal of Environmental and Engineering Geophysics, v. 5, n. 2, p. 31-38.

A 2-D MASW SHEAR-WAVE VELOCITY PROFILE ALONG A TEST SEGMENT OF INTERSTATE I-70, ST. LOUIS, MISSOURI

Thitimakorn, T. (University of Missouri-Rolla; thanop@umr.edu; 573 341-4616)
Anderson, N. (University of Missouri-Rolla; nanders@umr.edu, 573 341-4852)
Fennessey, T. (Missouri DOT; Thomas.Fennessey@modot.mo.gov; 573 526-4340)
Lauer, R. (Missouri DOT; LAUERR@mail.modot.state.mo.us; 314 340-4100)

ABSTRACT

Multi-channel surface-wave (MASW) control was acquired along a 6400 ft segment of interstate I-70 in downtown St. Louis, Missouri. The acquired MASW data set was processed and transformed into a 2-D MASW shear-wave velocity profile with a trace-spacing of 40 ft. Shear-wave velocity control extends from the surface to a depth in excess of 50 ft. The interpreted depth to acoustic bedrock along the 2-D MASW profile varies between 20 ft and 44 ft.

The interpreted 2-D MASW profile was compared to available borehole (depth to bedrock), cone penetrometer and seismic cone penetrometer control provided by the Missouri Department of Transportation. The 2-D MASW profile correlates very well with available geotechnical control, supporting the conclusion that the multi-channel surface-wave seismic technique can be used to generate reliable and interpretable 2-D shear-wave velocity profiles of the shallow subsurface.

INTRODUCTION

Multi-channel surface-wave seismic control (MASW data) was acquired along a 6400 ft segment of interstate I-70 in downtown St. Louis, Missouri (Figure 1). These data were processed (spectral inversion) and transformed into a 2-D MASW shear-wave velocity profile consisting of multiple traces (shear-wave velocity curves) spaced at 40 ft intervals. The initial output MASW shear-wave velocity profile extended to a depth in excess of 100 ft. The 2-D

MASW profile presented herein however, was truncated at a depth of 50 ft. This depth is suffi-

cient to image the interpreted top of bedrock ($\leq$44 ft) and provides for superior visual resolution.

The 2-D MASW profile was interpreted and compared to proximal borehole (depth to

bedrock), cone penetrometer and seismic cone penetrometer (SCPT) control provided by the

Missouri Department of Transportation (MoDOT). There were two primary objectives. The

first was to determine if the MASW shear-wave velocities were reliable. The second was to

determine if depth to acoustic bedrock could be accurately estimated on the basis of the

interpreted MASW profile.

Figure 1: Segment of I-70 study area (sheet 1/4).

OVERVIEW OF MASW TECHNIQUE
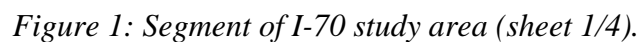
Types of Acoustic Waves: When an acoustic source (weight drop, dynamite charge, etc.) is

discharged at or near the surface of the earth, two fundamental types of acoustic waves (strain

energy) are produced: body waves and surface waves. Two types of body waves can propagate through an elastic solid (compressional waves and shear waves). Similarly, two types of surface waves can propagate along the earth's surface (Rayleigh waves and Love waves).

Compressional waves (or P-waves) propagate by compressional and dilatational strains in the direction of wave travel (Figure 2). Particle motion involves oscillation, about a fixed point, in the direction of wave propagation. Shear waves (or S-waves) propagate by a pure strain in a direction perpendicular to the direction of wave travel (Figure 2). Body waves are essentially non-dispersive over the range of frequencies employed for earthquake studies and seismic exploration (i.e., all component frequencies propagate at the same velocity). The propagation velocities of body waves are a function of the engineering properties of the medium through which they are traveling (Figure 2).

Love waves propagate along the surface of a layered solid (earth's surface) if the shear-wave velocity of the uppermost layer is lower than that of the underlying layer (e.g., unconsolidated strata overlying bedrock). Love waves are polarized shear waves with an oscillatory particle motion parallel to the free surface and perpendicular to the direction of wave motion (Figure 3). Love waves are dispersive, and are characterized by velocities between the shear-wave velocity of the shallowest layer and that of deeper layers. The amplitude of a Love wave decreases exponentially with depth. The lower component frequencies of Love waves involve particle motion at greater depth and therefore generally exhibit higher velocities.

Rayleigh waves propagate along the earth's surface (free surface). The associated particle motion is elliptical in a plane perpendicular to the surface and containing the direction of propagation (Figure 3). The orbital motion is in the opposite sense to the circular motion associated with a water wave, and is often described as retrograde elliptical. The amplitude of a

Rayleigh wave decreases exponentially with depth (Figure 3). Progressively lower frequency components of Rayleigh waves involve particle motion over progressively greater depth ranges (relative to free surface). Rayleigh waves in a heterogeneous medium (with respect to velocity) are therefore dispersive. The velocities with which the highest component frequencies travel are a function of the engineering properties of the shallowest sediment. The velocities with which progressively lower frequencies travel are functions of the varying engineering properties over a progressively greater range of sediment depths. In the "multi-channel analysis of surface wave" (MASW) technique, the phase velocities of the component frequencies are calculated. These data are then inverted and used to generate a vertical shear-wave velocity profile.

Rayleigh Waves: Rayleigh waves propagate along the free surface of the earth, with particle motions that decay exponentially with depth (Figure 3). The lower component frequencies of Rayleigh waves involve particle motion at greater depths. In a homogeneous (non-dispersive) medium, Rayleigh wave phase velocities are constant can be determined using the following equation:

$$\mathbf{V_R^6 - 8\beta^2 V_R^4 + (24 - 16\beta^2/\alpha^2)\beta^4 V_R^2 + 16(\beta^2/\alpha^2 - 1)\beta^6 = 0} \qquad \text{where:}$$

$\mathbf{V_R}$ is the Rayleigh wave velocity within the uniform medium
$\boldsymbol{\beta}$ is the shear-wave velocity within the uniform medium (also denoted Vs)
$\boldsymbol{\alpha}$ is the compressional wave velocity within the uniform medium (also denoted Vp)

In a heterogeneous earth, shear-wave and compressional-wave velocities vary with depth. Hence, the different component frequencies of Rayleigh waves (involving particle motion over different depth ranges) exhibit different phase velocities (Bullen, 1963). The phase velocity of each component frequency being a function of the variable body wave velocities over the vertical depth range associated with that specific wavelength. More specifically, in a layered earth, the Rayleigh wave phase velocity equation has the following form:

$$\mathbf{V_R}\,(\mathbf{f_j},\,\mathbf{C_{Rj}},\,\boldsymbol{\beta},\,\boldsymbol{\alpha},\,\boldsymbol{\rho},\,\mathbf{h}) = \mathbf{0} \quad (\mathbf{j} = \mathbf{1},\,\mathbf{2},\,\ldots.,\,\mathit{m}) \qquad \text{where:}$$

$\mathbf{f_j}$ is the frequency in Hz
$\mathbf{V_{Rj}}$ is the Rayleigh-wave phase velocity at frequency $\mathbf{f_j}$
$\boldsymbol{\beta} = (\boldsymbol{\beta_1},\,\boldsymbol{\beta_2},\ldots.,\,\boldsymbol{\beta_n})^{\mathbf{T}}$ is the s-wave velocity vector
$\boldsymbol{\beta_i}$ is the shear-wave velocity of the ith layer
$\boldsymbol{\alpha} = (\boldsymbol{\alpha_1},\,\boldsymbol{\alpha_2},\,\ldots..,\,\boldsymbol{\alpha_n})^{\mathbf{T}}$ is the compressional p-wave velocity vector
$\boldsymbol{\alpha_i}$ is the P-wave velocity of the ith layer
$\boldsymbol{\rho} = (\boldsymbol{\rho_1},\,\boldsymbol{\rho_2},\ldots.,\,\boldsymbol{\rho_n})^{\mathbf{T}}$ is the density vector
$\boldsymbol{\rho_i}$ is the density of the ith layer
$\mathbf{h} = (\mathbf{h_1},\,\mathbf{h_2},\ldots.,\,\mathbf{h_{n\text{-}1}})^{\mathbf{T}}$ is the thickness vector
$\mathbf{h_i}$ the thickness of the ith layer
$\mathbf{n}$ is the number of layers within the earth model

The spectral analysis of surface waves (MASW) technique is based on the relationship between Rayleigh wave phase velocities and the depth-range of associated particle motion. More specifically, in this technique, phase velocities are calculated for each component frequency of field-recorded Rayleigh waves (active monitoring). The resultant dispersion curve (phase velocity vs. frequency) is then inverted using a least–squares approach and a vertical shear-wave velocity profile is generated (Miller *et al*., 2000; Nazarian *et al*., 1983; Stokoe *et al*., 1994; Park *et. al.,* 2001; Xia *et al*., 1999).

MASW Field Technique: The acquisition of the "active" Rayleigh wave (surface wave) data was relatively straightforward (Figure 4). Essentially, 12 low-frequency (4.5 Hz) vertical geophones, placed at 10 ft intervals, were centered about station location #1 (Figure 1). Acoustic energy was generated at an offset (distance to nearest geophone) of 60 ft using a 20 lb sledge hammer and metal plate. The generated Rayleigh wave data were recorded. For "all intents and purposes", the entire 12-channel geophone array and source were then shifted (iteratively, and at 40 ft station intervals) along the entire test segment of interstate. At each "station" location, Rayleigh wave data were generated and recorded. (In actual fact, the MASW

data were acquired using a 24-channel seismograph. Data acquisition was not quite as straightforward as described above, however it was much more efficient.)

Processing of MASW Data: The acquired Rayleigh wave data were processed using the KGS software package SURFSEIS (Figure 5). Each set of Rayleigh wave data (12 channel data set for each station location) was transformed from the time domain into the frequency domain using Fast Fourier Transform (FFT) techniques. These field-based data were used to generate site-specific dispersion curves ($V_R(f)$ versus $\lambda_R(f)$) for each station location. The site-specific dispersion curves (**DCS**) generated from field-acquired Rayleigh wave data were then transformed into vertical shear-wave velocity profiles (**SASW** shear-wave velocity profile). Transformations were based on the assumption that Poisson's Ratio was 0.4.

(a) P-waves

$$\alpha = [(K + 4\mu/3)/\rho]^{1/2}$$
$$\beta = [\mu/\rho]^{1/2}$$
where:
α = P-wave velocity (Vp)
β = S-wave velocity (Vs)
K = bulk modulus
μ = shear modulus
ρ = density
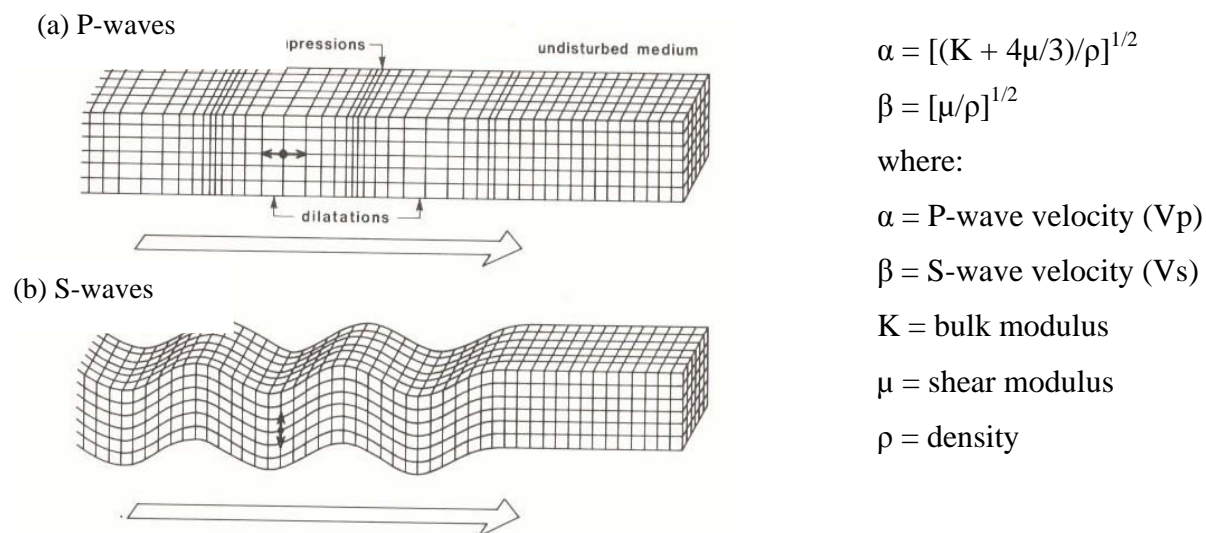
(b) S-waves

Figure 2: Particle motions associated with compressional waves
(P-waves; upper caption) and shear waves (S-waves; lower caption).

FIELD SITES: LOCATIONS AND GEOTECHNICAL DATA

MASW data were acquired along a 6400 ft paved segment of interstate I-70 (Figure 1). All of the SCPT sites and most of the borehole sites are off-line (re: MASW profile). For the purposes of analyses, borehole and SCPT data were "tied" to the closest MASW station location.

(a) Rayleigh waves
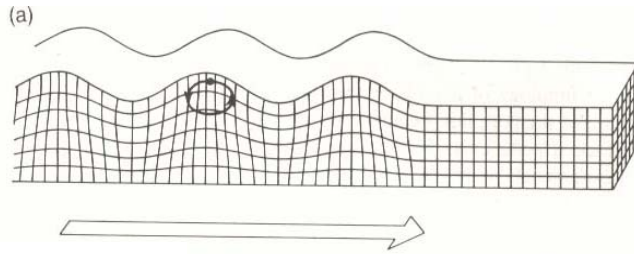
Rayleigh wave particle motion
- retrograde elliptical
- decreases exponentially with
  depth
- function of α and β
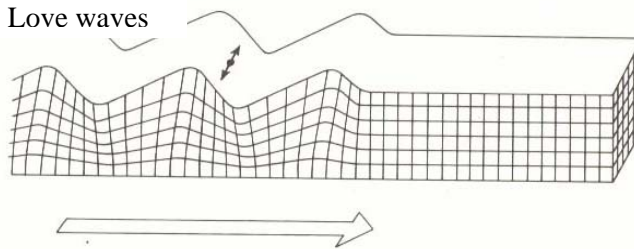
(b) Love waves

Love wave particle motion
- horizontal
- decreases exponentially
  with depth
- function of β

*Figure 3: Particle motions associated with Rayleigh waves
(upper caption) and Love waves (lower caption).*
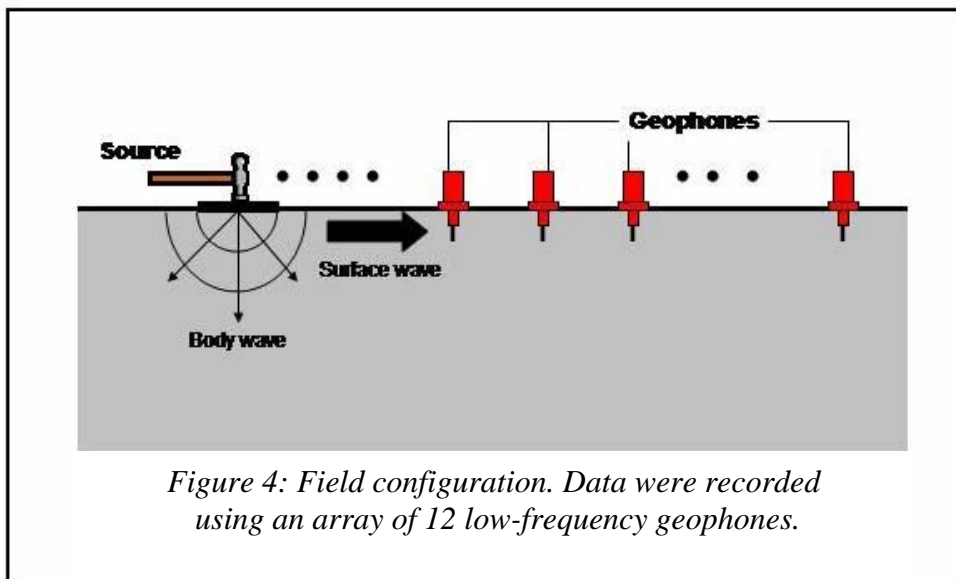
*Figure 4: Field configuration. Data were recorded
using an array of 12 low-frequency geophones.*
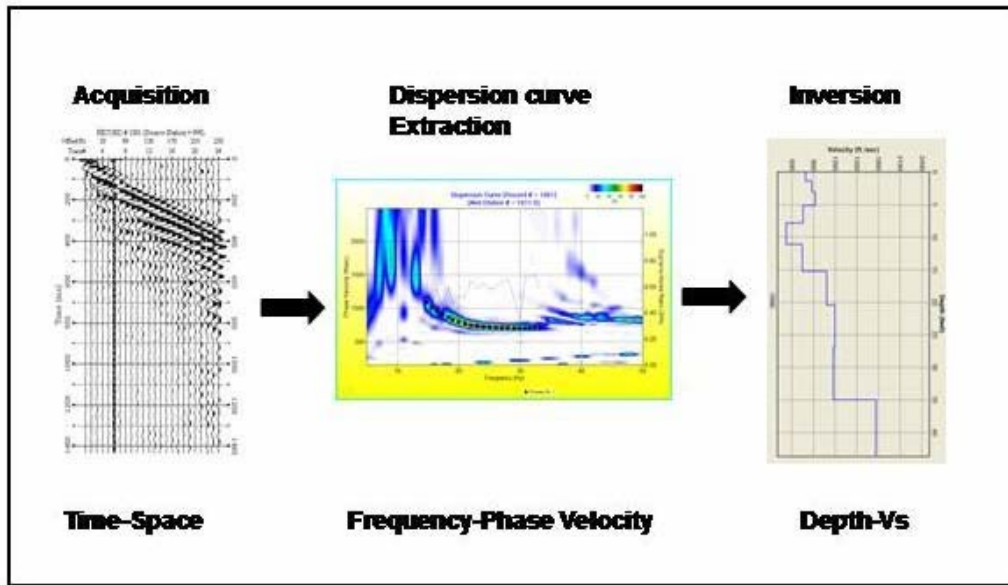
Figure 5: Dispersion curves were generated for each acquired Rayleigh wave data set. Each dispersion curve was transformed (inversion) into a shear-wave velocity vs. depth curve.

2-D MASW SHEAR-WAVE VELOCITY PROFILE

The interpreted version of the MASW shear-wave velocity profile is presented as Figure 6. The "horizon" correlated (with minimal smoothing) across the MASW profile (depths of 20-44 ft; Figure 6) is interpreted as "acoustic bedrock". (Acoustic bedrock, as mapped on the MASW profile, is characterized by shear-wave velocities in excess of 1000 ft/s.) The identification of acoustic bedrock (Figure 6) was based on the "ties" between the 2-D MASW profile and the limited borehole control (boreholes B-39, B-43 and B-44) initially provided by MoDOT. At these three borehole locations and at all other test locations (except SCPT Site A6440-10), "acoustic" bedrock represents the soil/limestone interface. (At SCPT Site A6440-10, the interpreted "acoustic" bedrock corresponds to the top of a dense sand immediately overlying bedrock.)
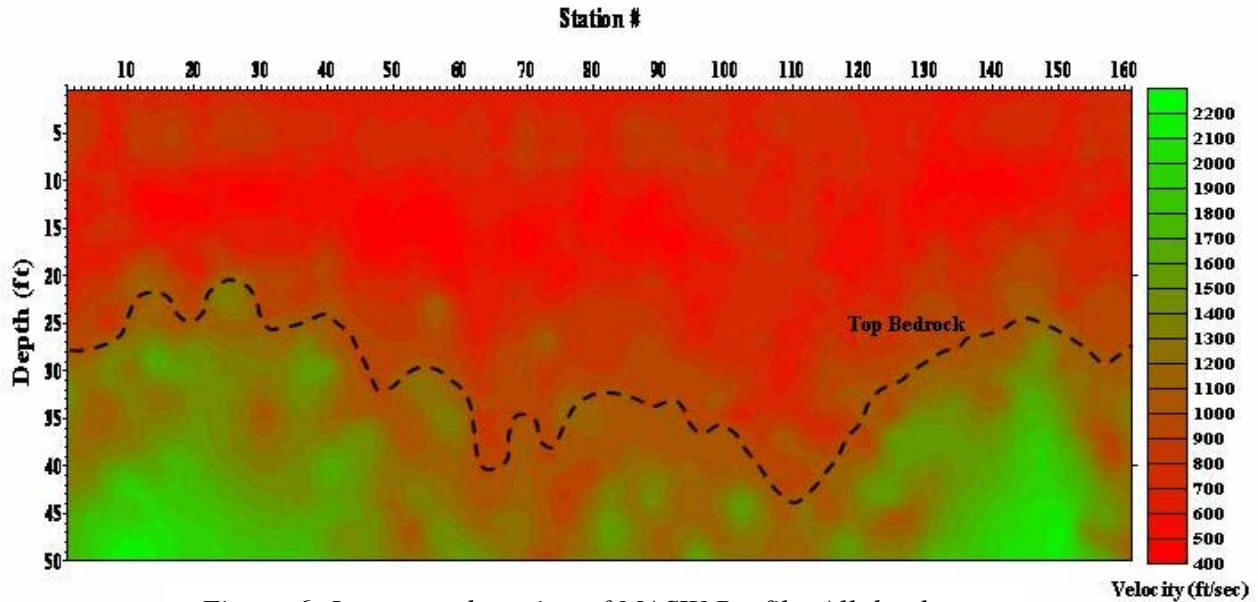
Figure 6: Interpreted version of MASW Profile. All depths are relative to top of pavement along MASW traverse.

Limestone bedrock in the study area is characterized by MASW shear-wave velocities that typically increase from 1000 ft/s to in excess of 1500 ft/s over vertical depths on the order of 15 ft (Figure 6). This increase in velocity with depth is consistent with the nature of limestone bedrock in the study area. More specifically, the uppermost limestone bedrock (<2 ft depth) is frequently described on MoDOT logs as highly weathered. The underlying limestone is typically described as gray, medium grained and medium hard. At many test sites multiple thin (<1 ft thick) clay layers were encountered within limestone bedrock. In general, the quality of limestone increased with depth from top of rock.

Depth to acoustic bedrock varies between 20 and 44 ft along the length of the MASW profile. Depths are believed to be accurate to within one-half of an MASW sample interval (accurate to within ~±2.5 ft). *Note: MASW depths to bedrock at all station locations were based on the interpretation of the smoothed acoustic bedrock horizon on Figure 6. Depths were not estimated from individual MASW curves.*

COMPARISON OF MASW AND BOREHOLE CONTROL

The interpreted MASW profile (Figure 6) was compared to available SCPT and borehole bedrock control (Figure 1). The first objective was to determine if the MASW shear-wave velocities were reliable. The second was to determine if the MASW-estimated depths to acoustic bedrock were accurate.

A total of six SCPT data sets and 19 boreholes (drilled to limestone bedrock) were included in the comparative analyses of the MASW profile. Two SCPT data sets and one borehole log are presented herein for the purposes of illustration.

The uppermost limestone bedrock (<2 ft depth) in the study area is typically described on MoDOT boring logs as highly weathered. The underlying limestone is typically described as gray, medium grained and medium hard. At many test sites multiple thin (<1 m) clay layers were encountered.

Borehole B-39: In Figure 7, MASW trace #84 is "tied" to borehole log B-39. The B-39 datum is at an elevation of 451.6 ft; the MASW datum is 453 ft.

The MASW trace #84 shear-wave velocity curve correlates well with the B-39 borehole log. More specifically, the uppermost 8 ft (comprised of
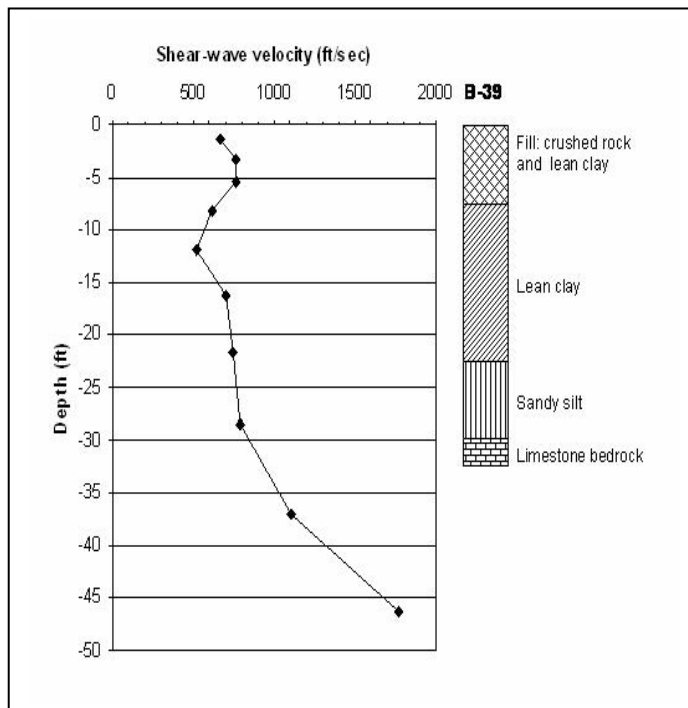
Figure 7: B-39 borehole lithologic log and MASW station #84. Datum elevation is 451.6 ft.

pavement and compacted fill) is characterized by MASW shear-wave velocities of between 600 and 700 ft/s; lean clay is characterized by velocities between ~450 and ~650 ft/s; sandy silt is characterized by velocities characterized by velocities in excess of 850 ft/s.

Limestone (acoustic bedrock) is characterized by shear-wave velocities that increase from 1000 ft/s to in excess of 1600 ft/s over 15 ft (31 ft - 46 ft; Figure 7). This is consistent with the nature of limestone bedrock in the study area. More specifically, the uppermost limestone bedrock (<2 ft depth) is often described as highly weathered. The underlying limestone is typically described as gray, medium grained and medium hard. At many test sites multiple thin (<1 ft) clay layers were encountered within limestone bedrock. In general, the quality of limestone increased with depth from top of rock.

The depths to limestone bedrock at the B-39 borehole location and MASW acoustic bedrock (29.5 ft and 32 ft respectively) correlate very well considering the test locations are separated by more than 50 ft. MASW shear-wave velocities are thought to be reliable because the estimated depth to acoustic bedrock at the MASW test site appears to be fairly accurate. (*Note: MASW acoustic bedrock is estimated to at a sub-pavement depth of 32 ft on MASW profile; Figure 7.*)

SCPT Site A6433-10 (Station 3+78.5, 44.7'RT, Elev. 463.0): SCPT site A6433-10 is located off-line (re: 2-D MASW profile; Figure 1) and more than 50 ft from station #87 (nearest MASW station). SCPT site A6433-10 is at an elevation of 463.0 ft; the MASW station #87 datum is at an elevation of 451 ft. The SCPT A6433-10 shear-wave seismic velocity curve and MASW station #87 are plotted in Figure 8. MASW station #87 ties the SCPT curve at a depth of approximately 12 ft.

Limestone bedrock was not encountered at the SCPT site, however it was encountered at a proximal borehole site (Station 3+66.7, 13.7'RT, Elevation 462.3) at a depth of 45.3 ft (417.0 ft

elevation). Bedrock at the SCPT A6433-10 site is therefore estimated to be at 417.0 ft elevation.

Depth to acoustic bedrock at MASW station #87 is estimated to be at an elevation of 418 ft

elevation. (*Note: MASW acoustic bedrock is estimated to at a sub-pavement depth of 33 ft on MASW profile; Figure 7.*) The difference between these two depths to bedrock is only 1.0 ft.

The uppermost ~8 ft (12-20 ft depth interval) of the subsurface at MASW station #87 location is characterized by MASW shear-wave velocities of between 650 and 850 ft/s (Figure 8). This zone is thought to consist primarily of pavement and compacted

Figure 8: SCPT curve for site A6433-10 and MASW station #87. Datum elevation is 463.0 ft.

fill (crushed rock and lean clay; Figures 10 and 14). The corresponding depth interval at the

SCPT site is comprised predominantly of clay, silty clay to clay, and clayey silt to silty clay.

The 20-45 ft interval (interpreted base fill – interpreted top acoustic bedrock; Figure 8) at

the MASW station #87 location is characterized by shear-wave velocities that vary from ~500

ft/s to ~1000 ft/. Only the uppermost 22 ft the corresponding depth interval was tested by the

CPT tool. CPT testing indicates this 22 ft interval is comprised predominantly of clay (~6 ft),

silty clay to clay (~6), clayey silt to silty clay (~7 ft), sandy silt to clayey silt (~1.5 ft), and silty

sand to sandy silt (~1.5 ft). It is characterized by SCPT shear-wave velocities ranging from ~ 250 ft/s to ~800 ft/s. The average SCPT shear-wave velocity is approximately 540 ft/s (Figure 8).

As noted, the MASW shear-wave velocities and the SCPT shear-wave velocities correlate reasonably well despite the physical separation between the two locations, the propensity for soil lithologies to vary laterally over short distances, and the fact that SCPT site is located on the embankment adjacent to interstate I-70, whereas the MASW site is on I-70. The MASW shear-wave velocities are believed to be reliable because the estimated depth to acoustic bedrock at the MASW test site appears to be fairly accurate. {Note that the SCPT curve is somewhat suspect because it has assigned an unreasonably high shear-wave velocity of 4560 ft/s to a 3 ft interval comprised mostly of clay, silty sand, sandy silt and sand (3.5-6.5 ft interval; not shown in Figure 8)}.

SCPT Site A6440-10 (Station 3+12.8, 6.3'RT, Elev. 463.3): SCPT site A6440-10 is located off-line (re: 2-D MASW profile; Figure 1) and more than 50 ft from station #110 (nearest MASW station; Figure 9). SCPT site A6440-10 is at an elevation of 463.3 ft; MASW station #110 is at an elevation of 460 ft. The SCPT A6440-10 shear-wave seismic velocity curve and MASW station #108 are plotted in Figure 9. MASW station #110 ties the SCPT curve at a depth of approximately 3 ft.

High-velocity (~2170 ft/s) sand was encountered at a depth of 45.5 ft (elevation of 417.8 ft; Figure 9) at the SCPT test site. The top of these sands represent acoustic bedrock. Acoustic bedrock at MASW station #110 is estimated to be at an elevation of ~416 ft. (*Note: MASW acoustic bedrock is estimated to at a sub-pavement depth of 44 ft on MASW profile; Figure 7.*) The difference between these two depths to bedrock is ~1.8 ft.

The uppermost ~6 ft (3-9 ft depth interval) of the subsurface at MASW station #110 location is - characterized by MASW shear-wave velocities of between 750 and 900 ft/s (Figure 8). This zone is thought to consist primarily of pavement and compacted fill (crushed rock and lean clay; Figures 10 and 14). The corresponding depth interval at the SCPT site is comprised predominantly of clay, silty clay to clay, and clayey silt to silty clay.
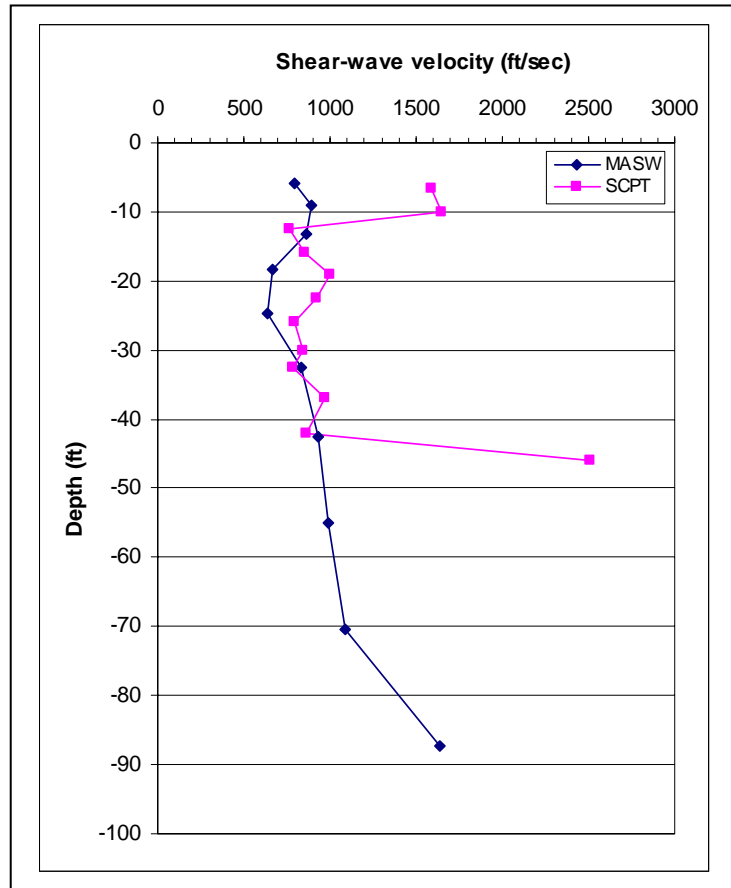
Figure 9: SCPT curve for site A6440-10 and MASW station #110. Datum elevation is 463.3 ft.

The 9-47 ft interval (interpreted base fill – interpreted top acoustic bedrock; Figure 9) at MASW station #110 is characterized by MASW shear-wave velocities that vary from ~600 ft/s to ~1000 ft/. The corresponding depth interval was tested by the CPT tool, which indicates this 37 ft interval is comprised predominantly of clay (~2.5 ft), silty clay to clay (~5), clayey silt to silty clay (~11 ft), sandy silt to clayey silt (~12 ft), silty sand to sandy silt (~2.5 ft), and sand to silty sand (~3). It is characterized by SCPT shear-wave velocities ranging from ~ 300 ft/s to ~980 ft/s, and underlain by dense sand with an SCPT interval velocity of 2110 ft/s (Figure 9).

As noted, the MASW and SCPT shear-wave velocities correlate reasonably well despite the physical separation between the two test locations, the propensity for soil lithologies to vary

laterally over short distances, and the fact that SCPT site is located on an embankment adjacent to interstate I-70, whereas the MASW site is on I-70. However, the SCPT velocities are somewhat suspect because of the presence of an interval of unreasonably low (~-2280 ft/s) within a 3 ft interval (3-6 ft; not shown), and an interval of unreasonably high shear-wave velocities (~1400 ft/s) within a 6 ft interval (6-12 ft; Figure 9) comprised mostly of clay, silty clay and clayey silt.

The MASW shear-wave velocities are believed to be more reliable than the SCPT velocities because of the presence of the anomalous SCPT velocity values and because the estimated depth to acoustic bedrock at the MASW test site appears to be fairly accurate.

Suite of Seventeen Borehole Locations Presented in Table 1: Seventeen boreholes are listed in Column B Table 1. Corresponding highway structures (Column A), borehole station locations (Column C), offsets (Column D), borehole elevations (Column E), borehole depths to bedrock (Column F) and borehole bedrock elevations (Column G) are tabled. Presented as well in Table 1 are the closest MASW station locations (Column H), and corresponding MASW datum elevations (Column I), estimated MASW depths to bedrock relative to MASW datum (Column J), and estimated MASW bedrock elevations (Column K). Depths in columns G and K can be compared directly.

The comparison of the borehole depths to bedrock (Column F) and the corresponding MASW estimated depths to acoustic bedrock (Column J), indicates that the MASW interpretations compare favorably to ground truth except in proximity to borehole A6440-13. Dense sand was encountered at an elevation of 415.3 ft (ASL) in the A6440-13 borehole. The top of this dense sand is thought to represent acoustic bedrock.

On average (including depth differential to acoustic bedrock at borehole A6440-13 and MASW station 110), MASW estimated depths to bedrock exceed borehole depths to bedrock (as per Figure 17) by ~0.7 ft. This average depth differential is remarkably small, given the variable depth to bedrock in the study area and the fact that the boreholes were not situated exactly on the centerline of the MASW traverse.

CONCLUSIONS

On the basis of the comparison of MASW-estimated bedrock depths and proximal ground truth (borehole control), it is concluded that the interpretation of the 2-D MASW shear-wave velocity profile is reasonably reliable (Figure 6). The implication is that the MASW shear-wave velocities are also reliable. Indeed, if this were not the case, the MASW horizons (as interpreted; Figure 6) would not correlate well (depth-wise) with available borehole control. It is recognized that all currently available borehole control is "off-line" and that comparative analyses are based on extrapolated "ties".

REFERENCES

Bullen, K.E., 1963, An Introduction to the Theory of Seismology: Cambridge University Press, 381 p.

Miller, R.D., Xia, J., Park, C.B., and Ivanov, J., 2000, Shear-wave velocity field from surface waves to detect anomalies in the subsurface: Geophysics 2000, FHWA and MoDOT Special Publication, 4:8.1–4:8.10.

Nazarian, S., Stokoe, K.H., and Hudson, W.R., 1983, Use of spectral analysis of surface waves method for determination of moduli and thicknesses of pavement systems: Transportation Research Record, **930**, 38-45.

Park, C.B., Miller, R.D., and Xia, J., 1999, Multichannel analysis of surface waves: Geophysics, **64**, 800-808.

Park, C.B., Miller, R.D., and Xia J., 1999, Multimodal analysis of high frequency surface waves: Proceeding of the Symposium on the Application of Geophysics to Engineering and Environmental Problems, 115-121.

Park, C.B., Miller, R.D., Xia, J., and Ivanov, J., 2000, Multichannel seismic surface-wave methods for geotechnical applications: Geophysics 2000, FHWA and MoDOT Special Publication, 4:7.1-4:7.11.

Stokoe, K.H., Wright, G.W., James, A.B., and Jose, M.R., 1994, Characterization of geotechnical sites by SASW method, *in* Geophysical Characterization of Sites ISSMFE Technical Committee #10, edited by R.D. Woods: Oxford Publishers, New Delhi

Xia, J., Miller, R.D., and Park, C.B., 1999, Estimation of near-surface velocity by inversion of Rayleigh waves: Geophysics, **64**, 691-700.

Highway Structure (Fig. 1)	Highway Structure Borehole Number (BH#)	Highway Station of BH	Offset of BH (ft)	BH Elev. (ft)	BH Depth to Bedrock (ft)	BH Bedrock Elevation (ft ASL)	MASW Station	Elevation of MASW Station (ft)	MASW Depth To Bedrock (ft)	MASW Depth to Bedrock (ft ASL)
A	B	C	D	E	F	G	H	I	J	K
A6427	A6427-4	6+66.3	54' LT	448.9	19.2	429.7	11	451	22	429
A6426	A6426-5	47+13.1	0.2' LT	445.6	21.7	423.9	22	447	22	425
	A6426-6	47+16.82	15' RT	445.5	22.5	423.0	21	447	23	424
A6422	A6422-5	31+60.6	16.6' LT	448.6	20.3	428.3	41	448	23	425
A6525	A6525-8	10+47.3	1.7' RT	448.3	23.0	425.3	42	448	24	424
A6423	A6423-7	357+21.3	21' LT	447.8	19.5	428.3	41	448	23	425
A6424	A6424-13	456+08	0.5' RT	449.3	24.1	425.2	45	448	25	423
A6433	A6433-4	2+03.8	26' LT	448.0	25.7	422.3	86	452	32	420
	A6433-5	2+03.8	C/L	447.6	25.6	422.0	87	451	33	418
A6430	A6430-9	293+94	30' LT	459.5	37.8	421.7	68	459	35	424
A6440	A6440-13	5+31.5	C/L	459.8	44.5 DS#	415.3	109	460	44	416
A6434	A6434-1	2+07.8	33.6' LT	436.5	26.3	410.2	141	439	26	413
	A6434-2	2+02.7	C/L	435.6	21.6	414.0	140	440	26	414
	A6434-3	2+00.9	26' RT	435.9	20.4	415.5	139	441	26	415
	A6434-4	2+28.5	C/L	436.6	22.4	414.2	141	439	25	414
	A6434-5	2+27.4	C/L	435.8	21.3	414.5	140	440	26	414
	A6434-6	2+25.7	51.7' RT	436.2	23.2	413.0	138	441	27	414

Table 1: A comparison of borehole depths to bedrock at seventeen additional borehole locations and corresponding estimated MASW depths to bedrock (* denotes depth to limestone bedrock; # denotes depth to dense sand.)

Remote Sensing Studies, Carroll and Tippecanoe Counties, Indiana
With Engineering Geology Applications

by Yinghui Sui, Huagen Liu and Terry R. West
Dept. of Earth & Atmos. Sciences
Purdue University, West Lafayette, IN 47907-2051
(trwest@purdue.edu)

ABSTRACT

Carroll and Tippecanoe Counties northcentral IN on the Wisconsin Tipton Till Plain, consist of gently rolling ground moraine, dissected by the Wabash River and its tributaries. Collectively the two counties have an area of about 880 square miles. Delphi is the county seat of the agricultural Carroll County wherein Lafayette is the County seat of the more populous Tippecanoe County.

Two remote sensing studies were conducted. The first (H.Liu) was a soil texture classification of Carroll County using Landsat Thematic Mapper data. Two methods were developed and applied 1) multi-category logistic regression models and 2) Support Vector Machines (SUMs). Two SUMs were applied, polynormal and Radial Basis Function. Analysis was based on selected training fields; 8x4.8 km area selected to train and evaluate models. The Maximum Likelihood Method was also used to obtain a classification for comparison.

The second study (Y.Sui) involved site evaluation for relocation of State Highway 25 through Carroll and Tippecanoe Counties. A new four-lane highway (northeast-southwest orientation) will be located near the center of each. Four alternate routes were evaluated based on engineering soils properties, topography and groundwater. Thematic Mapper data were analyzed and compared to STATSGO, the State Soil Survey Geographic data base for Carroll County, a digitized data base of the agricultural soils. Studies of the four alternate locations were conducted and the preferred route designated.

These two remote sensing studies of Carroll and Tippecanoe Counties illustrate how to provide useful information for engineering geology analysis.

INTRODUCTION

Two remote sensing studies were conducted in north-central Indiana in an area of gently rolling ground moraine. The first was a sophisticated soil classification of multispectral data for Carroll County (Liu, 2004) and the second, a study involving highway relocation for both Carroll and its adjoining neighbor, Tippecanoe County (Sui, 2004) (Figure 1).

STUDY ONE, DETAILED MULTISPECTRAL ANALYSIS, CARROLL COUNTY

Carroll County, Indiana, is located in the north-central part of the state, about 60 miles northwest of Indianapolis and 120 miles south of Chicago. It is nearly square in shape, about 21 miles on a side, with an area of 375 squares miles. Delphi, the county seat and largest city, is located west of center along the Wabash River.

Carroll County lies within the Tipton Till Plain, its topography a result of glacial deposition. It is characterized by a gently undulating to moderately rolling surface. During the Pleistocene,

1

glaciers flowed across Indiana from the north and northeast acting as the primary erosional agent to flatten the landscape. Erosional debris was deposited to form rolling ground moraine and occasional end moraines.

Below the glacial deposits, bedrock consists of Silurian and Ordovician aged sedimentary rocks. The Teays River Valley, developed prior to Pleistocene glaciation, trends across Carroll county as a buried stream valley paralleling the current-day Wabash River. Filled with coarse fluvial material it serves as an important aquifer in the area.

Carroll County generally consists of a flat plain dissected by the Wabash and Tippecanoe Rivers along with numerous creeks, streams, and ditches. The highest point in the county, about 840 feet MSL, occurs at its southeast corner, whereas the lowest is about 520 feet MSL located in the western part. Maximum relief occurs along the Wabash River Valley.

The major drainage channels are the Wabash and Tippecanoe Rivers, the latter flowing through the northwest part of the county. The Wabash River flows from northeast to southwest, and has many tributaries. The Tippecanoe River flowing from north to south enters the Wabash River several miles south of the county line in Tippecanoe County.

Soil is the most important natural resource in Carroll County, as agriculture comprises the predominant land use. Most of the county consists of cropland or pasture, but a few dairy farms exist. A dolomite quarry is found along the Wabash River and several sand and gravel pits occur along various stream valleys.

Water supply in the county is mostly ground water, obtained from glacial drift. The depth to water typically ranges from 150 to 250 feet (USDA, 1987).

Carroll County has a population, based on the 2000 census, of 20,165, with 3015 people residing in the county seat, and largest city, Delphi. This city serves as the principal market center for the rural and farming community. One federal highway (US421) and several major railroad lines serve Delphi as do three state highways. Most county roads are located along section lines, and many consist of bituminous pavements.

The predominant land use in Carroll County is agriculture with Delphi as the largest residential and industrial community. The smaller communities were originally located along railroad lines and state or federal highways. Three primary soil textures occur in the county; loam, silt loam and silty clay loam. These three textures account for about 90% of the surface soils and this research focused on how to classify or differentiate these three soil textures.

For detailed soil surveys, soil textures provide a primary information source for large land areas. These surveys are used extensively for highway planning and construction, waste disposal site selection, zoning, resource management, real estate development and environmental consideration. Conventional survey methods for measuring soil textures are not efficient, requiring significant time and labor, with numerous measurements needed to quantify the space-time relationship. By contrast, remote sensing provides a convenient method to survey, measure and monitor extensive landscapes.

From the 1970s, because of the rapid development of remote sensing techniques and their successful applications for large area observation, identification, and monitoring, remote sensing has played an increasingly important role in numerous specialties such as land use/land cover mapping, environment monitoring, resource preservation, agriculture, and forest protection (Condit, 1970; Cipra et al., 1980; Frazier and Cheng, 1989; Agdu et al., 1990; Moran et al.,

1992; White et al., 1997). In regard to soil surveys, remote sensing has received increased emphasis from the 1970s until the present.

The primary objective of this research was to develop methods for classifying the spectral properties of surface soil textures using Landsat Thematic Mapper (TM) images and to investigate the ability of Landsat TM images to classify surface soil textures from an engineering geology view point. Two methods were considered and analyzed; multicategory logistic regression and Support Vector Machines (SVM).

Multispectral Remote Sensing

Multispectral sensors used to measure spectral response of radiation were first developed in the 1960s (Jensen, 1996). Unlike photographic sensors, multispectral sensors form images by the process of scanning. In multispectral data, ground pixels are represented by a set of values that are measurements of spectral response. Each value corresponds to one spectral band. Because of its inherently quantitative property, multispectral data are ideal for analysis using computer techniques. Based on various different methods, statistical pattern recognition is regarded as an effective method for analyzing multispectral data (Swain and Davis, 1978). A pixel with n-band measurements can be classified and considered as a point in a n-dimensional feature space where each feature represents a spectral band. Based on the stochastic or random process approach, the characteristics of classes can be modeled. This approach has been proven to be successful for classifying multispectral data during the past three decades (Hsieh, 1998).

In the stochastic approach, the characteristics of a class are often summarized and parameters of classifier are estimated based on known samples, called training samples. The ratio of the number of training samples as compared to the dimensionality of the feature space has a significant effect on parameter estimation accuracy. When dimensionality increases, the required number of training samples needed to characterize the classes also increases. If not accomplished the classification becomes less accurate (Kuo, 2001). Theoretically, increasing the number of spectral bands (dimensionality) will increase the class separability, but there are a finite, fixed number of training samples and the accuracy of statistical parameter estimation decreases when dimensionality increases. This negative effect dilutes the class separability as dimensionality increases. Consequently, the classification accuracy often increases first and then declines when the number of feature spaces is increased. This is commonly referred to as the Hughes phenomenon (Hughes, 1968).

Landsat Thematic Mapper Images

The Thematic Mapper (TM) is a multispectral scanner onboard Landsat satellites, which are unmanned land surface observation satellite systems of the United States. NASA launched the first satellite ERTS-1 (originally called the Earth Resources Technology Satellite) in the Landsat series on July 23, 1972. On January 22, 1975, the second satellite was launched. Subsequently, NASA renamed ERTS as Landsat. Landsat-3 was launched March 5, 1978; landsat-4 on July 16, 1982, landsat-5 on March 1, 1984 and Landsat-7 on April 15, 1999. Landsat-6 was destroyed after its launch failed on October 5, 1993.

The six Landsats belong to three generations of technology with different satellites, orbital characteristics, and imaging systems. Table 1 shows orbital characteristics of the three generations of Landsat. The multispectral scanner (MSS) was the primary imaging system used in Landsat 1 through 3. Landsat 4 and 5 carried an improved imaging system called the Thematic

Mapper (TM) and the MSS. The imaging system on Landsat 7 is Enhanced Thematic Mapper Plus (ETM+).

TM provided multispectral imagery with a higher spatial, spectral, temporal and radiometric resolution than the MSS (Table 2). TM sensor includes the visible near-IR, mid-IR, and thermal-IR wavelength ranges. The spatial resolution is 30 m for bands 1 to 5 and 7, and 120 m for band 6. Radiometrically, the TM radiometric resolution is 8 bits. Table 3 provides a list of the seven bands of the TM along with a brief summary of the principal applications intended for each band.

Table 1. Orbit pattern and imaging systems for three generations of Landsat.

Feature	Landsat 1, 2, & 3	Landsat 4 & 5	Landsat 7
Altitude	920 km	705 km	705 km
Inclination	99.2°	98.2°	98.2°
Orbits per day	14	14.5	14.5
Number of orbits	251	233	233
Repeat cycle	18 days	16 days	16 days
Image sidelap at equator	14%	7.6%	7.6%
Crosses equator time	9:30 a.m.	9:30 a.m.	10:00 a.m.
Imaging systems:			
MSS	Yes	yes	No
TM	No	Yes	No
ETM+	No	No	Yes

Modified from Sabins (1977) with additional data.

Similar to Landsat 4 and 5, Landsat 7 orbits at an altitude of 705 km. It also has a sun-synchronous 98 degree inclination angle, 10:00 am descending equatorial crossing time and a 16-day repeat cycle. However, instead of Thematic Mapper, Enhanced Thematic Mapper Plus (ETM+) is the imaging system on Landsat 7.

Like TM, the ETM+ is a multispectral scanning radiometer, which provides high-resolution images of the earth's surface. Along with the capabilities of Thematic Mapper, the ETM+ has several new features. Added are a panchromatic band with 15m spatial resolution and a thermal IR channel with 60m spatial resolution. Moreover, it has on board, a full aperture, 5% absolute radiometric calibration.

Because of on board solar calibration and payload correction data for ETM+, ground personnel can correct the data radiometrically to an absolute accuracy of 5% and register a scene geometrically to within 250 meters. ETM+ provides spatial resolution of 15 meters in the panchromatic band, 30 meter in the VNIR and SWIR bands and 60 meters in the LWIR band (Table 4).

Table 2. Characteristics of Landsat imaging systems.

	MSS	TM	ETM+
Spectral region			
Visible and reflected IR	0.5 to 1.10 μm	0.45 to 2.35 μm	0.45 to 2.35 μm
Thermal IR	--	10.4 to 12.5 μm	10.4 to 12.5 μm
Spectral bands	4	7	8
Panchromatic band	--	--	0.52 μm to 0.90 μm
Terrain coverage			
East-west direction	185 km	185 km	183 km
North-south direction	185 km	172 km	170 km
Instantaneous field of view			
Visible and reflected IR	0.087 mrad	0.043 mrad	0.043 mrad
Thermal IR	--	0.17 mrad	0.082 mrad
Ground resolution cell			
Visible and reflected IR	79 by 70 m	30 by 30 m	30 by 30 m
Thermal IR	--	120 by 120 m	60 by 60 m
Panchromatic	--	--	15 by 15 m

Modified from Sabins (1997) with additional data.

Soil Classifications

The distribution of particle sizes in the soil is known as soil gradation, and forms the basis for soil classification. Soil particle sizes occur over a large range, from boulder size (10^3 mm) to extremely fine colloidal materials (10^{-5} mm). Several different soil classifications have been developed by various agencies and professional organizations for their specific applications. The common classifications are shown in Figure 2 (West, 1995).

The Wentworth scale widely used by geologists employs 2 mm as the primary unit and its subdivisions involve the base 2. It is commonly used as a comparison to the engineering and agriculture classifications. The primary textural classes are gravel, 4 to 2 mm; sand, 2 to 0.0625 mm; silt, 0.0625 to 0.0039 mm; and clay < 0.0039 mm.

The AASHTO (American Association of State Highway and Transportation Officials) classification is used mostly for highway studies and construction. Grain size designations are gravel > 2.0 mm; sand, 2.0 to 0.075 mm; silt, 0.075 to 0.005 mm; and clay < 0.005 mm. The U.S. Bureau of Public Roads (BPR) classification predated that of AASHTO as a highway classification. Its primary textural classes are gravel > 2.0 mm; sand, 2.0 to 0.05 mm; silt, 0.05 to 0.005 mm; and clay <0.005 mm.

Table 3. Thematic Mapper Spectral Bands (Sabins, 1997).

Band	Wavelength (µm)	Spectral Locations	Principal Application
1	0.45-0.52	Blue - green	Maximum penetration of water, which is useful for bathymetric mapping in shallow water. Useful for distinguishing soil from vegetation and deciduous from coniferous plants
2	0.52-0.60	Green	Matches green reflectance peak of vegetation, which is useful for assessing plant vigor.
3	0.63-0.69	Red	Matches a chlorophyll absorption band that is important for discriminating vegetation types.
4	0.76-0.90	Near IR	Useful for determining biomass content and for mapping shorelines.
5	1.55-1.75	Mid IR	Indicates moisture content of soil and vegetation. Penetrates thin clouds. Provides good contrast between vegetation types.
6	10.4-12.5	Thermal IR	Nighttime images are useful for thermal mapping and for estimating soil moisture.
7	2.08-2.35	Mid IR	Coincides with an absorption band caused by hydroxyl ions in minerals. Ratios of bands 5 and 7 are used to map hydrothermally altered rocks associated with mineral deposits.

Table 4. ETM+ Bands

Band	Wavelength (µm)	Resolution (m)
1	0.45-0.515	30
2	0.525-0.605	30
3	0.63-0.69	30
4	0.75-0.90	30
5	1.55-1.75	30
6	10.4-12.5	60
7	2.09-2.35	30
8	0.52-0.90	15

The ASTM (American Society for Testing and Materials) classification is a general-purpose soil classification used for numerous construction projects. Its primary textural classes are gravel > 4.75 mm; sand, 4.75 to 0.075 mm; silt, 0.075 to 0.005 mm; and clay < 0.005 mm. The USDA (U.S. Department of Agriculture) classification is widely used by agronomists and soil scientists for agricultural studies. Its primary textural classes are gravel > 2.0 mm; sand, 2.0 to 0.05 mm; silt, 0.05 to 0.002 mm; and clay < 0.002 mm. The boundary between silt and clay is 0.002 mm, which is considerably lower than that used in the Wentworth (0.0039), BPR (0.005) and the ASTM (0.005) classifications. Setting the boundary lower helps to insure that clay size particles are also clay minerals with their increased plasticity. This is because few non-plastic materials such as fine-sized quartz and feldspar grains occur below 0.002 mm (West, 1995). The Unified Soil classification is mostly used in construction projects except for highways, airports, and a few other specialized applications. In this classification, grains size smaller than 0.074 mm are referred to as fines. If the fines are plastic, they are termed clay, if the fines are non plastic they are considered to be silt.

Soils are divided into soil types based on soil texture. This involves the appearance or feel of a soil and is determined by particle size, shape, and gradation (West, 1995). A general texture description is determined by visual inspection but a sieve analysis is needed for detailed description and accurate classification. Once the percentages of sand, silt, and clay present in a given sample are known, charts such as Figure 3 and Figure 4 can be used to determine the soil classification. The primary textural classes are gravel, sand, silt and clay. The term loam is used to designate soils with essentially equal amounts of sand and silt. Sand and gravel are coarse textures, whereas silts and clays are considered as fine-textured soils. Triangular charts are used to describe soil textures; two triangular charts are shown in Figure 3 and Figure 4 for the Bureau of Public Roads and the USDA classifications, respectively.

For the Bureau of Public Roads classification analysis the three constituents sand, silt, and clay are represented. Given a grain size distribution this can be designated as a point on the diagram according to its constituent percentages of sand, silt, and clay. Grain size information is typically classified according to the Bureau of Public Roads diagram for highway studies. In Figure 4 the USDA classification grain sizes are sand, 2 to 0.05 mm; silt, 0.05 to 0.002 m; and clay < 0.002 mm. Because of the differences in the boundaries for the two classifications (Figures 3 & 4) a grain size distribution will plot at different locations on the two diagrams and may even result in having a different soil designation.

Conclusions

Remote sensing provides a convenient method to survey the distribution of surface soil textures. In this study, Landsat Thematic Mapper (TM) data were used to classify primary soil textures for Carroll County, Indiana. Landsat 7 TM data from March 25, 2000 were used in the study.

Three primary soil textures occur in Carroll County; loam, silt loam, and silty clay loam. These three soil textures account for about 90% of the entire county. Therefore, this study focused on how to classify these three soil textures. Figure 5 is a digitized map of soil textures in Carroll county based on NRCS data.

Two different classification methods were developed and analyzed: one using multicategory logistic regression models, and the other using Support Vector Machines (SVMs). Two kinds of SVMS were included, polynomial SVMs and Radial Basis Function (RBF) SVMs. They were all constructed based on selected training fields. A 5x3 mile (8x4.8 kilometer) area was selected in

the northern part of the county to train and evaluate the models. The Maximum Likelihood method was also used to obtain a classification for comparison purposes.

Feature space and sampling size were analyzed regarding their effect on classifier performance. A pixel with n-band measurements can be considered as a point in a n-dimensional feature space. Feature space showed a significant effect on the results of classifiers. Four best features of Landsat TM data were able to provide equal classification results as when all the TM bands were employed. Figure 6 is a soil texture map of the county based on Landsat TM bands 1, 5, 6 and 7. This map is similar to the one obtained when all eight bands are used.

Sampling size has a significant effect on multicategory logistic regression model classifiers and RBF SVMs classifiers. When more features are involved in the classification, a larger sample size is needed to obtain good results. By contrast, polynomial SVMs classifiers show no significant difference based on different sample size.

Both multicategory logistic regression models and SVMs classifiers showed good results in the soil texture classification. They provided an average testing accuracy of approximately 80%. Landat TM data also showed good capability in soil texture mapping. The best-fit classifiers were selected during the study and best-fit logistic regression models were applied to the whole county to obtain primary soil textures distribution maps. When compared with the Engineering Soils Map of Carroll County (1966), these generated maps confirm the general information of the 1966 map.

From the above summary, the following conclusions are reached:

1. Multicategory Logistic Regression Models and Support Vector Machines (SVMs) based on Landsat TM data show high potential for soil texture classification.

2. The best combination of four TM bands, can provide classification results that are as good as when all TM bands are used. The best combination is TM bands is 1, 5, 6, and 7.

3. Best multicategory logistic regression classifiers were obtained. TM bands 5, 6, and 7 occur in every model which indicates that these three bands are most important in classifying soil textures. This confirms the summary of Sabins (1977) in Table 3 that these TM bands are the soil-related bands. The fourth common band used in the models is band 1. This also confirms that TM band 1 is helpful in distinguishing soils (Sabins, 1997).

4. Three factors control the construction of Polynomial SVMs. They are polynomial dimension d, number of features, and sample size. The polynomial SVMs might not be generated if dimension d increases, number of features decreases, or sample size increases.

5. Polynomial SVMs with dimension d = 1 or d = 2 provide good classification results for soil textures.

6. γ is the controlling parameter of RBF SVMs. γ is generally less than 1. When γ decreases, the performance of RBF SVMs classifiers improves.

7. Feature space and sample size both affect the γ value at which the performance of RBF SVMs become stable. When feature space becomes smaller, the RBF SVMs reach stable performance at a larger γ value. When sample size becomes smaller, the RBF SVMs become stable at a smaller γ.

8. The best RBF SVM is accomplished with $\gamma = 0.003$ which includes all 8 TM bands.

9. Sample set size is crucial to the multicategory logistic regression models and RBF SVMs. Generally, a larger sample size is preferred in order to obtain better classification results.

10. Polynomial SVMs are not sensitive to sample size.

11. The soil texture classification maps using multicategory logistic regression models comply with the general details of the Engineering Soils Map of Carroll County (1966).

12. Presence of the end moraine shown on the Engineering Soils Map of Carroll County (1966) can not be verified in the TM data or on a recently published map by Indiana Geological Survey (2000).

STUDY TWO, HIGHWAY RELOCATION STUDY

In the second remote sensing study (Sui, 2003), the area of interest included Carroll County as well as the adjacent Tippecanoe County. Several highways cross the two county area: US52, US231, SR25 and SR43. The Wabash River along with its tributaries comprise the major drainage system.

Tippecanoe County has a land area of 322,000 acres or 503 square miles extending 24 miles north-south and 21 miles from east-west. Lafayette, the county seat, is located near the center of the county. The population of Tippecanoe County is about 152,000 (circa 2002) (Indiana Business Research Center, 2002).

About 81 percent of the county is in farmland and grains are the principal crops (corn and soybeans). Hogs, beef cattle, sheep, and a few dairy cattle are raised in the county, which also has a few vegetable farms. Because of urban and industrial development, the farmland acreage continues to decrease (NCSS, 1998).

Tippecanoe County is mainly a flat till plain dissected by the Wabash River and numerous other rivers, creeks, streams and ditches. Glaciation was the principal agent affecting the present landforms. The area was completely covered by ice during the Wisconsin glacial stage. As the ice receded to the north, melt-waters flowed across the county and formed terraces and outwash plains along the Wabash River and its tributaries.

The underlying bedrock in the western part of the county is Mississippian age siltstone and shale, and that in the northeastern part of the county is the New Albany Shale of Devonian age. Bedrock is exposed in many locations along Flint Creek in the western part of Tippecanoe County and along the Wabash River in its northeastern part.

The greatest relief in the county occurs along the Wabash River and its tributaries, and along the breaks between the uplands and the terraces and flood plains. The highest elevation, about 843 feet MSL is in the southeastern part of the county. The lowest elevation, about 473 feet MSL occurs at the point where the Wabash River leaves the county on its western edge.

The Wabash River cuts diagonally across the northern half of the county from the northeast to southwest. This river and its tributaries drain the entire county. Valleys ranging from 0.5 to 5 miles in width border the Wabash River. The valleys associated with its major tributaries range from about 50 feet to 0.5 miles in width. Bottomland areas near the mouth of these tributaries are commonly flooded several times in late winter and early spring (NCSS, 1998).

In 1987 the Indiana Department of Transportation (INDOT) began a feasibility study for a multi-lane highway, SR25 from Lafayette to Logansport. In 1995, the highway was approved and funded by Congress (INDOT, State Road 25 study).

In November 2001, INDOT prepared a Draft Environmental Impact Statement which was approved in August 2002. Four alternatives were provided for the new SR25. The purpose of the current study was to evaluate the four alternatives proposed by INDOT, considering the soil engineering properties, topography, and groundwater conditions in the area.

It is generally accepted in pavement design studies that subgrade soils with a high plasticity yield more highway durability problems than do low plasticity soils (Yoder and Witceak, 1975). The absolute elevation is not a major consideration in an area like northern Indiana, but the slope of the terrain is a concern. Greater slope changes require more cuts and fills. For the current SR25, undulation is great because of the rolling topography and the highway has limited sight distance. In the new SR 25 study, attention will be considered to slopes along the road. In this study area, the portion with groundwater depths less than 6.1 m (20 feet) comprise about 24 percent of the right of way. In keeping with the discussion above three parameters soil type, topography and groundwater conditions were considered in the selection process for the right of way location.

Soil Engineering Property Evaluation

The USDA (United States Department of Agriculture) soil map, and remote-sensing image (Thematic Mapper Data, March 25, 2000) were used to study the soil engineering properties. Remote Sensing study results were compared to the USDA soils map. If similar results were obtained for both, remote sensing could be used to extend mapping capabilities to locations where soil maps are not available.

The SSURGO (Soil Survey Geographic) database provides the most detailed information of soil, and it includes soil plasticity index values. In this study, the four alternative routes proposed for the new SR25 were digitized. To obtain the soil plasticity index of the soil for the four alternatives, the SSURGO detail soil map was clipped along the four digitized alternatives.

Using the SSURGO detailed soil map data, average soil plasticity index values were obtained for the four alternatives. The average for alternative one was 8.7; for alternative two, 8.7; for alternative three 9.0; and for alternative four, 9.1. The alternatives with the lowest plasticity index average were numbers one and two. The paired samples, provided t tests for comparison, which showed that alternatives one and two versus alternatives three and four were statistically significant (at alpha level of 0.05). This indicates that alternatives one and two are the best for highway construction based on soil plasticity and are therefore preferred over alternatives three and four.

Remote Sensing Image Analysis

The State Soil Geographic (STATSGO) database is a generalized soil survey map based on SSURGO. Since it is more general, it can be used to evaluate the results of remote sensing image classification at the first accuracy level. In STATSGO, each soil class is provided with the percentage of the hydrologic soil groups. In this study a new parameter $R = \dfrac{2A + B}{2D + C}$ was defined where A is sandy, free draining soil, D is clayey, poor draining soil and B and C are intermediate soil groups. The values for A and D were doubled to accentuate the difference between clay and sand. Based on the R values obtained, the soils in Tippecanoe and Carroll Counties were divided into six classes. Using this classification for Carroll County, training samples of the remote sensing image were collected. Supervised classification was accomplished using Erdas Imagine 8.5

A preliminary analysis was implemented for the classifications. The supervised classification provides a general idea of the soil distribution for the study area. However, the results did not match closely those of STATSGO (Fig. 7). Hence, further study based on this classification method was not justified and no additional work on this subject was conducted.

Digital Elevation Data Analysis

The topography study was based on the National Elevation Dataset, seamless 30-meter Digital Elevation Model (DEM) data for this area. Slope values are derived from the DEM. Results are consistent with the flat, planar nature of the study area. The area with slopes greater than 10 degrees equals 1.3%, areas with slopes from 5 to 10 degrees is 6.4% and the remaining 92.3% is less than 5 degrees.

In some cases the four alternatives proposed by INDOT overlapped and in other cases they remained separate. Separate sections of the alternatives were digitized to provide detailed information and the four alternatives have eight separate sections. After slope values were obtained, areas were clipped based on the eight separate sections. The results are summarized in Table 5.

Table 5. Slope Value Distributions for Individual Sections

Section No.	Number of Pixels	Average Slope (in degrees)
Section 1-1	443	0.43
Section 1-2	441	0.44
Section 2-1	183	1.00
Section 2-2	209	0.64
Section 3-1	110	2.04
Section 3-2	95	2.97
Section 4-1	2197	0.96
Section 4-2	2146	0.66

Alternative one consisting of Section 1-1, Section 2-1, Section 3-1 and Section 4-1 was evaluated. For Section 1-1, the average slope value is 0.43 and the count is 443; for Section 2-1, the average slope value is 1.03 and the count is 183, for Section 3-1, the average slope value is 2.04 and the count is 110; and for Section 4-1, the average slope value is 0.96 and the count number is 2197. In summary, the average slope value for alternative one including its separate sections is

$$\frac{0.43*443 + 1.03*183 + 2.04*110 + 0.96*2197}{443 + 183 + 110 + 2197}, \; = 0.93.$$ In the same way, the average slope

value for alternative two equals 0.93, alternative three is 0.70, and alternative four is 0.70. This shows that alternatives three and four are preferred over alternatives one and two because they consist of less steep slopes.

Groundwater Study

In this study, groundwater depth was determined based on the iLITH database which is obtained from a 1999 version of IDNR (Indiana Department of Natural Resources) water-well record database. Depths to the water level in well logs were interpolated. The smallest groundwater depth for the area is 0 feet, whereas the largest depth is 200 feet (61 m), shown in Figure 8.

The area of interest was defined as four 1000 meters wide polygons centered along each alternative and the polygons were merged together. The interpolated groundwater parameter theme was extracted from merged polygons to provide the groundwater information for the area of interest. For the area around the alternative routes, the greatest groundwater depth occurs in the west-southern part of the area of the four alternatives. The area with the smallest groundwater depth is found in the middle and northeastern part for the four alternatives. The greatest groundwater depth is 130 feet, and the smallest is 1 foot. Normally in highway construction, the top 1-2 feet (0.3-0.6 m) of top soil are stripped off and stockpiled for final dressing of the slopes. If in this process the groundwater table is intercepted a drainage system may be needed below the pavement, which will increase construction costs. During the highway construction, there is a concern for the portion where the groundwater depth is found only two feet or less below the surface.

Conclusions

The SSURGO database was used to obtain value for the plasticity index of the soil. The four alternate highway locations were evaluated. Based on results alternate one and two were favored versus alternates three and four.

The STATSGO digitized soil data set was used to prepare a classification of the study area based on remote sensing image. Soil categories were based on sandy soil, clayey soil and two intermediate varieties. The results did not match well with the STATSGO soils map so this endeavor was not studied further.

The digital elevation data were used to generate slope values for the four alternates. Alternates three and four were preferred over one and two because of reduced slope value.

Groundwater depth for the four alternatives was developed from the iLITH database from IDNR. Areas with the shallowest groundwater depth (less than one foot) were located there, presumably being the points where greater construction complications would occur.

REFERENCES CITED

Agdu, P.A., Fehrenbacher, J.D. and Jansen, I., 1990, Soil property relationships with SPO satellite digital data in east central Illinois, Soil Science Society of American Journal 54, 808-812.

Cipra, J.E., Franzmeir, D.P., Bauer, M.E. and Boyd, R.K., 1980, Comparison of multispectral measurements from some nonvegetated soils using Landsat digital data and a spectroradiometer, Soil Science Society of America Journal 44, 80-84.

Condit, H.R., 1970, Application of characteristic vector analysis to the spectral energy distribution of daylight and the spectral reflectance of American soils, Applied Optics 11, 74-86.

Frazier, B.E. and Cheng, Y., 1989, Remote sensing of soils in the eastern palouse region with Landsat Thematic Mapper, Remote Sensing of Environment 28, 317-325.

Hughes, G., 1968, On the mean accuracy of statistical pattern recognizers, IEEE Transactions on Information Theory IT-14, No.1, 55-63.

Indiana Geological Survey, 2000, Map of Indiana showing physiographic divisions.

Indiana Geological Survey, A GIS Atlas for Indiana, http://igs.indiana.edu/arcims/southwest/metadata/Indust_Minerals_pts_sw.html.

INDOT, State Road 25 Study, http://www.sr25study.com, verified on 6 December 2003.

Indiana Business Research Center, 2002, Tippecanoe County IN Depth Profile, http://www.stats.indiana.edu/profiles/pr18157.html, verified on 6 December 2003.

Jensen, J.R., 1996, Introductory digital image processing: a remote sensing perspective, 2 edn, Prentice-Hall, Upper Saddle River, N J.

Kuo, B.-C., 2001, Improved Statistics Estimation and Feature Extraction for Hyperspectral Data Classification, PhD thesis, Purdue University, West Lafayette, IN.

Lui, H., 2004, Soil Texture Classification Using Landsat TM Data, M.S. thesis, Purdue University, West Lafayette, IN.

Moran, S.M., Jackson, R.D., Slater, P.N. and Teillet, P.M., 1992, Evaluation of simplified procedures for retrieval of land surface reflectance factors from satellite sensor output, Remote Sensing of Environment 41, 169-184.

National Cooperative Soil Survey (NCSS), 1998, Soil Survey of Tippecanoe County, Indiana

Natural Resources Conservation Service (NRCS), 2001, Indiana aerial photographs. Data available at http://danpatch.ecn.purdue.edu/~caagis/ftp/gisdata/data.html.

Purdue University Joint Highway Research Project (PUJHRP), 1966, Engineering soils map of Carroll County, Indiana.

Sabins, F.F., 1997, Remote Sensing: principles and interpretation, 3 edn, W.H. Freeman and Company, New York.

Spangler, M.G., 1960, Highway Engineering Handbook, McGraw-Hill, New York, chapter 8.

Sui, Y., 2003, Engineering Geology and Remote Sensing Study Along Proposed Highway Location, SR25, Tippecanoe and Carroll Counties, Indiana, M.S. thesis, Purdue University, West Lafayette, IN.

Swain, P.H. and Davis, S.M., 1978, Remote Sensing: The Quantitative Approach, McGraw-Hill, New York.

USDA (U.S. Department of Agriculture), 1987, Soil survey of Carroll County, Indiana.

USGS, Soil Survey Geographic (SSURGO) Data Base, Data use Information http://tahoe.usgs.gov/files/ssurgo_database.pdf, verified on 6 December 2003.

USGS, GeoData Digital Raster Graphics, http://mac.usgs.gov/mac/isb/pubs/factsheets/fs08801.html, verified on 6 August 2003.

West, T.R., 1995, Geology Applied to Engineering, Prentice hall, Englewood Cliffs, New Jersey.

White, K., Walden, J., Drake, N., Eckardt, F. and Settle, J., 1997, Mapping the iron oxides content of dune sands, Namib Sand Sea, Namibia, using Landsat Thematic Mapper data, Remote Sensing of Environment 62, 30-39.

Yoder, E.J. and Witceak, M.W., 1975, Principles of Pavement Design, Second Edition, John Wiley & Sons, Inc.

CASE HISTORY OF THE SOUTH STREET SINKHOLE

FREDERICK, MARYLAND

By

A. David Martin

Chief, Engineering Geology Division

Maryland State Highway Administration

(410) 321-3107

dmartin@sha.state.md.us

ABSTRACT

During the early morning hours of September 23, 2003, a sinkhole opened in an area
that was adjacent to the eastbound lanes of I-70 in Frederick, Maryland. The sink was
110' long, 30-50'wide and 35' deep at the throat. The sink was located near a bridge that carried
the interstate over a city street, and a passenger railroad line. Part of the toe of the
interstate's approach embankment was undermined. Traffic on all three transportation facilities
was suspended during the rush hour while the sink was given a preliminary evaluation.

In order to restore service as quickly as possible, the sink was immediately backfilled
with crushed stone. To fill this sink, 2700 cubic yards of crushed rock were required, followed
by over 2000 cubic yards of low mobility grout that was pumped under the rock fill. A redesign
of the drainage for the highway, the railroad, and the city street was initiated.

INTRODUCTION

During the early morning hours of September 22, 2003, a sinkhole opened in the interchange for I-70 and South Street in Frederick, Maryland. The sink was 110' long, 30'-55' wide, and 35' deep at the throat. The initial backfill required 2700 cubic yards of quarry waste. The oval opening of the sink lay along the south facing bridge approach embankment for I-70 as it passes over South Street and a commuter railroad. The toe of the embankment was slightly undercut, and the eastbound lanes of the interstate were closed for a short period while the impact was evaluated. The railroad line was closed for a day, and South Street was closed for a week.

LOCATION

The subject area is just east of the City of Frederick, Maryland, in the southeast quadrant of the interchange for South Street and I-70. The interchange consists of dual spans of I-70 over South Street and a commuter railroad. The on and off ramps for eastbound I-70 are located in the southeast quadrant of the interchange. The on and off ramps for westbound I-70 are both located in the northeast quadrant. Figure I shows the locations of the features.

Figure I

GEOLOGIC SETTING

Frederick is located in the Piedmont Province of Maryland. The three physiographic provinces of the State of Maryland are the Coastal Plain, the Piedmont, and the Appalachian. The Piedmont Province covers most of central Maryland and is divided into an eastern and a western division. The eastern division is underlain by Precambrian high grade metamorphic formations, while the western division is underlain by low grade metamorphics, and Cambrian and Ordovician Limestones. The limestones are well folded and fractured and karst features abound. In the subject area, residual soils are sandy.

The sinkhole of this report is located near the axis of a double plunging syncline that is overturned to the west. The general strike of the folded formations is to the northeast. The saddle of the double plunging syncline is just to the northwest of the area of the subject sinkhole. A limestone quarry is operated to the southwest. A large northeast striking fault, is located about 100' east of the on ramp from South Street to eastbound I-70. This area is currently the most active karst area in the State of Maryland. Figure II shows the geology of the area. Mapped sinks are identified on the figure.
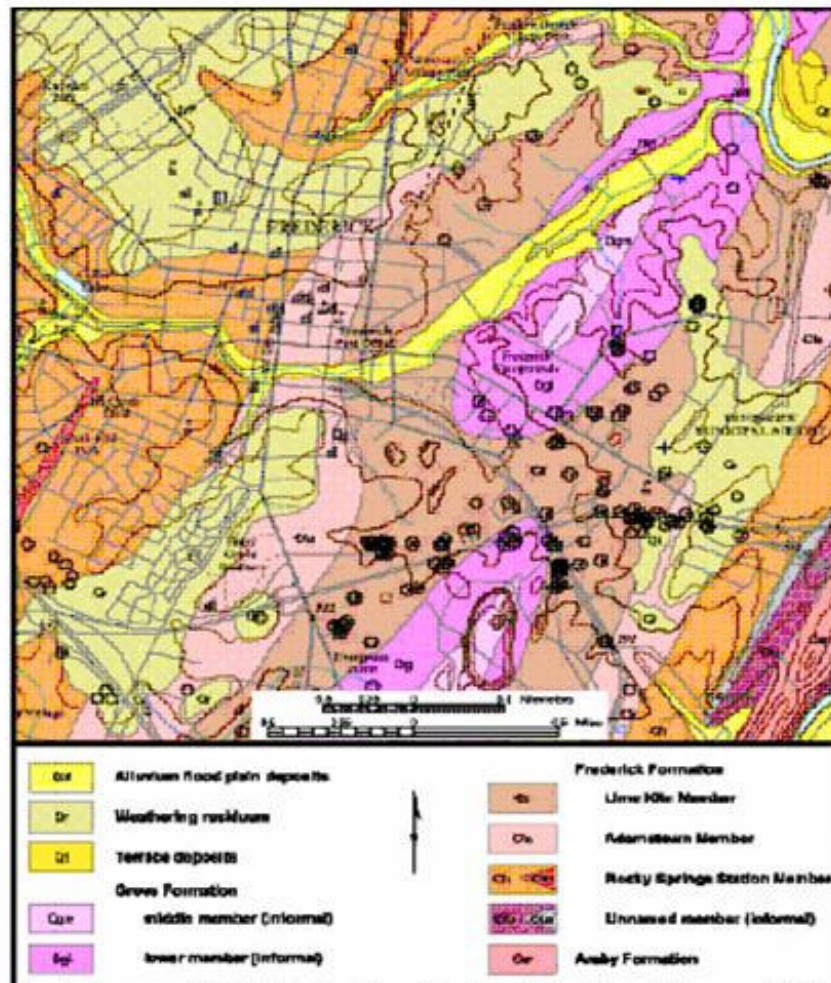
Geologic map with sinkhole locations (circles with hachures) for a part of the Frederick 7.5-minute quadrangle

Figure II by Brezinski

HISTORY

The City of Frederick was founded in 1745. It grew as a transportation hub for agricultural products from Central Maryland. Its location, which is just east of Blue Ridge, placed it on a colonial north-south traffic corridor, as well as an east-west corridor connecting Baltimore with Hagerstown and Cumberland. In 1760, a road connecting Frederick and Baltimore was completed. This road was eventually extended to Cumberland, Maryland through the use of several toll road segments. It became known as the Baltimore National Pike.

In 1806, Congress passed legislation that initiated the National Road to provide a connection for Wheeling to Cumberland, Maryland. This road, along with the existing toll roads between Cumberland and Baltimore made the Port of Baltimore available to handle trade to and from the Ohio River Valley. The National Road and the Baltimore National Pike ultimately became US 40 which was the main street for the City of Frederick. The interstate program provided I-70 to supersede US 40. I-70 passes Frederick on the south side and also acts as a bypass. I-270 was built to connect Washington DC with Frederick and I-70. The interchange for I-70 and I-270 is southwest of the City.

Frederick has grown to be the second largest metropolitan area in Maryland after Baltimore. Positioned 40 miles northwest of Washington, DC, it has become a home for many commuters who work in that city.

SINKHOLE HISTORY OF THE AREA

This area is within the zone of influence of the quarry noted above. The elevation of the quarry floor is currently at sea level (0) while the elevation of the rim ranges from 275' to 300' above sea level. The railroad line that parallels South Street has a history of almost constant sink activity up until it was grouted in 1999, as part of a track improvement program to make it suitable for commuter trains. No sinks have been experienced in the track area since that time. Figure III shows sinks that have been mapped since 1985. Those shown in red have occurred since 2000.

Figure III

HIGHWAY DRAINAGE SYSTEM

Surface drainage for much of Frederick City is to Carroll Creek which flows easterly through the City and empties into the southward flowing Monocacy River to the east of the City. The Monocacy joins the Potomac which flows to the Chesapeake Bay.

The construction of I-70 around Frederick City took place in the late 1950s and early 1960s. At that time, the drainage design philosophy was to replicate the existing surface drainage patterns as closely as possible and little or no thought was given to water quality and quantity management. Sediment and erosion practices were non-existent.

In the subject area, a well defined natural surface drainage system does not exist. Surface water leaves this area by infiltration or by dropping into sinkholes. At the time of I-70's construction, the use of existing sinkholes for drainage was a common, but not recommended practice.

The original drainage system of the interchange and surrounding area utilized a sinkhole located about 300' north of the interchange in the northeast quadrant. Drainage from the south of the interchange was collected within the southeast loop and piped north, under the interstate, to a swale that was piped under Monocacy Boulevard, a parallel city street to the sinkhole. Drainage from the northeast quadrant was piped east, under South Street, to join the northward moving water as it entered the pipe under Monocacy Boulevard

Since the completion of I-70, the receiving sinkhole was partially backfilled by adjacent property owners who were attempting to develop the area. Also, the City undertook several subsurface grouting operations in order to maintain the stability of Monocacy Boulevard. These activities resulted in a reduction in the sink's capacity to receive storm water, so that during heavy rain events, ponding occurs in the northeast quadrant of the interchange. This ponding often backs up through the pipe that is under I-70, to make additional ponding in the southeast quadrant. The infiltration of this water through the sandy residual soils can be rapid, and once a solution channel is found in the rock, it can quickly be exploited into a sinkhole. The subject sinkhole is the prime example of this process. (Figure IV) Of particular concern is the ponding that occurs on the north side of I-70 between the interstate and Monocacy Boulevard. Since the zone of influence of the quarry creates a steep ground water gradient to the southwest, it is felt that any sink that forms in that area will pass under the embankment for the interstate as it attempts to migrate towards the quarry.
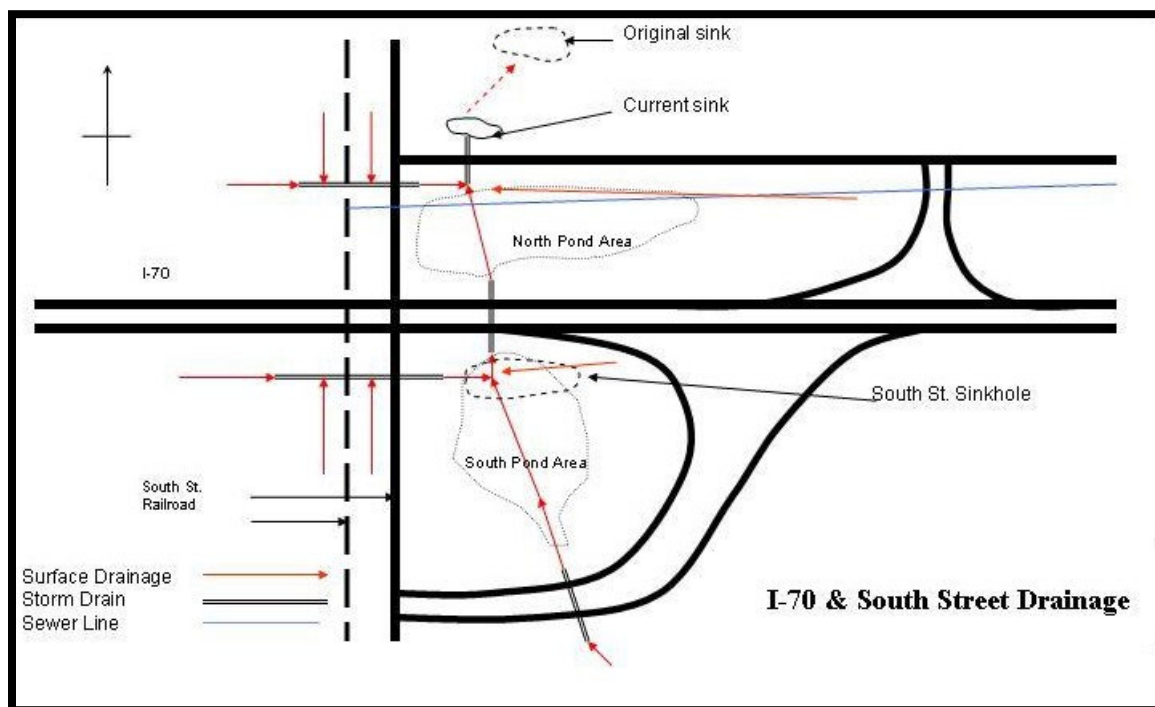
Figure IV

When built, the average daily traffic count for I-70 in this area was about 10,000. Today, it is over 70,000. I-70 is no longer able to handle the traffic volumes imposed upon it, so plans are under way to upgrade the interchanges and add lanes. With these improvements, modern storm water management is required. Since the utilization of sinkholes as recipients of highway runoff is not acceptable to either SHA, or the regulating agencies, the storm water for these projects is to be collected in lined ponds and pumped to Carroll Creek to the north of the project.

The Maryland State Highway Administration (SHA) has standard design elements that are applied to all of its projects in karst areas. These elements provide for all storm water and drainage facilities to be lined, and all pipes to be backfilled with flowable backfill. Existing

sinkholes are excavated and backfilled with large stone and/or Portland cement concrete. Repaired sinks that are under the pavement also are covered with a reinforced concrete slab. Subsurface pressure grouting with low mobility grout is employed for areas of potential sink activity. In extremely sensitive areas, instrumentation and reinforced pavements are used.

Figure V shows the planned improvements for I-70.
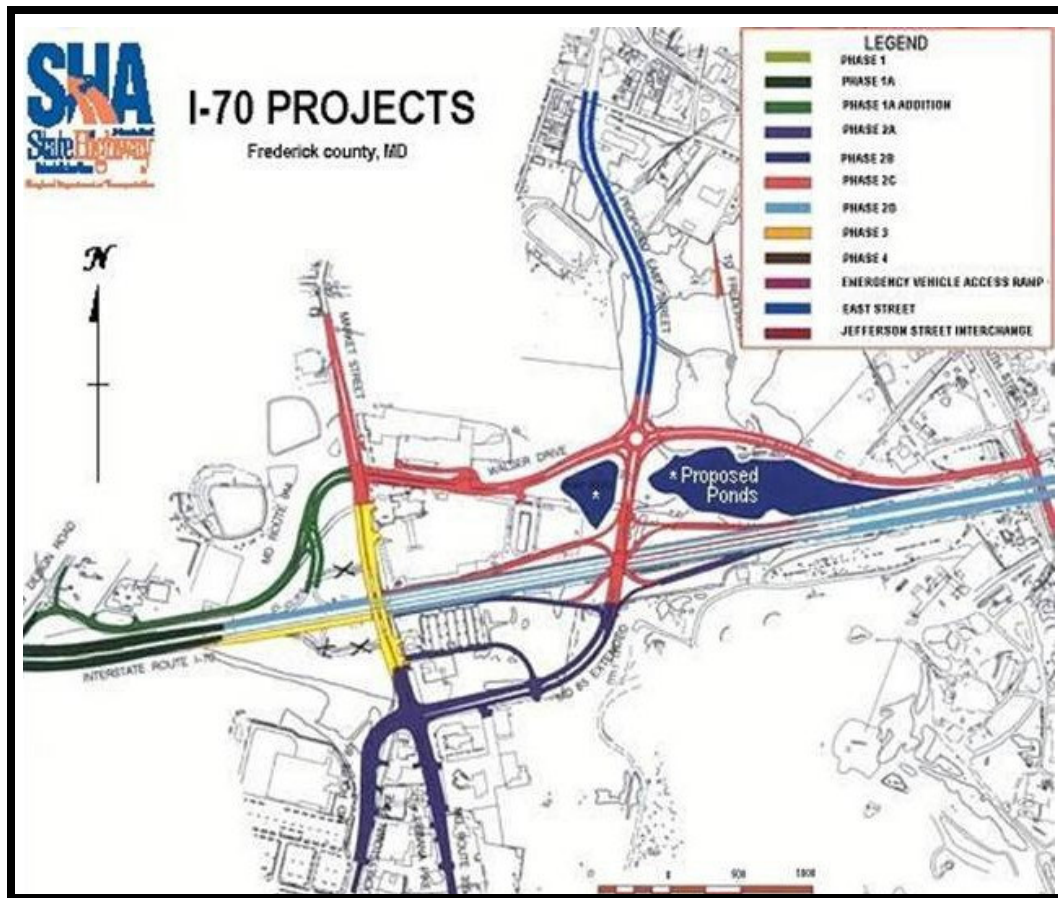
Figure V

FORMATION OF THE SOUTH STREET SINKHOLE

In Maryland, 2003 was the year of highest annual precipitation on record. Annual precipitation was 62.5" which is about 50% higher than the normal 41". This extremely moist year followed a two year period of drought where precipitation averaged about 20". In early September, Hurricane Isabel swept through this area and dropped about 2 ½" of rain. This was followed by a 5" rain about a week later. It appears that when these heavy precipitation events reach a rate of one inch per hour, the capacity of the receiving sinkhole is exceeded and ponding occurs. Infiltration through the sandy soils is relatively rapid, and when a solution feature is encountered, erosion of the overburden is prompt and swift. The South Street sink occurred in this fashion.

The cover collapse sink opened and rapidly grew to the dimensions of 110' long, 30'50' wide and 35' deep at the throat.

Rock was visible in the throat. The log of a nearby monitoring well (Figure VI) shows the response of the local water table to the massive infiltration.
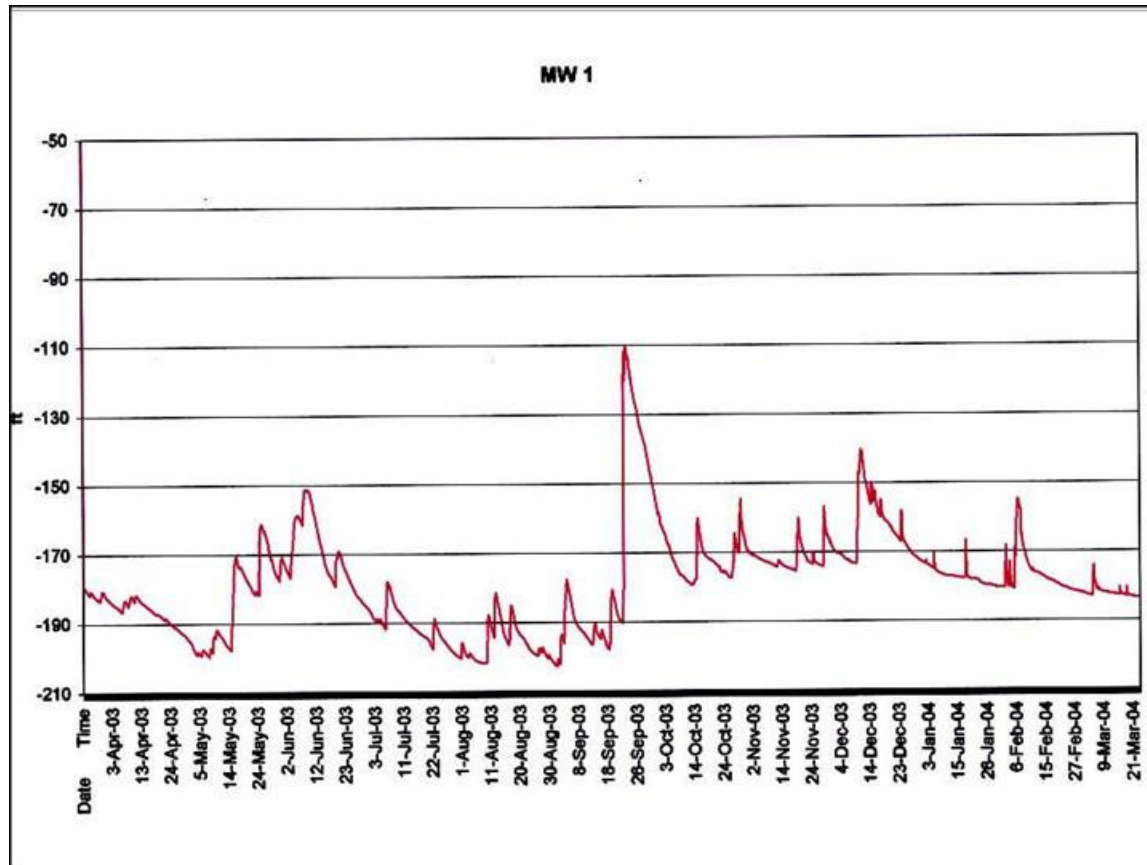
Figure VI - Monitoring Well Log

RESPONSE TO THE FORMATION OF THE SINKHOLE

The perimeter of the open hole was unstable and presented a threat to the stability of I-70 as well as to any efforts to work its vicinity. SHA decided to backfill the hole as soon as it was determined that the underground utilities (fiber optics) that were damaged by it could be abandoned. Quarry waste from the nearby quarry was dumped adjacent to the sink and pushed in with a dozer. This operation utilized 2700 cubic yards of the unsorted shot rock. Since it was not practical to remove the soil and expose a rock bottom, there was an undetermined amount of disturbed soil left under the backfill. SHA planned to pressure grout with low mobility grout at the top of rock.

The grouting operation commenced shortly after the backfill. Sixty-nine holes were drilled in a 15' by 15' grid, each hole drilled into 5' of rock. The final pattern consisted of five lines of holes

parallel to I-70, and one line of holes parallel to South Street. Depth to rock ranged from 20' to 100'. No groundwater was encountered. A total of 2045 cubic yards of grout was used. Grout takes per hole ranged from less than one cubic yard to 113 cubic yards. Fifteen of the holes took more than 50 cubic yards and 23 holes took more than 25 cubic yards of grout. The grouted zone is shown in Figure VII.
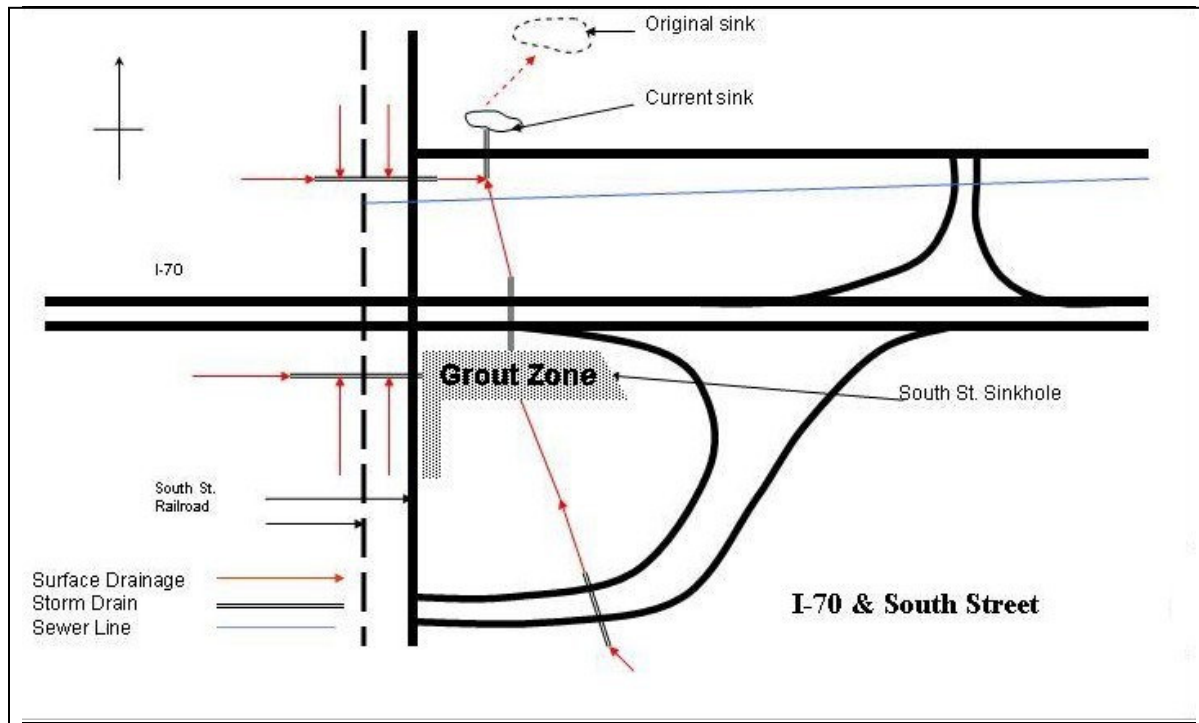
Figure VII

FUTURE OF THE HIGHWAY DRAINAGE SYSTEM

SHA recognizes that while backfilling and grouting provide immediate relief from the symptoms of the problem, the potential for more sinks will continue to exist until comprehensive measures to control the drainage in the area are implemented. Major storm events that have occurred after the grouting operation was completed have caused ponding in the sinkhole area. To date, no new sinks have appeared in the grouted zone. Should new sinks form beyond the perimeter of the grouted area, SHA will allow them to remain.

The ultimate plan for the area is to construct a lined pond, emptied by a pumping station that pipes the drainage directly into Carroll Creek. Since funding for that project has not been obtained, SHA is attempting to change the scope of nearby funded projects to include this pumping station and pond. Should that effort fail, SHA is looking at interim plans that provide for the use of injection wells to relieve the ponding problems. The injection wells may take the form of enhancing the present receiving sinkhole, or drilling a new well. The regulatory agency that needs to be satisfied in order to obtain a permit for the use of an injection well is the Maryland Department of the Environment (MDE). MDE's interpretation of the regulations is

that the highway drainage would have to meet drinking water standards before it would be permitted to be placed in an injection well. Needless to say, meeting drinking water standards would be impossible. Negotiations are under way. In the mean time, every storm is followed by an intensive inspection.

REFERENCES

Brezinski, David K., 2004, Stratigraphy of the Frederick Valley and its Relationship to Karst Development. Maryland Geological Survey

Vokes, Harold E., 1957, Geography and Geology of Maryland. Maryland Geological Survey

State Roads Commission, 1930, Report of the State Roads Commission of Maryland for the years 1927, 1928, 1929 and 1930

PHOTOGRAPHS

View of sink looking to the east. I-70 embankment on left.

View of sink looking to the west. Commuter rail line is just beyond the guard rail.

View of north pond area during heavy storm event. Gray water is due to quarry dust.

View of south pond area during heavy storm event. Note that the grouting has arrested the development of sinks for the time being.

View of receiving sinkhole during storm event.

THE EXPECTATIONS AND REALITIES OF
GEOPHYSICAL INVESTIGATIONS IN KARST

By
Joseph A. Fischer, Geoscience Services, Donald L. Jagel, Advanced Geophysical Services,
Joseph J. Fischer, Geoscience Services, and Richard S. Ottoson, Geoscience Services

ABSTRACT

Geophysical techniques have been utilized to characterize karst terranes for many years with mixed success. Although geophysical techniques have become increasingly sophisticated and are better able to resolve subtle subsurface features, the complexity of karst has continued to be extremely difficult to characterize and image consistently with the resolution desired by the engineering geologist/geotechnical engineer. Although the geophysicist may well feel that the resolution and interpretation are detailed, the results are often interpreted by the ultimate user as being vague, inconclusive, and sometimes unrealistic.

To increase the rate of success of a geophysical investigation in karst terrane, both the geophysicist and the engineer/geologist need to share an understanding of the type of subsurface karst features to be expected, the materials overlying the bedrock, local geologic structure, bedrock weathering patterns, and realistic expectations with regards to the resolvability of a specific size and type of feature within a given depth zone.

For this paper, the authors have simplistically divided solutioned carbonate rocks into three types: the semi-consolidated, lightly cemented corals of Florida and the Caribbean; the hard, flat-lying, well-consolidated limestones and dolomites found, for example, overlying the Inner Craton of the central United States; and the similarly hard, often tectonized carbonates of the valleys within the Valley and Ridge provinces of the eastern and western United States.

With cooperation and understanding throughout the geophysical investigation program's design, field data acquisition, interpretation of the results, and coordination of the results with a geotechnical investigation, it is possible to utilize the overall product in a useful subsurface evaluation. As discussed herein, geophysics cannot be used indiscriminately in all karst environments. Neither should the user or interpreter presume the available geophysical resolution for flat-lying, soft-rock carbonates is the same for a contorted Valley and Ridge karst site. Consideration of the hard data in the interpretation of the geophysical data is a necessity.

INTRODUCTION

The term karst is used in many ways throughout the world to describe a variety of landscapes. In as much as the term is synonymous with a region of Slovenia named Karst where pinnacled limestone spectacularly protrudes above the ground surface, the authors tend to think of karst as looking like Figure 1.

The term "karst" in the United States is applied somewhat broadly to terranes underlain by three basic types of subsurface materials. These are; a) geologically recent (Tertiary) coral-derived sediments, b) older (Paleozoic-Mesozoic) limestones and dolomites, both flat-lying and folded, and c) metamorphosed carbonates (marble). To effectively characterize the karst subsurface, one must understand the possible differences in material properties, solution potential and likely failure mode(s) in relation to proposed site use. Site exploration may be performed with conventional geotechnical and geophysical tools and procedures, but the investigation techniques, planning and interpretation require strong geologic input.

Figure 1: Chinese karst.

To complicate the situation, former flat-lying sediments have often been tilted by tectonic action during folding and cut by faults. In the authors' experience, faults and fractures usually provide a preferred path for the movement of acidic ground water, and apparently stressed and sheared zones are more susceptible to solutioning and weathering. A route or site generally lies across many beds with varying physical properties. In the more northerly areas of the country, the effects of glaciation further complicate this geologic picture from both an interpretation and design standpoint.

Simplistically, when working in the recent, often clastic "karst" of Florida and the Caribbean, one must be aware of not only the relatively low strength of the weakly cemented "limerock", but also the often low density and high porosity of the overlying sands, be they aeolian, marine or residual. Large cavities can be found in the limerock and both raveling and cover collapse sinkholes can be found (see Figures 2A and 2B).

Figure 2: Raveling sinkhole (A) and cover/cave collapse sinkholes (B) in flat-lying carbonates.

In dealing with the older Paleozoic-aged crystalline carbonates, different types of problems are found. For example, the relatively flat-lying rocks of the Central United States, perhaps best exemplified by the numerous studies of the Mammoth Cave, Kentucky area, generally fail from cave roof collapse (see Figure 2B) with often extensive and large secondary porosity features. Often, superimposed upon the strata are erosional or depositional features.
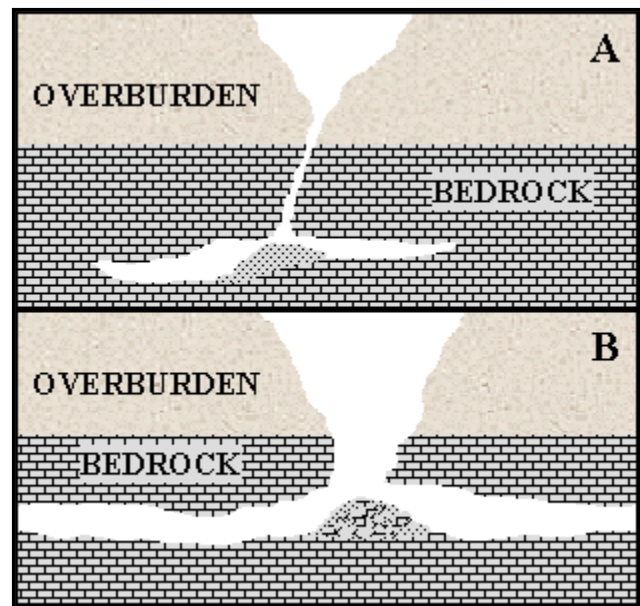
The folded and faulted Paleozoic carbonates found within the valleys of the Appalachian Mountain chain of the eastern United States (typical of Paleozoic carbonate rocks world-wide) offer a different design problem than the relatively flat-lying rocks of the Interior Craton. Cavities mostly develop along both bedding and shear zones that dip and are oriented in various directions. Zones stressed by folding often exhibit increased dissolution. Sinkhole formation is more often of the raveling-type with a subsurface that often looks like Figure 3, although cave collapse is not unknown.

Metamorphism has altered older, solutioned carbonates into marble and skarn. Essentially, from an investigatory standpoint, these older carbonates offer the same difficulties in evaluation as the aforementioned folded and faulted Paleozoic rocks. As
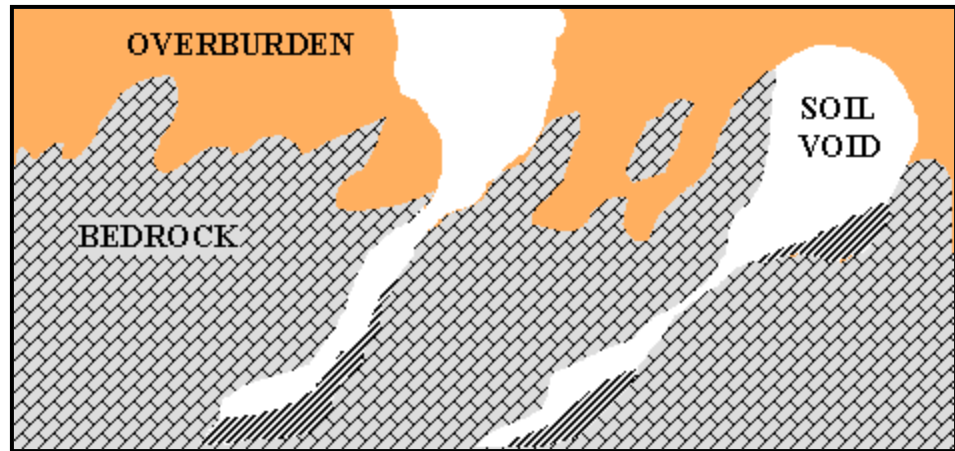
Figure 3: Raveling sinkhole in "bent" carbonates.

discussed subsequently, each of these solutioned carbonate terranes present different problems to investigators and designers. Of course, any of these difficulties must consider the nature of the planned construction. In relation to highways, there is obviously a need for geologic information for; 1) route selection, 2) constructing right-of-ways, 3) supporting pavements and structures, as well as 4) in evaluating, maintaining and remediating slopes.

Geophysical investigations have been used in all phases of roadway construction, from the planning to the remedial stages. Although often quite useful, the results are not always what the engineering design team envisioned. This can occur because of a lack of pre-survey planning, poor communication between the engineering team and the geophysicists prior to the investigation, misapplied geophysical techniques, poor understanding of the geologic regime, and/or a number of other variables.

The importance of planning and selecting appropriate geophysical methodologies as a part of an overall site characterization has been described previously (Benson, et al 2003). Aside from the geologic considerations when planning, factors that can also lead to the real or perceived success or failure of a geophysical investigation include time and budget constraints, pre-existing site conditions such as sources of cultural interference (traffic noise, underground and overhead utilities, etc.), and available space to conduct geophysical tests. Each of these considerations is very important to the geophysicists' ability to resolve large- and small-scale karst features.

Sinkhole occurrence (e.g., Moore, 1984 and Moore, 2003) in relation to highway performance has always been of concern. Investigation techniques have been discussed (e.g., Fischer and

Greene, 1991) and geophysical investigations described (e.g., Benson, et al, 1998; Hanna, et al, 2001; Stephenson, et al, 2003; and Adams, et al, 2003). Remediation of roadways in karst has also been addressed (e.g., Martin, 1995; Fischer and Fischer, 1995 and 1997; and Fischer, et al, 2001).

The following portions of this paper will attempt to address the technical issues introduced previously in relation to the need for interdisciplinary dialogues and realistic expectations.

"FLORIDA" KARST

Although not really true "karst" (i.e., Figure 1), the Paleogene and Neogene period carbonates of Florida and portions of the Caribbean have presented a major hazard from the standpoint of ground water protection and structural support. While older (Cretaceous period) rocks are found at depth in these "new" portions of the United States and Caribbean, the greatest concern to man has been the result of building above the more recent, lightly cemented coral sands or "lime rock".

Simplistically, these materials often have a relatively horizontally layered surface, as shown on Figure 2. The overlying sands are generally loose and may be derived from either quartz or coral. Underlying the upper deposits is generally soft lime rock, often with high secondary porosity.

Superimposed upon this section can be old, filled sinkholes, pockets of clayey or organic materials (Figure 4), and both collapse- and raveling-type sinkholes (Figures 2A and 2B). Strike and dip of the bedding are not particularly diagnostic in evaluating the geophysical data, but shear or fracture zones and failure types could be. Of concern from both the engineering and detection aspects are the possible existence of minor folds and the resultant fracturing and/or weathering.
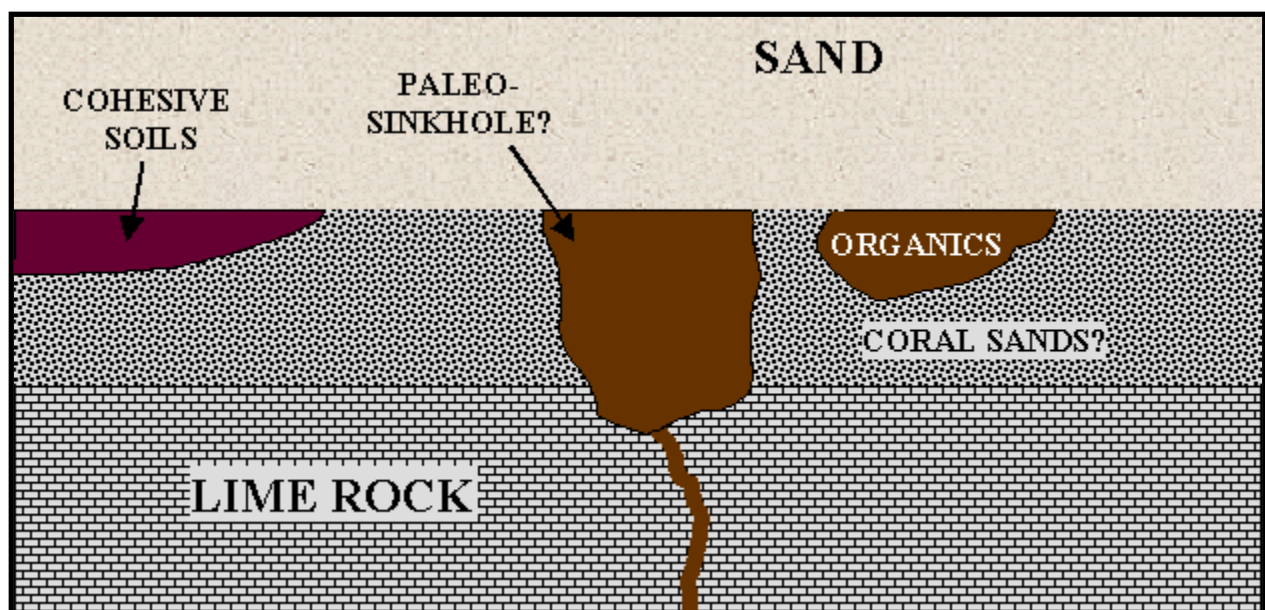
Figure 4: "Florida" karst conditions.

Geophysical investigation within this type of karst regime often targets the identification of shallow soil raveling, a depressed water table, abrupt dipping strata and bedrock voids. Methods that may be applicable, depending upon site-specific conditions, include ground penetrating radar (GPR), resistivity, spontaneous potential (SP), electromagnetics (EM), seismic reflection, and gravity.

Using a combination of complementary geophysical methods is generally recommended to increase the likelihood of a successful investigation. In this regime the geophysicist should target shallow features in the overlying sediments as well as deeper bedrock features (Yuhr, et al, 2003). Commonly, it is possible to identify medium- to large-scale karst features within this regime when detailed geophysical investigations using multiple methods are integrated with drilling or other direct sampling methods. However shallow, small karst features may still be beyond resolution unless directly encountered by a drill hole or test excavation. Thus, interpretation of the geophysical data usually requires some hard site data to identify or eliminate various different diagnostic features.

FLAT-LYING, HARD CARBONATES

Much of the central United States is underlain by hard, crystalline carbonates originally deposited during early Paleozoic time. These flat-lying rocks are common in the Interior Craton and generally continue from Kansas into western New York State. Numerous commercial caves in Kentucky and Ohio allow one to observe these limestones and dolomites in situ. A view overlooking the Mammoth Cave area of Kentucky looks like a moonscape in miniature or a World War I battlefield. A typical section often presented as representative of these materials is provided on Figure 5. In the northerly areas of the Craton, a mantle of glacial deposits can provide protection for the underlying carbonates, as well as sometimes masking diagnostic features that are usually evident in residual soils.

Figure 5: Section of "sinkhole plane" in flat-lying carbonate rocks.

Often, anhydrites are interbedded with the older carbonates and this can contribute to solution-related problems and hence, geophysical interpretation.
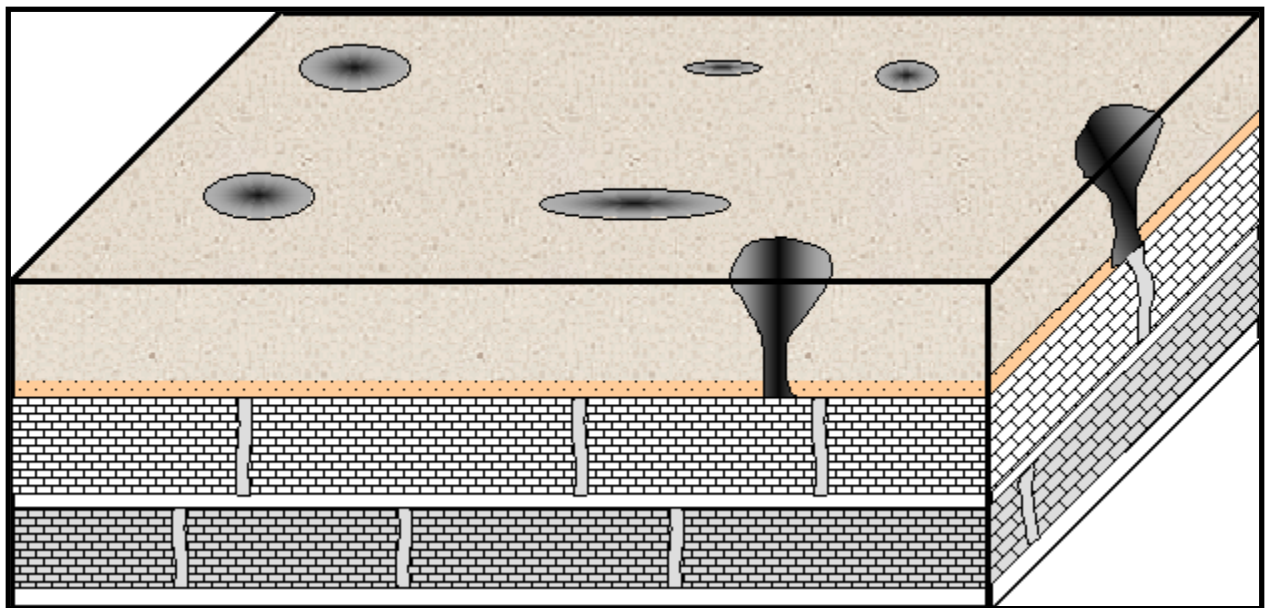
These carbonates are generally quite hard with unconfined compressive strengths on the order of 10,000 pounds per square inch (psi) or more. Solutioning is often controlled by the relative solubility of the different strata and variations in regional water levels with time. Thus, solutioning generally occurs along bedding (albeit, at different depths, depending upon previous ground water levels) with occasional control by fractures or faults.

Mapping of bedrock jointing patterns and faults in the area can be quite useful. Looking in local quarries and at aerial photographs can provide insight into joint strike and dip which can be very useful in identifying areas where potential sinkholes can form. Commonly the intersection point of two bedrock fractures weather more rapidly and provide a conduit to any solution voids below.

Geophysical targets in this regime commonly include weathered bedrock fractures, depressed bedrock surfaces and localized increases in overburden thickness, bedrock pinnacles, horizontal zones of anomalous electrical resistivity, anomalously low seismic velocities noted along the bedrock surface, electromagnetic (EM) conductivity anomalies, and gravity anomalies.

Methods that may be applicable depending on site-specific conditions and depth of interest include resistivity, seismic refraction or reflection, EM profiling, including very low frequency (VLF) EM, GPR, and gravity.

Factors that can adversely affect the resolvability of karst features in this regime include overburden thickness and composition, the presence of a thick saprolite layer, size and orientation of the karst feature, and whether the feature is clay-filled, water-filled or air-filled. The geophysical results should be integrated with other geologic and geotechnical information to evaluate whether the identified anomalies present a potential risk or may only preferential bedrock weathering that poses little risk.

FAULTED AND FOLDED, HARD CARBONATES

Folded and faulted Paleozoic Era dolomites and limestones are found in the Ridge and Valley Province of the eastern United States as well as in many similarly folded and faulted locales in the western United States. These environments present a more difficult geophysical target than either the flat-lying soft or hard carbonates previously discussed. A typical cross-section of the subsurface in these rocks is provided as Figure 6. Failure is most often of the raveling type (Figure 3), but cave collapse (Figure 2B) is not unknown.

These carbonates are a particularly difficult geophysical target. Often, the strata dip at very steep angles exposing a variety of beds at the bedrock surface over short horizontal distances. These conditions offer a variable geophysical landscape that differs with depth and azimuth. Cavities

can be large or small, and partially or fully filled with air, water and/or soil. Soft soil zones often exist atop the rock surface, and fracturing/solutioning are ubiquitous (see Figure 7).
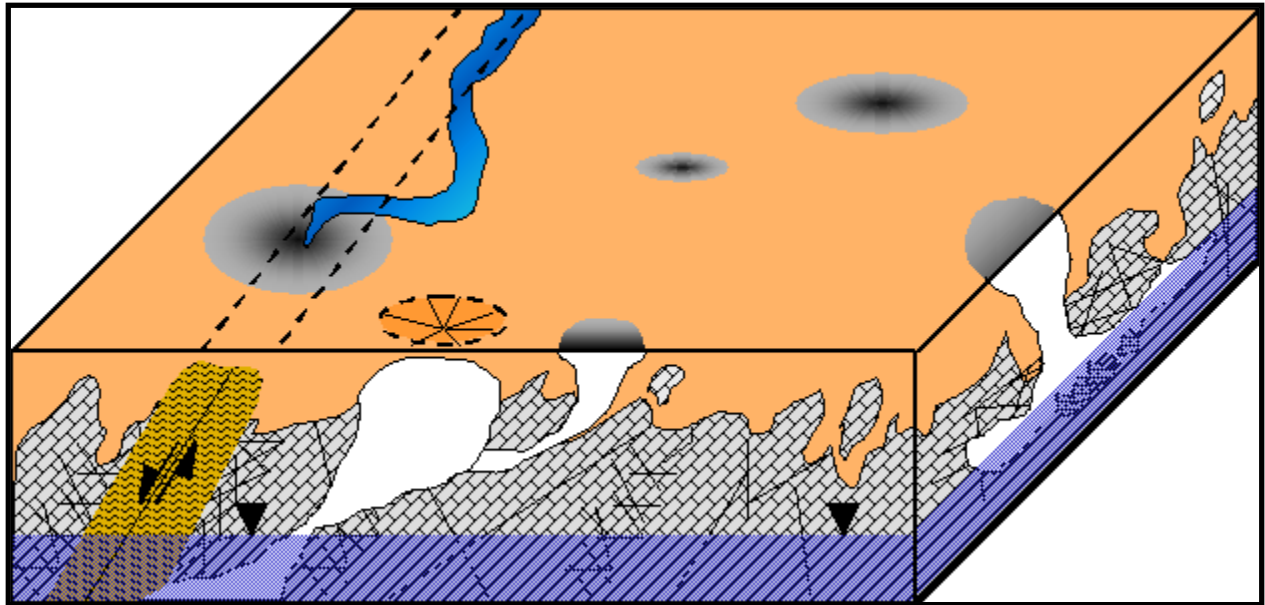
Figure 6: Typical subsurface section of "bent" carbonate rock.

Because of the small size of many of the karst features in this regime, it is very difficult to provide good resolution of these features for a reasonable cost. Furthermore, the many geologic variables and potential 3D effects can make interpretation difficult, even if anomalous geophysical responses can be detected.

Geophysical techniques such as resistivity, seismic refraction, gravity and EM methods provide bulk characteristics of a volume of the subsurface materials. Additionally, the amount of the volume increases

Figure 7: Exposed rock surface at "bent" rock karst site.

with depth thereby decreasing feature resolution with depth. As a result, the bedrock surface interpreted from geophysical data may appear smoother than it actually is and small voids may be beyond the resolution of the geophysical methodology applied.

To maximize the resolution of karst features requires finely spaced geophysical data collection, although the small size and complicated nature of the targets may be beyond the resolution of

any practical geophysical or drilling investigation. For example, Maule, et al (2000) completed 2D and 3D resistivity soundings and several test borings at a complicated shallow karst site in eastern Pennsylvania. They concluded "the combination of mud-filled and air-filled cracks and voids is probably too complicated to be mapped in detail by either resistivity or drilling".

Engineers unfamiliar with the limitations of geophysical methods may view such results as an unsuccessful investigation, however the geophysical results should be considered one (economical) piece of the puzzle needed to develop a rational site characterization. The geophysical results need to be integrated with other geologic and geotechnical information and not blindly dismissed as unreliable.

As with other types of karst regimes, multiple geophysical methods should be used to provide complementary information of potential targets. Methods commonly considered depending on site-specific conditions include resistivity, seismic refraction, EM, gravity and GPR. Often, GPR results are severely influenced by the presence of a clayey saprolite cover over the variable depth, variably weathered bedrock surface. In this regime, the practicing engineer or geologist that will use the geophysical results should anticipate that additional drilling and/or other direct sampling methods will be needed to further characterize the site. Even then, additional surprises will likely be encountered during any construction activities and experienced construction personnel are a must.

SUMMARY AND CONCLUSIONS

Simplistically, all karst terranes are not underlain by the same earth materials in a uniform depositional sequence despite their original sedimentary history. Therefore, before one can contemplate using geophysical investigative tools and procedures, there should be a general understanding of the subsurface target and the resolution necessary to identify the target and the need of the designers.

Thus, the initial planning stage for a site geophysical study includes research into the local geology, a review of aerial photography and/or satellite imagery, as well as a site reconnaissance with these data in hand. Hard data, e.g., test borings and test pits, should be considered part of the site investigation. Rarely can geophysical procedures be considered a stand-alone investigatory tool for highway route and facility sites.

With these preliminary concepts in hand, it is possible to consider the use of appropriate geophysical tools to expand and advance knowledge of the subsurface. The engineer/geologist that intends to make use of geophysical tools needs to have an understanding what methods are appropriate for the site-specific conditions and what are the realistic limitations of the methods to be applied prior to initiation of the investigation. However, one cannot ask for, expect to see, or demand miracles. Essentially, overall target resolution will vary with the nature of the subsurface, the amount of hard data available, the tools and procedures used, and the skill of the operator and interpreter.

The author's hope that this paper presents a realistic appraisal of the use of geophysical tools and their relationship to an overall site subsurface investigation program. First and foremost is the need for a coordinated interpretive effort by <u>all</u> involved with the clear understanding of the capabilities and limitations of every tool available, whether direct or indirect, as they apply to a specific site.

REFERENCES

Adams, et al, 2003. *Using GPR Reflection Patterns and NP Measurements to Predict Sinkhole Risk in Central Florida*, in Proc. of 54th Highway Geology Symp., Burlington, VT.

Benson, R.C., R.D. Kaufmann, L. B. Yuhr, D. Martin, 1998. *Assessment, Prediction and Remediation of Karst Conditions on I-70, Frederick, Maryland*, in Proc. of 49th Highway Geology Symp., Prescott, AZ.

Benson, R.C., L. Yuhr, R.D. Kaufman, 2003. *Some Considerations for Selection and Successful Applications of Surface Geophysical Methods,* in Proc. of 3rd International Conf. on Applied Geophysics, Orlando, FL

Fischer, J.A., and R.W. Greene, 1991. *Roadways in Karst Terrane*, in Proc. of 42nd Highway Geology Symp., Albany, NY.

Fischer, J.A. and J.J. Fischer, 1995. *Remediation for Highways in Karst*, in Proc. of 46th Highway Geology Symp., Charleston, WV.

Fischer, J.A. and J.J. Fischer, 1997. *Investigation and Remediation of Service Plaza Fuel Storage Tanks in Karst*, in Proc. of 48th Highway Geology Symp., Knoxville, TN.

Fischer, J.A., J.J. Fischer, and R.S. Ottoson, 2001. *Roadway Remediation – Case Histories in Karst*, in Proc. of 52nd Highway Geology Symp., Cumberland, MD.

Hanna K., A. Rock, and B. Hoekstra, 2001. *Three Dimensional Tomographic Imaging for Deep Foundation Integrity Testing*, in Proc. of 52nd Highway Geology Symp., Cumberland, MD.

Martin, A.D., 1995. *Maryland Route 31 Sinkhole*, in Proc. of 46th Highway Geology Symp., Charleston, WV.

Maule J.A., J.E. Nyquist, and M.J.S. Roth, 2000. *A comparison of 2D and 3D Resistivity Sounding in Shallow Karst Terrain, Easton, PA*, in 2000 Conf. Proc., Symp. on the Application of Geophysics in Engineering and Environmental Problems, Arlington, VA.

Moore, H.L., 1984. *Geotechnical Considerations in the Locations, Design, and Construction of Highways in Karst Terrain – 'The Pellissippi Parkway Extension', Knox-Blount Counties, Tennessee*, in Sinkholes: Their Geology, Engineering & Environmental Impact, A.A. Balkema, Boston, MA

Moore, H.L., 2003. *Recent Sinkhole Occurrences Along Highways in East Tennessee, A Historical Perspective*, in Proc. of 54th Highway Geology Symp., Burlington, VT.

Stephenson, J.B., R.D. Kaufman, J.A. Archer, C. Bertz and P. Bradley, 2003. *Environmental Investigation of a Diesel Spill in a Karst Area of Kentucky*, in Sinkholes and the Engineering and Environmental Impacts of Karst, ASCE.

Yuhr, L., R.C. Benson, R.D. Kaufman, D. Casto, and J. Jennings, 2003. *A Case History of a Large Karst Investigation*, in Proc. of the 3rd International Conference on Applied Geophysics, Orlando, FL.

Debris Flow Remediation

by

Erik J. Rorem, President & General Manager

Geobrugg North America, LLC
551 W. Cordova Road, PMB 730
Santa Fe, NM 87505
tel: (505) 438-6161   fax: (505) 438-6166
email: erik.rorem@geobrugg.com

Abstract

In the fall of 2003, devastating fires ravaged the terrain in the San Bernardino Mountains above San Bernardino, CA near the mountain towns of Crestline and Lake Arrowhead, CA. These fires left the steep slopes and drainages barren of trees and ground cover, exposing soil on these slopes to erosion. Despite emergency measures to hydro seed these slopes on a massive scale and various other mitigation efforts, unusually large rainfall in December 2003 produced several large scale debris flows and many smaller debris flows that resulted in loss of life and considerable property and highway damage, as was widely reported in the national media.

Following these events, Caltrans undertook emergency measures to install a series of flexible barriers installed at multiple sites, to control debris flows that are likely in the future. The primary section of road under consideration is a section of State Route 18 commonly referred to as "The Narrows." Along this section of road, 10 distinct debris flow channels upslope from and opening onto the roadway were identified for application of these barriers.

At each site, field observations were made by Caltrans to estimate expected volumes of debris and velocities from debris flow events, broadly characterize the expected debris flow compositions, measure channel geometry and determine barrier orientations. From this information, engineers at Geobrugg were able to dimension barriers appropriate for these conditions. Dimensioning of the barriers was completed using a general design concept developed from that learned in various field testing efforts, from back-calculating forces exerted on barriers from observations of performance of barriers that had been impacted to date in actual debris flow events in the field, and from verification of the concept using a unique computer simulation program that predicts barrier response and performance. Each site required a unique barrier design with differing barrier heights, capacities and support infrastructure.

Construction of these barriers commenced in May 2004 on a tight schedule for July completion. Due to the custom nature of the design for each site and unique materials for each, as well as a requirement for special colorization of all materials, meeting this schedule was a significant challenge but vital due to the importance of tourism in this area.

A general overview of the debris flow problem, the mitigation design process and the construction sequence for this project will be presented. A brief description of the various unique barrier types installed will be provided.

INTRODUCTION

Several natural debris flow events in the USA and around the world have demonstrated that flexible barriers can be effective at stopping debris flows. Barriers installed initially for the purposes of rockfall mitigation have been impacted by mudflows, debris flows, and small snow avalanches with the somewhat surprising result of the material being stopped with little or no damage to the barriers.

As a result of these observations, further research has been conducted in an attempt to identify the appropriate design parameters for such barriers, and to identify modifications to rockfall barriers necessary to make them appropriate for debris flow. Such research has included 1:1 field-testing with small artificially generated debris flows, as well as computer simulations modeling the behavior of barriers during such events.

This research has led to an initial dimensioning model for flexible barriers to be used for debris flow mitigation, which is currently being applied in numerous cases. In California, this concept has been applied to one project case involving 10 debris flow sites along a short distance of highway in the San Bernardino Mountains of Southern California. These barriers have been installed, but have yet to be impacted by actual debris flows. When these barriers are eventually impacted, the observations will provide invaluable information regarding performance, design assumptions, and maintenance requirements including cleanout.

OBSERVED EVENTS AND RESEARCH

Events

Compared to testing of rockfall protection barriers, testing of debris flow barriers can be very difficult and costly due to the high costs associated with actual 1:1 field-testing, the myriad of variables involved with debris flow, and the logistics of creating debris flows for testing purposes. Alternatively, observation of performance and identification of input variable values can be done relatively inexpensively and easily by observing actual impact events to barriers installed in the field, and then back calculating. Such events have occurred in the USA in

several instances, and in numerous cases around the world including mud and debris flow impacts as well as small snow avalanche impacts. These events have been used as cases to allow back-calculation of the mechanics and forces involved, as well as the response of the barrier to the impacts.

One case in particular can be outlined to illustrate this back-calculation process. In 1998, a temporary 1500 kJ barrier installed in Aobandoni, Japan to protect against rockfall during construction work being performed downstream, was impacted by a series of debris flow pulses. This barrier was 20 meters long and 5 meters tall. Three consecutive debris flow pulses impacted the barrier, completely filling it with approximately 750 m^3 of debris. Nearly 100% of the debris involved with the flow was retained by the barrier. During the impacts, the friction braking elements in the support ropes and upslope retaining ropes responded to varying degrees. Remaining effective height of the barrier after the event was approximately 70%, and net deflection was only 3 meters. Other than replacement of these braking elements and cleanout of debris, no other maintenance or repair was necessary. However, since this was a temporary installation, the barrier was disassembled and taken away, to be re-used elsewhere in the future.

Figure 1 - Aobandoni, Japan Debris Flow Impact. 5 meter tall barrier.

Due to the extreme nature of this event and the degree of key barrier element engagement, this case provided an excellent opportunity to back-calculate the mechanics of the event and the consequent response of the barrier. Because of the relationship between the amount of loading versus the degree of braking element response is well documented, it is a relatively simple matter to back-calculate the forces exerted on the support infrastructure. Similarly, loading data gained during 1:1 testing of rockfall barriers facilitates the ability to back-calculate debris flow loading, if the total amount of barrier deformation is known. Back-calculation of other such events has yielded similar relationships and results. This case and others have thus proven to be valuable

input for creation of a dimensioning concept for use of these barriers specifically for protection against debris flow.

Testing

At least two known 1:1 field tests have been conducted on flexible barriers to determine performance under debris flow loading. The first such test was conducted in 1996 at the USGS Debris flow flume in Blue River, Oregon. During 6 tests conducted at this site, various instrumentation was used to record flow velocities, forces on various barrier elements, and debris flow character and barrier response in a general way. The most important finding from these tests from a design standpoint was the fact that despite the relatively large openings of ring nets, they can be very effective for purposes of retaining even fine-grained mudflows. Additionally, the tests demonstrated that ring nets perform better than woven wire rope nets due to the higher flexibility, higher energy absorption, better load distribution to the support infrastructure, less need for repair, and better adaptability to the irregular terrain that can be expected in debris flow channels.

Figure 2 - USGS Debris Flow Flume

Figure 3 - Debris in Ring Nets During Test

Another test series was conducted in Lobenbach, Germany by the Technical University of Munich to test the performance of flexible barriers to impacts from torrents laden with woody debris. In these tests, a barrier was subjected to impacts from torrents laden with timber and other woody debris, allowing water to pass but restraining the debris. Copious loading data was collected from various instrumentation in the support infrastructure.

Data from these tests has been invaluable in determining the response of barriers to such loading, and thus has contributed to creation of the barrier dimensioning concept.

Simulations

A computer program called FARO developed as part of a Swiss Commission for Technology and Innovation project to simulate the response of ring net barriers to dynamic loading has also been useful in validating the barrier dimensioning concept. The program was initially developed to model point load impacts such as from rockfall, but it can also be used for loading from impacts covering a larger impact surface area such as with debris flows. The simulations were used to support and validate the back-calculations referenced earlier, and also to verify and validate the barrier dimensioning concept.
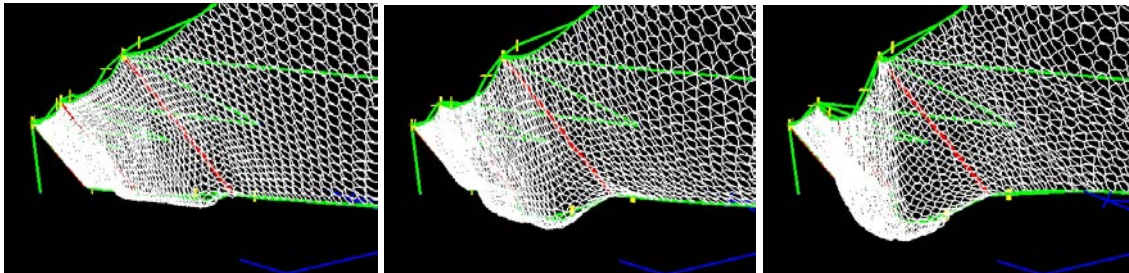
Figure 4 - Graphic Representation of FARO Simulation.

APPLICATION OF CONCEPT: CASE HISTORY

To demonstrate how this dimensioning concept can be applied, a recent project in California provides an excellent example from problem definition to design to completion.

Problem

In the fall of 2003 devastating wildfires ravaged countless acres of terrain in the San Bernardino Mountains near the mountain communities of Crestline and Lake Arrowhead, CA. These fires

Figure 5 - Typical Burned Terrain (courtesy Duffy)

left large areas completely devoid of all vegetation and ground cover, most of which involves

very steep mountainous slopes. This left the soils and debris on these slopes completely exposed to the elements, with nothing remaining to hold the soils in place.

Without question, the coming rainy season would produce numerous mud and debris flows in these areas. In anticipation of this, the California Department of Transportation (Caltrans) identified key areas where state highway numbers 18 and 138 would be vulnerable to such threats and stopgap measures were undertaken to minimize any potential damage to the highways and hazards to motorists.

Figure 6 - Debris Flow Channel, Site 7

Initial Mitigation Attempts

Various initial mitigation measures were undertaken, though just a few will be discussed herein. Some of these measures included a flexible rockfall and debris flow protection barrier, cable net slope drapes, and several so-called suspended mesh drapes across several drainage channels opening onto the road.

As expected, the rains came in December. However, at Christmas, the worst possible scenario emerged with a large storm event producing up to 4 inches of rain – far more than could be reasonably anticipated. As was widely reported in the media, this storm produced numerous mud and debris flows, not the least of which was the Waterman Canyon debris flow that killed 11 people camping in the canyon. Of course, none of the installed mitigation systems were nor could they be designed or intended for such an event, nor were they installed in that area. However, in the areas where these systems were installed, debris flow impacts were reported. Varying degrees of success were observed from these systems. The cable net drapes were very

effective in preventing large erosional events on the slopes, while on the other hand, the rockfall and debris flow barrier that was installed was only minimally impacted. Most of the suspended mesh drapes however were impacted by large amounts of debris.

Figure 7 – Debris in and Around Suspended Tecco Mesh Drape

Though these suspended mesh drapes did contain large amounts of debris, they were largely overwhelmed by the sheer volume of debris. In some cases, the debris flows effectively lifted the mesh and flowed underneath. In other cases, the bottom of the mesh was weighted down by accumulated debris such that much debris was retained, but the volume was too great and excess debris flowed around the sides of the drape. In only one case was there a true system failure, and this was due to failure of the rock into which that the lateral support anchor was placed. In the end, this section of road had to be closed due to the volume of debris on the road and damage to the roadbed, mostly in areas where no initial mitigation measures were placed.

Even though the suspended drapes were not entirely effective in keeping all debris material off the road, much was learned in terms of the degree of debris flows that could be expected and possible alternative mitigation methods appropriate for such events. Additionally, in the sense that more road damage did not occur than otherwise may have occurred, these systems served a useful purpose.

Figure 8 - Area Overwhelmed with Debris Flow (courtesy Duffy)

Subsequently, 10 channels along state route 18 in the area known locally as "The Narrows" were identified as being prone to debris flow and appropriate for protection with more substantial barriers.

Flexible Barriers Dimensioning

Flexible barrier system designs for debris flow are based on the basic designs of certified rockfall protection barrier systems. Since debris flow impacts have a large surface area of impact as opposed to the punctual loads associated with rockfall impacts, some adaptations to the barriers are necessary:

- Stronger support ropes (or more of them), and brake elements with higher capacities. Also, ring nets with a lower capacity can also be used due to the larger surface area of loading.
- Stronger anchorage.
- Protection system adjustable to different torrents

Several mechanical and rheological models have been proposed for analysis and prediction of debris flows. Due to the lack of field data for comparison, Rickenmann (2001) suggests using empirical relationships to establish the following parameters:

- Volume of debris flow
- Peak discharge
- Velocity at peak discharge
- Flow depth at peak discharge

- Density of material
- Impact time

With these parameters it is possible to calculate the impact energy of the flow. The kinetic energy capacities for flexible barriers are between 100 kJ and 3,000 kJ. However, for debris flows, the dimensioning energy cannot be compared with design energies of rockfall protection barriers, due to the differing mechanics and loading characteristics of the two types of events. To account for this, a safety factor of 1.5 is applied to the initial calculation of kinetic energy, as determined necessary from the back-calculation studies of loading versus barrier responses from observed events. After applying the requisite safety factor, design load kinetic energies could be determined for each site, as well as barrier geometries. These barriers can be used for debris flow involving up to 1,000 m^3 of debris having a maximum flow velocity of approximately 5 to 6 m/s.

Identification of the following parameters is necessary in order to apply the dimensioning model:

- Character of flow. Granular debris versus mudflow.
- Debris flow channel geometry.
- Longitudinal geometry of debris flow channel upstream from the barrier.
- Average width of channel at barrier location.
- Inclination of channel at barrier location.
- Estimated total flow volume.
- Estimated density of flow material.

For each of the 10 debris flow channels identified, Caltrans estimated the above parameters from site investigations. Engineers at Geobrugg then used this data to design barriers appropriate for each of the sites.

Specific Designs

Six basic designs were used of varying heights, depending on the volumes and flow energies anticipated and the geometry of the debris flow channel as illustrated below.

VX barrier: - No posts, since <12 meter channel width (fig.)
  - Top, middle and bottom support ropes, anchored at the sides.
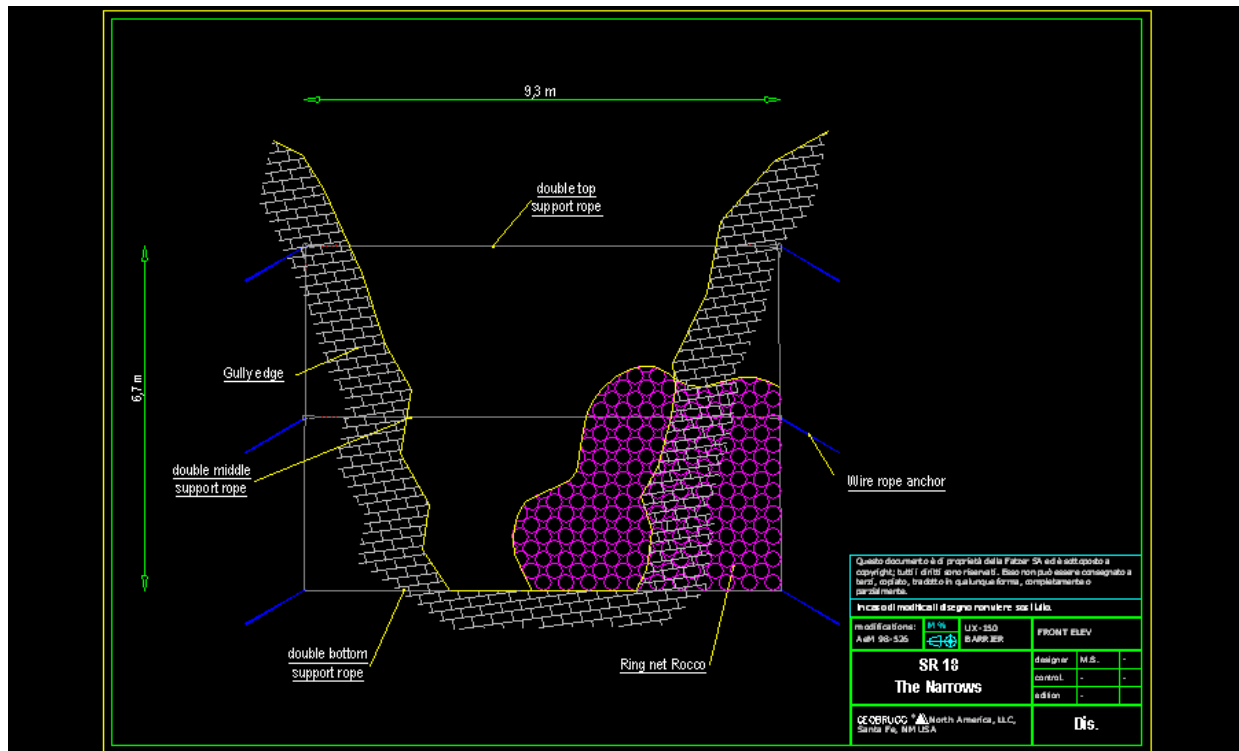
Figure 9 - General Schematic of VX Barrier, Site 6.

Site # 6:
- Calculated design kinetic energy = 700 kJ.
- Calculated necessary height = 6.7 m.
- Length across top = 9.3 m.

Site # 7:
- Calculated design kinetic energy = 200 kJ.
- Calculated necessary height = 8.0 m.
- Length across top = 10.0 m.

Figure 10 - Site 7, VX Barrier

VX+ barrier: -   Same as VX, with one middle post to support the long span (> 12 m.).
             -    Top, middle and bottom support ropes, anchored at the sides.

Site # 2:
- Calculated design kinetic energy = 400 kJ.
- Calculated necessary height = 5.0 m.
- Length across top = 22.0 m.

Site # 9:
- Calculated design kinetic energy = 1,000 kJ.
- Calculated necessary height = 5.0 m.
- Length across top = 17.3 m.

Site # 10:
- Calculated design kinetic energy = 300 kJ.
- Calculated necessary height = 4.0 m.
- Length across top = 14.0 m.

Figure 11 - Site 2, VX+ Barrier

Figure 12 - Site 9, VX+ Barrier

UXI-050 barrier: -   A variation of the RXI-050 rockfall barrier. 500 kJ capacity.

Site # 3:
- Calculated design kinetic energy = 250 kJ.

- Calculated necessary height = 3.0 m.
- Length across top = 20.0 m.

    Site # 8:
- Calculated design kinetic energy = 200 kJ.
- Calculated necessary height = 3.0 m.
- Length across top = 20.0 m.

UX-075 barrier: - A variation of the RX-075 rockfall barrier. 750 kJ capacity.

    Site # 5:
- Calculated design kinetic energy = 700 kJ.
- Calculated necessary height = 4.0 m.
- Length across top = 16.0 m.
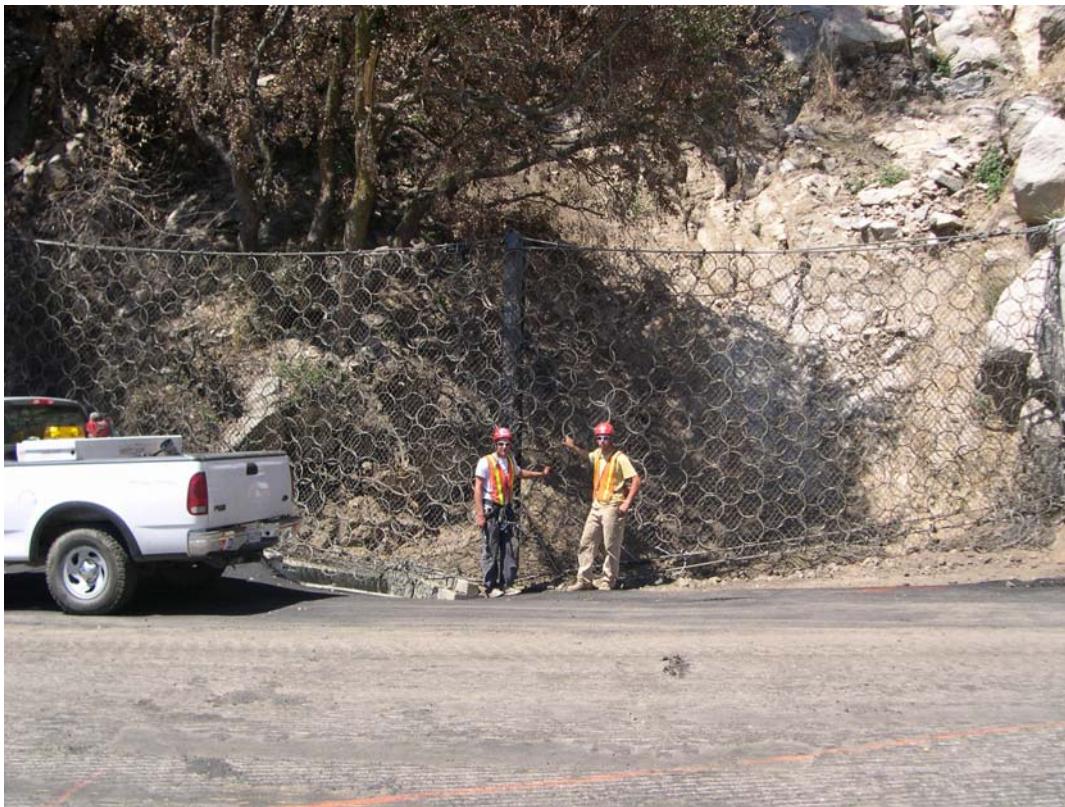
Figure 13 - Site 5, UX-075 Barrier

UX-150 barrier: - A variation of the RX-150 rockfall barrier. 1500 kJ capacity.

    Site # 1:

- Calculated design kinetic energy = 1,200 kJ.
- Calculated necessary height = 5.0 m.
- Length across top = 17.0 m.

  Site # 4:
- Calculated design kinetic energy = 870 kJ.
- Calculated necessary height = 4.0 m.
- Length across top = 16.0 m.

Figure 14 - Site 1, UX-150 Barrier

Special Considerations

One very important consideration for these debris flow barriers is that of ease of maintenance and cleanout. Some of these barriers will most certainly be significantly impacted, and once full of debris, it is imperative that the barriers be cleaned out in a timely manner so that they are ready for the next event. Since loaded barriers are under tension, an easy method of releasing the nets is necessary. Thus, a decision was made in the field to replace shackle connections of the nets to the side support ropes and from net to net, with a 5/16 inch seaming cable. When the nets are loaded with debris, this seaming cable can be cut, thereby releasing the nets from the side supports and each other, and allowing the debris to be extracted with excavating equipment. Due to the shackle connections of the ring nets to the top and bottom support ropes, the nets can be slid open like a curtain to some degree to help facilitate access to the debris. After cleanout, the nets can be slid back into place and the seaming can be replaced at insignificant cost.

Because this area is in the jurisdiction of the U.S. Forest Service (USFS), aesthetic impact of these barriers to the surroundings was an important consideration. The USFS thus required that the barriers and all related materials would need to be colorized to minimize the visual impact. All materials were thus colored a dark brown color, including posts, nets, hardware and attached chainlink mesh.

Figure 15 - Colorized Netting

In some instances where the bottom or side support ropes were not in close contact with the ground surface due to terrain irregularities, intermediate anchors were placed in order to ensure no large gaps would exist between the barrier surface and the ground.

Construction

Construction of the barriers commenced in May of 2004, and was completed July 19. In the interest of simplifying and expediting construction, and since a large airtrack rig was available for drilling, all anchors were installed with a 50 ton pullout strength. In reality, the required pullout strengths for all upslope and lateral wire rope anchors varied considerably between the various barriers, but it was considered more expeditious to simply install all anchors at this maximum requirement of 50 tons. After anchor and post foundation construction, erection of the

barriers was completed very quickly since most of the construction was at or near road grade allowing easy assembly.

CONCLUSIONS AND OUTLOOK

Field observations have proven that flexible barriers can be used to stop debris flows with debris volumes of up to 1,000 m^3. Due to the flexible nature of these barriers, they are ideal for mitigating such dynamic impacts in a cost effective, quick and relatively nonintrusive manner. A basic barrier dimensioning model based on back-calculations of prior impacts to barriers, 1:1 field testing and a novel computer simulation program has been created to help provide some objective basis for dimensioning such barriers.

The barriers installed at "The Narrows" for Caltrans will undoubtedly be significantly impacted during the next significant rain events. Because the availability of objective data to date regarding impacts to barriers is limited, it is planned to instrument at least one of these barriers. Data collected from this instrumentation as well as qualitative observations of the performance of these barriers will be invaluable for advancing the field of debris flow mitigation.

REFERENCES

DeNatale, J. S., Fiegel, G. L., Iverson, R. M., Major, J. J., LaHusen, R. G., Duffy, J. D. and Fisher, G. D., 1997, "Response of Flexible Wire Rope Barriers to Debris-Flow Loading." Proceedings of the First International Conference on Debris-Flow Hazards Mitigation.

Duffy, J., 2004, personal communication.

Frenez, T., Roth, A., and Kaestli, A., 2004, "Debris Flow Mitigation by Means of Flexible Barriers." Proceedings of the 10th Congress Interpraevent 2004, Trento, Italy.

Rickenmann, D., 2001, "Estimation of debris-flow impact on flexible wire rope barriers." Unpublished internal Geobrugg report.

Rimbock, A., Strobl, T., 2002, "Rope Nets for Woody Debris Entrapment in Torrents." Technical document of the Technische Universitat Muchen.

Volkwein, A., "Numerical simulation of highly flexible rockfall protection systems." Research project ETH Zurich.

A DETAILED STUDY OF THE NEW BALTIMORE LANDSLIDE ALONG PENNSYLVANIA TURNPIKE

Ryan S. Tinsley
Michael Baker Jr., Inc., 4301 Dutch Ridge Road, Beaver, Pennsylvania 15009

And

Abdul Shakoor
Department of Geology, Kent State University, Kent, Ohio 44242

Abstract

The New Baltimore landslide is an old (pre-1883?) landslide located along I-76 (Pennsylvania Turnpike) in Somerset County, Pennsylvania. The landslide, which extends approximately 2000 ft (616 m) upslope and 1000 ft (305 m) laterally, has been problematic for I-76 ever since its construction in 1940. Being an active landslide, it continues to move toward the east-bound lane of I-76 at a rate of approximately 3.5-5.0 inches (9-13 cm)/yr, which causes the shoulder to heave. Overall, the landslide can be classified as a translational failure with localized rock falls, rotational slides, and flows. The geology at the site consists of the Upper Devonian Catskill Formation that includes sandstone, siltstone, and claystone units.

The landslide was mapped in detail to show the presence of major and secondary scarps, tension cracks, drainage channels, and depressions. A subsurface investigation was conducted by American Geotechnical & Environmental Services, Inc. of Pennsylvania. It consisted of 18 borings, ranging in depth from 39.4 ft (12 m) to 118.1 ft (36), and installation of 15 piezometers, 11 Time Domain Reflectometry (TDR) cables, and 3 slope inclinometers. These instruments were monitored quarterly to investigate the pore water pressures at different depths and determine the location of the failure plane. The core from the boreholes was logged to establish the stratigraphy and to select samples for laboratory testing. The factor of safety against sliding was determined for varying drainage conditions.

The results of the study indicate that the primary failure is located along the bedding plane at an approximate depth of 10 ft (3 m) in the toe area and 75.5 ft (23 m) near the crest of the slope. The material along the failure plane is a nondurable (slake durability index < 37%), soil-like claystone of low shear strength. The instrumentation data show that the most significant movement and higher pore pressure occur in the months of February through May. For varying drainage conditions, the factors of safety range from 1.0 (for dry slope) to 0.9 (for maximum pore pressure measured along the failure plane). A number of stabilization alternatives were evaluated as possible remedial measures including rock dowels, drilled piles, slope re-gradation, provision of a catchment ditch and a protective barrier, and monitoring of the slide in combination with road maintenance.

Introduction

The New Baltimore Landslide is located at milepost 128 along the eastbound lane of the Pennsylvania Turnpike (I-76) in Somerset County, Pennsylvania (Figure 1). It is an old (pre-1883) landslide that is approximately 1000 ft (305 m) wide and extends 2000 ft (610 m) upslope. Overall, the landslide can be classified as a translational movement with localized rock falls, rotational slides, and flows. The landslide has several distinguishing features that indicate various episodes of movement inside the mobilized mass, the most prominent being the repetitious series of scarps and slumps within the hummocky terrain that extends from the toe to the crest of the slope. Throughout the slide mass comprising the hummocky topography of the lower section, there are numerous occurrences of disturbed rock blocks, tension cracks, minor scarps, and tilted trees. The landslide has posed a problem to the Pennsylvania Turnpike ever since the completion of its construction in 1940. It continues to move toward the Interstate 76 at an approximate a rate of 3.5 to 5.0 inches (9 to 13 cm) per year. The active nature of the landslide has led to a relatively large unstable rock mass at the toe of the slope and heaving of the east-bound lane shoulder as shown in Figures 2 and 3.   There have been numerous rock falls along the eastbound lane of I-76, like the one shown in Figure 4, that pose a constant threat to the Turnpike traffic.

The geology at the New Baltimore Landslide site consists of the Devonian-aged Catskill Formation that is approximately 1600 to 2000 ft (488 to 610 m) thick and is comprised of alternating units of sandstone, siltstone, and claystone (Flint, 1965). The sandstone is very fine-grained to fine-grained, and locally micaceous and conglomeratic. The siltstone is thinly to thickly bedded, micaceous, and agillaceous. The claystone is commonly silty, thinly to medium bedded, and variegated (McElroy, 2001). Alternating sequences of clayey siltstone to silty claystone are very common. The colluvial and residual soils consist of sandy silts with intermixed clay and fragments of claystone, siltstone, and sandstone. The landslide is located on the western limb of the Deer Park anticline, a major structural feature of the area. The axis of the fold strikes N 35 E and dips 15 to 25 degrees towards the northwest (McElroy, 2001).

Based on historical records provided by the Pennsylvania Turnpike Commission (PTC) (PTC, 2003), the New Baltimore Landslide appears to have been active since initial construction of the turnpike in 1940. The sketches and maps of the landslide drawn by the PTC in the 1940s indicate line and grade shifts due to slope movement. Periodically, the PTC established baselines to monitor surface movements, which is indicated on the older sketches. The PTC made an attempt to remediate the slope in the 1950s by cutting an approximately 40-ft (12 m) wide bench and providing a 1H:1V back slope extending to the initial head scarp. In 1972, Geomechanics, Inc., a geotechnical firm from Pittsburgh, completed a subsurface investigation consisting of three borings within the slide mass to locate the failure plane. In 1999, American Geotechnical & Environmental Services (AGES), Inc. were hired by the PTC to determine the location of the failure plane and the rate of the movement, and suggest possible remedial measures to prevent the mass movement from reaching the highway. The study presented herein incorporates the subsurface and instrumental data collected jointly with AGES, Inc.

Research Methods

Field Mapping, Subsurface Investigations, and Monitoring

The main and lateral scarps of the landslide were mapped to delineate the limits of the landslide. Also, minor scarps, tension cracks, depressions, and groundwater seeps were mapped to evaluate surface conditions. The site was visited periodically for more than one year to revise the map for the presence of groundwater seeps or newly developed tension cracks.

Detailed subsurface investigations were conducted in collaboration with the American Geotechnical and Environmental Services (AGES), Inc. as a part of investigation of the New Baltimore Landslide for the Pennsylvania Turnpike Commission (PTC). The main purpose of subsurface investigations was to sample the strata above, close to, and below the primary failure plane for laboratory testing and to install monitoring instrumentation to determine the location of the failure plane and evaluate the direction and rate of movement. Also, there was a need to monitor the fluctuations in the ground water conditions of the slide area. Eighteen vertical test borings were drilled to a depths ranging from 39 ft (12 m) at the toe and 118 ft (36 m) near the crest of the lower, more recent landslide. The test borings were aligned in two lines from toe to crest to get a full representation of stratigraphy of the lower slide area. Ten of the 18 boreholes were sampled continuously using an NX size (54 mm) core barrel.

The methods used to monitor the slope movement included the use of 3 transect lines, 3 slope inclinometers, and 11 time domain reflectometry (TDR) cables (Henderson, 2000). Fifteen vibrating wire piezometers were used to monitor the water table functions leading to the pore pressure variations (Henderson, 2000). Figure 5 shows the locations of the slope instrumentation within the slide mass. The slope instrumentation was monitored quarterly from August 1999 to May 2001. The data from slope inclinometers and the TDR cables indicated similar depths of the primary failure plane within the slide. Figure 6 shows the graphical outputs of both the TDR and slope inclinometer results at test boring 2. Tables 1 and 2 summarize the depths of the failure plane at various locations as indicated by the slope inclinometers and TDR cables. These results indicate that the primary failure plane is located within a weak claystone unit at an approximate depth of 10 ft (3.3 m) in the toe area and 75.5 ft (23 m) near the crest of the slope. Piezometric data suggest that the higher pore water pressures occur in the late winter and early spring months. Table 3 summaries the pore pressure readings near the failure plane.

Table 1: Depth of failure plane below the ground surface at various slope inclinometer locations.

Inclinometer	Depth of Failure Plane Below the Ground Surface
I-2	25 ft / 7.62 m
I-4	73 ft / 22.25 m
I-8	17 ft / 5.18 m

Table 2: Depth of failure plane below the ground surface at various TDR cable locations.

TDR Cable	Depth of Failure Plane Below Ground Surface
T-2	26-29 ft / 7.92-8.84 m
T-3	72-75 ft / 21.95-22.86 m
T-6	43-46 ft / 13.10-14.02 m
T-8	19-22 ft / 5.79-6.71 m
T-9	9-13 ft / 2.74-3.96 m
T-10	34-38 ft / 10.36-11.58 m

Table 3: Pore water pressure data from November 1999 through May 2001.

Date	Piezometer at I-2 (28.5 feet)	Piezometer at I-4 (75.5 feet)	Piezometer at I-5 (50 feet)	Piezometer at I-6 (45 feet)
Nov 9, 1999	0.37 psi	1.60 psi	0.40 psi	1.57 psi
Feb 8, 2000	0.52 psi	2.20 psi	0.61 psi	1.62 psi
Apr 3, 2000	0.25 psi	2.70 psi	1.03 psi	1.39 psi
Aug 7, 2000	0.34 psi	2.97 psi	0.54 psi	1.47 psi
Nov 16, 2000	0.26 psi	2.59 psi	0.36 psi	1.37 psi
Feb 28, 2001	0.36 psi	3.42 psi	1.13 psi	1.45 psi
May 3, 2001	0.44 psi	2.80 psi	Possible Shear of Cable	1.53 psi

Laboratory Investigations

Laboratory tests were conducted on the core samples to determine dry density, percent absorption, Atterberg limits, slake durability index, unconfined compressive strength, tensile strength, and shear strength parameters. All tests were conducted in accordance with American Society for Testing and Materials (ASTM, 1996) Standards, where applicable.   The purpose of laboratory tests was to characterize the materials involved in sliding and to obtain engineering property data needed for stability analysis. Two types of direct shear tests were conducted to obtain shear strength data, one involving shearing along the discontinuity and the other involving shearing through the intact rock. Competent sandstones and siltstones were failed along two saw-cut surfaces to simulate shearing along the discontinuity. The highly weathered, soil-like claystone, collected in the vicinity of the failure plane, was tested using intact cores.

Tables 4 and 5 summarize the engineering properties of various rock units. The sandstone samples, failed along the saw-cut surfaces, exhibit peak friction angle values ranging from 12 to 25 degrees and residual friction angle values ranging from 8 to 25 degrees. The peak and

residual cohesion values for the sandstones range from 166 to 286 psi (1144 to 1282 KPa) and 109 to 215 psi (751 to 1482 KPa), respectively. The siltstone samples that were failed along the saw-cut surfaces have peak and residual friction angle values of 21 to 31 degrees and 21 to 27 degrees, respectively. The peak cohesion values for the siltstone samples range from 0 to 171 psi (0 to 1179 KPa) whereas the residual cohesion is approximately zero psi. The siltstones with interbedded claystones have a peak and residual fiction angle value of 11 degrees, with peak and residual cohesion values of 240 and 136 psi, (1655 and 938 KPa), respectively. The weaker claystone samples that were failed in the intact state exhibit peak friction angle values of 21 to 22 degrees and a residual friction angle of 11 to 21 degrees. The peak and residual values of cohesion for the intact claystones range from 86 to 186 psi (593 to 1282 KPa) and 0 to 63 psi (0 to 434 KPa), respectively.   The peak values of strength parameters found in this study are in agreement with those reported by Geyer (1982).

Table 4: Strength properties of various rock units comprising the landslide mass.

Lithology	Unconf. Comp. Strength (psi)		Tensile Strength (psi)		Shear Strength Parameters			
	Range	Average	Range	Average	C_{Peak} (psi)	ϕ_{Peak} (psi)	$C_{Residual}$ (psi)	$\phi_{Residual}$ (psi)
Sandstone	15,897.5 - 29,396.2	22,646.0	1,449.0 – 3,368.0	2,408.0	166 – 286	12 – 25	109 – 215	8 - 25
Siltstone	14,493.5 – 21,576.9	18,034.0	650 – 1,521.0	1,085.0	0 - 171	21 – 31	0	21 - 27
Siltstone w/ interbedded claystone	4,582.8 – 8,316.9	6,451.4	500 – 1,394	947.0	240	11	136	11
Claystone	NT	NT	NT	NT	86 - 240	21 – 22	0 – 136	11 - 21

Table 5: Index properties of rock units comprising the landslide mass.

Lithology	Dry Density (pcf)		Aborption (%)	Slake Durability Index Id^2 (%)
	Range	Average		
sandstone	166.6-174.6	170.0	0.9-1.5	63.5-92.1
Siltstone	171.7-174.8	173.2	1.9-2.2	92.7-95.9
Siltstone w/ interbedded claystone	174.4-176.6	175.5	1.3-1.9	36.9-95.7
claystone	NT	NT	NT	25.0-92.8

Stability Analysis

Because of the planar nature of the failure surface indicated by the borehole data, a plane failure (sliding block) analysis was conducted to analyze the stability of the slope according to the procedure outlined in Hoek and Bray (1981). The following equation was used to compute the factor of safety (F.S.) against sliding:

$$F.S. = [cA + (W\cos\Psi p - U - V\sin\Psi p) \tan\phi)/ (W\sin\Psi p + V\cos\Psi p)]$$

Where:

c = cohesion (psf)

A = area of sliding (ft^2)

W = weight of block (lbs)

Ψp = angle of failure plane (degrees)

U = uplift pressure (lbs)

V = lateral pressure due to water (lbs)

Φ = friction angle (degrees)

For the purpose of analysis, the landslide was treated as one continuous block from the crest to the toe. Figure 7 shows the slope geometry for the cross-section used in the global stability analyses. The primary failure plane angle (ψ_p) was determined to be 16 degrees. The tension crack at the crest of the slope was assumed to be vertical. The cross-section shown in Figure 7 was analyzed for stability under varying drainage conditions including a dry slope and maximum pore pressure along the failure plane. The maximum pore water pressure along the failure surface was simulated by incorporating the piezometric data.

The stability analysis was conducted using different shear strength parameters. The analysis was first conducted using the residual strength parameters (c = 0 psf and ϕ = 21 degrees) of the weathered claystone as determined by the direct shear test. The results showed that the slope was stable (F.S.>1.0) under both dry and maximum pore pressure conditions. Since, the slope at the New Baltimore Landslide site has already failed and the slide continues to move throughout the year (under all drainage conditions), it was concluded that the friction angle for the weathered claystone used for stability analysis was high and was not representative of the field conditions. Therefore, a back analysis was conducted to determine the friction angle value for c = 0 psf and a safety factor equal to 1.0 under dry slope conditions. The back-calculated friction angle was determined to be 16 degrees. A second stability analysis was then conducted using c = 0 and the back-calculated value of friction angle of 16. Table 5 shows the results of stability analyses under varying drainage conditions with residual and back-calculated shear strength parameters. The back-calculated value of friction angle is in agreement with the commonly used friction angle values 12 to 16 degrees for similar claystones in southwestern Pennsylvania (Hamel, 1969).

The New Baltimore Landslide has been an active slide since the 1940's. Due to repeated shearing that has occurred along the primary failure plane, the lowest shear strength parameters are the most representative of the field conditions. With a c = 0 psf and ϕ = 16 degrees, the analysis produces an unstable slope under dry and maximum pore pressure conditions, which suggests slope movement throughout the year. The small difference in the factor of safety values for the dry and maximum pore pressure conditions is attributed to the relatively small value of maximum pore pressure compared to the dry weight of the large landslide mass. This is consistent with the slope monitoring data where periodic movement was recorded during a 1.5 year period.

Table 5: Results of plane failure analyses using residual and back-calculated strength parameters.

Drainage Conditions	F.S.		F.S.	
	ϕ=21	c=0	ϕ=16	c=0
Dry Slope	1.3		1.0	
Max. Pore Pressure along Failure Plane	1.2		0.9	

Remediation Alternatives

The New Baltimore Landslide is a very large failure that occupies more than 30 acres and poses a threat to the Pennsylvania Turnpike. Due to the nature and size of this slide, a variety of reinforcement, stabilization, and protective measures were evaluated as possible remediation alternatives. The alternatives were analyzed to evaluate their effectiveness in stabilizing the riving forces behind the lower section of the New Baltimore Landslide. The analyses were conducted to obtain a factor of safety of 1.5, which is generally considered adequate for permanent slopes (Pennsylvania Department of Transportation, 1993). A cost analysis was conducted to determine the most cost effective and feasible alternative. Table 6 provides the results of cost analysis along with a brief description and the advantages and disadvantages of each alternative as well as the results of this analysis.   The New Baltimore Landslide has been a slow moving landslide for the last 64 years. The slide has not caused any major accidents or deaths although the potential for such a hazard does exist. The slope can be maintained and monitored at minimal cost compared to the costs of remediation alternatives 1, 2, and 3.

Table 6: Cost analysis of potential remedial measures for the New Baltimore Landslide.

Remediation Alternative	Description	Advantages	Disadvantages	Estimated Cost
Rock Dowels	2.5 in diameter Ultimate stress=150 ksi Number of dowels =2102 Spacing = 7.3 ft	Requires no additional right of way (ROW) Minimal delay of traffic Achieved design factor of safety	Requires shoulder closure	$6,077,237.24
Drilled Piles	HP 12X84 Ultimate stress= 106 ksi Number of piles = 3000 Spacing = 5.6 ft	Requires no additional ROW Minimal delay of traffic Achieved design factor of safety	Requires shoulder closure Requires a large number of piles	$11,251,600.00
Regradation of Slope to A. 3H:1V B. 3.5H:1V C. 4H:1V	A. Removal of $514{,}007$ yd^3 of slide mass B. Removal of $855{,}349$ yd^3 of slide mass C. Removal of $1{,}324{,}046$ yd^3 of slide mass	Removes slide mass Design factor of safety not achieved Complete removal of slide including failure plane	Requires additional ROW Requires lane closure or lane shift for blasting - delay of traffic Requires a waste area	A. $5,016,177.50 B. $7,491,149.60 C. $14,288,841.70
Provision of Catchment Ditch and Protective Barrier	Cutting existing slope back to a 1H:1V Removal of $7{,}708$ yd^3 of slide mass Installation of concrete barrier for rockfall protection	Requires no additional ROW Provides rockfall protection Provides access for rockfall cleanup Less expensive compared to other alternatives	Requires lane closure/delay of traffic Requires a waste area Requires slope Instrumentation monitoring Does not improve global stability Requires slope Instrumentation warning system	$ 114,747.50
Maintenance and Monitoring	Annual rockfall clean up and shoulder repair Install additional slope instrumentation	Allows time to address needs for further investigation Least expensive in both short and long terms	Global stability is not addressed	$ 4,268.04/ year

Conclusions

Based upon the results of this investigation, the following conclusions are drawn:

1. The New Baltimore Landslide is an old, large, translational, and slow moving slide that covers more than 30 acres and extends on both sides of the Pennsylvania Turnpike. Localized rotational slides, rockfalls, and flow type movements are present throughout the slide mass that indicates its complex nature.

2. Subsurface investigations, slope inclinometers, and time domain reflectometry (TDR) cables indicate that the primary failure plane is located along the bedding plane within a weak claystone unit at an approximate depth of 10 ft (3 m) in the toe area (along east-bound lane of I-76) and 75.5 ft (23.0 meters) near the crest of the slope. The material along the failure plane is a highly weathered ($Id_2 \leq 37\%$), soil like silty claystone (ML-CL) of low shear strength.

3. The rate of movement of the slide ranges from 3.6 to 5.1 inches (9.1 to 13.1 cm) per year as indicated by the slope inclinometers. The maximum movement and the associated higher pore pressures occur in the late winter and early spring months.

4. The stability analysis, using a plane failure scenario, indicates a factor of safety of 1.0 or less for both dry and maximum pore pressure conditions.

5. The New Baltimore Landslide poses a continual threat to the Pennsylvania Turnpike. The common occurrences of rock falls, pavement heaving, and potential for a catastrophic failure make this landslide a serious hazard. The Pennsylvania Turnpike Commission continues to monitor the slide and maintain the roadway. However, remedial measures would be needed to stabilize the slope and minimize the risk of a large failure.

Acknowledgments

References

American Society for Testing and Materials, 1996, *Soil and Rock*: Annual Book of ASTM Standards, Vol. 4.08, Section 4, Philadelphia, PA, 1000 p.

Flint, N., 1965, *Geologic Map of Southern Somerset County, Pennsylvania*; Report C56A: Pennsylvania Geologic Survey, Harrisburg, PA, pp. 20-21.

Geyer, A. R. and Wilshusen, J. P., 1982, *Engineering Characteristics of the Rocks of Pennsylvania*: Pennsylvania Geological Survey, Harrisburg, PA, pp. 14, 17-20, and 59.

Hamel, J. V. and Flint, N. K, 1969, *Analysis and Design of Highway Cuts in Rock: A Slope Stability Study on Interstate Routes 279 and 79 near Pittsburgh, Pennsylvania*: Unpublished Ph.D. Dissertation, Department of Civil Engineering, University of Pittsburgh, Pittsburgh, PA, pp. 99-108.

Henderson, C., 2000, personal communication, American Geotechnical and Environmental Services, Inc., 440 Old Pond Road, Suite 301, Bridgeville, PA 15017.

Hoek, E. and Bray, J. W., 1981, *Rock Slope Engineering*: Institution of Mining and Metallurgy, London, 358 p.

McElroy, T. A., 2001*, Groundwater Resources of Somerset County; Pennsylvania*, CD-ROM: Open-File Report 2000-2002: Pennsylvania Geologic Survey, Harrisonburg, PA, pp. 33-42, 107-113.

Pennsylvania Department of Transportation, 1993, *Design Manual # 4*: Harrisonburg, PA, pp. B4-B18.

Pennsylvania Turnpike Commission (PTC), 2003, Pennsylvania Turnpike Maintenance Records: Work Order Detail Reports; PTC Western Regional Office, New Stanton, PA.

Washington SR 20 Rock Avalanche:
Monitoring, Characterization, and Analysis

R. Burk (URS, bob_burk@urscorp.com), N. Norrish (Wyllie & Norrish Rock Engineers),
S. Lowell (Washington State Department of Transportation – WSDOT), M. Molinari
(URS), R. LaHusen (U S Geological Survey – USGS), J. Schick (URS), B. Strickler
(URS), B. Duevel (URS) and M. McCabe (URS)

> URS Corporation, 1501 4th Avenue, Suite 1400, Seattle, WA 98101-1616
> Wyllie & Norrish Rock Engineers, 17918 NE 27th Street, Redmond, WA 98052
> WSDOT, PO Box 167, Olympia, WA 98504
> USGS, Cascade Volcano Observatory, 1300 SE Cardinal Court, Building 10,
> Suite 100 Vancouver, WA 98683-9589

Introduction

On November 9, 2003 a major rock avalanche occurred near Newhalem, Washington at Milepost 121.5 on State Route 20 (SR 20), the North Cascades Highway. Avalanche debris traveled from a source area over 2,000 feet in elevation above the highway down Falls Creek, Falls Creek chute and Afternoon Creek (Figure 1). Most of the debris, approximately 1,000,000+ cubic yards, was deposited in Afternoon Creek and did not reach SR 20. Lesser amounts of rockfall debris traveled down Falls Creek and Falls Creek chute forcing highway closure.

Following the rock avalanche, URS and Wyllie & Norrish Rock Engineers working with Washington State Department of Transportation (WSDOT) undertook a monitoring and investigation program. Initial work focussed on emergency activities and monitoring the source area of the rock avalanche to understand the nature of the hazards and to ensure that appropriate action was being recommended to protect the public.
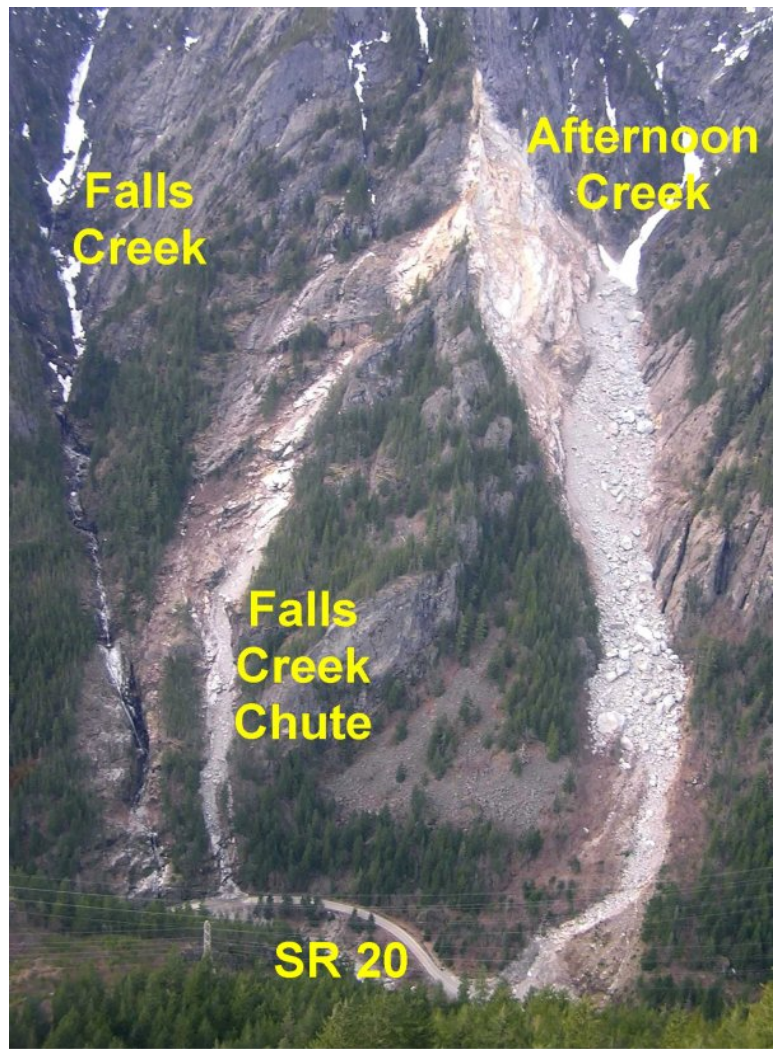

Figure 1. Overview of the slide area.

Initial concerns included:

> ➢ Remobilization of the rock avalanche debris entrained along Falls Creek and Falls Creek Chute.
> ➢ Risk of additional rock avalanches, especially if there was headward migration of the slide scarp towards Falls Creek
> ➢ Blockage of the Skagit River because of remobilization of the rock avalanche debris in Afternoon Creek.

A major unknown was whether slope failure was the first phase of activity of a larger event or was the primary event. The risk to the public prompted an emergency response by WSDOT and other agencies responsible for public safety.

A slope-monitoring program initially included visual observations, measurement of Skagit River water levels using a pressure transducer, collection of rainfall data, and survey prism monitoring. Later, a geophone and an automatic rain gage were placed in Afternoon Creek and geophones, extensometers and tiltmeters were placed in the source area of the rock avalanche. Data from all of these instruments were telemetered to an internet connection.

As the intensity of the emergency response abated geotechnical site characterization activities were undertaken to assist in the development of mitigation measures. Three primary types of mitigation efforts were considered: removal of the hazard, slope reinforcement, and protection of the highway.

Removal of the hazard might have included removal of blocks of rock that could potentially fall and reach the highway. This approach was rejected because of the difficulty of working high on the slope, some 2,000 feet above the highway, and the risk of creating progressive failure scarps that would further destabilize the mountainside and lead to a more severe hazard. Reinforcement on many rock slopes includes use of rock bolts and other mechanical means to increase rock mass strength. In this case the blocks are so large, and the construction access so difficult, that this measure was not considered feasible. This left protection of the roadway as the preferred mitigation measure. Six options to protect the roadway were developed

This paper describes the monitoring effort, site characterization, mitigation measures, discussion of rockfall modeling, and embayment slope design and conclusions.

Site Characterization

Monitoring

Given the potential consequences of additional activity, multiple methods of monitoring were required. Visual monitoring was begun immediately. Placement of survey prisms around the source area and the rock avalanche debris to allow monitoring of any continuing movement was accomplished as soon as practical. Prisms on the upper portions of the slope were placed using ropes or from a basket suspended on a helicopter

long line. Weather
conditions made prism
placement difficult,
however, before November
23, 2003 14 prisms and 2
backsight locations were
placed (Figure 2).

The URS/WSDOT Team
assisted the U S Geological
Survey (USGS) in setting up
a geophone in the Afternoon
Creek drainage with a
telemetered connection to
Seattle City Light (SCL)
and later to a satellite up-
link. This geophone was
intended to monitor any
large-scale movement of the
rock avalanche debris in
Afternoon Creek.

The USGS Water Resources Division set up a pressure
transducer in the Skagit River upstream from the mouth of
Afternoon Creek. Water levels above those associated with
spilling at Gorge Dam would be an indicator of blockage of
the Skagit River.
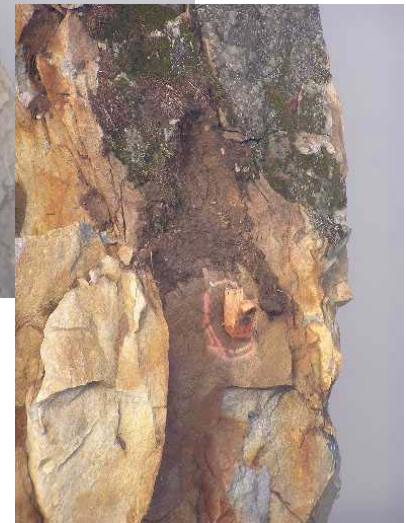
Figure 2 Prism A-4

Prism monitoring continued on a daily basis through the middle of January 2004.
Monitoring activities established that most of the rock slopes and the avalanche debris
were not moving in the time frame of the monitoring. However, movement observed on
one survey point (A11) allowed prediction of a large rockfall event that occurred on
December 19-20, 2003 as described below in the section on Subsequent Rock Fall and
Rock Avalanche Events.

Afternoon Creek Rock Avalanche Debris Stability

To assess the stability of the of the Afternoon Creek rock avalanche debris, dye trace
work, LIDAR/photogrammetric comparisons and computer modeling techniques were
used. Initial reports indicated that water was building up in the Afternoon Creek rock
avalanche debris. Inert, environmentally safe dyes were injected into Afternoon Creek to
help assess the hydraulic conductivity of this debris. Dye was placed at the head of the
slide debris and at the waterfall three-quarters down the slide using a helicopter.

LiDAR (light detection and ranging) data were collected on December 18, 2003 by Terra
Remote Surveys. These data allowed topographic maps and orthophotographs to be
prepared in early January 2004. LiDAR data allowed calculation of the amount of rock

avalanche debris in Afternoon Creek, measurement of the orientation of discontinuities, and provided a base map for planning mitigation measures.

Research into debris flows in British Columbia (Hungr et al, 1984,and Hungr, 1995; Hungr and Evans, 1996) have produced dynamic models in which the debris can be treated as a frictional, rheological or combination material to estimate the runout performance. DAN W a commercially available software package employs a fluid dynamic model based on the numerical solution of the St. Venant's equation of unsteady open-channel flow (Hungr, 1995), extended to account for mass changes during the flow process. The software allows the slide mass to be divided into a number of elements, and the forces on and displacements of these elements are estimated at successive intervals of time until displacements subside. The slope of the bed and the width and shape of the runout channel can be incorporated into the analysis, but the occurrence of sharp changes in channel direction cannot. The accuracy of the software has been checked by back analysis of various laboratory and full-scale debris flow events. However, calibration to local events in the region of interest is strongly recommended by the authors.

The software was used to examine the potential runout distances and possible risk to users of SR 20 if the debris in Afternoon Creek gorge was mobilized. The first step in the analysis was to select a material property model and associated debris parameters that would provide an accurate prediction of the initial rock avalanche runout. Selection of the frictional model, with parameters that include friction angle and pore pressure ratio, typically resulted in runout distances that far exceeded the observed distance. However, the Bingham rheologic model with a shear strength of 500 kPa and a viscosity of 15 kPa-seconds produced a good match between prediction and actual runout.

Next, these best-match parameters were used to assess the runout of the re-mobilized debris. If the base material was treated as a frictional material with a friction angle of 32 degrees and a near-100-year rainfall event pore pressure ratio of 0.25, the analysis predicts that the re-mobilized debris will travel to and a short distance down the Skagit River bed. For a lower pore pressure ratio of 0.10, or for a higher friction angle of 38 degrees for the bed material, the analysis predicts that the debris will not reach SR-20. The rates of displacement predicted by the software are relatively high, i.e. in the range from approximately10 to 20 meters per second. Later, drilling through the debris suggested that pore water values were expected to remain low even during high rainfall events and friction angles were estimated at greater than 38 degrees.

Subsequent Rockfall and Rock Avalanche Events

Subsequent to the initial slide on November 9th, rock debris was mobilized in Falls Creek on November 18th in an event that blocked SR-20. This event was associated with more than six inches of rain that fell between November 15 and November 18, 2003.
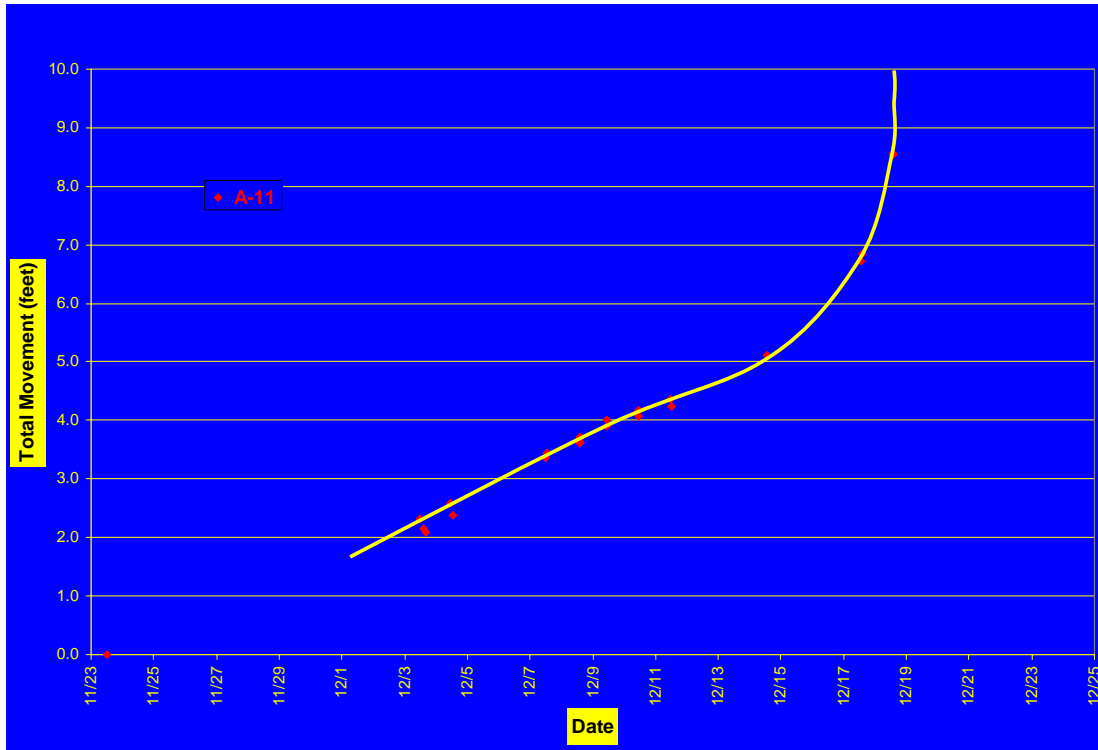
Figure 3. Total movement on survey prism A-11.

Minor rockfall events occurred on December 17 and 18th in Afternoon Creek, followed by an event in the early morning on December 19th that involved tens of thousands of cubic yards of material. Another major event occurred on December 20th while Norm Norrish was working at the survey shed. The event on December 19th was predicted by the URS Team, based on the increase in rockfall activity and the exponential increase in movement observed on survey point A11 (Figure 3). The rockfall was correctly predicted to fall into Afternoon Creek. The event on the 20th was heard, but clouds obscured the view.
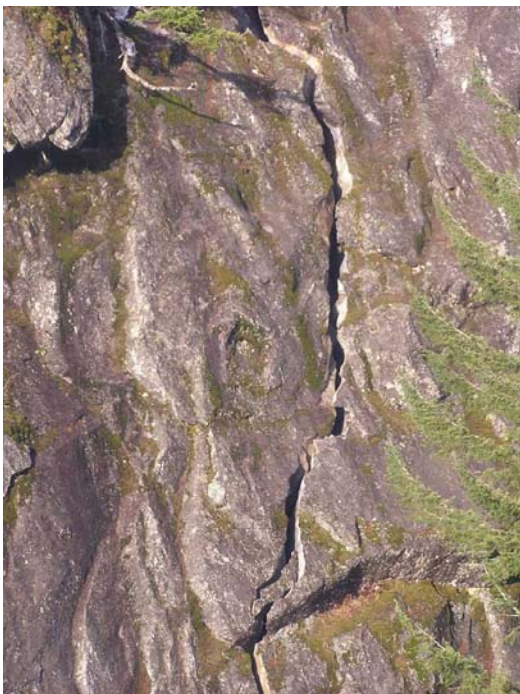
After the initial major slide on November 9th a new crack in intact rock developed below and to the west of the A4 block was observed. After the December the 19th and 20th event, the crack widened and increased in length (Figure 4).

Figure 4. Crack in previously intact rock up to approximately 1.5 feet wide adjacent to the main rock avalanche source area.

General Geology

The North Cascades represent a complex mosaic of crustal blocks (terranes) that have their origin offshore as sediments and volcanic rocks on the sea floor and in island arcs. These terranes were accreted piece by piece to the North American continent approximately 90 million years ago with associated crustal thickening and metamorphism. Much of the rock in the metamorphic core of the North Cascades began as molten rock that intruded the area just before or during this metamorphism. The rocks in the SR 20 project area are considered part of the Skagit Gneiss Complex (Haugerud, et al, 1991; Misch, 1966), one of the units in the metamorphic core. The Skagit Gneiss exhibits banding (metamorphic foliation and/or lineation), and the alignment of minerals indicates that the rocks, both the original material of the terranes and the invading plutons were being deformed as they were recrystallized (USGS, 2004). The bedrock in the SR 20 project area consists of an orthogneiss.

From an engineering viewpoint this geologic history provides the background to help understand the mechanisms involved in the slope failure that occurred on November 9, 2003. Because most of the rock in the project area is an orthogneiss it behaves mechanically in a relatively isotropic fashion. In many metamorphic terranes weaker metamorphic rocks such as schists take up strain. However, in this case the monolithologic nature of the rock, its strength (ISRM, strong to very strong), and the multiple periods of deformation combined to form discontinuities with multiple orientations.

Geologic Hazards

Geologic hazards that may influence SR 20 in the area of Falls Creek and Falls Creek chute include: Rockfall, Rock Avalanches, Debris Flows, Snow Avalanches. Steep (>30 degree) slopes over much of the drainage basin of Falls Creek and Falls Creek chute and direct pathways from high on the slope to SR 20 make rockfall a continuing geologic hazard. Although this hazard has always been present in this area in post-glacial time, there may be increased incidence of rockfall in the future, if progressive failures at the head of the main Afternoon Creek scarp continue to migrate to the west. Should this migration continue to occur it may subject the Falls Creek area to major rock avalanches.

When rockfall and/or rock avalanche debris accumulates on steep slopes it can under certain circumstances saturate and form debris flows. Such a situation occurred on November 19, 2003 in the Falls Creek chute, causing SR 20 to be closed. The total amount of loose rock and soil debris in the Falls Creek chute is roughly estimated as 50,000 to 75,000 cubic yards between SR 20 and elevation 1,300 feet. All of this material is overlying bedrock and over time is expected to be evacuated from the chute as part of debris flows or other similar mass wasting events.

Snow avalanches have historically traveled down Falls Creek and Falls Creek chute with an estimated recurrence interval of approximately 30 years (URS, 2004). Wet snow avalanches, common in this area, entrain soil and rock debris. Because of the additional

rock avalanche debris in the Falls Creek chute related to the November 9, 2003 event, the amount of rock and soil debris entrained in future snow avalanches will increase. Blocks as large as 30 feet in length can be transported by snow avalanches in Afternoon Creek (URS, 2004).

Origin of the November 9, 2003 Rock Avalanche Event

Slope failures frequently have multiple causes and the November 9, 2003 event is no exception. Topography, geologic structure, lithology, rock mass degradation, and groundwater all contributed to this failure. Pre-existing, glacially oversteepened slopes were located along the free face of a ridge that was freed from glacial support approximately 10-12,000 years BP. Multiple crosscutting faults were present along with a complex discontinuity network exploited by weathering processes. Late-glacial post-glacial weathering resulted in reduced discontinuity wall strength. Clay minerals produced by weathering of discontinuity walls and in fault gouge decreased rock mass strength and created a local aquitard. High water conditions created by rainfall events in October 2003 caused groundwater damming that further decreased rock mass strength. Because of the complex network of faults and discontinuities there does not appear to be a single kinematic explanation for the failure. It appears likely that toe failure during high water conditions caused the slope to progressively unravel along multiple fault and discontinuity surfaces.

An undated image taken prior to November 9, 2003 indicates recent slope failure activity based on vegetation, weathering indicators, and numerous boulders in the creek bottom that have apparently been transported by rockfall activity. The Afternoon Creek fan is laterally extensive and fan deposits were encountered to a depth of over 200 feet in a borehole that penetrated the Afternoon Creek rock avalanche debris (URS, 2004). At least two older rock avalanche deposits were identified in the fan area, near SR 20. All of these factors suggest ongoing post-glacial instability in the Afternoon Creek drainage.

Mitigation Measures

Overall hazard mitigation was approached by considering Removal, Reinforcement and Highway Protection. Removal of the hazard has a number of issues including access and safety issues for construction, the scale of removal that may be necessary, and the probability of success. Reinforcement options address many rock mass stability problems; however the scale of this site makes these options unfeasible. Protection, by moving the road or developing cover over the road was selected as most likely to provide cost-effective protection for SR-20. Under the general heading of protective measures three primary options were evaluated: Option 1 provides an embayment area for rockfall at Falls Creek, the area where SR 20 is most likely to receive direct impact from rockfall. This embayment would prevent most reasonably foreseeable rockfall events from reaching the road. Option 2 is a rock shed that would allow any rockfall, rock avalanche, snow avalanche, or debris flow events to pass over the road and into the Skagit channel. Option 3 involves moving SR 20 onto an embankment built in the Skagit channel, creating a basin to contain any mass wasting events.
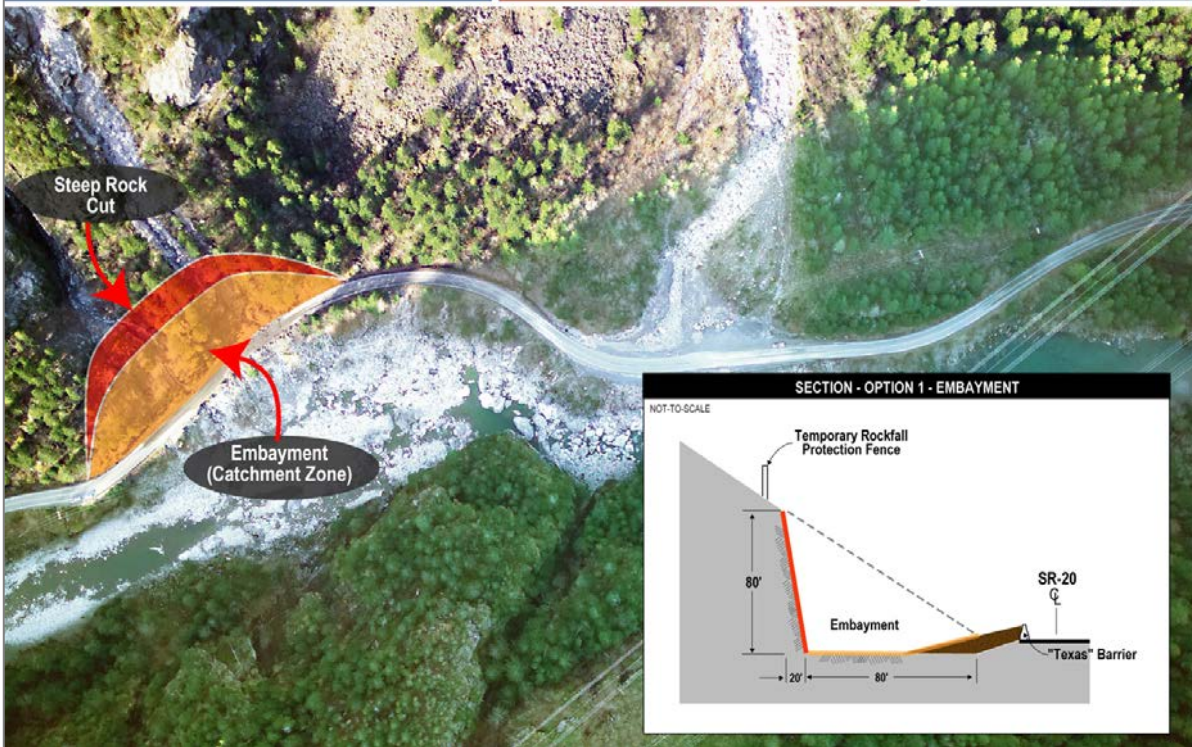
Figure 5

Figure 6
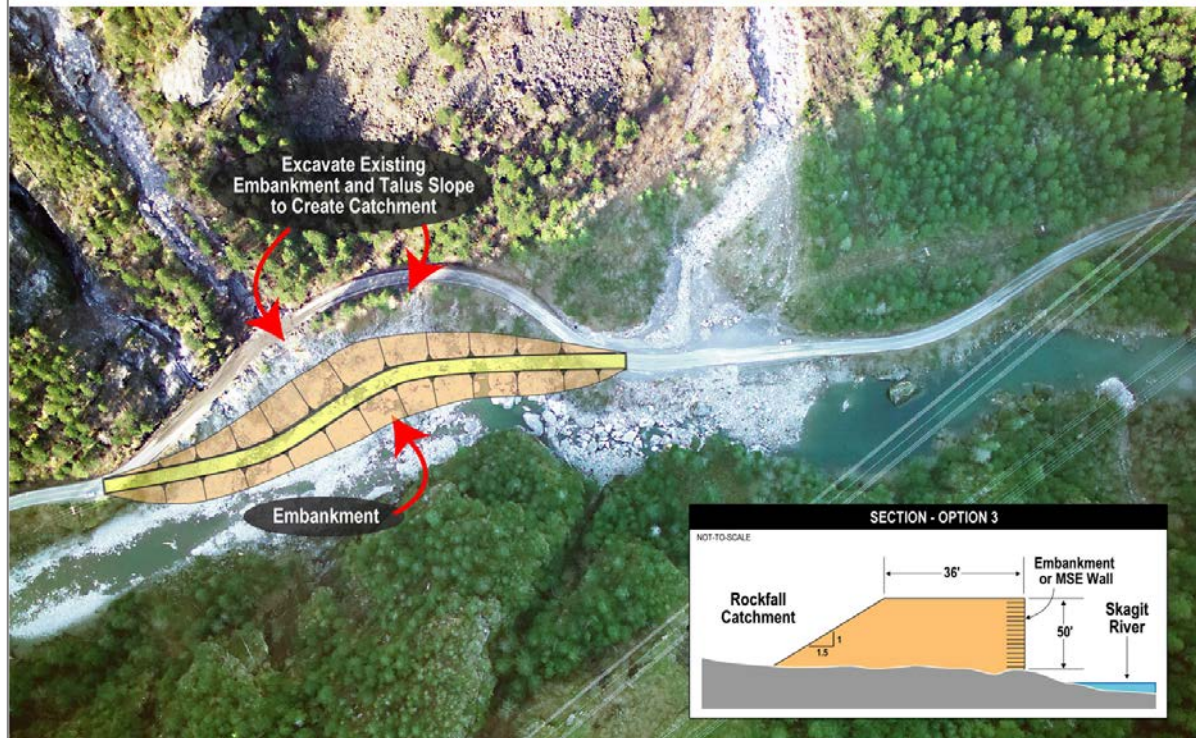
Figure 7

The geologic field reconnaissance work and the interpretation of aerial imagery assisted in the delineation of surficial deposits including colluvium, alluvium, and rock avalanche deposits. This work provided the basis for determining the surface characteristics of the materials for rockfall modeling and the areas where surficial deposits may need to be removed as part of rock cut development. LiDAR data collected by Terra Remote Surveys (Victoria, B.C.) provided a base for plotting field results, analysis of rockfall paths and for conceptual engineering design work. Rockfall modeling was performed using Colorado Rockfall Simulation Program, Version 4.0 (Jones, et al, 2000).

Structural mapping was focused on providing scan line and window surveys that measured discontinuity orientation, persistence, aperture, roughness, filling and wall strength. This information was combined with discontinuity measurements from borehole imaging and used in making recommendations for the proposed rock cut at the back of the embayment.

Four boreholes were drilled in the area of the proposed rock cut to investigate the depth of surficial deposits and to assess rock quality. Borehole imaging was performed using the CRUX Oriented Borehole Logging system (COBL). Borehole imaging uses an oriented downhole camera to provide a record of borehole conditions and allows discontinuities to be located and their orientation defined.

Option 1 – Design Support

Structural Mapping

Structural mapping was performed using window and scan line survey techniques. Four scan lines and three window surveys were completed as part of this mapping effort and a total of 313 features were catalogued. The work was completed in general accordance with ISRM Suggested Methods for Rock Characterization, Testing and Monitoring (Brown, 1981). Information regarding the bedrock structural fabric was incorporated into the kinematic analysis and rock mass stability assessment.

Borehole Imaging

Discontinuities observed in the COBL videos were initially mapped and their orientations calculated by Crux Subsurface. URS reviewed this analysis for completeness and further characterized the discontinuities based on the downhole photographic record and the borehole logs. This review identified four different features including mineral banding/foliation, joints, healed joints, and features that could not be distinguished as either banding or joints.

The structural fabric presented on the stereographic projections is generally consistent for three of the four boreholes. The structural fabric recorded in the record for B-2 is distinctly different from the other three and the surface mapping datasets. The dataset for this borehole has an apparent lack of distinct structural trends. The B-2 borehole described the rock core as highly fractured with hydrothermal alteration along the fractures, indicating that the borehole was drilled within a possible shear zone or fault.
Further review of the COBL photographs for B-2 suggests that a greater proportion of high angle joints were encountered in this borehole compared to the adjacent borehole B-4, located approximately 100 feet downslope. This indicates that the inferred fault structure proximal to B-2 is steeply dipping because a shallow dipping feature would have most likely also been encountered in the second borehole.

Rock Strength Testing

Point-load testing was conducted along with estimates of rock strength by field personnel. Laboratory testing was performed on core samples selected from each of the boreholes. Sample selection attempted to obtain a suite representative of typical rock mass strength for the orthogneiss. For comparative purposes to UCS results, the point load strength values were converted to equivalent UCS values using a correlation coefficient of 24 (Goodman, 1980) and a core size correction factor.

The orthogneiss based on the test results was classified as "R4-strong rock" in accordance with ISRM (Brown, 1981). The range of tested strength was from 3,500 psi (R3 - medium strong rock) to 21,400 psi (R5 - very strong rock). The strength testing was used as collateral data for slope stability analyses.

Rockfall Modeling

Methodology

The objective of rockfall modeling is to predict the trajectory and energy of discrete rock particles ("boulders") at points of interest along a two-dimensional slope profile. Although the algorithms to calculate these parameters are well developed, it remains that the simulation of rockfall using computer codes is an engineering challenge. This is because of the complex interaction of multiple variables that in many cases are empirically derived rather than rigorously measured. The simulations thus provide "probable" results that guide engineering judgment rather than absolute, deterministic results. Application of models can be made more rigorous through a site specific calibration process wherein documented rockfall events are numerically replicated.

A three-part study was performed using the Colorado Rockfall Simulation Program, (CRSP) Version 4.0 (Jones, et al, 2000) to predict the behavior of rockfalls originating from the upper rock slope near the scarp of the November 9, 2003 rock avalanche. The first part of the analysis attempted to analytically recreate the November 9, 2003 rockfall event thereby calibrating the model parameters for the second part of the analysis in which rockfall mitigation scenarios were analyzed. The third aspect of the modeling dealt with the reduction of rockfall risk during construction activities for an embayment excavated near Falls Creek.

Derivation and Calibration of Model

The simulation program required development of the following input parameters:

Slope Profile: A clearly evident rockfall path extends from a source area near elevation 2500 feet leading down Falls Creek Chute eventually to the SR 20 alignment some 2000 feet below. Using the LiDAR generated topographic maps, a profile was developed down the centerline of the sinuous path, with stationing assigned from the summit and increasing downslope to the south. The model did not incorporate the three-dimensional aspects of this path. It is noted that the inclination of the profile decreases from approximately 60° at the summit to 36° at the toe just above SR 20.

Rockfall Source: Based on aerial mapping and geologic hazard assessment, the conclusion was reached that further retrogression of the head scarp toward the west increased the probability of rockfall events traversing the Falls Creek chute rather than Afternoon Creek. Accordingly, the source area for the modeling was conservatively assigned to the vertical interval between elevations 2250 and 2680 feet

Rock Size: The rockfall associated with the November 9, 2003 event provided information on which to base an assessment of boulder size likely to reach SR 20 in the future. As shown, multiple intact fragments of the strong orthogneiss in the three to five-foot size range were present on the highway grade after the rockfall. In addition, one "mega-boulder" with a size of 8 x 8 x 14 feet reached SR 20 during this event.

Figure 8. Boulders on SR 20, November 9, 2003.

Rock Shape: Although the November 9, 2003 event yielded subangular boulders (Figure 8), for simulation purposes generally spherical shapes were assumed. This was regarded as a conservative assumption because of the greater ease of rolling. Consequently, for modeling purposes the following range of boulder sizes and shapes were considered:

Shape	Size	Weight[1] (tons)
Spherical	2.5-foot diameter	0.7
Spherical	5-foot diameter	5.4
Spherical	10-foot diameter	43
Cylindrical	8 x 8 x 14 feet	58

Notes: [1]. *Boulder weight is based on unit weight of 165 pcf.*

Initial Rock Velocity: For all simulations an initial velocity of $V_h = 1$ ft/sec and $V_v = - 1$ ft/sec was assumed consistent the default option in the CRSP program. This initial velocity would be consistent with a mild triggering event.

Rock Slope Roughness: This parameter has the greatest influence on the trajectory of rockfall events for a given slope profile. The LiDAR data facilitated incorporation of a high degree of slope roughness detail. This was accomplished by subdividing the overall profile into fourteen station intervals for assignment of appropriate material properties including roughness. For each of the fourteen slope intervals, the angular departures from the mean inclination were calculated over incremental lengths corresponding to the boulder sizes. Based on the distributions of these angular departures (mean and standard deviation) and on engineering judgment, roughness values were assigned to each station interval. The table below includes the roughness values assigned by slope interval and as a function of boulder size.

Interval No.	Restitution Coefficients		Profile Limits (feet)		Surface Material	Roughness Values "S" by Boulder Size (feet)		
	R_t	R_n	Start	End		2.5 ft	5 ft	10 ft
1	0.80	0.25	0	320	Rock - irregular, rough	1.0	1.25	2.0
2	0.65	0.12	320	360	Soil, firm	0.35	0.5	1.0
3	0.85	0.30	360	600	Rock - smooth, planar	0.35	0.5	1.0
4	0.80	0.25	600	880	Rock - irregular, rough	1.0	1.25	2.0
5	0.85	0.30	880	1020	Rock - smooth, planar	0.65	1.0	1.5
6	0.80	0.25	1020	1310	Rock - irregular, rough	1.0	1.25	2.0
7	0.75	0.20	1310	1500	Boulder field	0.65	1.0	1.5
8	0.85	0.30	1500	1550	Rock - smooth, planar	0.65	1.0	1.5
9	0.75	0.20	1550	1800	Boulder field	0.65	1.0	1.5
10	0.75	0.20	1800	2240	Boulder field	0.65	1.0	1.5
11	0.75	0.20	2240	2270	Asphalt (existing alignment)	0.4	0.62	1.0
12	0.65	0.12	2270	2360	Talus - road bank	0.35	0.5	1.0
13	0.75	0.20	2360	2650	Boulder field (Skagit channel)	0.65	1.0	1.5
14	0.80	0.25	2650	2700	Rock - irregular, rough	0.65	1.0	1.5

Coefficients of normal and tangential restitution: The manual for CRSP provides guidance for typical values to be used for the coefficients of normal and tangential restitution. As a starting point, values for the fourteen intervals were assigned based on the midpoints of the ranges suggested by CRSP. These values were subsequently down-rated to the values shown in the table above based on initial model calibration runs as discussed below.

Having developed the model input parameters, two rockfall events were used to calibrate the model. The first was the November 9, 2003 event wherein the following observations were deemed noteworthy:

> ➢ Few rock fragments came to rest beyond the center of the Skagit River channel
> ➢ The majority of the rockfall fragments came to rest on the existing SR 20 alignment .
> ➢ Multiple intact fragments on SR 20 were in the three to five-foot size range.

The second calibration event was the hand scaling that was performed in conjunction with installation of monitoring equipment on the mountainside. During scaling of the slope area that coincided with the potential rockfall source area, boulders in the two to five-foot size range were dislodged. Some of these boulders traversed to the lower slope near elevation 1,000 but did not reach SR 20.

On the basis of these two events, the restitution parameters were down-rated to the low end of the recommended ranges to account for greater energy loss at each impact along the rockfall path. The asphalt surface was further down-rated to reconcile with the observation that the boulder impacts punctured the surface. Following these modifications, the resultant model still predicted the boulders to have greater runout distances than observed. For example, the model predicted that between 60 and 90 percent of spherical boulders would traverse beyond the crest of the highway bank above the Skagit Channel and that there was only a four percent probability that a cylindrical boulder in the 58-ton category would stop on the SR 20 grade. Conversely, the model replicated the field observation that no rockfall fragments came to rest beyond the center of the river channel. The conclusion reached from the calibration exercise was that the model was appropriately conservative for the design of mitigation alternatives.

Application to Embayment Design

The "calibrated" CRSP model was applied to a variety of geometries for an embayment at the toe of the slope at the inboard shoulder of SR 20. The geometric variables for the embayment included:

> ➢ Embayment width (measured from hinge point of a new rock cut to the shoulder of the highway).
> ➢ Embayment elevation (measured relative to the elevation of the highway and facilitated through either raising the highway grade or lowering the embayment grade).
> ➢ Slope inclination for embayment cut (steep cuts are preferred for rockfall control).
> ➢ Incorporation of barriers (berms or rockfall control fences) between the embayment and the highway.

The CRSP parameters for the embayment cut slope and the embayment base were assigned assuming high quality, controlled blasting for the rock cut to minimize surface roughness and incorporation of an energy-absorbing granular blanket on the floor of the embayment.

Results of the mitigation analyses are presented below. Note that smallest boulder (2.5 feet) was determined to be inconsequential to the embayment design and was therefore not included in these analyses.

| EMBAY WIDTH (ft) | SLOPE HINGE POINT ELEVATION * | BARRIER TYPE | BARRIER LOCATION | PREDICTED EFFECTIVENESS | | | REMARKS |
				5 ft dia 5.4 ton	10 ft dia 43 ton	8x8x14ft 58 ton	
90	Road less 10 ft	Fence / 12 ft high	Shoulder	>99%	96.8%	88.0%	Base case - acceptable
90	Road less 10 ft	Berm / 20 ft high	20 ft left of shoulder	97.5%	94.6%	88.7%	Acceptable
90	Road less 20 ft	Berm / 10 ft high & 10 ft rock wall	20 ft left of shoulder	93.7%	88.9%	80.4%	Marginal
75	Road less 8 ft	Fence / 12 ft high	Shoulder	91.1%	74.7%	55.1%	Unacceptable
75	Road less 8 ft	Raise grade 10 ft	Shoulder	95.6%	92.9%	86.4%	Acceptable
75	Road less 8 ft	Berm / 20 ft high	20 ft left of shoulder	85.2%	79.2%	70.6%	Unacceptable
75	Road less 18 ft	Berm / 20 ft high	20 ft left of shoulder	80.3%	74.6%	68.1%	Unacceptable
75	Road less 18 ft	Raise grade 10 ft & 10 ft rock wall	Shoulder	96.2%	92.3%	88.0%	Acceptable

* Road elevation applies to current grade.

Acceptability of a specific design geometry was based on a performance criterion of about 90 percent predicted effectiveness meaning that the catchment zone provided by the embayment would intercept 90 percent of discrete rockfall events based on the input parameters to the CRSP model. Using this criterion, four of the analyzed geometries were rated as "acceptable."

Application to Rockfall Mitigation during Construction

During construction, a temporary rockfall hazard will be presented by the rock avalanche deposits that are contained within the Falls Creek chute. Subsequent to the November 9, 2003 event, this material partially remobilized during a period of heavy precipitation as a debris slide that buried the closed SR 20 to a depth of 10 to 15 feet. WSDOT plans to minimize slope grading thereby leaving the rock avalanche deposits in place and to specify a temporary rockfall control fence to be installed at an elevation of approximately 850 feet in addition to other measures to be implemented above the embayment crest.

To provide guidance on the capacity and height of the fence the calibrated CRSP model was modified to simulate a source area between elevations 1160 and 1300 feet corresponding to the upper rock avalanche deposits. The model was used to predict the energy and trajectory (bounce height) at the location of the proposed fence for spherical boulders with diameters of 2.5, 5 and 10 feet.

Embayment Slope Design

5.1 Structural Geology

Rock slope design for shallow excavations in strong rock, as is present at the embayment site, is controlled by the spatial relationship of discontinuities that can combine to form structurally-defined planar, wedge or toppling blocks and the viability for these blocks to translate out of the proposed slope face. The greater the persistence of the discontinuities that form the blocks, the greater the rock volume that may be involved in a potential failure. An absence of adversely oriented, persistent discontinuities means that structural failures will be local in nature and that they will not be a controlling factor for overall slope design.

As previously discussed, detailed structural mapping, borehole logging and borehole imaging (COBL) procedures were performed to characterize the structural geology in the vicinity of Falls Creek. It was noted that the data throughout the area is consistent with four or five common discontinuity sets but with differing relative frequencies. The most prominent discontinuities were Set 1 which is sub vertical and northeast – southwest trending (81°/308° to 84°/312°, dip/direction) and Set 2 which is shallow dipping toward the southwest (28°/232° to 23°/210°, dip/dip direction). When a persistence threshold was used to filter the mapping data, the dominance of these two discontinuity sets was readily apparent

The predominant discontinuity types are mineral banding/foliation, joints, and healed joints. Discontinuity surfaces typically were noted as planar and rough with little or no infilling. Only three features were mapped with infilling characteristic of shearing. Based on this generalized mapping information, for kinematic analyses discontinuities can be expected to exhibit a minimum frictional strength of at least 30°.

5.2 Kinematic Analysis for Slope Design

Kinematic analyses for rock slope design evaluate the orientation of potential structurally controlled failure modes (planar, wedge, topple) relative to the orientation of the proposed rock cut. For the embayment at Falls Creek, the majority of the cut slope will have its crest parallel to the SR 20 alignment. Thus, for design purposes the dip direction of the primary cut slope was set as 120°.
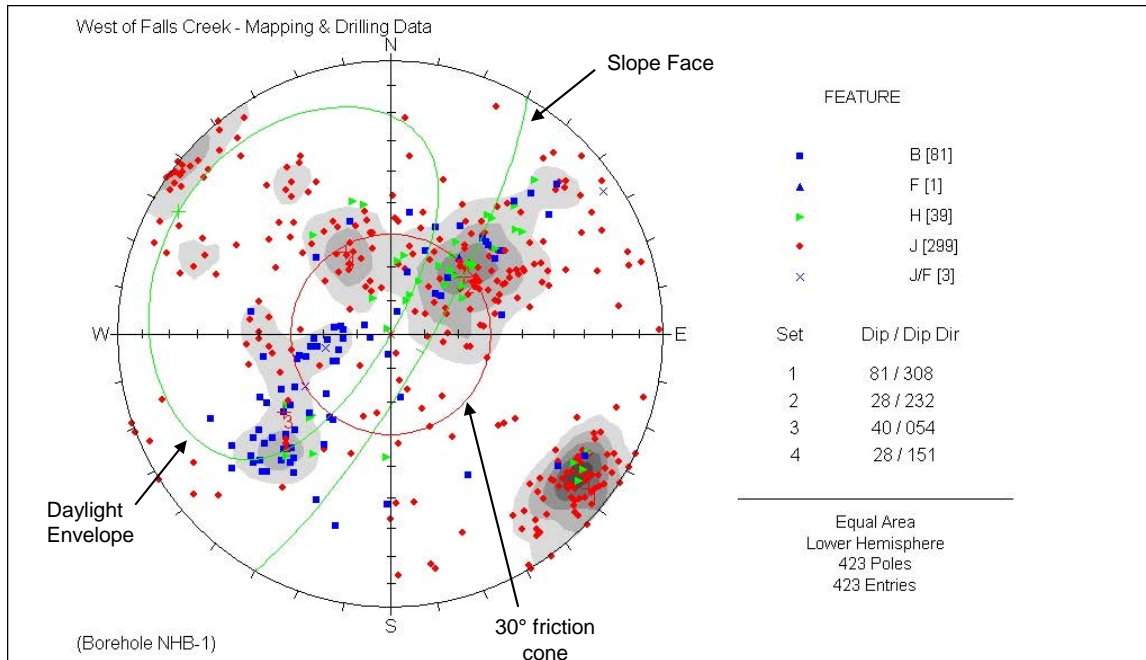
Figure 9. Stereogram for kinematic analysis.

Figure 9 superimposes the structural geology, slope face and minimum frictional strength for the primary southeast dipping embayment cut slope. For the purposes of the kinematic analysis, a steep slope inclination was selected consistent with the objective of avoiding rockfall impacts on the slope face (i.e. rocks will free-fall from crest to toe). The preferred slope configuration consisted of 1H:8V inclinations for assumed 30-foot lifts. Accommodation of the maximum inter-lift offsets allowed under WSDOT Standard Specifications results in an overall, toe to crest, slope inclination of 79° to 80° depending on the number of lifts.

Discontinuities with adverse orientations that could form planar or wedge-shaped failure blocks have poles that plot within the "Daylight Envelopes" and are shown to be limited in number and to consist of either metamorphic features associated with the rock genesis (see Set 3) or impersistent joints.

Conclusions for Option 1

Conclusions – Site Characterization

The site characterization program near the proposed embayment has yielded the following findings pertinent to slope design:

➢ The structural fabric of the bedrock is consistent over the length of the embayment with the exception of the conditions intersected in one borehole. The structural fabric of the bedrock is generally favorable for the excavation of steep slopes.

- Set 1 is the most dominant joint set mapped and is favorably oriented to provide a "break" surface for controlled blasting. In places Set 1 will dip into the proposed cut leading to localized block instability. Large-scale toppling is not anticipated along this structure because of spacing considerations.

- Borehole B-2 encountered 52 feet of unconsolidated rock avalanche debris and alluvium. The lateral and vertical limits of this deposit are not known with certainty. The material may be encountered in the cut slope for the embayment east of Falls Creek chute and in such a circumstance will pose a long-term stability issue. Even if the deposit is not intersected by the cut slope, its presence above the cut will pose a construction risk to the contractor.

- Afternoon Creek – Snow avalanches are expected to carry boulders up to 30 feet in length (URS, 2004). Slopes are too steep north of SR 20 to allow construction of a containment berm without a major earthwork project. A deflecting berm may narrow the area over which snow avalanches affect the road, however, this potential benefit is offset by allowing the snow and rock debris to accumulate to greater depths on the road.

Conclusions – Rockfall Simulation

The rockfall modeling using the Colorado Rockfall Simulation Program (CRSP) have demonstrated that:

- The slope profile, roughness and material properties incorporated in the "calibrated" model adequately replicated the results of the November 9, 2003 rockfall event adjacent to Falls Creek.

- Notwithstanding maintenance issues, the calibrated model has shown that it is impractical to intercept rockfalls in the lower Falls Creek chute above the grade of SR 20 because of the extreme impact energy requirements for mechanical devices (suspended nets or rockfall fences).

- An at grade catchment zone ("embayment") is the most practical, permanent rockfall protection approach.

- During construction, the rockfall hazard in the upper Fall Creek chute can be reduced through a temporary rockfall control fence located in the chute on a bedrock foundation near elevation 850 feet. The fence should have a capacity of 250 ft-tons and a height of eight feet.

References Cited

Brown, E.T., 1981, Rock Characterization and Testing: ISRM Suggested Methods; Pergamon Press, Oxford, 211p.

Evans, S.G. and Clague, J.J., 1999, Rock avalanches in glaciers in the Coast and St Elias Mountains, British Columbia; in Proc 13th Annual Vancouver Geotechnical Society Symposium, pp 115 – 123.

Goodman, R.E., 1980, Introduction to Rock Mechanics; John Wiley & Sons, 478p.

Haugerud, R.A., P. Van Der Heyden, R. Tabor, J. Stacey, R. Zartman, 1991, Late Cretaceous and early Tertiary plutonism and deformation in the Skagit Gneiss Complex, North Cascade Range, Washington and British Colombia: Geological Society of America Bulletin, v. 103, p. 1297-1307.

Hungr, O., 1995, A model for the runout analysis of rapid flow slides, debris flows, and avalanches. Can. Geotech. J., V.32, pp 610-623.

Hungr, O. and Evans, S.G., 1996, Rock avalanche runout prediction using a dynamic model, in Landslides, ed. Senneset, Balkema, Roterdam, pp. 233-237.

Hungr, O., Salgado, F.M. and Byrne, P.M., 1989, Evaluation of a Three-Dimensional Method of Slope Stability Analysis, Canadian Geotech. Journal, V.26, pp 679 – 686.

Jones, C.L., Higgins, J.D., and Andrew, R.D., 2000, *Colorado Rockfall Simulation Program (CRSP)*, Version 4.0, Colorado Department of Transportation, pp. 127.

Misch, P., 1966, Tectonic evolution of the northern Cascades of Washington State – a west-Cordilleran case history *in* A Symposium on the Tectonic History and Mineral Deposits of the western Cordillera: Canadian Institute of Mining and Metallurgy, Special Volume 8, p. 101-148.

RocScience Inc., 2001. User's Guide DIPS – Plotting, Analysis and Presentation of Structural Data Using Spherical Projection Techniques, Version 5.102, pp. 86.

Tabor, R.W., R.A. Haugerud, D.B. Booth, and E.H. Brown, 1994, Preliminary Geologic Map of the Mount Baker 30- by 60-Minute Quadrangle, Washington: U.S. Geological Survey Open File Report 94-403.

URS Corporation, 2004, Geotechnical Report SR 20 MP 121.5 Option 1 Embayment, prepared for Washington State Department of Transportation, May.

USGS, 2004, http://wrgis.wr.usgs.gov/docs/parks/noca/nocageol6.html

WSDOT, 2004. Standard Specifications for Road, Bridge and Municipal Construction, http://www.wsdot.wa.gov/fasc/EngineeringPublications/Manuals/SS2004.PDF.

Recent Developments, Same Old Problem: The Interstate 70 Sinkholes in Russell County, Kansas

By
Neil Croxton, Kansas Department of Transportation

In the summer of 1966, during construction of I-70 in Russell County, Kansas, two active sinkholes were discovered adjacent to the right-of-way. A third, smaller sinkhole was discovered in the late 1970's. The sinkholes are located within a one-mile section of the interstate and are the result of oilfield-related salt dissolution 1300 feet below the surface. As a result, the Kansas Department of Transportation has since been plagued by expensive repairs, poor public relations, and unsuccessful attempts to stop the subsidence.

A current regrading project through this area will bring the interstate back to grade for the first time since 1971. The bridge serving a county road that bisects the two larger sinkholes has already been dynamited and the road permanently closed. Up to 12 feet of fill is being added to the eastbound lanes.

As part of this project, KDOT has hired the Kansas Geological Survey to perform a geophysical survey of the area. Using high-resolution seismic reflection, two intersecting lines will be surveyed across the sinkholes. Salt and voids show up well in seismic reflection, and we expect to receive a clear picture of the subsurface. Using this information, we can hopefully reassure the public that Interstate 70 is safe, and learn how much of the 270-foot salt bed remains.

No other large sinkholes have developed in this area. We hope that the seismic survey shows a reason for the development of three sinks in such a short distance. If a trend or lineament can be detected that explains the unfortunate placement of the sinkholes, then perhaps in the future I-70 can be relocated to a safe alignment.

Slope Stabilization Using Recycled Plastic Pins

J.E. Loehr[1], J.J. Bowders[2], C-W Chen[3], K.S. Chandler[4], P.H. Carr[5], and T.W. Fennessey[6]

Abstract

Surficial slope failures, or nuisance slides, constitute a significant economic and manpower burden for many transportation agencies due to the frequent and recurring nature of the slides. The Transportation Research Board recently estimated that annual costs for stabilization of nuisance slides exceed the costs for repair of major landslides, which suggests that annual costs for repair of nuisance slides on the U.S. Highway System alone exceeds $100 million. An ongoing evaluation has shown the feasibility of using slender recycled plastic members for in situ reinforcement of surficial slides in slopes and embankments. This paper describes an ongoing evaluation of the technique and the results and conclusions derived from the evaluation to date. Topics covered include description of five well-instrumented field test sites, the construction equipment and techniques used to install the recycled plastic members, the performance of the field test sites to date, and the costs for the technique as compared to other methods.

Introduction

Slope failures and landslides constitute significant hazards to all types of both public and private infrastructure. Total direct costs for maintenance and repair of landslides involving major U.S. highways alone (roughly 20 percent of all U.S. highways and roads) were recently estimated to exceed $100 million annually (TRB, 1996). In the same study, indirect costs attributed to loss of revenue, use, or access to facilities as a result of landslides were conservatively estimated to equal or exceed direct costs. Costs for maintaining slopes for other

[1] Assistant Professor, Dept. of Civil Engineering, University of Missouri-Columbia, E2509 EBE, Columbia, MO 65203, 573-882-6380, eloehr@missouri.edu

[2] Professor, Dept. of Civil Engineering, University of Missouri-Columbia, E2509 EBE, Columbia, MO 65203, 573-882-8351, bowders@missouri.edu

[3] Graduate Research Assistant, Dept. of Civil Engineering, University of Missouri-Columbia, E2509 EBE, Columbia, MO 65203, 573-884-3862, cchy8@mizzou.edu

[4] Graduate Research Assistant, Dept. of Civil Engineering, University of Missouri-Columbia, E2509 EBE, Columbia, MO 65203, 573-884-3322, kscce1@mizzou.edu

[5] President, The Judy Company, Inc., 9133 Woodend Road, Kansas City, KS 66111, 913-422-5088, pcarr@judycompany.com

[6] Geotechnical Engineer, Missouri Department of Transportation, 1617 Missouri Blvd, Jefferson City, Missouri 65102

highways, roads, levees, and railroads maintained by government and private agencies such as county and city governments, the U.S. Forest Service, the U.S. Army Corps of Engineers, the National Parks Service, and the railroad industry significantly increase the total costs for landslide repairs.

A significant, but largely neglected, toll of landslides is the costs associated with routine maintenance and repair of "surficial" slope failures. Costs for repair of such slides were not explicitly included in the above referenced study because of limited record keeping for these types of slides by most state departments of transportation. However, the authors of the TRB study conservatively estimated that costs for repair of minor slides equal or exceed costs associated with repair of major landslides. This estimate is supported by the Missouri Department of Transportation's (MoDOT) experience with surficial slide problems, which are estimated to cost on the order of $1 million per year on average. Many other state departments of transportation have similar problems with similarly high, or even higher annual costs. All available evidence clearly indicates that the cumulative costs for repair of many surficial slides can become extremely large, despite the fact that costs for repair of individual slides are generally low. In addition, minor failures often constitute significant hazards to infrastructure users (e.g. from damage to guard rails, shoulders, or portions of road surface) and, if not properly maintained, often progress into more serious problems requiring more extensive and costly repairs.

The basic premise of the project described in this paper is that slender structural members manufactured from recycled plastics can be used to effectively reinforce slopes as illustrated in Figure 1. As shown in the figure, recycled plastic reinforcing members are installed in the slope to intercept potential sliding surfaces and provide the resistance needed to maintain the long-term stability of the slope. Using recycled plastic members for stabilization has several potential advantages over more common civil engineering materials. Plastic members are less susceptible to degradation by chemical and biological attack than other structural materials and are lightweight, meaning smaller installation equipment and lower transport costs. Plastic members also present less of an obstruction if future construction (e.g. underground utilities) must traverse a stabilized site. Using recycled plastics also has environmental and political benefits as it reduces the volume of waste entering landfills and provides additional markets for recycled plastic. Development of a cost effective means for using these materials while providing long-term stabilization therefore clearly has numerous advantages for agencies faced with maintaining numerous surficial slides. This paper summarizes the results of an ongoing project to evaluate the use of recycled plastics for stabilization of surficial slides. Additional details of the ongoing investigations can be found in Loehr et al. (2000), Chen (2003), Bowders et al. (2003), and Loehr and Bowders (2003).

Material Characteristics

The engineering properties of recycled plastic members are of paramount importance because of the potential for structural failure of the members due to the loads imparted on the members during installation or imposed by the soil following installation. An extensive testing program was therefore undertaken to develop a database of the engineering properties of recycled plastic members. The program included: (1) determining the basic engineering and

material properties of recycled plastic members; (2) determining how these properties change when the material is subjected to potentially detrimental environments; and (3) determining the potential variability of these properties within one product and among various products and manufacturers.
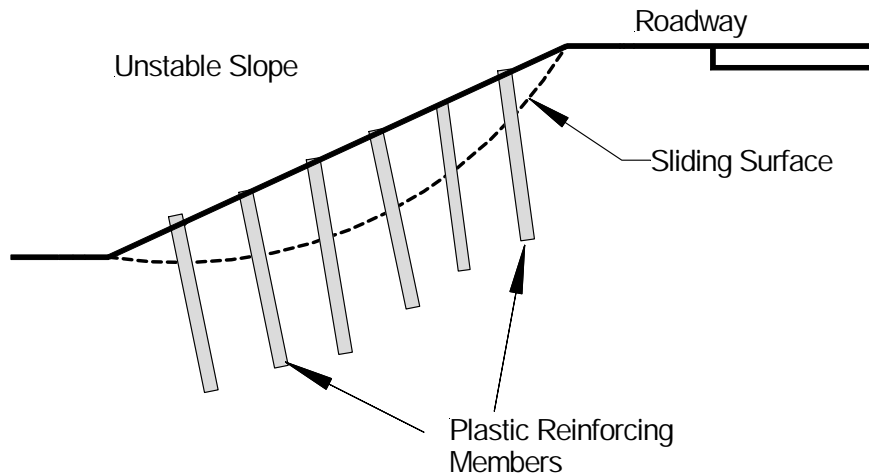

Figure 1.   Schematic of technique for stabilization of surficial slope failures using recycled plastic reinforcement.

Laboratory tests performed to evaluate the engineering properties of the recycled plastic members included uniaxial compression tests, four-point flexure tests, compressive creep tests, and flexural creep tests. When available, standard ASTM test methods for recycled plastic lumber products were followed with slight modifications to produce results more appropriate for the application of stabilizing earthen slopes. Laboratory tests were performed on specimens from three manufacturers. Members were divided into thirteen different batches according to the type of member, the manufacturer, and the condition of the member. All members were nominally 3.5-in. x 3.5-in. in cross-section by 8-ft in length. The principal constituent and manufacturing processes for each manufacturer varied as did the measured unit weights, which ranged from 52- to 68-pcf. Table 1 shows a summary of uniaxial compressive strengths measured on specimens of recycled plastics considered in the study.

Results obtained from the laboratory testing indicated significant variability in the engineering properties of the members. The variability stemmed both from simple variations in properties as are expected of any manufactured material as well as from variations attributed to distinct differences in material constituents and manufacturing processes. Compressive strengths of the recycled plastic members ranged from 1600- to 3000-psi with extruded products having strengths about 20 percent lower than compression-molded products. Values for the secant modulus of elasticity from uniaxial compression tests ranged from 80- to 190-ksi. Compression-molded products had the highest moduli of all products. Fiberglass-reinforced products were about 60 percent stiffer than unreinforced products. Flexural strengths ranged from 1300- to 3600-psi and flexural moduli varied from 90- to 250-ksi. Overall, compression-molded products were found to be significantly stiffer, and more brittle than extruded products. The recycled

plastic products were found to be creep sensitive. However, results of Arrhenius modeling performed as part of the project indicates that, at current field temperature and stress levels, creep failure is not expected for between 45 and 2000 years.

Table 1   Summary of uniaxial compressive strengths determined for recycled plastic members.

Specimen Batch	# Specimens Tested	Uniaxial Comp. Strength (psi)	
		Mean	Std. Dev.
A1	10	2784	128
A2	7	2948	117
A3	6	2824	88
A4	6	2621	295
A5	6	1634	200
A6	14	1602	105
A10	15	2219	154
A11	15	2301	139
A12	8	2085	84
A13	15	2380	330
B 7	15	2080	69
B 8	15	2500	191
C 9	15	2315	209

[1] stress calculated using initial cross-sectional area (A_0)

Field Test Sites

Field performance evaluations are being performed at five different test sites located across the state of Missouri. Table 2 summarizes the general characteristics of the field test sites. Figure 2 shows the general locations of the sites. In general, sites were selected from among the available sites to represent the range of conditions where frequent surficial slides are encountered. Slope angles at the respective sites ranged from 2.2H:1V to 3.2H:1V with slope heights ranging from 15-ft to 46-ft. Test sites included both excavated and embankment slopes.

Stabilization schemes utilized at each test site generally consisted of reinforcing members installed at uniform spacings across the former slide area(s). At sites established early in the project, members were installed at nominally 3-ft center to center spacing. At subsequent sites, several test "sections" were created at each site and members were installed at different spacings or in different arrangements to evaluate the potential for optimizing the technique. Figure 3 shows a plan view of the US36-Stewartsville site with the installed member locations shown. Members were installed either vertically or perpendicular to the face of the slope.

Site	MoDOT District	Slope Inclination (H:V)	Slope Height (ft)	General Characteristics
I70-Emma	2	2.5:1	22	Embankment slope with lean to fat clay
I435-Wornall Road	4	2.2:1	32	Embankment with lean clay over clay shale fill
I435-Holmes Road	4	2.2:1	15	Embankment with lean clay over clay shale fill
US36-Stewartsville	1	2.2:1	29	Excavated slope with lean clay over fat clay
US54-Fulton	5	3.2:1	46	Excavated slope in "ablation" till

Table 2   Summary of field test site characteristics.
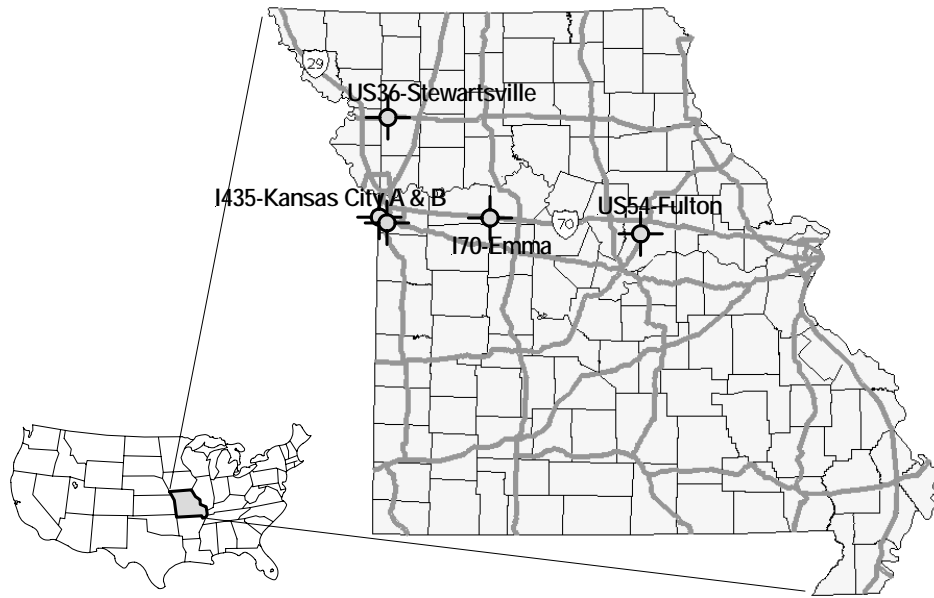

Figure 2.   Map showing general locations of field test sites.

Installation Technique

Reinforcing members were installed using a variety of equipment with variable success. Early attempts to install the recycled plastic members utilized a hydraulic hammer ("breaker") mounted on a rubber-tired backhoe shown in Figure 4. This rig proved to be generally unsuitable for installation of the recycled plastic members because the rubber-tired backhoe was difficult to maneuver on the slopes and because it was extremely difficult to maintain the alignment of the hammer and the reinforcing member during driving. The lack of a mechanism for maintaining the alignment of the hammer and the reinforcing member resulted in numerous members being ruptured in bending during installation.
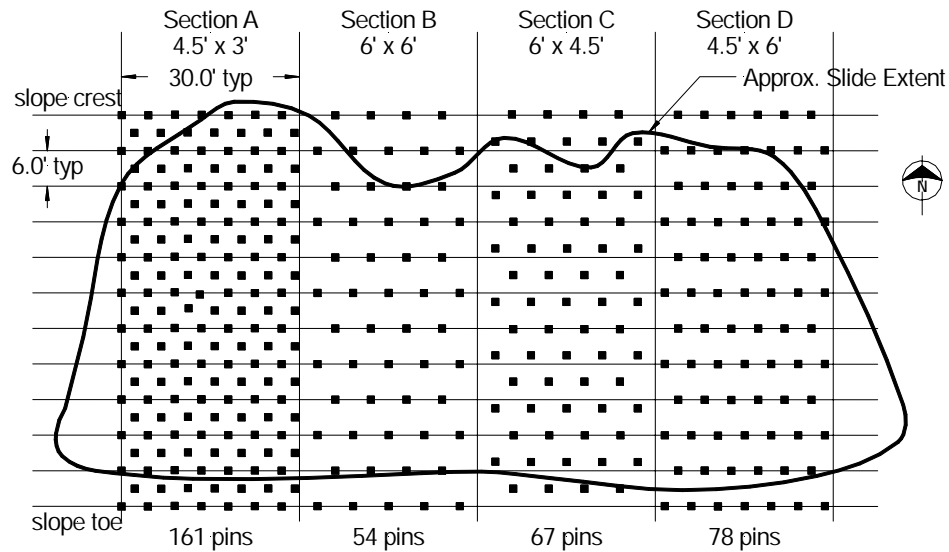
Figure 3.   Plan view of US36-Stewartsville site showing locations of reinforcing members.

Figure 4.   Backhoe-mounted hydraulic hammer use for initial installation attempts.

Subsequently, several types of equipment that include a driving mast to maintain the alignment of the hammer and the reinforcing member were utilized with much greater success. Figure 5 shows two such pieces of equipment. The majority of members at the field test sites were installed using track-mounted hydraulic or pneumatic hammer drills similar to the

equipment shown in the background of Figure 5. This type of equipment proved to be much more maneuverable on the steep slopes and provided sufficient percussion energy to install the members within a reasonable time frame. On the steepest slopes, the equipment had to be tethered to the top of the slope to maintain the position and orientation of the equipment during driving. A limited number of reinforcing members were installed using a simple drop-weight system mouted on a skid-steer loader as shown in the foreground of Figure 5. This equipment also proved to be very effective at driving the reinforcing members.

Figure 5.   Pneumatic hammer drill (background) and drop-weight hammer rigs (foreground) successfully used to install reinforcing members at field test sites

Installation rates achieved at the respective test sites generally improved as more experience was gained with installation and as minor improvements were made to the driving equipment. Installation rates at the early test sites were nominally 80 members per day for one piece of equipment. Installation rates at the later test sites generally exceeded 100 members per day and the peak installation rate was 140 members per day at the last test site (US54-Fulton site).

Field Performance

Following installation of the reinforcing members at the respective test sites, a suite of instrumentation was installed at each site to monitor the performance of the slopes over time. Instrumentation used at each site included slope inclinometers, standpipe piezometers, instrumented reinforcing members, and several types of soil moisture sensors. The instrumentation was regularly monitored to evaluate the performance of the stabilized slopes and the load transfer from the soil to the reinforcing members.

Figures 6 and 7 respectively show the observed maximum lateral deformations and the maximum mobilized bending moments from the instrumented reinforcing members as a function of time for the I435-Wornall Road test site. Data from the other test sites is generally consistent with that observed at the I435-Wornall Road site, although some of the slopes have yet to be subjected to periods of significant rainfall and therefore have yet to experience significant deformations or mobilization of resistance in the reinforcing members.
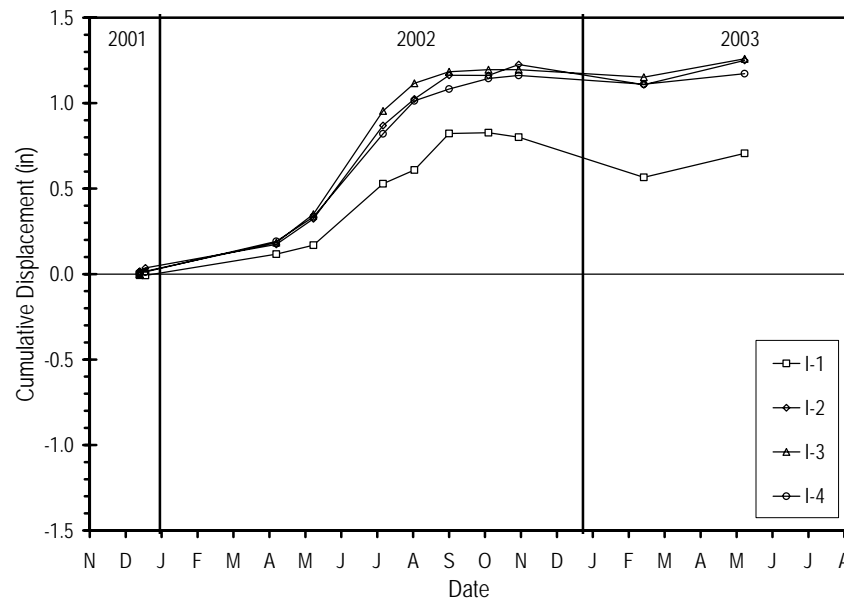

Figure 6.   Cumulative lateral deflections for inclinometers at the I435-Wornall Road test site.

In general, the observed field performance has consisted of a period of time following installation during which little movement was observed and minimal resistance was mobilized in the reinforcing members. This period generally corresponded with a period of below normal precipitation during which time the slope would have been stable without the reinforcement. Subsequent to this initial stage of performance, during the first period of above average rainfall at the respective sites, slope movements were observed to increase (Fig. 6). At the same time, the bending moments in the instrumented reinforcing members were also observed to increase (Fig. 7), which suggests that the resistance of the reinforcing members was being mobilized to maintain the stability of the slopes. This period was generally observed to continue until the resistance provided by the reinforcing members was sufficient to maintain the stability of the slope, at which point the lateral slope deformations were also observed to become essentially constant. Continued monitoring of the site following this initial "mobilization" stage have shown negligible additional deformations and essentially no increase in the observed bending moments even after additional periods of above normal precipitation. The magnitudes of deformations required to mobilize the resistance in the reinforcing members at the respective test sites varies somewhat but is on the order of 1-in to 1.5-in. Mobilized bending moments in the

reinforcement following the initial mobilization also vary but generally range from 20 to 50 percent of the average bending capacity of the members determined from laboratory tests.
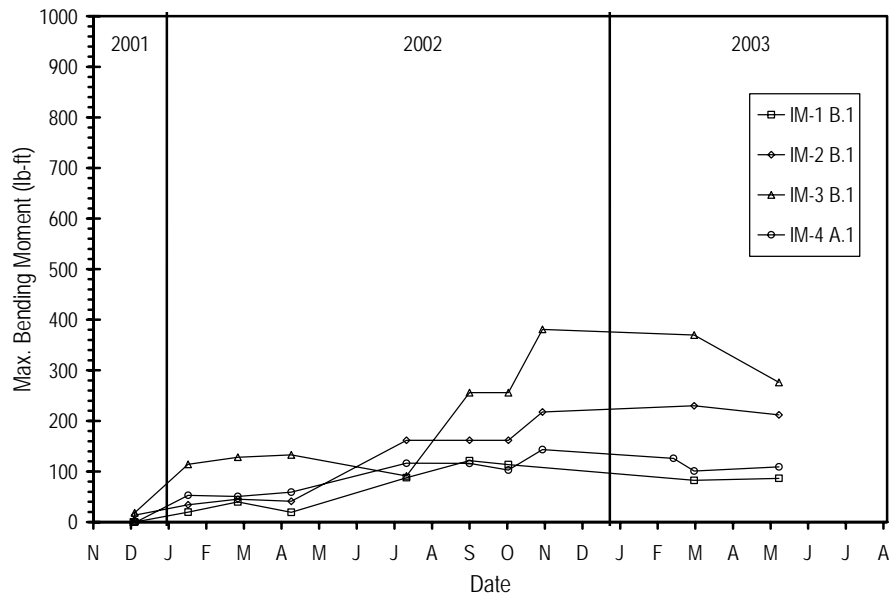

Figure 7.   Maximum mobilized bending moment in instrumented reinforcing members at I435-Wornall Road test site.

Overall, the performance observed at the field test sites to date suggests that surficial slides can be effectively stabilized using recycled plastic reinforcing members when members are placed on a 3-ft grid across the former slide area. Additional monitoring of test sections where members were installed at greater spacings is ongoing. To date, none of the stabilized test sections have experienced a failure. However, some of the sites have yet to be subjected to above normal precipitation for extended periods so it is premature to conclude that placing members at greater spacings will prove to be as effective.

Economic Considerations

Table 3 summarizes the results of cost analyses performed for each of the respective field test sites. As expected, the primary factor affecting the costs of the stabilization measures is the reinforcement spacing. Unit costs (per unit area of slope face) range from $4.20 to $4.60 per square foot when members are placed on 3-ft centers to as low as $1.00 per square foot when members are placed on 6-ft centers. Clearly there is a significant cost benefit to utilizing schemes with more widely spaced members. However, additional investigations are ongoing to evaluate whether such schemes can be effectively utilized to stabilize surficial slides. Regardless of the member spacing, however, the costs to stabilize slopes using recycled plastic reinforcement are very competitive with other common measures used to stabilize surficial slides.

Table 3.   Summary of cost analyses for stabilization of field test sites.

Field Test Site	Slope Section	Stabilized Area WxL (ft)	Member Spacing LxT[1] (ft)	Members Installed	Total Cost[2] ($)	Unit Cost[3] ($/ft^2)	Actual Cost[4] ($)
I70 Emma	S1	42x42	3x3	199	7960	4.5	11590
	S2	39x36	3x3	163	6520	4.6	
I435-Wornall		115x76	3x6; 3x3[5]	916	36640	4.2	44740
I435-Holmes		60x51	3x3	262	10480	3.4	18315
US36-Stewartsville	A	30x66	4.5x3	161	6440	3.3	14600
	B	30x66	6x6	54	2160	1.1	
	C	31x66	6x4.5	67	2680	1.4	
	D	32x66	4.5x6	78	3120	1.6	
I70-Emma	S3-A	25x48	4.5x3	95	3800	3.2	7960
	S3-B	25x36	4.5x6	35	1400	1.6	
	S3-C	25x36	6x6	30	1200	1.3	
	S3-D	25x36	6x4.5	38	1520	1.7	
US54-Fulton	A	34.5x75	4.5x4.5	113	4520	1.7	15040
	B	36x75	6x6	66	2640	1.0	
	C	36x75	3x3; 6x6[5]	97	3880	1.4	
	D	33x75	3x3	73	2920	1.3	
	E	40x75	10x10	28	1120	0.4	

[1] longitudinal (strike) spacing measured parallel to roadway by transverse (dip) spacing measured along slope
[2] total cost based on $20/member material costs and $20/member installation costs
[3] total cost divided by stabilized area
[4] actual costs paid for stabilization as part of the project
[5] mixed reinforcement configuration utilized

Conclusions

The following conclusions are drawn based on the results of the work presented in this paper:

1. The ongoing investigation has clearly demonstrated that recycled plastic reinforcement can be used to stabilize surficial slope failures.

2. Material properties of recycled plastic members can vary significantly depending on the specific constituents and process used to manufacture the members.

3. The most important feature of equipment used to install recycled plastic members in slopes is that the equipment has some system to maintain the alignment of the hammer and the reinforcing member to prevent damage to the members during installation.

4. The field performance of slopes at the field test sites indicates that lateral deformations of 1.0 to 1.5-in are required to mobilize the resistance in the reinforcing members. Such movements were generally not observed until the first extended period of above average precipitation at the respective field test sites.

5. Unit costs for stabilizing slopes using recycled plastic reinforcement are closely tied to the spacing at which the members are installed. Nominal costs for schemes with members placed at spacings of 3-ft center to center are $4 to $4.50. Additional monitoring and investigation is needed to establish whether less costly stabilization schemes can be effectively used to stabilize surficial slides.

References

Bowders, J.J., J.E. Loehr, H. Salim, and C-W Chen (2003), "Engineering Properties of Recycled Plastic Pins for Use in Slope Stabilization," *Transportation Research Record: Journal of the Transportation Research Board*, TRR 1849, pp. 39-46.

Chen, C-W (2003), *Engineering Properties of Recycled Plastic Pins for Use in Slope Stabilization*, Thesis submitted to the University of Missouri in partial fulfillment of the requirements of M.S. Degree, 118 pp.

Loehr, J.E., J.J. Bowders, and H. Salim (2000), *Slope Stabilization Using Recycled Plastic Pins – Constructability*, Missouri Department of Transportation, MoDOT RDT 00-007, 74 pp.

Loehr, J.E., and J.J. Bowders (2003), *Slope Stabilization Using Recycled Plastic Pins: Phase II – Assessment in Varied Site Conditions*, Missouri Department of Transportation, RDT 03-016, 214 pp.

Transportation Research Board (1996), *Landslides: Investigation and Mitigation*, TRB Special Report 247, A.K. Turner and R.L. Schuster editors, National Academy Press, 673 pp.

A Masonry Wall and Slide Repair Using Soil Nails and Rock Dowels

Drew Gelfenbein, Christopher Benda, PE and Peter Ingraham, PE

1.0 Background

In the middle of August 2003, Vermont experienced several days of very heavy rains which precipitated a slide failure on Vermont Route 73 in Forest Dale at approximately mile marker 6.36. A blocked culvert on the south side of VT 73 caused an overflow of water across the road surface and over an asphalt and wood curb down an embankment. This resulted in a significant amount of erosion, undermining of the road surface (Figure 1) and a washout of a timber cribbing retaining structure located on the top of a mortared masonry wall (Figure 2).

Figure 1: Undermining of north side of VT 73 in Forest Dale.

In the project area, VT 73 is constructed on a retained embankment in steep terrain formed in sub-vertically dipping schistose meta-greywacke. The embankment along a valley sidewall was originally built by constructing masonry retaining structures to span between a series of rock knobs. Soils mantling the rock in the valley consist of dense glacial till. The natural terrain was incised by the Neshobe River, which occupies the valley floor approximately 80 feet below and 100 feet north of the project retaining walls.

Figure 2: Washout of timber cribbing above mortared masonry wall. (View from road level)

After site visits by Vermont Agency of Transportation (VTrans) staff, it was decided that the laid up masonry wall immediately west of the slide area was also in desperate need of repair. The laid up masonry wall (Figure 3) was observed to have broken and missing blocks. Also the top of the wall was leaning out past the bottom of the wall an estimated 12-18 inches. During the 1970's the west end of the laid up masonry wall was replaced with a cast in place concrete wall. As both walls could be remediated by the same contractor, it was decided to repair both locations at the same time.

Golder Associates Inc. (Golder) was retained to perform the engineering design for both walls under a current On-Call Geotechnical Engineering

Figure 3: Laid up masonry wall, immediately west of slide area.

Services Contract. This included performing a site survey, designing a remediation for the wash out area and a shoring system for the laid up masonry wall.

2.0 Design

After discussions between VTrans and Golder, it was agreed that the old timber grade separation structure would need to be replaced and the masonry walls repaired. An approach consisting of a gabion basket retaining structure and soil nail/rock reinforcement repairs to the masonry walls was selected. This would entail clearing brush around the sites, removing loose soil, placing a layer of shotcrete (A pneumatically sprayed concrete with steel fiber reinforcement) to the surface of the walls, drilling 2 and 4 inch holes and installing 1 inch diameter, 75 ksi threaded bars. After the bars had been grouted and reinforcing mats placed an additional 5 inch layer of shotcrete was applied. A gabion basket retaining wall would then be built on the top of the mortared masonry wall in the wash out area to provide a stable slope back up to the road surface. A Gabion basket structure was selected to minimize the need for specialty construction, and allow participation of VTrans maintenance personnel in the construction to expedite the project. To support design of the structures, VTrans completed 6 standard penetration borings in the roadway behind the two walls.

Design of the gabion wall for the washout area consisted of a conventional retaining wall design for a sloping backfill condition. Soil strength values used included a friction angle of 32 degrees and zero cohesion used for the analysis and input into the GAWACWIN 2003 program for gabion wall design developed by Maccaferri Gabions Inc. The program results for a 30-degree back slope and a height of nine feet yielded a three tiered configuration as shown in Figure 4a. The Gabion wall was designed with a 6-degree batter, a shotcrete pad was incorporated to facilitate installation of the first course of Gabion baskets, and rock anchors were installed in the first tier of baskets to pin the wall to the supporting bedrock.

Support of the Gabion wall was checked using the program SLIDE developed by Rocscience. The analysis assumed that the existing masonry wall did not contribute to overall stability, only narrow sliver-type joint failures would be kinematically feasible because of joint orientations, and rock mass failure would occur as a circular failure. The critical cross section was analyzed for rotational stability and initially no rock anchors were considered in the analyses, with shear strength of the rock mass varied to evaluate the need for support. Assuming rock mass cohesion of 1500 pounds per square foot (psf), and a design rock mass friction angle of 40 degrees (conservative), the minimum calculated factor of safety was 2.1. While the calculated minimum factor of safety was adequate to support the Gabion wall, a pattern bolting design and shotcrete

facing (Figure 4a) were included to address potential variability in rock mass strength, seasonal groundwater fluctuations and long-term repair to the masonry wall that had started to ravel at the toe (Figure 7).
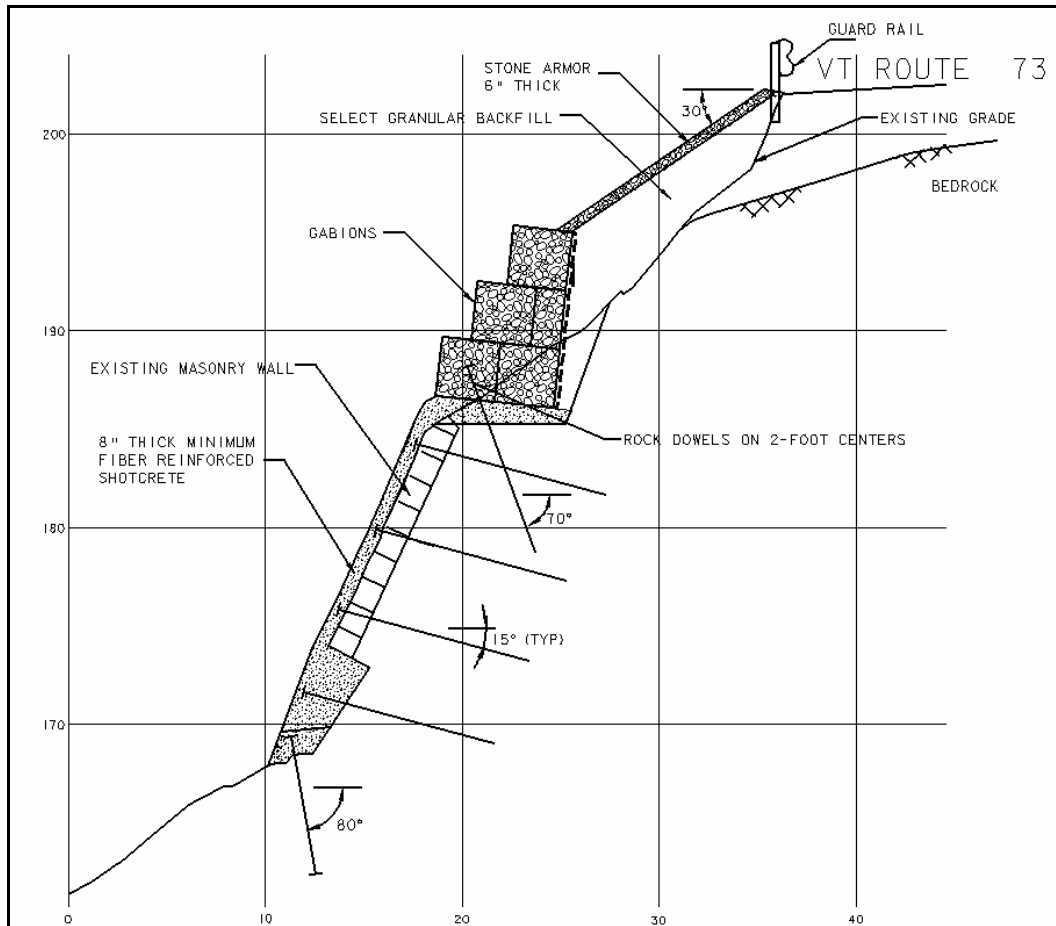

Figure 4a: Section view of mortared masonry wall.

Design of soil nail reinforcement of the masonry wall west of the washout assumed a 16-foot wall height with no batter and a surcharge load of 640 psf consistent with HS20-44 loading. The service load design followed the procedures outlined in the Federal Highway Administration (FHWA) "Manual for Design and Construction Monitoring of Soil Nail Walls" revised October 1998 (FHWA-SA-96-069R). Soil internal friction was assumed at 34 degrees and the soils assumed to be cohesionless (conservative). Global stability of the nailed soil block was checked using the program SLIDE. To account for variations in rock surface elevation, the soil nails were extended a minimum of 8 feet into sound bedrock at each nail location (Figure 4b).
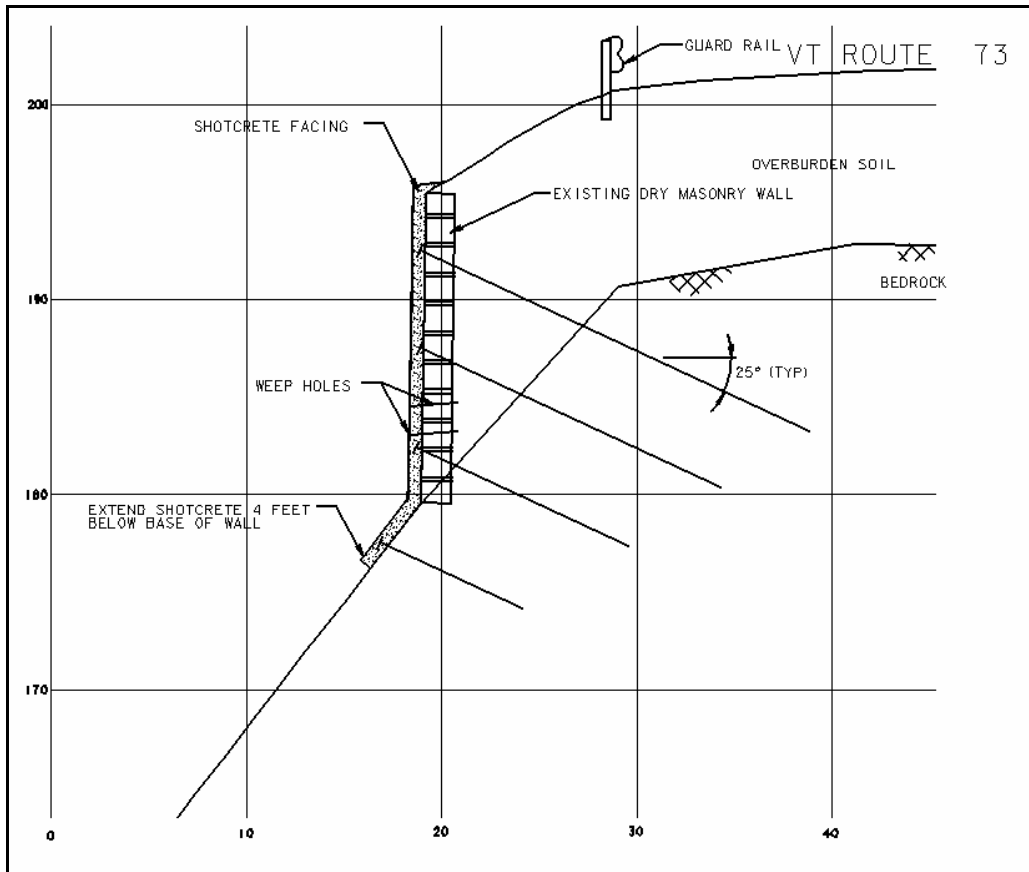
Figure 4b: Section view of laid up masonry wall repair

3.0 Construction

Due to the highly specialized nature of the rock reinforcement work and steep terrain at the two sites combined with the winter season quickly approaching, it was decided not to bid the project but to hire Janod Inc. (Janod) of Quebec, Canada under a force account contract. Janod specializes in rock scaling and drilling soil nails/rock dowels while on rappel and had completed a similar soil nail wall project on rappel for the New York State Thruway Authority two years earlier. Additionally, Janod has experience applying and protecting shotcrete in winter and inclement weather conditions (Figure 5).

Construction commenced on Wednesday October 15, 2003. Janod operated primarily with a five

Figure 5: Shotcrete being applied while on rappel.

man crew. It took approximately one day to clear out the brush around the two job sites. Weep pipe locations were chosen based upon visual inspection of the wall surfaces. If an area had visible moisture coming through the rock face a 3" PVC pipe was placed to provide drainage after the shotcrete was placed. A minimum three inch initial layer of shotcrete was applied to both retaining walls after they were cleaned to provide a secure working surface for personnel. The shotcrete was applied using a dry mix pumped through a hose and then mixed with high pressure water at the nozzle, just prior to exiting the hose.

The shotcrete was delivered in 2200 pound bags and suspended by a crane over the pump (Figure 6). The flow of the shotcrete was under constant supervision during the application. In some areas of the masonry walls the initial thickness of shotcrete was much greater than three inches due to inconsistencies in the rock face and void spaces

Figure 6: Shotcrete pump with a bag of shotcrete suspended over it.

Figure 7: Masonry wall below washout.

between the rocks (Figure 3). The initial layer of shotcrete not only provided reinforcement of the masonry walls during drilling operations, but also provided an even surface for soil nail bearing plates and other reinforcing elements. The raveled void below the mortared masonry wall at the washout area was also backfilled with shotcrete (Figure 7). With the start of winter weather and daily low temperatures of 30-40 degrees, thermal blankets were placed over the shotcrete at night, for a minimum of 2 days to prevent the concrete from freezing during the curing process.

Following application of the initial layer of shotcrete, the next step was to drill the holes for the soil nails and rock dowels. For design purposes, all of the 4-inch diameter holes with grouted bars were deemed to be soil nails, even when drilled for a minimum of 8 feet into competent rock. Two-inch diameter holes were

drilled for rock dowels, which were installed where bedrock was exposed at the slope surface. Rock dowels were also drilled a minimum of 8 feet into competent rock. Two sacrificial test soil nails were drilled, one located near each retaining wall. It was decided not to perform tests on nails installed through the existing masonry walls to avoid causing any further damage to the walls during the testing process. After the site was cleared of loose soil and vegetation, the edge of the laid up masonry wall and rock outcrops became more distinct. To accommodate the encountered field conditions, several soil nails were relocated or eliminated.

There were 20 holes drilled in each wall, for a total of 40 holes. All 20 of the holes drilled in the mortared masonry wall in the washout area were rock dowels, while in the laid up masonry wall 12 of the holes were soil nails and 8 were rock dowels. If a soil nail hole was found to have fracturing during the drilling process, the hole was drilled deeper in order to achieve a minimum 8 foot embedment depth into competent rock. If fracturing was encountered, a woven fiberglass "sock" was used on the outside of the 1 inch diameter threaded steel bar to prevent excess grout loss into the void spaces. The fiberglass socks (Figure 8) were used on 8 of the 12 soil nail holes. In the soil nail holes, centralizers, spaced no more than 5 feet apart, were placed on the threaded bars prior to placement.

Prior to the grouting of the production soil nails and rock dowels, soil nail bond verification tests were performed. Both test nails were tested to 1.5 times the design load of 4 kips per linear foot for pullout and creep. The test nails at both locations performed satisfactorily.
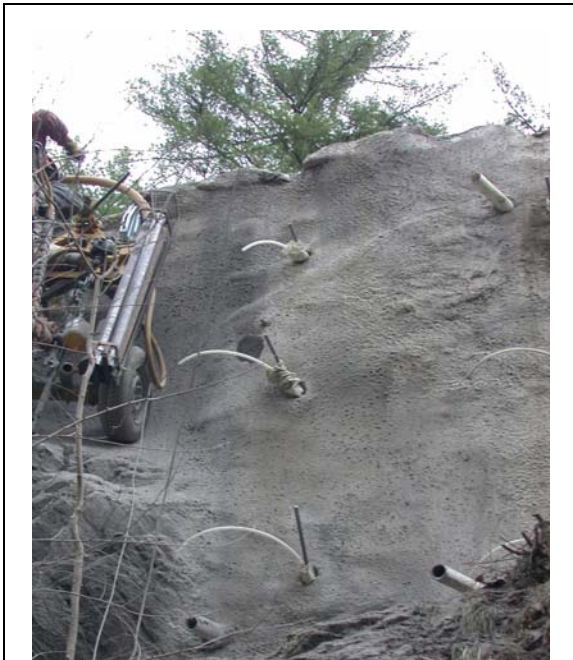

Figure 8: Fiberglass socks shown protruding from the top of soil nail holes.

The production nails were grouted in place using Sika 212 grout. The grout was tremmie pumped into the holes using grout tubes to ensure that the grout reached the bottom of the holes. Pumping continued until the grout flowed from the collar of the holes. If the level of the grout receded, additional grout was placed to bring the grout level up to the surface of the shotcrete wall face.

After the soil nails and rock dowels were grouted, welded wire fabric was placed over both walls. Reinforcing bar whalers were placed above and below each row of soil nails and rock dowels. A 3 foot piece of reinforcing bar was placed vertically on each side of each soil nail and rock dowel (Figure 9).

The final layer of shotcrete was then applied with a minimum thickness of 5 inches to encapsulate the reinforcing fabric and whalers.

Figure 9: Welded wire fabric and rebar on mortared masonry wall.

At the location of each soil nail/rock dowel several inches of shotcrete was built up, and then a 5 inch square bearing plate was wet set into the shotcrete followed by a hand tightened nut. The soil nails and rock dowels were *not* post-tensioned. Additional shotcrete was then applied to encapsulate the bearing plate and nut to achieve 5 inches of cover to prevent corrosion.

Six of the rock dowels installed in the top of the mortared masonry wall were designed to provide a support system for a gabion wall which was constructed to replace the failed timber crib wall. The six rock dowels were equally spaced at approximately 2 feet on center and installed with a 70° rake from horizontal.

The gabion baskets were assembled and constructed by VTrans personnel from the District 3 Brandon garage. The bottom row of 2 baskets was placed over the six rock dowels. They were filled 2/3 of the basket height with stone prior to a 5 inch bearing plate and nut being installed on the threaded rod. The remainder of the baskets were then filled with stone. Additional layers of gabion baskets were installed. Each layer of baskets was laced to one another and to the row of baskets below them. A granular backfill was compacted behind the gabion wall in 1 foot lifts. A Geotextile was placed behind the gabion wall and brought over the top of the granular backfill.

Stone fill was then placed on the geotextile to form the slope back up to the road surface. The final gabion wall can be seen in Figure 10.

The construction for both walls was completed in 13 working days. There were 714 yd^3 of shotcrete applied, 446 yd^3 to the laid up masonry wall and 268 yd^3 to the mortared masonry wall. A total of 251 feet of 1 inch diameter threaded bar was installed in the mortared masonry wall and 233 feet in the laid up masonry wall.

Figure 10: Completed Gabion wall

Materials Testing

The specifications required that the test procedures outlined in Table 1 be performed. Reinforced and un-reinforced pre-production test panels were fabricated prior to the start of shotcreting operations. Strength testing was conducted on shotcrete cores taken from the un-reinforced panels. Tests for absorption were conducted on cores taken from both reinforced and un-reinforced panels. The Sika 212 grout was only tested for compressive strength. Additionally, the VTrans Materials and Research Lab checked the thickness of the galvanization on a hex nut and a 5 inch square bearing plate even though there was no specific requirement for the galvanizing thickness. The average galvanization on the hex nut was 2.05 mil and 12.0 mil on the bearing plate. The galvanization measurements were performed using an Elcometer magnetic coating thickness gauge.

Material	Test Method	Minimum Requirement	Actual
Sika 212 Grout – Test Nails	AASHTO T106 – 3 days	1500 psi	2170 psi
Sika 212 Grout – Test Nails	AASHTO T106 – 28 days	3000 psi	5630 psi
Sika 212 Grout – Production Nails	AASHTO T106 – 3 days	1500 psi	3340 psi
Sika 212 Grout – Production Nails	AASHTO T106 – 28 days	3000 psi	5770 psi
Shotcrete – Compressive Strength	AASHTO T22 – 7 days	2000 psi	5350 psi
Shotcrete – Compressive Strength	AASHTO T22 – 28 days	4000 psi	8303 psi
Shotcrete – Absorption	ASTM C642	Less than 8%	8.70%
Shotcrete – Boiled Absorption	ASTM C642	Less than 8%	8.92%
1" Diameter Threaded Bar - Yield	AASHTO T244	75000 psi	81329 psi
1" Diameter Threaded Bar - Ultimate	AASHTO T244	100000 psi	115038 psi
1" Diameter Threaded Bar Elongation in 8 inches	AASHTO T244	7%	13.4%

Table 1, Laboratory Test Results

Conclusions

As a result of the collaborative effort between the VTrans, Golder and Janod, a repair concept and design were quickly implemented and project construction progressed very smoothly. The project was completed in less time than estimated and under budget. The finished walls can be seen in Figures 11 and 12.

Figure 11: Completed repairs to mortared masonry wall below slide area.

Figure 12: Completed repairs to laid up masonry wall.

US35/I 64 Interchange
Embankment and MSE Wall Design and Construction

Using Lightweight Backfill

James C. Fisher

West Virginia DOT

Abstract

US Route 35 in Putnam and Mason counties is currently being upgraded from two lanes to four lanes. As a part of this upgrade a new relocated Route 35 intersection with existing Interstate 64 is being constructed in Putnam County.

The construction of the project is within the valley of the ancient Teays River. The Teays River was an ancient stream, comparable in size to the modern Ohio River that once drained much of the east central U.S., including nearly two-thirds of Ohio. It was destroyed by the glaciers of the Pleistocene Ice Age about 2 million years ago. The edge of the glacier created a massive dam that blocked the northward-flowing Teays and created a major lake in southern Ohio eastern Kentucky and western West Virginia.

The lake waters rose to an elevation of nearly 900 feet, creating an intricate pattern of long finger lakes in tributary valleys. The deep valleys of the lake filled with sediment.

These thick lake deposits were encountered during the subsurface investigation for the project. These lake deposits required special design considerations for construction of the interchange.

The focus of this paper is the investigation and design consideration for construction of exit Ramp 5. This ramp required the most detailed geotechnical considerations for construction of the interchange. Due to the project geometric requirements, a large amount of fill was required on this ramp. An abutment for a flyover bridge over I-64 is to be located on top of the fill. Several design alternatives were considered, ultimately two Mechanically Stabilized Earth (MSE) walls were designed to meet the ramp's right of way, utility and geometric requirements. Special consideration was required for designing and constructing the embankment fill and backfill of the MSE walls over a thick and relative low strength soils deposits. Alternatives were studied in order to construct the fill and backfill and maintain stability considering the weak material that would be at the base of the embankment and MSE walls. It was decided to use a lightweight fill material in order to maintain stability of the embankment and MSE walls. Bottom ash, which is a waste product obtained from coal burning power plants, was chosen as the light weight material for inclusion in the fill and backfill.

Geologic Background of the Region

The Teays River was an ancient stream, comparable in size to the modern Ohio River, which once drained much of the east-central U.S., including nearly two-thirds of Ohio. It was destroyed by the glaciers of the Pleistocene Ice Age about 2 million years ago. Remnants of the valley of the Teays River are preserved as flat-bottomed valleys in hilly, unglaciated southern Ohio and West Virginia, and as deep valleys now filled with sediment. The Teays River system originated long before 2 million years ago, in the Tertiary Period, and had its headwaters in western North Carolina near Blowing Rock. It flowed northward across Virginia and West Virginia, where its course is marked by the valleys of the modern New River and the Kanawha River. From St. Albans, West Virginia, the Teays flowed westward to Wheelersburg, Scioto County, Ohio, and then northward to Chillicothe, Ross County. This valley segment is dramatically visible on satellite imagery.

Chillicothe marks the southward limit of glaciation in central Ohio, and the valley of the Teays disappears beneath glacial sediments (drift) at this point. However, by means of water wells and other data, the buried Teays valley has been traced beneath the glacial drift northwestward across Pickaway, Fayette, Madison, Clark, Champaign, Shelby, Auglaize, and Mercer Counties to the Ohio-Indiana border. At the Ohio-Indiana border the valley of the Teays appears to be continuous with a buried valley that has been traced westward across Indiana and Illinois, where it emptied into an embayment of the ocean, now occupied by the Mississippi River.

The earliest of three or more major glacial advances destroyed the Teays River system in western Ohio. The edge of the glacier created a massive dam that blocked the northward-flowing Teays and created a major lake in southern Ohio. The lake waters rose to an elevation of nearly 900 feet, creating an intricate pattern of long finger lakes in tributary valleys. Numerous ridge tops poked above the waters as islands.

This lake is estimated to have covered an area of nearly 7,000 square miles (modern Lake Erie has an area of 9,910 square miles) in southern Ohio and parts of West Virginia and Kentucky. It is named Lake Tight in honor of the pioneering study of the Teays system by Denison University professor William George Tight (1865-1910). Lake Tight is estimated to have existed for more than 6,500 years as interpreted from seasonal layers in the sediment deposited on the lake bottom. Eventually the waters of Lake Tight rose to an elevation sufficient to breach drainage divides and create new drainage channels, which in some cases were opposite in direction to the original Teays drainage.

These new drainage channels cut below the elevation of the Teays, forming a new drainage system known as Deep Stage. This event marked the beginning of the modern Ohio River drainage system, although it would require many further modifications from later glaciations to finally shape the present course of the modern Ohio River.
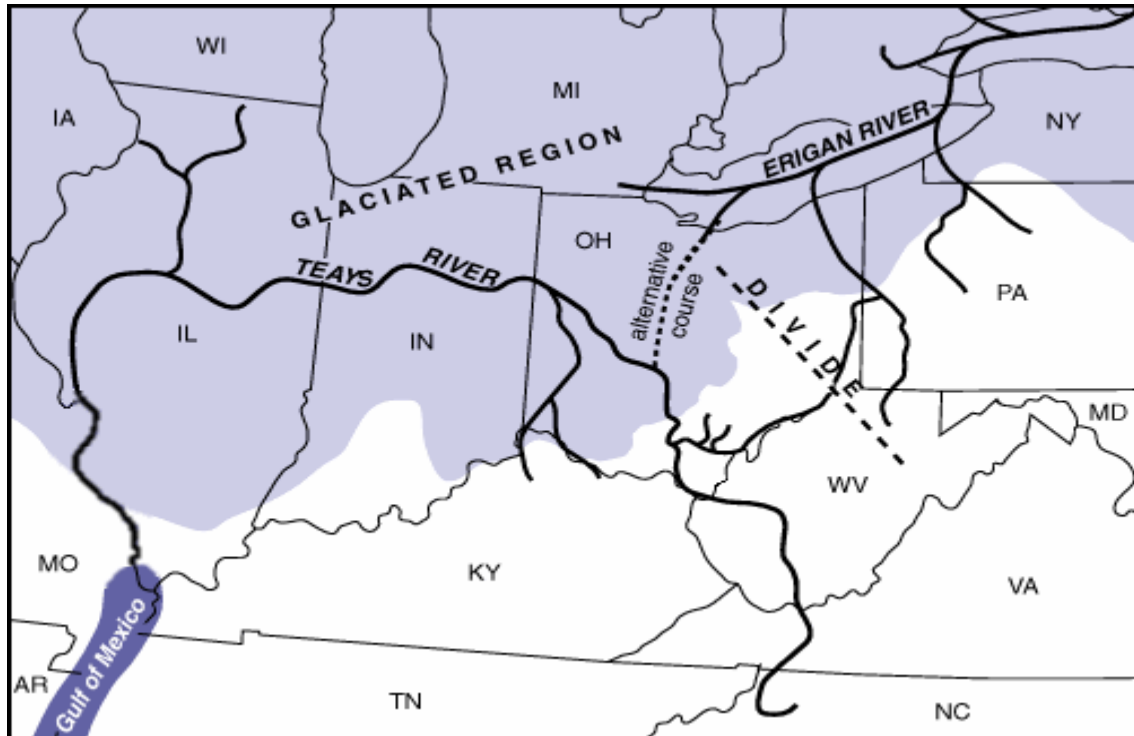
Classic interpretation of the preglacial Teays River

Geology Investigation of Project Site

H.C. Nutting Company performed the subsurface/geotechnical investigation under contract with Michael Baker Jr. Inc. (the Consulting Engineer). H.C. Nutting's scope of services included; reconnaissance of the proposed alignment, evaluation of the existing cut and fill slopes; logging of outcrops; a study of the published geologic data; test boring inspection during drilling operations; preparation of the final boring logs for laboratory evaluation and development of geotechnical recommendations for embankment construction and cut slope design. Based on H.C. Nutting's investigation, recommendations were made for constructing the embankments and cut slopes within the project limits. This papers focus is on the design considerations for Ramp 5 on the project. Due to the project geometric requirements, a large amount of fill was required on this ramp. An abutment for a flyover bridge over I-64 is to be located on top of the fill.

Subsurface Profile from the test borings

In the low lying valley areas of the site interbedded alluvial/lacustrine soil deposits were encountered. The encountered alluvial/lacustrine soils are considered highly compressible and have low to moderate shear strength. The thickness of the lakebed/alluvial deposits ranged from 25 to 77 ft. within the test borings. Typically the shallower lakebed deposits are associated with

the west and east sides of the valley and the deeper lakebed deposits are associated with the center portions of the north south trending valley that bisects the project area.

The lakebed deposits as encountered in the test borings were described as lean clay, silty clay fat clay and sandy clay with occasional interbedded silt and sand seams to partings. The AAASHTO classification of the lakebed soils was described as A-4 A-5 A-6 A7-5 and A-7-6 with occasional layers or seams of A-2-5, A-2-7.

The moisture contents of the lakebed soils ranged from 19 to 40% and were typically above 25%. Atterberg limit test performed on selected lakebed soil samples indicated liquid limits ranging from 24 to 61% and plastic limits ranging from 16 to 30%. Typically below a depth of 10 ft of the existing ground surface, the water content of the soil ranged from 4 to 16% above the plastic limit. Soils shallower than 10 ft typically were at or slightly below the plastic limit of the soil.

According to unconfined compression strength test the undrained shear strength of the soil ranged from 0.4 to 2.8 ksf and was typically below 1.8 ksf. These undrained shear strengths indicate very soft to stiff consistency. Consolidated undrained triaxial compression tests with pore water pressure measurements indicated effective cohesion values ranging from 20 to 50 psf and effective phi values ranging from 19 to 25 degrees.

Several one dimensional consolidation tests were also performed on the lakebed soil samples. The consolidation tests indicated compression indices ranging from 0.13 to 0.68 and recompression indices ranging from 0.02 to 0.14. From the consolidation data it was determined that the preconsolidation pressures within the lakebed soil samples ranged from 2 to 5 tsf with corresponding overconsolidation ratios ranging from 1 to 11 indicating both normally consolidated and over consolidated soils are present at this site. Typically, the overconsolidation ratios within the tested overconsolidated lakebed soil samples ranged from 2 to 5. The overconsolidation is likely due to desiccation and chemical reaction in the soil after it was deposited.

In order to construct the ramp and abutment, two very important design considerations had to be addressed: Settlement and Stability.

Embankment Settlement

Due to the compressible soils beneath the embankment, settlements associated with consolidation of the foundation soils was anticipated as the embankments were being built and for a period of time after completion.

The settlement of the foundation soil is a function of three items:

1.   The height of the embankment
2.   The thickness of the underlying soils
3.   The consolidation properties of the foundation soils.

As the height of the embankment increases, the stress increase in the foundation soils due to the embankment construction. The stress distribution to the embankment construction within the foundation soils were determined using Bousinessq theory. Due to the aerial extent and significant height of the embankment, the stress influence zone extended to bedrock with little stress dissipation at most locations. As a result the entire foundation soil profile contributes to the foundation soil settlement, and shallow soil improvement will not reduce settlement appreciatively.

The soil parameters for settlement analyses were based on laboratory consolidation tests performed on relatively undisturbed Shelby tube samples from various borings.   Time rate analyses were also performed using data from the consolidation test results and past experience in similar soils. Due to silt and sand partings, seams and layers encountered with the lakebed soils within the boring along the valley floor, two way and three way drainage was conservatively assumed. The following table provides an estimate of the settlement at Abutment 2.

Location	Embankment	Estimated	Estimated	Estimated
	Height	Total Settlement	Time for 50 %	Time for 90%
	(Feet)	(Inches)	Settlement	Settlement
			(Days)	(Days)
Abutment 2	35-42	22-30	60-120	400-500 #

This number could be reduced to 90-100 days with the installation of prefabricated vertical drains. (PVD)

Stability

 A large amount of fill was required for construction of Abutment 2 on top of Ramp 5
 (35-42 ft.). DOH require an allowable long term global safety factor of 1.5 be achieved adjacent to structures. Due to the deep lacustrine soil deposits encountered this safety factor could not be met. Soil deposits at the location of the abutment were 70 feet thick. Deep soil modifications were investigated to increase the allowable safety factor to 1.5.

The three initial soil modifications investigated consisted of:

1. Construction of a toe berm along the right side of the embankment toe.
2. Construction of a select embankment (rock) shear key below the toe of the right side embankment.
3. Stone columns along the toe of right side embankment

The toe berm extended beyond the construction limits and required the purchase of additional right of way. The short term global stability was less than 1.2 which would require staged construction.

The shear key required a minimum 40 ft. deep by 20 ft. wide excavation to meet the required design considerations. As a result of the excavation dewatering would have likely been required posing constructability issues. Additionally it was felt the shear key could dewater the surrounding soils, resulting in subsidence of the nearby structures.

The third option of placing a row of stone columns near the right toe of the approach embankment. This method achieved the safety factors requirements of the Department and appeared to be the preferred option.

All design alternatives required staged construction in order to dissipate excess pore pressure. Prefabricated vertical wick drains (PVD) should be installed to the bedrock (70 to 75 ft at the abutment) to aid in a more rapid dissipation of pore water, and aid in consolidation and shear strength gain in overburden soils in time. Piezometers were recommended to be installed to monitor and control the rate of staged construction.

The Department then requested H.C. Nutting to investigate constructing a Mechanically Stabilized Earth Wall (MSE) to catch the toe of the fill, and also study the placement of a light weight fill behind the wall and additionally as fill material for the embankment. Construction of the MSE wall would minimize the right of way concerns expressed with the previously studied alternatives. The placement of a light weigh fill would address the issues of stability and settlement.

H.C. Nutting was asked to evaluate the material and engineering properties of bottom ash as the light weight fill material. Bottom ash is the waste product obtained from coal burning power plant. John Amos power plant is located in close proximity to the project and was contacted on the availability of supplying approximately 150,000 tons of material. After the availability issue was established, Nutting was directed to proceed with their evaluation. Upon review of the test results of the bottom ash, the Department gave approval for Nutting to pursue a design consisting of installing an MSE wall and embankment using bottom ash as the fill material.

The Highway Department had previously used bottom ash as a backfill material on a MSE wall during the 1980's. At that time little investigation was performed on the electrochemical properties of bottom ash. The focus at the time was on direct shear results and unit weights. Bottom ash is well known to have a relative low unit weight and relative high ϕ.

Bottom Ash Electrochemical and Engineering Properties

WVDOH Electrochemical Specifications & Test Results	
Specifications	**Test Results**
Resistivity > 3000 ohm centimeter	5710-7344 ohm centimeter
Ph 5-10	5.5-6.5
Chlorides < 100 parts per million	Test Waived (Note 1)
Sulfates < 200 parts per million	Test Waive (Note 1)
Organic Content 1% Maximum	1.8 to 2.8 (Note 2)
Note 1 Test Waived: Specifications: If Resistivity is greater than 5000 than test is waived	
Note 2 Test Waived: Organic content judged to be inert	

Bottom Ash (Granular Backfill)			
Physical Properties		**Mechanical Properties**	
Specific Gravity	2.1-2.7	Maximum Dry Density	60-100 lbs/ft^3
Dry Unit Weight	45-100 lbs/ft^3	Optimum Moisture	12-24%
Plasticity	None	LA Abrasion	30-50%
Absorption	0.8-2.0 %	Sodium Sulfate Soundness	1.5-10%
		Shear Strength	38-42 ϕ
		California Bearing Ratio	40-70%
		Perm. Coefficient	10^{-2} - 10^{-3}

MSE Wall and Embankment Recommendations

The geometric requirements of the project required the MSE wall extend for a total length of 835 ft. The total height varied from 6 to 31 ft. The fill place above the MSE wall in the embankment required a 2 ft. cover of random material in order to encapsulate the bottom ash. The following table provides soil parameters that were used in the evaluation of the embankment and MSE wall.

Soil Type	Moist Unit Weight (pcf)	Saturated Unit Weight (pcf)	Effective Cohesion (psf)	Effective Friction Angle (°)	Total Cohesion (psf)	Total Friction Angle (°)
Soil Parameters Used In Global Stability Analyses						
Random New Fill	130	130	200	28	1200	0
Select Embankment	130	130	0	38	0	38
Crushed Stone	130	130	0	38	0	38
Compacted Bottom Ash	70	70	0	38	0	38
Fat Clay	119-120	119-125	50	23	800	0
Silty Clay	120	123	50-100	19-21	800	0
Lean Clay	120	120-123	50	23-25	800-1000	0
Silt and Sand	124	124		28-30	0	28-30
Bedrock	130	130	5000	0	5000-6000	0

Based on results of the unconfined compression strength test of the anticipated MSE wall foundation soils and methods outlined by FHWA LRFD design and construction guidelines, a nominal bearing capacity of 6700 psf was recommended. This was based on using the laboratory shear strength values of relatively undisturbed soil samples near the wall location. These results indicated undrained cohesion values of at least 1400 psf. The nominal bearing capacity is based on a layered analysis of compacted select embankment on No. 57 crushed stone material overlying the natural clay soil. The ultimate bearing capacity should have a resistance factor of 0.6 per the LRFD Manual. For ASD, an allowable bearing capacity of 3350 psf should be used. The MSE wall would require a 5, 4 or 3 ft. undercut below the proposed wall elevation. Locations of the undercut areas were delineated on the project plans. Long term factors of safety of 1.5 were analyzed and achieved for circular and translational failures.

For LRFD design, a nominal sliding resistance of 0.58 should be used based on the MSE wall bearing on compacted select embankment (borrowed rock). A sliding resistance factor of 0.9 should be applied per the AASHTO LRFD Manual.

The wall manufacturer is responsible for the internal stability of the wall, and is contacted by contractor that is awarded the project. The wall manufacturer must meet specifications approved by the department.

Additional Recommendations

H.C. Nutting recommended that locations under the bridge abutment in the embankment and under the highest portion of the MSE wall be monitored electronically for pore pressure, settlement and stability. Three locations were chosen for installation of piezometers to monitor the pore pressure. Two locations were chosen for the installation of the settlement sensors. Two locations were chosen for the installation of the slope inclinometers to monitor the stability. These areas were on the project plans. Special provisions were included in the project contract specifying requirements for the type of instrumentation and method of providing data to the Highway Department.

Construction Summary

The contract to construct the interchange was awarded to Kanawha Stone, Nitro West Virginia. Kanawha Stone contacted Foster Geotechnical to supply the MSE wall. The placement of the bottom ash in the fill and MSE wall was placed with no significant construction issues. The density of the placement of the bottom ash was controlled by establishing a target maximum dry density. PVD drains were placed on the project for a total 104,000 lf, of which only 13,656 lf required predrilling. Maximum measured settlement readings from the settlement sensors were 9 inches, at the abutment location. Piezometer readings were negligible during construction of the fill and MSE wall. No movement could be detected by the two installed slope inclinometers. Survey markers on the wall and fill are continuing to be monitored to determine if any additional settlement is occurring. The project is scheduled for completion during the fall of 2004.

As a side bar to the construction of the MSE wall, and after the contract was awarded, discussions within the Department questioned the long term affect of galvanized reinforcements behind MSE walls. Research and literature was studied to determine an approach to monitor the long term strength of the galvanized reinforcements. Foster Geotechnical supplied information on a program that California DOT had instituted to monitor the reinforcement in their MSE walls. Ca. DOT's program consists of installing test rods in their MSE Wall's. The test rods are located parallel to the plane of the primary reinforcements and their material properties match the primary reinforcement. The test rods are removed from the wall during specified times and there condition is evaluated. The author contacted Ca. DOT and was supplied with details of the installation and extraction procedures of the test rods. A change order was intimated with Kanawha Stone for the installation of 18 test rods. Three test rods are scheduled for removal on a schedule of three rods every five years. The first rods are scheduled for removal in 2010. Hopefully my colleagues in the Highway Department will keep abreast of the extraction of these test rods and provide the results to the Highway Community.

Acknowledgements

References

H.C. Nutting Report of Geotechnical Investigation U.S. 35/64 Interchange

FHWA Mechanically Stabilized Earth Walls and Reinforced Soil Slopes Design and Construction Guidelines

Hansen, Michael Geofact Ohio GES November, 1995

"The Ice Age in West Virginia" WVGES Mountain State Geology 1982) p 26-33

"Legacy from the Ice Age" WVGES Mountain State Geology 1987 p 29-32

Majizadeh, Hamran, Gary Bokowski and Rashad El-Mitiny. "Material Characteristics of Power Plant Bottom Ashes and Their Performance in Bituminous Mixtures: A Laboratory Investigation," Proceedings of the Fifth International Ash Utilization Symposium, U.S. Department of Energy, Report No. Metc/SP-79/10, Part 2, Morgantown, West Virginia, 1979.

Soil Nailing:
DOTs Warm Up to New Technology
By
Pat Carr
President, The Judy Company

Soil and rock nailing provides project owners and Departments of Transportation

economic benefits and a rapid means of retaining wall construction, slope stabilization

and excavation retention support. It is a relatively new construction technique, developed

and first used in Europe in the 1970s as a means of excavating and shoring tunnel roofs in

fragile rock conditions during construction. Soil and rock nailing used for retaining walls

and slope stabilization evolved from the tunnel shoring system, and DOTs across the

country are quickly discovering the technique is often advantageous over more

conventional retaining wall construction. Two very different DOT projects proved the

advantages of soil and rock nailing over conventional retaining wall construction in

Kentucky and Iowa.

A retaining wall of 63,000 s.f. was constructed on I-235 in Des Moines, Iowa as a

retaining means and back form for conventionally placed concrete and for pre-cast

concrete panels. The freeway was widened and exit and entrance ramps were added. Soil

nailing allowed excavation and construction to proceed in a minimum right-of-way.

Excavation proceeded very close to city streets and utilities and eliminated the necessity

or detours, lane closures, resulting in avoiding traffic congestion during construction.

On Route 119, in the mountains of eastern Kentucky, near Pikeville, an 8500 s.f.

retaining wall was constructed with a shotcrete finish that was sculpted and stained to

match the geologic look and conditions of the surrounding terrain. An historic cemetery located close by the proposed road prevented conventional excavation and benching and an alternative means of stabilization was needed. The decision to use soil nailing to retain the wall was made because of the technique's unique advantages of requiring minimal working space and it's ability to stabilize a slope without the need to find an anchorage zone for prestressing tie-back anchors.

The use of non-stressed nails instead of pre-stressed anchors was developed and used in Austria in the mid 1970s to stabilize and secure tunnel roofs as they were constructed in fragile rock conditions. Until then, as tunnels were excavated, rock was secured by installing pre-stressed rock bolts, similar to tie-backs, to tighten the tunnel roof rock, putting it in compression and creating a monolithic structure of the roof. Rock bolting is similar to tieback anchors used in shoring. Typically, a hole is drilled to a depth past the rock to be secured and into an anchor zone of competent rock able to handle the anticipated design load. A bolt with an end anchor is inserted. The anchor is then set and the bolt is tensioned using a plate and nut against the rock surface, compressing and thus tightening the rock influenced by the bolt. Finally, the bolt is grouted for corrosion protection and to lock in the tension. This is a very labor-intensive procedure. In addition, it involves moving the rock in the zone to be secured during compression. Austrian engineers in the early 1970s were faced with the construction of a tunnel with a fragile rock condition where there was hesitation about moving the rock. They decided to try an unstressed bolt, later called a nail. Holes were drilled and a bolt without an anchor was

inserted and grouted. They had decided to allow the rock to move, essentially allowing it "fail", in a sense, as the tunnel excavation proceeded. The theory was to engage residual stresses in the rock to act in friction along the grouted bolt mass in hopes that the rock would essentially secure itself. Residual stresses in the rock acted in friction on the grout mass around the nail, and the area of influence of the nail was stabilized. The tunnel was thus constructed in fragile rock where movement into compression was not permitted for fear of collapse, and a new technique, roof nailing, was born. From there, the process of rock nailing emerged for not only for tunnels, but was also applied to like rock fall protection and slope stabilization.. Rock nailing became the normal process to secure a tunnel roof and outcropping for slope protection because it was faster and more economical. There was now no need to set an anchor, grout in the anchor, tension the bolt, and then grout the tensioned section, saving labor and time. Construction costs dropped and schedules shortened. The new method of passive reinforcement of rock in tunnel excavation came to be known as the New Austrian Tunnel Method, or, NATM, and the procedure revolutionized the tunneling construction industry

Eventually, the process was successfully attempted in soil and rock retention. Tiebacks, the retention technique of choice, as with rock bolts, require the finding and reaching an anchor zone, setting the anchor and tensioning a bolt. With the correct soil and rock conditions, soil nailing is extremely rapid and economical, produces less noise, requires less labor, and can be installed in shorter depths requiring fewer easement and property issues. Since nailing uses the soil to be retained as its anchor instead of having to reach an

anchor zone, the technique allows complete geometric flexibility for shape and for changing field conditions.

Soil nailing projects generally follow the same procedure as with any retention technique. Geotechnical engineers, employed either by the contractor or the owner, design the soil nailing, taking into account soil compatibility and characteristics, strength requirements, and consideration for the surface wall load expected. The technique works in cohesive soils or soils with enough apparent cohesion to allow a vertical cut and a drilled hole to remain open for about 24 hours. Nailing is also excellent in weak or fragmented rock and in mixed-face conditions.

First, a field test program is initiated. Bolts are installed and tested for pullout resistance in various soils, chosen based on the geotechnical soils report. Pending results, bar lengths, hole diameter, bar spacing and depth are adjusted and retested to meet design requirements.

The process is top-down construction. A bench of four to six feet is excavated with a horizontal working surface needed of about twenty feet. Holes are drilled into the excavated face, typically ten to fifteen degrees below horizontal, and six to eight inches in diameter in soil and three to four inches in rock. For soil, cohesive soil is more suitable because the excavated bench needs to stand unsupported for the workday while the nails are installed and the facing is applied, and because the drill hole needs to be able to stay

open during nail installation. For those reasons it is important, actually critical, to excavate only what the crews can finish during a day.

Hole depth varies based on soil characteristics but typically penetrates the global failure plane and continues roughly another third of that distance. Hole spacing typically ranges from four to eight feet.

Retaining walls can be permanent or temporary, which plays a role in the materials used. Temporary retaining walls are often used during building construction to maintain an excavation until the structure's below grade stories are built. The exposed exterior walls of buildings or parking structures can be built top-down using soil nail construction. For this type of construction, floor reinforcement bars are added and stubbed out of the wall.

The nails are generally of grade150 steel and are continuously threaded so they can be cut and coupled to any length in the field as needed. Where the nails are to be permanent, they are generally epoxy coated or are equipped with a corrugated sheathing that has been factory grouted as an extra measure of corrosion protection. The encapsulation in grout also provides corrosion protection.

Once the holes are drilled, they are pumped full with grout, usually with a concrete pump from a ready-mixed truck. The grout, like the nails, follows the design specifications of the geotechnical engineer. Immediately following pumping, the nails, fitted with centralizers, are inserted into the grouted holes with enough bar protruding past the

surface to be fitted with an integrating device for the wall load, usually a bearing plate and nut.

To prevent hydrostatic buildup in permanent walls, a drainage system consisting of vertical and sometimes also horizontal drain strips are installed against the excavated face prior to placing the shotcrete. The system collects and funnels surface runoff and below grade water to the base of the wall to a drain system that carries it away from the wall.

Reinforcing is added over the drainage system, typically consisting of reinforcing bars and a welded wire fabric mat.

A load transfer device, usually a bearing plate and nut, is fixed onto the bar protrusion to transfer the anticipated wall load into the nail and finally into the soil. If a cast-in-place or sculpted wall is to be placed over the construction facing, Nelson studs are welded to the bearing plate as a load transfer device for the finish wall to the soil nails.

With the nails, drainage system, reinforcing, and load-bearing plates in place, the shotcrete surfacing is applied. A high-pressure concrete pump, usually the same one or type used to fill the holes, is used to spray the excavated face to the thickness designed. The spraying of shotcrete should always be performed by an experienced craftsman to assure all voids are filled and there is no "shadowing" behind the reinforcing steel. Temporary walls have a construction facing and as with excavation shoring are typically 4-6 inches thick. Permanent walls are typically 6-12 inches thick, depending on structural

requirements. For walls behind either cast-in-place concrete or pre-cast concrete panels, the surface can be left rough or trimmed with control wires. For permanent walls, hand finish troweling can be applied.

If a sculptured look is desired, as in the case of the Pikeville, Kentucky project, the structural facing is carved and later stained. After completing the construction facing, Nelson studs were fixed to the bearing plates and an 8-inch thick layer of shotcrete was placed working from a manlift. Following closely behind, sculptors on another manlift carved the shotcrete from the top down using hand trowels and brushes, emulating the natural rock formations of the area. After curing, the wall was stained, making the finished product look like a natural cut.

On the I-235 project in Des Moines, an 8 inch cast-in-place wall with rustication grooves was constructed over the shotcreted soil nail wall facing. The facing chosen matched other construction being performed along the freeway corridor.

To summarize, with the right soil and site conditions, soil nailing is a rapid and economical means of constructing earth retention support systems and retaining walls, with the following advantages

- Allows foundation construction in limited area, reducing easement issues
- Works through different soil strata
- Top-down construction
- Shorter drill holes than conventional tie-backs

- Smaller bar diameters at shorter lengths

- Retainage is secured laterally into the soil, eliminating piles and foundation footers

- Because of the small working area required, excavation for building or road construction can proceed simultaneously

- Passive, not pre-stressed, saving labor and time

- Grouting only once is required instead of twice as with pre-stressed anchor tie-backs

- Requires only cohesive soil or broken rock, does not need anchoring in competent rock

- Drainage system eliminates hydrostatic buildup

- Hard face shotcrete is applied and can be left rough, finish troweled, or sculpted and stained

- Forming and placing concrete wall unnecessary, saving labor, material, and time

- Soft facing can be applied instead of shotcrete for soil retention or slope stabilization

- Geometric flexibility because the nails are essentially anchored by the same soil it is intended to secure and anchor zones aren't necessary

We at the Judy Company support and encourage the consideration of this important geotechnical construction technique. Thank you for your time.

MONITORING SHALLOW SLOPE FAILURES IN THE OZARK PLATEAU USING TIME DOMAIN REFLECTOMETRY

Norman D. Dennis, Jr., University of Arkansas, Fayetteville, AR
Voon Huei Wong, MACTEC Engineering and Consulting, Birmingham, AL
Chongwei Ooi, CEI Engineering Associates, Bentonville, AR

Abstract

Time domain reflectometry (TDR) is gaining attention as a cost effective method to monitor mass movements in both soil and rock. It has been used successfully to monitor deep-seated failures in soil deposits and for monitoring many different kinds of movements in rock masses. However, its use in monitoring shallow failures in engineered cut slopes and embankments has been limited. The chief benefit of using this technology would be to remotely monitor the effectiveness of remediation measures. This paper describes a study, conducted in Arkansas' Ozark Plateau, in which TDR was used at various sites where shallow failures were imminent or had already occurred along highway cut slopes and embankments. Several types of coaxial cables were evaluated under field conditions to determine which type had the best potential for accurately depicting the location of failure slip surfaces. The monitoring at all sites consisted of grouted coaxial cables in combination with grouted inclinometer casing in which a probe inclinometer was used to establish a reference for movements in the slopes. Moisture contents were also determined using TDR methods. The TDR cables and moisture probes were monitored remotely through an automated data collection system while inclinometer data was collected manually on an intermittent basis. It was determined that all cable types performed differently in the field and each had certain installation and maintenance issues. Threshold movements, necessary to produce a distinguishable cable signature, were determined for several locations. Based on installations at four sites recommendations relative to cable type, installation procedures and the overall effectiveness of this monitoring method for shallow slope failures are given.

1. Introduction

On January 8, 1999, the Arkansas State Highway and Transportation Department (AHTD) opened the final section of a new interstate highway designated as Interstate 540 (I-540), which connected Ft. Smith to Fayetteville. The new 69km span, traversing the rugged terrain of the Ozark Plateau in Northwest Arkansas, has 13 major bridges and a 430m twin bored Tunnel. The overall cost for this project was $460 million equivalent to $6.7 million per kilometer ($11 million per mile), an expensive project for the area. During the construction of portions of the new highway, repair of slope failures and modifications to slide prone areas cost

approximately $65,000 per mile per year (Connelly et. al., 1999). Additionally, the state highway department has spent over $33 million on slope repairs for this section of road after only four years of service. These expenditures have made this section of I-540 not only the most expensive interstate ever built in Arkansas but also a high maintenance highway. As a result of this large investment in slope repairs, the State of Arkansas has become astutely aware of the need for proper repair techniques as well as the need to monitor the effectiveness of these repairs.

The issues with slope failures continue along this section of road, with the Highway Department documenting 37 new slope failures during the period May 2001 to May 2004 alone. In addition, an extension of this Highway system to the south through similar terrain promises more problems with slope stability. Currently, the principal remediation technique for failures in this area has been removal of failed material and replacement with rock or rock buttressing, which is a very expensive remediation technique. With the requirement for continual slope maintenance the Highway Department is seriously investigating more cost effective preventative measures for slope instability such as the installation of drainage systems and is interested in developing means to remotely monitor the effectiveness of these remediation systems.

2. **Monitoring Systems**

Historically, the monitoring of slope performance or the actual mass movements in slopes has been conducted with surveying instruments, inclinometers and even piezometers. These techniques, while accurate, require technicians to visit the site periodically to take or record physical measurements and often times the data must be interpreted to determine it's inferred meaning. Also, the periodic nature of these techniques can sometimes cause investigators to miss significant movements. Engineers have developed many systems that can monitor movements autonomously, but most are very expensive. Time Domain Reflectometry appears to be a cost effective technique that has been used successfully in the past to monitor movements in rock and deep-seated slope failures on an intermittent basis. This method promises to be an effective remote monitoring technique that can autonomously monitor the effectiveness of slope remediation measures on a continuous basis.

Time Domain Reflectometry, (TDR), is similar to radar in that is uses reflected energy to determine the location of anomalies in normal energy patterns. In the case of TDR, all of the system energy is confined to a waveguide or cable. A schematic diagram of a TDR system used to monitor deformations in slopes is illustrated in Fig. 1; while the actual hardware required to create the monitoring system is portrayed in Fig. 2. The TDR monitoring system essentially consists of a coaxial cable, grouted into a borehole, which traverses the anticipated shear surface of a slope failure. This system uses a pulse generator/receiver, called a cable tester to send a fast rise energy pulse through a coaxial cable. It then waits for energy from that pulse to be reflected from the end of the cable. Any anomalies or defects along the length of the cable, such as those produced by shearing will reflect a portion of the energy pulse. By knowing the propagation velocity of the energy pulse through the cable, the time of arrival of the reflected energy can be used to determine where the anomaly exists in the cable. While the TDR methods have been used successfully in the past to monitor mass movements in rock, [3] [4], or deep failures in soil masses [5] they have not been used to detect shallow failures like those occurring in the I-540 right-of-way. In addition, previous TDR research has not revealed the threshold movement necessary to produce a satisfactory TDR signature.
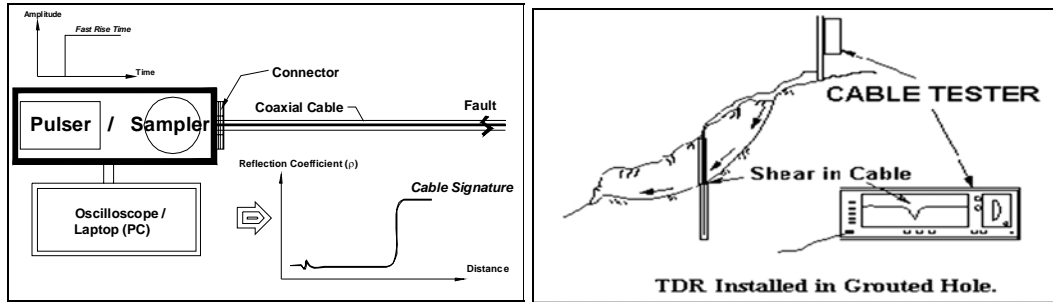
Figure 1 a.) Schematic of the monitoring of the energy pulse generated by the cable tester. b.) Schematic Diagram of TDR installation in an actively moving slope. (After Kane, 1996)

Figure 2. TDR hardware used in this study; Clockwise from top left, 16 channel data logger, cable tester, multiplexer, , analog cell phone, modem, complete field installation, TDR moisture probe.

3. Study Methodology

This study employed both inclinometers and a TDR system to monitor movements in slopes that were believed to be actively moving. Inclinometers were used as the absolute reference in the actively moving slope to determine the displacement required to produce a threshold signal from the TDR system. Efforts were also made to determine the most cost effective cable type to be used in the TDR application by comparing the reflected electrical signatures of four pre-selected coaxial cable types in the laboratory. Finally, TDR moisture probes were used in this project in an attempt to tie slope movement to increases in sub-surface moisture.

The initial site selected for study was a cut slope located at mile marker 46 of I-540. This slope consisted of between 2 and 5 meters of soil underlain by shale. The face of the slope was cut at 3 on 1 and had only sparse grassland type vegetation. This site was selected because a recent failure had occurred adjacent to it and there appeared to be a toe bulge forming at the specific location selected. The plan and profile of the cable installation is depicted in Fig. 3. Each row of the installation had four different cable types and an inclinometer installed in
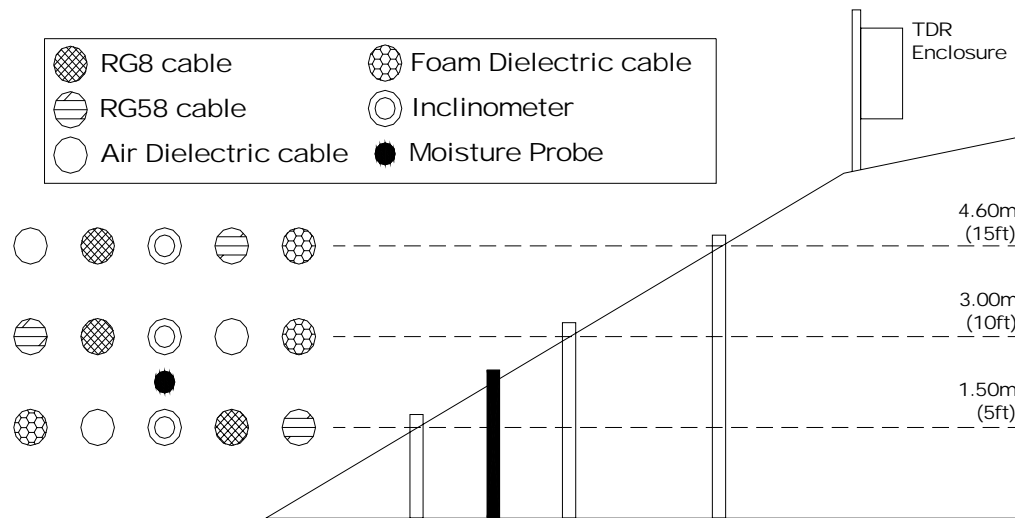

Figure 3. Schematic diagram of cable and inclinometer layout for the mile marker 46 site.

separate 200 mm boreholes with a weak sand-cement grout. The grout mixture was composed of 5 parts sand to one part cement with a water to cement ratio of 2.65. The four cable types selected for study, along with their associated connectors, are depicted in Fig. 4. The air-dielectric and foam cables are considered rigid cable while the RG8 and RG58 are considered flexible. Properties and costs of these cables are itemized in Table 1. The rigid cables were terminated about 300 mm above each borehole and connected to a length of flexible RG8 cable, which ran from the borehole to the data collection station. The flexible cables were run continuously from the bottom of the borehole to the collection station. All cable runs from the borehole to the data collection station were covered with a thin layer of soil for protection. The inclinometer casings were initially logged on a weekly basis and cable signatures from the TDR system were collected every two hours. The data logger of the TDR system had sufficient memory to store one week of cable signature data before the information had to be off-loaded.
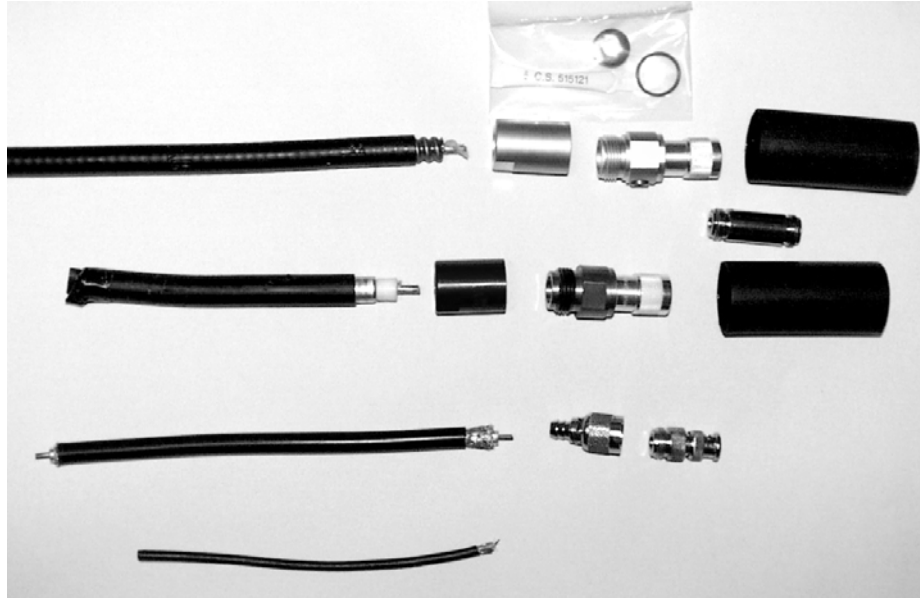
Figure 4. Cable types and connectors installed for this study.

Table 1. Summary of cable properties and costs for the cables types used in this study.

Cable Type	Diameter (mm)	Impedance (ohms)	Propagation Velocity (%)	Cable Cost (m)	Connector Costs (installation)
Air Dielectric	12.5	50	91.5	$13.50	$100.35
Foam Dielectric	12.5	50	81	$6.60	$40.32
RG8	12.5	50	82	$2.40	$9.20
RG58	9.5	50	66	$0.75	$3.80

After the first two months of operation it was concluded that the lack of activity at this site did not warrant the frequency of the collection efforts. As a result, TDR cables were scanned on a two hour frequency but data was only collected once a day and the frequency of inclinometer logging was reduced to once a month. The summary of a sample series of cable signatures for one year of monitoring at this location is displayed in Fig. 5. Each monthly signature has been manually offset by an impedance of 0.02 rho for display purposes. The baseline reading is at the bottom of the chart and it is obvious that none of the subsequent readings display any anomalies in the cable geometry. This set of readings is typical of all the readings taken at this site. Several issues arose with faulty connections and water intrusion into the air-dielectric cable that gave false indications of anomalies in cable geometries, but the locations did not match the movement recorded by the inclinometers and reason for the changes in impedance were isolated and corrected. A summary of the inclinometer readings for the same period is provided in Fig. 6. The maximum movement recorded in the top-row borehole by the inclinometer was only 4 mm. It became apparent after two full cycles of wet seasons that the portion of the slope selected for the study was not moving while areas on both sides of the

study area exhibited obvious signs of significant movement. It is likely that the grouted boreholes provided adequate reinforcement to this shallow failure so that the factor of safety remained well above one.
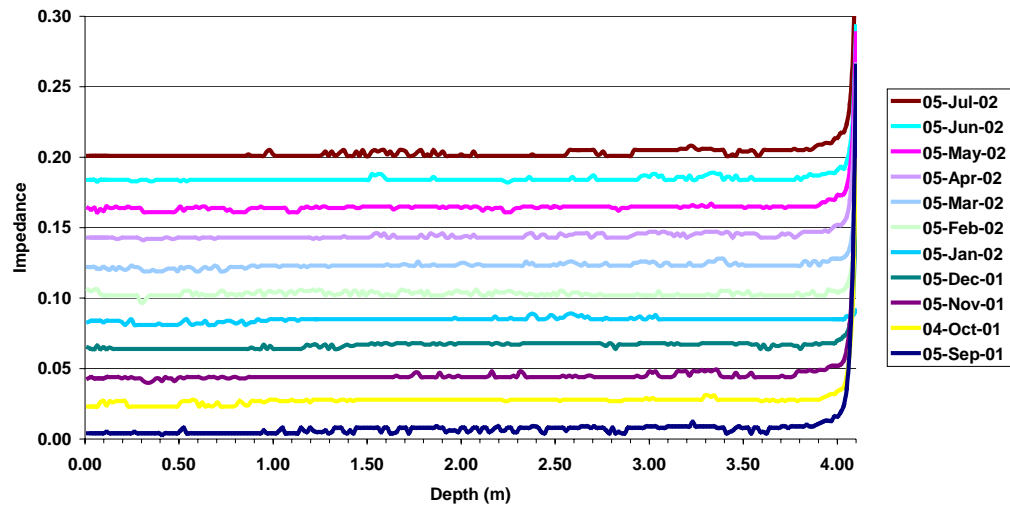

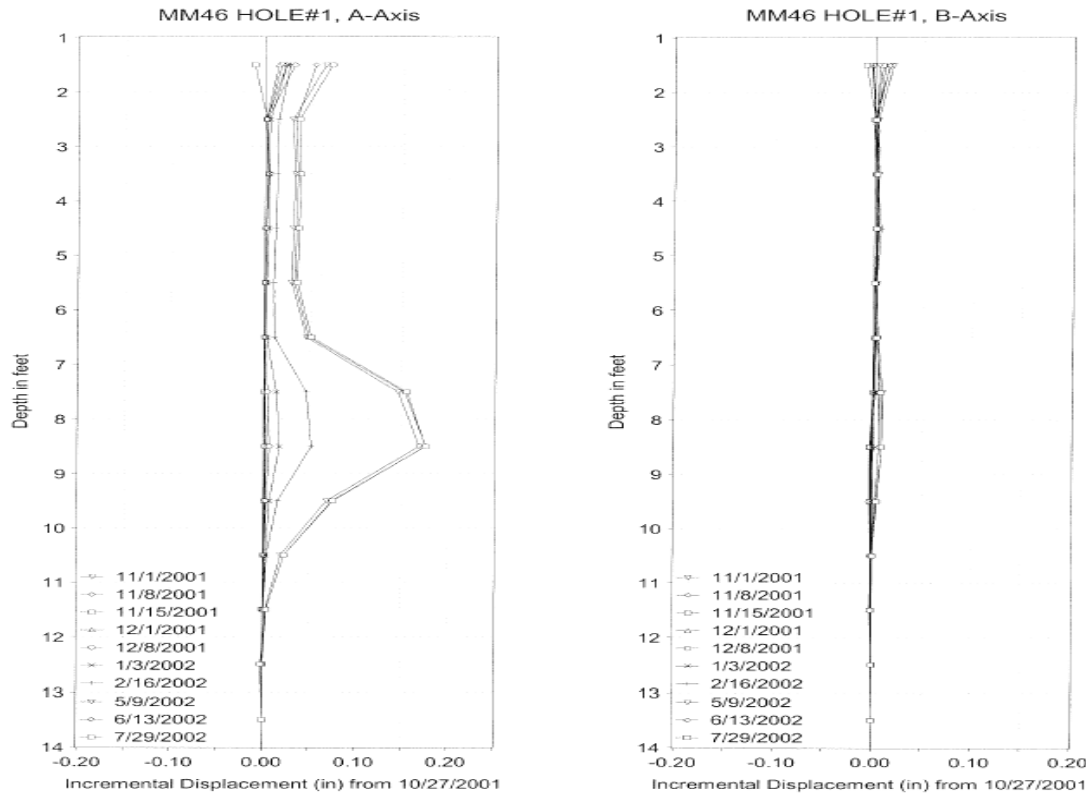Figure 5. Summary of signatures for the RG8 TDR cable installed in the top row at MM 46.

Figure 6. Summary of inclinometer readings for the top row at mile marker 46.

As a result of the discouraging field results at mile marker 46 a laboratory investigation was conducted to determine the amount of movement required along a shear surface to produce a noticeable "spike" in the TDR cable signature. A loading device, illustrated in Fig. 7 was created that could load three grouted cables in double shear at one time to a maximum deflection of 25 mm. A summary of the loading results for the foam dielectric cable is presented in Fig. 8. It is apparent from the information in Fig. 8 that at least 7 mm of deformation are required to produce a "spike" in the cable signature and that the spike increases
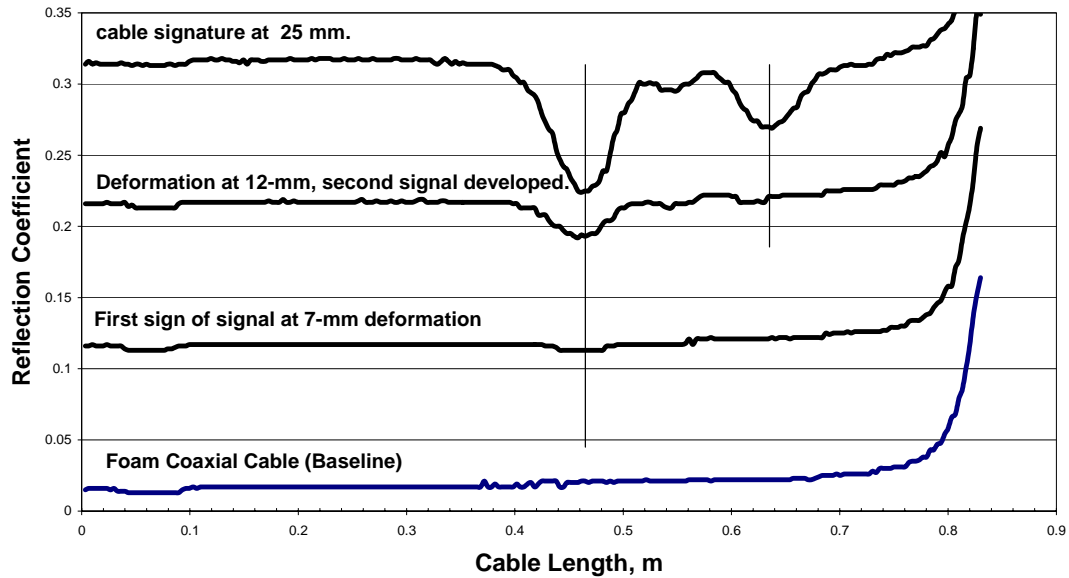

Figure 7 Results of laboratory shear testing for foam dielectric cable.

in magnitude as deformation increases. RG8 cable produced similar results, exhibiting the first noticeable spike at 5 mm of deformation. Both RG8 and foam dielectric cables produced a useful signature over the full range of deformations investigated. The results for RG58 and the air dielectric cable were not as pronounced and their useful range of deformation was limited. The first spike for the air dielectric cable did not occur until 10 mm of deformation and the cables shorted out after only 15 mm of total deformation. The RG58 cable exhibited a positive change in impedance at approximately 7 mm of deformation. This behavior is indicative of a failure of the outer conductor rather than a deformation of the insulating material. This cable exhibited the signature of a completely open outer conductor by 13 mm of total deformation. This laboratory investigation indicated that RG8 and foam dielectric cable gave the most useful results over the widest range of deformations. However, the decision was made to continue to test all four cable types in the field because of the success reported by others, [4], [5] for the air dielectric and RG58 cables. An additional finding of this laboratory study was that there appeared to be a nearly linear relationship between deformation and increasing magnitude of the spike in the cable signature for both the foam dielectric and RG8 cables Figure 8 illustrates the relationship between changes in cable impendence and deformation for the RG8 cable. The reflection coefficient results for the foam dielectric cable were similar to those presented for the RG8 cable.

Figure 8. Changes in reflection coefficient versus increases in deformation for RG8 coaxial cable.
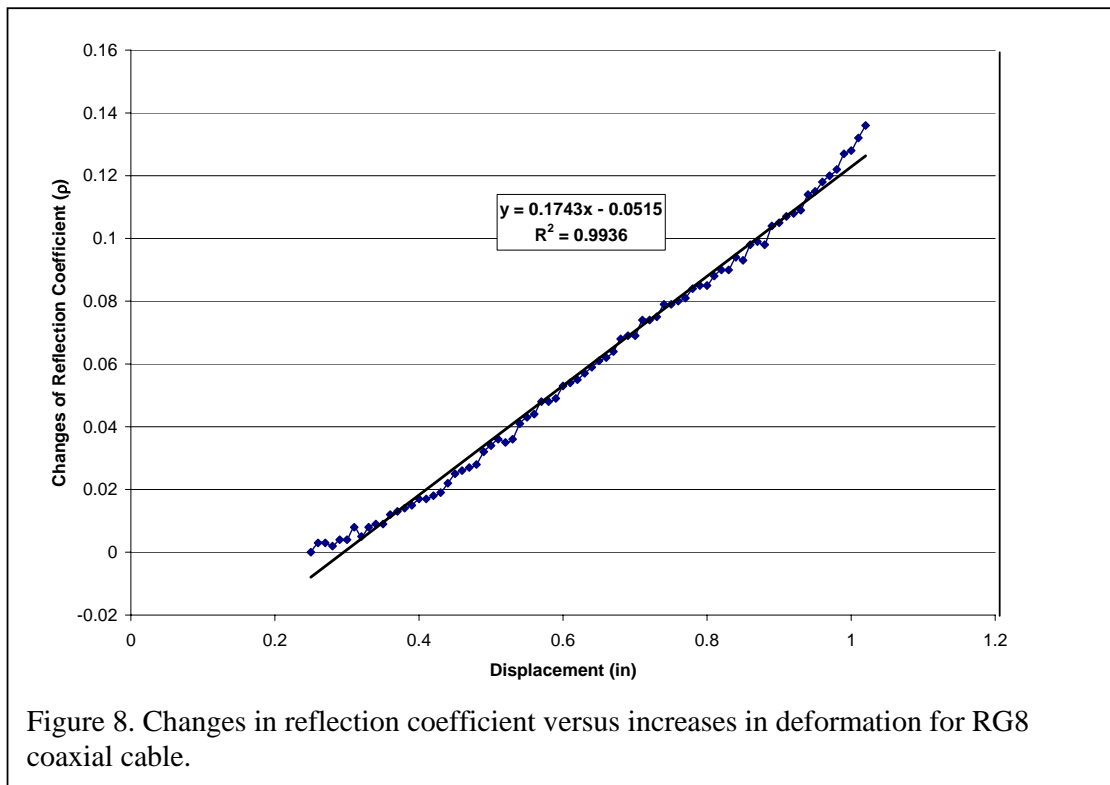
At the conclusion of the laboratory testing a new study area was selected for a revised installation of the TDR monitoring sytem. The new area was located at mile marker 50 on interstate 540. This was another 3 on 1 cut slope constisting of 3 to 5 meters of mixed clayes over shale. This slope had failed two times previously. Each time the failed material was simply pushed back into place with a bull-dozer. This slope was considered a very likely candidate as an actively moving slope. The schematic of the cable layout for this installation is illustrated in Fig. 9. .

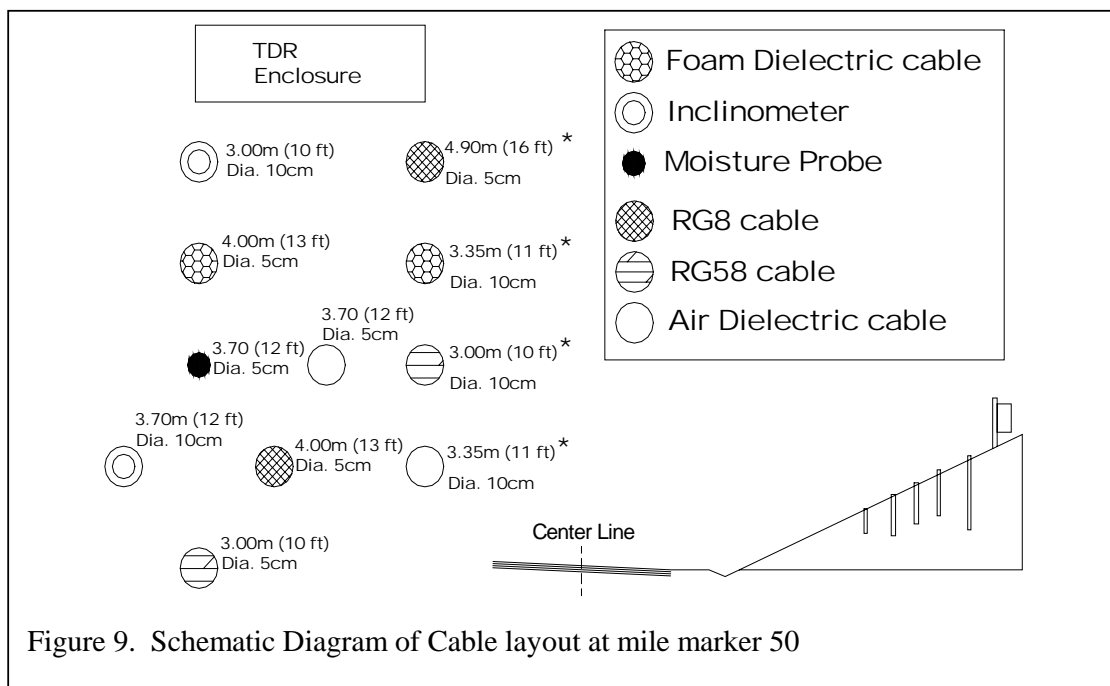Figure 9. Schematic Diagram of Cable layout at mile marker 50

Fig. 9 indicates that there are duplicates of each cable type installed essentially side by side. Initially all cables on the left side of Fig. 9 were grouted into 70 mm borehles using a weak cement-bentonite grout that constisted of 1 part bentonite to 1 part Portland cement with a water to cement ratio of approximately 4.0. Due to poor mixing of the grout and the high percentage of benonte in the grout mixtue, zones of very weak grout, (qu = 455 kPa) were created in the boreholes. After four weeks of monitoring this installation it was concluded that the grout would not develop sufficinet strength to deform the rigid cables. As a result, a second installation of cables, shown on the right side of Fig.9, was made. For this installation all cables were grouted into 100 mm boreholes with a cement-bentonite grout that consisted of 10 Kg bentonite, 43 Kg Portland cemtent and 150 liters of water in a portable 0.2 cu m concrete mixer. This gave a water to cement ratio of 3.5. This combination of grout and borehole diameter created a significantly weaker grout column than the sand-cement mixture used at mile marker 46, but the grout itself had a compressive strength of approximately 5500 kPa.

After approximately 12 months of monitoring the second installation, the TDR cables started to exihibit the characteristic "spike" associated with a developing shear surface. Inclinometer readings verified the location of the shear surface and the locations indicated by both monitoring systems matched well. A summary of the cable signatures for the foam dielectric cable from the second instllation is given in Fig. 9 and the correspnding inclinometer data is given in Fig. 10. It is significant to note that the TDR cable did not register the presence of a shear surface until August of 2003 and the deformation required to produce the "spike" was approximately 20 mm, as determined by the inclinometer. This was about 4 times the deformation required in the laboratory to produce a similar "spike" in the signal. None of the cables from the initial installation at this location ever exhibited a cable signature that varied form the baseline signature.
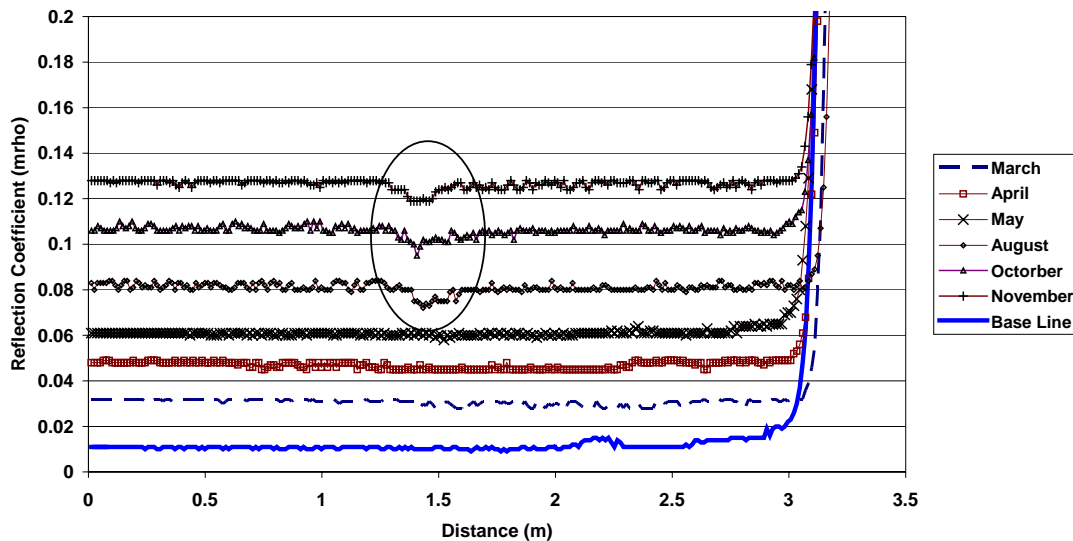

Figure 10. Comparison of waveforms for the second foam dielectric cable installed at mile marker 50 from March 2003 to November 2003.

In an attempt to verify the apparently large field deformation required to produce a spike in the cable signature a final installation of TDR cables and inclinometers was made.
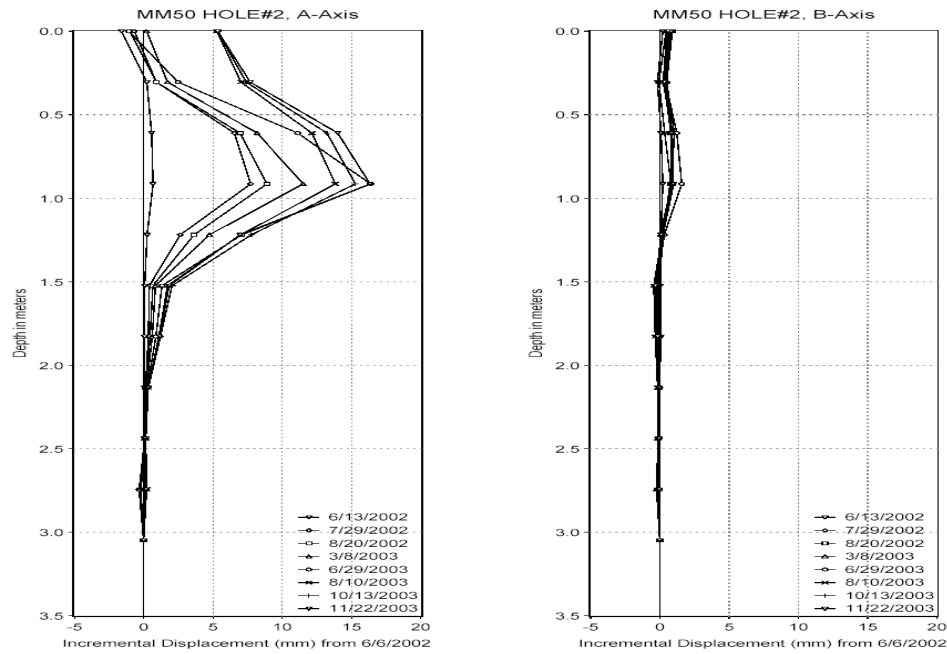
Figure 11. Summary of inclinometer data for the lower borehole at mile marker 50 on Interstate 540.

The installation was made in an actively moving slope near Batesville, Arkansas in June of 2003.   The prescence of a an ever widening crack in the sout bound lanes of US 167 provided evidence of the failure activity of this slope. Figure 12 illustrates the monitoring layout for this installation along with the proposed repair for the failing slope.This installation constisted of two RG8 cables grouted into 100 mm boreholes and two inclinometer casings
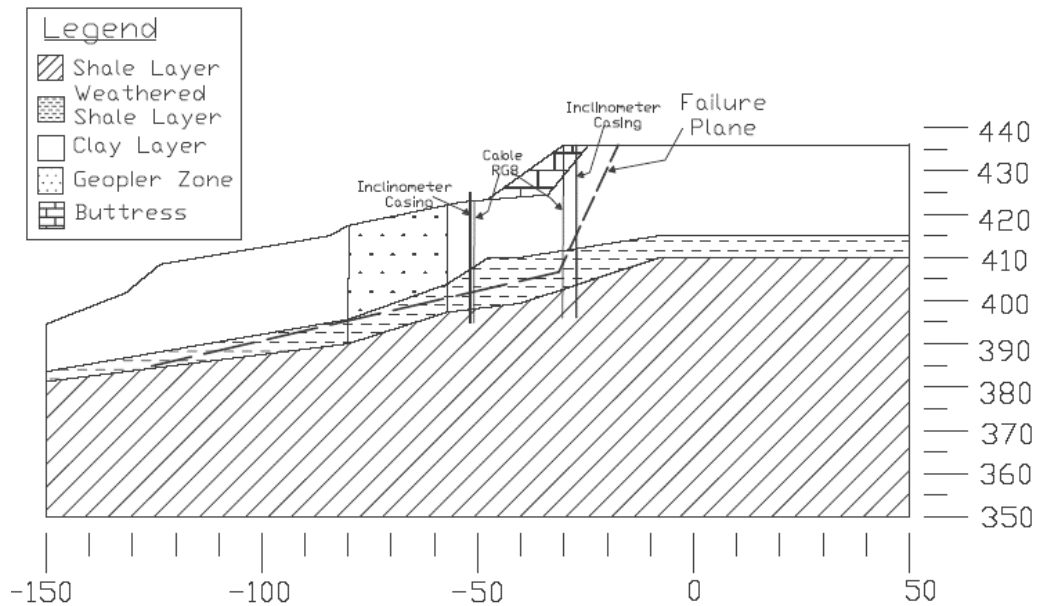

Figure 12. Cable and inclinometer installation schematic for Batesville, AR.

grouted into 200 mm boreholes. Cables were grouted with a cement bentonite grout consisting of 1 part bentonite to 2 parts Portland cemtent with a water to cement ratio of 2.7. The grout had a compressive strenght of approximately 8200 kPa. Illustrated in Fig. 13 are the incremental dispacements of the upper (a) and lower (b) inclinometer casings over the six month monitoring period. The upper inclinometer casing became mis-aligned during installation and the movement recorded was not primarily in the plane of the A axis, so a vector sumation of both te A and B axes is required to determin the absolute incremental movements. Figure 14 provides a summary of the TDR cable traces from the the upper cable installation. Inspection of Fig. 14 reveals that the first noticable anomoly in the cable trace was detectect in September of 2003. The cable traces, illustrated in Fig. 14 are for the same dates as the inclinometer data shown in Figure 14a. Of significance when comparing these two figures is the fact that the vector sum of the A and B axis movements along the shearing surface for the upper casing is almost 33 mm at the point in time when the TDR cable indicates movement. Note that in Fig. 13b the inclinometer data do not portray a clearly defined falure plane but rather a failure zone of about 1 meter in thickness. The corresponding TDR signatures in Fig. 15 for the lower cable, while distiguishable at movements exceeding about 25 mm, do not exhibit the clearly defined "spike" as those for the upper cable,shown in Fig. 13. This points to the fact the shearing must be confined to a very thin zone for the detection of movement using TDR to be effective. The increase in the required deformation to produce a "spike" at the Bateville site when compared to the threshold movement at mile marker 50 on I-540 is likely due to the significantly increased cable lenghts used at the Batesville site. At the Batesville site the cable run from the grouted
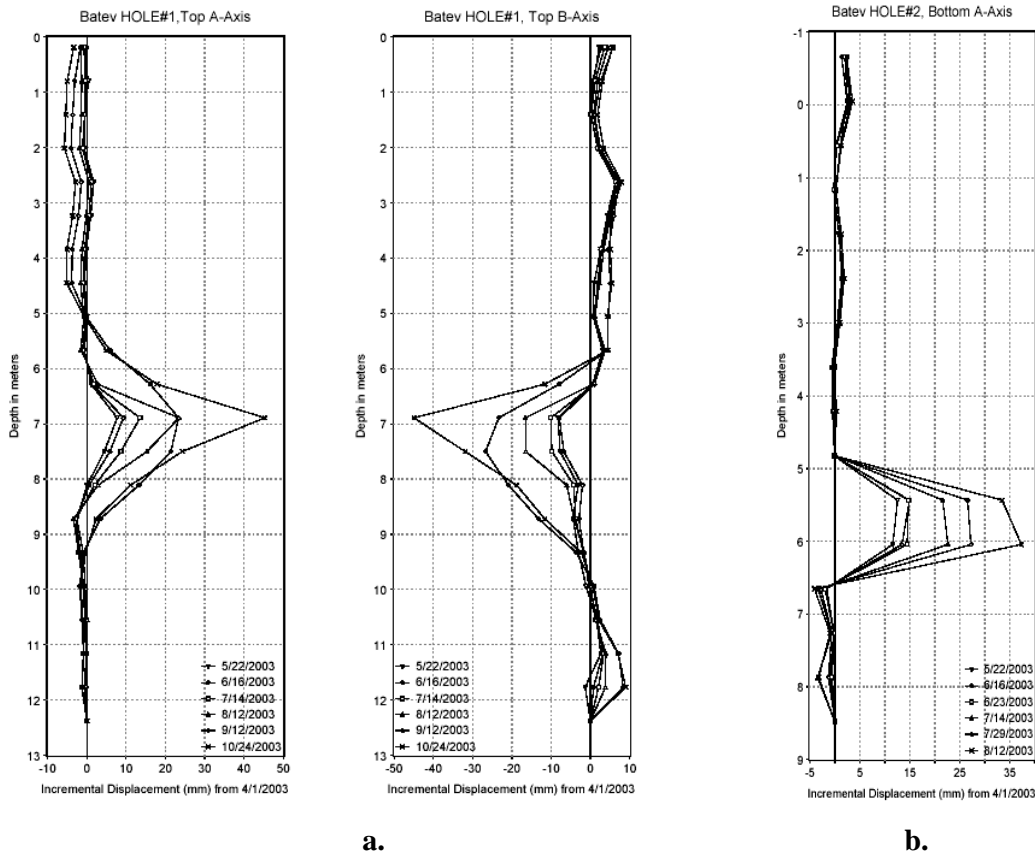

a.   b.

Figure 13. Summary of inclinometer readings for: a.) Upper casing. b.) Lower casing.

probe to the TDR enclosure was over 60 meters while it was less than 15 meters for the the site at mile marker 50. This icrease in length causes signal attenuation which in turn requires a more significant shearing action in order to observe any reflected energy.
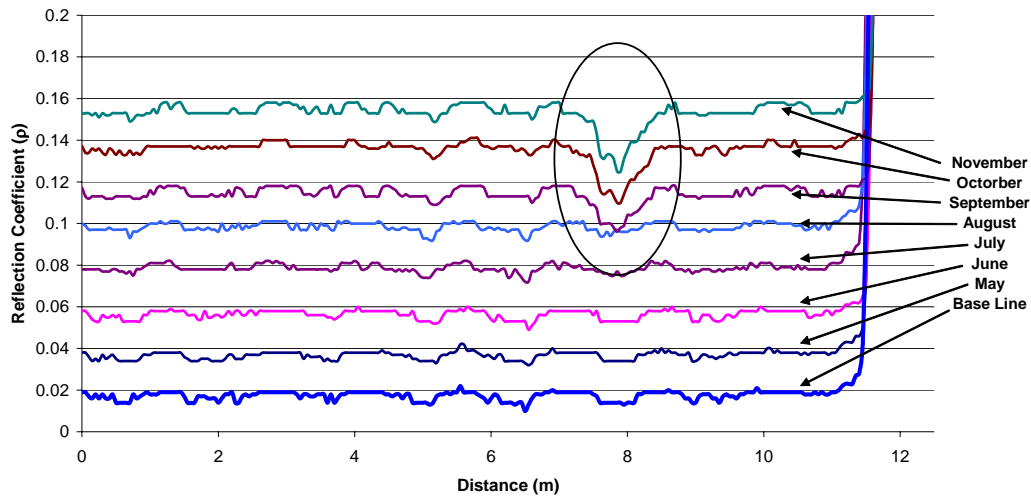

Figure 14. TDR cable signatures for the upper cable at the Batesville, AR site.
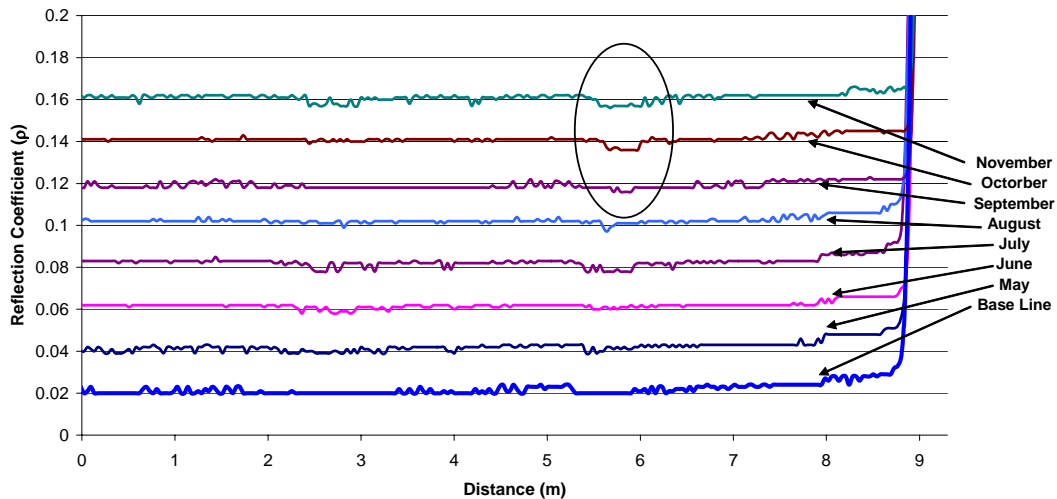
Figure 15 TDR cable signatures for the lower cable at the Batesville, AR site.

4. Conclusions

This study has illustrated that monitoring slope movements remotely with TDR techniques is a feasible alternative to more labor intensive methods like using survey monuments or probe type inclinometers. The installation of the TDR cables must be such that shallow failures are not reinforced to the point where movement is prevented by the strong grout columns. On the

other hand the grout must be stiff enough to deform the TDR cable. A balance of grout strength and borehole diameter must be achieved for satisfactory results. For this study grout strengths of 5500 kPa and higher produced satisfactory results with both rigid and flexible coaxial cable. Based on both laboratory and field studies it can be concluded that RG8 is perhaps the most cost effective cable to use for shallow installations it possesses good signal attenuation characteristic, has few installation and connection problems and it the cheapest in terms of material costs. The field TDR installations have verified that at least 20 mm and more likely 30 mm of deformation along the shear surface is required before the TDR cable will be able to record any anomaly or shear in the slope. Of significance is the fact that a complete autonomous TDR installation can be made for far less money than the purchase price of a probe type inclinometer. In addition, the labor costs to monitor the TDR installation for long periods are almost nil.

5. References

1 Connelly, J. B., Lemmer, R. E., Sims, W. J., Al- Shukri, H. J., Smith, P.N. and Dalby, JL (1999). "*Hazard Mitigation Plan, Clay County, Arkansas*", Clay County Disaster Preparedness Council, Piggot Arkansas, [Online] URL:http://quake.ualr.edu/HazardMitigation/claymitg-plan/Landslides.htm, Date Accessed June, 2002.

2 Kane, W. F., Beck, T. J., Anderson, N. O., and Perez, H. (1996). "Remote Monitoring of Unstable Slopes Using Time Domain Reflectometry." Proceedings, Eleventh Thematic Conference and Workshops on Applied Geologic Remote Sensing, ERIM, Ann Arbor, MI, II, 431-440.

3 Anderson, N and Welch, D (2000). "Practical Application of Time Domain Reflectometry (TDR) to Monitor and Analyze Soil and Rock Slopes," Geotechnical Measurements: Lab and Field: Proceeding of Sessions of Geo-Denver 2000 :August 5-8, 2000, Reston, Virginia: ASCE, Geotechnical Special Publication No. 106, pp.65-79.

4 O'Connor, K. M. and Wade, L. V., (1994). "Application of Time Domain Reflectometry in the Mining Industry," Proceedings of the Symposium and Workshop on Time Domain Reflectometry in Environmental, Infrastructure, and Mining Applications, Northwestern University, Evanston, Illinois, September 17-19, Washington, DC: U.S. Bureau of Mines USBM Special Publication SP 19-94, pp. 494-506.

5 Kane, W. F., Beck, T. J., and Hughes, J. J., (2001). "Applications of Time Domain Reflectometry to Landslide and Slope Monitoring," 2nd International Symposium and Workshop on Time Domain Reflectometry for Innovative Geotechnical Applications, Infrastructure Technology Institute Northwestern University, Evanston, Illinois

Design Considerations for Hybrid MSE/Shoring Retaining Walls

By Frank Harrison, P.E., Kimberly Morrison, P.E.,R.G., Golder Associates Inc., Lakewood, CO; Jim Collin, P.E., Ph.D., The Collin Group, Bethesda, MD; and Scott Anderson, P.E., Ph.D., FHWA, Lakewood, CO

Abstract:

In the last 20 years, use of MSE walls has risen substantially for roadway construction, including construction in steep or mountainous terrain. In steep terrain, their use has often been to allow for widening of an existing narrow roadway, by constructing an MSE wall on the outboard or "fill" side of the roadway. On some projects, the excavation to establish a working bench on which to construct the new MSE wall becomes substantial, and shoring methods have recently been employed to allow the excavation to proceed with traffic safely accommodated on one or more lanes of the existing roadway, above the excavation.

Should the stabilizing effect of the shoring system be accounted for in the subsequent design of the MSE wall? If so, how should engineers approach the design of these composite wall systems? FHWA is sponsoring a research project into these questions. Elements of the research completed to date will be presented and discussed, including both centrifuge scale model tests and a full scale test wall. Proposed design methodology and contracting strategies will be discussed.

OBSERVATIONS ON DRAINAGE AND STRENGTH CHARACTERISTICS OF MISSOURI ROADWAY BASE

Awilda M. Blanco[1], John J. Deeken[1], John J. Bowders[2], William Likos[3] and John P. Donahue[4]

ABSTRACT

For the last few decades, the design of pavement systems has not emphasized drainage. A majority of the damage seen in pavement systems is caused by poor subsurface drainage, often the result of base materials that are not providing adequate drainage. Until recently, in Missouri, two principal base course systems were used beneath the pavement. One was a 100 mm (4 in) layer of a well-graded aggregate with up to 15 percent fines, known as Type 5 base material. The alternate system included a 600 mm (24 in) layer of rock fill (onto which a 4 in layer of material with similar properties to the Type 5 base material is placed). A program of laboratory and in-situ testing was performed on six different Type 5 base materials in order to assess their drainage and strength characteristics. Drainage quality was also determined using pavement design software. In-situ hydraulic conductivities ranged from 2×10^{-3} to 4×10^{-5} cm/sec (6 to 0.6 ft/day). Laboratory hydraulic conductivities were in the range of 9×10^{-2} to 7×10^{-7} cm/sec (255 to 2×10^{-3} ft/day). The bases tested in this program averaged 1000 times lower hydraulic conductivities than typically accepted as good drainage of the pavement subsurface. In long-term flow tests (1 to 3 months duration), flow rates for the Type 5 base material decreased by roughly one order of magnitude. Cyclic triaxial tests on the base material exhibited undrained behavior and loss of strength even when tested under fully drained conditions. Given these findings, it can be anticipated that roads constructed with this base will perform poorly compared to roads with base materials providing adequate drainage. Inevitably, poor drainage translates into poor rideability and higher maintenance costs.

INTRODUCTION

Although the importance of well-drained pavement systems has been extensively documented (Cedergren 1974, Cedergren, 1994, Moulton, 1980), during the last twenty years the design and construction of such systems has emphasized strength performance over drainage. Water can flow into the base of pavements through joints, cracks, and from groundwater sources (Moulton, 1980). The presence of water, lack of drainage, and the cyclic loading due to vehicles result in high pore water pressures, which decrease the effective strength of the base and eventually cause pavement failure. Also, fine materials from the subbase and base can be pushed out of the pavement through cracks and joints, creating voids underneath the surface layer. If this layer is not adequately engineered, it can show signs of distress or failure soon after construction.

---

[1] Graduate Research Assistant, Department of Civil and Environmental Engineering, University of Missouri – Columbia

[2] Croft Professor, Department of Civil and Environmental Engineering, University of Missouri – Columbia

[3] Assistant Professor, Department of Civil and Environmental Engineering, University of Missouri – Columbia

[4] Research and Development Engineer, Missouri Department of Transportation

In Missouri, until recently two principal base course systems were used beneath the paving. The first was a well-graded aggregate known as Type 5 Base material. This material is compacted into a 100 mm (4 in) layer, and the pavement placed directly on this material. An alternate design consisted of using a 600 mm (24 in) layer of rock fill material as base layer, onto which a 100 mm (4 in) layer of material with similar specifications to the Type 5 base is placed, overlaid by the pavement. The main objective of this project was to assess the drainage and strength characteristics of the Type 5 materials by performing a program of laboratory (hydraulic conductivity, strength, and long term flow) and in-situ hydraulic conductivity testing.

MATERIALS AND METHODS

Bulk samples of the base materials were obtained from supplier quarries, on-site stockpiles and from compacted, in-place roadway bases around Missouri (Table 1). Based on Missouri's Department of Transportation's specifications (MoDOT, 1996), the Type 5 base material can have up to fifteen percent by weight passing the No. 200 sieve (Figure 1). The alternate rock fill material can have individual particles as large as 300 mm (12 in) and its interstices may be filled with a mixture of coarse aggregates to fines. Due to the poor constructability of the rock fill material, a 100 mm (4 in) layer of Type 5 base-like material is often placed as a working surface on top of the rock. It was anticipated that this layer would control the drainability of the pavement base system, thus testing was performed on the working surface material.

TABLE 1 Location of Base Course Samples and Details of Testing Performed.

Location	Date	Tests Performed	Source	Sampling Location	Type
Rt. 71, McDonald Co.	Sept. 2001	GS, LP, DRI, SST, CT	Lanagan Quarry	Quarry	Type 5
Rt. 13, St. Clair Co.	Sept. 2001	GS, LP, DRI, SST	Ash Grove Quarry	Quarry, field	Type 5
Rt. 63, Randolph Co.	Sept. 2001	GS, LP, DRI	Riggs Quarry	Stockpile at site	Type 5
Rt. 71, Nodaway Co.	Sept, 2001	GS, LP, DRI	Idecker Quarry	Stockpile at site, field	Type 5
Taney Co.*	Dec. 2001	GS, LP, DRI	Journegan Quarry	Stockpile at site	Rock Fill
Crawford Co.*	Dec. 2001	GS, LP, DRI	Unknown	Stockpile at site	Rock Fill
Boone Co.	Sept. 2002	GS, LTF	Boone Quarry	Quarry	Type 5

GS = grain size distribution; LP = laboratory permeability testing; DRI = on-site hydraulic conductivity testing using double ring infiltrometer; LTF = long term flow tests; SST = shear strength tests; CT = cyclic triaxial tests. * Only the cap material was tested.
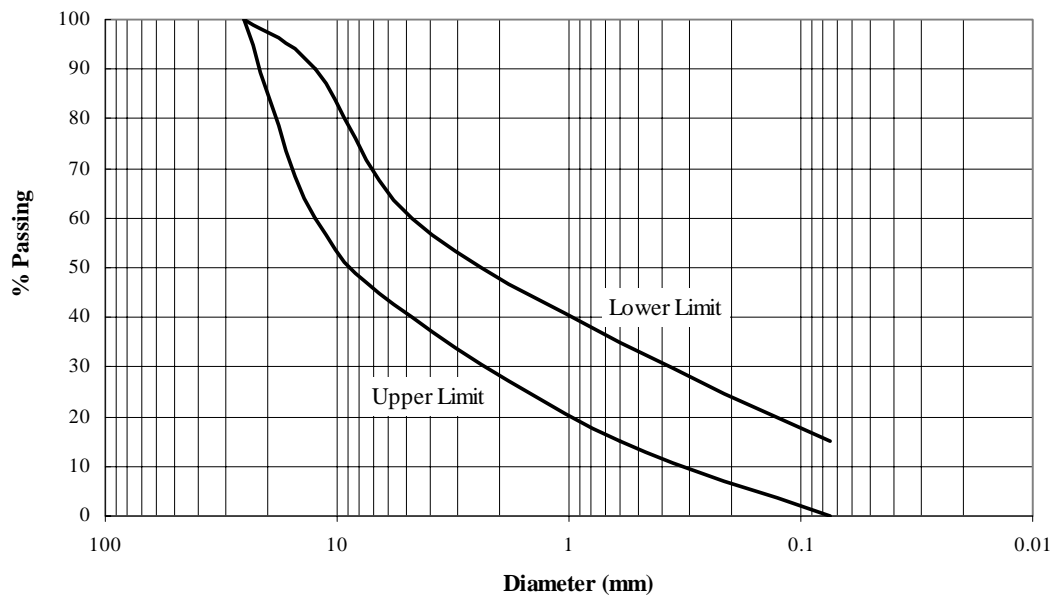
Figure 1 Limits of Type 5 Base specified gradations

The first step of the testing program was to determine the grain size distribution of each sample and compare it with the specified limit gradations provided by the Missouri Department of Transportation (Figure 1). Both dry and wet sieve analyses were performed, but due to the high abrasiveness of the material (Blanco, 2003) wet sieve analyses were deemed more appropriate.

The laboratory hydraulic conductivity test program included rigid-wall constant head tests and flexible-wall falling headwater - raising tailwater tests. The constant head tests were performed using a Marriotte tube, whereas the falling headwater - raising tailwater tests (ASTM 2000a) were performed using a panel board system with superimposed air pressures (Figure 2). Constant head tests were tried on 150 mm (6 in) diameter compacted specimens from every sample, but in some cases no flow was possible at the maximum available hydraulic head. Thus, testing was performed on all samples on 150 mm (6 in) compacted specimens using the flexible wall apparatus, except for the Boone Quarry material. This material has been extensively studied using the constant head permeameter by Prachantrikal (2001).

In-situ hydraulic conductivity measurements were performed using a double ring infiltrometer (DRI) (Figure 3). Each ring is embedded approximately 50 mm (2 in) into the base by carefully hand-excavating a slot, inserting the ring, and filling the annulus with bentonite paste. The DRI provides a direct determination of the infiltration rate in the material being tested (ASTM 1994).
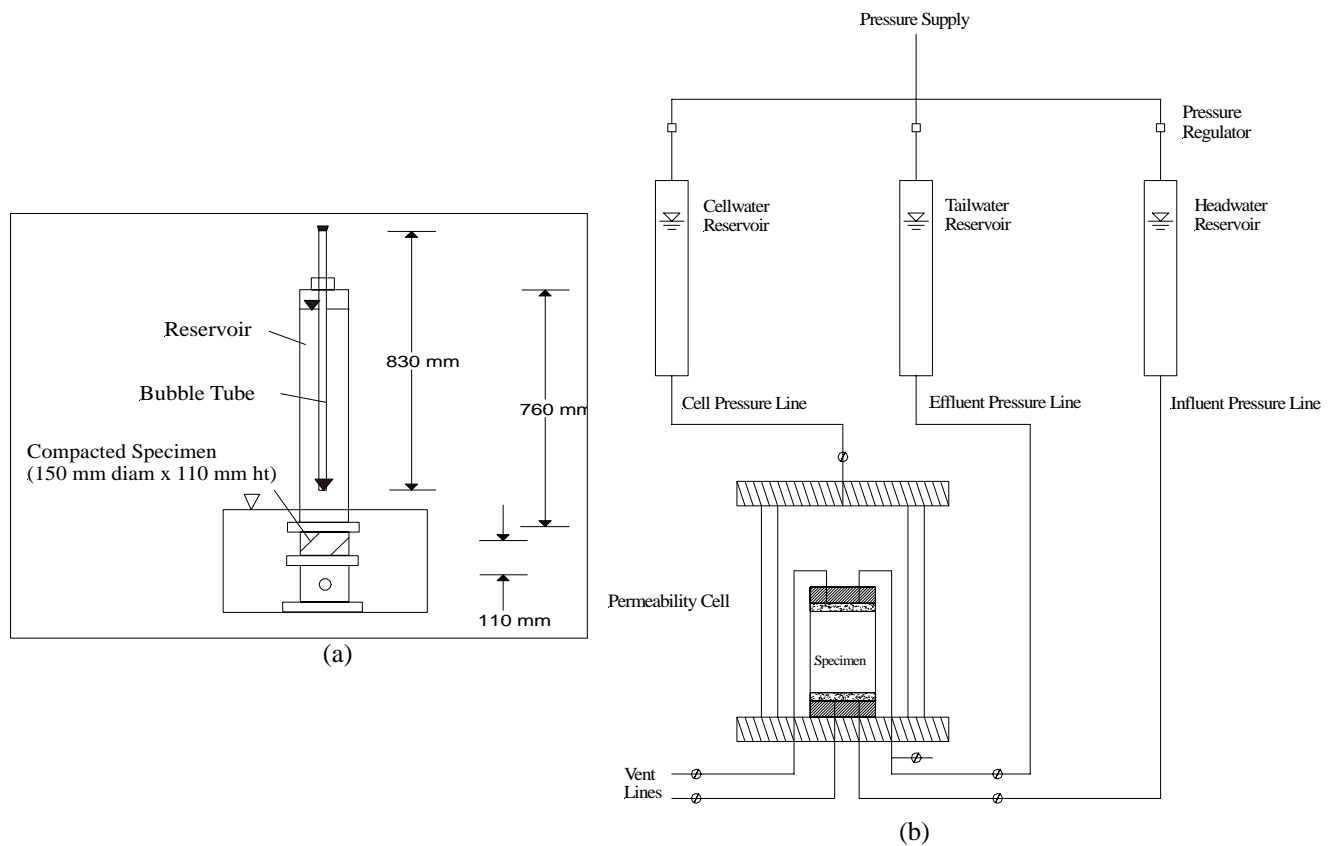
Figure 2 (a) Mariotte Tube for constant head testing (b) Panel board setup for raising tailwater falling headwater hydraulic conductivity tests
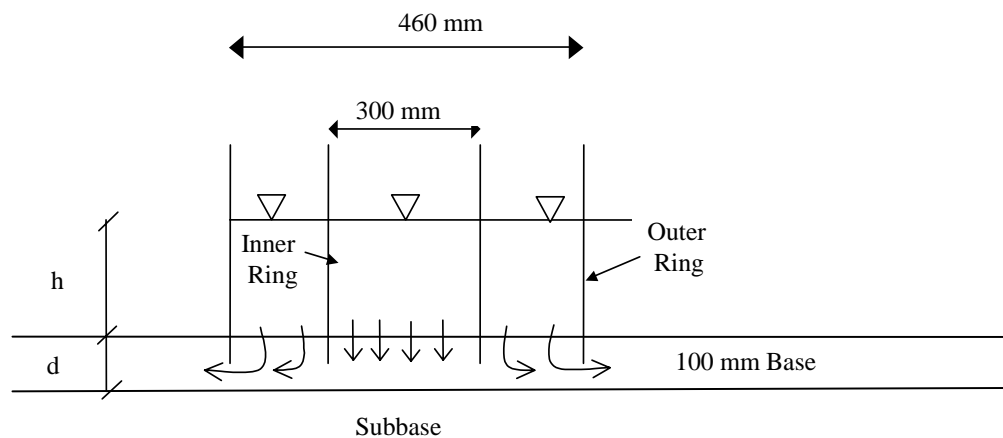

Figure 3 Cross section view of double ring infiltrometer (DRI)

The infiltration rate is defined as volume per time per unit area perpendicular to flow, or

$$I = \frac{Q/t}{A} \tag{1}$$

where I is the infiltration rate [L]/[T], Q is the volume of infiltrated fluid [L^3], t is the time of infiltration [T], and A is the area [L^2] where the fluid was infiltrated.

The hydraulic conductivity is determined by dividing the infiltration rate by the hydraulic gradient. To determine the hydraulic gradient, it was first necessary to determine if the infiltration measured was vertical or horizontal. For such purposes, the depth of the wetting front was determined and compared with the thickness of the base layer. If the depth of the wetting front was less than the thickness of the layer, the flow was assumed to be vertical. As testing time proceeded, the estimation of the depth of the wetting front was larger than the thickness of the base layer, thus the flow was assumed to be horizontal. The following equation was used to determine the hydraulic gradient:

$$i = (h+d)/d \tag{2}$$

where h is the height of water ponded above the base [L], and d is the depth of the wetting front [L] in the case of vertical flow. For horizontal flow, hydraulic gradients for lengths of flow (d) of 1.5 m (5 ft) and 3m (10 ft) were determined. For comparison purposes, the hydraulic gradient was calculated assuming full-depth saturation of the base to determine the vertical hydraulic conductivity; these values were similar to those measured in the laboratory. The hydraulic conductivity is then calculated as:

$$k = \frac{I}{i} \tag{3}$$

where k is the hydraulic conductivity [L]/[T], I is the measured infiltration rate and i is the hydraulic gradient.

Drainage Requirements in Pavements 2.0 (DRIP 2.0) (Applied Research Associates, 2002) is a computer program developed by the United States Department of Transportation and the Federal Highway Administration (FHWA) for the design of subsurface drainage. DRIP 2.0 provides a rating (Excellent to Poor) of a pavement's drainage system based on variables including infiltration, pavement geometry, and the drainage characteristics of the pavement's substructure. For this study, an infiltration based on a 50 mm (2 in) rain event and infiltration coefficient of 0.67, were held constant. The geometries used included a cross sectional slope ranging from 0.005 to 0.020, and a longitudinal slope ranging from 0.005 to 0.040. The width of the road was assumed to be 8.5 m (28 ft) and the distance from the edge of the pavement to the edge drain was assumed to be 1.2 m (4 ft). The average unit weight of the base was assumed to be 21.2 kN/m^3 (135 lb/ft^3) and specific gravity of solids of 2.65. Laboratory-measured and field-

measured hydraulic conductivity values were used for the analysis, although the DRIP program also allows the user to input the grain size distribution of the material to determine its hydraulic conductivity based on Moulton's equation (Applied Research Associates, 2002). The code analyzes all the variables based on the AASHTO Guide for Design of Pavement Structures and determines the time required for 50 percent drainage under a constant infiltration rate. The times to drain for the resulting scenarios for the laboratory and field measured hydraulic conductivities were determined and rated (by DRIP 2.0) for pavement performance.

Long term, rigid wall-constant head flow tests (Table 2, Figure 4) were performed on Boone Quarry specimens over a period of 2 months. The main objective of these tests was to determine the effect of the supporting layer and fines content on long term flow through MoDOT Type 5 base material. To fulfill these objectives, 13 cm (5.25 in) high, 10 cm (4 in) inside diameter compacted specimens prepared with 6 and 15 percent (dry weight) material passing the No. 200 sieve were tested using various lower boundary conditions (Table 2). The geotextile used was a non-woven needle punched geotextile (E.O.S = 0.202 in). After approximately 2 months of flow, the specimens were allowed to gravity drain, and grain size analyses were performed on the top and bottom half of each specimen to determine the fines distribution and if any fines migration had occurred.

Table 2 Long Term Flow Specimens.

Specimen No.	Percent Fines	Boundary Condition
1	6	Wire Mesh and Geotextile
2	6	Wire Mesh and No. 200 Screen
3	15	Wire Mesh Only
4	15	Wire Mesh and No. 100 Screen
5	15	Wire Mesh and No. 200 Screen
6	15	Wire Mesh and Geotextile

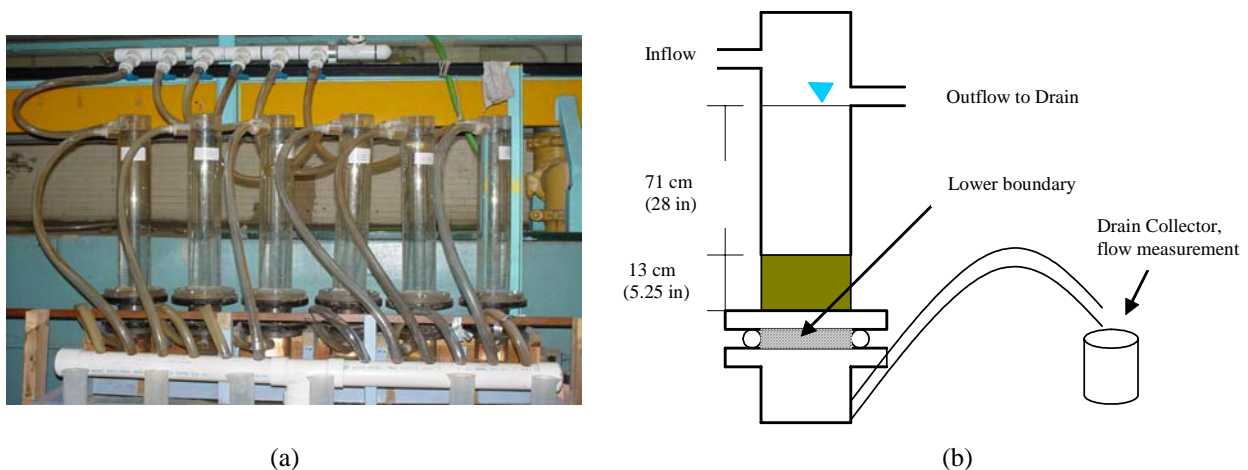(a)   (b)

Figure 4 Long term flow test apparatus (a) Equipment and water inlet (b) Schematic of individual testing cell

The effective stress shear strength properties of Lanagan Quarry base material were determined by performing consolidated-undrained triaxial tests with pore pressure measurement ($\overline{CU}$) on 14.2 cm (5.6 in) high and 7.4 cm (2.9in)-diameter specimens. To mimic the worst case scenario (saturated base material) and due to testing methodology, the specimens were tested under completely saturated conditions. Based on the time needed to reach 100 percent consolidation, the specimens were sheared at a strain rate of 1.5 percent per hour. Specimens were sheared under effective consolidation stresses of 14, 28, and 42 kPa (2, 4, and 6 psi) and to a maximum axial strain of 30 percent (Parra and Blanco, 2002).

Stress and strain controlled cyclic triaxial $\overline{CU}$ tests were performed to determine the shearing behavior of compacted specimens from Lanagan Quarry. Sample dimensions, gradation, test preparation, and saturation process for the cyclic triaxial tests followed the same procedures as for the $\overline{CU}$ type triaxial tests. The strain rate was set to 1000 percent per hour to mimic the cyclic effect produced by traffic loads as closely as possible. Stress-controlled tests were set to stop when reaching either of the following criteria: a maximum strain of 20 percent or one hundred loading cycles. Samples at an effective stress of 14 kPa (2 psi) were loaded to stresses corresponding to 20 percent, 40 percent, and 60 percent of the maximum principal stress difference as determined from static $\overline{CU}$ tests, respectively; and reloaded at about 5 percent to 10 percent of the maximum principal stress difference.

Strain-controlled tests consolidated under effective confining stresses of 14 and 28 kPa (2 and 4 psi) respectively, were set to shear to 100 load cycles at low strains in the range of 1 percent to 4 percent. A strain rate of 1000 percent per hour was again used (Parra and Blanco, 2002). Drained, cyclic triaxial, strain controlled tests (CD) were also performed on saturated samples of compacted, Type 5 base materials.

RESULTS AND DISCUSSION

Grain size distributions were determined for all the specimens. Forty-four percent of the specimens tested had more than 15 percent fines (Figure 5, Table 3). The percent fines was in the range of 12 to 19 percent (dry weight). The differences in fines content between materials were expected due to the different sources of the materials and the differing amounts of handling each material received prior to sampling.

Values for the coefficients of uniformity and gradation are presented in Table 3, as well as the USCS and AASHTO soil classifications. The coefficients and soil classifications were determined using information based on the wet sieve analysis, although for some materials D_{15} and D_{10} values had to be extrapolated from the grain size distribution plots. Both coefficients of uniformity and gradation show the materials to be well-graded sands with considerable silt-sized particles.
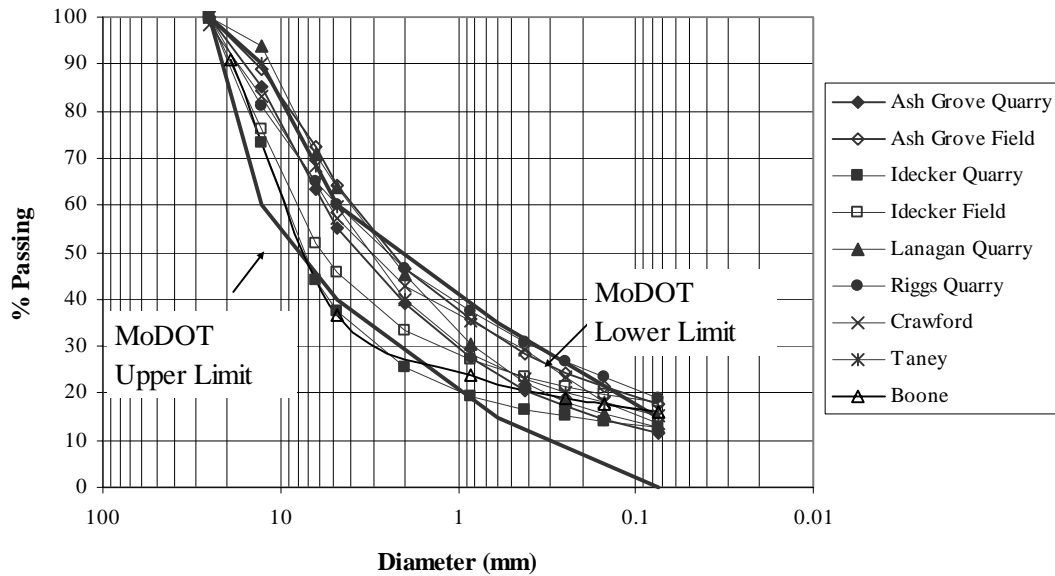
Figure 5 Grain size distributions for materials tested based on wet sieve analysis

Table 3 Material Properties, Type 5 Base and Alternate Rock Fill.

Source	D_{60}	D_{30}	D_{15}	D_{10}	C_u	C_z	% Pass	γ_{dmax}	OMC	Void	Soil Classification	
	(mm)	(mm)	(mm)	(mm)			#200	(pcf)	(%)	Ratio (e)	USCS	AASHTO
Ash Grove Quarry	5.3	1	0.20	**0.05**	106.0	3.8	12	136.5	7.0	0.21	GP-GM	A-1-a
Ash Grove Field	3.8	0.5	**0.10**	**0.02**	190	3.3	17	136.5	7.0	0.21	SM	A-1-b
Idecker Quarry	9.1	2.7	0.25	**0.02**	455.0	40.1	13	125.0	10.0	0.32	GM-GC	A-1-a
Idecker Field	8.0	1.3	**0.03**	**0.01**	800	21.1	18	125.0	10.0	0.32	GM/GM-GC	A-1-b
Lanagan Quarry	4.0	0.8	0.10	**0.04**	100.0	4.0	13	141.0	6.5	0.17	SM	A-1-a
Riggs Quarry	4.8	0.4	**0.04**	**0.02**	237.5	1.7	19	137.0	8.0	0.21	SM	A-1-b
Crawford Co.	5.1	0.5	0.10	**0.05**	102.0	1.0	14	138.7	8.0	0.19	SM	A-1-a
Taney Co.	4.8	1	0.08	**0.02**	237.5	10.5	15	138.9	7.7	0.19	SM	A-1-a
Boone Co.	9	2.1	**0.05**	**0.004**	2250	122.5	16	135	8.1	0.22	GM	A-1-b

Values in bold represent grain sizes extrapolated from grain size distributions based on wet sieving
OMC = Optimum moisture content
Porosity = e/(1+e)
25.4 mm = 1 in
0.157 kN/m^3 = 1 lb/ft^3

Results of laboratory and field hydraulic conductivity tests are shown in Figure 6. In general, all laboratory compacted specimens were tested in the Marriotte device; however, the sensitivity of the device is about 10^{-4} cm/sec (0.3 ft/day) below which, accurate hydraulic conductivity measurements are difficult to discern. Therefore, specimens that exhibited hydraulic conductivities lower than approximately 10^{-4} cm/sec (0.3 ft/day) were removed from the Marriotte tube, set up in a flexible-wall permeameter and re-tested. Laboratory-measured

hydraulic conductivities ranged from 10^{-2} cm/sec to 10^{-7} cm/sec (28 to 3×10^{-4} ft/day) (Figure 6). In general, the in-situ hydraulic conductivities ranged from 10^{-3} cm/sec to 10^{-5} cm/sec (3 to 0.03 ft/day).
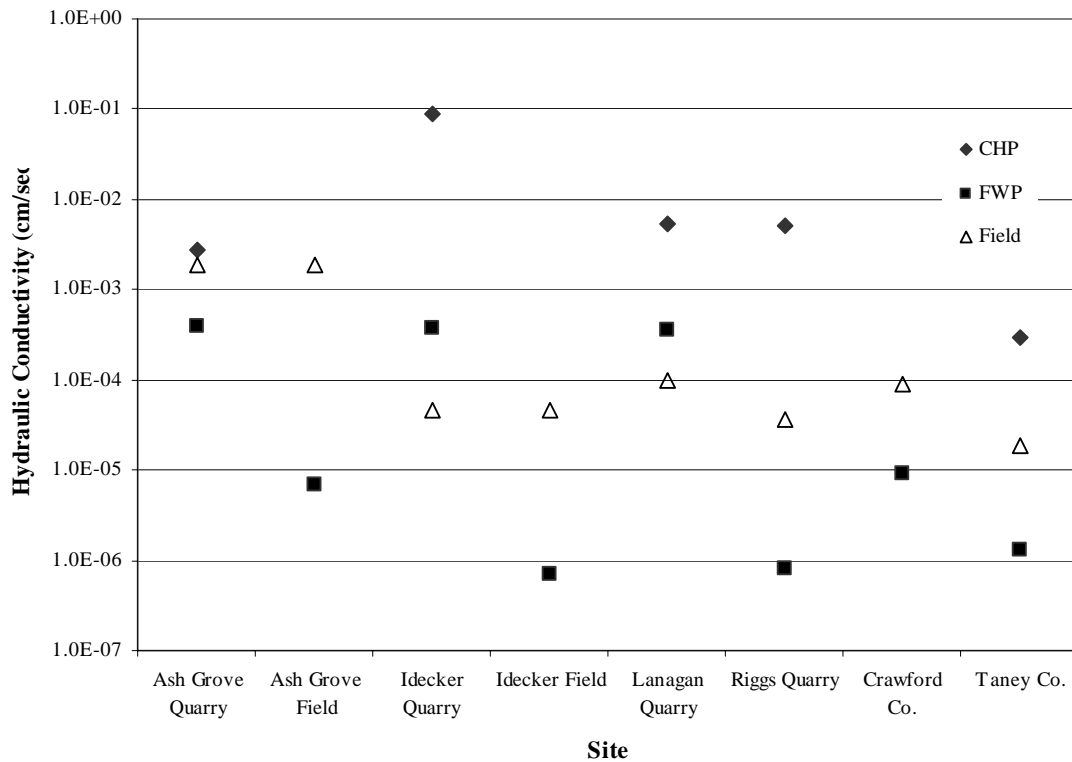

Figure 6 Laboratory and field measured hydraulic conductivities, CHP = constant head test, FWP = falling headwater – raising tailwater test, Field = Double Ring Infiltrometer test

Differences between laboratory and field hydraulic conductivity values can be explained by the laboratory and field compaction methods, limitations of the hydraulic conductivity testing equipment, and differences in size of areas tested. First, although the laboratory specimens were compacted near optimum Proctor conditions, it is possible that the final conditions of the laboratory specimens did not adequately represent those of the field-compacted specimens. The laboratory compaction was performed using a static compactor (ASTM 2000b); however, the field compaction was performed with self-propelled vibrating equipment. Second, during permeability testing in the Marriotte device, piping of some fine particles (occasionally large amounts) was observed. While such piping will increase the hydraulic conductivity of the laboratory specimens, no such piping was observed in the field tests. Furthermore, it is possible that sidewall leakage occurred during testing on the Marriotte device, again increasing the measured hydraulic conductivity. Given these three observations, it is understandable that the field hydraulic conductivity would tend to be lower than the laboratory-measured hydraulic conductivity (from the Marriotte device).

Most of the hydraulic conductivities measured in the flexible-wall permeameter (6 cases) were lower than the field values. This is probably due to the larger volume of material tested during the field procedure. The in-situ test involved a specimen area of 700 cm^2 (110 in^2) while the lab test specimen was about one half that size. Thus, the field test was more likely to include macro-discontinuities than the lab specimen, resulting in higher measured hydraulic conductivities.

The results of the DRIP 2.0 analyses showed that pavement slope had negligible effect on the drainage performance, at least for drainage systems having hydraulic conductivities in the range of the materials tested in this project (10^{-2} to 10^{-7} cm/sec) (28 to 3×10^{-4} ft/day). Times required to drain for the different materials are presented in Table 4. Time to drain values based on laboratory -measured hydraulic conductivities (constant head permeameter) ranged between 0.1 days and 1540 days. Those based on field-measured hydraulic conductivity ranged between 13 days and 1766 days. Although values for hydraulic conductivity were entered in the analysis, the porosity of the materials was determined using wet grain size analysis information. Small variations in hydraulic conductivity can double the time to drain, and most of the times to drain based on the field hydraulic conductivity tend to be higher than the times based on laboratory values. The only exception is the material from Crawford, for which the laboratory hydraulic conductivity values presented were determined using the flexible wall permeameter. As shown in Table 4, the best rating of drainage found for both laboratory and field hydraulic conductivity values was good, which corresponds to pavement systems that take longer than one day for achieving 50 percent drainage.

Table 4 Laboratory and Field Hydraulic Conductivity and Time to Drain Values Based on DRIP 2.0 Analyses for Quarry Samples, Type 5 Base and Capping Material on the Alternate Rock Fill.

	Measured k values		Time to Drain		Quality of Drainage	
Material	Laboratory k (cm/sec)	Field k (cm/sec)	Laboratory (days)	Field (days)	Laboratory	Field
Ash Grove	2.8×10^{-3}	1.9×10^{-3}	8.9	13	Poor	Poor
Idecker	8.8×10^{-2}	4.6×10^{-5}	0.1	253.7	Good	Very Poor
Lanagan	5.4×10^{-3}	9.7×10^{-5}	2.4	223.3	Fair	Very Poor
Riggs	5.2×10^{-3}	3.7×10^{-5}	1.1	163.9	Good	Very Poor
Crawford*	9×10^{-6}	9.1×10^{-5}	1540	154	Very Poor	Poor
Taney*	3.0×10^{-4}	1.9×10^{-5}	158	1766	Poor	Very Poor

1cm/sec = 2835 ft/day

*Values calculated assuming a 700 mm (2.3 ft) base layer

Long term flow results show a one order of magnitude decrease in hydraulic conductivity in approximately 70 days of testing (Figure 7). As expected, specimens with higher amounts of fines showed lower hydraulic conductivities. Also, as the opening size of the boundary condition decreases, the hydraulic conductivity also decreases. The hydraulic conductivity values measured are comparable to those measured using the laboratory constant head permeameter.

The same testing issues as those of the laboratory constant head permeameter are responsible for the higher long term flow hydraulic conductivity values when compared to those measured using the laboratory Marriotte device, flexible wall permeameter, and those measured in the field.

Flow was disrupted on three occasions: on day 4, day 15, and day 28. The specimen with 15 percent fines and wire mesh boundary condition was the most affected by these disruptions. The large increase in hydraulic conductivity that occurred after the second disruption is due to piping of the fine material through the specimen and the wire mesh, allowing water to move freely throughout the specimen. This also reflects on the high hydraulic conductivity at the end of the test, even though this specimen had the highest amount of fines.
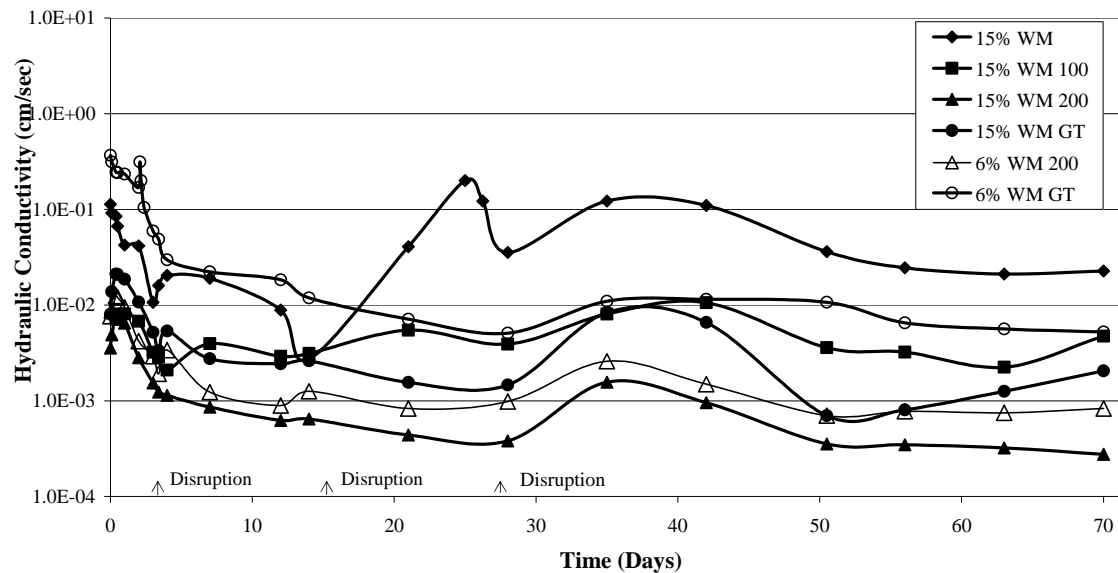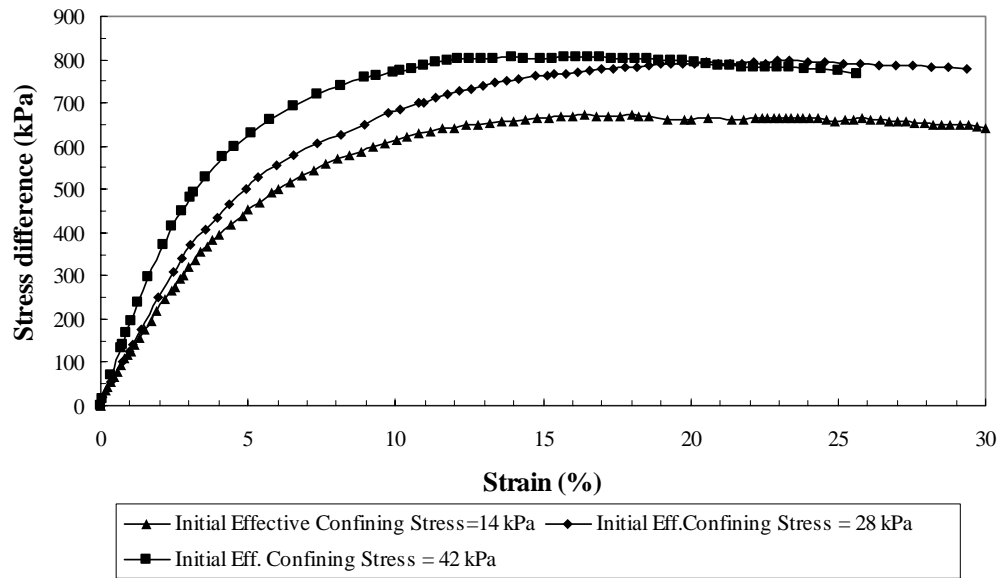

Figure 7 Long term hydraulic conductivity versus time, Boone Quarry material, with various end conditions
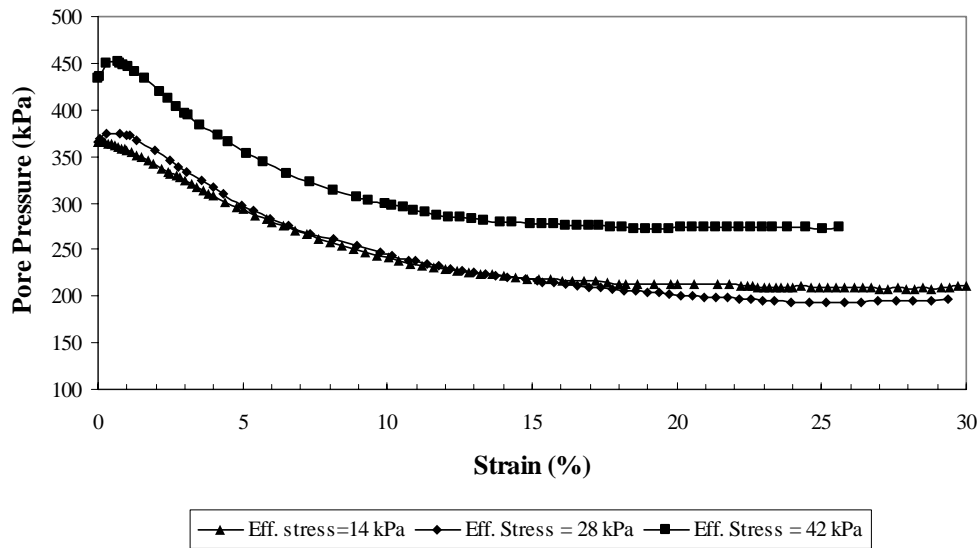
Results of $\overline{CU}$ tests on Lanagan Quarry specimens are presented in Table 5. The strength tests performed indicated that the material compacted at optimum water content has no cohesion intercept and has an effective internal friction angle of 42 degrees, values representative of highly dense granular soils. As shown in Figures 7(a) and (b), the stress difference–strain relationship was non-linear and continuously increasing until about 15 percent strain after which it leveled out. The pore pressures increased slightly at the start of the test (1 percent strain), then decreased during testing until they leveled off at approximately 20 percent strain, which again represents the typical behavior of dense granular soils under undrained conditions.

Table 5 Triaxial Test Results for Lanagan Quarry Material Based on Maximum Stress Difference Criterion.

| Max γ_{dry} kN/m^3 (pcf)	OMC (%)	Sample No.	σ_3' kPa (psi)	Molding w (%)	Test w (%)	$\sigma_1' - \sigma_3'$ kPa (psi)	Peak ε (%)	ϕ'	c'
		1	13.8 (2)	6	8.9	97.4 (14.1)	16.2		
141.4 (22.2)	6	2	27.6 (4)	6.5	8.7	115 (16.7)	20.4	42	0
		3	41.4 (6)	6	9	116.6 (16.9)	12.7		

(a)

(b)

Figure 7 (a) Stress difference versus strain, Lanagan Quarry material $\overline{CU}$ tests (b) Pore pressures versus strain

The stress difference-strain response to cyclic loading under stress-controlled conditions was similar to the response observed in the static $\overline{CU}$ triaxial tests. Increased pore pressures were evident at the start of the test, and then decreased throughout the remainder of the test, even during unloading (Parra and Blanco, 2002). Failure was defined by excessive bulging at 20 percent strain.

Under strain-controlled conditions, bulging was not experienced at low strains. Figure 8 shows the results of the strain-controlled cyclic triaxial test performed at an effective confining stress of 28 kPa (4 psi) to strains ranging between 1 percent and 4 percent. This specimen experienced a small drop in pore pressure during the first load cycle, after which the pore pressures started to increase until the end of the test. Consequently, strength degradation caused a flattening of the stress difference-strain curve slope, which progressed with every load cycle. After applying twenty load cycles, the principal stress difference attained was only about 10 percent of the initial maximum principal stress difference in the first cycle and the stress difference-strain curve had flattened out. Loss of strength is evident from the second cycle onwards.
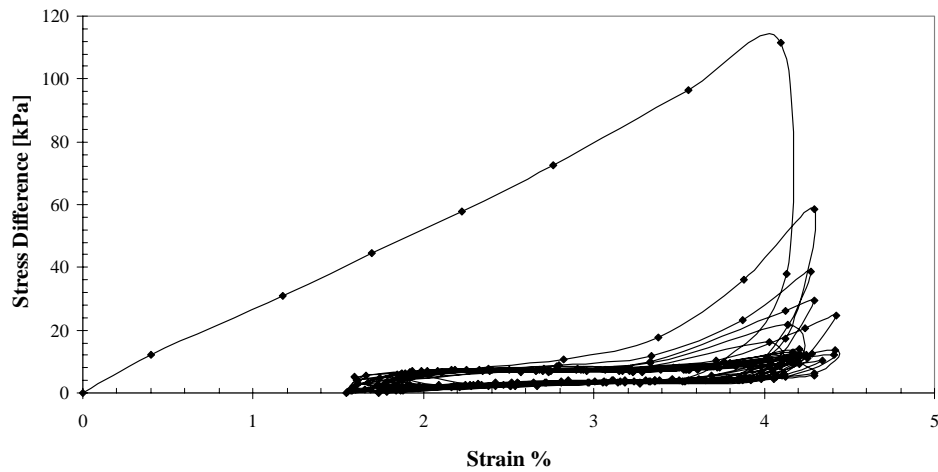
(a)
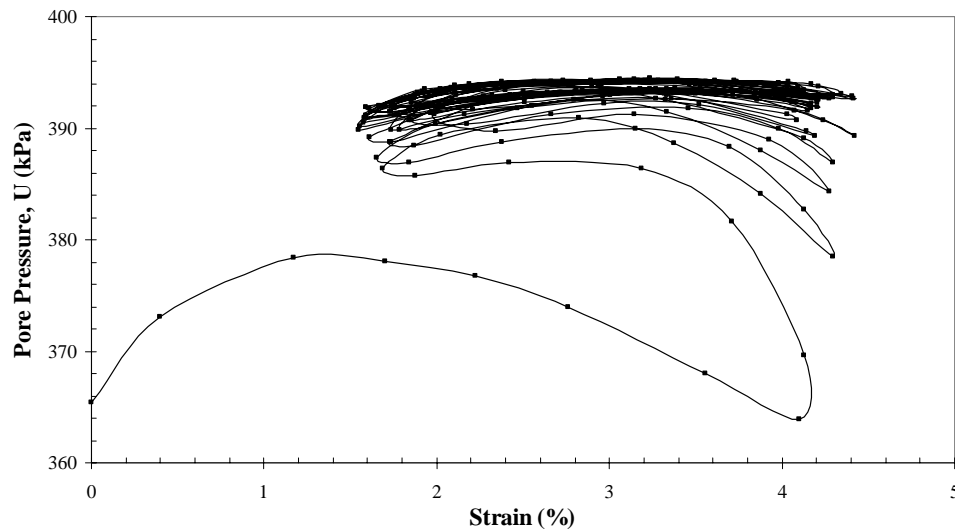
(b)

Figure 8 Strain-controlled undrained cyclic triaxial test results at initial effective confining stress of 28 kPa (4 psi), (a) Stress difference versus strain, (b) Pore pressure versus strain.

The Type 5 base material is a drainage layer, so its behavior under drained condition was also studied. A drained, cyclic triaxial test was performed on a specimen from Lanagan Quarry. As shown in Figure 9, the material shows an almost complete loss in strength after the 10th load cycle. Compression occurs at the beginning of the test, during the first half minute. As the test progresses, the specimen dilated, which reflects a behavior very similar to that of an undrained material (Figure 7).
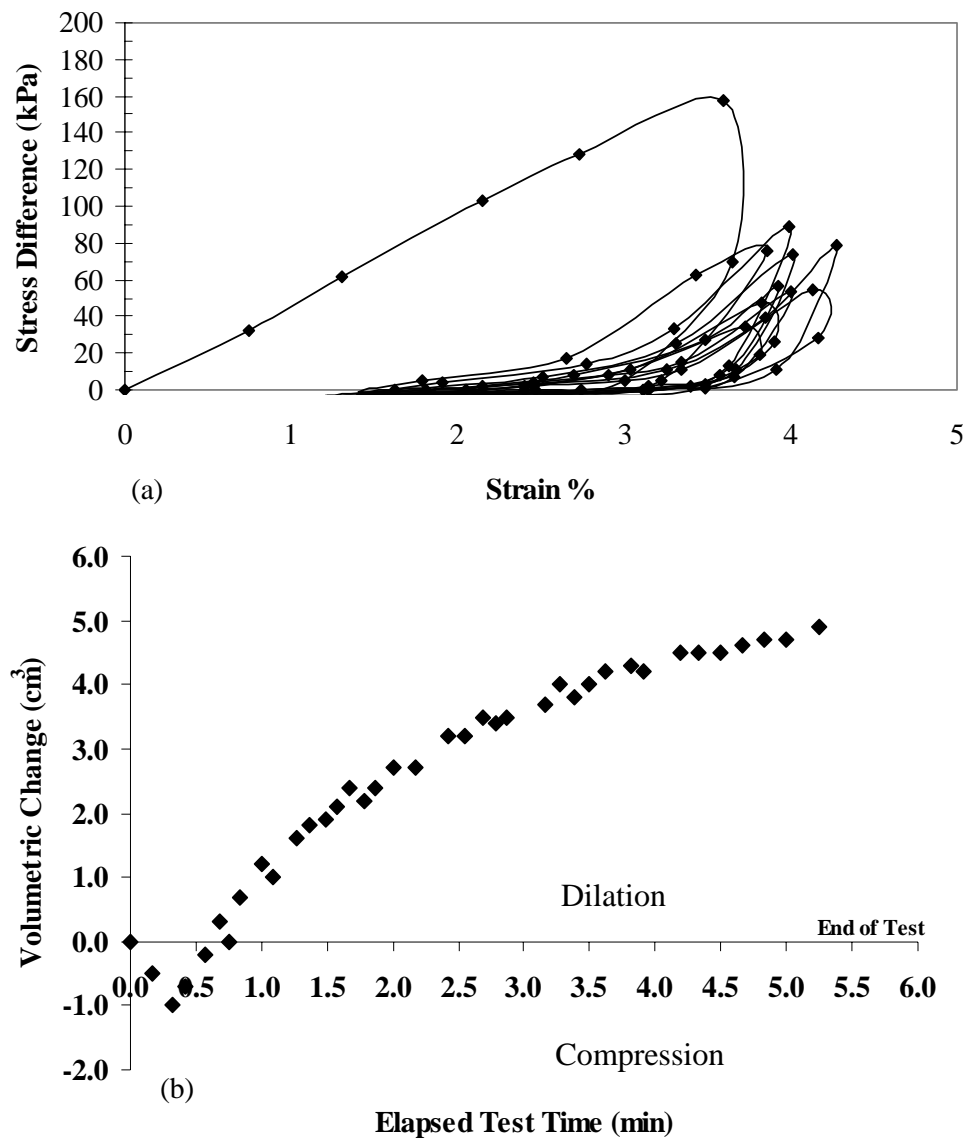

Figure 9 Strain controlled, drained cyclic triaxial test with initial confining stress of 14 kPa (2 psi) (a) Stress difference versus strain (b) Volume change versus time of test

PRACTICAL IMPLICATIONS

One of the best ways to prevent damage to roads is to allow for complete and rapid drainage of any water that infiltrates into the pavement system. The specifications for the base materials used in roads should provide for the use of more permeable materials, or provide for alternate means to provide sufficient drainage, e.g. geocomposites. Strength and hydraulic conductivity testing should be performed on these new materials or systems to determine if they are capable of removing the water that might infiltrate the pavement system in a timely manner, and if it will be strong enough to support the loads imparted during construction traffic and subsequently by the pavement layers and traffic.

CONCLUSIONS

Cedergren (1989) suggests a minimum hydraulic conductivity of 1 cm/sec (2835 ft/day) for materials to be used for high permeability base layers in pavement systems. The National Highway Institute (1999) also recommended a hydraulic conductivity of 0.35 cm/sec (1000 ft/day) for materials used in high permeability base layers in pavement systems. A program of in-situ and laboratory testing was performed on Missouri's Type 5 base material to assess its drainability and strength characteristics. In-situ hydraulic conductivities ranged from $2x10^{-3}$ to $4x10^{-5}$ cm/sec (6 to 0.1 ft/day). Laboratory hydraulic conductivities were in the range of $9x10^{-2}$ to $7x10^{-7}$ cm/sec (255 to $2x10^{-3}$ ft/day). The bases tested in this program averaged 1000 times lower hydraulic conductivity than typically necessary or recommended for good drainage of the pavement subsurface. The drainage quality of the materials was determined using the DRIP 2.0 software based on laboratory and field hydraulic conductivity values. Drainage quality ranged from good (1 case) to very poor (5 cases). Long term flow tests indicated that the hydraulic conductivity decreased one order of magnitude in an approximate 2 month period, and that the layer underlying this material will affect its drainage behavior.

Strength testing ($\overline{CU}$) showed that the material behaves as a dense, granular soil, showing contraction at the beginning of shearing and dilation afterwards. In undrained stress-controlled cyclic triaxial tests, the material showed a gain in strength, but failure was reached by excessive bulging. In undrained, strain-controlled cyclic triaxial tests the specimen lost most of its strength after 20 load cycles. Results of drained, strain-controlled cyclic triaxial test showed a behavior very similar to those specimens tested under undrained conditions, i.e., a dramatic loss in strength within a few load cycles.

Based on the hydraulic testing results and strength testing results, the Type 5 base material used in Missouri's roadways is not drainable. Other materials or composites should be introduced in the design to create a more permeable base layer and thus a more resistant and longer-lasting pavement system.

ACKNOWDEDGEMENTS

RERERENCES

American Society for Testing Materials (1994) *Standard Test Method for Infiltration Rate of Soils Using Double-Ring Infiltrometer*, D 3385-94, Section 4, Vol. 4.08

American Society for Testing Materials (2000a) *Standard Test Methods for Measurement of Hydraulic Conductivity for Saturated Porous Materials Using a Flexible Wall Permeameter*, D 5084 Sect. 4, Vol. 4.09

American Society for Testing Materials (2000b) *Standard Test Methods for Laboratory Compaction Characteristics of Soil Using Standard Effort (12,400 ft-lbf/ft^3 (600 kN/m^3))*, D 698-00, Sect. 4, Vol. 4.08

Applied Research Associates (2002). *Drainage Requirement in Pavements Version 2.0 (DRIP 2.0)*. FHWA Contract No. DTFH61-00-F-00199, Users Manual

Blanco, A. (2003). Drainage Performance of Missouri Roadway Bases. Masters Thesis, Department of Civil and Environmental Engineering, University of Missouri – Columbia

Cedergren, H.R. (1974). *Drainage of Highway and Airfield Pavement*. John Wiley and Sons, Inc., New York

Cedergren, H.R. (1989). *Seepage, Drainage and Flow Nets*, Third edition, John Wiley and Sons.

Cedergren, H.R. (1994). America's Pavements: World's Largest Bathtubs. *Civil Engineering*, Vol. 64, pp. 56-58

Missouri Department of Transportation (1996) *Materials Specifications*, Section 1007.

Moulton, L. (1980) Highway Subdrainage Manual, Report, TS-80-224. FHWA, U.S. Department of Transportation

Parra, J. and A. Blanco (2002). Hydraulic and Strength Performance of Missouri's Type 5 Base Material. *Proceedings, Transportation Scholars Conference*, Iowa State University

Prachantrikal, W. (2002) Hydraulic Conductivity of Type 5 Base Rock. Master Thesis, Department of Civil and Environmental Engineering, University of Missouri - Columbia.

USE OF LIME KILN DUST FOR STABILIZATION OF FINE-GRAINED SUBGRADE SOILS

Timothy D. Shevlin

Civil & Environmental Consultants, Inc., 333 Baldwin Road, Pittsburgh, Pennsylvania 15205

And

Abdul Shakoor

Department of Geology, Kent State University, Kent, Ohio 44242

Abstract

Common methods of treating poor quality subgrade soils are either to replace the poor quality soils by crushed stone or stabilize them with chemical agents such as lime or Portland cement. A relatively new agent of soil stabilization that has appeared in the market is lime-kiln dust (LKD), a byproduct of lime production. However, for a large-scale application of LKD, the pertinent engineering properties of LKD, and LKD-soil mixtures, must be documented.

A bulk sample of fine-grained subgrade soil (CL) was obtained from milepost 113 along Pennsylvania Turnpike (Interstate 76) and was evaluated for Atterberg limits, moisture-density relations, permeability, unconfined compressive strength, and California bearing ratio (CBR). The permeability, unconfined compressive strength, and CBR tests were performed on samples compacted to a minimum of 95% of maximum dry density (MDD) and within 2% of optimum water content (OWC). The soil was then mixed with three different types of LKD, designated as Graymont LKD, Strasburg LKD, and synthetic LKD, as well as with pure lime, and the mixtures were tested for Atterberg limits, moisture-density relations, permeability, unconfined compressive strength, and CBR. Each LKD was mixed with the soil at 2%-10% LKD by weight, at 2% intervals. The mixtures were also evaluated for strength gain over an 81-day curing period. Finally, Eades and Grim pH procedure was performed as a chemical check of the minimum amount of LKD required to stabilize the soil.

The results of the study show that the permeability of the LKD-soil mixtures generally increases by one order of magnitude, compared to the pure soil, at all LKD contents used. The LKD-soil mixtures gain most of their strength at 6% LKD content with unconfined compressive strength values increasing from 55 psi for pure soil to 90 psi-100 psi for the 6% LKD-soil mixtures. At longer curing periods of 27 and 81 days, the strength increases to as much as 150 psi. The CBR values increase from 4.5% for pure soil to 35%-40% for all LKD mixtures at LKD contents greater than 4%. According to Eades and Grim procedure, 4% LKD content was found to be sufficient to bring the pH to the required value of 12.45. Finally, no significant differences were found between the LKD materials tested. These results indicate that LKD is a viable material for stabilization of fine-grained soils.

Introduction

Soils constitute one of the most widely used materials for engineering construction. Buildings, bridges, dams, tunnels, roads, and highways are just a few examples of the engineering structures that are built on or through soil material. Often times, the in-situ soils are not of the proper quality for construction and need to be stabilized. Stabilization is the natural or artificial process by which soils are made stronger and more resistant to deformation under applied loads (Spangler and Handy, 1973). Some problems associated with construction on or through soils are: excessive settlement, volume changes (shrinking and swelling), frost susceptibility, corrosiveness, and loss of strength due to saturation (West, 1995). A variety of methods can be used to improve soil properties with mechanical compaction being the most frequently used method (Holtz and Kovacs, 1981; Moseley, 1993; Schaefer, 1997; Day, 1999). Other ground improvement methods include removal and replacement, dewatering, freezing, grouting, preconsolidation, and the addition of chemicals.

The use of chemicals in ground improvement has been practiced extensively for thousands of years. Specifically, the application of lime for soil stabilization has been dated back to Ancient Roman and Greek times (McDowell, 1959; Bell, 1996). Also, several other chemicals have been used for ground improvement including Portland cement, bentonite, fly ash, and a variety of salts (Moseley, 1993; Ferguson, 1993; Nicholson and Kashyap, 1993; Schaefer, 1997; Day, 1999). Also, some waste materials that have been tested for explicit use as stabilization agents include scrap tires, fly ash, bottom ash, foundry sand, lime sludge, and sewer sludge (Hart et al., 1993; Black and Shakoor, 1994; Shakoor and Chu, 1998; Fransisco, 2001).

During highway construction, some form of ground improvement is almost always necessary to improve the quality of pavement subgrades. The subgrade is the bottom-most layer of the pavement system normally composed of the original ground or a fill material (Spangler and Handy, 1973; West, 1995; Day, 1999). In many cases the subgrade soil is of poor quality and inadequate with respect to load carrying capacity. This can be due to soil conditions that are too wet, too loose, or both, and, therefore, the subgrade soil needs to be stabilized. Probably the most common and traditional method to treat highway subgrades is to over excavate and replace the poor quality soil with crushed stone, but this can be very expensive. For this reason fly ash and lime, either separately or in combination, have been used for some time as chemical agents in the stabilization of highway subgrades.

Another product that is starting to be commercially marketed for soil stabilization is lime kiln dust (LKD), a byproduct from lime production. The Pennsylvania Turnpike Commission has used LKD as a subgrade stabilization agent on a limited basis during the reconstruction of the Pennsylvania Turnpike. The active ingredient in LKD is calcium oxide (CaO, quicklime). Therefore, the description of the clay-lime reaction discussed below also holds true for LKD. It should be noted that the lime reaction is complex and the description that follows is quite simplified (Boyton, 1966; Transportation Research Board, 1976; Transportation Research Board, 1986; Little 1995). The process of hydrating lime (CaO), shown in the following reaction,
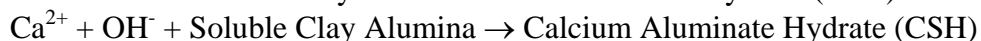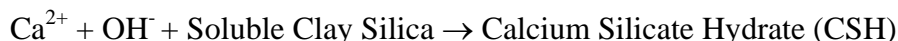
makes the lime disassociate into Ca^{2+} and OH^- that is followed by the formation of calcium hydroxide {$Ca(OH)_2$, hydrated lime}.

$$CaO + H_2O \rightarrow Ca^{2+} + 2OH^- + heat \rightarrow Ca(OH)_2$$

When lime becomes hydrated and reacts with clay soil the first two processes to occur are cation exchange and flocculation/agglomeration (Thompson, 1975; Transportation Research Board, 1986; Bell, 1996; Mathis, 1999; Qubain et al., 2001). Cation exchange is simply the exchange of different cations in a system. Flocculation is edge-to-face attraction of the clay particles in fine-grained soils. These two processes happen very rapidly.

In a clay-water system the highly negative charge of the clay particle surface attracts water, a dipolar molecule, and positively charged ions creating a diffuse water-ion layer. When lime is added, the free Ca^{2+} ions react with the diffused water and weak ion layer between the clay sheets. The ion exchange between the Ca^{2+} ion of the lime and the weaker ions attracted to clay particles helps reduce the thickness of the diffuse water layer and consequently causes flocculation of the clay particles. Flocculation helps increase the shear strength of the soil. Also, the ion exchange dries out the soil by reducing the ability of the clay particles to hold a thick diffuse water-ion layer, therefore, lowering the plasticity of fine-grained soils. Ion exchange and flocculation almost immediately improve the engineering properties of soil including plasticity, workability, uncured strength, frost susceptibility, and load carrying capacity (Thompson, 1975; Bell, 1996; Mathis, 1999; Qubain et al., 2001).

The long-term strength gain associated with lime stabilization of clay soils is due to the pozzolanic reactions shown below. The pozzolanic reaction produces the cementitious products,

$Ca^{2+} + OH^- + $ Soluble Clay Silica $\rightarrow$ Calcium Silicate Hydrate (CSH)
$Ca^{2+} + OH^- + $ Soluble Clay Alumina $\rightarrow$ Calcium Aluminate Hydrate (CSH)

namely calcium silicate hydrate (CSH) and calcium aluminate hydrate (CSH). These products form when the correct moisture and pH conditions are met and there is a sufficient amount of pozzolans, fine-grained siliceous and aluminous materials, to react with the Ca^{2+} ion (Ferguson, 1993; Nicholson and Kashyap, 1993; Little, 1995). The above reactions are very dependent on pozzolan content and, therefore, the mineralalogy of the soil in question or the amount of artificial pozzolans (flyash or LKD) added to a soil greatly influence the results. When strictly lime is used to stabilize a soil and no artificial pozzolans are added, the soil must have the correct mineralalology for the pozzolanic products, CSH and CAH to form. If the amount of silicates and aluminas (clay minerals) available is not sufficient, as can be the case for eastern soils shed from the Appalachian Mountains, artificial pozzolans can be added by using fly ash or LKD to allow for the pozzolanic reaction to occur more readily.

Limited research on the use of LKD for soil improvement, conducted by Qubain et al (2001), has shown that unconfined compressive strength and California Bearing Ratio (CBR) both increase with the addition of LKD. Although these findings are encouraging, the use of LKD has not been researched in detail. Due to chemical variation of LKD between various

manufacturers, it is essential that additional research be conducted to evaluate the variability of LKD from different suppliers.

Objectives

The objectives of this investigation were as follows:

1. Determine the engineering properties of LKD-soil mixtures, containing 2% to10% LKD by weight, for the purpose of finding the optimum LKD content for three different types of LKD material obtained from three different sources.

2. Investigate the effect that long-term ambient curing has on the unconfined compressive strength of LKD-soil mixtures.

3. Determine if there was variation in the performance of LKDs with respect to their source.

Methodology

Sample Collection

A sample of a fine-grained clay soil, weighing approximately 500 lbs (230 kg), was collected from the subgrade of the westbound lanes of I-76 through Pennsylvania, near milepost 113. This particular section of the highway was under construction at the time of sampling. Seven lime kiln-dust (LKD) samples were obtained with the help of the personnel from Pennsylvania Turnpike Commission. Based on an evaluation of the chemical characteristics of the seven LKD samples, provided by the suppliers, three were chosen for the study. These included a low-end LKD, a high-end LKD, and a synthetic LKD (50%, lime, 50% flyash), the low-end and high-end referring to the available CaO (Table 1). The LKD samples were designated as the Strasburg LKD, Graymont LKD, and synthetic LKD, respectively. A quicklime sample was also chosen to serve as a control and will be referred to as the Annville lime in the following discussion. The main factors that control the chemical constituents of LKD are the original stone used to produce the lime, the type of coal used to fire the kilns, and the strength of the blowers used to contain the lime kiln dust waste.

Laboratory Tests

Laboratory tests were performed to determine Atterberg Limits, moisture-density relationships, permeability, unconfined compressive strength, and California bearing ratio (CBR) of the subgrade soil and LKD-soil mixtures. In addition, the Eades and Grim pH procedure was performed on LKD-soil mixtures. Except for the Atterberg limits tests and the Eades and Grim pH procedure, the tests were conducted on compacted samples of LKD-soil containing 0% to 10% LKD by weight, at 2% intervals. All samples were compacted to at least 95% of maximum

Table 1: LKD additives used as the soil stabilizing agents.

LKD Sample	Total Lime CaO (%)	Active Lime CaO (%)	Total Pozzolan (%)
Graymont	52.1	26.0	13.3
Strasburg	67.0	44.0	8.5
Synthetic*	49.6	47.3	37.0
Quicklime	95.4	90.8	2.4
FlyAsh (Class F)	3.8	3.8	71.5

* Synthetic: 50% Hatfield Flyash + 50% Annville Lime

dry density (MDD) or greater and within 2% of optimum water content (OWC). The samples for unconfined compression test were cured for varying time intervals to evaluate the time-dependent gain in compressive strength. All laboratory tests were conducted in accordance with the American Society for Testing and Material (ASTM) procedures (ASTM, 1996), where applicable.

Summary of Results

Results of Engineering Tests

The subgrade soil has a natural water content of 14.8%, a MDD of 111.0 pcf (1781.6 kg/m^3), and an OWC of 12.5%. According to the Unified Soil Classification System (USCS), the subgrade soil can be classified as clay of low plasticity (CL). The as delivered water content values of all the pure LKD samples are 0.0%, and their gradations are different from one another.

Addition of the LKD materials to the subgrade soil increases the liquid limit (LL) and plastic limit (PL) values compared to the pure soil except for LKD-soil mixtures with 2% Strasburg LKD in the case of LL, and 2% Graymont LKD in the case of PL. The LL and PL values tend to increase up to 6% LKD content and then decrease as LKD dosage increases to 10% for all the LKD materials. The plasticity index (PI) generally decreases with increasing amounts of LKD (Table 2, Figure 1). The addition of LKD to the pure soil changes the USCS classification from a clay of low plasticity (CL) to a silt of low plasticity (ML) in all cases except for the Graymont LKD-soil mixtures at 2% and 10% LKD content, as well as the Synthetic and Strasburg LKD-soil mixtures at 2% LKD content.

Mixing the LKD material with the pure soil at concentrations of 2% to 10% by weight generally decreases the MDD (Figure 2) and increases the OWC (Figure 3), but the trends observed were not consistent. When compared to the MDD of the pure soil, the MDD of the Graymont LKD-soil mixtures continually decreases with the exception of the 6% mixture. The Strasburg LKD decreases the MDD at doses of 2% and 4%, after which the MDD increases sharply at 6% LKD content before decreasing again at higher LKD contents. The MDD of the

Table 2: Atterberg limits of the LKD-soil mixtures at various LKD contents.

| LKD Type	Atterberg Limits	LKD Content			
		0%	2%	6%	10%
Graymont					
	Liquid Limit	32.7	34.5	40.0	35.0
	Plastic Limit	18.7	18.2	28.5	21.2
	Plasticity Index	14.0	16.3	11.5	13.8
Strasburg					
	Liquid Limit	32.7	31.9	34.5	36.5
	Plastic Limit	18.7	22.5	23.9	25.3
	Plasticity Index	14.0	9.4	10.6	11.2
Synthetic					
	Liquid Limit	32.7	36.5	38.5	35.1
	Plastic Limit	18.7	21.7	26.3	23.9
	Plasticity Index	14.0	14.8	12.2	10.9
Annville Lime					
	Liquid Limit	32.7	23.5	38.0	36.3
	Plastic Limit	18.7	23.8	25.2	24.8
	Plasticity Index	14.0	8.7	13.8	11.6
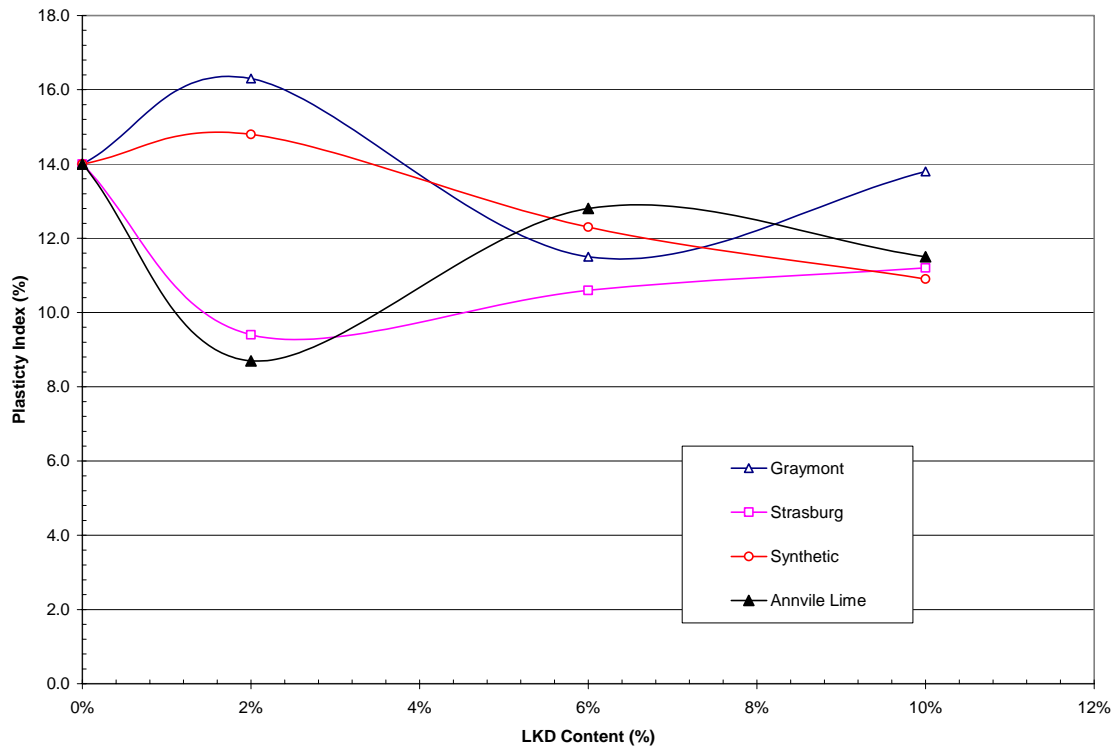
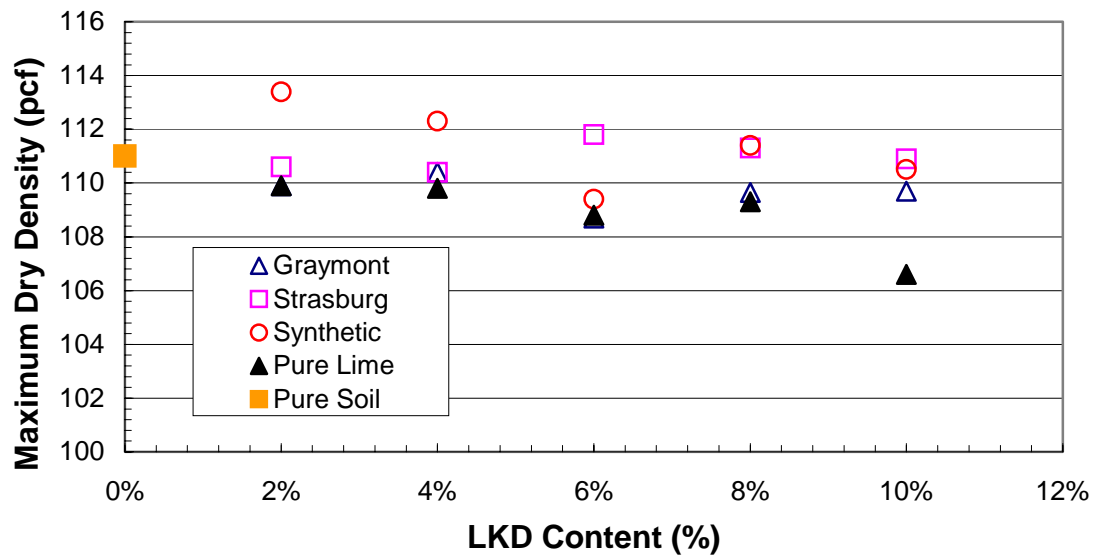Figure 1. Effect of increasing LKD content on plasticity index of the subgrade soil.

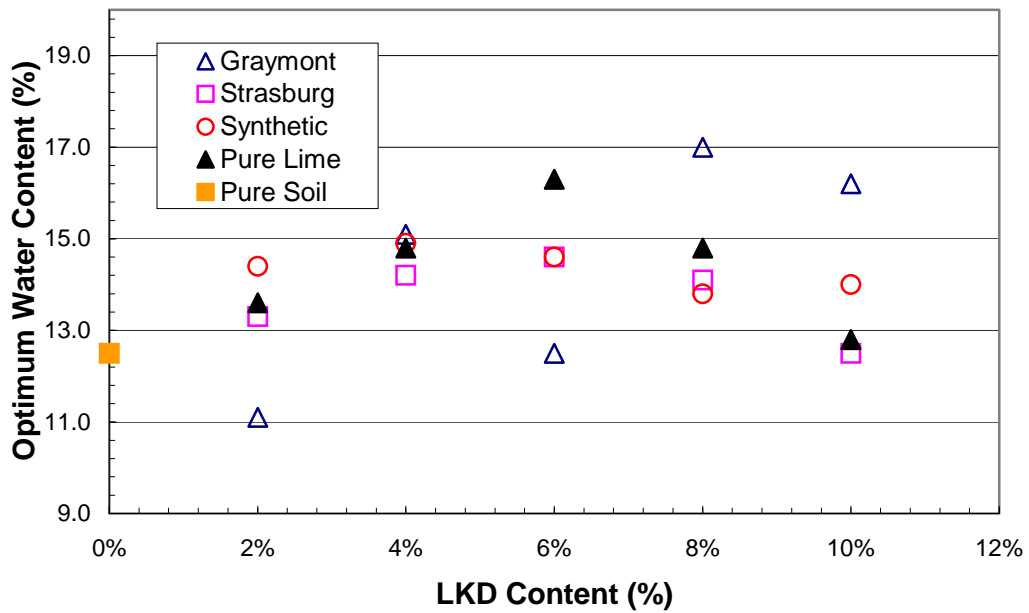Figure 2. : Relationship between maximum dry density and LKD content.

Figure 3. Relationship between optimum water content and LKD content.

synthetic LKD-soil mixtures increases from that of the pure soil and then decreases, with a sharp drop at 6% Synthetic LKD content. Finally, the trend of MDD of the Annville lime-soil mixtures shows a continuous decrease in a linear fashion except for a slight deviation at 8% lime content.

The trend of OWC with respect to increasing LKD content is relatively more consistent (Figure 3). The OWC is almost always higher than that of the pure soil, with the exception of the following LKD-soil contents: Graymont LKD at 2% and 6%, and Strasburg LKD at 10%. The OWC generally increases until 6% LKD content and then decreases, but the OWC values remain higher than the OWC of the pure soil (12.5%).

The permeability values of all the LKD-soil mixtures, from 2% to 10% LKD, are similar to those for soils of poor drainage characteristics such as glacial tills, silts, and loess (Table 3, Figure 4). The Strasburg LKD-soil mixture is the most permeable with a permeability value of 1.74E-05 cm/sec (3.43E-05 ft/min) at 2% LKD content which decreases to approximately 1.50E-06 cm/sec (2.9E-06 ft/min) at 8% and 10% Strasburg LKD content. All the other LKD mixtures, at all dosages from 2% to 10%, consistently exhibit permeability values between 1.0E-06 cm/sec (1.9E-06 ft/min) to 2.0E-06 cm/sec (3.9E-06 ft/min). The pure soil has a permeability of 2.77E-07 cm/sec (5.45E-07 ft/min), nearly impermeable.

Strength values for all the LKD-soil mixtures follow very similar trends. The unconfined compressive strength values increase with increasing LKD content and gradually level off at 6% LKD content and above (Table 4, Figure 5). The unconfined compressive strength of the pure soil is 55.3 psi (381.2 kPa). The strength values for the Strasburg LKD-soil and Graymont LKD-soil mixtures at LKD contents of 6% and above are consistently in the range of 90.0 psi to 100.0 psi (620.5 to 689.4 kPa), whereas the strength values for the synthetic LKD-soil and Annville lime-soil mixtures at 6% LKD contents and higher are generally near 80 psi (551.5 kPa).

CBR values for all the LKD-soil mixtures tested are very close (Table 5, Figure 6). Mixtures at a 4% LKD content show an increase by 30% points compared to a CBR value of 4.5% for the pure soil and stay in the range of 35% to 40% at LKD contents of 4%, 6%, and 10%. The exception is the 6% Strasburg LKD-soil mixture with a CBR value of 28%. However, the Strasburg LKD-soil mixture at 8% LKD content has the highest CBR value of 45%.

Table 3: Permeability values of the LKD-soil mixtures at various LKD contents.

	Permeability (cm/sec)					
LKD Content	0%	2%	4%	6%	8%	10%
Graymont	2.66E-07	2.65E-06	1.56E-06	2.80E-06	1.09E-06	1.28E-06
Strasburg	2.66E-07	1.74E-05	8.36E-06	6.91E-06	1.40E-06	1.77E-06
Synthetic	2.66E-07	1.24E-06	2.88E-06	1.11E-06	1.77E-06	2.21E-06
Annville Lime	2.66E-07	1.60E-06	1.97E-06	1.02E-06	5.20E-07	8.25E-07

Results of the Eades and Grim pH Procedure

The Eades and Grim pH procedure indicates the minimum amount of LKD that is needed to satisfy cation exchange and all initial short-term reactions (Little, 1995). The minimum amount refers to the point at which there is enough CaO to saturate the water, bringing the pH to 12.45. After the short-term processes are satisfied, any excess CaO will start to react and form pozzolanic agents adding to the long-term strength gain. The results of the Eades and Grim pH procedure are shown in Table 6 and Figure 7. The pH of the pure soil was found to be 8.25. The Annville lime sample is the only material used in this study for which the pH value of the 2% mixture exceeded 12.45, reaching a value of 12.53. The Graymont, Strasburg, and synthetic LKDs have pH values of 11.99, 12.26, and 12.26, respectively, at 2% LKD content. All of the LKD-soil mixtures reach a pH of 12.45 when LKD is added at amounts of 4% and greater.
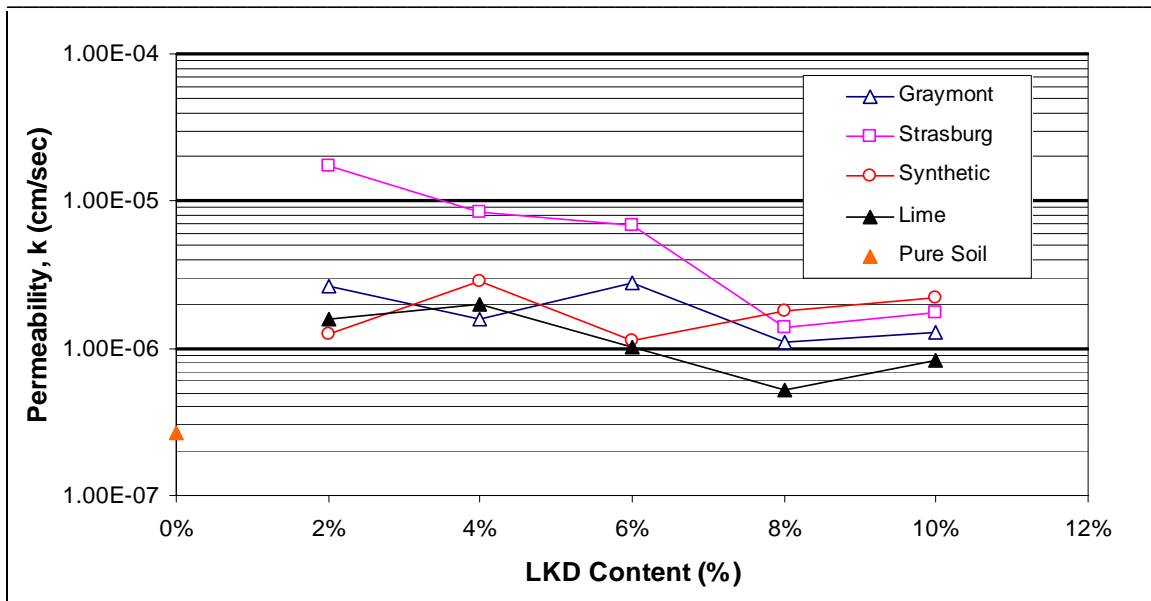
Figure 4. Relationship between permeability and LKD content.

Table 4: Unconfined compressive strength values of the LKD-soil mixtures at various LKD contents.

LKD Content	Unconfined Compressive Strength (psi)					
	0%	2%	4%	6%	8%	10%
Graymont	55.3	43.6	74.7	93.1	96.5	91.9
Strasburg	55.3	74.7	78.0	91.9	98.1	96.5
Synthetic	55.3	63.9	70.1	78.9	81.0	82.5
Annville Lime	55.3	66.8	79.4	81.5	91.9	79.4
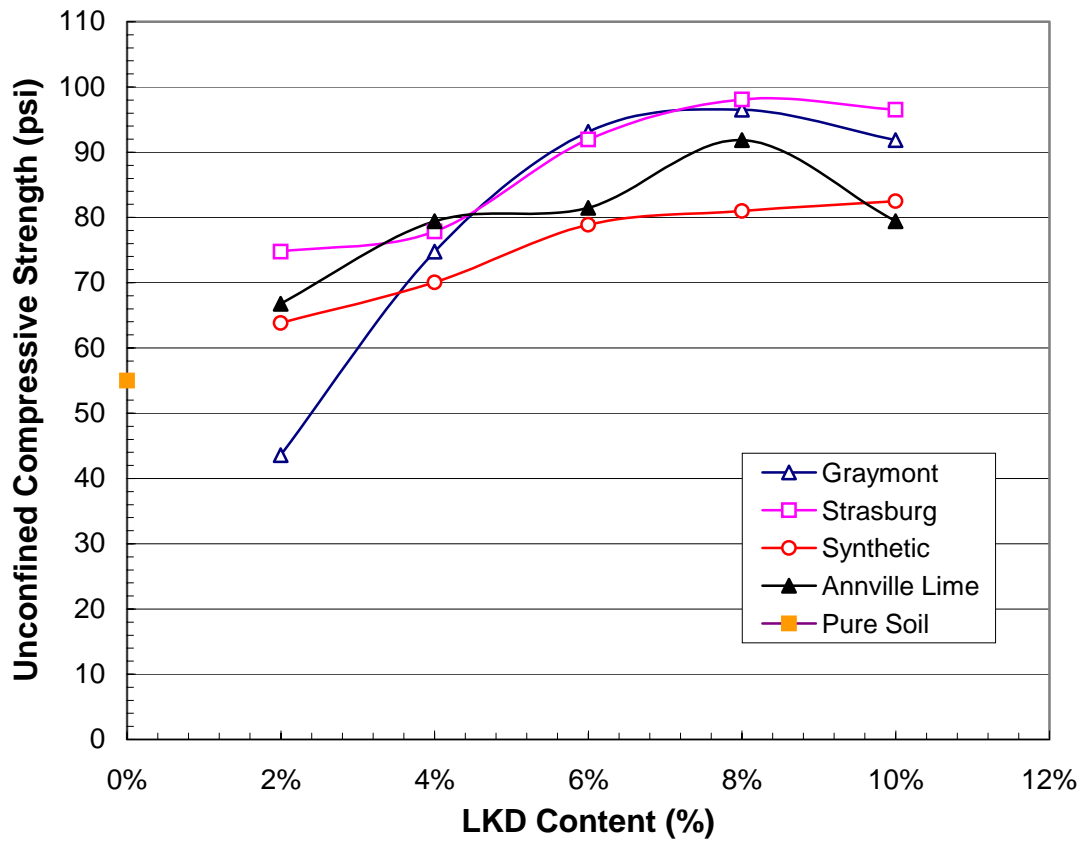
Figure 5. Effect of LKD content on the unconfined compressive strength of LKD-soil mixtures.

Table 5: CBR values of the LKD-soil mixtures at various LKD contents.

	California Bearing Ratio (%)			
LKD Content	0%	4%	6%	8%
Graymont	4.5	36.7	39.7	39.0
Strasburg	4.5	40.0	29.0	45.0
Synthetic	4.5	39.3	37.3	35.0
Annville Lime	4.5	35.7	35.6	40.0

Application of this procedure to the LKD-soil mixtures used in this study shows that all of LKDs reach the minimum amount of LKD needed to satisfy short-term stabilization of the subgrade soil at a dosage of 4%, although pure lime has enough active CaO at a 2% dose.
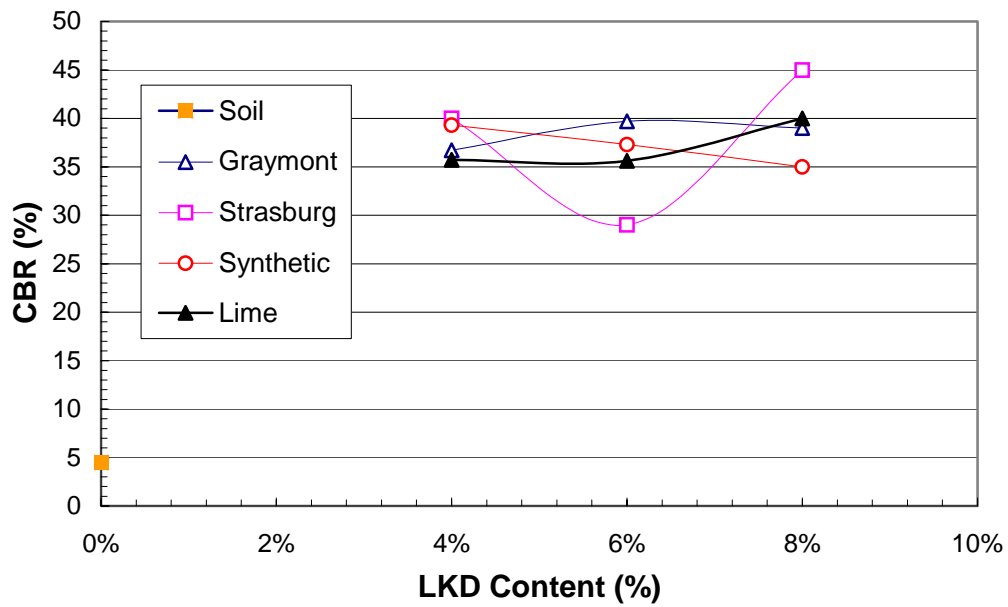
Figure 6. Effect of LKD content on the CBR of LKD-soil mixtures.

Table 6: Values of pH measured during the Eades and Grim pH Procedure.

LKD (%)	pH				
	Soil	Graymont	Strasburg	Synthetic	Lime
0	8.25	NA	NA	NA	NA
2	NA	11.99	12.26	12.26	12.53
4	NA	12.43	12.49	12.5	12.47
6	NA	12.49	12.49	12.49	12.5
8	NA	12.5	12.49	12.46	12.5
10	NA	12.55	12.5	12.51	12.52

NA: Not applicable (sample does not exist)

Results of Time-dependent Unconfined Compression Testing

A very important aspect of using LKD for soil stabilization is the length of time that the LKD-soil mixtures are allowed to cure. Time is integral to strength gain because the cementing agents, calcium silicate hydrate (CSH) and calcium aluminate hydrate (CAH), are products of the

long-term pozzolanic reaction and they continue to grow as the curing time increases. According to the TRB State-of-the-Art Report 5 (TRB, 1986), the pozzolanic reaction is dependent on soil mineralogy and soil reactivity. A soil is considered to be reactive if after 28 days of curing the increase in the unconfined compressive strength of the soil is greater than 50 psi (344.7 kPa) and non-reactive if the strength gain is less. However, if a soil is non-reactive it does not mean that pozzolanic activity does not take place (TRB, 1986). It has been shown that with a long enough curing period and a reactive soil, pozzolanic strength gains can be as high as 400 psi (2757.9 kPa) (TRB, 1986; Little, 1995). The main factors that influence strength gain include the type of soil, amount of lime added, curing temperature, and length of curing time.

The time-dependent strength gain portion of this study was performed to investigate how the strength of LKD-treated soils changes with time. The clay soil was mixed with a 6% dose of each of the LKD materials. The mixtures were then compacted to at least 95% of MDD and within 2% of OWC, and allowed to cure for 9, 27, and 81 days at ambient conditions. The ambient conditions for this study consisted of a temperature of $23^{o}C$ ($73.4^{o}F$) and a relative humidity of 95%, achieved by use of a humidity-control chamber. Results of time-dependent unconfined compression testing show that strength increases with time (Table 7 and Figure 8). All of the LKD treated samples exhibit a sharp increase in strength between 3 and 9 days of curing beyond which the relationship between strength and curing time becomes asymptotic. All of the samples have unconfined compressive strengths of more than 100 psi (689.4 kPa) after a 9-day curing period. For the Graymont LKD, Strasburg LKD, synthetic LKD, and Annville lime-soil mixtures, the strength values increased to 106.9 psi (737.0 kPa), 146.5 psi (1010.0 kPa), 117.8 psi (812.2 kPa), and 158.3 psi (1091.4 kPa) after 81 days of curing, respectively. It should be noted that the Graymont LKD-soil sample had the least amount of strength gain throughout the entire 81-day curing period. This could be due to the fact that the Graymont LKD is the lower-end member LKD material with 26% active CaO, but further study would be needed to verify this explanation. Also, the compressive strength of the Graymont and synthetic LKD-soil mixtures cured for 81 days are lower than the compressive strengths of the mixtures cured for 27 days. The reason for this is not clear and can possibly be attributed to small variations from sample to sample or to experimental error.

Table 7: Unconfined compressive strength of 6% LKD-soil mixtures cured over varying periods of time at ambient conditions.

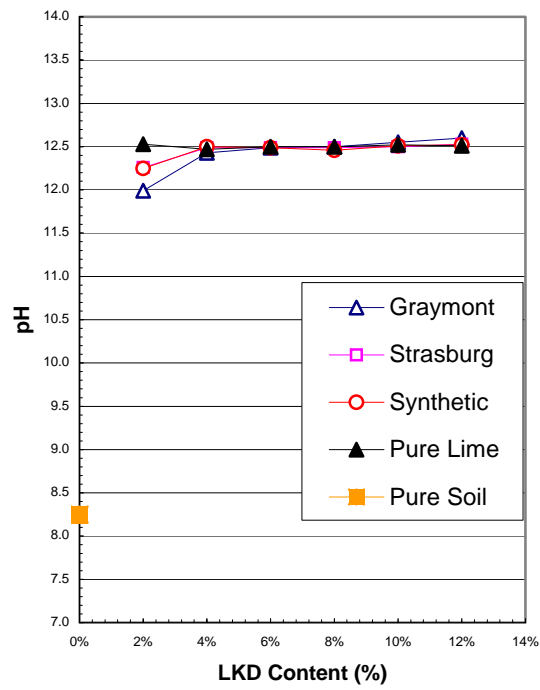| LKD	Unconfined Compressive Strength (psi)			
	3-Day	9-Day	27-Day	81-Day (avg)
Graymont	91.9	121.4	115.2	106.9
Strasburg	87.2	147.9	143.3	146.5
Synthetic	79.4	144.8	154.1	117.8
Pure Lime	84.1	138.6	152.6	158.3

Figure 7. Effect of LKD content on pH values of LKD-soil mixtures
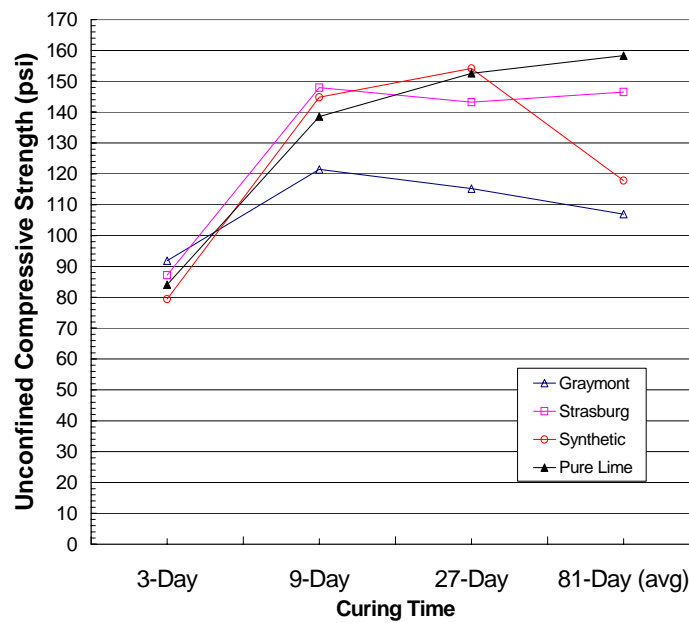tested according to the Eades and Grim pH Procedure

Figure 8. Unconfined compressive strength values for 6% LKD-soil samples
cured for 3, 9, 27, and 81 days under ambient conditions.

Discussion

Optimum Lime Content Needed to Improve Engineering Properties of LKD-Soil Mixtures

An evaluation of the optimum amount of LKD can be divided into two categories. The first category is modification or soil change that improves the engineering properties of the subgrade soil in response to the rapidly occurring reactions of hydration and flocculation. The second category, stabilization, involves strength related criteria, such as unconfined compressive strength, associated with the pozzolanic reaction. The results of the strength-gain tests described above indicate that the proper LKD dosage required to modify as opposed to stabilize the subgrade soil is different depending on the purpose of the stabilization effort. The tests performed in this study evaluate specific engineering properties, which are optimized at different LKD contents.

The optimum LKD content, as indicated by the Atterberg limits tests performed in this study, is 6%. This dosage of LKD reduced the soil plasticity most consistently amongst the LKD materials used and is, therefore, the most dependable dosage. The implication of soil plasticity reduction is that the soil becomes less susceptible to detrimental changes induced by changing water content and, at the same time, the soil becomes more workable, expediting construction.

Permeability increases slightly with the addition of any amount of LKD after a 3-day curing period. This increase is related to the ion exchange and flocculation of the clay soil. These processes cause the soil to become less plastic, and siltier in nature. Therefore, when compacted, the flocculated soil is more permeable because pore spaces become more connected. The unconfined compressive strength of the soil has the most significant gain with the addition 6% LKD and does not continue to gain significant strength with higher doses. In this study, a compressive strength of 100 psi (689.4 kPa) was considered to be the desired value. The target strength of 100 psi (689.4 kPa) is not met after a 3-day curing period, but the observed strengths come close to the required strength at 6% LKD content and above. The CBR, an indication of shear strength, increases significantly. Finally, the Eades and Grim pH procedure suggests that 4% LKD is the minimum amount of LKD necessary to modify the subgrade soil.

Based on the results of this study, 4% LKD appears to be the minimum amount needed to improve the engineering properties that are related to short-term soil modification. These improvements include plasticity reduction, improved workability, immediate strength increase, and reduced potential for volume change (TRB, 1986; Little, 1995). The optimum LKD content for strength gain after 3 days of ambient curing is achieved with the addition of 6% LKD.

With respect to long-term strength gain, the samples tested reached compressive strength values greater than 100 psi (689.4 kPa) after a 9-day curing period. The samples containing the Strasburg LKD, synthetic LKD, and Annville lime reached a compressive strength of approximately 140 psi (965.2 kPa). The Graymont LKD sample reached an unconfined compressive strength value of just over 120 psi (827.3 kPa). The 27-day curing period resulted in a slight improvement compared to the 9-day strength, with strength values just above 150 psi

(1034.2 kPa) for the samples containing the synthetic LKD and Annville lime. The samples containing Graymont LKD and Strasburg LKD showed no additional gain in strength with 27 days of curing. After 81-days of curing, only the pure lime sample increased in strength to just under160 psi (1103.1 kPa), the Strasburg sample held in the range of 140 psi to150 psi (965.2 kPa to1034.2 kPa), and the samples containing the Graymont and Synthetic LKDs dropped in strength.

As discussed previously, the pozzolanic reaction is the main source of long-term strength gain because of the formation of the cementing agents CSH and CAH. Although the samples cured for 3 days do not reach the desired strength of 100 psi (689.4 kPa), the time-dependent strength gain portion of the study shows that with a slightly longer curing time of 9 days there is significant increase in strength above 100 psi (689.4 kPa). Furthermore, although the strengths increased above the target value of 100 psi (689.4 kPa) after 9 days, there was an insignificant increase in strength with longer curing periods of up to 81 days.

Performance Variability of Various LKD Materials

An important aspect of this study was to find out if there was a variation between LKD materials of different characteristics with respect to their ability to stabilize subgrade soils. To accomplish this three different LKDs and pure lime, of varying CaO and pozzolan contents, were evaluated with respect to improvement in the engineering properties tested this study. The results of the engineering tests indicate that there is little variability between the LKDs used in this study. The Atterberg Limits, permeability, and CBR tests all yield results that are almost exactly the same with respect to the different LKDs. The unconfined compression test after 3 days of curing show that the samples containing the Strasburg and Graymont LKDs perform slightly better whereas the results of unconfined compression testing of samples cured for longer time periods indicate that the Graymont LKD-soil samples perform the poorest with the other three LKDs exhibiting similar results. However, Strasburg LKD was found to be easy to work with because of its relatively coarser grain size.

Pure lime was used for comparison purposes in this study because it has been tested extensively and proven as a viable stabilizing agent for clay soils. All of the previous studies that the results of this study were compared to were performed on soils treated with pure lime. It is important to note that the LKD materials used in this study performed similar to pure lime. This suggests that LKDs with lower levels of available CaO can be relied upon as stabilization agents.

Limitations of the Study

The study presented herein has several limitations. These include: 1) results of laboratory tests were not verified by any field testing with respect to stabilizing ability of the LKD materials; 2) only one type of subgrade soil was used; and 3) there was very limited replication of the laboratory tests.

Conclusion

Based on the results of this study, it can be concluded that LKD is a viable agent for stabilization of poor quality, fine-grained subgrade soils. The optimum amount of LKD needed for stabilization depends on the goal of stabilization. For modification of subgrade soil, a 4% by weight dosage of LKD may be adequate whereas 6% LKD content is required for more complete stabilization. Modification of soil, related to short-term processes of ion exchange and flocculation, reduces the water retention capability of the fine-grained soil and improves the related engineering properties such as plasticity characteristics, workability, shrink-swell potential, and shear strength related to textural changes (TRB, 1986; Little, 1995). Complete stabilization, where the available CaO, after satisfying the short-term processes, combines with silica to generate the cementing agents CSH and CAH, helps meet the required unconfined compressive strength and CBR criteria.

Aknowledgments

References

American Society for Testing and Materials, 1996, Soil and Rock; Dimension Stone Geosynthetics: Annual Book of ASTM Standards, vol. 4.00, section 4, Philadelphia, PA. 1000 p.

Bell, F.G., 1996, Lime Stabilization of Clay Minerals and Soils: *Engineering Geology*, vol. 42, pp. 223-237.

Black, B.A., and Shakoor, A., 1994, A Geotechnical Evaluation of Soil-Tire Mixtures for Engineering Applications: proceedings, First International Congress on Environmental Geotechnics, Edmonton, Canada, pp. 617-623.

Boyton, R.S., 1966, Chemistry and Technology of Lime and Limestone: John Wiley & Sons, New York, New York. 531 P.

Day, R.W., 1999, Geotechnical and Foundation Engineering: Design and Construction, McGraw-Hill Companies, Inc., Highstown, New Jersey, 748.

Ferguson, G., 1993, Use of Self-Cementing Fly Ashes as a Soil Stabilization Agent: In Flyash for Soil Improvement, Sharp, K.D., (ed.). Geotechnical Special Publication No. 36, American Society of Civil Engineers, New York, NY., pp. 1-14.

Fransisco, B.H., 2001, A Geotechnical Evaluation of the Potential Use of Selected Waste Materials for Lime Spoil Stabilization: unpublished research, Masters Thesis, Kent State University, 119 P.

Hart, M.L., A. Shakoor, and T.P. Wilson, 1993, Characterization of Lime Sludge for Engineering Applications, *Waste Management*, vol. 13, pp. 55-63.

Holtz, R.D. and W.D. Kovacs, 1981, An Introduction to Geotechnical Engineering: Prentice Hall, Englewood Cliffs, New Jersey, 733 P.

Little, D.N., 1995, Handbook of Stabilization of Pavement Subgrades and Base Courses with Lime: Kendall/Hunt Co., Dubuque, Iowa, 219 P.

Mathis, H., 1999, Soil Modification and Lime Stabilization Utilizing Lime:, Dravo Lime Company, Kentucky, pp. 1-40.

McDowell, C., 1959, Stabilization of Soils with Lime, Lime-Flyash and other Lime Reactive Material: *Highway Research Board, Bulletin 231*, Washington, DC, pp. 60-66.

Moseley, M.P., 1993, Ground Improvement: CRC Press, Inc., N.W., Boca Raton, Florida, 218 p.

Nicholson, P.G., and V. Kashyap, 1993, Flyash Stabilization of Hawaiian Soils: In Flyash for Soil Improvement, Sharp, K.D., (eds.). Geotechnical Special Publication No. 36, American Society of Civil Engineers, New York, NY., pp. 15-29.

Qubain, B.S., E.J. Seksinsky, and J. Li, 2001, Incorporating Subgrade Lime Stabilization into Pavement Design: *Transportation Research Record,* pp. 3-8.

Schaefer, V.R., (ed.), 1997, Ground Improvement, Ground Reinforcement, Ground Treatment, Developments 1987-1997: Geotechnical Special Publication No. 69, American Society of Civil Engineers, New York, NY., 615 p.

Shakoor, A., and Chu, Chien-jen, 1998, Suitability of Soil-Tire Fill Mixtures as a Lightweight Fill for Highways, 8th International Association of Engineering Geologists Congress Proceedings, Vancouver, B.C., Canada.

Spangler, M.G., and R.L. Handy, 1973, Soil Engineering: 3rd Edition: Intext Educational Publishers, New York, 748 p.

Thompson, M.R., 1975, Soil-Lime Mixtures for Construction of Low-Volume Roads: *Special Report Presented by Transportation Research Board*, pp. 149-165.

Transportation Research Board (TRB), 1976, State of the Art: Lime Stabilization, Reactions Properties, Design, Construction TRB Circular, National Academy of Sciences, Washington, D.C. p. 30.

Transportation Research Board (TRB), 1986, State of the Art Report 5: Lime Stabilization: Reactions, Properties, Design, and Construction. TRB, National Research Council, Washington, D.C. 59 P.

West, T.R., 1995, Geology Applied to Engineering, Prentice Hall, Englewood Cliffs, New Jersey, pp. 542.

Exploding Roads in Texas: an Ounce of Prevention is Worth a Pound of Cure

[1]Pat Harris, Ph.D., P.G., [2]Stephen Sebesta, and [3]Joré von Holdt

Abstract

Texas has spent tens of millions of dollars in the last twelve years repairing heaves caused by calcium-based stabilizer use in sulfate-bearing subgrade soils. The sulfate minerals react with lime or cement to form reaction products that expand approximately 2.5 times the original volume. This study focuses on identification of problematic soils in the field (ideally prior to construction), steps to take with sulfate laden soils, and remediation of pavement failures. We developed a procedure to assess the potential for sulfate problems prior to construction. Three-Dimensional swell tests were performed on sulfate-bearing samples at concentrations of 0, 1000, 2000, 3000, 5000, 7000, and 12,000 parts per million (ppm) to determine limits for effective lime stabilization. We identified alternative stabilization and construction techniques for high sulfate soils. Use of geologic maps, visual observation, and measurement of sulfate content with a colorimeter can identify areas at risk of developing sulfate-induced heave. Results of our 3-D swell experiments indicate that up to 3000 ppm sulfates can be stabilized with traditional lime techniques. Modified construction techniques like mellowing, single instead of double lime application, and higher molding moisture contents (2% above optimum moisture) can treat up to 7000 ppm sulfates. Use of a ground granulated blastfurnace slag cement and lime mixture can be used to treat sulfate concentrations in excess of 10,000 ppm. This research is being implemented by the Texas Department of Transportation in the form of new test procedures for field identification of sulfates, and revision of construction guidelines in sulfate-bearing soils.

---

(1) Associate Research Scientist, Texas Transportation Institute, Materials and Pavements Division, 405 Spence St., College Station, Texas 77843-3135; Telephone: (979) 845-5845; e-mail: pat-harris@tamu.edu

(2) Associate Transportation Researcher, Texas Transportation Institute, Materials and Pavements Division, 405 Spence St., College Station, Texas 77843-3135; Telephone: (979) 458-0194; e-mail: s-sebesta@tamu.edu

(3) Technician #1, Texas Transportation Institute, Materials and Pavements Division, 405 Spence St., College Station, Texas 77843-3135; Telephone: (979) 847-8998; e-mail: j-vonholdt@tamu.edu

INTRODUCTION

The Texas Department of Transportation (TxDOT) has spent tens of millions of dollars over the last twelve years repairing sulfate-rich subgrade soils stabilized with lime or cement. Soluble sulfate minerals in the soil react with calcium-based stabilizers (lime/cement) to form ettringite which results in a large volume increase that generates heaves like this one on US 67 near Waxahachie, Texas (Figure 1).

Figure 1. Vertical heaves generated after a rainfall event is the product of lime stabilization of a sulfate-rich subgrade.

Cement and concrete researchers (*1*) have recognized problems with sulfates for decades. Sherwood (*2*) reported problems with sulfates in lime and cement stabilization of soils. However, until the mid 1980's sulfate induced heave in soils received little attention. Formation of ettringite was the cause of heaving in a case study from the southern United States (*3*). Mitchell's Terzaghi Lecture was the first time sulfate induced heave received national recognition (*4*). He stressed the importance of physicochemical and biological changes in soil mechanics in a case study of a parking lot in Las Vegas that heaved two years after construction. Mitchell reported ettringite and thaumasite were the cause of failure. Hunter explained many of the physicochemical details concerning sulfate heave (*5*).

Petry and Little (*6*) reported the first sulfate-induced heave in Texas. They identified four locations with sulfate-induced heave and discovered problems associated with testing soils for sulfates (*6*). The Texas Transportation Institute (TTI) has worked on several forensic investigations where sulfate-induced heave was determined to be the cause of failure. Inconsistencies in sulfate data were noted during these investigations (Harris, unpublished data).

Hunter determined that a unique set of conditions exists when a clay-bearing, sulfate rich soil is stabilized with lime (*5*). He identified four constituents that are essential for sulfate-induced heave: water, aluminum, calcium, and sulfur. When these four ingredients are present and the pH is above 10, then the conditions are right for forming ettringite.

Sulfate is the key ingredient for causing heave. TxDOT currently uses a gravimetric technique (Tex-620-J) to measure sulfate in soils. If the sulfate levels are greater than 2000 parts per million (ppm), then TxDOT does not recommend calcium based stabilizers for subgrade stabilization. California uses a similar gravimetric technique to measure soil sulfate concentrations greater than 2000 ppm (Little, unpublished data).

Previous research has focused on mechanisms of sulfate heave. However a few studies examined swell caused by lime stabilizing sulfate-rich soils. Mitchell and Dermatas systematically added sulfates ranging from 3000 to 62,000 ppm to artificial kaolinite- and montmorillonite-rich soils (*7*). This study focused on extremely high sulfate concentrations and extended curing times (generally 30 days). In 1999, another study evaluated the effects of ground granulated blastfurnace slag as a stabilizer in an artificial kaolinite and sulfate rich soil and a natural sulfate bearing Kimmeridge Clay (*8*). This study examined extremely high sulfate concentrations (11,200 ppm sulfate is the lowest) as well.

Field recommendations in Texas have been based solely on empirical data (field experience). In Texas, sulfate concentrations as low as 3000 ppm have caused problems with heaving. The research reported in this paper focuses on adding very low sulfate concentrations (0, 1000, 2000, 3000, 5000, 7000, 10,000, and 12,000 ppm) to a natural soil to measure three-dimensional (3-D) swell.

Vertisols underlie a large portion of the Texas Coastal Plain (*9*), home to some of Texas' most densely populated cities. A sulfate-poor soil of the Vertisol order with a P.I. of 24 was chosen for the swell experiments: low concentrations of sulfate were added to various samples.

There are three main objectives to this research: (1) assess the different techniques for measuring sulfates in subgrade soils; (2) determine what sulfate content is too high for traditional lime stabilization (no mellowing) and how effective mellowing, double lime application, and increased moisture content are at reducing swell in high sulfate soils; and (3) determine what alternatives can be used in soils with sulfate concentrations too high to be treated with lime.

BACKGROUND
Sulfate Detection

Bower and Huss (*10*) used conductivity to measure sulfate content in soils. They mixed 10 to 20 g of air-dried soil with distilled water. The water dissolved the gypsum; acetone was then added to reprecipitate the gypsum. The reprecipitated gypsum was washed to remove salts (NaCl, etc.) and then redissolved in distilled water. The conductivity was measured and compared to a calibration curve to determine gypsum concentration in the soil.

Studies of sulfate-bearing soils at TTI have yielded conflicting results for the amount of sulfate present in a soil. For example, a soil subjected to a rapid field conductivity test proposed by Bredenkamp and Lytton (*11*) would give results typical of a low sulfate soil, however additional testing of the soil would give a value typical of high sulfates. After reviewing the conductivity test and TxDOT Test Method Tex-620-J some questions were raised about the accuracy of the techniques.

Conductivity

Conductivity is a measure of how well a solution will carry a current (i.e., pass electrons usually via ions). Two factors influence conductivity: first, the number of displaceable electrons each ion carries (e.g., an anion with a –2 charge will carry twice as many electrons as an anion with a –1 charge); second, the speed at which each ion travels through the solution (*12*).

The conductivity of a solution is the sum of the conductivities of the ions present; it cannot distinguish between different types of ions. For example, if two salts (halite and gypsum) are present in a soil, gypsum ($CaSO_4 \cdot 2H_2O$) will dissolve releasing Ca^{2+} and $(SO_4)^{2-}$ ions while halite ($NaCl$) will add Na^+ and Cl^- to the solution. Both salts will contribute to the conductivity. Also at higher concentrations the ions may form some un-ionized molecules which will reduce the conductivity (*12*).

Colorimetry

A review of the environmental testing and water quality sales literature revealed another technique for sulfate analysis. This test was designed to measure sulfate concentrations in natural waters, but we thought that the test could be adapted to soils. It operates on the principles of colorimetry (measure degree of absorption of light transmitted through the sample by human eye) or spectrophotometry (when an instrument measures the light transmitted).

The colorimeter/spectrophotometer consists of four parts: a light source, a filter, a detector, and a sample. The light source consists of an LED because the wavelength does not shift with changes in temperature. The filter removes all light except wavelengths of interest and the detector determines how much light is transmitted through the sample.
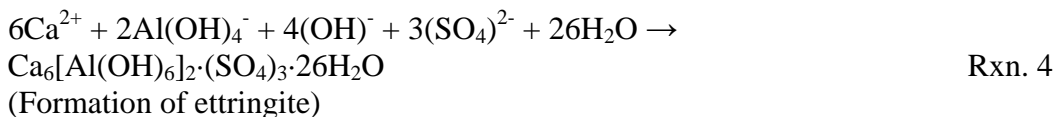
Sulfate-Induced Heave Reactions

The most severe heaves reported in Texas were observed at Joe Pool Lake near Dallas *(6)*. Burkart et al. identified certain geologic formations that possess high sulfates and that gypsum was the most common sulfate in Dallas area soils *(13)*. Researchers at LSU looked into the possibility of anhydrite ($CaSO_4$) converting to gypsum in a humid environment as the heave mechanism: heave was actually due to formation of ettringite in the cement-stabilized soil*(14)*.

It is important to recognize that gypsum is not the only problematic sulfur-bearing mineral in soils. Pyrite (FeS_2) is a sulfide mineral that alters to gypsum ($CaSO_4 \cdot 2H_2O$) under the right conditions and creates similar problems. Dubbe et al. reported five case histories where pyritic shales are oxidized to sulfates causing heave and concrete deterioration *(15)*. Pyrite derived sulfate was documented as the cause of heave in Portland cement stabilized minestone *(16)*. Oxidation of pyrite-bearing Eagle Ford shale in north Texas is the source of sulfates in many soils from that region *(13)*.

Ettringite, with a chemical formula of $Ca_6[Al(OH)_6]_2 \cdot (SO_4)_3 \cdot 26H_2O$, requires special conditions to form. At standard temperature (25ºC) the pH has to be above 10, and a source of water is critical for the 26 moles of water in the mineral structure: a source of aluminum, sulfur and calcium are also required to form ettringite. Stabilizing sulfur bearing clay-rich soils with lime or cement satisfy all of the above criteria. Lime and cement both raise the pH to above 12. A pH above 10.5 causes dissolution of clay minerals and releases aluminum into the system. Water may be supplied from a number of sources. It may be supplied during the stabilization process, occur as precipitation after stabilization, or be supplied from the groundwater or adjacent reservoirs. Calcium is released by the lime and cement during stabilization and the sulfur is supplied from sulfide and/or sulfate bearing soils or water.

Following is an abbreviated geochemical reaction model from Hunter *(5)*:

$Ca(OH)_2 \rightarrow Ca^{2+} + 2(OH)^-$ Rxn. 1
(Ionization of lime; pH rises to 12.3)

$Al_4Si_4O_{10}(OH)_8 + 4(OH)^- + 10H_2O \rightarrow 4Al(OH)_4^- + 4H_4SiO_4$ Rxn. 2
(Dissolution of kaolinite at pH > 10.5)

$CaSO_4 \cdot 2H_2O \rightarrow Ca^{2+} + SO_4^{2-} + 2H_2O$ Rxn. 3
(Dissolution of gypsum)

$6Ca^{2+} + 2Al(OH)_4^- + 4(OH)^- + 3(SO_4)^{2-} + 26H_2O \rightarrow$
$Ca_6[Al(OH)_6]_2 \cdot (SO_4)_3 \cdot 26H_2O$ Rxn. 4
(Formation of ettringite)
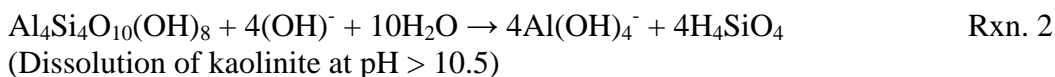
Reactions 1 and 2 occur in any lime-stabilized kaolinite-bearing soil. Addition of lime to the soil causes the pH to rise to approximately 12.3 and releases large amounts of calcium to the soil. Clay minerals are unstable at a pH above 10.5 so the clays start breaking down into aluminum hydroxide and silicic acid. Sulfate and calcium ions (reaction 3) are supplied by the dissolution of gypsum. The only other elemental requirement for the formation of ettringite is water. Ettringite only forms in a high pH ($\approx$ 10-12) environment. Once the pH drops below 10 ettringite stops forming. In this example, kaolinite is the aluminum source and gypsum is the sulfur source, but aluminum may be derived from dissolution of any clay mineral and sulfur may be derived from any sulfur-bearing mineral as previously discussed. Gypsum is used as the sulfur-bearing mineral in this example and it appears to be the dominant sulfur-bearing mineral responsible for sulfate-induced heave in Texas soils *(13)*.

METHODS
Sulfate Detection
To evaluate the accuracy of each sulfate measuring technique, a two-step process was developed. First, laboratory-manufactured samples with known sulfate concentrations were tested using different methods. Secondly, real soil samples were tested to identify possible interferences with natural samples.

To test the adequacy of the methods for quantifying sulfates, gypsum was added to samples in two size fractions (passing #200 sieve, and passing #10 retained on #40 sieve) at the following concentrations: 0, 1000, 2000, 3000, 5000, and 12,000 parts per million (ppm) sulfate. The different sizes represent reactive sulfates found in natural soils in Texas.

Sulfate-Induced Heave 3-D Swell Samples

A soil from the Vertisol order was selected for swell measurements to determine what concentrations of sulfate are too high for stabilization with lime in Texas. Vertisols have high shrink-swell potential due to smectitic clay minerals *(9)*. This soil was selected because (1) it is typical of lime-stabilized soils in Texas, and (2) it did not have any detectable sulfates (less than 100 ppm).

We dried the soil in a 140ºF (60ºC) oven to a constant weight and pulverized it to pass a #4 sieve as outlined in ASTM D 698. We then determined the engineering properties of the soil: a plasticity index of 24 was determined by ASTM D 4318, an optimum lime content of 6% determined by the Eades and Grim test *(17)* or ASTM D 6276, and the optimum moisture content (ASTM D 698) using 6% lime is 22%.

We added two different sulfate compounds to the soil: sodium sulfate (Na_2SO_4) and gypsum ($CaSO_4 \cdot 2H_2O$). The sulfates were added to samples at concentrations of 0, 1000, 2000, 3000, 5000, 7000, and 12,000 parts per million (ppm).

The researchers applied the sulfate to individual samples by four different techniques to represent different scenarios observed in the field. The sodium sulfate was added to the mixing water of some samples and dissolved and it was added to the water bath of other samples and dissolved to represent sulfates being added via an external water source (water truck) and from the groundwater, respectively. The gypsum was added directly to the soil in a solid state in two grain sizes 1) passing the #200 sieve, fine-grained (F.G.) and 2) passing the #10 sieve and retained on the #40 sieve, coarse-grained (C.G.). These size fractions were chosen because they are representative of the more reactive sulfates found in natural soils in Texas. Grain size is an important issue because the larger the grains, the longer it takes for them to dissolve and react.

The samples were molded to Proctor density using a Superpave Gyratory compactor and placed in 3-D swell tests.

Confirmation of Swell Reaction Products

Following swell testing of at least 45 days, the samples were dried in a 140ºF (60ºC) oven until a constant weight was reached. The samples were then measured again for volume change.

To determine if formation of ettringite was contributing to the swell of samples, X-ray diffraction (XRD) was performed on selected samples with a Rigaku X-ray diffractometer under the following operating conditions: we used Cu kα radiation at a scan speed of 0.75º/minute with a step of 0.02 degrees. A bulk sample analysis was performed on selected samples to identify reaction products: a side-loading random powder mount was used to reduce preferred orientation of minerals *(18)*.

A JEOL 6400 scanning electron microscope (SEM) with a Princeton Gammatech energy dispersive spectrometer (EDS) was used to observe crystal habit (shape) and location of reaction products. We operated the SEM at a beam current of 15 kV and 10 mm working distance to maximize EDS results.

RESULTS
Sulfate Detection
        A colorimeter powered by a nine volt battery measured sulfate concentrations of
manufactured soils prepared with 0, 1000, 2000, 5000, and 12,000 ppm sulfates. We sampled
each soil 10 times and measured the sulfate content with the colorimeter for a total of 50
measurements. These results are plotted against TxDOT test method Tex-620-J results for the
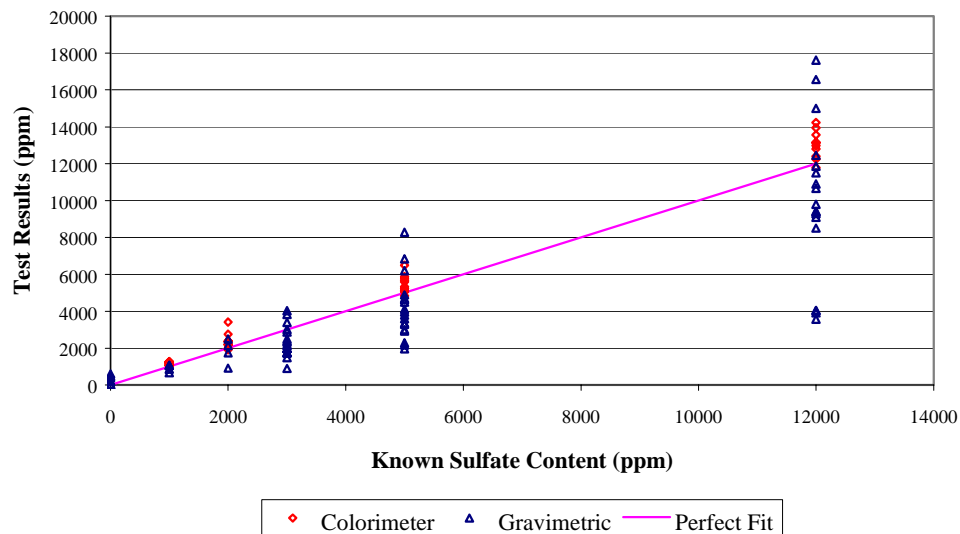manufactured soils in Figure 2.

Figure 2. Sulfate measurement results using the colorimeter versus the TxDOT method.

        Conductivity of sulfate standards was measured to generate a calibration curve (pink
squares in Figure 3). Final conductivities of 61 natural soil samples from different parts of Texas
were also plotted, as blue diamonds, on Figure 3. The graph illustrates that the conductivities of
the soils at the various sulfate concentrations correlate very well with the calibration curve.

Three-Dimensional Swell Experiments
        Figure 4 shows three-dimensional swell through time. The bottom curve illustrates how
lime treatment of the soil with no sulfates results in greatly reduced swell over the unstabilized
soil (top curve). This is exactly what one would expect for lime treatment and indicates that lime
is doing its job. The curves between the two control samples show that increasing amounts of
sulfate, from 3000 to 12,000 ppm in the form of coarse-grained gypsum, result in progressively
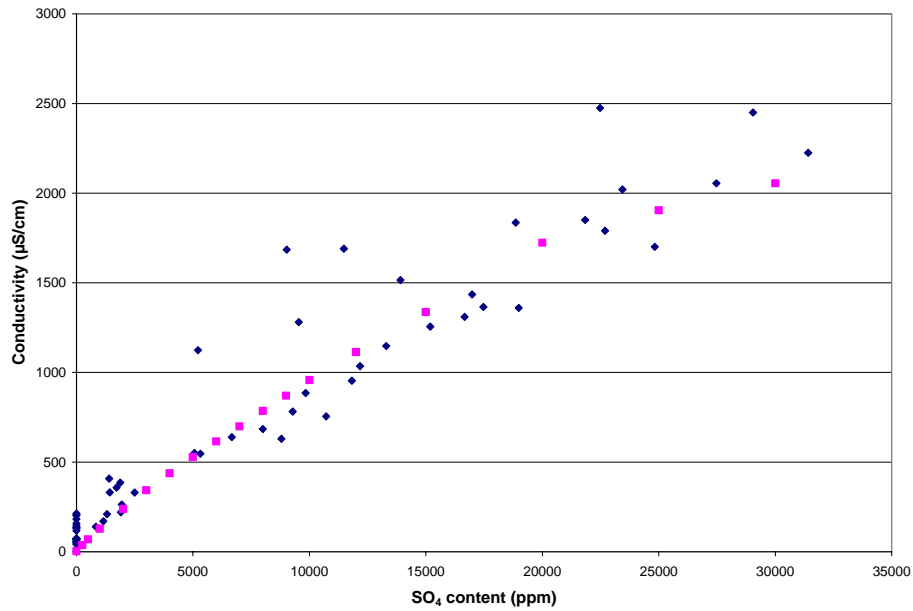more swell.

Figure 3. Conductivity of sulfate standards (pink squares) plotted against the conductivity of sulfate-bearing soils (blue diamonds) at a 1:20 soil to water dilution ratio.
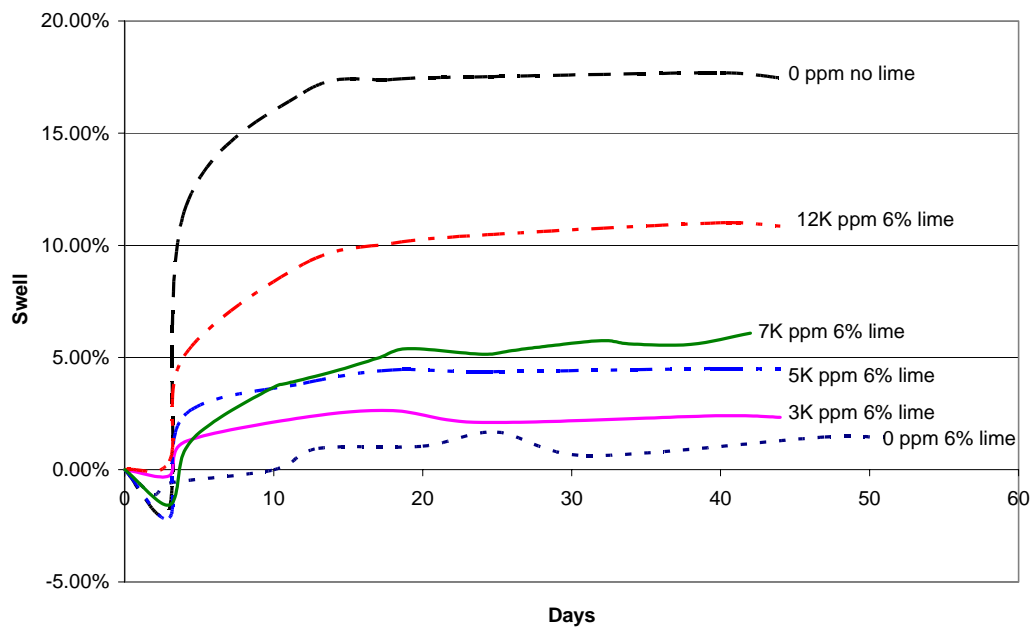

 Figure 4. Results of 3-D swell experiments on a Vertisol bearing concentrations of gypsum ranging from 0 to 12,000 ppm sulfate.

Effect of Mellowing on 3-D Swell

Following the results of the above swell measurements, we wanted to evaluate how effective higher moisture contents, double lime treatment, and mellowing are at reducing swell. Mellowing involves mixing the lime with the sample and allowing it to react (mellow) for a time of 1 to 3 days before compaction. Figure 5 shows how three days of mellowing reduces the overall 3-D swell for samples bearing 7000 and 10,000 ppm sulfates supplied via the molding water. Some interesting points to note from Figure 5 are: (1) everything else equal, higher molding moisture contents (2% above optimum moisture) reduced swell, (2) all other factors equal, single application of lime reduces swell better than double application (adding 6% lime and mellowing for three days is better than adding 3% lime and mellowing for three days then adding another 3% lime and compacting), and (3) three days mellowing results in acceptable (less than 2%) 3-D swell for 7000 ppm sulfates, but unacceptable swell for 10,000 ppm sulfates.
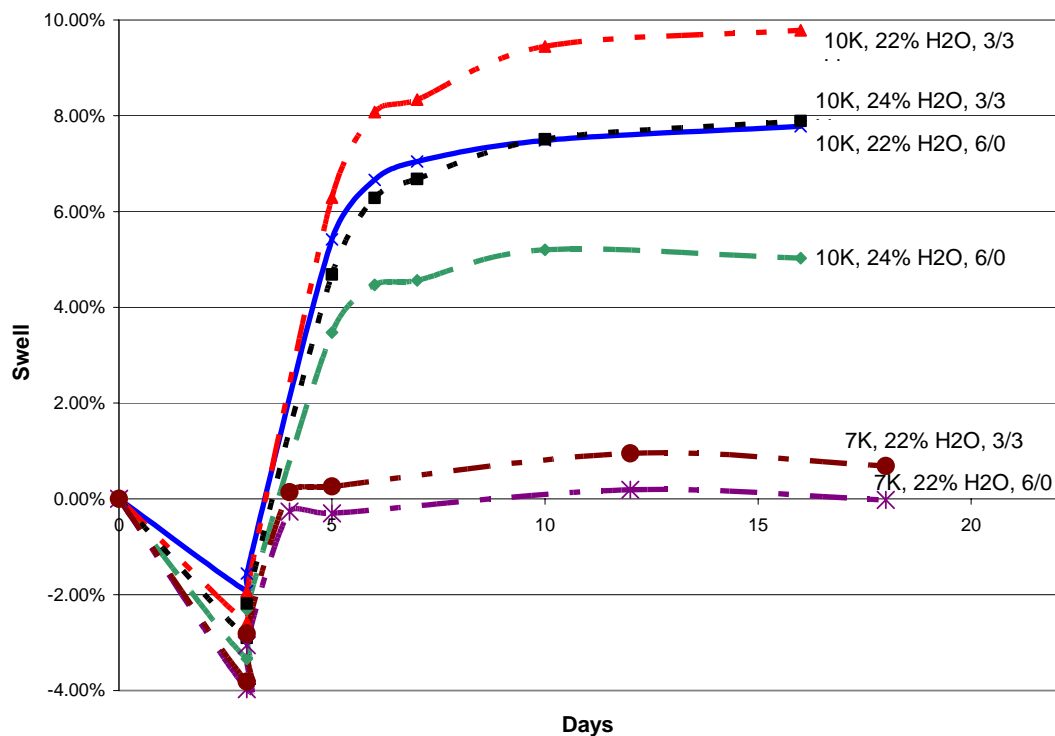

Figure 5. Results of 3-D swell for sulfate dissolved in molding water and mellowed for three days.

Alternatives to Lime

At sulfate concentrations of 10,000 ppm and higher, we wanted to identify alternatives to lime stabilization. An alternative that has shown promise in Europe (*8*) is the addition of a ground granulated blastfurnace slag (GGBFS). Based upon the European research (*8*), the researchers identified three mixtures to run 3-D swell experiments on. The soil was mixed with concentrations of 1 wt. % hydrated lime and 5 wt. % slag (1L5S), 3 wt. % hydrated lime and 3 wt. % slag (3L3S), and 6 wt. % hydrated lime and zero slag (6L0S). Replacing one half of the lime (3%) with GGBFS results in a significant decrease in 3-D swell, but replacing 5% of the lime with GGBFS results in a 35% decrease in 3-D swell. These great swell reductions occurred without mellowing or moisture contents above optimum.
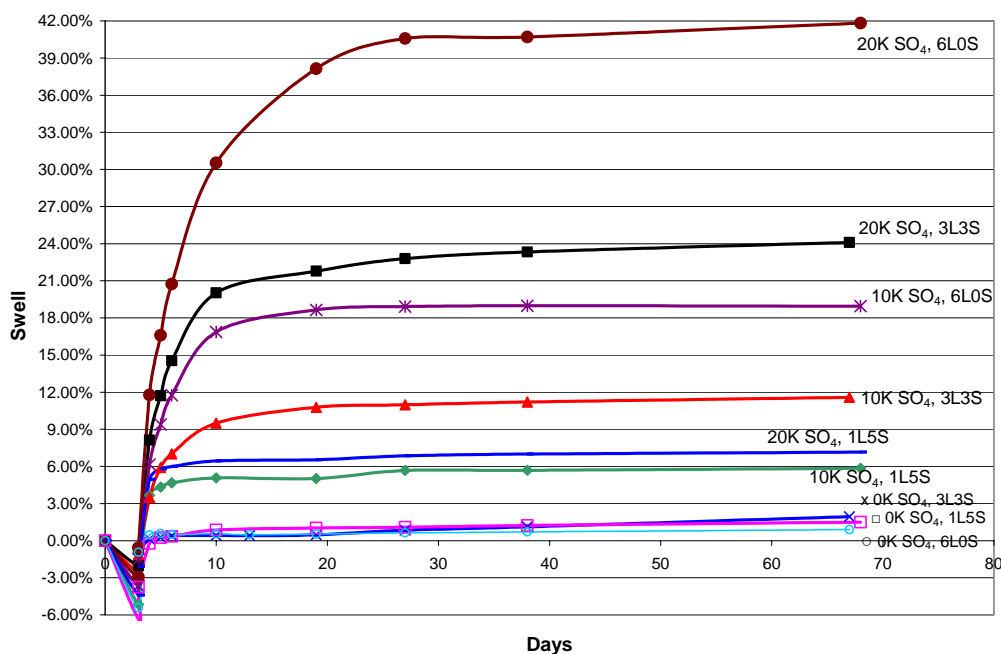
Figure 6. Comparison of 3-D swell for high sulfate levels and mixtures of lime and ground granulated blastfurnace slag (GGBFS) at optimum moisture and with no mellowing.

DISCUSSION
Sulfate Detection

Conductivity measurements are easy to perform and consistent results can be obtained between different laboratories (Harris, unpublished data). What can affect conductivity measurements are a dirty or improperly calibrated cell or a malfunctioning meter. Temperature fluctuations can also cause conductivity measurements to drift and not yield a stable reading.

Conductivity of sulfate standards was measured to generate a calibration curve (Figure 3). Final conductivities of various soils from Texas were also plotted on Figure 3. The graph illustrates that conductivities of soils at the various sulfate concentrations correlate very well

with the calibration curve. However, as illustrated in Figure 3, natural soils contain other ionic compounds that may dissolve and contribute to the conductivity which would result in an overestimation of the sulfate content.

The colorimetric technique (light transmitted through a sample) if not run under exact conditions may be subject to error from some of the following sources: maintain a constant solution temperature, acidity of solution, size of $BaCl_2$ crystals, amount of $BaCl_2$ added, time of stirring, rate of stirring, and the time that the suspension stands before a measurement is taken. The glass vials should be kept clean and free of oils from human hands to ensure consistent light transmittance through the sample.

In contrast to Tex-620-J, the colorimetric technique proved to be highly repeatable. To define the 95 percent confidence interval for true sulfate content to within ±10 percent of the true known value for concentrations of sulfates at 1000 ppm, only three tests are required with this technique. At 5000 ppm, only four tests are needed. This is in sharp contrast to Tex-620-J, which requires 43 tests, at 5000 ppm. At lower desired accuracy levels such as ±20 percent or ±30 percent, only one test is needed with the colorimeter. The higher precision of the colorimeter is graphically illustrated in Figure 2. It is clear that, with repeat testing, the colorimeter results are much less dispersed than Tex-620-J.

Factors Causing Swell

The three-dimensional swell experiments show a very nice trend of increasing swell with increasing sulfate content. As illustrated in the background most sulfate-induced heave is attributed to the formation of ettringite and/or thaumasite. The question is can the swell we obtained in our experiments be attributed to formation of ettringite and/or thaumasite?

We can rule out the formation of thaumasite in our experiments because it requires temperatures below 15ºC to form *(5)*: all of our experiments were conducted in the range of 22 to 25ºC.

Selected samples were analyzed by XRD and SEM to determine if deleterious reaction products actually formed in the lime-stabilized samples. Figure 7 are partial XRD patterns from 8º to 17º two-theta for a lime-stabilized sample that initially contained gypsum (dashed line) and an unstabilized gypsum-bearing sample (solid line). The unstabilized sample contains a sharp peak at 7.51 Å that is absent in the lime-stabilized sample: this peak confirms the presence of gypsum. The broad peak at 7.16 Å is the (001) kaolinite peak and is present in both samples. The two peaks at 9.66 Å and 5.57 Å are diagnostic of ettringite and are only present in the lime-stabilized sample. The presence of these two peaks and the absence of the gypsum peak in the lime-stabilized sample illustrates that gypsum is being used to form the highly expansive mineral ettringite. The XRD patterns confirm that ettringite was formed in the swell tests.

SEM analysis of the lime-stabilized and unstabilized gypsum-bearing samples confirmed the XRD results. Radiating fibrous crystals typical of ettringite were observed throughout the lime-stabilized material and were absent in the unstabilized materials. EDS analysis of the radiating fibrous crystals revealed calcium, aluminum, and sulfur in rations typical of ettringite.
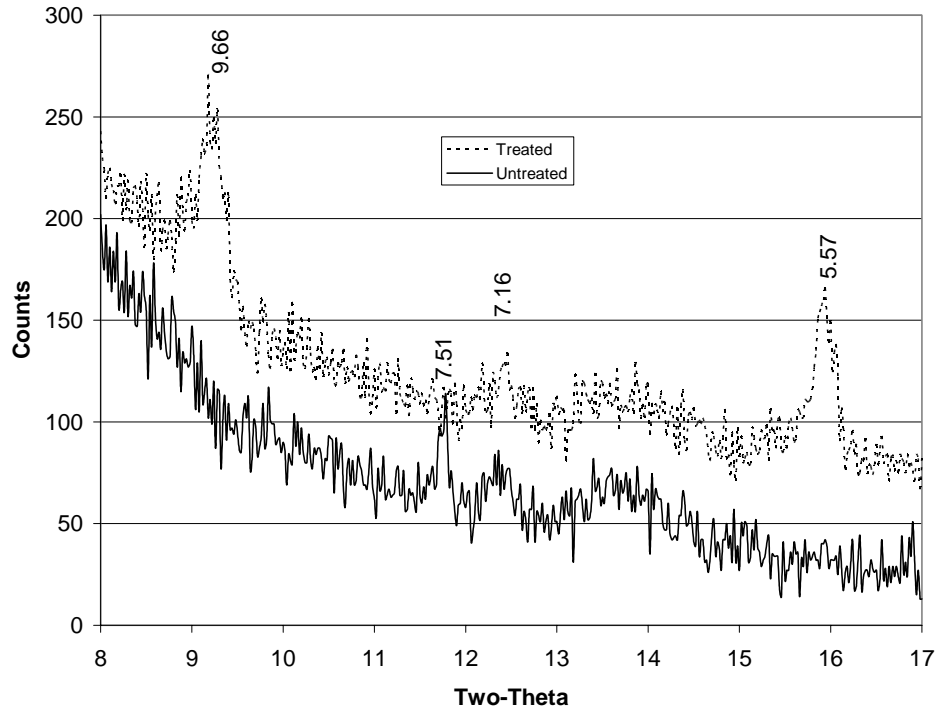
Figure 7. Partial XRD patterns of an unstabilized gypsum bearing soil (solid line) and a lime stabilized (dashed line) soil.

Upper Sulfate Limit for Conventional Lime Stabilization

After consulting various geotechnical engineers, we were unable to determine how much volumetric swell was unacceptable. Therefore, we decided to use the amount of swell experienced by the lime-stabilized soil without any sulfates as the cutoff. This was approximately 1.5% 3-D swell (Figure 4). However, TxDOT decided that 2.5% swell was acceptable which correlates with 3000 ppm sulfates. This implies that no special requirements are needed if sulfate concentrations are 3000 ppm or less.

Let us add a word of caution, one must be certain that there is a limited supply of sulfate ions. For example, suppose there is a body of water adjacent to a new road construction site where sulfates have been detected, but the sulfate concentrations are less than 3000 ppm. A full geotechnical investigation should be conducted to determine the source of the sulfate. If sulfate is being supplied from the body of water, then sulfate could be continuously supplied to the stabilized layer and eventually result in a disruption in the highway.

Effect of Mellowing on Upper Sulfate Limit

From the many swell experiments conducted, researchers determined that 7000 ppm sulfates can be safely treated by adequately mellowing the soil after lime treatment (Figure 5). However, we tested 10,000 ppm sulfates (Figure 5) but the swell was too high using 6% lime, 24% moisture,

and up to three days mellowing. We are speculating that increasing sulfate content requires more time to form deleterious reaction products: this would also be true for coarser grained sulfates.

Figure 8 shows how the soluble sulfate content decreases with time (mellowing). The graph indicates that for up to two days mellowing lime treatment for the three fine-grained gypsum samples similarly reduced the soluble sulfate, but after two days the curves deviate. After two days the three percent lime at 24% moisture treatment ceased to remove sulfate because all of the lime had reacted. At day three, another three percent lime was added and sulfate started reacting again, which explains why double application of lime resulted in more swell than single application. Three percent lime was not enough to remove all of the sulfates, so addition of the lime and compaction restarted the sulfate reaction, resulting in swell. The curve for six percent lime at 22% moisture also takes longer to react all the sulfates, which is consistent with observations that lower moisture contents result in more swell. The six percent lime at 24% moisture removed the soluble sulfate more rapidly and was enough to react with all of the sulfates. We speculate that the additional water dissolved the sulfate more rapidly and reacted with the lime to form ettringite.
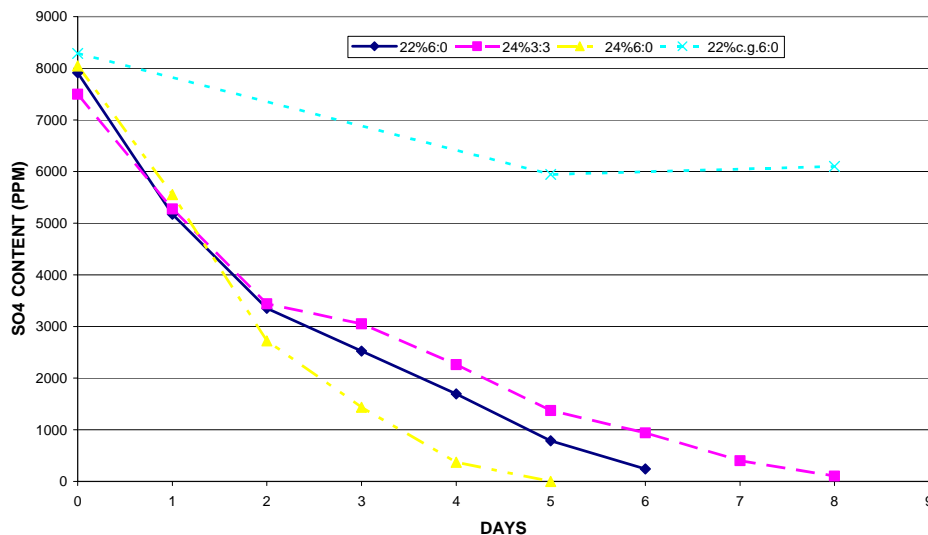
Figure 8. Observations of sulfate content changes over time in soil following lime treatment.   The soil contained 7000 ppm coarse- (c.g.) and fine-grained sulfate.

Effect of Molding Moisture on Swell

The Lime Association recommends adding from 3 to 5% above the optimum moisture content to give plenty of water for the sulfate to react. They also recommend compacting the soil at this higher moisture content (Eric Berger, unpublished data). The project management committee determined that 2% above optimum moisture was the practical limit for construction purposes; therefore our experiments evaluated mellowing and compaction at 2% above optimum. As evident in Figure 3, the higher moisture content always resulted in less 3-D swell.

Hunter's (*5*) investigation of soils in Las Vegas identified that 24% of the swell was due to formation of ettringite/thaumasite and the remainder to an increase in voids since the soil was initially in a heavily compacted state. Many investigators (*7, 8, and 19*) have noted that decreased density may reduce swell by allowing the expansive minerals to form in the additional void space. This was our observation; at the higher moisture content the samples could not be compacted to maximum density resulting in more void space for the deleterious minerals to expand into. A one-tail t-test showed that the mean densities are statistically different with a P value of 3.4 X 10^{-12}. This is analogous to air entrainment in cement paste to allow deleterious reaction products to expand into the voids without disrupting the concrete. However, Figure 8 shows that higher moisture contents result in more rapid removal of soluble sulfates, so we believe that reduced swell is due to a combination of more voids and a faster reaction rate removing more of the sulfate from the system before compaction.

Effect of GGBFS on Swell

The ground granulated blastfurnace slag reduced the sulfate-induced heave substantially. Previous investigations by Wild et al. (*8, 21*) illustrated that GGBFS reduces swelling of lime stabilized sulfate-bearing soils. Four major components are required for excessive swelling, water, lime, alumina, and sulfate (*8*). According to Wild et al. (*8*) slag partially substitutes for the lime and the depletion of lime restricts the formation of ettringite and reduces swelling.

SUMMARY AND CONCLUSIONS

With at least 124 counties in Texas that have the potential to develop sulfate problems and all of the sulfate heave problems reported from around the country, accurate detection and remediation of sulfate problems is imperative.

- The conductivity test is a good technique for identifying possible sulfate-rich soils, however, it will give high values in a soil containing other salts. This test is simple and can be rapidly performed in the field. This technique is recommended as a good screening tool. If there are high conductivities (>200 µS final conductivity at a 1:20 soil to water dilution ratio), then perform laboratory testing to determine if sulfates are causing the high conductivity readings.
- The colorimetric technique should be used in a laboratory or field office setting under controlled conditions.

Berger, Little, and Graves *(20)* stated that below 3000 ppm sulfates there is little concern for swell with lime stabilization, from 3000 to 5000 ppm sulfates are of moderate concern, 5000 to 8000 ppm sulfates pose a moderate to high risk and sulfates greater than 8000 ppm are generally too high for lime stabilization. Their results are based upon experiences in the field and our experimental results correlate very well with the recommendations of these researchers.

Results of this study from systematic addition of sulfates of known concentration to a Vertisol and lime stabilization reveal the following:

- Using a typical east Texas soil, the sulfate cutoff for traditional lime stabilization, where the lime is added to the soil and immediately compacted, is 3000 ppm. This is in accord with other researchers recommendations *(6,20)*.
- Coarse-grained sulfates require more time to form deleterious reaction products than fine-grained sulfates as illustrated in the slope of the mellowing curve (Figure 8).

- Use of a mellowing period up to 3 days after lime application works for concentrations up to at least 7000 ppm for fine-grained sulfates.
- Mellowing of 3 days at 2 percent above optimum moisture and 6 percent lime did not result in acceptable swell with 10,000 ppm sulfates.
- Using a moisture content above optimum results in lower swell due to a combination of lower compaction density (so more voids are available for reaction products to form in), and faster removal/reaction of sulfates.
- Application of all of the lime at once and then mellowing reduces 3-D swell better than adding half of the lime and mellowing followed by addition of the other half of the lime.
- Substituting GGBFS for lime significantly reduced 3-D swell for concentrations up to at least 20,000 ppm.

ACKNOWLEDGMENT

REFERENCES

1) Lea, F.M. *The Chemistry of Cement and Concrete*. Chemical Publishing Company, Inc., New York, 1971.
2) Sherwood, P.T. Effects of Sulfates on Cement and Lime-Stabilized Soils. In *Highway Research Board Bulletin* 353, TRB, National Research Council, Washington, D.C., 1962, pp. 98-107.
3) Schlorholtz, S., and T. Demirel. Quick Lime-Gypsum Interactions in Stabilized Soil Bases for Concrete Highways. *Cement and Concrete Research*, Vol. 14, No. 4, April 1984, pp. 529-532.
4) Mitchell, J.K. Practical Problems from Surprising Soil Behavior. *Journal of Geotechnical Engineering Division, ASCE*, Vol. 112, No. 3, 1986, pp. 259-289.
5) Hunter, D. *The Geochemistry of Lime-Induced Heave in Sulfate Bearing Clay Soils* (Dissertation) University of Nevada, Reno, 1989.
6) Petry, T.M., and D.N. Little. Update on Sulfate-Induced Heave in Treated Clays: Problematic Sulfate Levels. In *Transportation Research Record 1362*, TRB, National Research Council, Washington, D.C., 1992, pp. 51-55.
7) Mitchell, J.K., and D. Dermatas. Clay Soil Heave Caused by Lime-Sulfate Reactions. In *Innovations and Uses for Lime*, ASTM STP 1135, Americam Society for Testing and Materials, Philadelphia, 1992, pp. 41-64.
8) Wild, S., J.M. Kinuthia, G.I. Jones, and D.D. Higgins. Suppression of Swelling Associated with Ettringite Formation in Lime Stabilized Sulphate Bearing Clay Soils by Partial Substitution of Lime with Ground Granulated Blastfurnace Slag. In *Engineering Geology*, Vol. 51, 1999, pp. 257-277.

9) Gustavson, T.C. *Microrelief (Gilgai) Structures on Expansive Clays of the Texas Coastal Plain – Their Recognition and Significance in Engineering Construction.* Geological Circular 75-7, Bureau of Economic Geology, Austin, Texas, 1975.

10) Bower, C.A., and R.B. Huss. *Rapid Conductometric Method for Estimating Gypsum in Soils.* U.S. Department of Agriculture, 1948.

11) Bredenkamp, S., and R. Lytton. *Reduction of Sulfate Swell in Expansive Clay Subgrades in the Dallas District.* Report 1994-5. TTI, Texas Department of Transportation, 1995.

12) Robinson, J.W. *Undergraduate Instrumental Analysis*. 2nd ed. Marcel Dekker, Inc., New York, 1970.

13) Burkart, B., G. C. Goss, and J. P. Kern. The Role of Gypsum in Production of Sulfate-Induced Deformation of Lime-Stabilized Soils. In *Environmental and Engineering Geoscience*, Vol. V, No. 2, 1999, pp. 173-187.

14) Roy, A., L. Wang, R.K. Seals, and J.B. Metcalf. *Stabilization Techniques for Reactive Aggregate in Soil-Cement Base Course.* Louisiana Transportation Research Center Report # 366, Baton Rouge, Louisiana, 2003.

15) Dubbe, D.D., M.A. Usman, and L.K. Moulton. Expansive Pyritic Shales. In *Transportation Research Record 993*, TRB, National Research Council, Washington, D.C., 1997, pp. 19-27.

16) Thomas, M.D.A., R.J. Kettle, and J.A. Morton. Expansion of Cement-Stabilized Minestone Due to the Oxidation of Pyrite. In *Transportation Research Record 1219*, TRB, National Research Council, Washington, D.C., 1989, pp. 113-120.

17) Eades. J.L., and R.E. Grim. A Quick Test to Determine Lime Requirements for Soil Stabilization. In *Highway Research Record 139*, TRB, National Research Council, Washington, D.C., 1966, pp. 61-72.

18) Moore, D.M., and R.C. Reynolds. *X-Ray Diffraction and the Identification and Analysis of Clay Minerals.* Second edition, Oxford University Press, New York, 1997.

19) Kota, P.B.V.S., D. Hazlett, and L. Perrin. Sulfate-Bearing Soils: Problems with Calcium Based Stabilizers. In *Transportation Research Record 1546*, TRB, National Research Council, Washington, D.C., 1996, pp. 62-69.

20) Berger, E., D.N. Little, and R. Graves. (2001) Technical Memorandum: Guidelines for Stabilization of Soils Containing Sulfates. http://www.lime.org/publications.html. Accessed July 28, 2003.

21) Wild, S., J.M. Kinuthia, R.B. Robinson, and I. Humphries. Effects of Ground Granulated Blastfurnace Slag (GGBS) on the Strength and Swelling Properties of Lime Stabilized Kaolinite in the Presence of Sulphates. In *Clay Minerals*, Vol. 31, 1996, pp. 423-433.

Subsurface Surprises in a Fast-track Design/Build Project

By Patrick H. Poepsel, PE and James M. Sheahan, PE

BACKGROUND

A new design/build highway project is nearing completion at Fort Leonard Wood Military
Reservation in Pulaski County of central Missouri. An aerial view of a portion of the project
area is provided in Figure 1. The project involves the design and construction of 4.5 miles of
2-lane highway, including earth fills up to 90 feet in height, two-sided cuts up to 70 feet, sidehill
cuts up to 150 feet, a 483-foot long bridge, and ancillary drainage structures. The highway and
related features were designed and constructed in general accordance with current Missouri
Department of Transportation (MoDOT) and AASHTO specifications and standards.

Figure 1: Aerial View of Project Area

The design/build project was a joint venture with Bloomsdale Excavating, Inc. and HDR, Inc. under contract with the U.S. Army Corps of Engineers – Kansas City District. Geotechnology, Inc. performed the supplemental geotechnical work, geophysical testing and the observation and testing of earthwork.

The preliminary information provided to bidders indicated that the high fills for the new roadway could be constructed with rockfill. In addition, the preliminary alignment of the roadway was selected to avoid an existing landfill. Following the Notice to Proceed, a different set of circumstances became apparent. This paper describes several key issues that arose during the design phase of the project, specifically:

- The lack of available rock with the borrow areas required the use of highly plastic residual clay with gravel as fill for all embankments;

- An evaluation of the short and long term strengths and stability of the recompacted residual clay as embankment fill;

- A method specification was developed to produce a well-compacted, stable fill material with a strength similar to that which was derived in the lab testing and assumed in the stability analyses;

- The limits of the landfill was found to extend into the footprint of the roadway embankment which posed problems with stability and settlement;

- Several alternatives were evaluated to stabilize the landfill and deep dynamic compaction was selected and implemented to safely support a 50-foot high embankment.

A discussion of the performance of the embankment construction using the residual clay and the method specification will also be presented.

GEOTECHNICAL STUDIES

The results of a preliminary geotechnical investigation was provided in the design/build bid documents and consisted of making 195 exploratory test borings along the roadway corridor. The borings were taken generally every 200 feet along the centerline and at the right and left outside ditch lines. Some portions of the corridor were not drilled due to difficult access conditions.

During the bid preparation phase, the need for supplemental borings were identified to fill in these gaps in the coverage of data and to refine the estimate of soil and rock quantities available for use as fill. Shortly after the Notice to Proceed and the commencement of the supplemental work, it became apparent that competent rock was not continuous below the top of rock elevations shown in the preliminary report. A total of 90 supplemental borings were necessary to adequately investigate the presence of rock and determine the engineering characteristics of the residual clay as fill for the project.

Geophysical methods were performed to provide additional subsurface information in estimating the depth and limits of the existing landfill near Hollow Creek. Electromagnetic and resistivity surveys were selected for this purpose.

SITE CONDITIONS

Physiographic and Geologic Setting

The following description of the physiographic and geologic setting was obtained from the Geotechnical Data Report by Geotechnology, Inc. of Kansas City, Missouri.

"The proposed West Gate Access Road is located on the Salem Plateau, which is a sub-province of the Ozark Plateau in south Missouri. The Salem Plateau consists of rolling uplands with local relief of 100 to 200 feet, and karst activity. The most common karst features throughout the region include sinkholes, caves, abundant springs and lost streams.

The Salem Plateau consists of flat-lying to gently dipping Ordovician sedimentary rocks of sandstone, dolomite, shale and limestone. The surficial deposits generally consist of residual soil, loess, colluvium, and alluvium. Residual soil consists of silty and sandy clay to very cherty silty clay derived from in-situ weathered bedrock in the upland areas. Loess deposits consist of wind-blown silty loam. Colluvial material derived from mass wasting of residuum and loess occurs on most steep slopes in the area. Recent alluvial fill and older terrace deposits occur on the flood plains and tributaries. The surficial soils are underlain by the bedrock units, from youger to older, Jefferson City Dolomite, Roubidoux Formation, and Gasconade Dolomite."

The potential seismic exposure of the site is low and its impacts on the project are minor. The peak ground acceleration corresponding to a 90% probability of not being exceeded in 50 years was 0.05g.

Surface Features

The terrain of the project area is typically rugged with relatively steep hillside slopes and relatively narrow valleys between ridges. The majority of the construction will be situated where the ground cover is primarily native grasses, trees, and and a few unpaved access roads. The existing ground surface elevations along the alignment vary from about 785 to 1150 feet, MSL. The side slopes of the existing terrain are on the order of 1.5 to 2 (horizontal : 1 (vertical).

Subsurface Conditions

The results of the geotechnical investigations indicated that the project corridor is underlain by variably thick residual soils and variably weathered bedrock consisting mainly of dolomite with some sandstone.   Some granular alluvial deposits are present in several drainage areas.

Residual Soils

Residual soils were encountered at or near the surface in all areas along the alignment except within the alluvial valleys of Hollow Creek and Roubidoux Creek. Thickness of the residual soils ranged from 4 to over 77 feet. The residual soils are classified as fat clay (CH) with gravel or clayey gravel (GC) in accordance with the Unified Soil Classification System (ASTM D2488). The fat clay portion is soft to hard in consistency, and has liquid limits that range from 50 to 130, and plasticity indices from 15 to 25. The percent passing the #200 sieve was found to range in general from 15 to as high as 60%. The gravel portion of the soil matrix generally varied from 15 to 60%. Where encountered, the relative density of the clayey gravel ranged from medium dense to very dense. Standard Penetration Test values varied from 2 to over 100 blows per foot (bpf) in these materials.

Some thin layers of hard dolomite and sandstone were noted within the residual soil. Thickness of the intermittent rock layers varied between 1 and 8 feet and their locations were generally random in nature.

Alluvial Deposits

The alluvial deposits at Hollow Creek generally consist of a mixture of clay-sand-gravel. Thickness of the clay-sand-gravel varies from 22 to 35 feet at the boring locations. Some thin

zones of stiff, fat clay and dense sand and gravel were noted in the borings. The existing landfill materials were buried within the upper zones of these alluvial deposits.

Bedrock

The bedrock that underlies the project area consists of Jefferson City Dolomite of the Ordovician System. This formation includes variably weathered dolomitic rock with intermediate layers of sandstone and chert nodules. The dolomite is gray to tan, thin to thickly-bedded, fine to medium grained, and weathered to moderately hard.

Samples of NQ2 rock cores in the bedrock have Rock Quality Designations (RQD) that range from 0 ("very poor") to 96 ("excellent") and average about 61% based on 30 determinations. These RQD values would classify the rock as having a "fair" rock mass quality according to the AASHTO (1999) specifications. Unconfined compressive strengths were found to range from 3100 to 14900 psi and averaged about 8300 psi.

Groundwater

No groundwater was encountered in any of the borings completed along the alignment except in the vicinity of Roubidoux Creek and Hollow Creek. The water table was anticipated to be below the proposed depths of cuts along the entire alignment. No springs or wells were noted in the vicinity of the project.

Existing Landfill

The presence of an existing landfill was noted on the grading plans provided in the bid documents. The only information available at that time was that the landfill is composed of household waste from the 1950's and that the waste was placed in a series of excavated trenches and backfilled.

Subsequent investigations were completed to better define the vertical and lateral extent of the landfill, as well as to investigate its constituents. Geophysical methods (3-D resistivity and electromagnetic surveys), test excavations with a backhoe, and test borings were completed for this purpose.

The results of these investigations indicate that the landfill materials consist of miscellaneous paper, plastic, glass, brick and metal items. Geophysical data showed that the landfill may range in depth from 15 up to 30 feet below the existing ground surface. A total of 18 borings were advanced at the site to confirm the findings of the geophysical surveys. The thickness of the landfill materials was observed to range from about 5 to 13 feet at the boring locations and averages about 10 feet. The landfill material was generally encountered just below the ground surface to a maximum depth of about 13 feet. The average thickness of the landfill was about 8 to 10 feet.

No bio-degradable items were observed in the borings and test excavations. Since the landfill is thought to be about 50 years old, the decomposition of potentially degradable materials is assumed to be complete at this time (Fassett, 1994).

SPT blow counts in the landfill materials were taken to provide an indirect, qualitative assessment of the strength, compressibility and density of the constituents. Values of SPT blow counts were found to range from 2 to 9 bpf, indicating that the landfill materials are in a loose and compressible state.

EARTHWORK

Borrow Materials in Cuts

The supplemental borings indicate that the majority of the materials present within the cut areas consist of residual soil comprised of highly plastic clay and gravel-sized chert and limestone. These soils were classified as fat clay (CH) and clayey gravel (GC) in accordance with ASTM D 2488. Some isolated zones of fat clay were noted without the presence of gravel. Relatively thin lenses of dolomite and sandstone were noted in the borings within the residual soils. Thicker layers of dolomite bedrock were encountered in only a few cut locations.

Based on these findings, the earthwork quantities showed that the fills for the embankments must be constructed entirely with the fat clay with gravel. The construction of roadway embankments up to 90 feet high with this material is preferably made using rock fill to control settlements and provide stability. It was our understanding that fills of this height comprised entirely of highly plastic residual clay were unprecedented in this part of Missouri. Therefore, testing to evaluate the compaction and strength characteristics of the residual clay was conducted.

Compaction Characteristics

Laboratory compaction tests were performed on bulk samples of the residual clay after the gravel was screened off. Five Standard Proctor tests (ASTM D 698) showed maximum dry densities ranging from 93 to 114 pcf with optimum moisture contents varying from 16 to 26%. It was determined that this wide range of values was due primarily to the varying amounts of gravel within the soil being tested.

Method Specification for Acceptance of Fills

Due to the presence of a high percentage of gravel within the residual soils used in fills, obtaining accurate, consistent, and reliable field density results with the nuclear gauge for field verification of compaction was not feasible. The high gravel content makes the sand cone and rubber balloon methods inappropriate for density testing. In addition, the gravel correction procedures cannot be applied to adjust the field density measurements described in ASTM D 4718, since the correction is only valid for gravel contents less than 20%.

Section 203.3.5 in the MoDOT Specifications states, "*Material of a gradation having more than approximately 20% retained on a 3/4-inch sieve will generally be considered too rocky for satisfactory density testing.*" and *"During compaction, each layer shall have the moisture content controlled such that, in the judgment of the engineer, any silt and clay fraction is in a plastic state.*" Because of this, a method specification was necessary to determine the required number of passes and lift thickness to achieve the specified compaction for fills with over 20% gravel. In addition, moisture control was critical to ensure that proper compaction was obtained.

The method specification for acceptance testing of fills was developed to produce a structural fill that achieves the MoDOT requirement of at least 95% of maximum dry density as determined by the Standard Proctor test (ASTM D 698). The moisture content of the fill soils ranged between -2 and +4% of the optimum moisture as determined by the referenced compaction test.

Acceptance criteria for fills consisted of (1) a visual verification of fill placement and compaction procedures, and (2) moisture content testing. The specified compaction was achieved using a requirement of non-movement of the fill surface under compactive effort and corresponding moisture content within the acceptable range. All fill soils covered under the

method specification were required to contain at least 20% gravel. For fills with less than 20% gravel, the conventional nuclear density testing will be performed.

The following procedure was used to establish the method specification:

1. Construct a test fill in the presence of the geotechnical engineer, the field technician that will observe the production fills, the earthwork contractor, personnel from the USACE, and other interested parties. The test fill can be incorporated into the final embankment.
2. Place and spread a loose lift of fill.
3. Compacted the fill with several passes and probe the fill after each pass to evaluate its stiffness.
4. Collect several samples to determine the in-place moisture content of the fill.
5. Estimate the percent gravel based on field observation of the test fill.
6. If the moisture is in the acceptable range, there will be a point in the demonstration where no further increase in stiffness and associated density will be achieved with additional passes of the compactor. The number of passes that produces this maximum compaction will be noted and used as the requirement for that piece of equipment.
7. Perform a test fill for each compactor proposed for use.

Based on experience and observation of the test fills, it was concluded that three to four passes of a Caterpillar 825C compactor would be required to achieve the required compaction. A minimum of three passes was be used for all compactors.

Continued observation of the production fills and sample collection for determining moisture contents were conducted by the field technician. Where possible, the moisture and dry unit weight was tested in the field with a nuclear moisture-density gauge. The testing was performed

in accordance with ASTM D 2922 and D 3017. Except for fills containing soils with less than 20% gravel, results of the nuclear gauge testing was not be used as acceptance criteria for the fill.

 The nuclear density guage was used in the field to test fills with less than 20% gravel. The test results showed that the compaction requirements could be achieved with three passes of the compactor if the moisture was within the acceptable range. Less than 2.5% (12 of 517) of the field tests failed using this criteria, with most of the tests occurring within a week's time. It is not clear what casued this series of failed tests.

Overall, the method specification proved to be fairly successful in achieve compaction in fill for the full range of gravel contents.

EMBANKMENT DESIGN

Evaluation of Strength and Stability

The short and long term stability of the embankments are strongly dependent on the shear strength of the recompacted residual soils. The strength of fill was investigated using the results of UU and CU bar triaxial compression testing on samples recompacted in the laboratory to 95% of the maximum dry density. The tests were performed on the finer portion of the samples since the gravel was screened before sample preparation.

Therefore, the impact of the granular fraction on soil strength was not accounted for in these results. Judgment and experience in similar materials were used to estimate the contribution of gravel to the composite shear strength of the clay and gravel mixture.

Based on test results and assessments, the following strength parameters were used in the slope stability analyses:

Material	Total Stress (UU)		Effective Stress (CU bar)		
	c (psf)	φ (degrees)	c' (psf)	φ' (degrees)	γ (pcf)
Embankment fill	1750	0	200	28	130
Landfill waste	200	20	200	20	50
Granular alluvium	0	34	0	34	120
Dolomite	Note (2)				

Note (1) - c is cohesion, φ is the angle of internal friction, and γ is the moist unit weight.

Note (2) – Failure surfaces not allowed to extend into the dolomite.

Stability of Fills over Residual Soil

Slope stability analyses were performed for both short term (end of construction) and long term (drained) conditions for compacted fill placed over in situ residual soils. Long term conditions were evaluated using effective strengths and short term conditions were estimated from the total stress results of the laboratory strength testing.

The numerical analysis of the stability of the fill slopes was performed using the computer program PCSTABL. The PCSTABL program uses limit equilibrium techniques to estimate the minimum factors of safety against deep-seated instability. The modified Bishop's method of analysis was selected to evaluate the factor of safety for the most critical circular arc failure surface.

Recommendations for the steepest allowable fill slopes were based on the minimum factors of safety (FS) shown below.

- CASE 1 – End of construction: Minimum FS = 1.3 (total stress analysis)
- CASE 2 – Long-term drained: Minimum FS = 1.5 (effective stress analysis)
- CASE 3 – Earthquake A = 0.05g: Minimum FS = 1.0 (total stress analysis)

The alignment for the new roadway included fills of up to 90 feet in maximum height at centerline. The majority of the fills are between 30 and 60 feet in height. The fills included both full-section embankments and side-hill fills placed on a sloping ground surface. The results of the stability analyses indicate that 2:1 slopes could be used up to a maximum fill height of 60 feet, and that 2.5:1 slopes were needed for heights greater than 60 feet.

Stability of Fills over Existing Landfill

For the purpose of slope stability analyses, the subsurface profile beneath the embankment was assumed to consist of 10 feet of stabilized landfill material overlying 15 feet of alluvium and dolomite bedrock. The contribution of the alluvium to the strength of the landfill material in the trenches was conservatively neglected. Groundwater was assumed at a depth of 5 feet below the ground surface.

The strengths for the existing landfill waste were estimated from a reference article (Fassett, 1994) and the values used are considered the state-of-the-practice and conservative for the evaluation of landfill stability. Strengths of improved landfill material following deep dynamic compaction were estimated assuming compaction and addition of fill materials.

The block failure method of analysis using Rankine theory to determine active and passive portions of the sliding surfaces was selected to evaluate the factor of safety for the most critical sliding block failure surface. The analyses demonstrate that long term stability criteria cannot be met with construction of an embankment with 2:1 side slopes over the unimproved landfill.

Settlement of Existing Landfill

Accurate prediction of the magnitude and time-rate of settlement of landfill materials under the imposed embankment load is a very difficult task. Some published data on typical compressibility parameters are available, but show a wide range of values as would be expected.

Based on this data and engineering judgment, it was estimated that the total settlement of the unimproved landfill material beneath the 50-foot high embankment could be on the order of 2 to 3 feet. Research has shown that the majority of the settlement in the landfill will occur as the embankment fill is placed and during the first three to six months after placement (Fassett, 1994).

Stabilization of the Existing Landfill

General

The roadway alignment and profile require that a 50-foot high embankment and a triple box culvert be constructed in the area of an existing landfill. Stabilization of the landfill is required for the following reasons:

- Confirmed presence of weak landfill materials under a large portion of the embankment;
- No known precedent for construction of a new highway over an existing landfill without its removal or in-place stabilization;
- Risk of deep-seated slope failure; and
- Risk of excessive total and differential, short and long-term embankment settlement and cracking of the pavement.

Evaluation of Alternatives

Several alternatives were considered for landfill stabilization. These alternatives include:

- Removal and replacement of landfill
- Geofoam blocks as lightweight fill
- Surcharging
- Geogrid reinforcement and earth buttress
- Deep dynamic compaction

Removal and Replacement of Landfill

An effective method to eliminate the potential for excessive long term settlements and slope instability is to completely remove the waste and replace it with structural fill. This was not considered an option due to excessive costs of excavating, handling, and transporting waste.

Geofoam Blocks as Lightweight Fill

Geofoam blocks have been successfully used as lightweight fill to support roadways over weak and compressible foundation soils. Geofoam consists of low density expanded polystyrene blocks that meet the requirements of ASTM C 578. The geofoam blocks are typically manufactured in dimensions of 4 foot width, 8 foot length and 2 foot depth, and can be easily cut in the field to almost any shape.

Unit weights of the geofoam range from 1.0 to 1.5 pcf, or about 1% of the unit weight of soil or rock fill. The shear strength of the geofoam is on the order of 1000 to 1250 psf, which is comparable to that of stiff clay. Therefore, short and long term total and differential settlement

of the landfill material under the imposed weight of the geofoam embankment will be negligible and slopes will be stable. Construction time can be considerably reduced by using geofoam instead of traditional earth fill.

The primary drawback of using geofoam is expense, most of which is material cost (about $40-45 per cubic yard). Due to the excessive cost, this alternative was not considered feasible.

Surcharging

Surcharging of the landfill was considered a feasible alternative if staged construction was permitted to allow a significant gain in strength of the landfill materials and instrumentation was implemented to measure slope movements and settlements. Depending on the level of surcharge, the delay in construction could be as much as 12 to 18 months. Based on this delay in construction and a remaining moderate to high risk of excessive settlement and deep-seated slope failure, the surcharge option was not recommended.

Geogrid Reinforcement and Buttress

Layers of heavy duty geogrid and a blanket of crushed rock can be placed over the footprint of the landfill to bridge over soft areas within the existing landfill. The geogrid system does assist in minimizing differential settlements, but will not reduce the magnitude of settlements and will not adequately improve the deep-seated stability of the embankment and landfill material. To obtain adequate stability, an earthen berm or buttress would be required beyond the toe of the embankment to act as a counter balance weight to rotational instability.

The costs and time associated with this alternative make it feasible, but the associated risk, particularly of settlements that will impact the embankment and pavement performance, was still moderate to high. Therefore, the geogrid and buttress option is not recommended.

Deep Dynamic Compaction

The process of deep dynamic compaction (DDC) is a ground modification technique that involves the raising and dropping of a heavy weight (tamper) in a prescribed pattern to improve potentially unstable or weak ground with high energy impacts. The DDC method has been successfully implemented as a ground improvement technique on a number of transportation projects across the U.S (FHWA, 1995). Research has shown that DDC increases the strength and greatly reduces the compressibility of landfills.

DDC is most effective in granular soils that are above the water table and are less than 40 feet in thickness. Similar improvement was expected in the landfill materials at this site due to the depth and makeup of the landfill deposits. The magnitude of long term settlement would be reduced, and the associated risk of damaging differential settlements would be very low. The densification and addition of fill materials increases the strength of the improved landfill materials and the factor of safety against slope instability.

A compacted layer of fill would have to be placed on the ground prior to DDC activities to prevent pumping of the landfill materials upon impact of the falling weight. Craters formed by the falling weight would be filled with the typical fill materials on site.

Another added advantage of DDC is the ability to pinpoint soft areas and increase the applied impact energy in those zones to create a more uniform and increased stiffness for the embankment fill, thereby reducing the risk of differential settlement.

The costs associated with this alternative were considered reasonable (about $1 per square foot) and the method was considered very effective. In addition, the time frame is accommodating, making DDC a feasible alternative.

Recommended Alternative – Deep Dynamic Compaction

A comparison of alternatives was performed that included an assessment of relative cost, schedule and associated risk. A summary of these findings is presented below.

Alternative	Estimated Cost	Effectiveness in reducing long term settlement	Risk of damaging differential settlement
Surcharging	$50,000	Fair to poor	Moderate to high
Geogrid / buttress	$75,000	Poor	Moderate
DDC	$250,000	Good to Very good	Low
Geofoam	$2 million	Excellent	None

Based on this assessment, deep dynamic compaction was recommended for stabilization of the landfill. Before DDC activities began, a layer of fill was placed and compacted over the entire site to provide a stable working surface. DDC activities consisted of a series of low energy drops over the whole site to pinpoint soft areas for subsequent higher energy drops. The drops were continued until no further compression of the landfill material was observed. At the completion of high energy drops, fill was placed in the craters and a final "ironing pass" would be made over the whole site.

The design of DDC for the landfill was performed in accordance with recommendations of the

FHWA (1995). For an improvement depth of 15 feet, a tamper weight of 10 tons, and drop

heights ranging from 40 to 50 feet, an estimated 3 passes of 8 to 10 drops over a grid spacing of

10 to 13 feet would provide the required unit applied energy to compact the landfill to 100% of

Standard Proctor energy. The actual DDC methods employed at the site varied slightly

depending on the observed performance as operations proceeded. A view of the DDC process

performed at the landfill is shown on Figure 2 below. A view of the completed embankment

over the stabilized landfill is shown in Figure 3 below.

For landfill materials that are stabilized with DDC, settlements can be reduced significantly.

(Drumheller, 2003), and should be on the order of 1 or 2 inches. No monitoring of the settlement

was performed.

Figure 2: Deep Dynamic Compaction of Landfill

Figure 3: Embankment Construction over Landfill

CONCLUSIONS

The construction of the fills proved to be fairly successful using the residual clay and the method specification. In general, the compaction requirements were generally met with the three passes of the 825C compactor. When the required compaction wasn't achieved, the moisture of the fill was generally several points below optimum. The fill was typically reworked and water added as needed to achieve compaction with up to two or three additional passes. The retesting of failed portions of the fills all resulted in acceptable compaction.

The stabilization of the landfill with DDC was also considered to be very successful. The DDC was completely quickly and construction of the embankment and box culvert was allowed the

process shortly thereafter. The subgrade surface beneath the footprint of the embankment was non-yielding and provided a firm base for the placement of fill. At the time of this writing, the embankments had a healthy cover of vegetation and none showed any signs of distress, cracking or sloughing.

Figure 4: View of Completed 70-high Embankment at 2.5:1

 REFERENCES

AASHTO (1999), <u>AASHTO Standard Specifications for Highway Bridges</u>, Sixteenth Edition, 1996, with interims through 1999.

Drumheller (2003), Personal communication with Joe C. Drumheller, Densification, Inc.

Fassett (1994), "Geotechnical Properties of Municipal Solid Waste and Their Use in Landfill Design," by J.B. Fassett, G.A. Leonards and P.C. Repetto, proceedings of Waste Tech '94, Landfill Technology, January 13-14, 1994.

FHWA (1995), <u>Dynamic Compaction</u>, Geotechnical Engineering Circular No. 1, Federal Highway Administration, 1995.

MoDOT (2000), <u>Bridge Design Manual Section 3.74</u>, Missouri Department of Transportation, Revisions to 2000.

MoDOT (1999), <u>Missouri Standard Specifications for Highway Construction</u>, Missouri Highways and Transportation Commission, 1999.

<u>STABL User Manual</u>, Joint Highway Research Project, JHRP-75-9, Purdue University/Indiana Department of Highways.

Granites of the United States and Relationships
Pertaining to their Use as Aggregate

By: George H. Davis, R.G.
Geotechnical Liaison
Missouri Department of Transportation

Abstract

Granites of the United States possess many petrologic textures and varied petrochemistry. Both texture and chemistry pertain to their use as aggregate in highway pavements. Long-term performance of pavements that use granites depends upon petrologic texture of the granite, its chemistry, exposure to weathering and effects of thermal and pressure metamorphism on stone.   Most all engineers possess the mistaken impression that granite, due to its ability to perform as a monument stone and its reputation for hardness and resistance to weathering, is a stone that is superior to other types of aggregate in concrete or asphalt pavements.   This is true for some granitic rocks, but only those chosen carefully by the materials staff for a project will perform adequately in pavements.

 By International Union of Geological Sciences definition, granites possess phaneritic (coarse-grained) texture with specified percentages of quartz, alkali feldspars (which includes orthoclase, anorthoclase, and 'perthite'), and plagioclase feldspar. Muscovite and biotite micas, amphiboles, and accessory minerals may also be present, as allowed by definition. The percentage of minerals in granite aggregate has direct effect on particular physical engineering characteristics of aggregate stone, as well as durability. The textural characteristics of granite may augment or detract from a stone's suitability for use.

Few engineering studies exist of granitic aggregate used in pavement stone that relate to problems faced by highway agencies after pavement installation. Relating pavement study results to physical test results and granite aggregate physical and textural characteristics is difficult for this reason. The Missouri Department of Transportation has tested granitic stone for use as aggregate since 1997. Granite aggregate tested came from a variety of sources and states. Additional information on other sources has also been collected to draw conclusions based on texture, mineralogy, physical testing results, and chemical test results. Granite and other igneous rock samples and test results have been collected from Arkansas, Missouri, Oklahoma, Texas, Georgia, Arizona, Colorado, Vermont, Tennessee, and Virginia. Comparisons of physical testing results, chemical testing results, textural analysis, and hand sample examination has led to formulation of a number of interesting and perhaps important generalizations for an engineer or geologist to consider in selecting or recommending a particular type of stone for use as paving aggregate. These generalizations are outlined here for the first time.

Previous Work

Several workers have reported correlations of chemical testing results or mineralogic analysis with physical-testing results. Tugrul and Zarif (1999) reported that the influence of textural characteristics of a stone appears to be more important than mineralogy in comparisons of engineering characteristics. They used thin-section petrography to identify mineralogy of rocks chosen for study, and then tested representative samples for specific gravity, dry and saturated unit weight, water absorption, effective and total porosity, sonic velocity, Schmidt hardness, point-load strength index, uniaxial compressive strength, and modulus of elasticity. Their correlations were characterized by simple regression analysis, determining that types of grain contact, grain (mineral) shape, and grain size significantly influenced physical properties of granitic rock. Although the parameters listed influence selection of granitic aggregate, they do not effectively characterize rocks for a single end use, such as road aggregate.

Dossey and others (1990) reported on the use of chemical testing to quickly estimate preliminary concrete properties versus age before comprehensive sampling and testing. Their report was later integrated into an overall procedure for classification of coarse aggregates (Peapully and others, 1994), based on properties affecting pavement performance. Regression models were developed to predict 28-day concrete properties from chemical composition of coarse aggregate used in the concrete mix. Concrete mixes were formulated to simulate field conditions, using type I cement, and were allowed to cure at 75° F and 40 percent relative humidity. Twenty different aggregates were used, including granite. These were characterized chemically by X-ray-diffraction, fusion, and coulometric techniques. Physical properties measured were compressive strength, tensile strength, modulus of elasticity, and shrinkage on drying. Upon completion of all tests, correlation analysis was performed, using Pearson product-moment correlation to determine the degree of dependence or interdependence of the individual chemical components of test aggregates. Because only one granite sample was analyzed, conclusions cannot be drawn at any level of certainty. Regardless of an insufficient sample population, the overall study exhibited a good agreement between predicted and measured modulus of elasticity for Portland-cement concrete made from granite.

Davis (2004) reported a tentative correlation between CIPW normative minerals calculated from chemical laboratory data and physical test results, which was used as the basis for this study.

Defining Granite as a Term

In this report granite is defined as: a plutonic rock which possesses mineral percentages recognized by the International Union of Geological Sciences (IUGS), which is: between 20 and 60 percent quartz overall, containing alkali feldspar and/or plagioclase in varying proportion. Grain size is visible to the naked eye, which is known as phaneritic texture. Alkali feldspar includes: orthoclase, microcline, sanidine, anorthoclase, and 'perthites' (even though 'perthites' is actually orthoclase/plagioclase intergrowth, it can be assumed that perthitic textures for all practical purposes behave as orthoclase in aggregate stone).

This is a major difference in terminology between the term 'granite' as used by geologic professionals and 'granite'of quarrymen, stone cutters, and monument stone and facing stone dealers. Granite in the latter sense is an extremely hard rock usually of igneous or metamorphic origin that may contain quartz, feldspar, and/or mica in predominance. In this sense, many stones such as gneisses, syenites, and even serpentinites are considered to be 'granite' (Pepitone, 2004).

Examples of Granites and Similar Igneous and Metamorphic rocks

Several granites that were tested are shown in the following figures. Others are shown to illustrate similarity or dissimilarity to the concept of what granite represents in terms of aggregate suitability. The granites depicted herein are referred to by their proper stratigraphic name in keeping with the conventions of the U. S. Geological Survey and state geologic surveys around the United States.
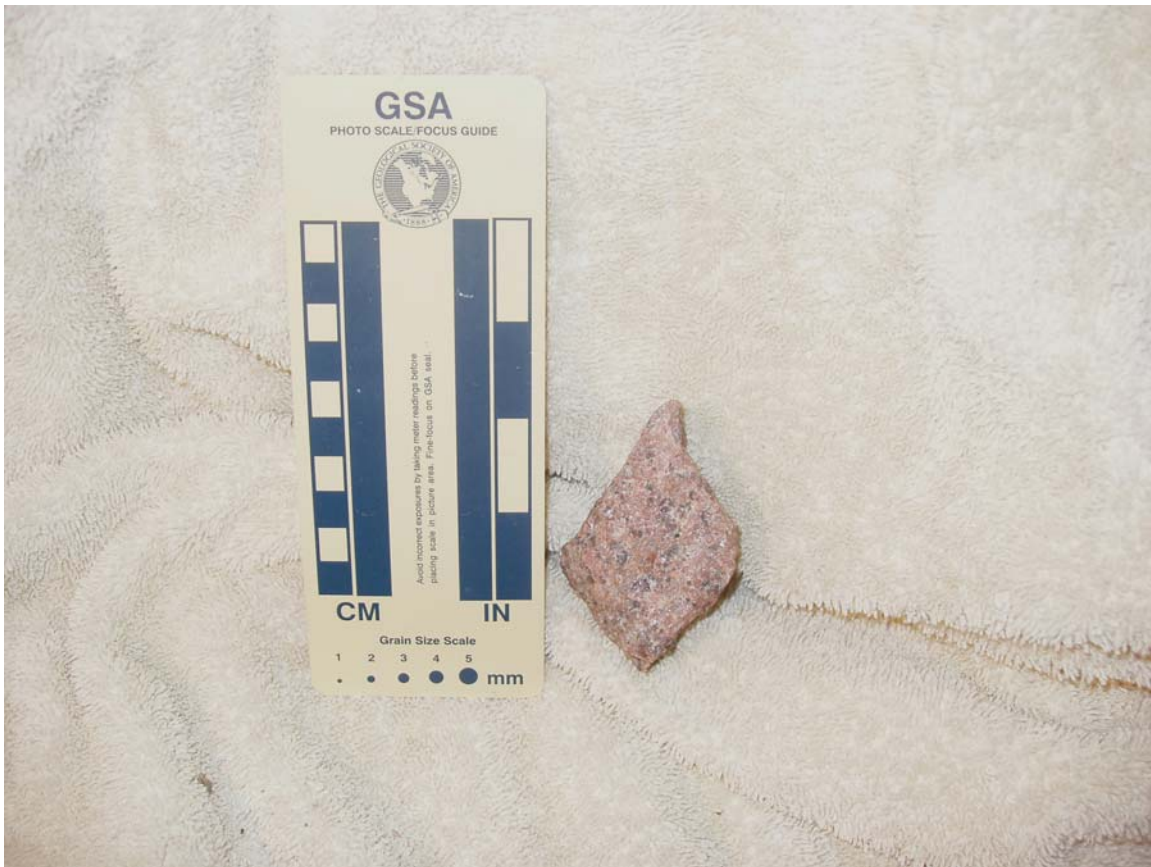

Figure 1. Graniteville Granite. This granite is a coarse-grained granite from southeast Missouri. It fits the mineralogic definition of what a granite is. In contains orthoclase feldspar (pink or flesh-toned in color), quartz, and plagioclase feldspar. These three minerals make up 95% of the rock or more. This sample is from the Missouri Red Quarry at Graniteville, Missouri.

The first two granites in these figures are from southeast Missouri, from the Graniteville Granite (Figure 1), and from the Butler Hill Granite (Figure 2). Both are true granites by definition, and have been extensively used in building and monument stone. They are also suitable for road aggregate purposes. The Graniteville has been found to meet MoDOT's test minimums for Los Angeles Wear Percentage, for absorption, and for specific gravity, thus meeting its asphalt criteria for Superpave stone. What makes the Butler Hill potentially different from the Graniteville is the texture and mineralogy of the rock unit. The Graniteville granite consists mainly of orthoclase feldspar and plagioclase with quartz. Mafic minerals such as biotite are largely restricted to joints that occur in the granite mass (Tolman and Robertson, 1969). Albite that occurs as microperthite in the granite is coarse and suggestive of a replacement texture for the rock. Only small percentages of biotite, pyrite, and albite alone as the primary plagioclase are present.

Figure 2. Butler Hill Granite from southeast Missouri. This granite is similar to Graniteville, except that it possesses muscovite mica and has a peculiar type of texture, known as 'rapakivi'. In this texture, rims of orthoclase surround larger grains and phenocrysts of plagioclase. The reverse is referred to, rather unimaginatively, as 'anti-rapakivi'. Butler Hill Granite possesses both rapakivi and anti-rapakivi textures. The upper sample shown here also possesses a large ragged-edged *xenolith* of unknown composition.

The Butler Hill granite contains approximately 40 to 60 percent orthoclase microperthite and microcline, with quartz comprising an average of 30 percent. This puts the Butler Hill granite well within the granite field of the IUGS classification as granite. Biotite and hornblende have been reported from the Butler Hill, within the confines of Hawn State Park near Piedmont, Missouri. (Lowell, 1976). The author has also collected Butler Hill Granite with hornblende and biotite near Fredericktown, Missouri.

The third figure is another type of granite also from southeast Missouri, the Breadtray Granite. This granite differs in both texture and mineralogy from both the Butler Hill and the Graniteville Granites. Several locations near Farmington, Missouri were sampled for their potential utility to MoDOT for coarse aggregate stone.

Figure 3. Breadtray Granite from southeast Missouri.

There are other types and textures of Missouri granites exposed in southeast Missouri as well. Data from coreholes and outcrops indicates that the area of the St. Francois Mountains is composed of granites and rhyolites intruded and extruded during the Precambrian, occurring in structural ring-complex features. Based upon field relationships, petrographic, geochemical, and aeromagnetic data, six separate ring-type intrusions have been identified in addition to 12 central plutons and a caldera-subsidence structure (Kisvarsanyi, 1976.)

Figure 4. Troy Granite from Meridian Aggregates Mill Creek Quarry, Oklahoma

The Troy Granite from Oklahoma is coarse-grained granite, similar to the Graniteville and Butler Hill granites, primarily composed of quartz, plagioclase feldspar (chemical testing results from MoDOT and the University of Minnesota's Rock Analysis Laboratory, [UMRAL] reveals plagioclase composition ranging from albite to labradorite), and orthoclase. Localized relationships with rocks in Oklahoma include a conformable relationship with the Burch Granodiorite, a magmatic codifferentiate of the same pluton. Further south in Oklahoma is the Tishomingo Granite, which (as it was analyzed chemically and petrographically by MoDOT) was determined to be a granodiorite. The use of the term 'granite' for the Tishomingo is actually correct, since the relative percentages of plagioclase and orthoclase indicated by chemical analysis and CIPW normative interpretation are borderline to the granite-granodiorite break, and since the presence of exsolved plagioclase in the orthoclase constituent of the stone creates a micrographic to graphic texture and perthitic to microperthitic texture.

Figure 5. Tishomingo Granite from Meridian Aggregates' Snyder facility, southern Oklahoma. Macroscopically, the graphic texture of the granite is readily visible.

Additional granitic and granite-like rocks appear in the following figures along with commentary regarding their origin, their rock chemistry, and observations regarding their relative worth as coarse aggregate in both concrete and asphalt. They serve as examples of what granite 'is' and what granite 'is not' to the reader.

Careful determinations by hand sample, petrographic analysis, and chemical analysis must be made to determine the true nature of a granite which is being investigated as a possible aggregate source. Determinations of strength and durability may be made by the appropriate physical testing, and absorption and specific gravity of the stone should also be determined.
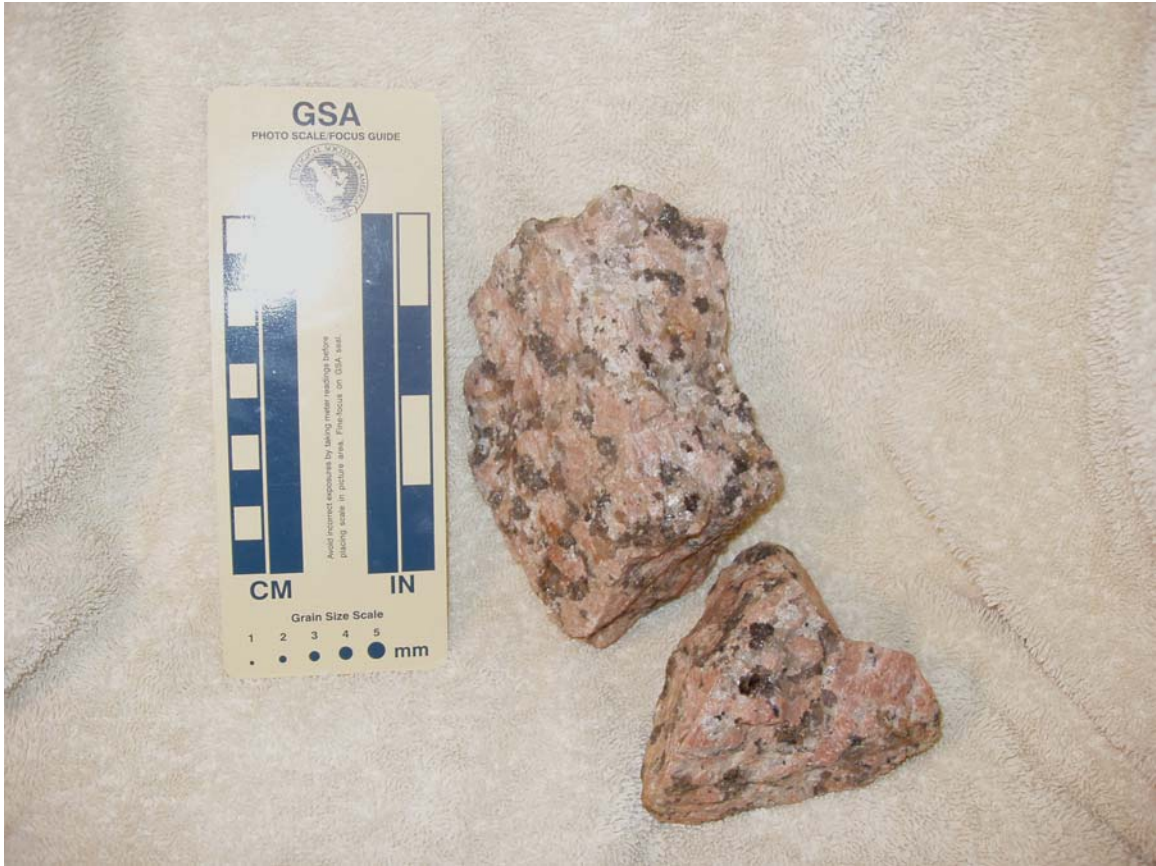
Figure 6. Town Mountain Granite from near Marble Falls, Texas. This is a good example of a dimension-quality stone which should also possess excellent attributes as aggregate stone. Its coarse grain size will add to its overall inherent strength. Visible biotite mica and hornblende may be regarded as accessory minerals in the stone, but these minerals may not prove to be deleterious. The stone has shown an excellent service life as monument and facing stone, appearing as the primary stone which was used to construct the Texas State Capital Building in Austin, Texas.

Figure 7. Cranberry Gneiss from eastern Tennessee. This rock, though it contains orthoclase, quartz, and plagioclase in similar proportions to granite, may not be an ideal aggregate stone for paving purposes. It is a metamorphic rock which has undergone stress. This stress may render it susceptible to alkali-silica reactivity (ASR) in a concrete pavement. Additionally, the stone possesses foliation planes that are markedly prominent enough to where it may increase the percentage of flattened and elongated particles in a crushed stone product. This would render it largely unsuitable for asphalt paving stone unless a sufficiently small gradation was found to decrease the overall percentage of flattened and elongated particles in an asphalt pavement. Gneisses can form from a variety of igneous and sedimentary rocks, thus, it is not always clear what rock is the precursor to the final metamorphic gneiss. Impurities in a variety of forms may also be present, as is the norm for many metamorphic rocks.

Figure 8. Quartz monzonite from the Burkeville Pluton and Luck Stone, Incorporated's facility in Burkeville. Quartz monzonite is marginal to granite, and often possesses favorable characteristics for use as aggregate in asphalt.

Thin-section petrography

Thin sections of granite when examined under polarized light reveal striking details not immediately evident during hand-sample examination. Point counts of grains and averaging of grain size allows a good estimation to be made of the gross mineralogy of nearly any sample that correlates well with chemical testing. Textures not evident in hand samples may also be revealed, or microscopic analogues of macroscopic textures may also be present. Accessory minerals are quickly identified by a trained observer.

Petrographic testing also may allow rapid determination of potential deleterious mineralogy in stone used as aggregate. Some minerals, actually beneficial in either asphalt or concrete mixes, may also be identified. Reasons for abnormally low performance or unexpectedly good performance in pavements may also be identified. Since the composition of granite is relatively simple, the minerals present determine the overall performance of the stone, and relative proportions dictate variations within a known set of variables.

Some of the more common minerals that occur in granite as accessories occur in small percentages or trace amounts, but may be quite deleterious in pavement. Pyrite, hematite, and magnetite all may contribute to reactions that contribute to or trigger pavement degradation. Quartz, though it is a major component of granite, must not be stressed or altered after melt crystallization for it to be used effectively in concrete pavements.

Of the granite samples collected, only two were analyzed petrographically to determine the relative presences of potential deleterious minerals which might affect stone quality, and sulfide and sulfate minerals, and to determine the presence or absence of stressed silicate minerals which would deleteriously affect the use of the granite in concrete. The two samples analyzed were from the Troy Granite and the Tishomingo Granite, both from the state of Oklahoma.   Figures that appear below illustrate some of the characteristics of these granites. It was found after relative percentages of constituent minerals were determined that these percentages agreed with CIPW normin recombinations of mineralogy in a general way.
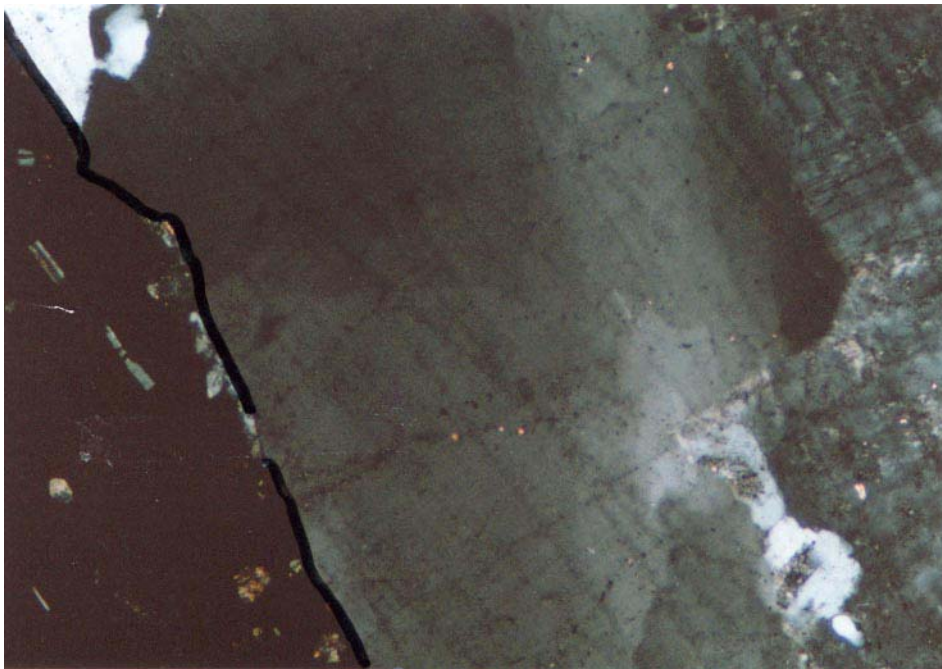

Figure 9. Margin of basalt intrusion and granite, Troy Granite, Meridian Aggregates' Mill Creek Quarry, Johnson County, Oklahoma. The basalt to the left of the photomicrograph was intruded after the emplacement of the granite pluton. Undulatory extinction in quartz grain on right-hand side of photomicrograph is indicative of stress from injection of basaltic dike adjacent. This renders the stone suspect for use in concrete due to ASR (alkali-silica reactivity) until further tests are performed. Crossed polars, 100X.

Figure 10. Undulatory extinction in pleochroic biotite grain also indicative of stress from dike injection of basalt. Troy Granite, Meridian Aggregates' Mill Creek Quarry. Johnson County, Oklahoma. Crossed polars, 100X.
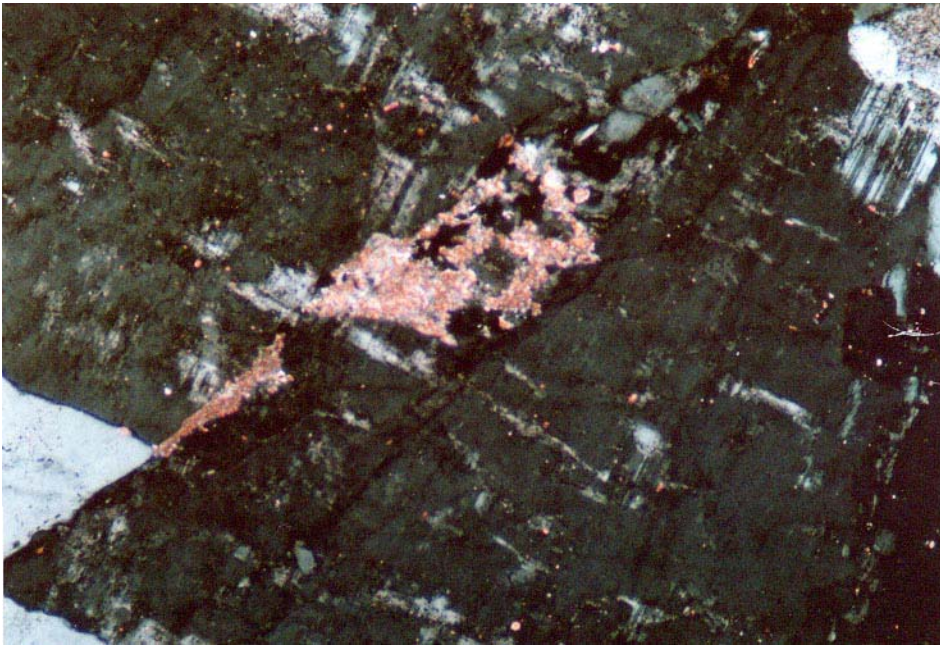

Figure 11. Adjacent orthoclase feldspar grains with fracture-filling calcite (note high birefringence) indicative of in-situ weathering and deposition of calcium bearing fluids by meteoric groundwater.   Note albite twinning on (112) surface of plagioclase grain in upper right hand of photomicrograph. Troy Granite, Meridian Aggregates' Mill Creek Quarry, Johnson County, Oklahoma. Crossed polars, 100X.

Figure 12. Quadrilateral sphene (titanite) grain as accessory mineral enclosed by quartz in graphic granite. Note micrographic texture on left side of photomicrograph. Granite from Meridian Aggregates Long Mountain (Snyder) facility, Jackson County, Oklahoma. Crossed polars, 100X.

Physical Testing Results

The data used obtained from physical testing in this study is shown in Table 1. Some of the granite samples chosen for use in this study were not submitted in sufficient quantity for testing of the required parameters, but are listed as they denote the location of each sample. Samples without state names under "Location and Notes" are from Missouri. Sample 9 data was obtained courtesy of the Elberton Granite Association.   Sample 10 data was obtained with the cooperation of the Vermont Department of Transportation, and Sample 11's data was obtained from the Arkansas Highway and Transportation Department. Samples 17 through 19 had data made available by one of the nation's largest aggregate producers, Luck Stone, Inc. Physical test data for Samples 1 through 6 came to MoDOT through the courtesy of the Missouri Department of Natural Resources' Geologic Survey and Resource Assessment Division (GSRAD).

Several of the samples were not granite. They were analyzed in the hope that the relationships found would be sufficiently robust to be applicable to other types of igneous rocks as well.

Table 1. Physical Test Data of Granites Used in Study

Sample No.	L.A. Wear, in percent	Absorption, in percent	Specific gravity	Location and notes
1	13.72	0.89	2.59	Graniteville granite outcrop near Bismarck
2	23.52	0.62	2.58	Van Buren Granite quarry near Big Spring
3	11.55	0.32	2.62	Mill Springs Granite quarry
4	20.52	0.39	2.6	Graniteville granite quarry
5	19.92	0.29	2.63	Missouri Red granite quarry
6	27.34	0.23	2.62	Butler Hill Granite near Knob Lick
7	28	1.1	2.65	Mill Creek Quarry, OK
8	18	0.8	2.58	Snyder Quarry, OK
9	NR	0.092	2.67	Elberton Granite, GA – Elberton Granite Assoc. data
10	30.6	0.8	2.64	Barre Granite, VT – Vermont DOT data
11	27	0.3	2.63	Pulaskite, AR - AHTD data
12	NR	NR	NR	Hill O'Mera Granite Quarry, Butler Hill Granite
13	NR	NR	NR	Knob Lick Granite Quarry
14	NR	NR	NR	Klondike Hill Quarry – Pilot Knob Felsite
15	23.54	0.5	2.6	'Missouri Red' granite quarry MoDOT check of Sample No. 5
16	27	0.4	2.62	Pulaskite, AR - MoDOT data; check of Sample No. 11
17	32.9	0.61	2.8	Luck Stone, Greene Co, VA
18	28.5	0.75	2.6	Luck Stone, Boscobel facility, VA
19	37.9	0.53	2.63	Luck Stone, Burkeville facility, VA

Chemical Testing Results

The results of chemical laboratory testing for this study are shown in Table 2.   Samples 1 through 6 were data made available by Missouri GSRAD (Davis, 2004). The Elberton Granite Association made data available for Sample 9. Sample 16's data came from Granite Mountain Quarries, in Sweet Home, Arkansas.   Data for Samples 17, 18, and 19 were contributed by Luck Stone, Incorporated. All other samples were analyzed at Missouri DOT's Central Laboratory in Jefferson City, Missouri.

Table 2. Chemical analyses of samples used in study.

[NR—not reported]

Elemental oxide weights, in percent									
Sample No.	CaO	MgO	SiO_2	Al_2O_3	Fe_2O_3	MnO	Na_2O	K_2O	TiO_2	Total
1	1.05	0.39	69.61	14.36	4.29	0.04	4.49	3.82	0.79	98.84
2	0.43	0.28	73.19	10.78	3.65	0.03	5.47	4.17	NR	98
3	0.57	0.17	72.94	12.66	4.02	0.03	4.03	4.19	0.65	99.26
4	0.8	0.29	73.04	12.38	3.95	0.04	3.63	4.28	NR	98.41
5	0.73	0.06	73.64	12.75	2.77	0.02	3.91	4.79	1.39	100.06
6	0.37	0.06	75.29	11.44	2.44	0.01	3.37	4.34	0.9	98.22
7	0.4	0.3	73.54	12.22	3.8	NR	3.31	4.51	0.24	98.32
8	0.56	0.17	72.71	12.73	4.88	NR	3.4	4.76	0.23	99.93
9	1.94	0.45	69.83	16.56	1.36	NR	4.74	5.03	NR	100.38
10	7.37	0.35	66.02	16.06	2.47	NR	2.55	4.37	0.43	97.65
11	7.92	0.28	61.72	18.88	2.67	NR	3.11	5.15	1.05	100.78
12	6.28	0.012	72.26	13.68	1.83	NR	2.14	4.36	0.22	100.97
13	7.98	0.27	69.61	12.6	3.3	0	2.43	3.34	0.4	101.06
14	6.17	0.06	72.8	12.21	1.88	NR	2.22	4.2	0.18	100.34
15	0.67	0.04	76.55	12.1	1.55	NR	3.51	4.72	0.08	99.22
16	1.27	1.19	60.3	19.93	4.67	NR	6.25	5.3	1.1	100.01
17	3.52	0.82	62.07	20.36	7.24	NR	0.41	1.5	NR	95.92
18	1.56	0.66	71.66	13.18	1.9	0.05	3.61	3.95	0.23	96.8
19	1.8	0.8	72	14	1.8	0.5	3.6	4.6	0.3	99.4

Synthesis of Generalizations

Once both chemical and physical test data were obtained, a number of attempts at correlation were made to attempt to use the data to predict potential performance results in terms of durability or other parameters. Previous work by Dossey et al. was closely examined to determine the pertinence of their procedures to that being attempted by MoDOT.

Dossey and others (1990) created a procedure that correlated the physical test results of concrete made from particular types of aggregate with groups of oxides that occurred most often together in various forms of aggregate. A correlation analysis was run to

determine which oxides were independent or correlated with each other to determine chemical associations, which they claimed indicated that the oxides exist naturally together as ores. Their groups were:

Group 1	Group 2	Group 3	Group 4	Group 5
SiO_2	CaO	MgO	Fe_2O_3	Al_2O_3
	CO_2		MnO	TiO_2
				Na_2O
				K_2O

These artificial groupings to determine end result concrete properties via regression analysis, though achieving the desired result did not truly reflect the mineralogy of the stone tested. For instance, though lime (CaO) and carbon dioxide (CO_2) appear in Group 2 logically as occurring together in calcite ($CaCO_3$), the primary constituent in limestone that was tested, these two oxides appear outside of the aggregate test group in other types of aggregate as other minerals. In granite, the lime constituent most likely would be a component of plagioclase, since calcite is rare in most granites, except as a secondary mineral deposited upon fracture surfaces. Several other possible discrepancies for igneous rocks also occur in the study, such as the failure to associate alumina (Al_2O_3) and silica (SiO_2), which is a common occurrence in igneous rock, as these both occur in feldspars. Dossey's group only tested one granite, which indicates a bias towards limestones and dolomites in their study. They do not adequately address granites and granitic composition, let alone other igneous rocks.

To characterize the possible mineralogic composition of granite and the aggregate used in our study, we chose a method useful in determining magmatic chemistries, the normative procedure of Cross, Iddings, Pirsson, and Washington (Cross et al., 1902). This procedure is often used to determine the degree of silica saturation in igneous rocks, relating the various amounts of oxides to known mineralogies that occur in igneous rocks. In this procedure, oxides are theoretically recombined to form artificial minerals, or normins, which represent actual minerals in an igneous rock. Normins may or may not correlate to the actual mineralogy of a sample. The procedure applied by Henderson for achieving silica balance in the normative procedure was used. Normins calculated from the chemical analyses completed or reported in Table 2 are shown in Table 3. The normins are italicized in keeping with current convention. See Table 4 for a list of abbreviations for normins.

The data may be arrayed in a suitable format for comparisons between individual samples to identify similarities and discriminate discrepancies. Groups of samples may also be arranged from known rock units to determine ranges of characteristics, and conclusions drawn from the grouped arrangements

Table 3. Normins calculated from chemical analyses by CIPW short-form normative method. See Table 4 mineral names given for CIPW normins.

Sample No.	il	or	ab	an	co	mt	fs	en	q	hm	wo	di	ac	hy	lc	ne	ol
	il	*or*	*ab*	*an*	*co*	*mt*	*fs*	*en*	*q*	*hm*	*wo*	*di*	*ac*	*hy*	*lc*	*ne*	*ol*
1	1.5	22.61	37.94	5.2	0.93	1.25	0.77	0.97	26.15	0	0	0	0	0.97	0	0	0
2	0	24.68	32.17	0	0	0	0	0.69	28.04	0	0.09	1.5	12.38	0	0	0	0
3	1.23	24.79	34.06	2.64	0.52	1.16	1.1	0.41	31.56	0	0	0	0	1.51	0	0	0
4	0	25.67	28.51	1.83	0.52	0.72	1.21	0.15	37.61	0	0	0	0	1.36	0	0	0
5	0	28.3	33.06	3.11	0	0.81	1.41	0.15	30.4	0	0	0.4	0	1.08	0	0	0
6	1.72	25.29	30.65	3.98	0.33	1.14	0.47	0.92	33.21	0	0	0	0	1.19	0	0	0
7	0.48	26.68	27.98	1.97	1.16	1.11	1.49	0.74	38.51	0	0	0	0	2.23	0	0	0
8	0.44	28.13	28.71	2.78	0.97	0.74	2.81	0.42	32	0	0	0	0	3.23	0	0	0
9	0	29.74	40.09	9.04	0	0.39	1.12	0.67	18.1	0	0	0.47	0	1.56	0	0	0
10	0.51	11.2	21.54	26.77	0	0.72	0.78	0.89	30.25	0	2.35	3.39	0	0	0	0	0
11	1.99	30.47	26.3	22.26	0.06	0	0	0	10.18	0.48	6.29	1.5	0	0	0	0	0
12	0.41	25.79	18.08	14.82	0	0.53	0	0	32.76	0	5.96	1.68	0	0	0	0	0
13	0.76	19.77	20.54	13.59	0	0.95	0	0	30.55	2.66	9.17	3.3	0	0	0	0	0
14	0.35	24.84	20.59	10.93	0	0.56	0	0	34.59	0	7.48	1.48	0	0	0	0	0
15	0.15	27.91	29.66	3.3	0	0.09	0	0.1	36.64	1.18	0	0	0	0.1	0	0	0
16	2.1	31.35	51.25	6.28	1.6	3.02	0	0	0	0	0	0	0	0	0	0.85	4.8
17	0	8.85	3.45	17.43	11.66	2.11	3.58	2.03	43.57	0	0	0	0	5.6	0	0	0
18	0.44	23.34	30.5	0.41	0.41	0.56	0.64	1.64	31.26	0	0	0	0	2.29	0	0	0
19	0.58	27.18	30.44	8.45	0	2.62	1.14	1.99	27.98	0	0	0.41	0	2.94	0	0	0

Table 4. Standard abbreviations used to identify CIPM artificial minerals or normins.

Abbreviation	Mineral	Abbreviation	Mineral	Abbreviation	Mineral
Il	ilmenite	*fs*	ferrosilite	*Ac*	acmite
or	orthoclase	*en*	enstatite	*Hy*	hypersthene
ab	albite	*q*	quartz	*Lc*	leucite
an	anorthite	*hm*	hematite	*Ne*	nepheline
co	corundum	*wo*	wollastonite	*Ol*	olivine
mt	magnetite	*di*	diaspore	*Pl*	plagioclase

One intent of this study was to document correlations between chemistry and physical property data and to verify that mineralogy is a control on the quality of aggregate. A relationship is present for Missouri granites where increased *pl* normin content is associated in a corresponding decrease in the percentage of wear as determined by the Los Angeles wear or abrasion test. This potential correlation was initially recognized with only six samples from Missouri, and could only have been considered tentative at best (Davis, 2004). Additional data was collected from producers and other sources where Los Angeles wear (LAW) can be predicted from *pl* normin using this regression equation (Fig. 13):

$$LAW = -1.02 * pl + 56$$

The regression on *pl* explains 72 percent of the observed variation (at the 95 percent confidence level) in LAW based on date from 13 quarries and sample locations. Equation 1is more likely to be valid for granites of the Precambrian mid-continent, particularly Oklahoma and Missouri. Of possible concern is a possible suggestion of heteroscedasticity relationship between pl and LAW when pl is greater than 35 percent. This is shown by increased scatter of points about the low end of the regression line (Fig. 9) and may invalidate the use of regression (Rock, 1988). This may suggest that the regression relationship loses validity where computed pl become large or may simply be due to chance given the small data set size.

Correlation of Los Angeles Wear Percent to pl CIPW Normin Percent

$$\text{\% Los Angeles Wear} = -1.0152\ pl\ \text{normin\%} + 55.706$$
$$R^2 = 0.7175$$
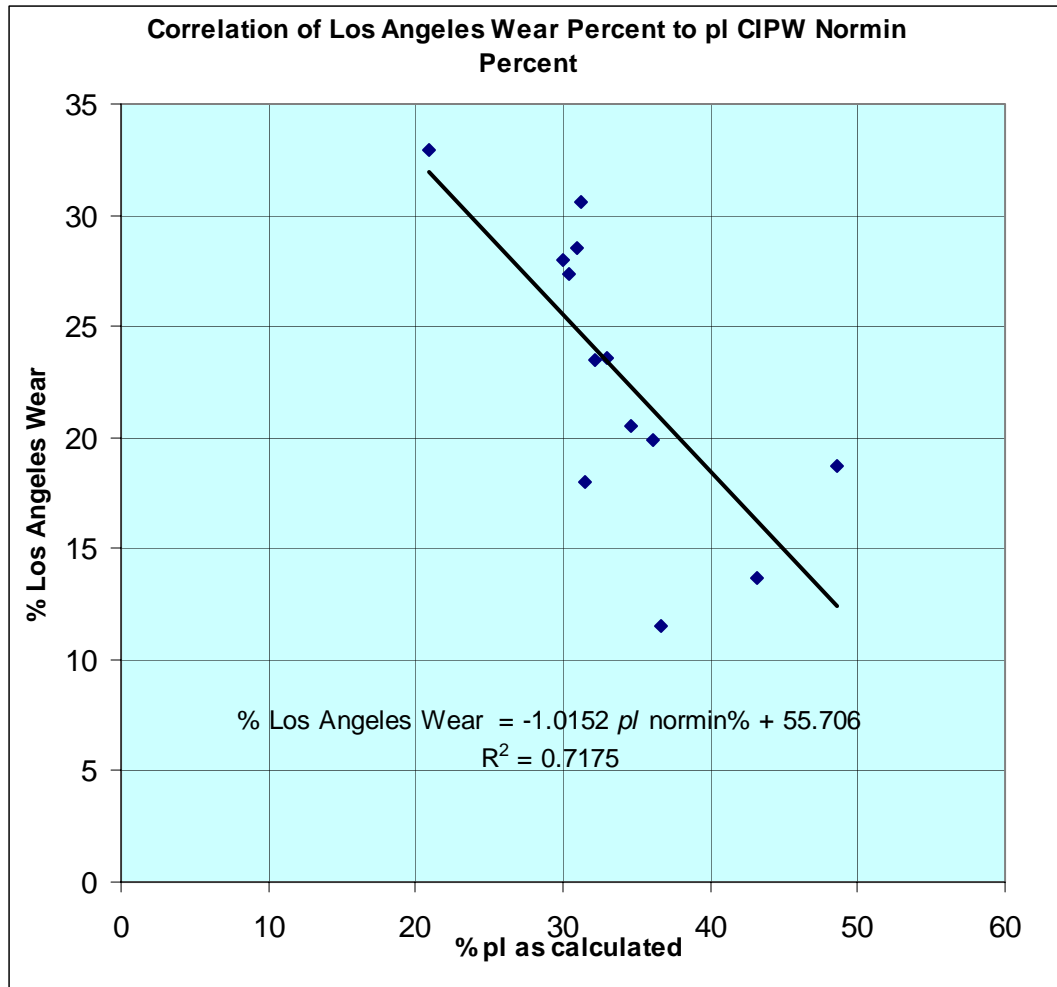
Figure 13. Proposed Correlation between Los Angeles Wear Percent and normin *pl* as determined by CIPW normative procedure.

It can be seen from the foregoing discussion, that there are four major criteria to consider when the engineering properties of granites are discussed. The first major criterion is mineralogy. As can be tentatively shown with the use of the CIPW normin, an inverse linear regressive relationship exists between Los Angeles Wear percent and plagioclase content in a granite. Increased plagioclase content (up to a tonalite composition) corresponds to a decreased Los Angeles Wear percent, and the durability of the stone correspondingly is markedly better. Durability is one of the most primary factors to consider in both concrete and asphalt pavements. Increased amounts of ferromagnesian minerals in the stone increase its susceptibility to weathering, and decrease a potential aggregate's durability. Anhedral grains of quartz in granitic rock seem to exhibit no effect on its overall durability. The mineralogy also has a direct effect on the stone's adhesive properties for asphalt oils. Grain surfaces on perthitic feldspars are particularly susceptible to fresh angular breaks due to the mixed mineralogy of albite and potassic

feldspar present. With plagioclase feldspar, the albite (0112) twinning surface, which exhibits many parallel lines on an aggregate grain's surface, also yields a ragged edge for asphalt oil to adhere to. By contrast, quartz, which breaks with conchoidal fracture surfaces, does not adhere well to asphalt (Nieminen,1987).

The second primary criterion, which is often overlooked by quarrymen and engineers, is the geologic setting of the stone. Some granites possess better physical test characteristics than other granites of identical petrochemistry and mineralogy. This is due to the stresses or degree of geological weathering that the granites have been exposed to. An example of stressed granite was collected from the Meridian Aggregates' Mill Creek Quarry that exhibits characteristics of both stress and weathering. Localized areas in the quarry have been intruded by tholeiitic basalt dikes in dike "swarms". Stresses from the intrusion is exhibited in thin section by quartz which possesses undulatory extinction under crossed polars, indicative of a stone which might be susceptible to alkali-silica reactivity, or ASR, when used in concrete (Leming, 1996).

Texture of aggregate stone is a third criterion to consider when considering the potential of granitic rock for use. Granitic rocks may have grain sizes that vary throughout the sample, or the grain sizes may be largely uniform.   Finer-grained granites have better potential for asphalt since rough fresh surfaces result from crushing. This allows asphalt oils to adhere better to the stone. Rapakivi textures, perthitic intergrowths of albite and potassic feldspar, and graphic or micrographic textures also add to the overall tendency of asphalt to adhere to the stone.

The final criterion for consideration is the intended use of the stone. Nearly all granites with favorable engineering test results for asphalt should perform well in asphalt pavements.   Strength and durability imparted as a result of texture and mineralogy is coupled with fresh angular faces from crushing and then added to a mixture of asphalt oil which produces asphalt pavement. Strength of an asphalt pavement made with granitic aggregate is as durable, flexible, and has a pavement life as long as the asphalt oil allows. This can easily be contrasted with asphalt pavement constructed with dolomite or limestone aggregate, which may often contain deleterious materials or flattened and elongated particles which detract from overall pavement utility and service life.

These generalizations add knowledge to the degree of care with which even granitic stone must be chosen when considered for use in concrete and asphalt pavements. Successful pavement construction starts with aggregate selection. Granite is aggregate that is worthy of consideration for both concrete and asphalt pavements.

References Cited

Davis, George H., 2004. "Tentative Correlation between the *pl* (plagioclase) CIPW Normin and LA Wear Percent – An Example From Precambrian Midcontinent Granites", pp 69-75 in: Proceedings of the 38th Forum on the Geology of Industrial Minerals, St. Louis, Missouri, April 28-May 3, 2002. Missouri Department of Natural Resources Geological Survey and Resource Assessment Division Report of Investigations No. 74. 310pg.

Cross, C.W., Iddings, J.P., Pirsson, L.V., and Washington, H.S., 1902, "A quantitative chemico-mineralogical classification and nomenclature of igneous rocks". Journal of Geology, v.10, p.555-690.

Dossey, Terry, Castedo, Humberto, and McCullough, B.F., 1990, Cement, concrete, and admixtures, 1990: Transportation Research Record No. 1284, 98 p.

Kisvarsanyi, E.B., 1976. "Missouri Precambrian Revisited: Progress in Studies of Precambrian Geology 1961-1976, pp.66-80 in: Kisvarsanyi, Eva, B. (ed.), 1976. Studies in Precambrian Geology with a Guide to Selected Parts of the St. Francois Mountains, Missouri. Missouri Department of Natural Resources Division of Geology and Land Survey Report of Investigations No. 61. 190 pg.

Leming, M.L., 1996. "Alkali-Silica Reactivity: Mechanisms and Management" in : Mining Engineering, Dec. 1996, pp.61-64

Lowell, Gary R., 1976. "Petrography of Precambrian Rocks in the Hawn State Park Area, Ste. Genevieve County, Missouri", pp. 140-147 in: Kisvarsanyi, Eva, B. (ed.), 1976. Studies in Precambrian Geology with a Guide to Selected Parts of the St. Francois Mountains, Missouri. Missouri Department of Natural Resources Division of Geology and Land Survey Report of Investigations No. 61. 190 pg.

Niemenen, P., 1987. Kiven Ja Bitumen Valisesta Tartunnasta ["Adhesion Between Stone and Asphalt"] Finnish Transport and Road Research Laboratory Report No. 16. 35pg.

Peapully, Srikrishna, Zollinger, D.G., and McCullough, F.B., 1994, Procedure for classification of coarse aggregates based on properties affecting performance: Texas Transportation Institute Research Report 1244-9, 113 p.

Pepitone, Mary G., 2004. "Stone: Solid As Ever", special article in Kansas City Star, issue of May 16, 2004.

Rock, 1988, Numerical geology—a source guide, glossary and selective bibliography to geological uses of computers and statistics: New, York, Springer-Verlag, 427 p.

Tolman, Carl F., and Robertson, Forbes, 1969, Exposed Precambrian Rocks in Southeast Missouri (Contribution to Precambrian Geology No.1) , Missouri Geological Survey and Water Resources Report of Investigations No. 44. 68pg.

Tugrul, A., and Zarif, I.H., 1999, Correlation and textural characteristics with engineering properties of selected granitic rocks from Turkey: Engineering Geology, v. 51, p. 303-317.

Abstract

Grout Stabilization of Compressible Embankment Fills Beneath Bridge Approach Slabs, SR51 HOV Lanes Design-Build Project, Phoenix, Arizona

Daniel N. Fréchette, Ph.D., P.E.
AMEC Earth & Environmental, Inc.
3232 W. Virginia Avenue
Phoenix, Arizona 85009
Tel. 602-272-6848
email: daniel.frechette@amec.com

Nicholas J. LaFronz, P.E.
AMEC Earth & Environmental, Inc.
3232 W. Virginia Avenue
Phoenix, Arizona 85009
Tel. 602-272-6848
email: nick.lafronz@amec.com

The Arizona Department of Transportation State Route 51 (SR51) HOV Lanes Design-Build Project between Interstate 10 and Shea Boulevard in Phoenix, Arizona involved modification of the northbound and southbound lanes of the existing SR51 urban freeway to provide new traffic lanes for high-occupancy vehicles. Six elevated bridge crossings of major arterial streets and an irrigation canal within the southern four miles of SR51 were originally constructed in the mid- to late-1980s, and subsequent compression of the predominantly fine-grained clayey approach fills (with a maximum thickness near 30 feet) had created severe "bump at the end of the bridge" conditions. Initially, the scope of the HOV Lanes project included a force account allowance for stabilization by deep compaction grouting of the existing compressible embankment fill soils followed by jacking of the settled approach slabs by grout injection to restore the slabs to their original grades. Both techniques were to utilize low-slump Portland cement grout injected under pressure up to a maximum of 400 psi. Pre-grouting subsurface geotechnical investigation was performed by both the ADOT Oversight Team and the Designer-Builder in an effort to establish the depth, lateral extent and characteristics of the compressible fill soils at the six crossings. Clayey fill soils with standard penetration test N-values as low as 1 (blows/foot) were encountered, and voids beneath the approach slabs up to about 7 inches in depth were identified under several of the slabs in the course of the investigations.

Evolution and development of the design-build project, Oversight Team reviews of Designer-Builder submittals, and consideration of the existing approach slab and bridge structure conditions all led to selection of an intrusion grouting technique using high-slump grout injected under moderate pressures as the preferred method of fill stabilization and void filling. A total of 1,462 grout and re-grout holes and 12,876 lineal feet of drilling were completed, and 36,688 cubic feet of grout was injected at pressures up to about 300 psi with the majority of the grout injected at pressures below 100 psi. Grout hole depths ranged from 3 to 29 feet, and the average grout take was 2.9 cubic feet/lineal foot of grout drill hole for the project. Post-grouting geotechnical investigation consisted of confirmation borings in all grouted fill zones after the initial round of grouting, and re-grouting was performed in fill zones not meeting minimum density requirements. Shallow intrusion grout injection and filling of under-slab voids also were completed as the last stage of grouting work. Through field trials, approach slab jacking was deemed impractical given the slab conditions and the high-slump grout utilized.

Bridge abutment walls, wingwalls and the walls and roof of two equipment underpasses at the irrigation canal were instrumented and monitored with strain gages and tiltplates, as well as visually monitored, full-time during grouting. Grout sampling, casting of cylinders and compressive strength testing also were completed.

Mine Paste-Soil Backfills
A New Application of Paste Technology

By
Michael Thompson, Golder

Mitigation of disused land over abandoned coal mines is becoming increasingly important as pressure to develop 'brown-field' and marginal sites increases. Due to the often large volumes of backfill required and the increasing environmental costs associated with quarrying new materials, not to mention consuming valuable landfill capacity when disposing of mine and other bulk wastes, the economical production of mine backfill from 'waste' materials is an attractive alternative.

During 2003, $1.5M of mitigation has been carried out using paste backfill in abandoned coal mines beneath parts of an 800 ha proposed resort complex and residential development in Canmore, Alberta. Land has been reclaimed for a diverse range of uses, from parkland to highways to residential buildings. Waste overburden materials, sourced from the development of the area, have been processed and mixed with between two and five percent cement to produce highly flowable, non-segregating, low compressibility fills. Unlike traditional reclamation using concrete, where the flow characteristics are determined by cement content, selective mixing of different overburden types effectively produces a wide range of slump and flow properties at similar water and cement concentrations.

The cost of the backfill is between a third and a half the cost of comparable concrete, with up to a 75% reduction in the number of boreholes required for injection compared with low–strength concrete. The paste-soil backfill reduces the impact on the environment by using waste materials from surface, less new materials for concrete and cement and reclaims high value land for development.

Recent Development of Geosynthetic-Reinforced Column-Supported Embankments

Jie Han**,** Ph.D., P.E.
Associate Professor, Civil, Environmental, & Architectural Engineering (CEAE) Department, the University of Kansas, 2150 Learned Hall, 1530 W. 15th Street, Lawrence, KS 66045, jiehan@ku.edu

James G. Collin, Ph.D., P.E.
The Collin Group, 7445 Arlington Road, Bethesda, MD 20814, jim@thecollingroup.com

Jie Huang
Graduate Research Assistant, Civil, Environmental, & Architectural Engineering (CEAE) Department, the University of Kansas, 2150 Learned Hall, 1530 W. 15th Street, Lawrence, KS 66045

ABSTRACT: Geosynthetic-reinforced column-supported embankments (GRCSE) have emerged as an effective alternative to conventional geotechnical solutions when constructing on soft soils. This paper provides the state of the art review of recent developments in the use and design of GRCSE. The review includes load transfer mechanisms, failure modes, design considerations, numerical analyses, and applications of GRCSE systems. The review concludes that GRCSE systems are most suitable for situations with a very soft soil underlain by a stiff soil layer or bedrock, when new fill with a certain minimum thickness is needed, rapid construction is necessary, and strict total/differential settlements are required. The common applications of these systems include bridge approach, roadway widening, and railroads or highways across soft soil. Soil arching, tensioned membrane or stiffened platform (or beam) effects, and relative stiffness effects between columns and soil are identified as the load transfer mechanisms above the pile caps or columns. Three common soil arching models are used for estimating the soil arching ratio and the average vertical stress above the geosynthetic reinforcement by assuming vertical slip surfaces, a rigid conical (axisymmetric) or triangular prism, and semi-spheres. A few tensioned membrane theories are available for estimating the strain and the tension developed in the geosynthetic reinforcement. Due to the complexity of the systems, numerical methods are considered as an effective way for analyzing these systems.

INTRODUCTION

When designing embankments over soft soils, geotechnical engineers must address design concerns related to potential bearing capacity failures, intolerable total and differential settlements, large lateral pressures and movement, and slope instability. A variety of techniques are available to geotechnical engineers to address the above concerns (Magnan, 1994). These techniques include pre-loading or staged construction, using light-weight fill, over-excavation and replacement, geosynthetic reinforcement, soil improvement techniques, and pile-supported embankments. The advantages and disadvantages of these techniques are discussed in the paper by Magnan (1994).

Among these techniques, geosynthetics (such as geogrids and geotextiles, made of polymer materials) as reinforcement have been adopted to reinforce soft foundations, slopes, and embankments. Geosynthetics have a high tensile strength that soils do not have. The function of the geosynthetics for embankments over soft soils is to increase bearing capacity, reduce differential settlement, and prevent slope instability. Many studies have shown that geosynthetics can be used for reducing differential settlements, however, they have limited contributions in reducing total settlements of embankments over soft soils.

In the column-supported embankment system, the columns carry most of the loads from the embankment and the soil is only subjected to small loads. The benefits associated with the use of column-supported embankments are as follows: (1) allows construction of the embankment in a single stage without prolonged waiting time, (2) significantly reduces total and differential settlements, (3) reduces or eliminates global stability concerns.

Column-supported embankment systems have been used with or without geosynthetic reinforcement. A system without geosynthetic reinforcement is referred to herein as the conventional column-supported embankment (CCSE) system while the system with geosynthetic reinforcement is referred to as the geosynthetic-reinforced column-supported embankment (GRCSE) system (Figure 1). For a CCSE, inclined columns are commonly used near side slopes to carry the lateral thrust from the embankment. In addition, columns need to be closely spaced and/or have large column caps in order to transfer surcharge loads through soil arching to the columns and minimize deflection of the soil between column caps and the deflection being reflected to the embankment surface. Shen and Miura (2001) proposed using varying lengths of piles to solve differential settlement of roads on soft soil in Japan. In the GRCSE system, the geosynsthetic reinforcement carries the lateral thrust from the embankment, creates a stiffened fill platform to enhance the load transfer from the soil to the columns, and reduce the differential settlement between pile caps. One single high strength geosynthetic layer may be placed over the column caps or columns acting as a tensioned membrane or multiple layers of geosynethtics with adequate strengths may be placed within granular fill to form a load transfer platform. As a result, the GRCSE system does not require inclined columns, large column caps, and close column spacing. Therefore, the GRCSE system creates a more cost-effective solution.
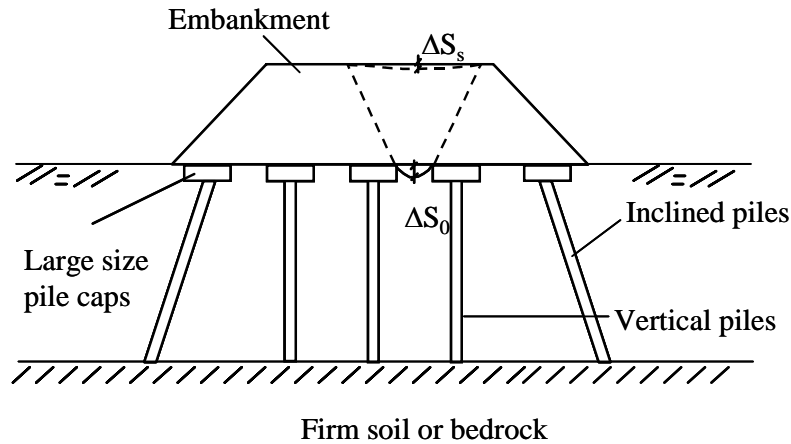
(a) Conventional column supported embankments
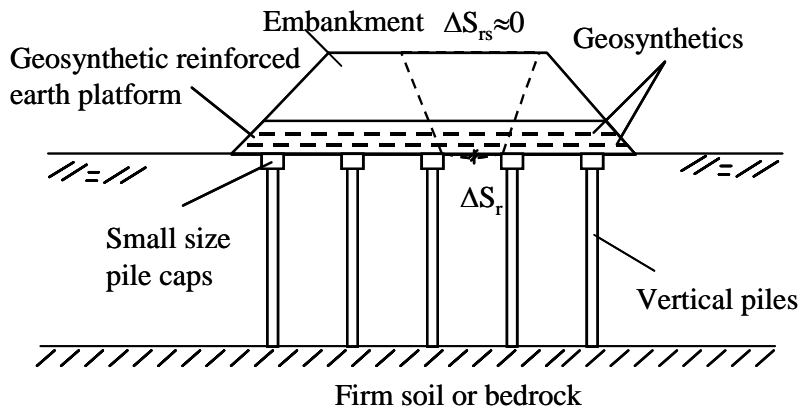
(b) Geosynthetic reinforced column supported embankments

Figure 1. Column-Supported Embankments

In addition to concrete piles and timber piles, vibro-concrete columns (VCC), deep mixed columns, rammed aggregate piers, or stone columns as columnar systems in ground improvement have been used for embankment support as well. The GRCSE systems have been used for a number of applications worldwide, which include: bridge approaching embankments; low height embankments; roadway widening; retaining wall foundation support; storage tanks foundation support; and building foundation support, etc.

Today, there are a several methods available for the design of GRCSE systems that provide very different designs for the same design parameters. There is a need to develop a rational design method for this emerging technology that more accurately predicts GRCSE performance. Several research activities have been going on in the United States in the past

few years, which include the FHWA pooled fund project – "Column-Supported Embankments" by Collin and Han, the National Deep Mixing Program project by Han – "Development of Design Charts for Geosynthetic-Reinforced Embankments over Deep Mixed Columns

MECHANISMS OF LOAD TRANSFER

The interactions among column, foundation soil, embankment fill, and geosynthetic reinforcement can be described as follows. Under the influence of fill weight, the embankment fill mass between columns has a tendency to move downward, due to the presence of the soft foundation soil. This movement is restrained by shear resistance from the fill above the columns. The shear resistance reduces the pressure acting on the geosynthetic but increases the load applied onto the columns. This load transfer mechanism in this case was termed the soil arching effect by Terzaghi (1943).

Compared with the unreinforced case, the inclusion of geosynthetic reinforcement is expected to reduce the displacement of the embankment fill between the columns. The reduction of the displacement would reduce the shear stresses in the embankment so that the effect of soil arching in the embankment would be minimized. As a result, the load transferred by soil arching to the columns is reduced. At the same time, however, the load on the columns may be increased by the vertical components of the tension force in the reinforcement. A single geosynthetic layer behaves as a tensioned membrane while a multi-layer system acts as a stiffened platform (or like a beam) due to the interlock of reinforcement with the surrounding soil. Giroud et al. (1990) and British Standard BS 8006 (1995) proposed similar rational for estimating the tension in geosynthetic reinforcement acting as a tensioned membrane. Wang et al. (1996) considered multiple geosynthetic reinforcements in soil providing an addition of apparent cohesion.

Soil arching and tensioned membrane effects also depend on the relative stiffness of the columns to the soil. A rigid column promotes the differential settlement between the columns and the soft soil so that there is more soil arching and tensioned membrane effect. Han and Gabr (2002) have confirmed these phenomena in their numerical analysis.

In summary, the mechanisms of load transfer can be considered as a combination of soil arching, tensioned membrane or stiffened platform effects, and relative stiffness effects between columns and soil. The load transfer contributed by each mechanism depends on a number of factors including number and tensile stiffness of geosynthetic reinforcement layers, properties of embankment fill and foundation soils, and moduli of column materials and soil.

POTENTIAL FAILURE MODES

If not properly designed, the GRCSE system may have the following possible failure mechanisms, failure of foundation soil, failure of columns and caps, failure of geosynethetic reinforcement, and slope instability.

Failure of foundation soil

When CSE are constructed over soft soil, the soft soil between the columns may fail due to

low bearing capacity. The inclusion of geosynthetic reinforcement above the columns reduces the load transmitted to the soft soil.

Failure of column and caps

The columns and caps under the embankment may have the following possible failures modes:

- Column caps punching through embankment fill
- Tilt of column caps
- Flexural and/or shear failure of column caps
- Compression failure of column shafts
- End-bearing failure of columns
- Bending failure of columns
- Shear failure of columns

The inclusion of geosynthetic reinforcement would increase the resistance against the punching of column caps, minimize the chance of tilt of column caps and bending failure of columns by reducing lateral thrust from the embankment. However, it may require more flexural and shear capacities of column caps and load capacities of columns since more load is transferred onto the column caps and columns.

Failure of geosynthetic reinforcement

The geosynthetic reinforcement above column caps may fail due to rupture or pullout from the soil especially when the reinforcement is near the edge of the embankment. The reinforcement can also experience excess elongation due to low modulus and/or creep deformation. The tension in a geosynthetic layer when acting as a tension membrane would be reduced as the deflection/elongation of the reinforcement increases (i.e., stress relaxation).

Slope instability

The embankment system may encounter the following possible slope instability situations:

- Lateral spreading due to the thrust from the embankment
- Local slope instability
- Slope instability outside the first row of piles
- Slope instability through piles
- Global slope instability below piles

DESIGN CONSIDERATIONS

Percent coverage or improvement ratio

Based on the performance investigation of conventional pile-supported embankments, Rathmayer (1975) recommended design criteria as shown in Figure 2. The required percent coverage of pile caps, defined as the percentage of the total area of pile caps to that of foundation footprint, depends on the quality of fill materials. For columnar systems, the

percent coverage is equivalent to area improvement (or replacement) ratio. The percent coverage of pile caps for thirteen actual GRCSE is plotted in Figure 2 for comparison purposes (Han, 1999). As shown in Figure 2, the area replacement ratio with geosynthetic reinforcement is much lower than that suggested by Rathmayer (1975) for the conventional CSE. The percent coverage of the GRCSE systems is consistently less than 20%. The reduction of percent coverage creates a more economical solution for embankment systems. The percent coverage or area improvement ratio for GRCSE embankment systems mostly ranges from 5% to 30% (Han, 2003).
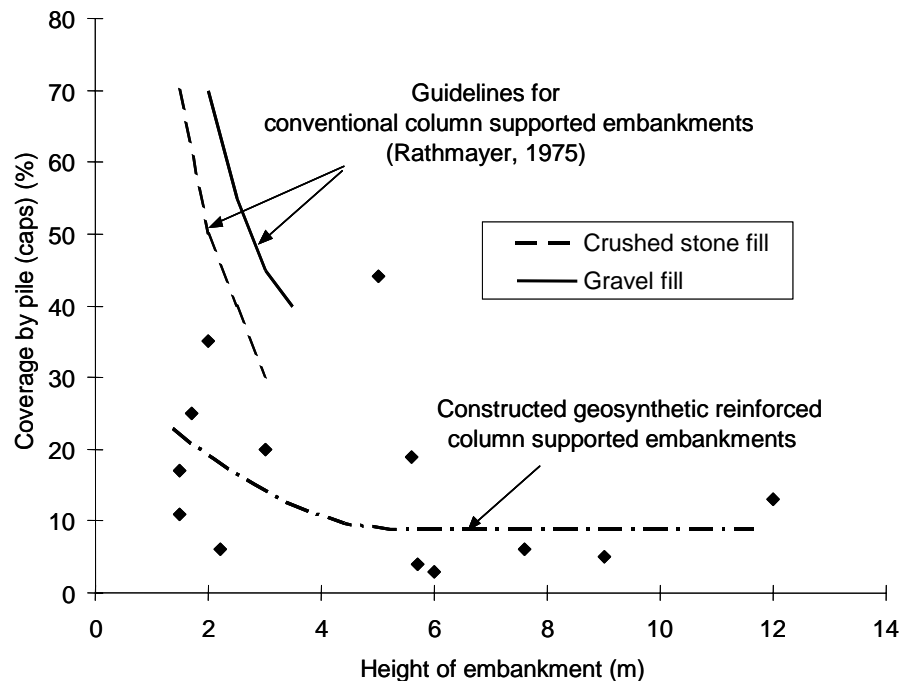
Figure 2. Percent Coverage of Pile Caps for Pile-Supported Embankments (Han, 1999)
Stress above geosynthetic reinforcement

The stresses applied on the soil (in CSE) and geosynthetic reinforcement (in GRCSE) between columns are reduced due to the soil arching effect. In GRCSE, the stress below the geosynthetic reinforcement is further reduced by the geosynthetics membrane effect. In almost all the related publications, the stress applied on the geosynthetic reinforcement is a key variable for computing the tension in geosynthetic reinforcement. Most current design methods ignore the soil resistance below the reinforcement, in other words, a void is assumed below the reinforcement. There are three categories of methods for computing the distributed stress above the geosynthetic reinforcement

1. Soil wedge method

This method has been adopted by a number of researchers, such as Carlsson (1987), Card and Carter (1995), and Svanø et al. (2000). The model is presented schematically in Figure 3. The weight of soil wedge is assumed carried by the geosynthetic reinforcement above the pile caps. Carlsson (1987) assumed $\theta = 15^{\circ}$ and Card and Carter (1995) used $\theta = 22.5^{\circ}$. Card and

Carter (1995) used this θ angle based on the condition that three geogrid layers are spaced at a certain distance and within the triangular area to form a composite load transfer platform with granular fill. Svanø et al. (2000) recommended the θ angle should vary from 15.9° to 21.8° and be calibrated.
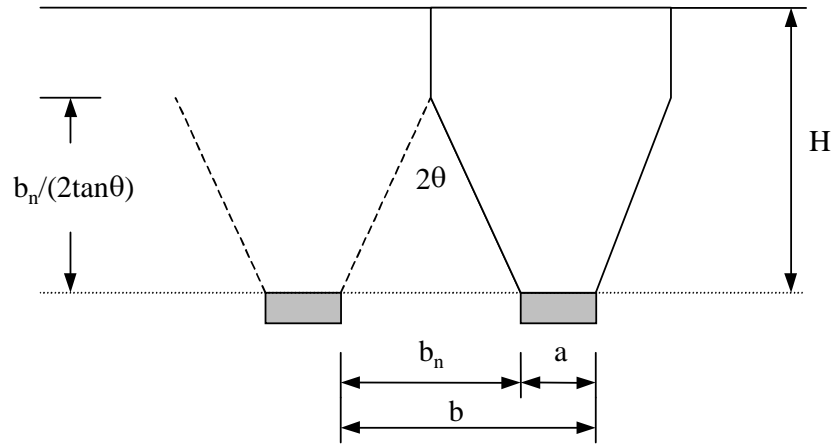

Figure 3. Soil Wedge Model

Carlson (1987) proposed a 2D approach with the height of the embankment above the triangular area so that the weight per unit length can be calculated by

$$w = \frac{(b-a)^2}{4\tan 15^\circ}\gamma \qquad (1)$$

where w = the weight per unit length of reinforcement;
    a = the width of square pile caps;
    b = the center-to-center spacing of piles;
    γ = the unit weight of fill.

Svanø et al. (2000) suggested that the load on the geosynthetic reinforcement is eventually carried by the two strips between column caps. These two strips have a width equal to that of the caps and a length equal to column spacing. They are perpendicular to each other if the columns are installed in a square pattern. This proposed method considers the 3-D effects. The weight per unit cap side length can be calculated by

$$w_s = \frac{\gamma}{2a}\left\{b^2H - \frac{1}{6\tan\theta}\left[(a + H\tan\theta)^3 - a^3\right]\right\} \qquad (2)$$

where w_s = the weight per unit pile cap side length;
    a = the width of square pile caps;
    b = the center-to-center spacing of piles;
    γ = the unit weight of fill;
    H = the height of the embankment;
    θ = the angle depicted in Figure 3.

If the height of the embankment is greater than $(b-a)/(2\tan\theta)$, $H = (b-a)/(2\tan\theta)$ should be substituted in Equation (2).

For multiple geogrid layers in the fill platform, Card and Carter (1995) suggested that each geogrid layer should be designed to carry the weight of the fill above within the soil wedge. Collin (2003) detailed the procedures for designing multiple geogrid layer-reinforced fill platform as a stiffened beam of reinforced soil that distributes the load from the embankment above the load transfer platform (i.e., stiffened beam) to the columns below the platform.
The Collin procedure is based on the following assumptions:

- The thickness (h) of the load transfer platform is equal to or greater than the clear span between columns (b-d), where d is the diameter of columns.
- A minimum of three layers of extensible (geosynthetic) reinforcement is used to create the load transfer platform.
- Minimum distance between layers of reinforcement is 20 cm.
- Select fill is used in the load transfer platform.
- The primary function of the reinforcement is to provide lateral confinement of the select fill to facilitate soil arching within the height (thickness) of the load transfer platform.
- The secondary function of the reinforcement is to support the wedge of soil below the arch.
- The entire vertical load from the embankment above the load transfer platform is transferred to the columns below the platform.
- The initial strain in the reinforcement is limited to 5%.

The vertical load carried by each layer of reinforcement is a function of the column spacing pattern (i.e., square or triangular) and the vertical spacing of the reinforcement. If the subgrade soil is strong enough to support the first lift of fill, the first layer of reinforcement is located 0.15 to 0.25 m above subgrade. Each layer of reinforcement is designed to carry the load from the platform fill that is within the soil wedge below the arch. The fill load attributed to each layer of reinforcement is the material located between that layer of reinforcement and the next layer above.

The uniform vertical load on any layer (n) of reinforcement (w_{Tn}) may be determined from the equation below:

$$w_{Tn} = [(b-d)_n{}^2 + (b-d)_{n+1}{}^2] \sin 60° \, h_n \, \gamma / [(b-d)_n{}^2 \sin 60°], \quad \text{triangular spacing} \quad (3)$$

$$w_{Tn} = [(b-d)_n{}^2 + (b-d)_{n+1}{}^2] \, h_n \, \gamma / (b-d)_n{}^2 , \quad \text{square spacing} \quad (4)$$

where b = the center-to-center spacing of columns;
      d = the diameter of columns;
      h_n = the height of soil above or between the reinforcement which is carried by the reinforcement;
      γ = the unit weight of platform fill.

2. Semi-spherical soil arching model

Hewlett and Randolph (1988) assumed the soil above the pile caps forms a semi-spherical soil arching as shown in Figure 4. The design considers possible failure of soil arching either at the crown of the arch or at the top of the column. The soil arching ratio, defined as the stress above the reinforcement to the overburden stress by the embankment, can be determined as the greater of the values in the following two equations:
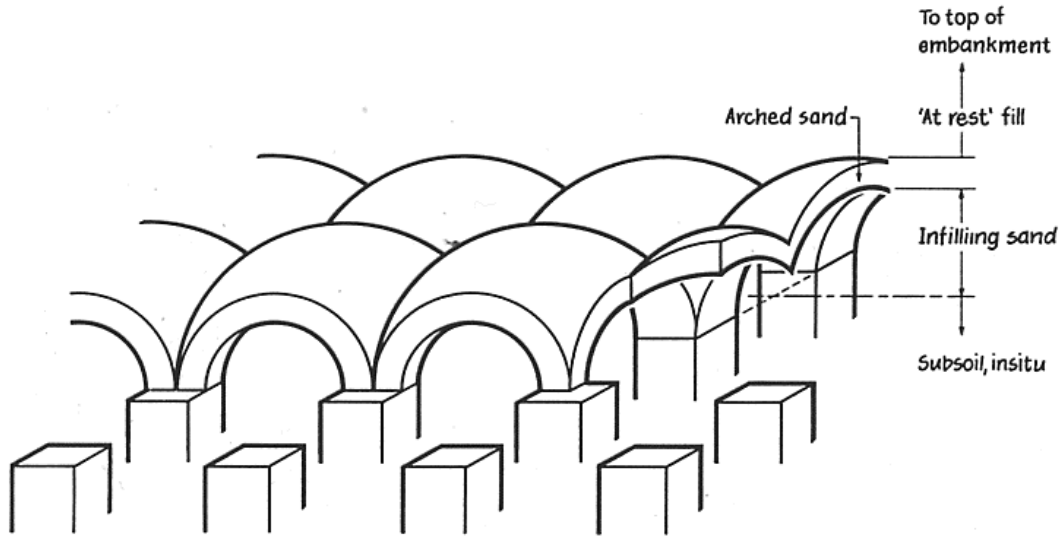

Figure 4. Soil Arching Model Proposed by Hewlett and Randolph (1988)

At the crown,

$$\rho = \left(1 - \frac{a}{b}\right)^{2(K_p-1)} \left[1 - \frac{b}{\sqrt{2}H}\left(\frac{2K_p-2}{2K_p-3}\right)\right] + \frac{b-a}{\sqrt{2}H}\left(\frac{2K_p-2}{2K_p-3}\right) \tag{5}$$

At the pile cap,

$$\rho = \frac{1}{\left(\dfrac{2K_p}{K_p+1}\right)\left[\left(1-\dfrac{a}{b}\right)^{1-K_p} - \left(1-\dfrac{a}{b}\right)\left(1+\dfrac{a}{b}K_p\right)\right] + \left(1-\dfrac{a^2}{b^2}\right)} \tag{6}$$

where   a = the width of pile cap;
         b = the spacing between centers of pile caps;
         H = the height of embankment;
         K_p = the coefficient of passive earth pressure.

Hewlett and Randolph (1988) suggested that the thickness of well-compacted high grade fill ($K_p > 3$) should not be less than the spacing of piles.

3. Vertical conduit soil arching model (British Standard BS8006)

The British Standard BS8006 considered the columns acting similar to buried rigid pipes in a conduit. The average vertical stress on the top of the column is estimated using Marston's formula for positive projecting subsurface conduits:

$$\sigma_c = p\left(\frac{C_a a}{H}\right) \tag{7}$$

$$C_a = \frac{1.95H}{a} - 0.18 \quad \text{for end-bearing columns}$$

or

$$C_a = \frac{1.5H}{a} - 0.07 \quad \text{for frictional and other columns}$$

where σ_c = the average vertical stress on the top of the column;
   p = the overburden stress at the base of the embankment;
   C_a = the arching coefficient;
   a = the width of square column;
   H = the embankment height.

The stress applied on the geosynthetic reinforcement between columns is dependent on the height of the embankment. The distributed load carried by the reinforcement between columns can be determined by

For H > 1.4(b-a):

$$w = \frac{1.4b\gamma(b-a)}{b^2 - a^2}\left[b^2 - a^2\frac{\sigma_c}{p}\right] \tag{8a}$$

For 0.7(b-a) ≤H≤1.4(b-a):

$$w = \frac{b(\gamma H + q)}{b^2 - a^2}\left[b^2 - a^2\frac{\sigma_c}{p}\right] \tag{8b}$$

$$w = 0 \text{ if } \frac{b^2}{a^2} \le \frac{\sigma_c}{p} \tag{8c}$$

where w = the distributed load per unit length of reinforcement;
   q = the uniform surcharge on the surface of the embankment;
   other symbols are defined in Equation (7).

Strain and tension in geosynthetic reinforcement

Geosynthetic reinforcement under applied stresses behaves as a tensioned membrane. A number of methods are available to estimate the strain and tension developed in the geosynthetic reinforcement.

1. Catenary method

The method presented in the reference (John, 1987) included the calculation of the strain and tension developed in the geosynthetic reinforcement:

$$\varepsilon_r = \frac{1}{2}\sqrt{1 + 16\frac{\Delta S_r^2}{b_n^2}} + \frac{b_n}{8\Delta S_r^2}\ln\left(\frac{4\Delta S_r^2}{b_n} + \sqrt{1 + \frac{16\Delta S_r^2}{b_n^2}}\right) - 1 \tag{9}$$

and $\quad T_r = \frac{1}{2}(\sigma_{sr} - \sigma_s)b_n\sqrt{1 + \frac{b_n^2}{16\Delta S_r^2}}$ (10)

where ε_r = the strain developed in the geosynthetic reinforcement;
ΔS_r = the maximum deflection of the geosynthetic reinforcement;
b_n = the net spacing between the pile caps (b-a);
T_r = the tension developed in the geosynthetic reinforcement;
σ_{sr} = the average vertical stress on the geosynthetic reinforcement;
σ_s = the average vertical stress (soil resistance) below the geosynthetic reinforcement;

The average vertical stress on the geosynthetic reinforcement can be determined based on the methods discussed above. Again, John (1987) assumed $\sigma_s = 0.15\gamma H$ (γ = the unit weight of the embankment fill and H = the height of the embankment). The procedures to determine the strain and tension developed in the geosynthetic reinforcement are as follows: (1) assume a maximum deflection of the geosynthetic reinforcement; (2) use Equation (9) to calculate the strain in the geosynthetic reinforcement; (3) calculate the tension in the geosynthetic reinforcement using Equation (10); (4) use the calculated tension and the tension-strain curve of the geosynthetic reinforcement determined in the lab to calculate the strain; (5) adjust the maximum deflection to repeat the procedures until reaching convergence if the calculated strains in Step (2) and Step (4) do not match.

2. Carlson's method

Carlson (1987) suggested a simple formula to compute the maximum deflection of the geosynthetic reinforcement over a 2-D span as follows:

$$\varepsilon_r = \frac{8}{3}\left(\frac{\Delta S_r}{b - a}\right)^2 \tag{11}$$

where ε_r = the strain developed in the geosynthetic reinforcement;
ΔS = the maximum deflection of the geosynthetic reinforcement;

b = the center-to-center spacing of piles caps;
a = the width of pile caps.

The tension developed in the geosynthetic reinforcement is calculated by

$$T_r = \frac{\gamma(b-a)^3}{32\Delta S_r \tan 15^\circ}\sqrt{1+\frac{16\Delta S_r^2}{(b-a)^2}}$$ (12)

where T_r = the tension developed in the geosynthetic reinforcement;
     γ = the unit weight of the embankment fill;
     ΔS = the the maximum deflection of the geosynthetic reinforcemetn;
     b = the center-to-center spacing of piles caps;
     a = the width of pile caps.

Rogbeck et al (1998) proposed the following 3-D modification factor to account for 3-D effects:

$$f_{3D} = \frac{a+b}{2a}$$ (13)

where f_{3D} = the 3-D modification factor;
     a = the width of the pile caps;
     b = the center-to-center spacing of piles.

Equation (13) is used to multiply Equation (12) to obtain the tension in the geosynthetic reinforcement accounting for 3-D effects.

3. BS8605 method

The method proposed in the BS8605 standard for estimating the tension in geosynthetic reinforcement between columns is as follows:

$$T_r = \frac{w(b-a)}{2a}\sqrt{1+\frac{1}{6\varepsilon_r}}$$ (14)

where T_r = the tension in geosynthetic reinforcement;
     w = the distributed load per unit length;
     a = the width of column/column cap;
     b = the center-to-center spacing of column;
     ε_r = the strain in geosynthetic reinforcement.

The BS8605 standard recommends an upper limit of 6% initial tensile strain in geosynthetic reinforcement for a general case and a reduced limit necessary for a low height embankment to prevent differential settlement at the surface of the embankment. In addition, the standard recommends a maximum creep strain of 2% over the design life.

4. SINTEF's method

Svanø et al. (2000) at SINTEF suggested that the elongation over the pile caps should be included in the calculation of the strain in the geosynthetic reinforcement. They proposed the following formula:

$$\varepsilon_r' = \varepsilon_r \left(1 + \alpha_T \frac{a}{b-a}\right) \tag{15}$$

where ε_r' = the "corrected" strain in the geosynthetic reinforcement;

ε_r = the strain considering a free span between the net spacing of column caps;
a = the width of column caps;
b = the center-to-center spacing of columns;
α_T = the tension ratio, which is defined as

$$\alpha_T = \frac{T_{rc}}{T_r} \tag{16}$$

where T_{rc} = the average tension in the geosynthetic reinforcement over the column caps;
T_r = the average tension in the geosynthetic reinforcement over the free span.

Svanø et al. (2000) did not provide any guidelines to determine the α ratio. However, the numerical study by Han and Gabr (2002) and Han et al. (2005) showed that the tension in the geosynthetic reinforcement above the column caps or columns is higher than that over the free span. Svanø et al. (2000) proposed the following equation to estimate the tension developed in the geosynthetic reinforcement:

$$T_r = \frac{w}{2}\sqrt{1 + \frac{1}{6\varepsilon_r'}} \tag{17}$$

where T_r = the tension developed in the geosynthetic reinforcement;
w = the distributed load above the geosynthetic reinforcement (two strips), which is calculated using Equation (2);
ε_r' = the corrected strain in the geosynthetic reinforcement, which is calculated using Equation (15);
b = the center-to-center spacing of piles.

5. Giroud et al. method (1990)

The tensioned membrane theory by Giroud et al. (1990) was developed for a geosynthetic layer over a sinkhole. Collin (2003) suggested the use of Giroud et al (1990) method to determine the tensile load in the reinforcement as a function of the amount of strain in the reinforcement. The tension in the reinforcement is determined from the following equation:

$$T_{rpn} = w_{Tn}\, \Omega\, D/2 \tag{18}$$

where: D = the design spanning for tension membrane, $D = (b-d)_n$ for square column spacing,
$D = (b-d)_n \tan 30°$ for triangular column spacing;
b = the center-to-center spacing of columns;
d = the diameter of the columns
Ω = the dimensionless factor provided in Table 1.

Table 1. Values of Ω

Ω	Reinforcement Strain $(\varepsilon)\%$
2.07	1
1.47	2
1.23	3
1.08	4
0.97	5
0.90	6

APPLICATIONS

The main purpose for the use of the GRCSE system is to transfer the fill loads through piles to a deeper and firm soil layer or rock beneath the soft deposit to reduce embankment settlements and instabilities. This system is most suitable for the situations where

- rapid construction is necessary;
- strict total and/or differential settlement is required.
- soft soil is underlain by a firm soil layer or bedrock;
- and or new fill with certain thickness is needed.

The GRCSE systems have been used for a number of applications worldwide, which include:

- bridge approaching embankments;
- retaining walls foundation support;
- roadway widening;
- storage tanks foundation support;
- low height embankment;
- building foundation support.

Selected case studies are discussed below.

Bridge approach embankments

Reid and Buchanan (1984) reported that this technique was used for preventing differential settlement between an approach embankment constructed over soft soil and a bridge abutment supported by long piles (Figure 5). Piles with varying lengths and spacing were designed for transiting the settlement from near zero at the bridge abutment to a relatively large settlement at the transition from the CSE to the unsupported embankment on the soft soil.   The

geosynthetic layer was placed to minimize the differential settlement between piles at the pavement surface. Two similar projects were reported by Broms and Wong (1985) using timber piles and geotextiles to support bridge approach embankments.
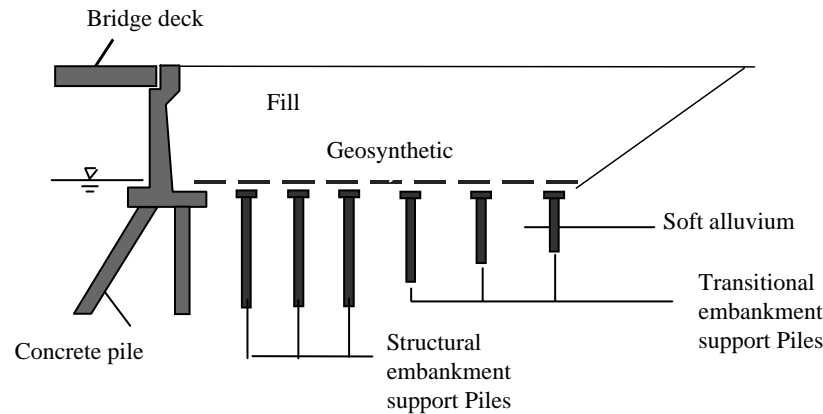
Figure 5. Bridge Approach Support Piling (Reid and Buchanan, 1984)

Retaining walls

An expansion of a highway in the northern area of Sao Paulo, Brazil included the construction of five geogrid-reinforced segmental retaining walls (SRW) with heights ranging from 2.0 to 8.2m. Fine-grained soil with 60 to 70% passing No. 200 sieve (LL<40, PI<20) was used as reinforced fill in these walls. To prevent potential buildup of pore water pressures in the reinforced fill, a drainage system with non-woven geotextile strips in the reinforced fill was installed. A portion of these walls were built on a 9m thick organic silt and clay deposit with SPT blow counts of 0 to 1. Jet-grout columns were selected for improving the very soft soil condition. The original design required 1.2m-diameter jet-grout columns spaced 2.0m on the centers. A geogrid-reinforced fill platform was introduced to enlarge the spacing of columns to 3.0m. These walls were instrumented and their settlements and lateral movements were monitored during the construction up to 90 days after the start of the construction. The typical cross-section of an SRW on a geogrid-reinforced fill platform supported by jet grout columns is illustrated in Figure 6.
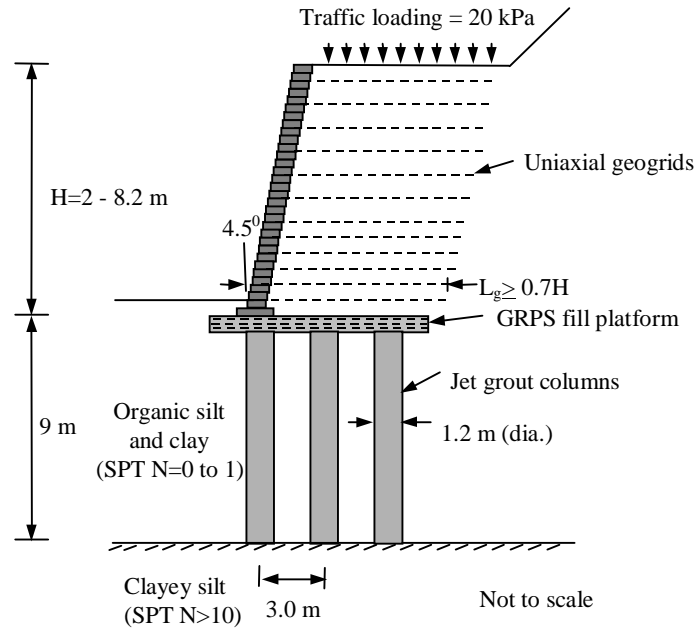
Figure 6. Typical Cross Section of SRWs on the GRPS System (Alzamora et al., 2000)

Roadway widening

Differential settlement is commonly an issue when a new embankment is constructed adjacent to an existing embankment for roadway widening. For most cases, the existing embankment has completed the settlement. The addition of the new embankment would induce not only relatively large settlement itself but also the settlement for the existing embankment. The GRCSE system was used in a project as shown in Figure 7 for preventing differential settlement between a new embankment over soft soil and an existing embankment. This project required not only the widening of the existing roadway but also the raising of the existing roadway elevation to approach a bridge. Vibro-concrete columns with enlarged column heads were used in this project.

Storage Tanks

As shown in Figure 8, the GRPS system was used in conjunction with vibro-concrete columns to minimize total and differential settlements for a storage tank founded over 3.0 to 4.5 m soft organic silt and peat (Shaefer et al., 1997). Three layers of geogrid were placed above the vibro-concrete columns to form the load transfer platform. A similar idea was adopted to construct other storage tanks in Scotland (Thorburn et al., 1984). Instead of geosynthetic-reinforced fill platform, a 150mm thick reinforced concrete membrane was placed over the piles and within the granular fill.
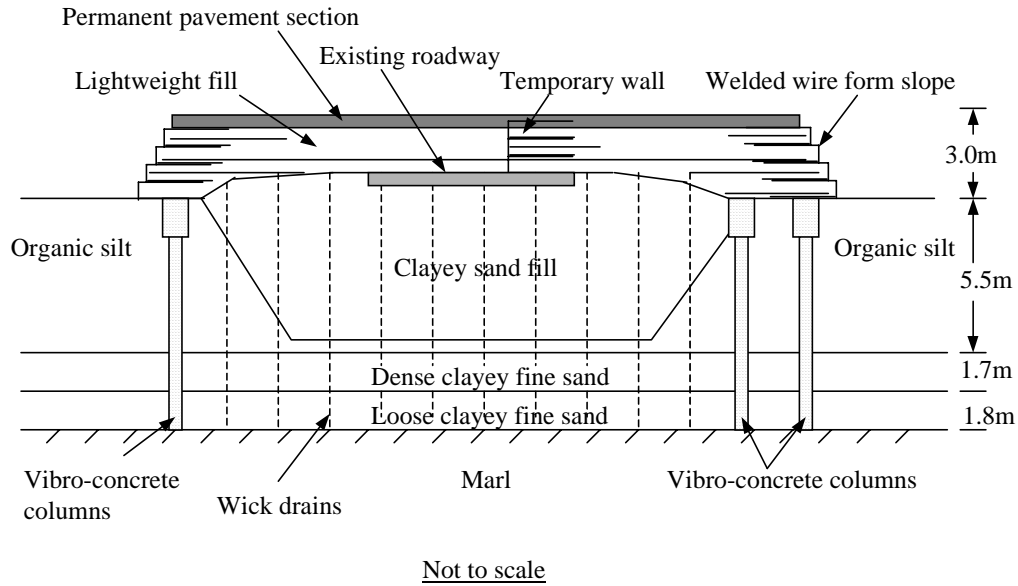
Figure 7. Typical Cross Section of Widening Roadway (Han and Akins, 2002)
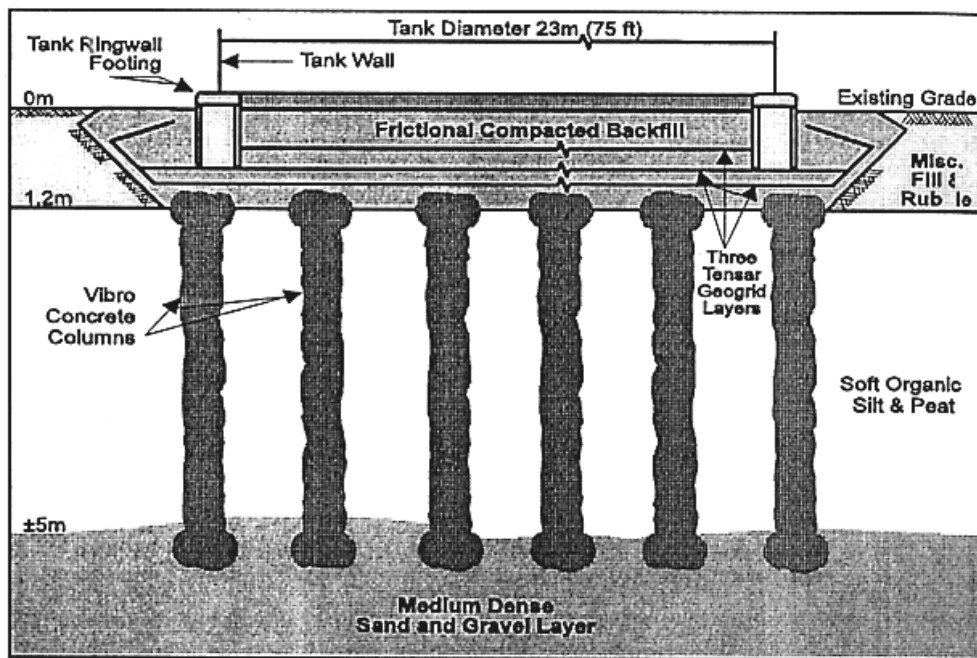
Figure 8. Storage Tank on A Geogrid-Reinforced and VCC-Supported Foundation (Shaefer et al., 1997)

Low height embankment

The major challenge of constructing a low height embankment over piles is the differential settlement between the pile caps to be reflected to the surface. The influence

of traffic loading on the settlement also becomes important. A two-lane 10m wide pavement with 2m wide sidewalks on each side was constructed on a soft foundation in Japan. The soft foundation consisted of a 4m thick peat layer with moisture content of 500% and a 4m thick clay layer. Deep mixing (DM) soil-cement columns were installed to improve the soft foundation. As shown in Figure 9, the DM columns were 800mm in diameter and spaced at 2.1m. They had an unconfined compressive strength of 1MPa. A single layer of geogrid was placed on the top of the DM columns. A relatively low (1.5m) embankment (pavement section) was constructed above the geogrid layer. The improvement ratio of 11% was used in this project, which is much less than 50 to 70% coverage of pile caps required in accordance to Rathmayer (1975) for the same height of embankments. The settlements on the top of the columns and the mid-span between the columns at the level of the top of the columns were monitored over a 15-month period. The measured results showed that differential settlements developed between the columns. The maximum differential settlement reached 15mm. In addition, The measured strains in the geogrid layer increased with the differential settlements but less than 0.5%.
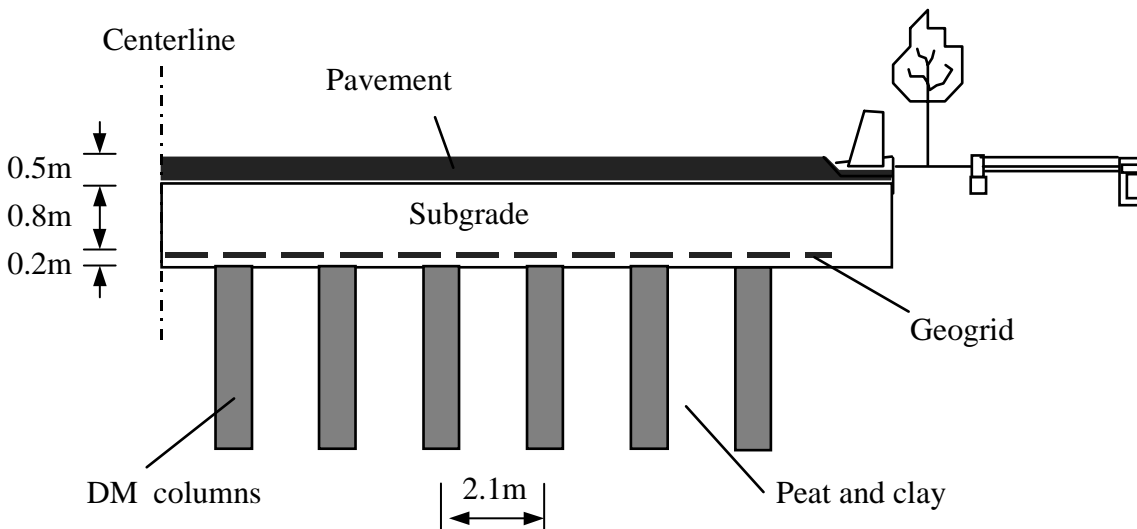
Figure 9. Low Height Embankment over Deep Mixed Columns (Tsukada et al., 1993)

Railroads

Due to the need for upgrading approximately one hundred-year-old railway between Berlin and Magdeburg, Germany, to withstand trains at a speed of 160km/h and higher loads, a geogrid-reinforced and pile-supported railway embankment was constructed over soft organic soil as shown in Figure 10. The details of this project can be found in the literature by Brandl et al. (1997) and Alexiew and Gartung (1999). Numerical analysis was conducted by Huang et al. (2005) to model this geosynthetic-reinforced pile-supported embankment and found the 3-D numerical method is reasonably accurate to estimate the maximum settlement below the geosynthetic layer and the maximum tension in the geosynthetic layers.
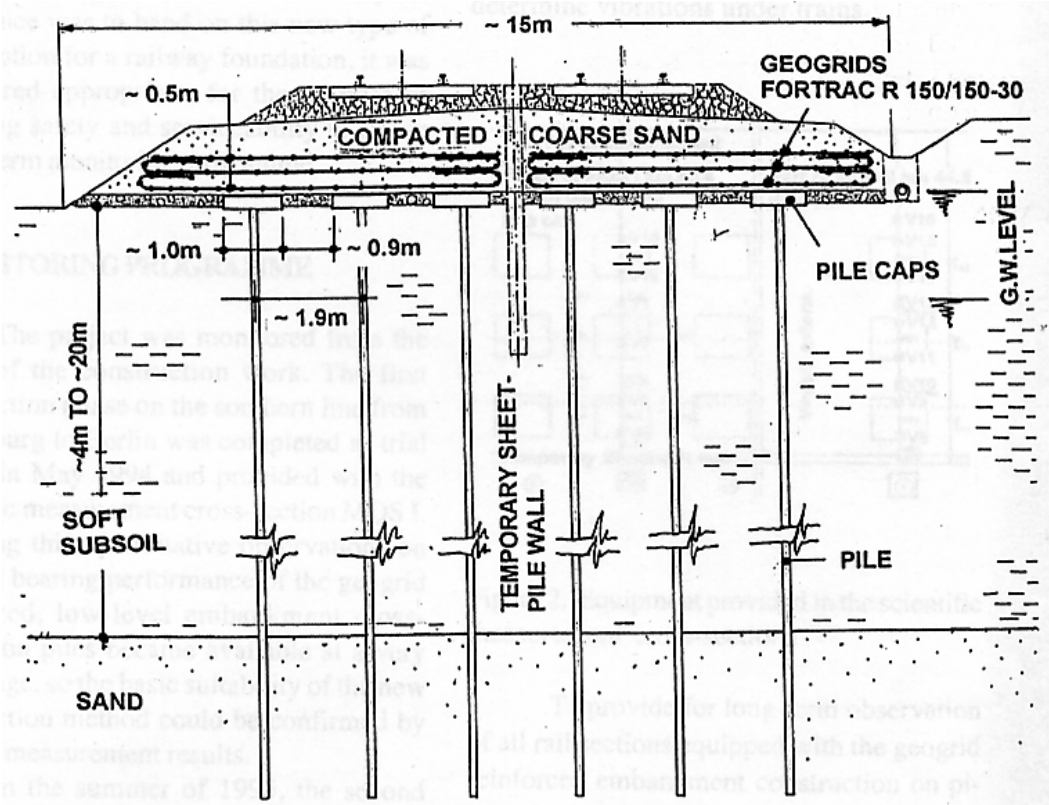
Figure 10. Railway on Geogrid-Reinforced and Pile-Supported Embankment (Alexiew and Gartung, 1999)

Buildings

Han and Akins (2002) reported the use of this GRCSE system for a building constructed on uncontrolled fill. Due to the highly variable uncontrolled existing fill and new fill with non-uniform thickness to be placed, the total and differential settlements are the major concern for this project. The GRCSE system was constructed to provide a stiffened platform to bridge over questionable underlying soils and mitigate differential settlement as shown in Figure 11. This project was designed based on numerical analysis and the predicted settlements were close to the measured. This was one of the earliest applications using geosynthetic-reinforced pile-supported fill platform for buildings.
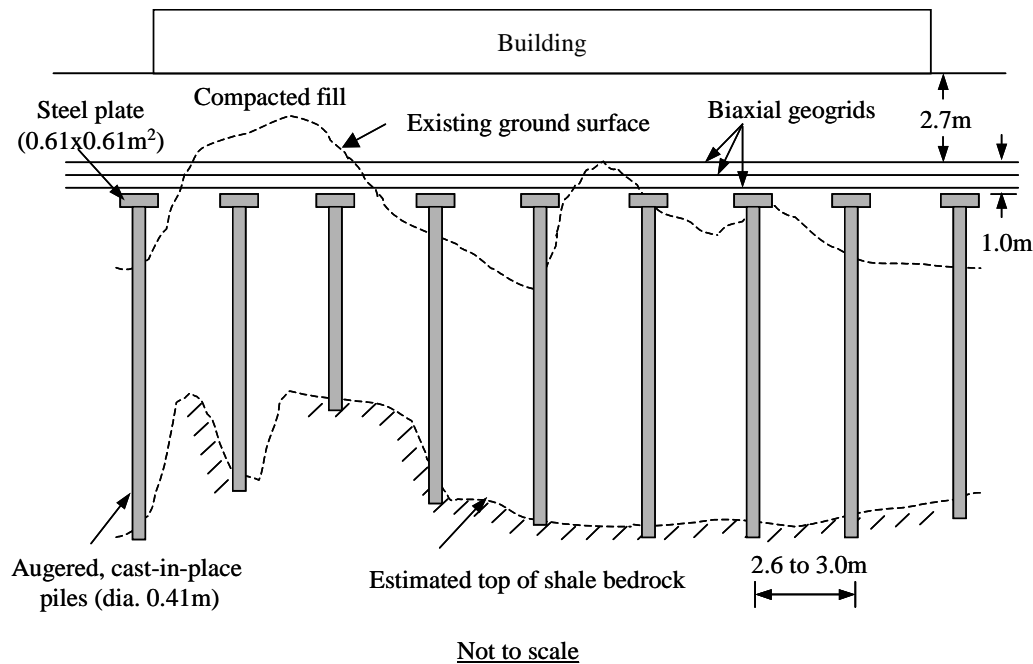
Figure 11. A Building on the GRPS System (Han and Akins, 2002)

CONCLUSIONS

The following conclusions may be drawn:

(1) GRCSE systems are most suitable for situations with a very soft soil underlain by a stiff soil layer or bedrock, new fill with certain thickness needed, rapid construction necessary, and strict total/differential settlement required;

(2) The common applications of these systems include bridge approach, roadway widening, and railroads or highways across soft soil;

(3) The use of geosynthetic reinforcement significantly reduces the required percent coverage or improvement ratio of the columns. The percent coverage or improvement ratio mostly ranges from 5% to 30%;

(4) Possible failure modes of these systems include failure of foundation soil, columns and caps, geosynthetic reinforcement and slope instability. The slope instability includes lateral spreading, local slope stability, general slope stability, and global slope stability;

(5) Soil arching, tensioned membrane or stiffened platform effects, and relative stiffness effects between columns and soil are identified as the load transfer mechanisms above the column caps or columns;

(6) Three common soil arching models are used for estimating the applied stress above the geosynthetic reinforcement;

(7) Tensioned membrane theories with different assumptions of deflected shapes are used for estimating the strain and the tension developed in geosynthetic reinforcement.

REFERENCES

Alexiew, D. and Gartung, E. (1999). "Geogrid reinforced railway embankment on piles – performance monitoring 1994 – 1998." *Proc. of Geossintéticos'99*, Rio de Janeiro, Brazil, 403-411.

Alzamora, D., Wayne, M.H., and Han, J. (2000). "Performance of SRW supported by geogrids and jet grout columns." *Proceedings of ASCE Specialty Conference on Performance Confirmation of Constructed Geotechnical Facilities*, Geotechnical Special Publication No. 94, ASCE, 456-466.

Bell, A.L., Jenner, C., Maddison, J.D., and Vignoles, J. (1994). "Embankment support using geogrids with Vibro Concrete Columns." *Proceedings, 5th International Conference on Geotextiles, Geomembranes and Related Products*, 1, Singapore, 335-338.

Brandl, H., Gartung, E., Verspohl, J., and Alexiew, D. (1997). "Performance of a geogrid-reinforced railway embankment on piles." *Proc. of the 14th ICSMFE*, Hamburg, 3, 1731-1736.

British Standard BS 8006 (1995*). Code of Practice for Strengthened/Reinforced Soils and Other Fills*, British Standard Institution, London, 162p.

Broms, B.B. and Wong, I.H. (1985). "Embankment piles." Third International Geotechnical Seminar – Soil Improvement Methods, Singapore, 27-29 November.

Card, G.B. and Carter, G.R. (1995). "Case history of a piled embankment in London's Docklands." *Engineering Geology of Construction*, Geological Society Engineering Geology Special Publication, No. 10, 79-84.

Carlsson, B. (1987). *Reinforced soil, principles for calculation*. Terratema AB, Linköping. (In Swedish)

Colin, J.G. (2004). "Column Supported Embankment Design Considerations." *Proc. University of Minnesota 52nd Annual geotechnical Engineering Conference*, Minneapolis, Minnesota.

Collin, J.G. (2003). *NHI Ground Improvement Manual – Technical Summary #10: Column Supported Embankments*.

Fluet, J.E., Christopher, B.R., and Slaters, A.R. (1986). "Geosynthetic stress-strain response under embankment loading conditions." *Proc. 3rd Int. Conf. on Geotextiles*, Vienna, Vol. 1, 175-180.

Giroud, J.P., Bonaparte, R., Beech, J.F., and Gross, B.A. (1990). "Design of soil layer-geosynthetic systems overlying voids." *Geotextiles and Geomembrane*, Elsevier, 9(1), 11-50.

Han, J. (1999). "Design and construction of embankments on geosynthetic reinforced platforms supported by piles." *Proceedings of 1999 ASCE/PaDOT Geotechnical Seminar*, Central Pennsylvania Section, ASCE and Pennsylvania Department of Transportation, Hershey, PA, 66-84.

Han, J. and Akins, K. (2002). "Case studies of geogrid-reinforced and pile-supported earth structures on weak foundation soils." *Proc. of International Deep Foundation Congress*, Geotechnical Special Publication No. 116 – *Deep Foundations 2002*, edited by O'Neill and Towsend, ASCE, Orlando, 668-679.

Han, J. and Gabr, M.A. (2002). "A numerical study of load transfer mechanisms in geosynthetic reinforced and pile supported embankments over soft soil." *Journal of Geotechnical and Geoenvironmental Engineering,* ASCE, 128(1), 44-53.

Han, J. (2003). *Development of Design Charts for Geosynthetically Reinforced Embankments on Deep Mixed Columns.* Interim Report I – Literature Review, submit to National Deep Mixing Cooperative Research Program, 123p.

Han, J., Huang, J., and Porbaha, A. (2005). "2D numerical modeling of a constructed geosynthetic-reinforced embankment over deep mixed columns." GeoFrontiers Conference, Austin, TX, Jan.

Hewlett, W.J. and Randolph, M.F. (1988). "Analysis of piled embankments." *Ground Engineering*, 21(3), 12-18.

John, N.W.M. (1987). *Geotextiles*. Blackie, Glasgow and London.

Magnan, J. (1994). "Methods to reduce the settlement of embankments on soil clay: a review." *Foundations and Embankments Deformations*, ASCE, Geotechnical Special Publication No. 40, 77-90.

Marston, A. and Anderson, A.O. (1913). "The theory of loads on pipes in ditches and tests of cement and clay drain tile and sewer pipe." Bulletin No. 31, Iowa Engineering Experiment Station, Ames, Iowa.

Pham, H.T.V., Suleiman, M.T., and White, D.J. (2004). "Numerical analysis of geosynthetic-rammed aggregate pier supported embankment." Geo-Trans Conference, Los Angles, CA, July.

Rathmayer, H. (1975). "Piled embankment supported by single pile caps*." Proceedings, Istanbul Conference on Soil Mechanics and Foundation Engineering*, 283-290.

Reid, W.M. and Buchanan, N.W. (1984). "Bridge approach support piling*." Piling and Ground Treatment*, Thomas Telford Ltd, London, 267-274.

Rogbeck, Y., Gustavsson, S., Södergren, and Lindquist, D. (1998). "Reinforced piled embankments in Sweden-design aspects*." Proc. 1998 Sixth International Conference on Geosynthetics*, 755-762.

Schaefer et al. (1997). *Ground Improvement, Ground Reinforcement, Ground Treatment Developments 1987-1997*. Geotechnical Special Publication No. 69, V.R. Schaefer et al. (ed.), 616p.

Shen, S. L., and Miura, N. (2001). "A technique for reducing settlement difference of road on soft clay." *Computer Methods and Advances in Geomechanics*, *Proc. 10 IACMAG*, Vol.2, Edited by C.S. Desai et al., A.A. Balkema, 1391-1394.

Stewart, M.E., Navin, M.P., and Filz, G.M. (2004). "Analysis of a column supported test embankment at the I-95/Route 1 interchange." Geo-Trans 2004 Conference, Los Angles, CA, July.

Svanø, G., Ilstad, T., Eiksund, G., and Want, A. (2000). "Alternative calculation principle for design of piled embankments with base reinforcement*." Proc. 4th International Conference on Ground Improvement Geosystems*, Helsinki, June.

Terzaghi, K. (1943). *Theoretical Soil Mechanics*, John Wiley & Sons, New York, 66-75.

Thorburn, S., Laird, C.L., and Randolph, M.F. (1984). "Storage tanks founded on soft soils reinforced with driven piles." *Piling and Ground Treatment*, Thomas Telford Ltd, London, 157-164.

Tsukada, Y., Isoda, T., and Yamanouchi, T. (1993). "Geogrid Subgrade Reinforcement and deep foundation Improvement: Yono City, Japan." *Proceedings, Geosynthetics*

Case Histories, International Society for Soil Mechanics and Foundation Engineering, Committee TC9, 158-159.

Wang, M.C., Feng, Y.X., Jao, M. (1996). "Stability of geosynthetic-reinforced soil above a cavity." *Geotextiles and Geomembranes*, Elsevier, 14, 95-109.

Zanzinger, H. and Gartung, E. (2002). "Performance of a geogrid reinforced railway embankment on piles.""Geosynthetics -–7th ICG, Delmas, Gourc, and Girard (eds.), Swets & Zeitlinger, Lisse, 381-386.

INVESTIGATING THE POTENTIAL IMPACTS OF PAST MINING ACTIVITIES, ON THE WIDENING OF SR 68, MOHAVE COUNTY, ARIZONA

Robert Cummings, P.E., Saguaro GeoServices, Inc. [1]
Nick Priznar, Arizona Department of Transportation[2]
presented at the
55th Highway Geology Symposium, Kansas City, Missouri, September 2004

ABSTRACT

A proposed expansion of Arizona State Route 68 in northwestern Arizona (Figure 1), required due to dramatic growth in the Laughlin, Bullhead City, and Las Vegas areas, was realigned to avoid undermined areas of the Arabian Mine group. The Arabian is an inactive underground mine that recovered precious metals from pre-1917 into the 1930s, using the shrinkage stoping method. Workings exposed at the surface (inclined shafts, drifts, open cuts, and stopes) were within a few hundred feet of the (then) two-lane highway. The mine was developed along a vein system that roughly parallels the highway, and the workings, including large, open voids, extended in the direction of the highway. In 1991, a mine survey and underground reconnaissance confirmed the presence of large open stopes. Deeper reconnaissance was not possible because the workings were flooded. However, the observations raised questions about the long-term stability of the deeper workings, thought to underlie or adjoin future roadway improvements. Cross hole acoustic tomography, conducted under a cooperative agreement between ADOT and the U.S. Bureau of Mines, disclosed the presence of underground voids approximately in the expected locations, but could not resolve the exact dimensions of the voids, nor the condition of the surrounding rock. Inasmuch as future stability of the workings could not be assured, especially given a history of domestic water extraction from the workings and statements of future mining intentions by the property owners, a decision was ultimately reached to relocate the expanded, four-lane SR 68 in an area known to be free of undermining.
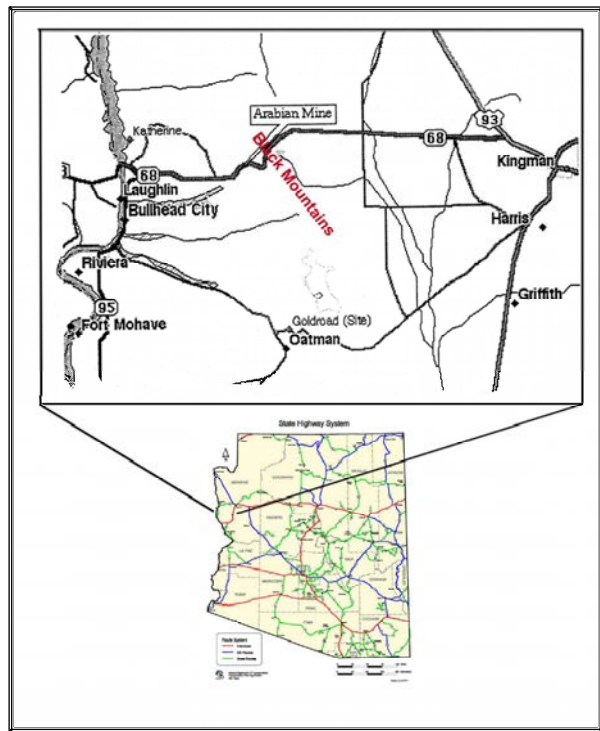
Figure 1 – Project location

---

[1] President, Saguaro GeoServices, Inc., P.O. Box 44154, Tucson, AZ 85733

[2] Engineering Geologist, Materials Group, 1221 North 21st Avenue, Phoenix, AZ 85009

BACKGROUND

In northwestern Arizona, Arizona State Route 68 runs from a point north of Kingman westward into Bullhead City. The project area (Figure 1) is along SR 68 about 9 miles east of Bullhead City, at the Arabian Mine. It is in the southwestern foothills of the Black Mountains, which are part of the Basin and Range Physiographic Province on the eastern flank of the Lower Colorado River Corridor.

The project area is situated in the arid Mohave Desert Region where the annual precipitation averages a little more than 5 inches per year. During the summer months, temperatures can easily exceed 100 degrees. Because of the climate of the region, soil cover is poorly developed and chiefly confined to slope debris and Quaternary alluvial soil deposits (Figure 2). Desert vegetation is quite sparse, and most of the individual plants are small. Desert vegetative species primarily consist of creosote, catclaw, and thorny ocotillo, with occasional palo verde and ironwood trees.

Figure 2 – Physiography near the Arabian Mine

Geologic Setting

The Black Mountains are dominantly composed of three sequences of middle to early Tertiary aged volcanic rock. In order of deposition they are known as the: Patsy Mine, Golden Door, and Mount Davis volcanic sequences. These volcanic deposits occur in varying unconformable and/or faulted contact with an older Precambrian metamorphic and igneous complex locally known as the Katherine Granite.

Regional faulting consists of two dominant sets of northwest to southeast trending faults, which appear to roughly parallel the orientation of the Black Mountain Range. According to Longwell (1963), "Most of the faults are normal, but at least two of the largest have reverse displacement along much of their exposed lengths. Blocks between the faults are generally tilted, and in the tilting movement several large faults were rotated to low angles of dip." In contrast to these regional trends, the project area exhibits an exceptionally persistent northeast to southwest trending, east dipping set of discontinuities we have referred to as the Arabian Fault Zone. These structures separate the Precambrian Katherine Granite Complex from the Tertiary volcanic sequence.

The region has been widely explored for precious mineral deposits over the past 150 years. According to Faulds and others (2000), Miocene dikes and veins of rhyolite, andesite, quartz, and calcite, have intruded pre-existing easterly dipping faults and are associated with mineralization in the Katherine District. Outcrops in the vicinity of the Arabian Fault Zone

appear to support this observation. A portion of a recent geologic map (Figure 3) shows the local geology.

Changes in base level and meandering of the Colorado River have created additional Tertiary alluvial sediments in the form of river and lake deposits isolated from the existing incised drainage channel. Uplands consist of a dissected pediment, alluvial fan and bajada morphology with overlapping terrace deposits, which are interrupted by relic monoliths of weirdly shaped volcanic materials that punctuate much of the region's slopes.
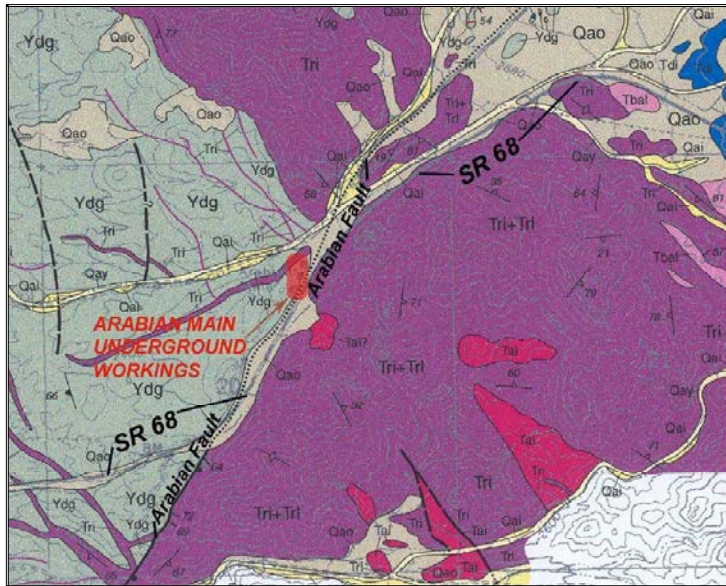
Figure 3 – Area geology (after Murphy, 2003)

Development of the SR 68 Corridor

The exact origin of the route is lost to history; however, it lies very near overland trails utilized by the Captain Lorenzo Sitgraves survey expedition exploring a transcontinental railroad route in 1851.

Although it is now hard to envision, the Colorado River was for many years a navigable waterway. As early as 1871, ships from San Francisco sailed to Mexican ports in the Gulf of California. There, goods and passengers transferred to shallow draft steam powered boats to travel to numerous points along the Colorado River. A site now known as Katherine Landing provided primitive embarkation facilities to the military and mining pioneers of latter part of the 19th century.

As local roads developed, they tended to originate from sites near the river and migrate away to livestock watering facilities or centers of commercial interest. Therefore, until late in the 19th century, unimproved dirt roads connected the river to mining properties along routes most easily accommodated by terrain. During those years, the complete isolation of the district resulted in mining companies shipping their ores to Europe for processing.

Construction of the Atchison Topeka and Santa Fe Railroad redirected commercial interests towards the railhead at Union Station (eastern foot hills of the Black Mountains). A primitive road was established (by 1909) to connect the mining supply center in Chloride, Arizona over Union Pass to Nevada via a ferry across the Colorado River. This route is shown on a map that is part of USGS Bulletin 397, and is probably part of the Katherine Mine Road or the road to Hardyville.

Until the 1940s, there was no graded roadway past the Arabian Mine, along what then became

Figure 4 – USBR construction of what is now SR 68

SR 68. The US Bureau of Reclamation undertook significant modernization to the former routes during the construction of Davis Dam (circa 1942-1953) (Figure 4). The regrading and paving facilitated transportation of power generating equipment (by tractor trailer), from the established railheads over the Black Mountains to the dam site on the Colorado River.

ADOT Project No. S-10(1) constructed in 1946 established a 24' wide, 2.5" thick mixed bituminous surface on varying thickness of select base course for 26 miles over mountainous terrain. The highway plans recommended 1.5:1 fill slopes and a 4.5% to 5% grade. The plans indicated that the new highway would overlie existing abandoned mine workings in the vicinity of Arabian Wash.

The westbound descent from the summit of Union Pass consists of almost 12 miles of 5% - 6% grade that terminate on the outskirts of Bullhead City. Within the last 30 years, a tremendous increase in the region's population and transportation infrastructure has resulted from the gambling and tourist industry in Laughlin Nevada. Traffic demands, combined with the long, unbroken steep grade to Union Pass and the high summer temperatures, created long queues of traffic, and mandated modification of the two lane rural road. Some climbing lanes were developed in the early 1990s, but none in the Arabian mine area. In 1992 a portion of the highway just south of the main underground workings was realigned to improve a hazardous curve and correct a site distance limitation. At the time, project designers became aware of past mining activities and the history of the road being constructed over abandoned workings.

In the late 1980s, ADOT began working on a corridor study to develop a comprehensive solution to the increasing demand. The final recommendation was a four lane divided highway with 38 ft paved roadways and 46 ft to 16 ft medians. Opposite the mine, two new westbound lanes would be added. As the project developed, concern about potentially hazardous conditions led to the investigation of the Arabian Mine and Rising Fawn underground mine workings close to the roadway alignment.

Arabian Mine History and Development

The Arabian Mine property consists of three patented claims (southwest to northeast, the Perry, Rising Fawn, and Resaca), and a large group of adjoining unpatented claims including the New Philadelphia (Figure 5), which adjoins the Resaca on the northeast, in Section 20, T21N, R20W. The Rising Fawn was staked just after the turn of the century and was followed soon after by the other patented claims. By 1915 considerable underground workings had been developed and the major shafts on the property (including the Philadelphia Nos. 1 and 2, and the R-A, R-1 and R-2 shafts) had been sunk, along with several hundred feet of drifting.
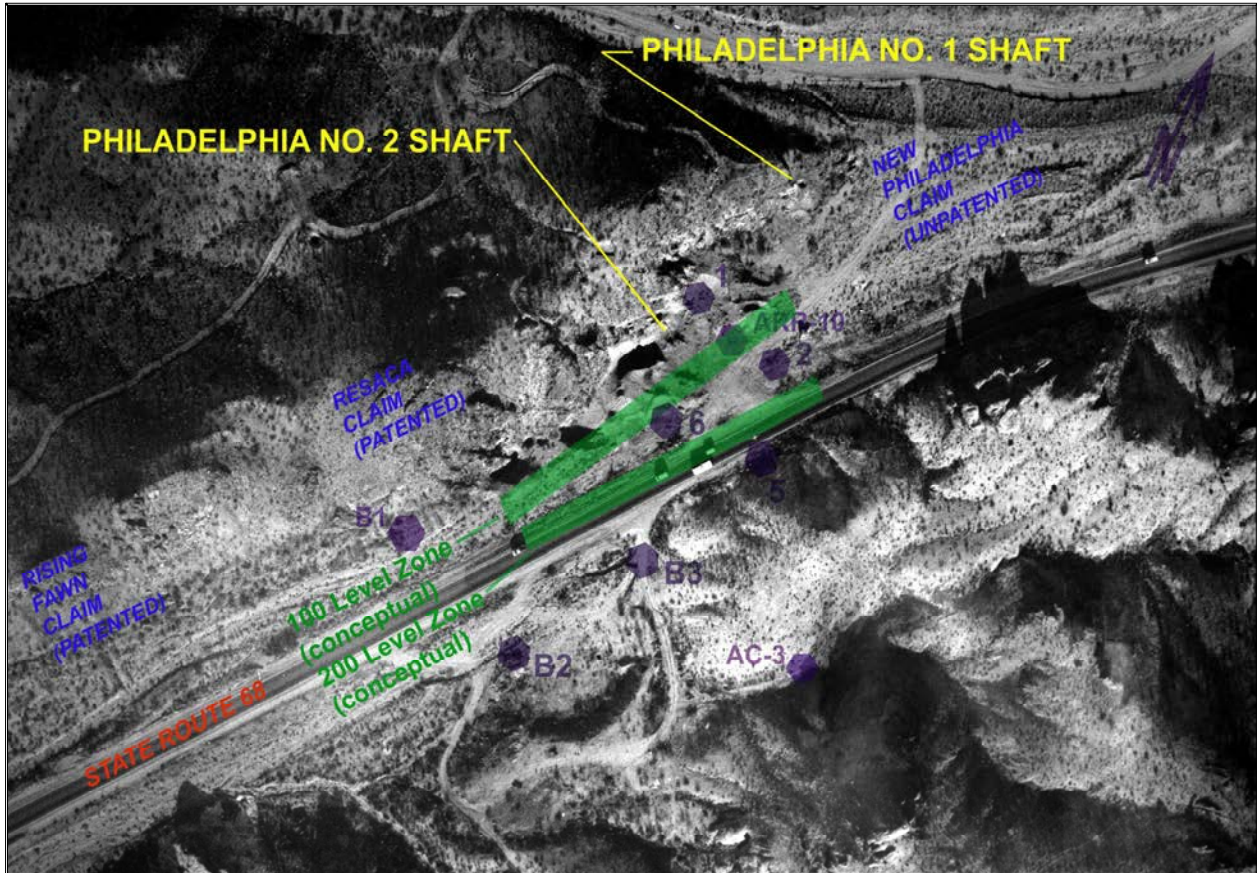
Figure 5 – Arabian Mine features. The SR 68 new lanes would be west of the existing.

The main mine was worked intermittently into the 1930s. The principal mined commodity was gold, occurring largely as free gold within a crushed quartz matrix. Production reportedly reached 50 tons per day during some periods of operation; altogether, production was in the neighborhood of 50,000 tons.

Apparently, early production and mine access were through the R-1, R-A, and R-2 shafts. Careful cross-checking of field conditions against the records show that stoping conducted after 1930 (probably between 1934 and 1938) has obliterated these shafts.
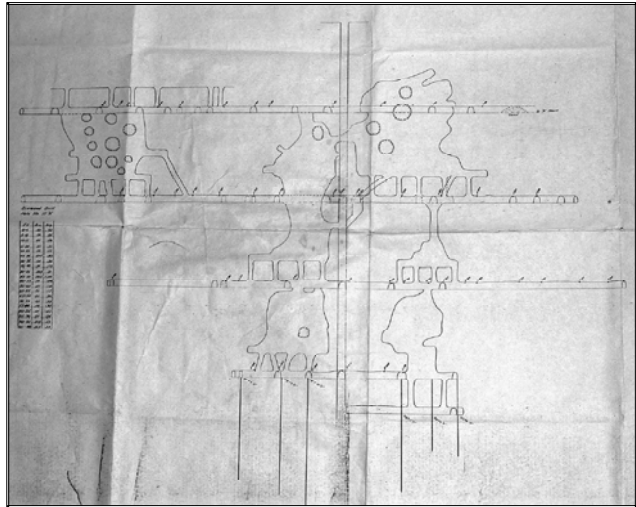
Figure 6 – Stope map by G.F. Chock, 1938

Following a dispute with the former mine owners, the Mines Company developed the Philadelphia No. 1 and Philadelphia No. 2 shafts on an adjoining claim to the northeast. The No. 2 became the main production shaft for the operation. This shaft was 280 ft deep by 1915, according to old mine reports. Sometime after 1930, a survey by a G. F. Chock (undated but traced by a Fred W. Becker in November 1938) was used to generate a longitudinal section in "the plane of the vein", and is the only depiction of the stopes developed (Figure 6). This section shows the Philadelphia No. 2 to extend below 300 ft, with levels and stoping to what appears to be the 250 ft level. Other records indicate that the Philadelphia No. 2 Shaft reached 500 ft, but there are no records indicating stoping to this depth. The shaft was originally timbered through a muck pile and is inclined about 60 degrees just below the collar, flattening with depth to about 53 degrees. Most of the records agree that levels exist at 100 and 200 ft; other records mention levels at 80 ft and one map shows a sublevel originating along the Philadelphia No. 1 Shaft at 60 ft. The 100-level drift between the Philadelphia No. 1 and Philadelphia No. 2 shafts was reported as caved in 1931, and there are no reports that it was reopened.

Stoping was reportedly accomplished through shrinkage methods. In addition to the stopes shown on the Chock survey, several large stopes break open to the surface as tabular voids 5 to 15 ft across with random pillars (refer to Figure 6), dipping moderately, and widening beneath the surface. These surface stopes were probably the ones that removed the R-1, R-2, and R-A shafts, and were extracted after Chock did his survey. This indicates that at the Arabian, as with most abandoned metal mine projects, the available records typically portray the underground openings; undocumented workings exist.

Figure 7 – Crosscut ending in gravel off the Philadelphia No. 1 shaft

Underground, the workings run chiefly along the strike. Crosscutting is indicated on old maps to have reached the footwall contact with the granite and the hanging wall contact with the gravel (Figure 7). This means that there is an efficient subsurface hydraulic connection between ground water and the workings. In fact, the workings are flooded below the 100 level and water has been extracted – in small quantities – in the past. Because of the flooding, none of the mine levels

below the 100 level can now be accessed without extensive pumping of the mine. Water levels now are very similar to those reported in the records from as long ago as the 1930s.

Other miscellaneous workings, including several shafts and an adit extending back into the granite footwall mass, are found several thousand feet southwest of the main mine workings. The shafts are presently filled a short distance below the surface. The hilltop behind the workings contains numerous trenches, shallow prospect pits, and short adits, all of which are above the main shaft elevations (Figure 8).

Figure 8 – Panoramic view of Arabian Mine site with realigned curve at extreme left

According to USBM Information Circular 6901 (1936) the mine was taken over by a new owner in 1933. In that year the mine produced 593 oz gold and 1,156 oz silver. In 1935, mining was actively proceeding.

Also, in 1934-1935, gold was recovered from a surface operation known as the Arabian Cut, on the Rising Fawn claim a little over 1,000 ft south of the underground workings, opposite the future curve realignment (Figure 9). According to the Arizona Department of Mineral resources in a report dated October 9, 1940, some development took place in the Philadelphia No. 1 shaft by new owners.

Figure 9 – Arabian Cut

Production essentially ceased in 1942 due to the Gold Order. Reportedly, new owners have intermittently recovered small quantities of ore since 1980. Various major mining companies reviewed the property over the years but none has undertaken more than exploratory boreholes. In the 1990s, the mine owners commissioned studies of open pit potential in the former Arabian Cut area.
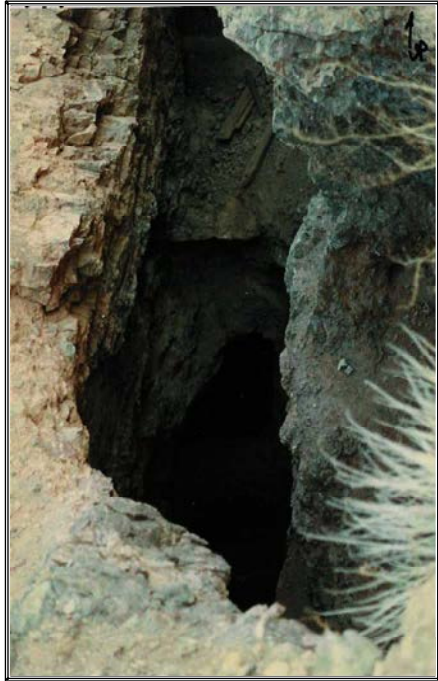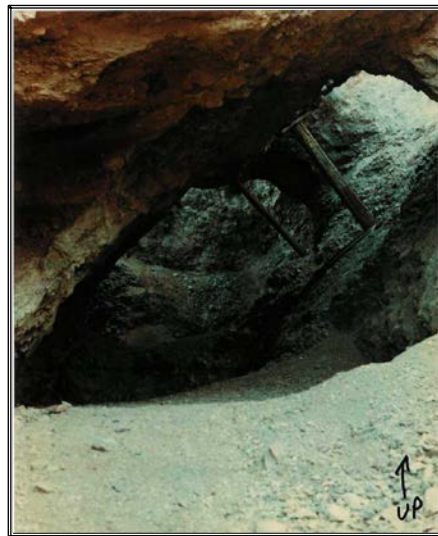
Figure 10 – Stopes open at surface

Figure 11 – Stopes used for water extraction

By the time it came under consideration for roadway widening, the Arabian Mine had not been worked for some time. Some open stopes were evident at the surface (Figure 10). Other workings consisted of shallow holes connecting former stopes (Figure 11, note small diameter polyethylene pipe used to extract water).

By the time ADOT commenced its studies, open stopes and shafts had stood for decades; some had remained open since the mine's period of active operation (compare Figures 12 and 13, next page), with remarkably few changes. Fencing of these very hazardous openings had deteriorated to where it was almost totally ineffective in denying casual public access. ADOT installed chain link fencing and razor wire to mitigate the hazards.

Mine Geology

The mine was developed along a steeply dipping rhyolite dike that intruded an older granitic mass, apparently along a significant fault zone. The shallower portions of the hanging wall of the dike contact gravel fill that comprises the adjacent wash (see Figure 14, next page, and Figure 7). Inasmuch as the wash drains a considerable portion of the surrounding upland terrain, the mine was wet during the period of operation, reportedly making about 35 gpm. Even today, the mine pool can be seen from the surface in some open stopes.

Lausen's (1931) description of the Arabian Mine geology was referenced for the study since most of the underground workings are inaccessible:

"At this time, a rhyolite-porphyry dike intrudes, and along the hanging wall of this dike, the rhyolite tuff has been faulted against the dike. The vein occurs in the dike, close to the fault and strikes northeastward while the dip is 82 degrees to the southeast. A mineralized zone, thirty feet wide and consisting of a number of quartz stringers, occurs in the rhyolite dike and, to a certain extent, in the granite footwall. The individual veinlets of this zone vary in width from a fraction of an inch up to twelve inches or more. The veinlets are chiefly quartz, but in some places, consist of coarse-grained gray calcite."
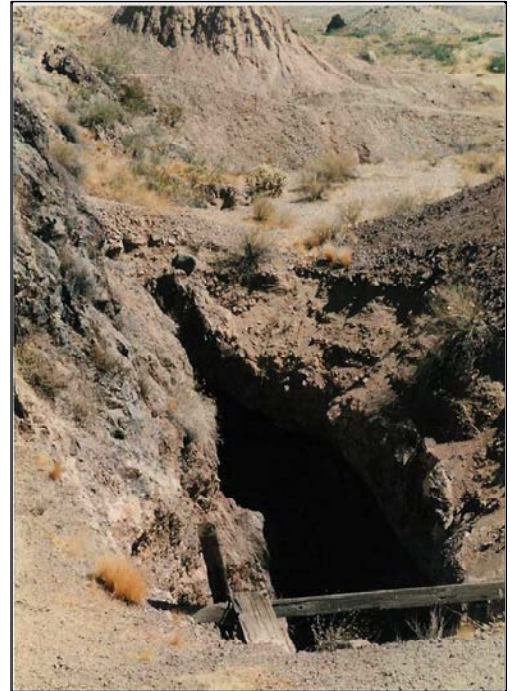
Figure 12 – 1930s view of stope and headframe

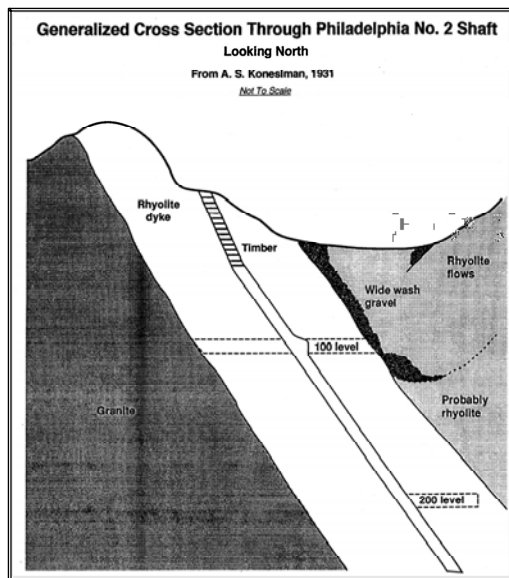Figure 13 – 1990s view of area in Figure 12

Figure 14 – Conceptual cross section through Arabian vein

The deeper portions of the dike hanging wall are in fault contact with porous rhyolite tuffs. The mineralized zone reportedly averaged about 30 ft wide, chiefly within the dike but also extending into the granite footwall, consisting of quartz stringers. Although Lausen notes that the Arabian vein dips 82 degrees overall, the inclinations of the main production shafts, the Philadelphia No. 1 and Philadelphia No. 2 shafts, do not match the steep inclination of the vein, but have a shallower slope in their accessible reaches.

APPROACH

The study of the mine and its potential impacts on the expansion of SR 68 began with a literature search.   Shortly thereafter, in order to relate the physical position of the workings with the proposed alignment, and also to ascertain the present condition of the workings, a mine survey and reconnaissance was contracted. That work led to a program of geotechnical borings and cross-hole geophysics to further resolve the underground conditions. Attempts were made to

secure a borehole video camera capable of obtaining imagery of suitable quality in the water-filled stopes. No suitable equipment was located that met the budget and time constraints at the time.

LITERATURE REVIEW

As part of the corridor analysis it was necessary to review the original construction documents from the 1942 road building efforts. It was discovered that the roadway had been built over abandoned mine workings. Examination of the vicinity during a field review identified several areas that exhibited unsecured mine workings of significant depth.

Beginning in the early 1990s, a search was conducted at the local historical society to determine if any of the original engineering documents had survived and was now part of the public record. The property owner was contacted to determine what materials were available for review. The U.S. Bureau of Land Management was researched to locate land and mineral survey maps and notes. Additionally many other state and federal agencies were contacted that may have details about the mining activity at the project area and in the region. Technical journals, newspapers, and district reports were also investigated for published articles that related details about the production activity of the mine.

Figure 15 -- Arabian Mill circa 1930

Fortunately, some underground mine surveying records had been preserved as historic documents, for assessment of the general geometry of the mine workings and mining methods. Unfortunately, development on the property had continued beyond the survey date and there was a lot of speculation about what progress had been made before the mine was closed in the 1940s. Not unexpectedly, some records were found to conflict with others, and it became difficult to separate factual from anecdotal information. Reliable information came from the few photographs available from the mine's period of operation (for example, Figures 15 and 16) and some authoritative reports whose data were confirmed by other records. The most serious information gaps related to the actual depth of mining, the widths of stopes at the close of active mining, and the actual inclinations of the Philadelphia No. 2 shaft and the stopes. These are critical factors in ascertaining the degree of undermining of the highway. In addition, the records contained hazy references to a connection
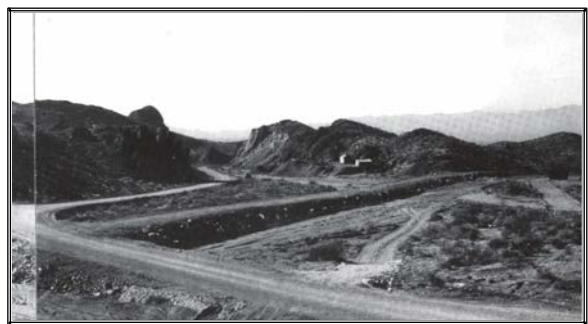

Figure 16 – Mine site and mill (unknown date)

between the main workings and the workings on the Rising Fawn claim, including a reference to a 60-ft-deep shaft that may have underlain the roadway near the realigned curve.

Despite the shortcomings, the literature survey offered an opportunity to at least qualitatively relate the location of underground mine workings to that of the highway corridor. A dependent resurvey of the original land lines with recorded ties to the main shafts was attempted. Most of the original survey monuments were no longer in existence; therefore, only an approximate location was possible. It was determined that further study of the mine maps should be made in conjunction with underground reconnaissance.

Figure 17 – Accessing the Philadelphia No. 1 shaft and removing hazardous ladders

MINE SURVEY AND RECONNAISSANCE

In 1991, ADOT contracted with the Tucson office of Engineers International, Inc. (EI), an engineering firm that specialized in mine stability and mine subsidence, to document the occurrence and condition of accessible underground workings with respect to the proposed roadway improvements and right of way. Accessible portions of the underground workings were inspected, mapped and surveyed to the extent that safe access permitted. From this information, additional confidence was gained in extrapolating the location of the inaccessible workings from the available records and surveys. The underground workings were inspected under a Site Safety Plan for confined space entry written by EI and approved by ADOT.

Figure 18 – Philadelphia No. 2 shaft in 1991

Subsurface access was obtained using ship's ladders. At the Philadelphia No. 1 Shaft, the ship's ladder was hung over a pipe framework placed over the shaft collar (Figure 17). The Philadelphia No. 1 shaft collar timber was found to be in good condition. Hazardous old ladders and other debris were hoisted out of the shaft and discarded. The ladders were later destroyed to prevent unauthorized replacement of these hazards into the shaft. At the Philadelphia No. 2, there was no safe way to set the pipe framework without disturbing an old timber loading platform and the debris atop it (Figure 18). Instead, pins were set at the collar to affix the shaft ladder at the surface. Concern for damaging the shaft collar timber, and the very limited working room around the collar, prevented more than 35 ft of ship's ladder from being lowered into the
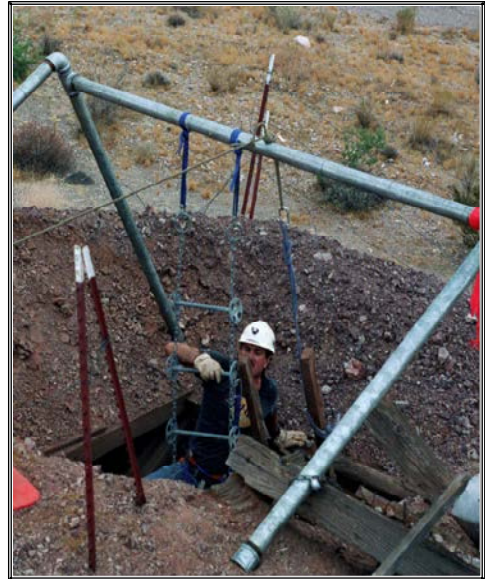
Philadelphia No. 2 shaft. Further access had to be gained by climbing down the shaft's old steel rail. Safety considerations prevented the transport of gear needed for deeper ventures. This limited the investigation of the No. 2 shaft to horizontal, continuous, and foot-accessible workings.

Because not all portions of the underground workings were accessible, it was not feasible to directly observe and measure the position, dimensions, and condition of the deeper workings, some of which were apparently developed subsequent to the available records. The underground survey pertained to those workings that were safely accessible without extraordinary effort.

The scope entailed an initial reconnaissance and site briefing, the underground survey with photographic documentation, and the preparation of mine level maps and cross sections showing the relation of the workings to surface features. Standard mine surveying methods were used. The general conditions of the accessible workings were observed and recorded with notes and photographs. The initial reconnaissance included an overall site inspection with notation of all surface features according to station and offset from roadway plans provided by ADOT. The principal surface workings were tied into the existing survey control.

Figure 19 – 100 Level stope off the Philadelphia No. 2 shaft

Workings recorded in the survey, or indicated in the records, were depicted on maps and cross sections, relative to the location of the roadway corridor. The assessment of the integrity of the mine workings and the likelihood and character of potential threats to the roadway due to the presence of the workings underneath (particularly the stopes), could not, because of the flooding, be observed directly. Underground observations did show that the stopes could not be accurately described as regular, tabular voids that have consistent orientations (Figure 19).

Comparison of the old records with present conditions reveals that the Philadelphia No. 2 shaft no longer collars at the same elevation it originally did. Shaft timbers once extended about 44 ft below the collar; they presently stop a little over 10 ft down, apparently from unrecorded mining of the dump material that once comprised the shaft walls. The remaining timber was found to be mostly loose and hanging, with free-running gravel behind, making mine entry hazardous. The inclination was measured at 48-50 degrees, slightly steeper in the timbered portion.

The Philadelphia No. 1 shaft is inclined downward at an angle of 57 degrees. It opens at the bottom into a chamber (Figure 20, next page) that probably served as the shaft station and loading station. Rock conditions in the shaft itself are excellent. Branching drifts appear to be the same ones shown on a 1916 survey map, which corresponds quite closely to the results of the

EI survey. None of the Philadelphia No. 1 workings appears to persist as far as the roadway. The furthest drift to the east is nearly filled to the back and stops at the contact with the gravel (see Figure 7). The entire level seems to be above the water level at all times, and there are no drips or seeps, although some locations of minor past seepage were noted. The gravel is very dense and compact, and tends to fall in chunks. It may be weakly cemented. The ribs in general are drummy and the rhyolite, though silicified and intensely fractured or crushed without much clay, is fairly soft. One fault contains as much as 1 ft of slickensided, clayey gouge, and has spalled moderately (Figure 21). The stability of the workings is probably attributable mostly to the absence of rock stress, owing to the shallow depth.

Figure 20 – Chamber at bottom of Philadelphia No. 1 shaft, with crosscut ahead

From the No. 2 shaft, it was seen that the stopes are very extensive both down the dip and along the strike. It was possible to discern the continuation of the 100 level past the stope in both directions, although reaching them was impossible due to interfering workings and loose zones.

The accessible portions of the 100 level agree closely with Chock's and other maps. However, it appears that an ore chute was added above the stope on the south side of the No. 2 shaft that is not shown on any maps, and this suggests an unknown shallower stope and some deeper workings. To the north, the 100 level has been partially filled with muck. To the south, the level cannot be accessed from the shaft. To do so would require
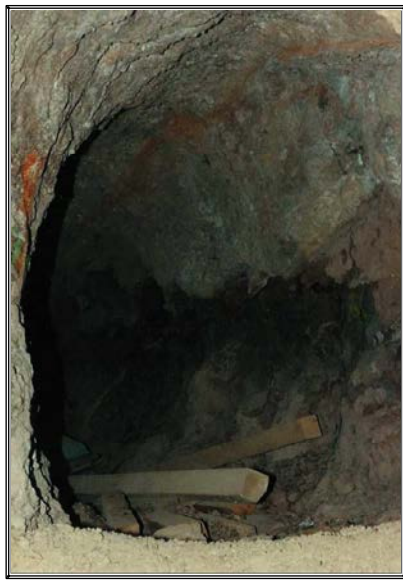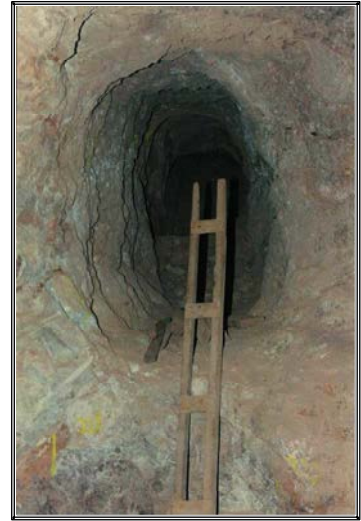

Figure 21 – Rib spalling in fault zone, 60-level drift off the Philadelphia No. 1 shaft

traversing a loose muck slope at the top of a deep, water filled stope. The drift appears to be open (Figure 22) but it doglegs to the left. Therefore, conditions beyond remain unclear.

Accessible stopes were generally open, despite prevalent raveling and drummy ribs. No large slabs or extensive cracking was noted. The striking feature of the stopes in terms of assessing their dimensions and stability is the irregularity in dimension perpendicular to the dip. Vertical distances to the stope backs range up to an estimated 40 ft
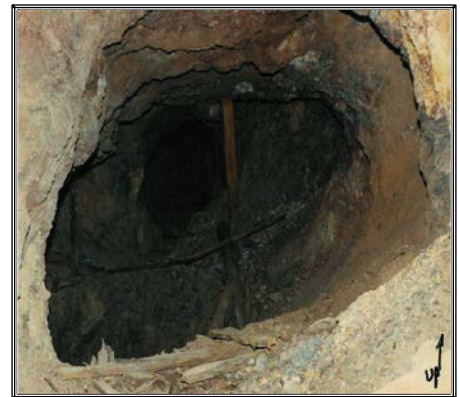

Figure 22 – 100 level drift south from Philadelphia No. 2 shaft

and stope widths range between 10 ft and an estimated 40 ft. Apparently, stopes were widened along ore shoots that may have been elongate perpendicular to the general structural trend. <u>There are no level maps that depict the dimensions of the stopes in this direction</u>, although it appears that the Chock longitudinal section may be a good source of estimated stope lengths along the strike. One report (circa 1915) describes a "hanging wall ore shoot" at the 200 level as being about 35 ft wide, which may be indicative of stoping widths. Stopes next to the shaft were observed to disappear into the water for as far as could be seen (Figure 23).
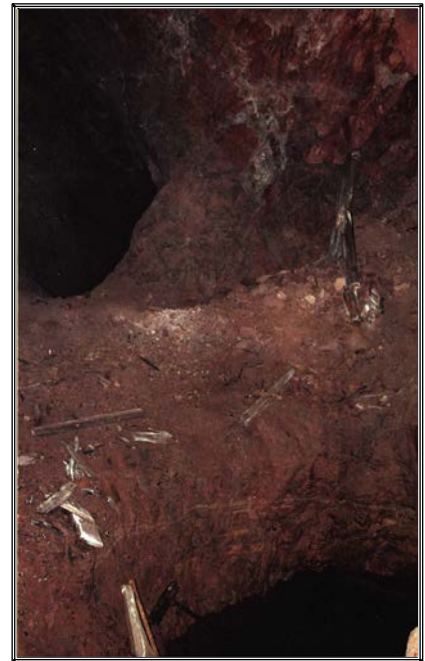
Surface reconnaissance revealed numerous short adits, shallow prospect pits, and sampling trenches. None of the other workings could be proven to connect with the main Arabian Mine or the stopes that were part of the Philadelphia Group, despite historical accounts of more extensive underground workings. It was concluded that most of the shallow workings that are no longer visible were either mined through using surface methods (the "Arabian Cut" – see Figure 9 – a benching operation along the surface expression of the vein nearly 150 ft high and 60 ft wide, that was mined in the 1930s), were proposed but never built, or were reclaimed in earlier phases of roadway construction. Vague references to a connection, between the main mine workings and shallower workings to the south, could not be confirmed.

Figure 23 – Water-filled stope off Philadelphia No. 2

Where underground observations were possible, stope as well as drift deterioration appeared to be a progressive occurrence characterized by raveling and sloughage, rather than large-scale block failures. Rock mass strength was observed to be low in much of the rock, and faults with gouge were seen to have considerable spalling and sloughage. Little timber remains except in the shafts, and timber was probably minimally used in drifts due to its scarcity in the area. Stulls were used sparingly as stope support, if at all. The principal mode of stope support seems to have been pillars of natural rock, probably relatively barren vein material. All the pillars within the stopes observed are hourglassed to some degree; the smaller pillars more severely than the larger ones. This indicates that sloughage from the sides of pillars has been occurring. However, the length of time that the workings have remained open argues that the sloughage process is very slow overall, and should remain so unless major changes occur. Where the hanging wall is an extrusive, massive rhyolite, extensive spans could be maintained.

It was concluded that the proposed new road alignment, to the west of the existing, would be underlain by stopes and drifts whose orientations, dimensions, or stability could not be observed directly. It was recognized that even substantial ground failures in single drifts would not affect highway integrity. No such drifts would occur shallow enough beneath the alignment to cause subsidence because the miners consistently avoided crossing through the gravels, according to

the few cross-sections available. It was noted that failures of single drifts have occurred on the 60 and 100 levels and there is no evidence of surface subsidence.

On the other hand, the potential for failure of stopes, and the effect any such failures might have on the ground surface, were of concern. The stopes accessed are open or water-filled; there is no indication that any were backfilled. Observed stopes are large enough that their collapse could affect the surface significantly.

Several sources of potential underground collapse were identified that could lead to surface disturbance. Major changes in water level could introduce further sloughing of pillars or may cause pore pressure changes within the gravels, perhaps leading to collapse of certain areas. Excessive blasting vibration from future mining or road construction, placement of thick fill atop the mine workings, seismic events leading to slippage along faults, introduction of fluids (mine leachate or other) into the mine, and other mechanisms leading to stress regime change, were identified as possible triggering mechanisms for stope instability.

The surface expression of underground stope failure could not be pinpointed in this case; it may range from zero to considerable. The considerable vertical extent of the workings, the presence of faults and other discontinuities that dip moderately to steeply, the presence of weakly-consolidated gravels, and the relatively shallow depths of the larger stopes beneath the road, indicate that stope collapse would be very likely to affect the surface. Surface movements of feet to tens of feet could very well occur as a result of massive stope collapse, particularly if the collapse occurred at shallower depth so that collapsed material could move downward through water-filled workings. It was recognized that proper construction blasting at the distances under consideration would not be likely to trigger the scale of stope collapse that would be prerequisite to large-scale ground movement, unless that collapse were already imminent.

Based on the recommendations from the subsurface reconnaissance, ADOT arranged for a subsurface drilling and geophysical program. It also fenced the hazardous workings, took steps to limit the extent of water withdrawal from the workings, and instituted criteria to limit construction blasting vibrations in the area.

INVESTIGATIVE BORINGS AND ACOUSTIC TOMOGRAPHY

In 1992 the Arizona Department of Transportation (ADOT) and the U.S. Bureau of Mines (USBM) jointly entered into a Cooperative Research and Development Agreement (CRADA), to test, at the Arabian mine, a prototype cross well tomographic system's ability to identify shallow voids at abandoned mines. The USBM prototype system consisted of a high frequency ceramic-piezoelectric, cylinder-bender, transducer source, and a wall locking, triaxial acoustic receiver.

(The following description is abstracted from Killoran, 1992.)

Acoustic Tomography

Cross well acoustic tomography methods (geotomography) were developed by the oil and gas mineral exploration industries to produce a better image, based on velocity, of the geologic structure between two boreholes. In cross well tomography, a transmitter probe is placed in a borehole and electrically excited to produce an acoustic wave. This wave propagates through the rock mass to a receiver probe in another borehole. The receiver signal is recorded and evaluated for the first arrival travel time.

Since the velocity of an acoustic wave is dependent on the media through which it travels, the arrival time represents the fastest path the wave can travel through the intervening rock mass. This implies that the acoustic wave travels the shortest path through the media. If a void, filled with air or water is present between the transmitter and the receiver, the first arrival travel time will be greater than if no void is present because the first arrival path will travel around the mine opening. By placing the transmitter and the receiver at numerous depths in the boreholes, a cross section of travel times can be recorded.

Tomography programs are then used to construct an image of the two-dimensional cross section between the boreholes using the first arrival travel times, the transmitter and receiver probe depths, distance between boreholes, and an initial estimate of the velocity field. The cross section is divided into rectangular "pixels" with a velocity associated with each pixel. The tomography program traces a ray path through the pixels from the transmitter to the receiver and computes the travel time. After all the ray paths have been computed, the velocity values are adjusted to minimize the differences between the measured travel times and the computed travel times. Geological and man-made subsurface features between the boreholes can then be interpreted from the final velocity distribution shown on the tomogram.

Supplemental Borings

To facilitate the cross well geophysical tests, ADOT provided seven vertical, reverse circulation boreholes at the Arabian mine site (Figure 3). The borings were drilled in two phases. Phase 1 borings were drilled to obtain information concerning the extent of the main workings (Figure 5 - labels 1, 2, 5, and 6). Phase 2 was drilled in an attempt to determine the extent of the underground workings to the southwest (Figure 5 - B1 through B3). The first phase borings were cased with plugged schedule 40 PVC pipe. However, the PVC would not maintain a constant head of water above the ground water table. The second phase borings were cased with plugged schedule 40 steel pipe and did maintain water to top of the casing. However, the steel casing attenuated the high frequency signal and inhibited a clear reception at the receiver.

The Phase 1 borings and tomographic profiles were partially successful in identifying underground workings below the ground water table. Mine voids were intercepted in Borings 2 and 5, probably corresponding to stopes extending between the 100 and 200 levels. In Boring 2, a 16 ft high void was first intercepted at a depth of 103 ft (undoubtedly a stope) and another void 4 ft high was intercepted 16 ft below the bottom of the first, corresponding either to a stope

irregularity or a drift. In Boring 5, an 11 ft high void, probably another stope, was encountered at a depth of 218 ft.

Interpretation

One successful tomographic profile is indicated in Figure 24. The darker red zones are low-velocity areas interpreted as open or water filled voids.

There was some confusion when considering the depths at which these voids were encountered, which seemed too shallow for the mine levels designated. However it must be remembered that the records indicate that levels were designated relative to the original collar down the main production shaft, and that it was determined that around 30 ft (slope distance) of the Philadelphia No. 2 shaft collar is missing, so all levels would occur around 25 ft shallower on that account.
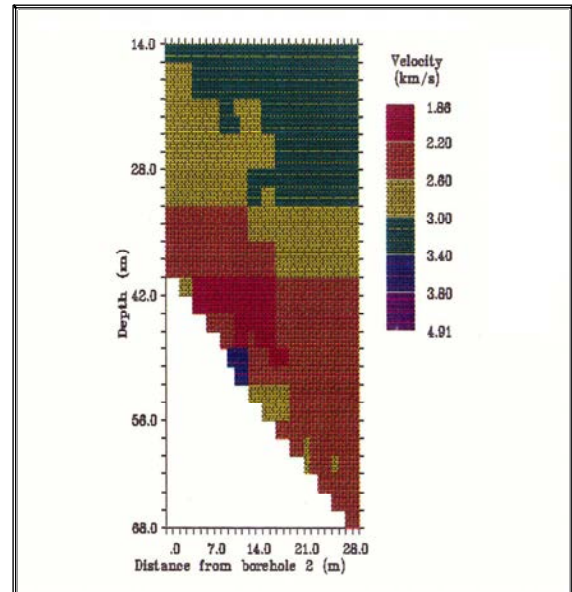

Figure 24 – Tomographic profile between boreholes 2 and 5

When the tomographic profile shown in Figure 24 is plotted against the most plausible interpretation of the extent of stopes between the 100 and 200 levels, together with the geologic interpretation drawn from available boring logs and geologic cross sections, a close agreement is obtained.
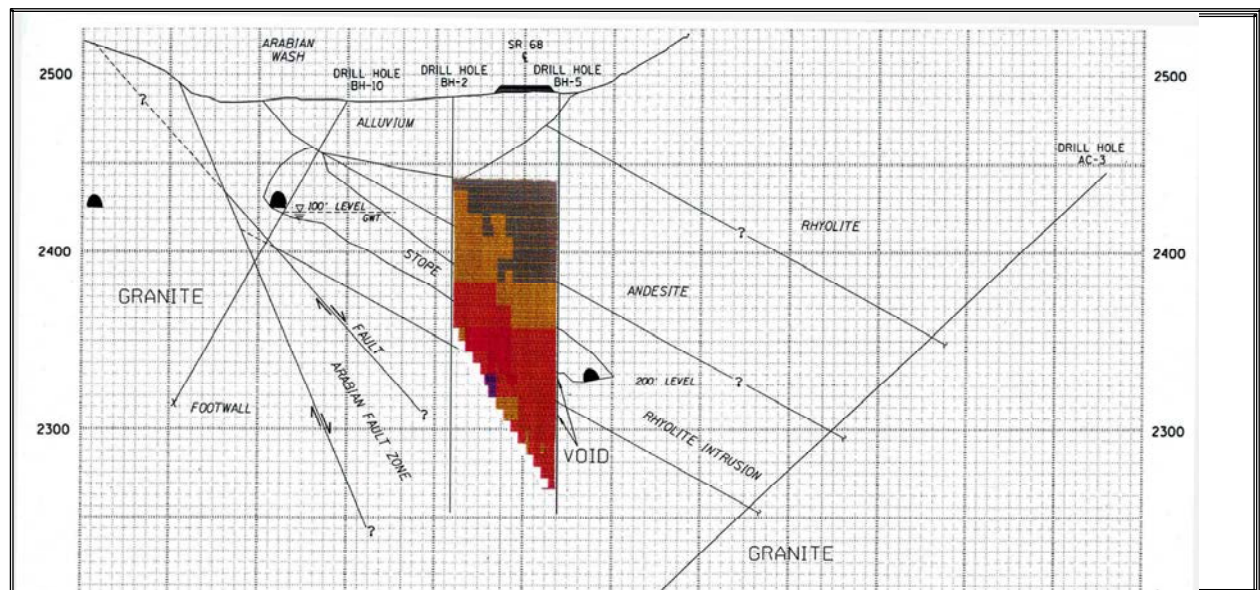

Figure 25 – Geologic interpretation of tomography between borings 2 and 5

Figure 25 shows regions corresponding to the gravel fill in the wash bottom, and to the occurrence of voids representing a large stope. Moreover, the tomography data shows that the hanging wall rock may be only a few meters thick, as indicated by the separation between the top of the low velocity (red) zone and the zone (green) representing low-velocity earth materials (possibly weak gravel or altered/weathered andesite). This condition is shown on the cross section to directly underlie the existing SR 68. The expansion would have provided a new westbound set of lanes, which would appear to the left of the roadway prism diagrammed in the cross section. That location would clearly have been underlain by shallower mine workings, overlain by thinner hanging wall rock, in turn overlain by gravel. Note that the groundwater table was observed just below the 100 level.

The Phase 2 borings and associated tomographic profiles did not produce completely reliable data and no conclusive interpretation was given by the USBM. However, altogether the tomographic images of the flooded underground workings suggested that voids are much more extensive than what was anticipated from the surviving mine records.

CONCLUSIONS

Just as permanent civil structures are designed and constructed for higher reliability than transient industrial facilities (like mines), the standard of "geotechnical stability" is higher where public highways are concerned. It is within this framework that the potential impact of the Arabian Mine had to be evaluated. Assuring the convenience and safety of the traveling public was, and remains, the paramount concern for ADOT.

The Arabian Mine, like most deep metal mines, is both geologically and geometrically complex. Unfortunately, despite years of records review and field work, practical constraints prevented developing the subsurface geotechnical data needed for a thorough evaluation of mine opening stability. The range of potential spans and depths was too great and too uncertain, and geotechnical parameters could not be reliably derived for the pillars and surrounding rock, not to mention the faults. Furthermore, inconsistencies in the available records limited the reliability of the information developed. To resolve this, a lengthy and expensive subsurface investigation would have been required.

Nonetheless, the data clearly showed that not only is the existing highway undermined, but the new, realigned highway would also be undermined. This would occur at a shallower depth, where a greater percentage (perhaps more than 75%) of the overburden thickness is represented by weakly cemented gravel. In addition, direct observations disclosed spalling, pillar hourglassing, locally weak, heavily fractured to shattered and clayey rock conditions, and a groundwater table that, while fairly stable in the past, could produce pore pressure changes in the mine support structure should it fluctuate in the future. Although there is no proven history of subsidence other than that induced on purpose as the result of overhead stoping, this does not assure future stability for the development of a public transportation corridor.

Distress to the support system in a mine as the result of ground water level fluctuation (not necessarily complete drying, which can have even more severe effects) results from a pressure imbalance within the supporting rock, because the openings depressurize more rapidly than the surrounding rock can drain. Instances of subsidence induced by surface or ground water disturbance are not unheard of, although they are not commonly reported. The authors know of several (published and unpublished) instances of the collapse of mine structures due to ground water withdrawal or drastic ground water level changes. This possibility added concern for building a new highway over the mine.

There are engineering solutions to the potential for subsidence. Mine backfilling was considered but dismissed due to the cost, time required, and the fact that it would sterilize the mineral estate, necessitating what was assuredly going to be the difficult task of negotiating the property's value with the mine owner(s). Likewise, applying an engineering solution at the surface ("subsidence-proofing") the highway was known to be complicated due to the high subsidence factors that would have to be considered, and the remoteness of the site.

Figure 26 – "North" realignment

At other, more constrained sites, perhaps such engineering solutions could not be avoided. In this case the argument for relocation was compelling, though it is often most convenient to expand the existing corridor rather than relocate it. In the end, the decision was taken to realign the highway to the north (Figure 26), through public land (and a few unpatented claims) known to be free of undermining. As it turned out, in part because the new construction could take place without interference from existing traffic, and in part because further right-of-way acquisition did not have to be negotiated with the current Arabian Mine owner(s), the eventual cost of construction proved to be less than the projected cost of the improvements within the existing corridor.

ACKNOWLEDGMENTS

REFERENCES

Cummings, R.A., 1991, Arabian Mine Survey and Reconnaissance: Final Report and Deliverables, ADOT Contract No. T92-0119-00 to Engineers International, Inc., Project No F-068-1-402, TRACS H273401D

Faulds, J. E., House P. K., 2000, Geology of the Laughlin Area, Clark County, Nevada: Open File Report 2000-6, Nevada Bureau of Mines and Geology

Gardner, E. D., 1936, Gold Mining and Milling in the Black Mountains, Western Mohave County, Ariz.: Information Circular 6901, U.S. Dept. of the Interior, U.S. Bureau of Mines

Gerity, G. E., 1998, Evaluation of the Gold Resources at the Arabian/ Philadelphia Mine, Mohave County, Arizona: unpublished report from Pioneer Engineering, Littleton CO

Killoran, L. K., 1993(?), Cross Well Acoustic Tomography to Locate Abandoned Mines and Subsidence Failure: U.S. Bureau of Mines, Denver Colorado

Lausen, Carl, 1931, Geology and Ore Deposits of the Oatman and Katherine Districts, Arizona: Arizona Bureau of Mines Bulletin No. 131, 126 p.; also, Arizona Bureau of Mines Geological Series, No. 6; University of Arizona Bulletin, v. 2, No. 2.

Lang, Nicholas P., C.F. Miller, J.E. Faulds, W. Cribb, 2001, Eruptive History Of The Union Pass Volcanic Center, Colorado River Extensional Corridor, Northwest Arizona: Cordilleran Section - 97th Annual Meeting, and Pacific Section, American Association of Petroleum Geologists (April 9-11), Session No. 21, New Insights in Igneous and Metamorphic Petrology and Volcanology

Longfellow, C. H., 1963, Reconnaissance Geology Between Lake Mead and Davis Dam, Arizona – Nevada: Shorter Contributions to General Geology, Geological Survey Professional Paper 374 - E

Murphy, R. T., J.E. Faulds, F. L. Hillemeyer, 2003, Preliminary Geologic Map of the North Half of the Union Pass Quadrangle, Mohave County, Arizona: Nevada Bureau of Mines and Geology

Schrader, F.C, 1909, Mineral Deposits of the Cerbat Range, Black Mountains, and Grand Wash Cliffs, Mohave County, Arizona: U.S. Geological Survey, Bulletin 397

U. S. Bureau of Reclamation, 1955, Davis Dam and Power Plant, Technical Record of Design and Construction: Davis Dam Project, constructed 1942-53

U.S. Bureau of Mines, Denver Research Center, 1995, Final Report, Cross Well Geophysical Investigation of the Arabian Mine, Mohave County, Arizona: Cooperative Research and Development Agreement CRDA – 6200 – 0022

PHILOSOPHY OF EVALUATING SURFACE-FAULT-RUPTURE HAZARDS IN THE PUGET SOUND REGION, WASHINGTON

Jeffrey R. Keaton[1] and David H. McCormack[2]

INTRODUCTION

Recent and on-going neotectonic research have led to discoveries in the Puget Sound region that are both dramatic and exciting for the geoscience community, and sobering and alarming for local governmental agencies and the land development community. LiDAR (an acronym for _li_ght _d_etection _a_nd _r_anging) technology with post-processing tree and building removal to produce high-resolution bare-earth digital elevation models (DEM, or DGM for digital ground model) was used to identify scarps of the Seattle fault on Bainbridge Island in the late 1990s. Subsequent trenching documented several surface rupture events within the last 3,000 years. As LiDAR coverage becomes available for more of western Washington, and other heavily vegetated areas in tectonically active regions, the number of documented active faults is expected to increase. In the fall of 2003 and spring of 2004, aeromagnetic anomalies and LiDAR lineaments were used by the U.S. Geological Survey as the basis for projecting hypothetical extensions of strands of the Southern Whidbey Island fault 25 km (16 mi) across Snohomish County into the rapidly growing region north of Seattle. Although surface-fault rupture has not been documented and may not have occurred, the Southern Whidbey Island fault has been shown to be active on Whidbey Island within the last 3,000 years.

The authors participated in discussions in July 2004 that should have focused on hazards associated with potential fault rupture at locations of proposed structures, but instead focused on the nature and significance of a nearby lineament. The purpose of this philosophical discussion is to draw attention to potential surface-fault-rupture hazards in western Washington, put fault-rupture hazards in the context of paleoseismology, and promote awareness of important distinctions between geologic research for scientific discovery and geologic investigation for site characterization and development. The distinction will become relevant as the state and local governmental agencies develop regulations for siting buildings and other facilities in areas of active faults and develop guidelines for evaluating surface-fault-rupture hazards in Washington.

SURFACE-FAULT-RUPTURE HAZARDS

A growing body of geologic information is facilitating identification of locations of late Quaternary and Holocene fault traces in the Puget Sound region. Faults identified to date include strands of the Seattle fault, Utsalady fault, Strawberry Point fault, Southern Whidbey Island fault zone, Tacoma fault, and Olympia fault. Results of research trench data released by the U.S. Geological Survey since the late 1990s demonstrate that scarps identified by examination of LiDAR data were created by post-glacial faulting. Interpretation of trench exposures indicates that the faults are Holocene and have

[1] AMEC, 1290 North Hancock Street, Suite 102, Anaheim, CA 92807
[2] Aspect Consulting, 811 First Avenue, Suite 480, Seattle, WA 98104

recurrence intervals in the range of hundreds to thousands of years. Clearly, the faults that have been exposed in trenches excavated by the U.S. Geological Survey in the Puget Sound region are *active faults* by all definitions of the term, and would be included in special studies zones as defined by the State of California (Alquist-Priolo Special Studies Zones Act) or the State of Utah.

Surface-fault-rupture hazards are those hazards caused directly by fault displacement at the ground surface. Historical earthquakes of moderate and large magnitude have occurred without being accompanied by displacement along faults at the ground surface, and, therefore, none of the damage from these earthquakes was fault-rupture damage. To be sure, many historical earthquakes of moderate and large magnitude have been accompanied by surface-fault displacement, and damage did occur to facilities that straddled the rupture zone. By rupture zone, we mean concentrated, discrete displacement along fault planes, as well as distributed displacement along minor faults, and folding or warping without discrete or distributed displacement.

A reasonable assumption is made in evaluating faults for surface-rupture hazards that future faulting will occur along pre-existing fault planes and be generally consistent with past surface-rupture events. Existing surface-fault-rupture hazard regulations include setback distances for structures so that they will be some distance away from active faults. Arbitrary distances of 15 m (50 ft) for structures for human occupancy to 60 m (200 ft) for siting hazardous waste facilities (Code of Federal Register Title 40 Part 264 Section 18) have been used in some regulations; however, the Utah guidelines use non-arbitrary factors (the geometry of the fault, the slope of the ground, and the importance of the structure) to calculate setback distances as small as 4.6 m (15 ft).

The generally good performance of buildings subjected to small displacements in liquefaction-induced lateral spread landslides has been used to justify exempting from setback requirements faults having less than 100 mm (4 in.) of displacement. The Utah guidelines do not categorically exempt such faults, but they acknowledge that risk-reduction options, such as foundation reinforcement, may take the place of setbacks in some instances. Therefore, the main questions to be answered in evaluating surface-fault-rupture hazards should be:

(1) Are fault planes and/or zones of deformation located at or near proposed structures? If so, then
(2) What was the direction and amount of displacement that occurred during past surface-rupture earthquakes on the local fault? And
(3) What are the limits of the zone of surface-fault rupture and associated deformation?

PALEOSEISMOLOGY

Paleoseismology, or earthquake geology, seeks to determine more details about active faults than needs to be determined in most surface-fault-rupture hazard evaluations. In general, paleoseismology focuses on geologic evidence of recency and recurrence of

surface-faulting earthquakes. Therefore, the main questions to be answered in paleoseismic evaluations are:

  (1) Are lineaments actually fault planes and/or zones? If so, then
  (2) What is the age of the youngest geologic unit that is cut by faulting?
  (3) What is the age of the oldest geologic unit that is undisturbed by faulting?
  (4) Does evidence exist in the geologic record for more than one surface-faulting event? If so, then
  (5) What are the age relations and amounts of displacement of the geologic units?
  (6) What range of earthquake magnitudes could have produced the faulted units in the geologic record?

SITE CHARACTERIZATION VERSUS SCIENTIFIC DISCOVERY

The answers to surface-fault-rupture hazard questions and to paleoseismology questions are contained in the geologic record and are available for exposure in trench excavations and subsequent interpretation. In some cases, surface-fault-rupture hazard questions can be answered adequately from knowledge included in published and/or unpublished geologic information, direct and indirect geologic observations (geologic mapping, aerial photograph examination, and LiDAR interpretation), and/or subsurface information derived from test pits, borings, or cone penetrometer soundings. Test pit exposures and stratigraphic interpretation of borehole samples and cone penetration resistance values can provide useful information for interpreting continuity of geologic formations that can provide the basis for professional judgments regarding the location or absence of faults.

Reliable geologic maps that show sites for development to be remote from traces of active faults provide an adequate basis for dismissing surface-fault-rupture hazards from further consideration without the need for subsurface data. In other cases, surface-fault-rupture hazard questions can be answered adequately only by careful direct geologic observation and interpretation of trench exposures.

In all cases, paleoseismology questions can be answered adequately only by careful direct geologic observation and interpretation of trench exposures. Furthermore, such trench exposures must be in optimum locations to expose geologic deposits that are meaningfully old, as well as meaningfully young, to allow the age of the most recent displacement to be bracketed by the stratigraphy.

In short, paleoseismology trenches need to be excavated where the best geologic information is located. Site development trenches must be excavated on property under the control of the entity seeking to develop the site.

In the early days leading to development of modern paleoseismology techniques, the primary issue was earthquake ground motion, not surface-fault-rupture hazards. Earthquake design of critical facilities, such as nuclear power plants, was based on an understanding of historical seismicity (earthquake catalog data) and prehistoric seismicity interpreted from the geologic record. The answers to paleoseismology questions were

vital to these types of projects because of the contribution to ground motion that could add significantly to the cost of design and construction. Consequently, the emphasis of paleoseismology evaluations focused on determining if geologic structures were faults, and if the faults were active faults.

The guidelines for evaluating surface-fault-rupture hazards in California (California Geological Survey Note 49) focuses on recency and recurrence of faulting along existing faults. Perhaps this focus was in reaction to attempts by some consulting geologists to show that traces of faults exposed in trenches at some sites were too old to be classified as active, but off-site geologic information had already established the fact that the fault was active. The California Geological Survey was charged with the task of mapping all Holocene faults in the state. These faults, and special studies zones around them, became the basis for the regulatory framework for managing hazard related to surface-fault rupture.

The guidelines for evaluating surface-fault-rupture hazards in Utah (Utah Geological Survey Miscellaneous Publication 03-06) were developed years after the California guidelines had been published. Consulting geology practice in Utah included a number of professionals who had worked in California under California regulations. The issue of using off-site geology to make a judgment about the degree of activity of on-site faults is included in the Utah guidelines. The Utah guidelines also provide a practical approach to evaluating on-site surface-fault-rupture hazards.

The Utah guidelines summarized their approach in two figures. One figure shows the boundary of a site, and the other figure shows the footprint of a building. The assumption is that active faults are located somewhere in close proximity to the site or building. Trench locations are sketched on the figures to provide guidance on where to excavate trenches on the site to evaluate surface-fault-rupture hazards. In the case of the site boundary, the purpose of trenching is to identify fault locations and zones of deformation so that appropriate setbacks can be established for layout of structures on the site that avoid the surface-fault-rupture hazard. In the case of a site where building locations have been selected, the purpose of trenching is to demonstrate that the building footprint is free from fault-rupture hazards. Trench excavations typically extend beyond the building footprint by a distance equal to the appropriate setback. If fault traces or zones of deformation are exposed in such trenches, adjustments must be made to the location of the structure or its design; whereas, if no fault traces or zones of deformation are exposed, then the structure is considered to be free from surface-fault-rupture hazards.

The Utah guidelines specifically note that the guidelines are intended for use in siting new buildings for human occupancy, rather than for use in siting lifelines (highways, utilities, pipelines), which commonly must cross faults. The commonly accepted approach to mitigating surface rupture hazards for many lifelines that must cross faults is to develop emergency repair plans in the event that damage occurs as a result of surface rupture. Other types of lifelines, particularly natural gas or refined products pipelines, have accepted design procedures for minimizing or eliminating the risk of loss of pressure integrity for design-fault-offset events.

CONCLUSIONS

The discussions in July 2004 in which the authors participated tended to focus on the significance of a projected lineament instead of on hazards associated with potential fault rupture at locations of proposed structures. We believe that the projection of the lineament probably is unrelated to active tectonics and recommended using excavations at and around proposed structures to verify our judgment that the structures were not subject to risk of damage from surface-fault rupture. Our recommendation was criticized because it "did not get to the question." That "question", of course, was entirely related to whether the projected lineament is an active fault, rather than to the safety of proposed structures located more than 150 m (500 ft) away from the projected lineament.

The U.S. Geological Survey released their interpretation that a projected lineament might exist in the vicinity of the proposed structures in the spring of 2004, several months after the site had been selected and facility locations had been defined. The approach we recommended to our client was to conservatively assume that the lineament actually was a fault, and that the fault was active. Given that conservative assumption, then two conclusions follow:

1) The only benefit resulting from geologic evaluation of the lineament would be information supporting an interpretation that it was either NOT a fault or NOT an ACTIVE fault, and
2) Excavations at specific structure locations would be adequate to address the issue of surface-fault rupture hazards at those locations.

We further recommended that geologic observations during final design and construction would be reasonable because of our belief that the projected lineament was not tectonic, and its distance from the proposed facilities in the event that it were a tectonic feature.

Earthquake ground motion for design of proposed structures at the facility evolved with the identification of the projected lineament, also. The original intent was to use the International Building Code, including its ground motion estimates, for design. A site-specific probabilistic seismic hazard analysis conducted by a Seattle-based consultant considered the nearby lineament to be an active fault with assumed reasonably conservative maximum magnitude and slip-rate parameters. The resulting ground motion estimates were significantly higher than the building code design values. The client was willing to accept the cost implications of the conservative assumptions because the cost of delay outweighed the higher cost of design and construction.

The State of Washington and local governmental agencies in the Puget Sound region are beginning to face the issue of how to incorporate surface-fault-rupture hazards into natural hazard mitigation strategies. Undoubtedly, guidelines developed in California and Utah will be examined as Washington develops its own guidelines. As professional geologists who have worked on research projects, we eagerly look forward to new paleoseismic information being released and for opportunities to participate in geologic

'trench parties' to examine and debate the evidence for past earthquakes in the Puget Sound region.

However, as professional geologists who provide consulting services to private-sector and local-government-agency clients, we feel strongly that the practical approach to evaluating surface-fault-rupture hazards must be included in Washington guidelines. It is simply not reasonable for guidelines to require that developers determine recency of faulting and recurrence of prehistoric earthquakes as part of the process of demonstrating that their buildings do not straddle active fault traces. It is similarly not reasonable for guidelines to require that developers investigate off-site locations as part of the process of demonstrating that their buildings do not straddle active fault traces, any more than it would be reasonable for off-site land owners to be required to give access permission for such investigations.

Until the State of Washington or local governmental agencies develop zones for special geologic studies around known or suspected traces of active faults, we believe that a reasonable approach for qualified engineering geologists to use consists of the following steps:

(1) Determine the location of the site with respect to known or suspected traces of Holocene faults (post-glacial faults in the Puget Lowland) based on available data from the U.S. Geological Survey, Washington Department of Natural Resources, and universities
(2) Understand the layout of the development being proposed
(3) Make a judgment regarding the need for on-site evaluation of surface-fault-rupture hazards
(4) Make a judgment regarding the type of on-site evaluation that is appropriate
(5) If trenching is appropriate, select trench locations with respect to site boundaries and building footprint layouts, paying attention to the likely age of deposits that will be exposed in the shallow subsurface, and other practical factors, such as wetlands, depth to ground water, existing utilities, pavement, past grading, and archaeological sites
(6) Interpret the results in the context of available geologic data
(7) Make a judgment regarding surface-fault-rupture hazards at the site
(8) Report the results in a format that permits reasonable independent review of the investigative process and conclusions.

We further recommend that part of the surface-fault-rupture hazard evaluation process include notifying geologists representing reviewing agencies of planned trenching and inviting them to visit the sites while trenches are open. This procedure has been helpful In Utah in facilitating regulatory review regarding issues such as appropriateness of trench locations, meaningfulness of exposed stratigraphy, and reasonableness of interpretations and recommendations.

Geological and Design Considerations for Replacement of Suspension Cable Anchorages, Bear Mountain Bridge, Hudson River, New York.

Danny J. Van Roosendaal and Andrew F. McKown

Haley & Aldrich, Inc.
465 Medford Street, Suite 2200
Boston, MA 02129-0414

INTRODUCTION

The Bear Mountain Bridge is a landmark structure familiar to many in the greater New York area. It is located on the Hudson River approximately 40 miles north of New York City, as shown in Figure 1. Figure 2 is a photograph 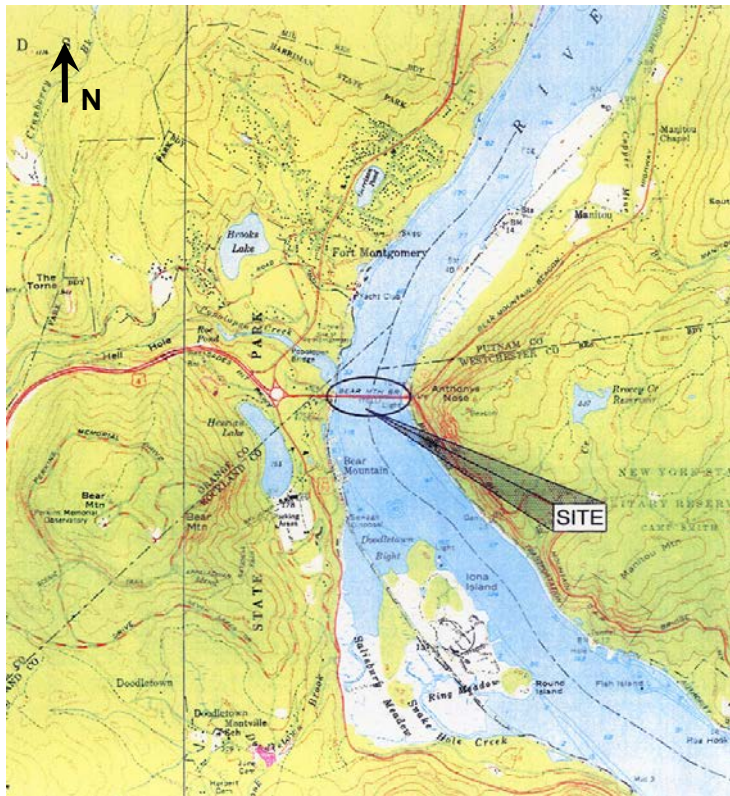of the Bear Mountain Bridge showing the two-lane suspension bridge spanning the Hudson River between Bear Mountain on the west and Anthony's Nose Mountain on the east. The total bridge length is approximately 2,255 feet between anchorages, with a main suspended span of 1,632 feet and two simply supported side spans of 210 feet each. The existing cables were spun in 1924 and carry a working load of approximately 14,000 kips each. Four concrete filled rock tunnels, 82 ft to 119 ft long, currently provide anchorage for the four support cables.

Figure 1: Site location map.

Stress corrosion cracking was recently detected in some of the wires. Although the cracking is not an immediate threat to the structural integrity of the bridge, the discovery has prompted a comprehensive Main Cable Strengthening Study to evaluate alternatives for future cable strengthening or replacement, and carry the preferred alternatives to the conceptual design phase. Such cable supplementation or replacement scenarios would require the design and construction of anchorages for the new cables. This paper presents the results of the investigation of replacement anchorages for the strengthened cables.

SITE GEOLOGY

The Bear Mountain Bridge is in the "Hudson - Reading Prong" section of the New England Upland physiographic province, sometimes called the Hudson Highlands. Generally, this section consists of ancient metamorphic rocks with a northeast to southwest trending pattern of faults and shear zones. The present zigzag course of the Hudson River through the Highlands is supposed to follow several of the eroded faults and shear zones. Also, the Ramapo-Timp Pass fault systems through this area are believed to be the axis of current minor earthquake epicenters.

Figure 2: The Bear Mountain Bridge crossing the Hudson River (looking south). Anthony's Nose Mountain is to the left.

At the western anchorages on Bear Mountain, bedrock consists of granitic gneiss and pegmatite that are associated with the Canada Hill formation. Bedrock is of the Precambrian age. Any formerly existing younger rocks have long since been eroded away. In outcrops, bedrock appears massive, but its geologic history indicates that it should also be heavily fractured. Gneiss was typically fresh, hard to very hard, fine- to very coarse-grained, with varying amounts of biotite and garnet. Pegmatite consists of massive quartz–feldspar intrusive granitoid with varying amounts of biotite and garnet. Joints were primarily moderately-dipping to very high-angle. Rock core recovery ranged from 92 to 100 percent of core run. Rock Quality Designation (RQD) ranged from 72 to 100 percent of core run.
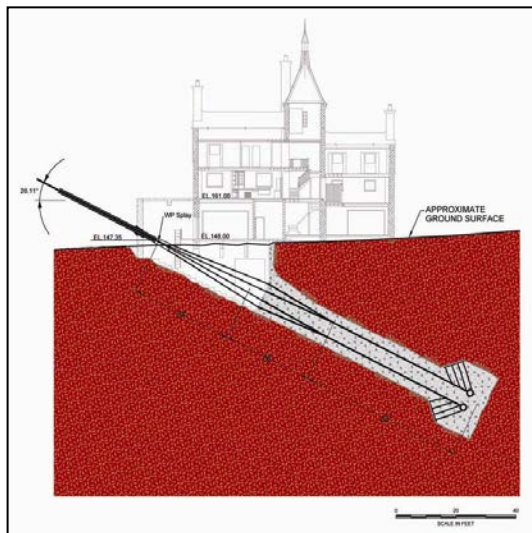

Figure 3: Schematic section of existing western anchorages situated near the toll facility.

In the immediate vicinity of the eastern anchorages on Anthony's Nose Mountain, bedrock consists of calc-silicate gneiss, calc-schist and lesser amounts of pegmatite. These rocks are associated with either the Grenville or Canada Hill series. As exposed at ground surface, the rocks range from massive to highly weathered. The rocks are susceptible to weathering because of their lime-rich composition, mica content, and prevalence of steep intersecting brittle faults which allow for groundwater percolation. The Timp Pass fault, a regional mapped fault system, is exposed in the vicinity of the east anchorage where brittle faulting overprints older metamorphic fabrics. Two other faults, or shear zones, are exposed immediately to the east of the anchorage pits. In the immediate vicinity of the existing anchorages, strikes of joints

and foliation features in the bedrock are generally parallel to the Hudson River and dips are downward to the east from about 35 to 80 degrees.

EXISTING ANCHORAGES

Figure 4: Existing eastern cable anchorages at the base of Anthony's Nose Mountain.

The western anchorages are situated near the toll facility and Bridge Administration Building, as shown in Figure 3, which is a section of the southwest anchorage. The eastern anchorage pits are situated above the roadway level on the steeply sloping side of Anthony's Nose, as shown in Figure 4.

Figure 5 shows that each of the four anchorages consists of steel eye bars embedded in concrete in a rock tunnel. Each tunnel has 36 steel bars, 14 inch by 1.75 inch, which transmit the cable load to two cast-steel base plates. These base plates bear on bedrock near the base of the tunnel, as shown in the photograph in Figure 6 (New York State Bridge Authority, 1999). The 11-foot long base plates are at 45 degree angles to the tunnel axis, and are approximately 4 feet above the base of the tunnel. According to record drawings, the tunnel shaft is approximately 9 feet wide by 11 feet high and the bell at its base is approximately 22 feet wide. Each pair of anchorage tunnels are spaced 61 feet apart, center to center. The four anchorage tunnels range in length from 82 ft to 119 ft.

The booklet, "Bear Mountain Bridge, The History," (New York State Bridge Authority, 1999) states that the main suspended span was constructed before the tunnels were concreted (Figure 7). Therefore, it is assumed that the cable loads are transferred to the bottom of the anchorage tunnel, rather than in side shear along the tunnel shaft. A finite-element model of the existing anchorage was performed to determine the zone of influence of this load transfer process to minimize interference between the existing and replacement anchorages. Figure 8 is a stress-distribution plot from the finite element modeling showing that the zone of influence extends approximately 30 ft from the existing anchorages.
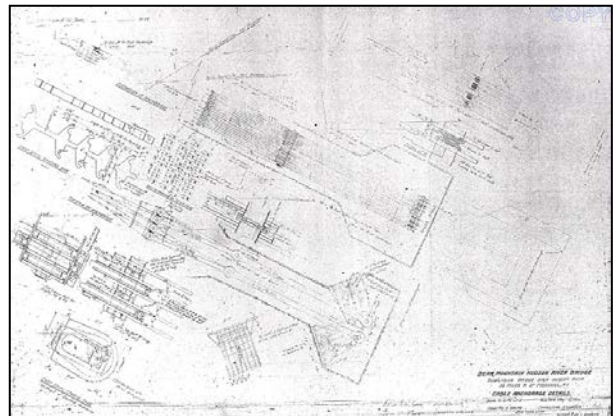

Figure 5: Reproduction of 1923 design drawing for the existing anchorages. Provided by the New York State Bridge Authority.

REPLACEMENT ANCHORAGE EVALUATION

Four foundation types were originally considered for new anchorages: anchor blocks, rock tunnels, drilled shafts, and rock anchors. Rock anchors were the only alternatives advanced to conceptual design. Some of the advantages of the rock anchors over the other anchorage types included: 1) elimination of significant drilling and blasting near the existing anchorages, 2) the use of smaller and easier to use equipment, and 3) the most economical cost of construction.

Design considerations for the rock anchors include compatibility with existing anchorages, depth and bond length of the rock anchors, and rock anchor layout details. The study also included an evaluation of precedent for the use of rock anchors for similar structures, corrosion protection of the rock anchors, and inspection methods for the installed anchors.

Rock Anchors Conceptual Design

An example conceptual design for an anchorage replacement using rock anchors is shown in Figure 9 (Amman & Whitney, 2004). Construction of the replacement anchorage includes the excavation of an approximately 20 ft wide ramped pit, casting of a concrete load transfer disk in the bottom of the pit, and installation of twelve 1,200 kip rock anchors through the load transfer disk. Our evaluation showed that the excavation and installation of rock anchors for the replacement cable and supplementary cable alternatives should not interfere with the existing anchorages. Although some of the rock anchors will be installed into the zone of influence of the existing anchorages, the installation of each anchor impacts a very small volume of rock surrounding the anchor. Thus, anchor installation within the zone of influence should have minimal impact on the existing anchorages.

Figure 6: 1924 photograph showing end bearing castings in the anchorage tunnel. From "Bear Mountain Bridge – The History," by the New York State Bridge Authority.

FHWA Geotechnical Circular No. 4 – Ground Anchors and Anchored Systems (FHWA, 1999) states that there is no practical limit to capacity of individual strand anchors, due to the ability to add strands until the desired capacity has been achieved. Assuming a group of twelve anchors, each anchor would require 35 strands to meet the capacity of 1,200 kips (assuming 0.6 inch strands, using Grade 270 steel wire).

The recommended total anchor lengths ranged from 90 ft to 115 ft. The un-bonded anchor lengths were estimated by determining the size of the rock cone that is needed to resist the combined working load of the anchor groups, which are 14,400 kips for the replacement cable alternative and 7,200 kips for the supplementary cable alternative. A 70 degree included angle

was assumed for the cone. Vertical forces are resisted by the weight of the cone only.
Horizontal forces are resisted by the frictional resistance on the surface of the cone. For the
various cases analyzed, the required un-bonded anchor lengths were governed by the horizontal
resistance requirements, using a minimum safety factor of 2.0, and ranged from 65 ft to 90 ft.
The 25 ft nominal bond lengths were determined following the Recommendations for Pre-
stressed Rock and Soil Anchors (Post Tensioning Institute, 1996).

Rock Anchor Layout

Design and constructability considerations dictate the following rock anchor layout criteria:

- **Rock Anchor Borehole Diameter:
  12 inches.** This nominal size is based on a
  1,200 kip anchor. The anchor will include
  35 – 0.6 inch diameter strands and a
  6 to 8-inch diameter PVC sheath, and a
  2 inch borehole annulus for grouting.

- **Minimum spacing between rock anchors:
  4 feet minimum, 6 feet desirable.** This
  dimension is based on a driller's ability to
  drill a straight borehole. For 100 feet deep
  boreholes, a 3 percent tolerance is
  achievable. Thus, two rock anchors should
  be at least 6 feet apart to avoid intersection of
  boreholes.

- **Minimum anchor head clearance: 2 feet
  minimum, 4 feet desirable.** This distance
  reflects the size of a steel bearing plate and
  the room needed to install jacks for future
  lift-off tests. The bearing plate for a 1,200

*Figure 7: Photograph showing concreting
of west anchorage. From "Bear Mountain
Bridge – The History," by The New York
State Bridge Authority.*

kip anchor will be approximately 24 inches square. A jack for lift-off test is
approximately 22 inches diameter, with a lifting plate to one side.

- **Splayed Anchors.** Anchors can be splayed several degrees from a normal axis to
  widen the separation distance between boreholes. By doing so, the anchor heads
  can be spaced closer together than the six feet recommended above.

- **Staggered Anchors.** For individual anchors, most load transfer and stressing of
  the rock mass will occur within the first 10 to 15 ft of the bonded zone. To avoid
  the concentration of these stressed zones within the anchor group, the length of
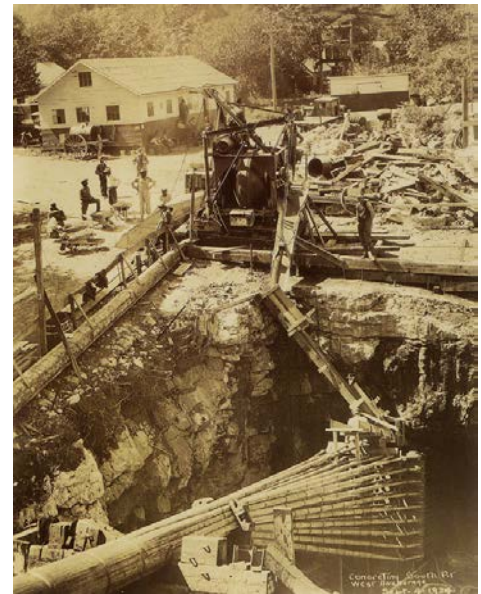 the un-bonded zones of individual anchors in the anchor group will be staggered

by approximately 5 ft. These staggered lengths will create a 10 ft difference in the unbonded length and total length of any adjacent anchors.

- **Anchor Head Accessibility.** Rock anchor bearing surfaces and heads will be accessible. This configuration will allow for long term testing and monitoring of individual rock anchors, as discussed below.

Precedent for Use of Rock Anchors

Although we are not aware of precedent for the use of rock anchors for the main cable anchorage on major suspension bridges, our evaluation indicated that there is sufficient precedent for the use of rock anchors in critical transportation structures. Large capacity, permanent rock anchors are commonly used in bridges and dams. One manufacturer that we contacted provided a list of 40 projects that included the use of epoxy coated strand anchors for bridges and dams dating back to

Figure 8: Stress distribution plot from a finite element analysis of the eastern anchorage.

1985. It is our understanding that most of these installations were for the seismic retrofit of bridge and dam foundations or for the stabilization of older dams. Notable bridge cases include the Golden Gate and Benicia-Martinez bridge seismic retrofits performed in California. Where reported, the number of strands per anchor ranged from one strand to as many as 61 strands. Several cases, including the two California Bridges, used 35 or more strands per anchor.
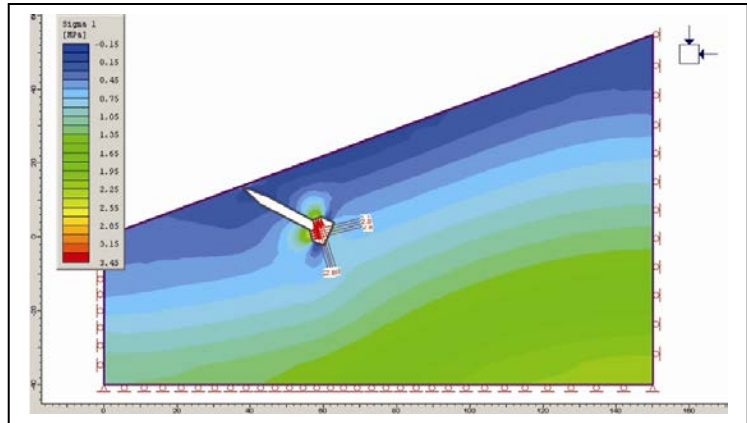
Corrosion Protection of Rock Anchors

The study included an evaluation of the design life and corrosion protection for the rock anchors. FHWA Circular 4 (FHWA, 1999) defines two classes of corrosion protection for rock anchors:

- Class I (Encapsulated Tendon), which includes a trumpet and cover for the anchorage, two layers of encapsulation (grease and grout filled sheaths) in the un-bonded zone, and grout-filled corrugated sheath or fusion-bonded epoxy coating in the bonded zone.

- Class II (Grout protected tendon), which includes a trumpet and cover for the anchorage, a single grease-filled or heat shrink sheath in the un-bonded zone, and cement grout cover in the bonded zone.

According to FHWA Circular 4, most reported anchor failures due to corrosion have occurred within 2 meters of the anchorage. Thus, guarding against corrosion of the anchorage is a critical component of the corrosion-protection system. Following the selection matrix presented in FHWA Circular 4, Class I corrosion protection is warranted for rock anchors used to anchor suspension cables at the Bear Mountain Bridge, because the structure is permanent and there are serious consequences of failure of the anchorage system.

Inspection Methods for Rock Anchors

The study also included an evaluation of potential inspection methods for the installed rock anchors. The Transportation Research Board has recently published NCHRP Report 477 "Recommended Practice for Evaluation of Metal-Tensioned Systems in Geotechnical Applications" (TRB, 2002). This publication specifically addresses non-destructive testing (NDT) of in-place rock and ground anchors and prediction of remaining service life of such anchors. The study concluded that two mechanical NDT methods (impact echo and ultrasonic tests) and two electrical methods (half-cell potential and polarization measurements) are viable alternatives for ND testing of installed metal tensioned systems. The electrical methods require electrical isolation of the structural element and the presence of a conducting electrolyte. The mechanical methods may be limited to bar elements, depending on the type instrument used.

Of particular note in the NCHRP report is the discussion on the monitoring of new installations. The report states that for new installations, provisions can be made for access to the heads of the elements and for electrical isolation of elements to facilitate NDT testing. Also, the report states that significant improvement can be made to new installations to facilitate ND testing for corrosion. Such improvement may include installation of reference electrodes along the length of the elements, or installation of strain gages at various locations along the element. These improvements would allow for careful monitoring and documentation of the onset and progression of corrosion over time.

Finally, if several rock anchors are used to support an anchor block, the system will include a certain degree of redundancy with respect to individual anchor capacity. Such redundancy would facilitate the use of actual lift off testing of individual rock anchors to confirm that the anchors are still carrying the design load. The ability to perform such tests is viewed as an advantage over single point anchors such as a tunnel.

CLOSING AND ACKOWLEDGEMENTS

The Main Cable Strengthening Study included an evaluation of the use of rock anchors for the replacement or supplementation of the existing suspension cables for the Bear Mountain Bridge across the Hudson River in New York State. This study has shown that rock anchors are feasible for the replacement cable anchorages and are compatible with the existing cable anchors.

The Bear Mountain Bridge is owned and operated by the New York State Bridge Authority, which has funded this study. The designers for the Main Cable Strengthening Study are Ammann & Whitney Consulting Engineers, Inc. of New York, New York. Haley & Aldrich of New York, working as sub-consultants to Amman & Whitney, provided foundation recommendations for anchorages for the conceptual phase of the project. Geologic mapping was performed by Dr. Charles Merguerian, of Duke Geological Laboratory, and Haley & Aldrich of New York.
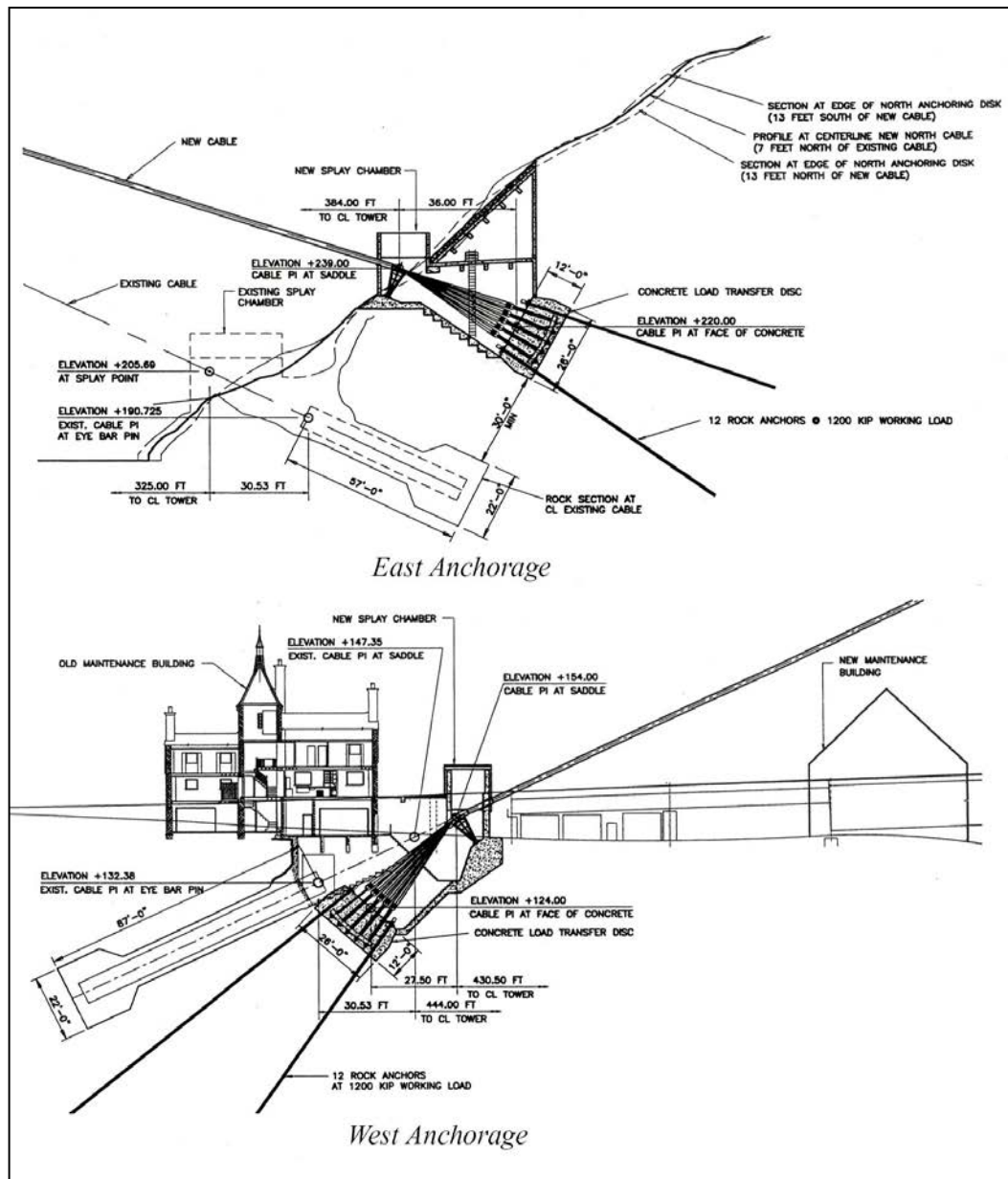

Figure 9: Example conceptual designs for replacement cable anchorages.
(Amman & Whitney, 2004)

REFERENCES

1.   New York State Bridge Authority, 1999, Bear Mountain Bridge – The History, Informational Pamphlet Published by the NYSBA.

2.   Amman & Whitney, 2004, Main Cable Strengthening Study for the Bear Mountain Bridge over the Hudson River in New York, prepared for the New York State Bridge Authority.

3.   FHWA, 1999, Geotechnical Circular No. 4 – Ground Anchors and Anchored Systems, Publication No. FHWA-IF-99-015

4.   Post Tensioning Institute, 1996, Recommendations for Prestressed Rock and Soil Anchors

5.   Transportation Research Board, 2002, Recommended Practice for Evaluation of Metal-Tensioned Systems in Geotechnical Applications, NCHRP Report 477

Rockfall Closure Impact and Economic Assessment for Rockfall Sites in Tennessee

Vanessa Bateman
Tennessee Department of Transportation
6601 Centennial Boulevard
Nashville, Tennessee 37243-0360
615-350-4137
vanessa.bateman@state.tn.us

Abstract

Rockfall problems in Tennessee have traditionally been dealt with by the Tennessee Department of Transportation (TDOT) on a reactive basis. Rockfall sites along state highways and interstates in Tennessee have sometimes required expensive remediation and have resulted in traffic accidents and serious injuries to motorists. Because of these problems, recommendations made by Federal Highways, and the success of other states implementation of a hazard rating system, the Tennessee Department of Transportation chose to implement a rockfall hazard rating system. A project to locate and rate hazardous sites along Tennessee state routes and interstates is currently in progress and will be complete in 2005. However, this system, while identifying potentially hazardous sites, does not provide a good method for comparing the cost of mitigation and the impact of road closures due to rockfall. Thus another step is needed to provide TDOT planners with the tools needed to proactively address rockfall problems in Tennessee. After the initial detailed hazard rating other assessments are being made. The Rockfall Closure Impact addresses the impact on the roadway system if a rockfall incident were to occur. The Economic assessment provides a first estimate of mitigation costs and identifies "hazard reducers," a list of tasks that TDOT maintenance can incorporate into their workflows to provide some mitigation of rockfall sites until a larger project can be let. As with the TRHRS (Tennessee Rockfall Hazard Rating System), field data collection is completed with the use of PDA (personal digital assistant) forms and all of the data is incorporated into the larger GIS environment designed for use with the Rockfall Project.

If an unlimited amount of money were available, all high hazard sites would be obvious choices for repair. By keeping the TRHRS, an assessment of the impact of a rockfall should an incident occur (Rockfall Closure Impact) and a basic cost estimate in separate components, planners have better tools to allocate limited highway dollars and begin a systematic effort to address mitigation of high hazard sites.

Introduction

Rockfall incidents along state highways and interstates in Tennessee have sometimes required expensive remediation and have also resulted in traffic accidents and serious injuries to motorists (Royster, 1979; Moore, 1986). However, historically the Tennessee Department of Transportation (TDOT) has responded to rockfall problems on a reactive basis. In order to act in an active and systematic manner, TDOT approved the development of the Tennessee Rockfall Management System. The primary components of this system are:

1) A database for storage of rockfall information,
2) A GIS for viewing and analyzing rockfall data in a spatial manner,
3) A rockfall hazard rating system used to rank sites in order of hazard,
4) Development of computerized field data gathering methods,
5) Economic tools for assessing the impact of a rockfall incident, and
6) Tools for cost estimating of mitigation.

Phase I of the project involved the assessment of five counties in Tennessee, testing of the hazard rating system, updates to the database, development of field procedures and the development of a preliminary GIS (Drumm *et al*, 2002). The five counties were surveyed to classify rock slopes into "A", "B" or "C" slopes as described in the *Rockfall Hazard Rating System Implementation Manual* and shown in Table 1. All identified "A" slopes were then rated using the updated Tennessee Rockfall Hazard Rating System (TRHRS).

Table 1.   Preliminary Rating System
(Pierson, Davis and Van Vickle, 1990)

Class Criteria	A	B	C
Estimated Potential for Rockfall on Roadway	High	Moderate	Low
Historical Rockfall Activity	High	Moderate	Low

This rating system, based on the RHRS developed in the state of Oregon, uses a modified section for the site geology.   While keeping the same basic scoring system and range as the RHRS, the TRHRS explicitly notes the types of geological failure modes present at a site. Instead of two failure types the Tennessee system has five: plane shear, wedge, differential weathering, raveling and toppling/bedding release. Other factors such as abundance (i.e. percentage of the slope effected) and block size are taken into consideration. Like the RHRS, the TRHRS also considers site characteristics such as the roadway width, average vehicle risk, height of slope, ditch effectiveness, decision site distance, water on the slope and rockfall history (Drumm *et al*., 2002**)**.

Phase II of the project, still underway, will provide detailed ratings for all identified "A" sites across the state and will be completed in the winter of 2005. A final implementation of the GIS, updated PDA forms, and an Oracle Spatial database will also be completed by that date. The development of this system is a joint project between researchers at the University of Tennessee, Virginia Tech and the Tennessee Department of Transportation.

Development of the Rockfall Closure Impact (RCI) rating system

The RHRS and derivative systems, such as the TRHRS were designed to rank sites in order of hazard to the public. They do not take into account the costs of mitigation for rated sites, or the impact of a rockfall event on the traffic flow. Some rock slopes may only shed small rocks, which are a hazard to the public, but are easily removed. These events may not be as critical as larger potential failures with significant road closures. In 1987, a rockfall problem along I-40 in North Carolina, just across the Tennessee border, completely closed the interstate for over four months. While five people were injured in the original incident, seven people were killed in truck related accidents on the detour route during this closure. These deaths were attributed to the poor level of service offered by the state highway used as a detour (DiMillo, 1988). It is precisely issues such as facility degradation, raised by the I-40 rockfall incident, that are not addressed by the RHRS and its derivative systems. While completing a survey of a state as recommended by FHWA will yield locations of hazardous sites and a systematic method for ranking those sites, it does not consider the traffic impacts of lane and road closures, nor does it address the cost of mitigating these sites. It is for this reason that the Rockfall Closure Impact (RCI) and cost assessment tools were developed. It is meant as a supplement to the TRHRS, accounting not only for hazards presented actively by rockfall, such as a car striking or being struck by a falling rock, but also hazards presented passively by rockfall such as road and lane closures. With a ranking based on active rockfall hazards, an assessment of the impact of rockfall closures on the traveling public as well as a rough estimate of the cost of mitigation, planners can make far more informed decisions as to the placement of limited highway dollars.

While the RHRS and derivative systems do not really address these issues, the Unstable Slope Management from the Washington Department of Transportation takes some of these factors into account. This system in use for both landslides and rockfall looks at some different categories than the RHRS and realted systems. The UMS focuses more on the impact to the highway facility. A table detailing the rating system used with the UMS can be seen in Table 2.

Table 2. Rating System for the Unstable Slope Management System
(Lowell and Morin, 2000)

Criterion	Point=3	Points = 9	Points =27	Points = 81
Problem Type: Soil	Cut, or Fill Slope Erosion	Settlement or Piping	Slow Moving Landslides	Rapid Landslides or Debris Flows
Problem Type: Rock	Minor Rockfall, Good Catchment	Moderate Rockfall, Fair Catchment	Major Rockfall, Limited Catchment	Major Rockfall, No Catchment
Average Daily Traffic	<5000	5000-20,000	20,000 – 40,000	>40,000
Decision Site Distance	Adequate	Moderate	Limited	None
Impact of Failure on Roadway	<50 ft	50 – 200 feet	200 – 500 feet	>500 feet
Roadway Impedance	Shoulder Only	1/2 Roadway	3/4 Roadway	Full Roadway
Average Vehicle Risk	<25% of the Time	25-50% of the Time	50-75% of the Time	>100% of the Time
Pavement Damage	Minor – Not noticeable	Moderate – Driver must sloe	Severe – Driver must stop	Extreme – Not Traversable
Failure Frequency	No failures in the last five years	One failure in the last 5 years	One failure each year	More than one failure each year
Annual Maintenance costs	<$5,000 per year	$5,000 - $10,000 per year	$10,000 - $50,000 per year	>$50,000 per year
Economic Factor	No detours required	Short detours <3 miles	Long Detours >3 miles	Sole Access, no Detours
Accident in Last 10 years	1	2-3	4-5	>5

Some of the factors, however, are not really adoptable within the State of Tennessee. The Annual Maintenance Costs and the Accidents in the Last 10 years are not information currently collected by the Tennessee Department of Transportation, nor are they likely to be in the near future. Decision Site Distance, Impact of Failure on Roadway, Average Vehicle Risk and Failure Frequency are categories accounted for within the RHRS and the TRHRS. Some of these, such as Impact of Failure on Roadway are accounted for within the Average Vehicle Risk in the RHRS as it includes the slope length in the Average Vehicle Risk calculation (Pierson, Davis and VanVickle, 1990). The UMS also does not address the degradation of roadway facility and does not include a cost estimates for mitigation of particular sites. It sacrifices some of the detail from the RHRS in order to simplify the system. The UMS does not gather enough information for preliminary cost estimates and does not gather the geological detail present in the TRHRS. Therefore, a supplement to the TRHRS was developed as a means of rating the impact of a rockfall incident at the "A" sites.

Rockfall Closure Impact (RCI)

Like many of the previous hazard rating systems in the United States, the RCI is designed to rank sites in order of hazard. It also keeps the exponential scoring system used with the RHRS and proposed by Wyllie (1987). The RCI is made up of five factors, ADT, Detour Length, Impedance, Duration of Impedance and Facility Degradation. For each site, a score is generated from each of these five factors and is summed up for a final score. The details of the scoring system can be seen in Table 3.

Table 3.   Rockfall Closure Impact

Criteria	Score = 3	Score = 9	Score = 27	Score = 81
ADT (Average Daily Traffic)	Little Traffic ADT>300	Some Traffic ADT 300-1000	Moderate Traffic ADT 1000-3000	Major Traffic ADT >3000
Impedance	Shoulder	1 lane	2 lanes	>=3 lanes or Total
Impedance Duration	Hours	1 Day	Days	Weeks
Detour Length	Very Short <1 mile or lane still open	Short 1-2 miles	Medium 3-4 miles	Long or None >4 miles
Facility Degradation RF-DF= DOF	0	1	2	3

DOF=Degree of Facility (RF=Degree of Road Facility; DF= Degree of Detour Facility)

0 = Local Roads / 1 Lane Road
1 = 2 Lane, no shoulder
2 = 2 lane, adequate shoulder
3 = 3 lane
4 = 4 lane
5 = 4 lane, divided highway, 5 lane highway
6 = Interstate

The total RCI score is an indicator of the size and significance of a rockfall event. Higher RCI scores mean that a rockfall incident will have a higher impact on traffic and the surrounding communities. The system compares the "most likely worst case event." It provides a means for estimating both the extent and duration of road closures.

Traffic counts were set to reflect the rural nature of some critical Tennessee roadways. Many areas in the state do not have the high traffic volume of the cities. Impedance provides an estimate of the amount of road that will be closed. Impedance Duration gives the length of time that a roadway may be affected. A single day road closure is far less significant than one that stretches over several weeks or months. Detour length reflects the additional travel time needed to get around a closed road. If the road can remain open after an incident, the site receives the lowest score. A detour of more than 4 miles would receive the highest score.

Facility degradation is a measure of the change in service level from the original road to the detour facility. Thus if traffic is detoured from an interstate (RF=6) to a three lane road (DF = 3), the degree of facility (DOF) becomes 3 and the slope receives a score of 81 for Facility Degradation. This factor accounts for the change in capacity of the two different routes. If interstate traffic is re-routed along a two lane, rural highway, as happened with the I-40 interstate closure, the traffic problems and additional hazards are obvious.

Mitigation Cost Assessment

However, while the TRHRS establishes a ranking for rockfall hazard and the RCI establishes a ranking for rockfall impacts, no planning tool is complete without the ability to measure the costs of a site. The cost notes form developed serves several functions; it gathers information on possible mitigation alternatives, acts as the basis for the mitigation cost estimates performed in the office and also provides a list of tasks that can be sent out to district maintenance offices. It provides quick guidance for different mitigation strategies that might be used and provides a rough estimate of the amount of slope that could benefit from a particular repair. An experienced geotechnical engineer or geologist can fill out both these forms quickly based on the detailed hazard rating and a single visit to the site.

Table 4.   Cost Notes Form

Minor Repair Options	Amount of Option			
Hand Scale Slope?	>10% of Slope Face	10-30% of Slope Face	30-60% of Slope Face	>60% of Slope Face
Machine Scale Slope?	>10% of Slope Face	10-30% of Slope Face	30-60% of Slope Face	>60% of Slope Face
Remove Vegitation?	>10% of Slope Face	10-30% of Slope Face	30-60% of Slope Face	>60% of Slope Face
Any Ditch Effectiveness?				
Clean Out Ditch?	Few Rocks <1 truckload	Some Rocks 1-2 truckloads	Many Rocks 2-3 truckloads	Major cleanup >3 truckloads
Select Trim Blasting?	>10% of Slope Face	10-30% of Slope Face	30-60% of Slope Face	>60% of Slope Face
Major Repair Options	Amount of Option			
Recut Slope to State Standards?	>10 % of Slope Length	10-30% of Slope Length	30-60% of Slope Length	>60% of Slope Length
Extra ditch width needed?				
Any structures taken?	Type and number			
Rockfall Fence?	>10 % of Slope Length	10-30% of Slope Length	30-60% of Slope Length	>60% of Slope Length
Draped Wire Mesh?	>10% of Slope Face	10-30% of Slope Face	30-60% of Slope Face	>60% of Slope Face
Retaining Wall?	>10 % of Slope Length	10-30% of Slope Length	30-60% of Slope Length	>60% of Slope Length
Field Estimation of Best Repair				
Field Estimation of Secondary Repair				
Comments				

As with the other components of the Tennessee Rockfall Management System, personal digital assistant (PDA) forms were developed in order to facilitate fast and accurate data gathering and storage in the field.   These assessments are being completed behind the rockfall hazard rating teams from the University of Tennessee and Virginia Tech for all identified "A" sites.

The cost note form is used as the basis for the mitigation estimates calculated in the office. Using the information gathered with the cost notes form as well as the geometry and geology details provided by the TRHRS, a cost estimate worksheet included in the rockfall database was filled out for each "A" site visited. A standard table of rockfall mitigation components with estimated costs was also developed. This cost list is based on average bid prices paid by the Tennessee Department of Transportation for projects completed since 1999 (TDOT, 2004). Several older projects, with prices adjusted for inflation and personal communications with rockfall mitigation vendors were also used in order to compile the list.

A standard worksheet for rockfall mitigation methods is included in the database. This worksheet allows the user to enter the individual items, prices and quantities needed for a particular mitigation strategy. The worksheet calculates the total cost per item and per site. Multiple strategies can be entered, however, the mitigation strategy chosen for the cost estimate and summary data is the cheapest feasible option. A mitigation strategy, which, in the judgment of the geologist or engineer evaluating the site, has a high probability of failure, shall not be used. Figure 1 shows an example of the calculations used to arrive at an estimated mitigation cost.

Figure 1:   Screen Shot of Cost Estimate Form in Rockfall Database

Note that these costs are preliminary and are not meant to supersede the detailed work that would be needed before site mitigation were to be attempted. It is done without cross sections and by visual inspection of the site. A more detailed exploration may be required before an actual contract to repair a site would be let.

Results and Discussion

Ninety-nine of the "A" sites in 20 counties identified by UT and Virginia Tech field crews have been evaluated. These sites are clustered in middle Tennessee in TDOT Region 3. Sites in the northernmost counties of Region 2 were also included. Because interstates in Regions 2 and 3 have not yet been assessed, only one interstate rock cut was included in this data set.

Figure 2:   Location of 99 Sites in 20 Counties, Region 2-4 "A" Sites
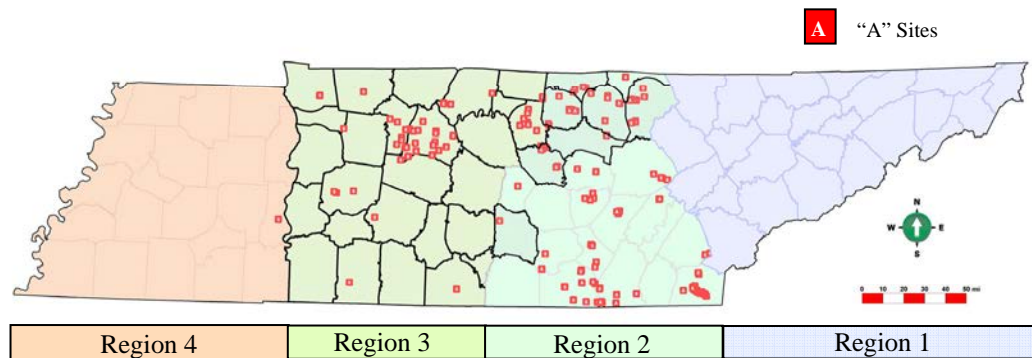
It should be noted that the analysis presented here is not the total data set that will be available on completion of the project. The data set comprises "A" sites from 20 counties and is used in order to demonstrate the capabilities of the system and methods. Figure 3 shows a bubble plot of the sites comparing the Rockfall Closure Impact (RCI) score with the Tennessee Rockfall Hazard Rating (TRHRS) score along with mitigation costs for these sites.

Figure 3: Rockfall Hazard Score vs. Rockfall Closure Impact
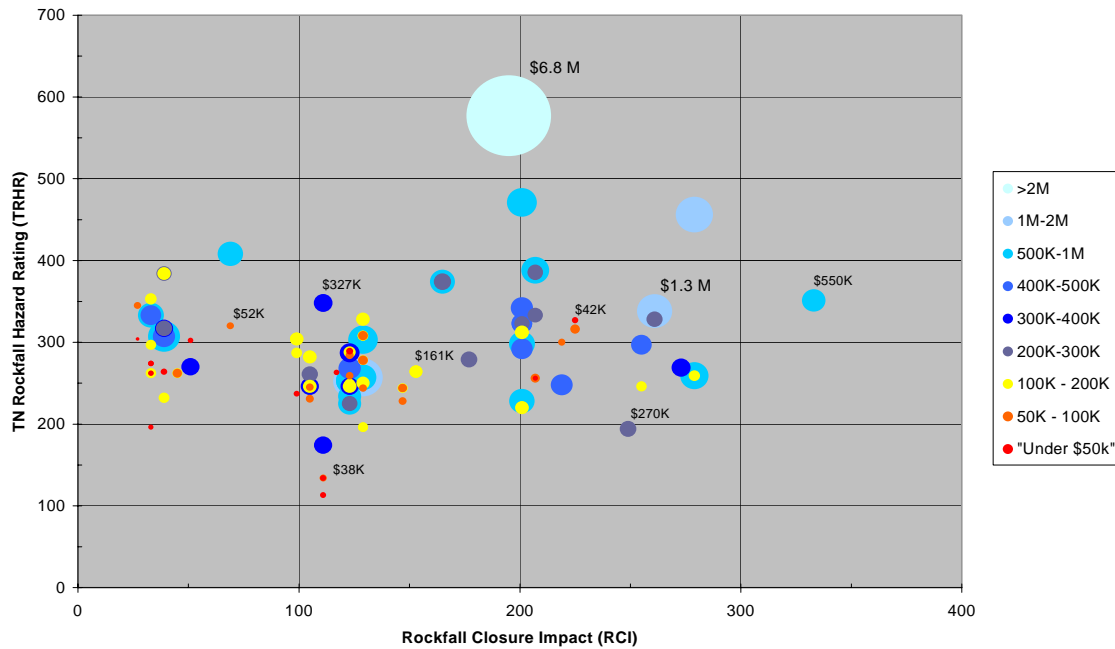
Estimated mitigation costs range from a low of just $14,000 to a high of $6.8 Million. The site with the highest cost had only a moderate RCI score, though it had the highest TRHR Score. While the majority of the lower cost sites also have lower RCI and TRHR scores, not all of these lower cost sites have low hazard and low rockfall impact. Table 5 shows the 19 sites, out of the 99 evaluated, which have both a high RCI score (over 200) and a high TRHR Score (Over 300). The first three sites shown have repair costs under $100,000, have a high rockfall hazard rating and will also have a high impact in case of a rockfall incident. These sites are significantly less expensive to mitigate than others, which also present similar hazard and rockfall impact scores.

Table 5. Sites with both High RCI and High Hazard Scores

| #	File Number	RCI		Hazard		Mitigation Cost
1	67SR084001006.50LRF	225	High	327	High	$42,525
2	19SR011001010.60RRF	219	High	300	High	$52,185
3	67SR294001001.40RRF	225	High	316	High	$94,250
4	44SR135001008.40LRF	201	High	312	High	$196,910
5	71SR084001012.20LRF	207	High	386	High	$219,695
6	71SR084001012.20RRF	207	High	333	High	$224,755
7	25SR085001007.90RRF	207	High	385	High	$226,800
8	41SR438001009.40LRF	201	High	323	High	$232,990
9	11SR001001006.30LRF	261	High	328	High	$250,397
10	16SR002001003.80RRF	201	High	323	High	$400,725
11	16SR002001003.80LRF	201	High	323	High	$400,775
12	83SR041001004.50RRF	201	High	342	High	$472,450
13	83SR041001004.10LRF	333	Very High	351	High	$525,020
14	67SR052001021.30RRF	207	High	388	High	$754,010
15	44SR135001007.10RRF	201	High	471	Very High	$850,520
16	11SR001001006.40LRF	261	High	338	High	$1,189,031
17	19SR001001002.40LRF	279	High	456	Very High	$1,317,855
18	80SR024001009.90RRF	261	High	384	High	$3,282,000
19	80SR025001008.60LRF	297	High	491	Very High	$5,267,030

Also worth noting are sites 5 and 14. They have almost identical hazard and RCI scores, yet the sites have a mitigation cost difference of $534,000. Table 6 shows the 18 sites that have a low RCI or a low Hazard Score. Here we can see that there are a number of sites which, while having a high hazard score, are low consequence failures. Some of these have high mitigation costs and likely would not be the first to be chosen for repair. Sites 20-23 have a low RCI impact score, but a high hazard score and a very low mitigation cost. Site 20 has an estimated mitigation cost of $14,000. This rock cut is only 12 feet in height at 180 feet in length, but has no ditch and very poor site distance. The impact to the road network is small and a failure at this location will not close the road. The higher hazard number and very low mitigation cost make the site an excellent candidate for early prioritization. Also of note are sites 24 and 31, which have high RCI scores. These two roads will be closed for some time in the event of a failure, both have a high ADT (average daily traffic) and there are no good detours. However, there is a $188,500 difference in their estimated mitigation costs.

Table 6. Sites with either Low RCI or Low Hazard Scores

| #	File Number	RCI		Hazard		Mitigation Cost
20	56SR056001002.10RRF	27	Low	304	High	$14,050
21	67SR052001021.90LRF	51	Low	302	High	$31,220
22	20SR100001009.95LRF	69	Low	320	High	$52,490
23	56SR056001002.20RRF	27	Low	345	High	$55,050
24	80IO040010254.00RRF	327	Very High	192	Low	$82,467
25	56SR262001008.80LRF	33	Low	353	High	$133,150
26	19SR012001008.40RRF	99	Low	304	High	$169,200
27	44SR135001010.40LRF	39	Low	384	High	$173,000
28	19SR012001008.40RRF	99	Low	304	High	$174,400
29	44SR135001010.40LRF	39	Low	384	High	$231,060
30	44SR135001008.60LRF	39	Low	317	High	$254,000
31	19SR024001001.80RRF	249	High	194	Low	$270,980
32	44SR135001008.60LRF	39	Low	317	High	$320,840
33	44SR135001012.70LRF	33	Low	333	High	$407,000
34	44SR135001012.10LRF	39	Low	307	High	$470,800
35	21SR141001002.90RRF	69	Low	408	Very High	$622,400
36	44SR135001012.70LRF	33	Low	333	High	$641,850
27	44SR135001012.10LRF	39	Low	307	High	$962,800

Costs can also easily be presented in aggregate, by roadway, county, region or maintenance district. Figure 4 illustrates this with a graph of the total mitigation cost for all rockfall sites evaluated to date by county.

Figure 4: Total Mitigation Costs by County
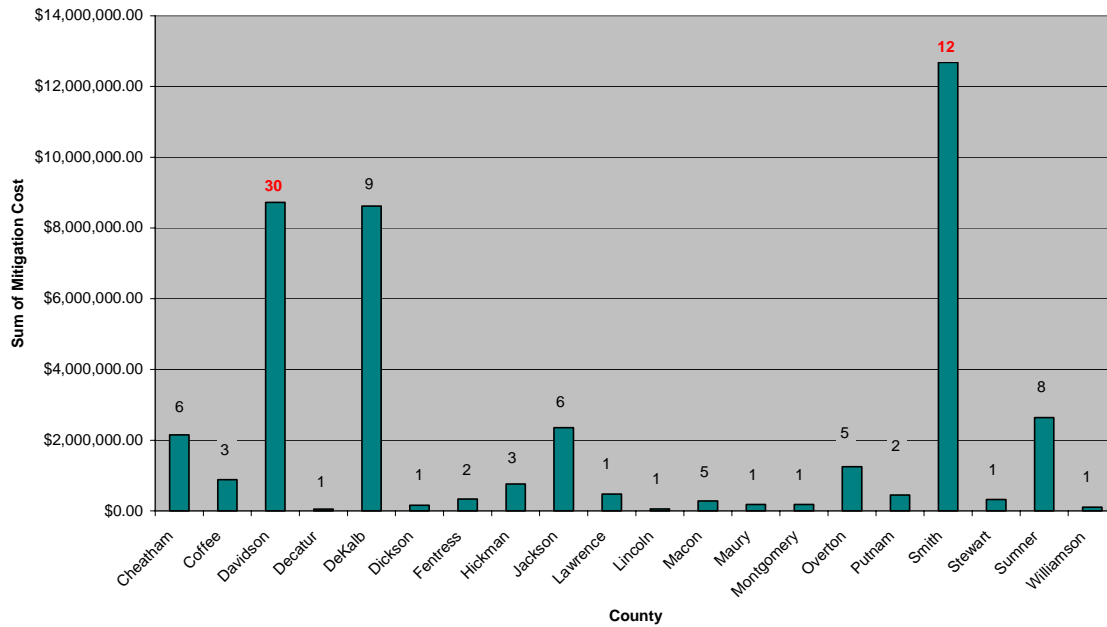
The total cost of rockfall mitigation in Davidson County is spread over 30 sites. Dekalb County, with a similar total cost, has only 9 sites. The most significant county identified thus far is Smith County, with an estimated mitigation cost of over $12.9 million dollars. Eighty-percent of that figure represents mitigation costs from only 3 sites. Figure 5 shows a similar graph, but with the results grouped by a selected set of roads. Here the average cost of rockfall sites along a particular road are shown along with the total cost of rockfall mitigation for all sites evaluated to date. Many other types of analyses are possible with the system including comparisons of TRHR score per mile of roadway, RCI score per mile of roadway as well as other types of spatial analysis.

Figure 4: Mitigation Costs by Route Number
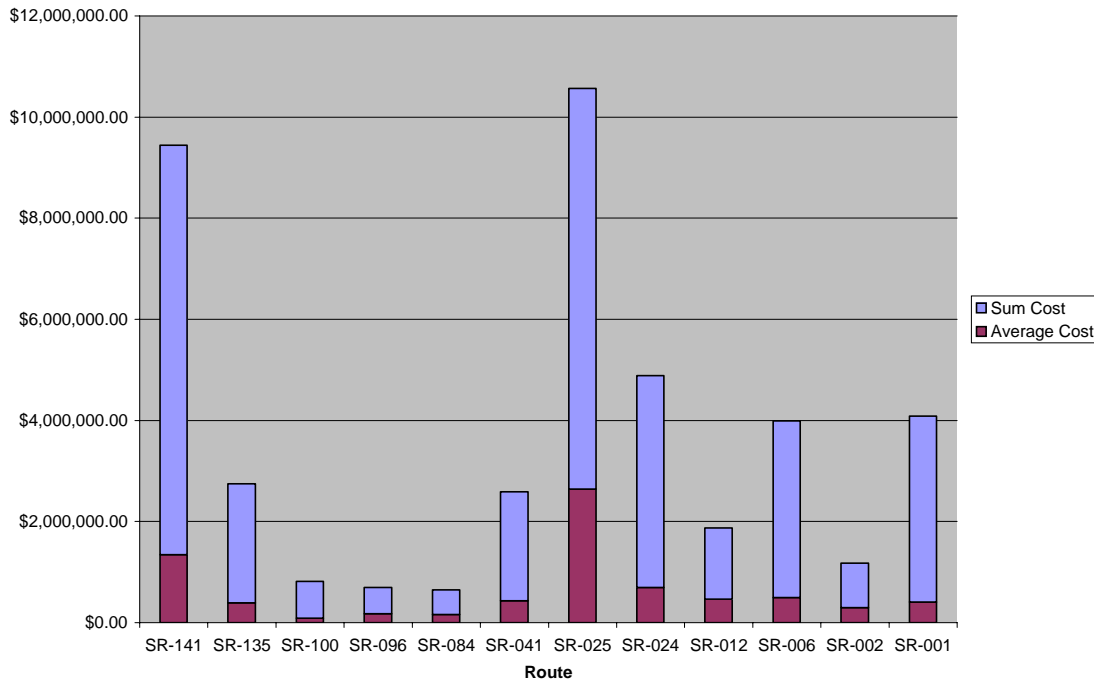
Unsurprisingly, many of the high rockfall hazard sites identified to date also have a very high price tag for mitigation. If an unlimited amount of money were available, these high scoring hazard sites would be obvious choices for repair. Because there is not, we need tools for sorting and intelligent prioritizing of sites based on available funds. The site with the highest hazard score may not give the best return if it has a very high cost and low impact of the traffic system. A critical roadway, which may be shut down for weeks at a time because of a rockfall event, might well receive priority over a site with a high hazard, but a low impact in case of an incident. The RCI component acts as a predictor for the consequence of a rockfall incident should one occur.

There is no set formulae to take into account exactly which site should be mitigated first, because that depends upon a number of factors that cannot be easily quantified ahead of time. For one thing, the amount of money available to devote to rockfall mitigation can make a huge difference. If $5 million were allocated this might take care of several counties. However, if only $100,000 were allocated to repair rockfall in a county, the choices are far more limited. By keeping the TRHRS, RCI and Cost categories in separate components, the impact of these three factors becomes more obvious. As funds become available and priorities are established, the system gives planners much better information for resource allocation.

References

Bateman, V.C., 2002, Managing Rockfall Hazard: The Tennessee Rockfall Hazard Database, Unpublished Masters Thesis, University of Idaho, 193 pages.

Burnett, Jim, 1988. Safety Recommendation. Letter from the National Transportation Safety Board to Robert E. Farris of the Federal Highway Administration.

DiMillo, A., 1988, Section 4.92 Rockfall Hazard Mitigation from, *A Quarter Century of Geotechnical Research*, Federal Highway Administration Report Number FHWA-98-13X, Washington, DC.
Web link: *http://www.tfhrc.gov/structur/gtr/century/chap04/chpt04.htm*

Drumm, E.C., Dunne, W. M., Mauldon, M., Bateman, V. Rose B., Bellamy, D., Vandewater C. (2001) "*Rockfall Management System (RMS) for Tennessee*", presented at the Southeastern Transportation Geotechnical Engineering Conference, Roanoke, VA

Drumm, E.C., M. Mauldon, W.M. Dunne, V.C. Bateman, D. Bellamy, C. Vanderwater, B. Rose, 2002, *Rockfall Management System for Tennessee: Final Report – Phase I*, Tennessee Department of Transportation, Division of Materials and Tests, Geotechnical Engineering Section, Nashville, TN.

Lowell, S. and P. Morin, 2000. Unstable Slope Management: Washington State. *Transportation Research News*, Volume 27, Transportation Research Board, Washington, D.C.

Moore, H., 1986. Wedge Failures along Tennessee Highways in the Appalachian Region: Their Occurrence and Correction. *Bulletin of the Association of Engineering Geologists*. Volume 23, Number 4, pp. 441-460.

Oliver, L. 2001. Personal Communication. TDOT - Division of Materials and Tests, Geotechncial Engineering Section, Nashville, TN.

Pierson, L., S. Davis and R. Van Vickle, 1990. *Rockfall Hazard Rating System Implementation Manual*. Federal Highway Administration Report FHWA-OR-EG-90-01, Federal Highway Administration, Washington, D.C.

Royster, D.L, 1979, Landslide Remedial Measures, *Bulletin of the Association of Engineering Geologists*, Vol. XVI, No. 2.

TDOT, 2004. Average Unit Bid Prices 1999-2003, Tennessee Department of Transportation, Construction Division.
Web link: http://www.tdot.state.tn.us/construction/specs.htm#AVERAGE%20BID%20PRICES

Vandewater, C. (2002) "*Geologic Controls on Rockfall Potential for Road-cuts in Middle and East Tennessee*", Master of Science Thesis, University of Tennessee, Knoxville, TN

Wyllie, D., 1987. Rock Slope Inventory/Maintenance Programs. *FHWA Rockfall Mitigation Seminar*, 13th Northwest Geotechnical Workshop, Portland Oregon.

Iowa Department of Transportation – Soil Survey Use of GPS, GIS with GPS, and Automation Applications for Soils Design

Matthew Trainum, Geologist
Soils Design Section, Office of Design
Iowa Department of Transportation

The Iowa Department of Transportation (IDOT) includes in the letting plans of major road construction projects, a set of boring plan and soil profile sheets of the proposed alignment. These sheets are prepared by the Soils Design Section of the Office of Design and are for Contractor bidding purposes and general use during construction. With the advent of using Global Positioning System (GPS) for survey, the Soils Design Section began in 1997 to use GPS locating and electronic data collection for all major projects.

The methodology implemented was to utilize a small laptop meeting military specifications for ruggedness, GPS software, and a mobile GPS unit with receiver/transmitter antennae for "real time" differential GPS, based on signal correction from Coast Guard Beacons within/adjacent to the state of Iowa. A predetermined boring layout is constructed in Computer Aided Design Drafting (CADD) software on a defined coordinate system. This design file is then loaded onto the laptop/GPS unit setup for the visual navigation of the Soil Survey Crew.

The Soil Survey Crew locates each boring site, recording the State Plane Coordinates (easting (X) and northing (Y)) and then opens up a database form, an in-house developed program, for the input of soils information (i.e. field descriptions, sampling information, soil parameters, etc).

Currently, the GPS software being used allows for the display of the boring layout as a geo-referenced graphic file. The IDOT is, at the time of this abstract, currently pursuing a GPS tool to work within Geographic Information System (GIS) software, used by most offices/sections of IDOT for initial review and analysis of projects. This GIS software allows for "on the fly" display of other images, of differing coordinate systems (i.e. USGS topographic maps, Geo-referenced aerial photos and design files, etc), into a predetermined coordinate system. The use of a GPS tool within the versatile capability of the GIS software is not only for greater visual information for the Soil Survey Crews, but also for better communication with property owners.

In addition to improving field work with a better GPS setup, the Soils Design Section is also moving to the automation of the plan and profile soil sheets. This is an in-house developed program. The process combines all soil information for a project; field collected data (i.e. X and Y coordinates, descriptions, depths, water levels, etc) and lab testing data (i.e. AASHTO classifications, sieve analysis, LL, PL, PI, etc), into a single database. With an automated assignment of predetermined soil layer material types, multiple forms are created for drawing the information on plan view, profiles, and cross sections (i.e. the borings symbols and identifications, layer lines, soil patterns, soil descriptions, etc). This information is then subject to final review and manual "override" by the Geotechnician, Geologist, and/or Geotechnical Engineer. The process will significantly decrease the amount of office work in design preparation.

Evaluation of Some Geologic Factors Affecting the Quality of Limestone Construction Aggregate*

By

Jason Mckirahan [1, A], Robert H. Goldstein[1], and Evan K. Franseen[2]

[1] Department of Geology, University of Kansas, Lawrence, KS 66045
[2] Kansas Geological Survey, University of Kansas, Lawrence, KS 66047

**[A] Present Address: Marathon Oil Company, 5555 San Felipe,
Houston, TX 77056**

Introduction

Carbonate aggregate producers and municipalities, state, and federal agencies are increasingly recognizing the need to understand the variables that affect the quality of material used for aggregate in construction. In many parts of the United States, where limestone and dolomite are the primary source of aggregate available, issues of aggregate durability are of prime concern. In eastern Kansas for examples, certain municipalities have required the use of far distant "hard-rock sources" of aggregate because of questions about consistency in the quality of the local sources of limestone aggregate. This has adversely affected a major Kansas industry and has the potential of adding significantly to costs of portland cement concrete pavement construction projects. It is clear that much remains to be learned about the factors that control the durability of limestone aggregate, and that research must be completed in order to assure consistent sources of durable limestone aggregate in Kansas and in other parts of the country.

The goal of this study is to evaluate geologic and physical properties of limestone aggregates in an attempt to find criteria that can be used to quickly and efficiently identify highly durable aggregates and those subject to decay over time. Most past concrete aggregate-related research in Kansas has concentrated on a type of deterioration known as d-cracking. D-cracking is characterized by fine, closely spaced, parallel cracks that have blue, black, gray, or white deposits in the crack at the pavement surface. It typically develops parallel to joints or cracks in the pavement. (Crumpton *et al.*, 1994).

An early study related to d-cracking was conducted by the Kansas Department of Transportation (KDOT) in 1944 and suggested a significant relationship between coarse aggregates and d-cracking. As a result, the sizes of aggregate used in pavement concrete were reduced, resulting in improved pavement performance. In 1973 Bukovatz *et al.* presented the results of another study on d-cracking and again concluded that coarse aggregates, and specifically coarse limestone aggregates, were a main cause of d-cracking. They stated that pavements that contained more than 35 percent coarse limestone aggregates were more likely to be d-cracked than pavements with less than 35 percent coarse limestone aggregates. Most pavements without limestone coarse aggregate were rated as good.

Best (1974) reported the results of a seven-year study with the goal of finding a specific cause for d-cracking. Although this study concluded that the exact cause of d-cracking still remained a mystery, it was suggested that the freezing and thawing of water within the pavements was a main contributor. This study also supported the previous suggestion that coarse, limestone aggregates were a cause of the problem.

Based on the results of the early studies and those reported by Bukovatz and Crumpton (1981), KDOT adopted new requirements for selecting limestone

aggregates. The plan adopted was to evaluate each quarry, subdivided into beds, and to approve or reject each individual bed based upon the results of laboratory freeze-thaw testing of concrete beams containing the coarse limestone aggregate from each bed (Wallace & Hamilton, 1982). Those aggregates that meet a minimum set of requirements concerning durability, freeze-thaw resistance and expansion are considered class 1 aggregates and are approved for use as construction grade material. The testing system outlined by the 1982 report is used today, and the use of aggregates meeting the established criteria has reduced occurrences of d-cracking. The tests are costly and time consuming, however, taking a minimum of six months to perform.

Research on geologic parameters that affect aggregate quality has been carried out for decades to identify more time-efficient methods to determine aggregate quality. Efforts have included thin-section petrography, rock texture classification, insoluble residue, clay content and type, pore size and distribution of porosity, and various geochemical analyses (e.g. Shaffer *et al.*, 2004; Oyen *et al.*, 2001; Lasemi and Smith, 1999; Chyi *et al.*, 1999; West, 1998; Bliss, 1998; Fountain *et al.*, 1996; Shakoor *et al.*, 1982; Biggs, 1966; Hiltrop and Lemish, 1960). Although the efforts to date have provided some insight into factors affecting aggregate quality, there is much more to be learned.

This paper reports on one project in our continuing efforts to identify geologic parameters that can be used to distinguish quality aggregates more easily. During the preliminary stages of the project several quarries currently producing class 1 limestone aggregate in eastern Kansas were visited. The units examined included the Tarkio Limestone, the Merriam and Spring Hill Limestones, the Argentine Limestone, and the Farley Limestone. Based on preliminary observations of outcrops and hand samples at the start of this study, specific geologic variables to be discussed, seem to affect whether a unit passes or fails the class 1 aggregate physical tests. These variables allowed the development of several general working hypotheses testable in the Farley Limestone.

(1) Micrite (microcrystalline calcite) -rich, phylloid-algal lithologies consistently produce durable aggregates.
(2) Fine-grained, matrix-rich limestones tend to pass, whereas coarser carbonate grainstones with coarse cements tend not to pass.
(3) High amounts of acid-insoluble residue in the rock has a negative impact.
(4) Distinct, sharp stylocumulates and shale beds have little or no impact on durability, whereas diffuse stylocumulates have a negative impact.
(5) Argillaceous limestones tend to fail testing; therefore the presence of clay minerals in the insoluble residues has a negative impact.
(6) Abundant, coarse, sparry calcite in the rock has a negative impact.

(7) Pyrite-rich, dark colored limestones, and those weathering with a strong
orange color tend to be poor in quality. These limestones are those most
likely rich in ferroan calcite, ferroan dolomite, and ankerite.

This study uses the Farley Limestone as a test case because it varies
significantly both laterally and vertically in aggregate quality and allows initial testing
of the first six of the hypotheses. If an understanding of how geologic factors interact
to produce high-quality rock in the Farley is established an analog for other similar
limestone units in different locations can be developed.

Methodology

To gather data on the various geologic variables, detailed measured
stratigraphic sections were described in eight quarries. Included in these sections were
both active and inactive quarries from which KDOT has produced both class 1 and
nonclass 1 aggregates from the Farley Limestone. All stratigraphic sections were
measured at or near the locations from which KDOT had recently tested aggregates.
Also included in the stratigraphic study were descriptions of outcrops and drill cores.
These sections helped fill gaps between quarry exposures so that a more accurate
stratigraphic reconstruction of the field area was possible. Information obtained
includes bedding nature, preliminary lithologic classification, fossil types, and the
percentage of the rock volume composed of sparry calcite. Descriptions of outcrops
also emphasized determining the percentage of each stratigraphic interval that
contained clay-rich zones. Shale beds, concentrated stylocumulates, diffuse
stylocumulates, and disseminated argillaceous material were documented. Percentages
of the total section that contained each form of argillaceous material were recorded.
The different types of clay-rich zones are discussed in greater detail below.

After stratigraphic sections were measured and described in the field, samples
were collected. For each of the stratigraphic sections, hand samples were collected,
and polished slabs and thin sections were made. These slabs and thin sections allowed
a more accurate, detailed description of each lithology using the Dunham classification
for carbonate rocks (Dunham, 1962). The descriptions include dominant depositional
fabric, identification of fossils and other carbonate grains, and a more accurate
estimation of the percentage of sparry calcite.

In addition to hand samples, 10 bulk rock samples of 250 pounds each were
collected and turned over to the Materials and Research Division of KDOT for
physical testing according to their established guidelines and procedures. After initial
crushing of these ten samples, 3 pounds of the crushed aggregate was obtained from
KDOT for each sample. This split included both $^3/_8$ and $^1/_2$ inch crushed aggregate.
Independent tests conducted on the crushed aggregates included determining acid
insoluble residue percentage, grain-size distributions of insoluble residues, x-ray

identification of residues, and thin-section petrography to examine lithologies and spar content.

KDOT Physical Tests

Ten 250 pound rock samples were obtained from the Farley Limestone in Johnson and Wyandotte counties and were identified as sample numbers KU-1 to KU-10. These samples were then tested by KDOT using the normal testing protocols proscribed by KDOT to determine aggregate durability. Physical test data for samples recently tested by KDOT from the Farley Limestone are also used in the study. These samples are referred to as KDOT-1 to KDOT-20. Stratigraphic sections were measured and described at or near the site of the KDOT sampling, so their test results could be compared directly to field observations.

The following sections summarize the parameters measured by the physical tests conducted by the Materials and Research Division of KDOT. The results of these tests constitute the data that are compared to data on geologic variables.

Absorption

Absorption is a measure of porosity and permeability of an aggregate sample and is determined as part of the physical tests conducted by KDOT. The reported value is given as a percentage of weight gain after soaking the aggregate in water for 24 hours.

Modified Freeze-Thaw Test (Soundness)

The modified freeze-thaw test (soundness) is used as the first cut to determine whether an aggregate will undergo additional testing. The test determines an aggregate's resistance to freezing and thawing and is performed on raw aggregate that has been size graded and weighed. The aggregate is size graded so that only $^1/_2$ and $^3/_8$ inch aggregates are tested. Following 25 cycles of freezing and thawing, the aggregate is size graded again and reweighed to determine how much mass the original sample has lost. The reported freeze-thaw value is the percentage of the aggregate's original mass that is retained after 25 cycles of freezing and thawing. If the modified freeze-thaw value is 0.85, the value reported in this study would be 85 percent. This indicates the sample lost 15 percent of its mass due to degradation from freezing and thawing. At present, KDOT requires a minimum modified freeze-thaw value of 0.85 to continue with testing. If samples do not have a 0.85 modified freeze-thaw value, they are classified as nonclass 1, and no further tests are conducted on that aggregate.

L.A. Wear Test

The L.A. wear test examines the resistance to degradation by abrasion and impact of the limestone aggregates using the ASTM Test C131-89. It is done by size

grading the aggregates, weighing them, and tumbling them in a large rotating drum with several large steel balls. Following the test, the aggregate is resized and weighed again. The value reported indicates the percentage of the original mass lost due to size reduction from degradation by abrasion and impact. This test is not typically useful in classifying aggregates relative to durability.

Expansion

Expansion percentages are determined as part of ASTM Test C666-92 Procedure B. It is accomplished by making three concrete beams out of the limestone aggregate to be tested and a standard cement mix. Two pins are placed in the beams, and after the beam is cured a precise measurement of the distance between the pins is measured. The beam is subjected to cycles of freezing and thawing; at periodic intervals the beam is examined and the distance between the pins is remeasured. The value reported is a percentage of expansion over the original measurement. KDOT currently uses an average of 0.02 percent expansion for the three beams as the maximum expansion limit allowed for class 1 aggregate.

Durability Factor

Durability factor is used to indicate an aggregate's durability and resistance to freezing and thawing. The durability factor is determined using ASTM Test C666-92 Procedure B. The value is related to the percent change in the fundamental transverse frequency of the beams, which is reported as the relative dynamic modulus of elasticity. The modulus of elasticity is a ratio of stress to strain in the elastic region and is an overall measurement of stiffness of a material. The durability factor measures the change in stiffness of the beams after a specified number of cycles of freezing and thawing. Currently, KDOT requires a durability factor of at least 95 to qualify an aggregate as class 1.

Lithologic Parameters

The following sections summarize the specifics of lithologic parameters that were compared to the results of the KDOT physical tests.

Lithology

Lithology was determined by examination of outcrops, hand samples and thin sections. Aspects of lithology considered include depositional fabric (Dunham textural classification), matrix type, fossils, and grain types. Comparing lithology to KDOT physical tests allows for identification of lithologies that might consistently produce durable aggregates. Lithologic examination also allows conclusions concerning the importance of micrite and microspar versus coarser cement (sparry calcite). Although

these lithologic properties are qualitative in nature, there is potential for the identification of characteristics that are important in aggregate durability.

Spar Content

Accumulations of coarse spar (clear, crystalline calcite) constitute 10 to 60 percent of the limestones in the Farley. These spar accumulations resulted from either cementation of pore space or neomorphism of micrite matrix. In the Farley Limestone, sparry cement is found in fractures, in molds, and in original pore spaces between or within grains. Neomorphic spar fabrics are also common in the Farley Limestone and dominated by microspar and pseudospar fabrics with crystals defined by Folk (1965) to be in the range of 4 to 50 micrometers in size.

Bulk Spar Percentage

For the purpose of this paper, bulk spar percentage is defined as the percentage of the rock composed of visible, coarsely crystalline material including fracture fillings, spar-filled fossil molds, replaced fossils, and any spar-filled interparticle porosity (Figure 1). Estimates of spar content were made from examination of quarry outcrops and from cut and polished hand samples. Any visible accumulation of spar larger than approximately 0.5 mm was considered in the estimate. The value reported is an estimate of the total percentage of the rock volume that is composed of spar.

Average Spar Crystal Size and Crystal Form

By examining thin sections made from hand samples of each rock subjected to KDOT physical tests, average spar crystal size for each sample was determined. Because 80 to 90 percent of micrite matrix in the rocks of the Farley Limestone was recrystallized to microspar or pseudospar, those crystals finer than 50 micrometers are considered matrix and are not included in the estimates of average crystal size. Also noted during examination of thin sections were various types and shapes of spar present in the rocks. Table 1 is a summary of how the spar was classified and described.

Spar Percentage of Crushed Aggregates (Aggregate Spar)

As defined for this paper, spar percentage of crushed aggregates, referred to as aggregate spar, refers to the percentage of rock composed of spar following crushing and sorting of the original rock. This estimate includes only spar coarser than 50 micrometers. Any spar finer than 50 micrometers is considered matrix and therefore is not included in this percentage. Whereas the bulk spar percentage discussed above is determined from outcrops and hand samples, the aggregate spar percentage was estimated following petrographic examination of splits of aggregate samples subjected

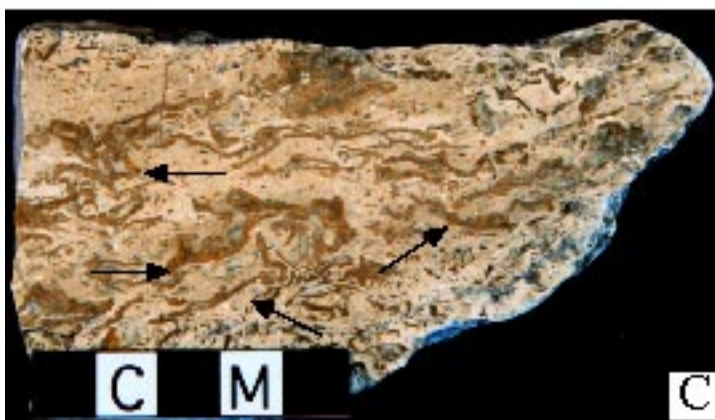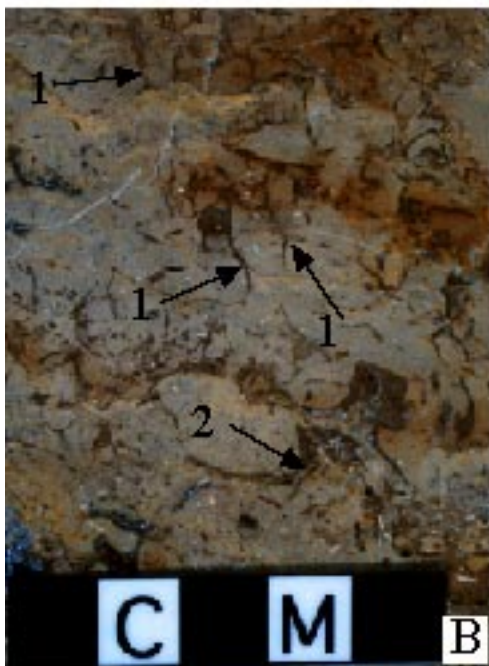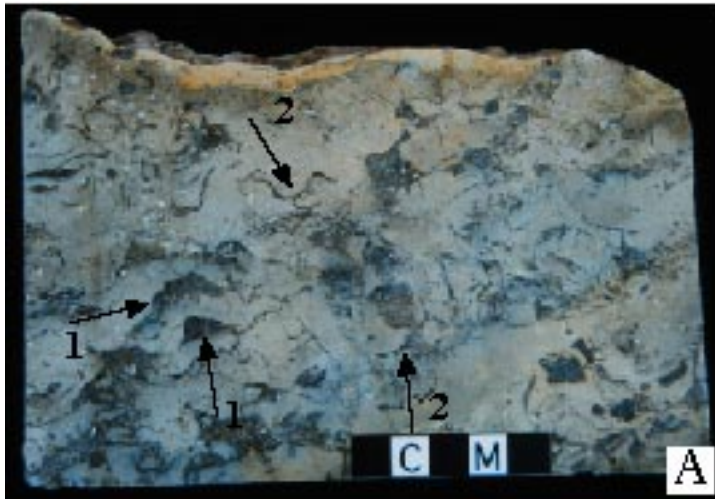**Figure 1.** Hand samples showing different types of spar accumulations found in the rocks of the Farley Limestone. (A) Phylloid algal wackestone with spar in shelter pores (1) and phylloid algal molds (2). (B) Phylloid algal wackestone with spar dominantly in fractures (1) and phylloid algal molds (2). (C) Phylloid algal packstone with spar found almost exclusively in phylloid algal molds (arrows).

Spar Type	Crystal Shape	Crystal Size	Boundary Shape
Sparry Cement	Equant: crystals have essentially equal length and width Bladed: length to width ratios are between 1.5:1 and 6:1 Fibrous: length to width ratio is greater than 6:1	Wide range of crystal sizes ranging from approximately 50 microns to several millimeters.	Intercrystalline boundaries of equant crystals are typically planar with even contacts. Irregular boundaries are present in small (under 70 microns) equant crystals and on some bladed crystals.
Neomorphic Spar	Exclusively equant crystals	Microspar: equant crystals of 5-10 microns. Pseudospar: equant crystals of 10-50 microns	Neomorphic spar is typically found in mosaics of microspar or pseudospar with crystal boundaries of an irregular nature.

Table 1. Table of spar characteristics observed in the rocks of the Farley Limestone.

to KDOT physical tests in order to deal with differences before and after crushing. Because this property is obtained from crushed aggregates, data were only available for those 10 samples for which crushed aggregates were available (KU-1-KU-10).

Clay Percentage and Type

All data concerning clay percentages and forms for all rocks studied were compiled from field observations and laboratory testing.
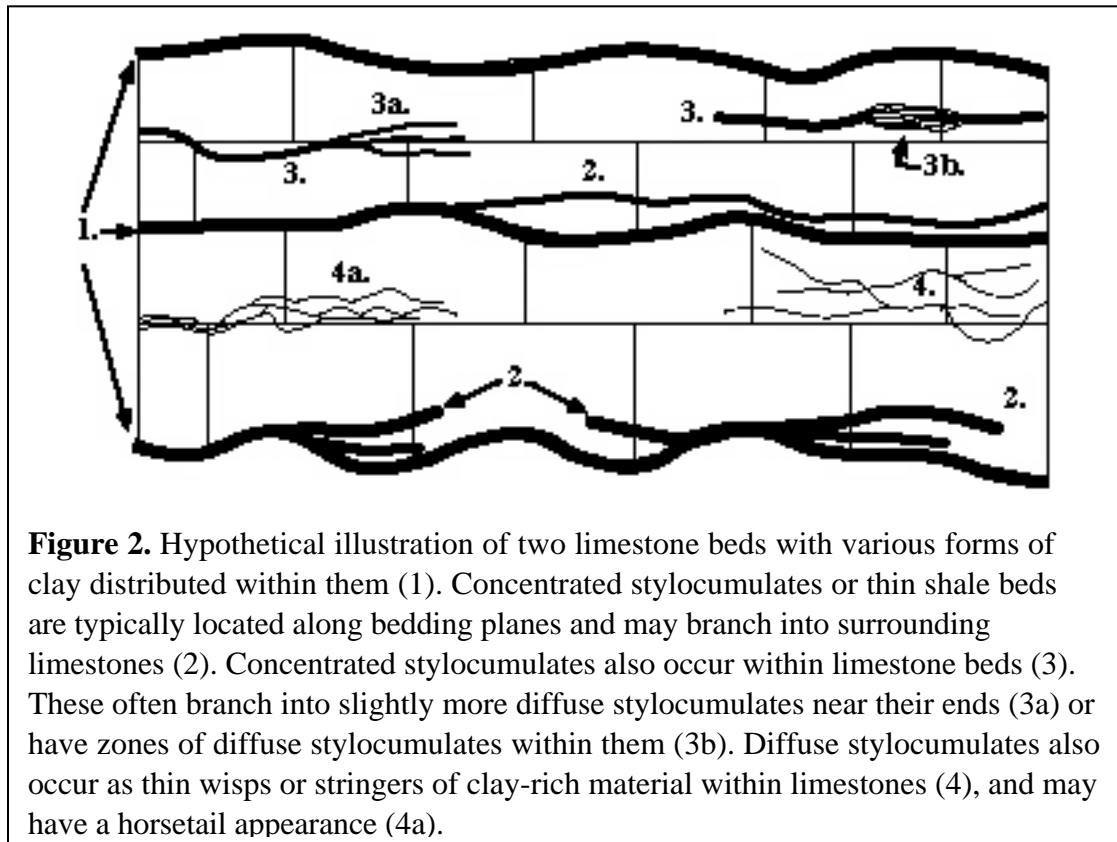
Total Percentage of Clay-Rich Strata

The total percentage of clay-rich strata is an estimate of the total thickness of the stratigraphic interval that contains any type of clay-rich zone. To calculate this value, estimates of the thickness of individual beds that contained any clay-rich material were made. From these estimates of clay content of individual beds, a total percentage of clay-rich strata was calculated for each stratigraphic interval.

Clay Distribution

Clay is typically distributed within a stratigraphic interval as shale beds, concentrated stylocumulates, diffuse stylocumulates, and disseminated material. Commonly it is found in concentrated clay-rich seams or stylocumulates defining bedding planes or within individual beds (Figures 2, 3). Shale beds and concentrated stylocumulates were identified by their size, shape, and relationship to the surrounding carbonate. The concentrated stylocumulates are typically ≥ 5 mm thick and are dominantly planar to slightly undulose with uniform thicknesses along their

lengths. The seams generally have sharp to slightly gradational contacts with surrounding carbonate and commonly contain fossil material. Concentrated stylocumulates and shale strata are easily identified because they can be removed from the surrounding carbonate with a hammer or pick or by crushing the rock. This is possible because there is little carbonate within the clay-rich area and it is easily separated from the surrounding limestone. Therefore, this occurrence of clay generally does not become a part of the aggregate because it is crushed into fine particles.

Some clays are in diffuse stylocumulates spread out within limestone beds (Figures 2 & 4). These diffuse stylocumulates are composed of numerous subparallel microstylolites and have a wispy to patchy appearance commonly dying out into the surrounding limestone. Because the diffuse stylolites are composed of numerous microstylolites spread throughout the limestone, they cannot easily be separated from the surrounding limestone with a pick or by crushing the rock.

Figure 2. Hypothetical illustration of two limestone beds with various forms of clay distributed within them (1). Concentrated stylocumulates or thin shale beds are typically located along bedding planes and may branch into surrounding limestones (2). Concentrated stylocumulates also occur within limestone beds (3). These often branch into slightly more diffuse stylocumulates near their ends (3a) or have zones of diffuse stylocumulates within them (3b). Diffuse stylocumulates also occur as thin wisps or stringers of clay-rich material within limestones (4), and may have a horsetail appearance (4a).
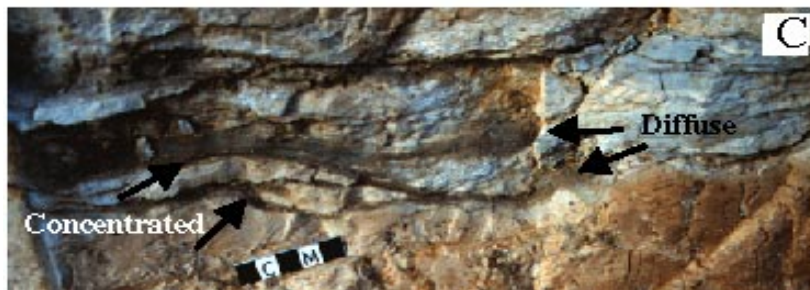
Figure 3. Photos of concentrated stylocumulates as they appear on outcrop. (A) Thin shale bed located between bedding planes.(B) Concentrated stylocumulate that branches into thinner and slightly more diffuse stylocumulates from left to right. (C) Concentrated stylocumulate that becomes more and more diffuse from left to right. The clay on the left would likely separate from the limestone in crushing whereas that on the right would likely remain in the aggregate after crushing.
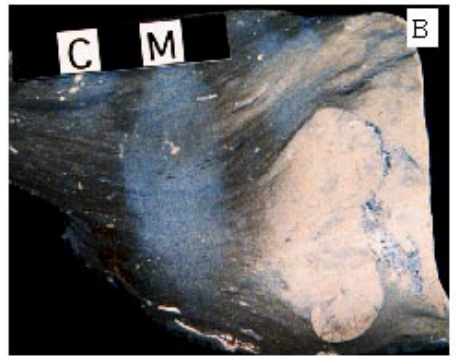
Figure 4. (A) Photo of thin, diffuse stylocumulates on outcrop. The irregular pattern, thinness and distribution throughout the limestone would likely cause these clay-rich zones to become part of the aggregate following crushing of the rock. (B) Hand sample of argillaceous skeletal wackestone (locality SRS) showing the stringy, and wispy nature of the diffuse stylocumulates. These wisps of clay-rich material will not be separated from the limestone when the rock is crushed.

Figure 5. Photo of a bed of phylloid algal wackestone with completely disseminated argillaceous material throughout its thickness. This from of clay is recognized by the bluish-gray color it imparts to the rock. Due to the disseminated nature of the clay, it will become part of the aggregate following crushing of the rock.

Because of its diffuse nature and distribution throughout limestone beds, this occurrence of clay generally will be retained in the crushed aggregates

Clay also occurs as completely disseminated argillaceous material in limestone. In these occurrences there are no visible discrete seams or stylolites. Instead, this clay distribution is typically recognized in outcrops by the bluish-gray color the disseminated clay imparts to the rocks (Figure 5). Like diffuse stylolites, argillaceous material that is completely disseminated throughout the limestone cannot be separated from the limestone and will become part of the crushed aggregate.

Insoluble Residues

Data on insoluble residue percentages of aggregate samples KU 1 to KU-10 were determined by the author, whereas percent insoluble residue for aggregate samples KDOT 1 to KDOT-20 were determined by the Materials and Research Division of KDOT as part of their testing protocol. Other data concerning insoluble residues, including grain size distributions and compositions, were determined for samples KU-1 to KU-10 only.

Percent Insoluble Residue

Percent insoluble residue represents the weight percent of aggregate composed of acid insoluble residue determined by digesting crushed aggregate samples in dilute hydrochloric acid, weighing the filtered residues, and calculating the total percentage by weight.

Insoluble Residue Grain Sizes & Aggregate Clay Percentage

Grain size distributions of the insoluble residues were determined for each aggregate sample tested for this study (KU-1 to KU-10). This was accomplished by weighing the residues, dispersing them in water, and sieving them. Following sieving, the mass of each fraction retained on the sieves and the mass of the fine fraction that passed through the finest sieve was determined and a percentage of the original sample was calculated for each grain size.

Using the percentage of each sieved residue composed of clay-sized material, a value was calculated that represents the weight percentage of the original aggregate mass composed of clay-sized material. This value is referred to as the aggregate clay percentage. Insoluble residue grain size data were not available for samples taken by KDOT.

Insoluble Residue Composition

Mineralogical compositions of insoluble residues of samples KU 1 to KU-10 were determined using x-ray diffractometry. These data were not available for samples taken by KDOT.

Results

In order to evaluate the hypotheses outlined at the beginning, data concerning the geologic variables must be evaluated relative to the results of the KDOT physical tests. Durability factor is the most important measurement in determining if an aggregate is a class 1 aggregate. For this reason, geologic variables are compared to the results of ASTM Test C666-92, Procedure B, which KDOT uses to determine durability factor. Other important test results used in KDOT's determination of whether an aggregate qualifies as class1 include the expansion percentage and the modified freeze-thaw (soundness) ratio. Therefore, some geologic variables were also compared to these results and correlations are discussed where applicable. Because durability factor is so highly correlated to expansion percentage (Figure 6), however, it is apparent that in most cases only one of these variables need be compared to lithologic parameters. Alternatively, because the results of the modified freeze-thaw
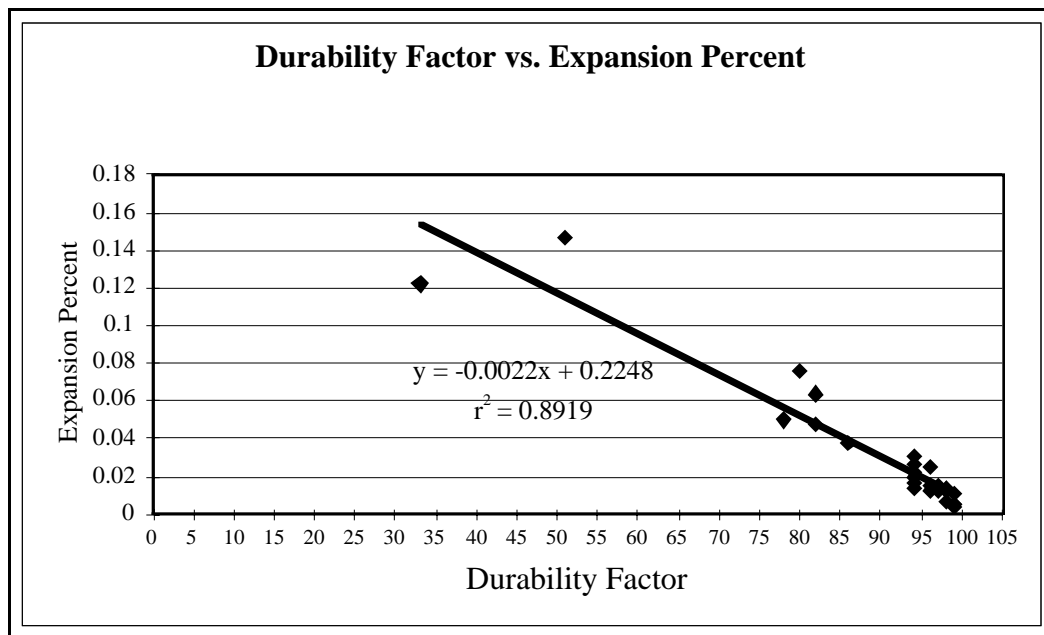

Figure 6. XY plot illustrating the relationship between durability factor and expansion percentage (n = 25).
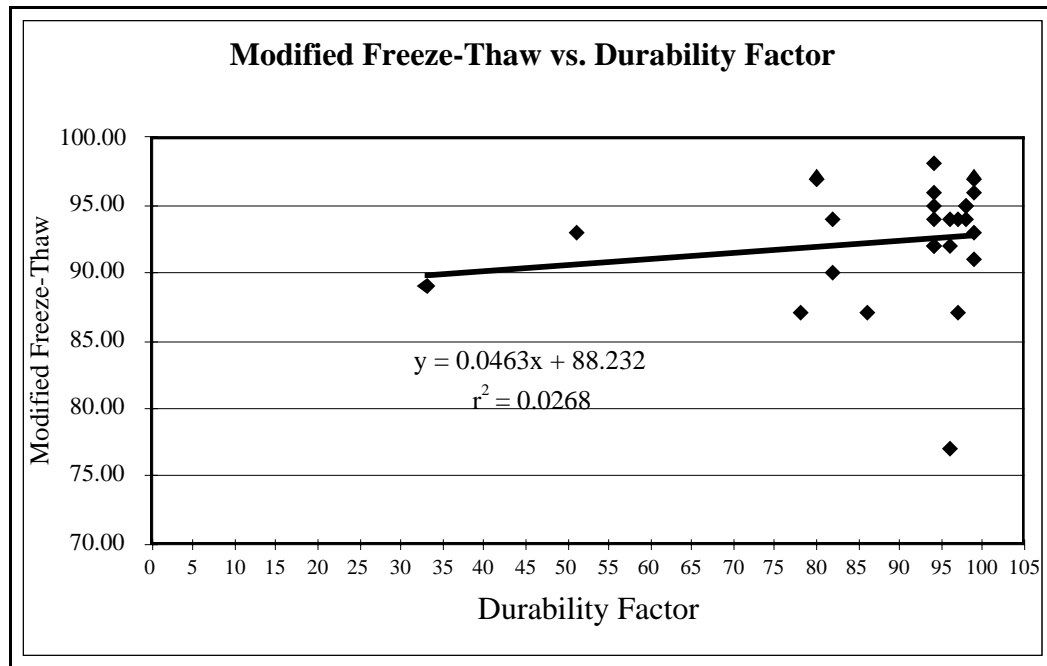
Figure 7. XY plot showing the relationship between durability factor and modified freeze-thaw (soundness) value (n = 30).

test essentially do not correlate to durability factor (Figure 7), the soundness test may either be reflecting an influence of different variables or may suggest that the soundness test is in need of further evaluation.

To compare most data to the durability factor, simple XY scatter plots were compiled. Then, using simple linear regression, any possible correlations or trends were examined. Although the regression data are not meant to represent rigorous statistical testing, they provide the means to simply evaluate trends useful for indicating those variables that may play a significant role in aggregate durability. In the future, as more comprehensive data are accumulated, these data may be conducive to multivariate statistical analysis. For other, more qualitative data such as lithology, spar types, and clay form, comparisons were made by categorizing the data into classes and compiling histograms.

Lithology

The rocks tested for this study (samples KU-1 to KU-10) and other recent KDOT tests (samples KDOT-1 to KDOT-20) are of six different lithologies (Table 2). Of the thirty aggregates examined in the study, 25 had durability-factor data. Nineteen of those 25 aggregates are phylloid-algal lithologies. Of those nineteen, eight

Lab. #/Sample #	Sample Source	Lithology	Dominant Matrix or Cement	Dominant Grain Type(s)	Dblty Factor
97-3685/KU-1	SRS L. Frly	Argil. Sk. Wckstn	Pseudospar & Microspar	Skeletal Fragments (Bryozoan, Crinoid, Brachiopd)	NC
97-3686/KU-2	SRS U. Frly	Phyl. Algal Wckstn	Micrite & Microspar	Phylloid Algae	94
97-3687/KU-3	SRO L. Frly	Skel. Grnstn	Equant Cement	Skeletal Frags., Quartz Grains, Peloids	97
97-3688/KU-4	SRBS L. Frly	Oolite	Isopach., Micrite, Eqnt Cement	Ooids, Peloids, Skeletal Fragments	98
97-3689/KU-5	SRBS U. Frly	Phyl. Algal Wckstn	Peloidal Micrite & Microspar	Phylloid Algae, Bryozoans	99
97-3690/KU-6	RQ U. Frly	Phyl. Algal Pckstn	Peloidal Micrite & Microspar	Phylloid Algae	96
97-3858/KU-7	SRS U. Frly	Pel. Sk. Pckstn	Equant Cement	Micritized Peloids, Skel. Frags (Crinoids, Brachs)	96
97-4058/KU-8	HM L. Frly	Skel. Wckstn	Micrite & Microspar	Fusulinids, Brach. & Bryozoan Frags.	97
97-4059/KU-9	HM U. Frly	Phyl. Algal Wckstn	Peloidal Micrite & Microspar	Phylloid Algae	99
97-4060/KU-10	HM U. Frly	Osagia, Brach Wckstn	Micrite & Microspar	Osagia, Brach Frags, Phylloid Algae, Ooids	82
95-0634/KDOT-1	SRS U. Frly	Phyl. Algal Wckstn	Peloidal Micrite	Phylloid Algae	98
95-634-P/KDOT-2	SRS L. Frly	Phyl. Algal Wckstn	Microspar & Micrite	Phylloid Algae Frags, Bryozoans, Brachs, Crinoids	94
93-4579/KDOT-3	SRO U. Frly	Phyl. Algal Wckstn	Peloidal Micrite	Phylloid Algae, Bryozoans	78
93-4579/KDOT-4	SRO U. Frly	Phyl. Algal Wckstn	Peloidal Micrite	Phylloid Algae, Bryozoans	86
94-0607/KDOT-5	SRBS M. Frly	Mixed Lith.	Equant Cement & Micrite	Peloids, Ooids, Skel. Frags.	82
94-0607/KDOT-6	SRBS U. Frly	Phyl. Algal Wckstn	Peloidal Micrite	Phylloid Algae, Bryozoans	80
94-2268/KDOT-7	HM U. Frly	Phyl Algal Wckstn	Peloidal Micrite	Phylloid Algae	99
94-2268/KDOT-8	HM U. Frly	Phyl Algal Wckstn	Peloidal Micrite	Phylloid Algae	99
94-2268/KDOT-9	HM U. Frly	Phyl Algal Wckstn	Peloidal Micrite	Phylloid Algae	98
94-2268/KDOT-10	HM L. Frly	Phyl Algal Wckstn	Microspar & Micrite	Phylloid Algae, Peloids, Skel. Frags.	94
94-2268/KDOT-11	HM L. Frly	Sk. Wckstn	Micrite & Microspar	Fusulinids, Bryozoan & Brach. Frags.	NC
93-4579/KDOT-12	SRO M. Frly	Sk. Grnstn	Equant Cement	Skel. Frags., Quartz Grains, Peloids	NC
95-634-P/KDOT-13	SRS L. Frly	Mixed Lith.	Equant Cement	Peloids, Crinoid Frags, Skel Frags.	NC
81-0083/KDOT-14	LQ L. Frly	Arg. Phyl. Algal Wckstn	Micrite & Microspar	Phylloid Algae, Brachiopods	33
81-0083/KDOT-15	LQ L. Frly	Arg. Phyl. Algal Wckstn	Micrite & Microspar	Phylloid Algae, Brachiopods	51
81-0083/KDOT-16	LQ U. Frly	Phyl. Algal Wckstn	Peloidal Micrite	Phylloid Algae	94
81-0083/KDOT-17	LQ U. Frly	Phyl. Algal Wckstn	Peloidal Micrite	Phylloid Algae	94
97-2114/KDOT-18	OAQ U. Frly	Phyl. Algal Wckstn	Peloidal Micrite	Phylloid Algae	96
97-2114/KDOT-19	OAQ U. Frly	Phyl. Algal Wckstn	Peloidal Micrite	Phylloid Algae	94
97-2114/KDOT-20	OAQ U. Frly	Phyl. Algal Wckstn	Peloidal Micrite	Phylloid Algae	NC

Table 2. Information regarding lithology of each aggregate source. Information includes locality and stratigraphic unit from which each sample was taken, lithology, matrix or cement type and dominant grain type. Also given are durability factors for each aggregate (NC= not calculated).

have durability factors of at least 95, six have durability factors of 90 to 94, and only five fall within the 0 to 89 range (Figure 8).

Coarser grained, micrite-poor lithologies such as skeletal grainstone (KU-3) and skeletal, peloidal packstone (KU-7) have durability factors of at least 95. Finer grained, micrite or microspar matrix-rich lithologies such as skeletal wackestone (KU-8) and phylloid algal wackestone (KU-5) also have durability factors of at least 95. Therefore, it does not appear possible to predict durability based exclusively on the variation in Dunham-classified lithologies in the Farley Limestone. Instead, the results of durability testing indicate that both matrix-rich lithologies such as phylloid-algal wackestone and skeletal wackestone-packstone and matrix-poor lithologies such as skeletal grainstone produce durable aggregates. This indicates that aggregate quality is largely controlled by factors other than lithologic composition. It does seem, however, that matrix-rich lithologies such as phylloid-algal wackestone and skeletal wackestone-packstone generally produce durable aggregates.
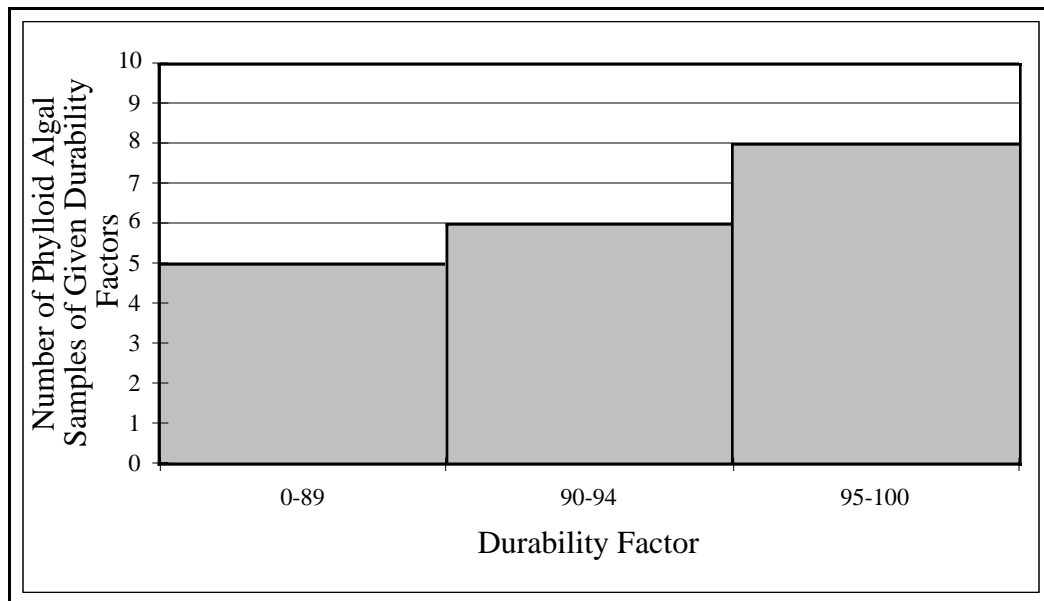

Figure 8. Histogram showing the number of samples of phylloid-algal limestone within durability-factor categories.
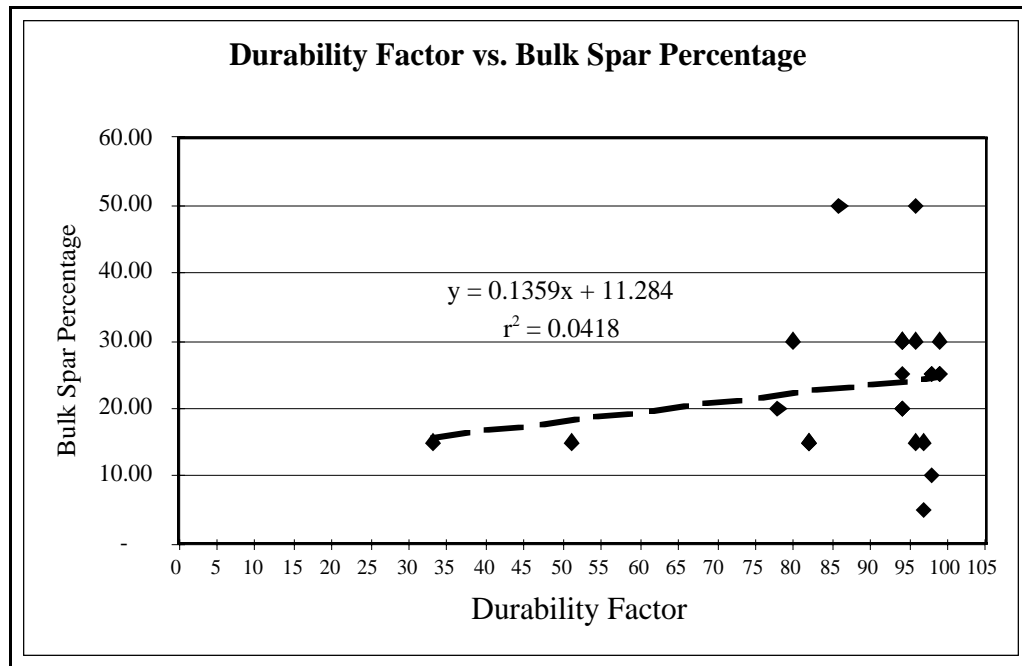
Figure 9. XY Plot showing relationship of durability factor to bulk spar percentage (n = 25). The weak relationship suggested is that as bulk spar percentage increases, durability increases.

Bulk Spar Percentage

The relationship between bulk spar percentage and durability factor is shown in Figure 9. Although the statistical correlation is weak, using the data to evaluate the trend visually is useful. The possible relationship suggested by the regression line is the higher the bulk spar percentage the higher the durability factor, but the fit is so weak we must conclude that, within this data set, there is no real relationship between bulk spar percentage and durability. It is possible, however, that within a larger data set with greater variance a stronger correlation may be established.

Average Crystal Size

The relationship between average crystal size and durability factor is illustrated in Figure 10. This variable was evaluated by determining the average crystal size for each aggregate and then dividing the data into two classes: (1) average crystal size in spar-rich aggregates ($\geq$ 25 percent bulk spar) and (2) average crystal size in spar-poor aggregates ($<$ 25 percent bulk spar). As with the durability factor-bulk spar percentage relationship, the correlations are weak. The regression lines for both classes vaguely suggest that as average crystal size decreases, durability increases.

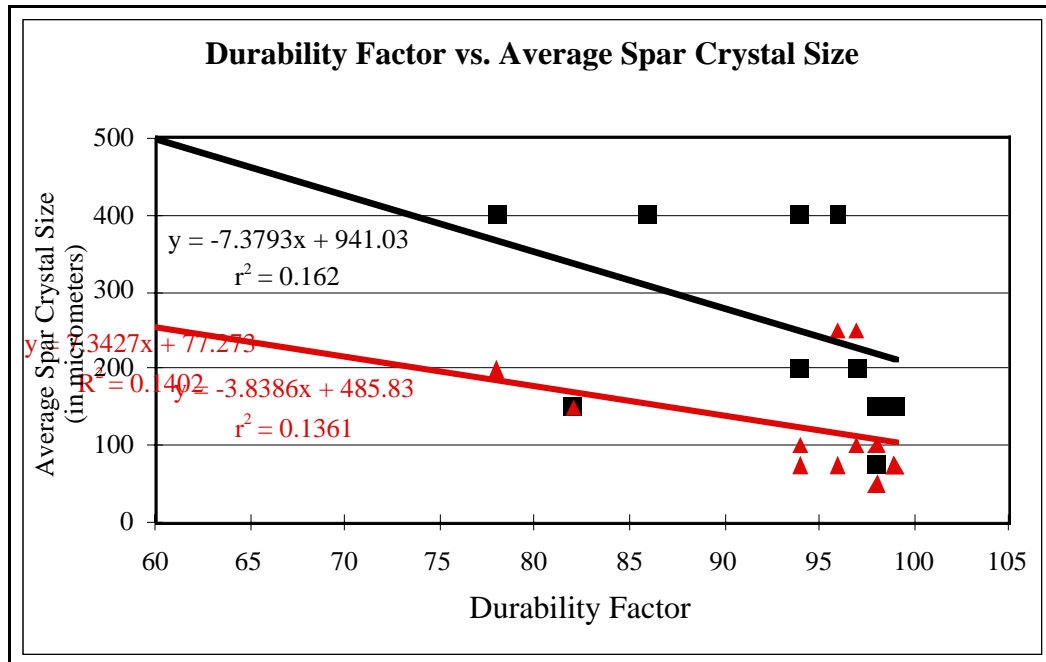**Figure 10.** XY plot showing the relationship between average crystal size (in micrometers) and durability factor. Red data points represent spar-poor samples (n = 12) and black are spar-rich samples (n = 12).
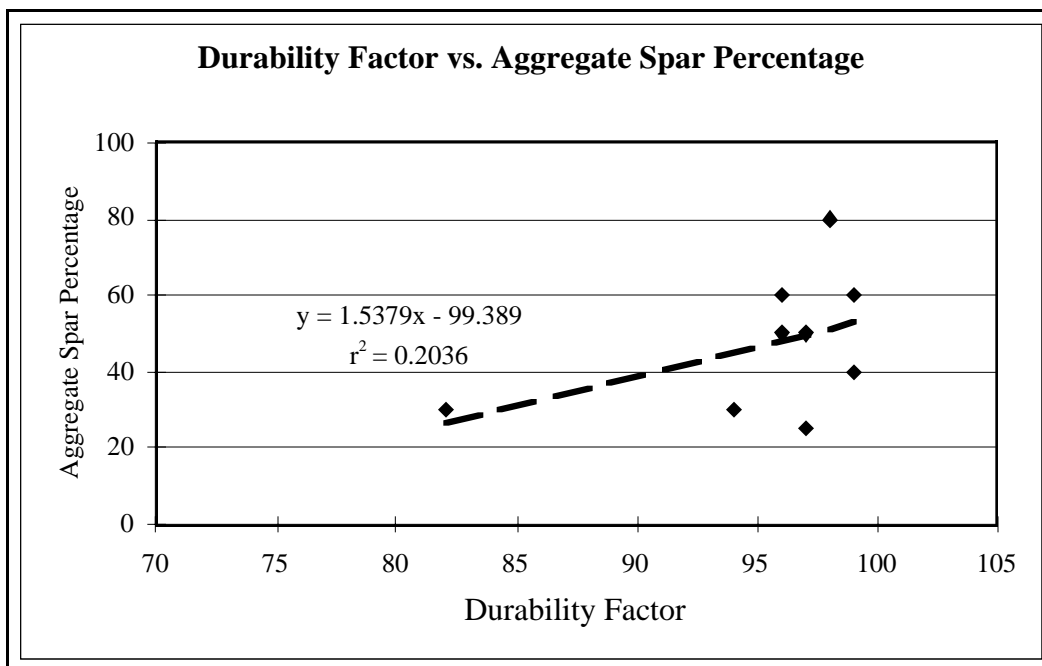

Figure 11. XY Plot comparing the total aggregate spar percentage to durability factor (n = 9). The regression line suggests a weak relationship; the higher the aggregate spar percentage the higher the durability.

Although the correlations are weak, they are stronger than the correlation between bulk spar percentage and durability factor.

Aggregate Spar Percentage

Comparison between durability factor and aggregate spar percentage (Figure 11) shows a slightly stronger correlation than in the other comparisons of bulk spar percentage and average crystal size. Although the plot shows that one data point dominates the correlation, the fit of the regression line suggests that the higher the percentage of aggregate spar, the higher the durability. We must, however, conclude that within this data set, there is no useful correlation. But again, examination of this variable within the context of a larger data set with greater variance may illustrate a more useful correlation.

Total Percentage of Clay-Rich Strata and Distribution of Clay

Comparing the total percentage of clay-rich strata to durability factor provides one of the stronger correlations. The fit of the regression line in Figure 12 suggests that the lower the total percentage of clay-rich strata the higher the durability factor. The correlation between outcrop clay percentage and expansion percentage also produces a relatively strong correlation and suggests that the higher the outcrop clay percentage the higher the expansion (Figure 13). These two plots compare the total clay percentage, including shale beds, concentrated stylocumulates, diffuse stylocumulates, and disseminated argillaceous material, to durability factor and expansion percentage. Because shale beds and concentrated stylocumulates are likely to be removed from the limestone during quarrying and crushing, however, correlations between the total percentage of clay-rich strata and durability factor and expansion percentage are not the best representations of the actual aggregate composition. Instead it would be more beneficial to evaluate the impact of only those occurrences of clay that become a part of the aggregate.

For this reason, a separate estimate was made of the percentage of the strata that contains only diffuse stylolites. Additionally, because the number of samples that contained enough disseminated clay to be detectable in outcrop is low, disseminated material was also included in this estimate so that the value is a total percentage of diffuse and disseminated clay. These values offer the closest approximations of the actual composition of the aggregate and best illustrate the impact of clay and its distribution on aggregate durability. When the percentage of strata that contains both diffuse and disseminated clay is compared to durability factor, the suggested correlation is stronger than that between total percentage of clay-rich strata and durability factor (Figure 14). Additionally, if the percentage of rock that contains diffuse stylolites and disseminated argillaceous material is compared to expansion percentage, another relatively good correlation is suggested (Figure 15).

Percent Insoluble Residue

    Evaluation of insoluble residue data suggests possible trends and relationships, but the correlation is relatively weak. The relationship observed between total percent insoluble residue and durability factor suggests that the lower the insoluble residue percentage the higher the durability factor (Figure 16). A similar, slightly stronger correlation exists between expansion percentage and insoluble residue percentage (Figure 17). These are the relationships we would expect to see based on the relationship of durability factor and expansion to percent clay. The fact that the correlations related to insoluble residue percentage are considerably weaker than those related to total clay percentage creates a possible contradiction if it is assumed that the bulk insoluble residue percentage should be a reflection of the total percentage of clay-rich strata.

    The bulk insoluble residue percentage of the aggregates is not a direct measure of the amount of clay in the rocks. Instead the insoluble reside percentage is a measure of not only the amount of clay in the rocks but also includes things such as quartz, feldspar and organic residue. Therefore, rocks appear to contain no clay can in fact

Durability Factor vs. Total Percentage of Clay-rich Strata

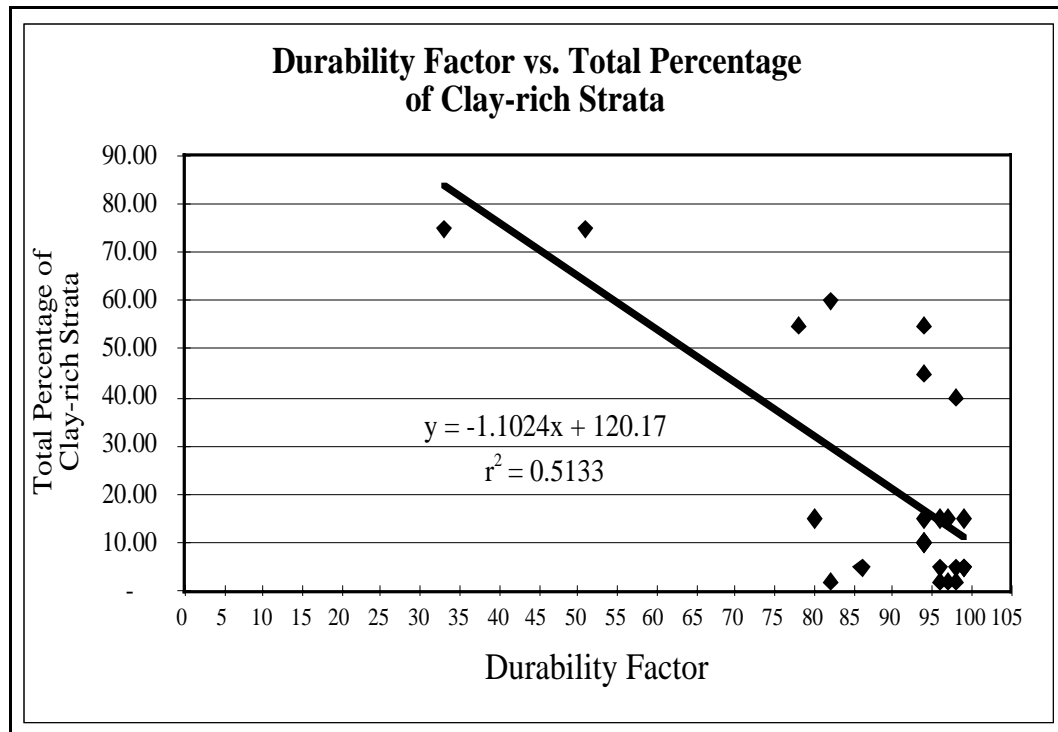$$y = -1.1024x + 120.17$$
$$r^2 = 0.5133$$

Figure 12. XY plot comparing durability factor to total outcrop clay percentage (n = 25). This percentage includes concentrated stylocumulates, diffuse stylolites, and disseminated argillaceous material.
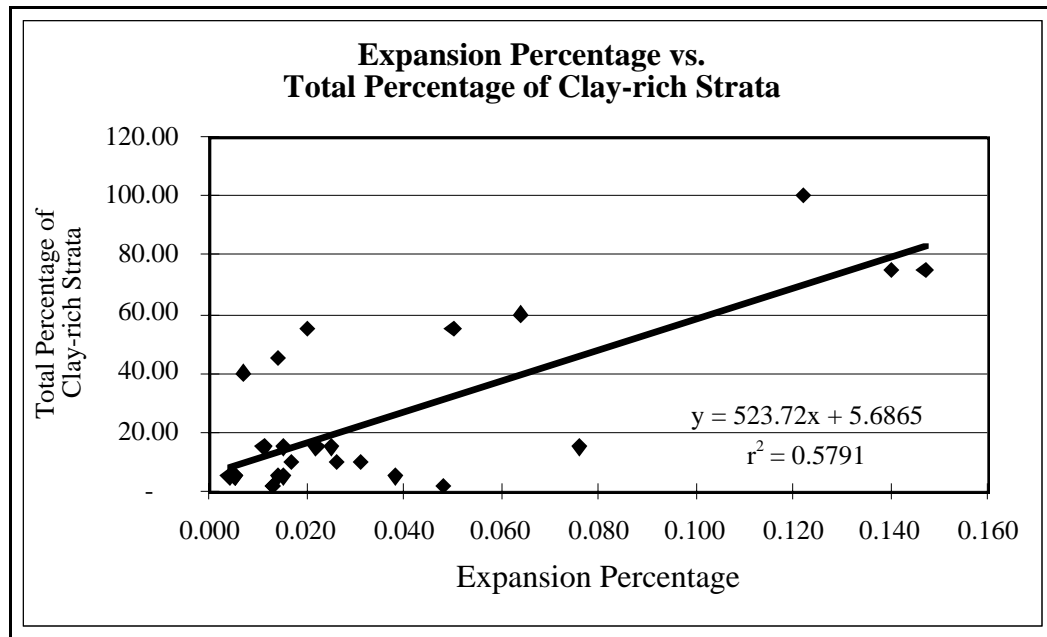
Figure 13. XY plot comparing expansion percentage to total outcrop clay percentage (n = 26). This percentage includes all three forms of clay.

have significant amounts of insoluble residue. For example, samples KU-3 and KU-4 have low total clay percentages (2 percent) but relatively high insoluble residue percentages (9.22 percent and 13.32 percent respectively). This indicates that some lithologies that have little to no clay visible on outcrop may contain insoluble materials other than clay, such as quartz, feldspar or organic residue. Furthermore, because insoluble residue percentages are calculated by weight percent, if there is abundant quartz or feldspar in the residue, the insoluble residue percentage is skewed towards the high side because these minerals are heavy relative to clay minerals.

The difference in correlations between insoluble residue percentage and total percentage of clay-rich strata indicates that the presence of minerals such as quartz and feldspar have a much less negative impact on durability factor than do clay minerals. This suggestion is further discussed and supported in the following section.

Figure 14. XY plot comparing durability factor to the percentage of rock that contains only diffuse stylolites and disseminated argillaceous material (n = 25).

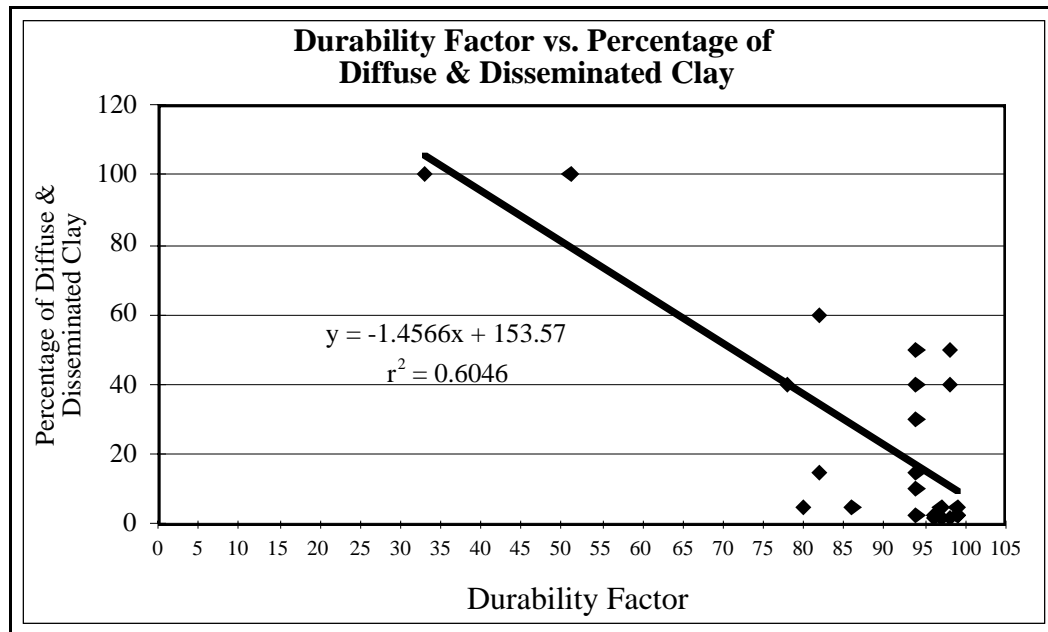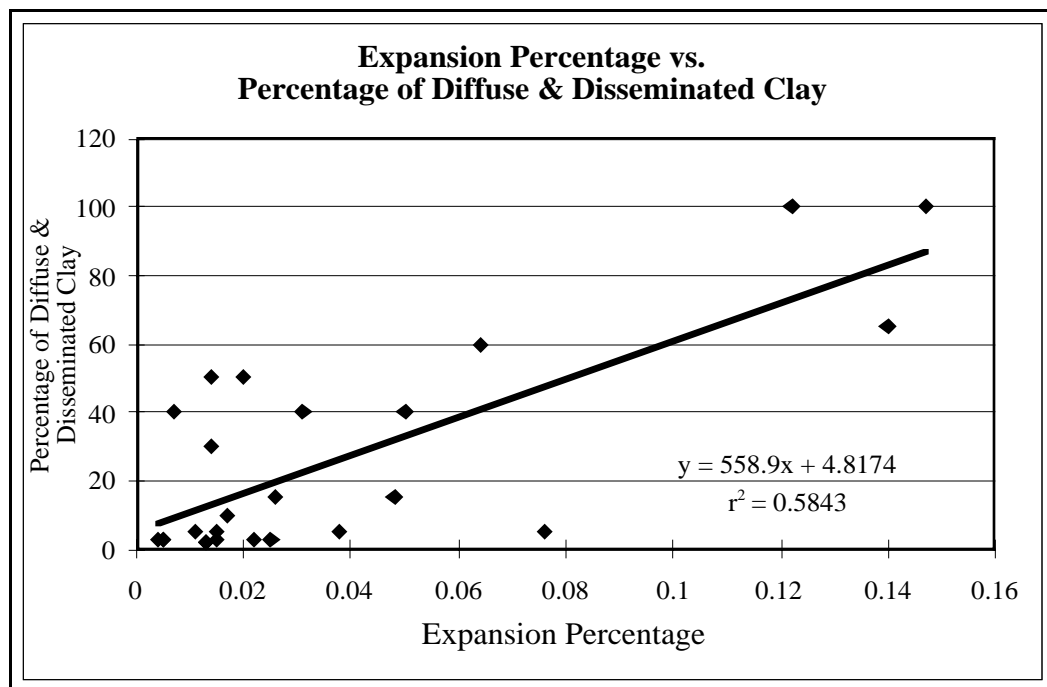**Figure 15.** XY plot comparing expansion percentage to the percentage of rock that contains only diffuse stylolites or disseminated argillaceous material (n = 26).
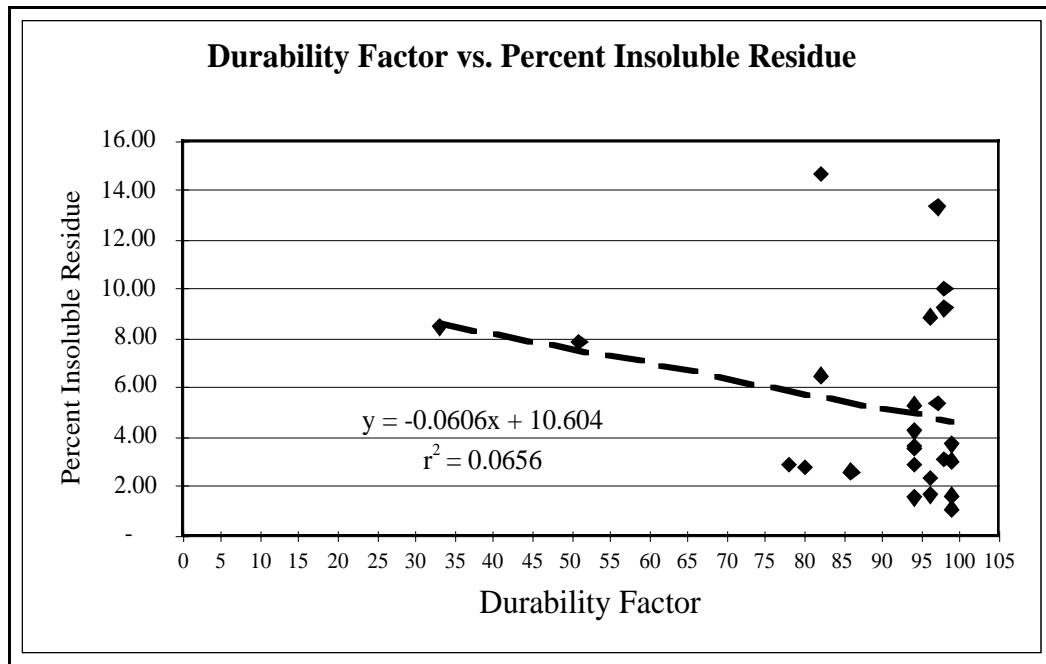
Figure 16. XY plot showing the relationship between durability factor and percent insoluble residue (n = 25).
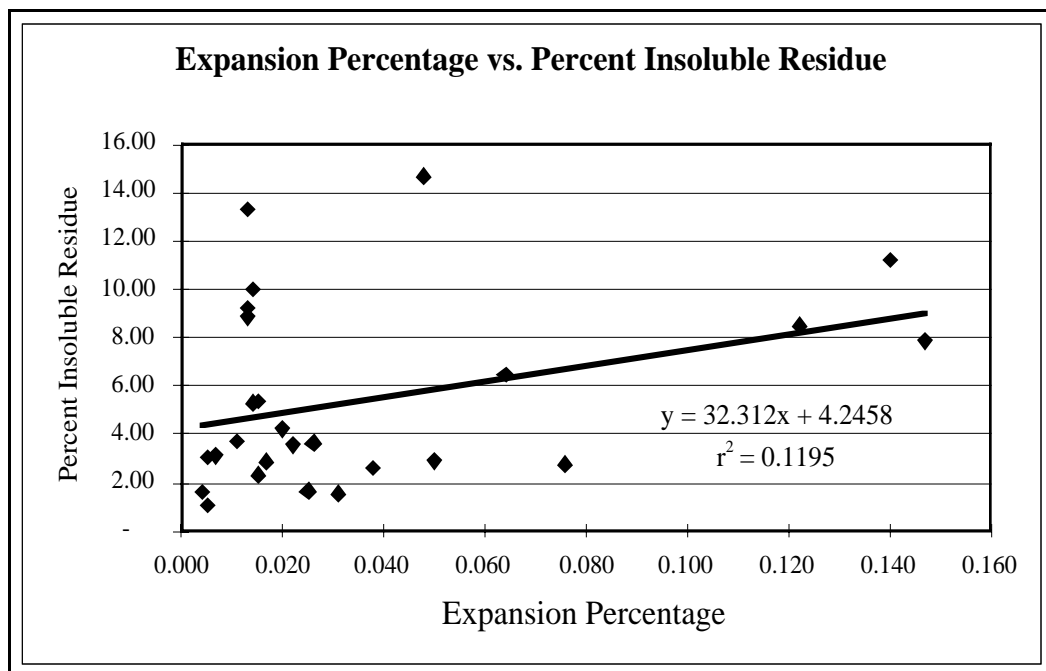

Figure 17. XY plot showing the relationship between expansion percentage and percent insoluble residue (n = 26).

Insoluble Residue Composition & Aggregate Clay Percentage

All residues examined contain quartz and feldspar, and all but one residue contains illite/mica. Other clay minerals in residues include smectite and kaolinite (Table 3). Comparison of residue mineralogy with durability factor and expansion percentage, although not a quantitative comparison provides useful information.

Of those aggregates that have durability factors below 95 (KU-2, KU-10) or had testing terminated due to poor performance (KU-1), all contain three detectable clay minerals: illite, smectite, and kaolinite (Table 3). Additionally, these aggregates that contain three identified clays in their insoluble residues also have the highest expansion percentages (Table 3). There is also an apparent relationship between durability and the aggregate clay percentage in those aggregates that contain the three detectable clay minerals. The aggregate that contains the three clays and has the highest aggregate clay percentage (9.73 percent) is KU-1. This aggregate performed so poorly that testing was terminated due to degradation and no durability factor was calculated. There was however, an expansion percentage calculated for this aggregate and it was much higher than those expansion percentages calculated for the other aggregates (Table 3).

Lab. #/Sample #	Quartz	Feldspar	Illite/Mica	Smectite	Kaolinite	Durability Factor	Expansion %	Agg. Clay %
97-3685/KU-1	X	X	X	X	X	NC	0.14	9.73
97-3686/KU-2	X	X	X	X	X	94	0.02	3.64
97-3687/KU-3	X	X	X			97	0.013	6.44
97-3688/KU-4	X	X	X			98	0.013	7.4
97-3689/KU-5	X	X	X			99	0.011	3.18
97-3690/KU-6	X	X	X	X		96	0.015	1.97
97-3858/KU-7	X	X	X		X	96	0.013	8.04
97-4058/KU-8	X	X	X		X	97	0.015	3.87
97-4059/KU-9	X	X				99	0.005	3.02
97-4060/KU-10	X	X	X	X	X	82	0.064	5.8

Table 3. Composition of each insoluble residue for which x-ray diffractometry data were obtained. Also shown are the calculated durability factors (NC = not calculated) and expansion percentages for each of the ten aggregates, as well as the calculated aggregate clay percentages.

The seven remaining aggregates have durability factors of at least 95. Of these seven, three (KU-6, KU-7, KU-8) contain a combination of only two detectable clay minerals in the residues, illite and smectite or illite and kaolinite. Although these aggregates have similar expansion percentages, a connection may exist between the presence of smectite and lower durability. Aggregate KU-6 contains smectite but has a relatively low percentage of aggregate clay (1.97 percent), whereas aggregates KU-7 and KU-8 contain higher aggregate clay percentages (8.04 percent and 3.07 percent respectively) and contain no smectite. Although, aggregate clay percentages do not

indicate the percentage of smectite exclusively, it is reasonable to infer that smectite is present in higher proportions (as are the other clay minerals) in aggregates with higher aggregate clay percentages. This suggests that the presence of smectite, even in small quantities, may negatively impact durability more than does the presence of other clay minerals in higher quantities.

Three aggregates (KU-3, KU-4, KU-5) contain only one detectable clay mineral, and one aggregate (KU-9) contains no detectable clay minerals. These aggregates all have the highest durability factors (97 or higher) and the lowest expansion percentages. Two of these four aggregates contain high aggregate clay percentages (6.44 percent and 7.4 percent). Apparently having only illite or lacking smectite or kaolinite indicates the potential for high durability as long as some clay percentage is not exceeded, but this critical percentage is unknown at this time.

Absorption

The absorption value is a measure of the porosity and permeability of an aggregate. The correlations between durability factor and absorption are weak or nonexistent (Figure 18), and the correlation between expansion percentage and absorption is only slightly stronger (Figure 19). The fit of the regression lines suggest that the lower the absorption percentage the higher the durability factor and the lower the expansion percentage, but the correlations are so weak that, within this data set, we must conclude that there is no relationship between absorption and durability or expansion.

Discussion

KDOT requires class 1 aggregates to meet three specifications: (1) a modified freeze-thaw ratio of 0.85 (85 percent) or greater; (2) a durability factor of 95 or higher; and (3) an expansion percentage of 0.02 percent or lower. Therefore, determining which geologic variables seem to have a direct affect on these three physical properties is important in recognizing what KDOT recognizes as durable aggregate. Because the correlations examined between modified freeze-thaw value and the geologic properties were all weak to nonexistent, however, the following discussion will concentrate on the comparisons that were made to durability factor and expansion percentage.
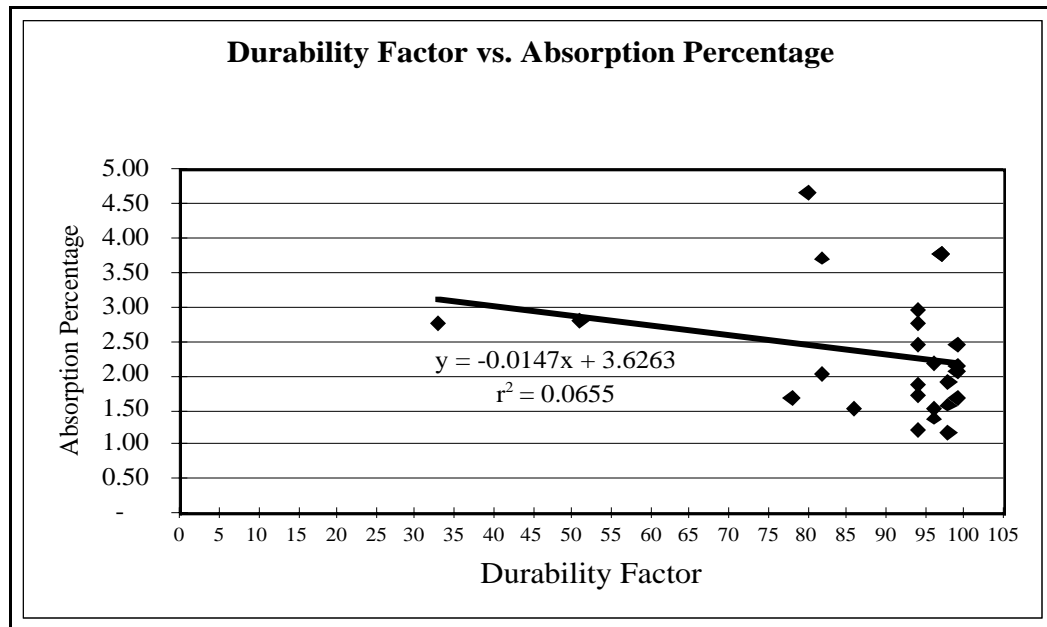
Figure 18. XY plot showing the relationship between durability factor and absorption percentage (n = 25).
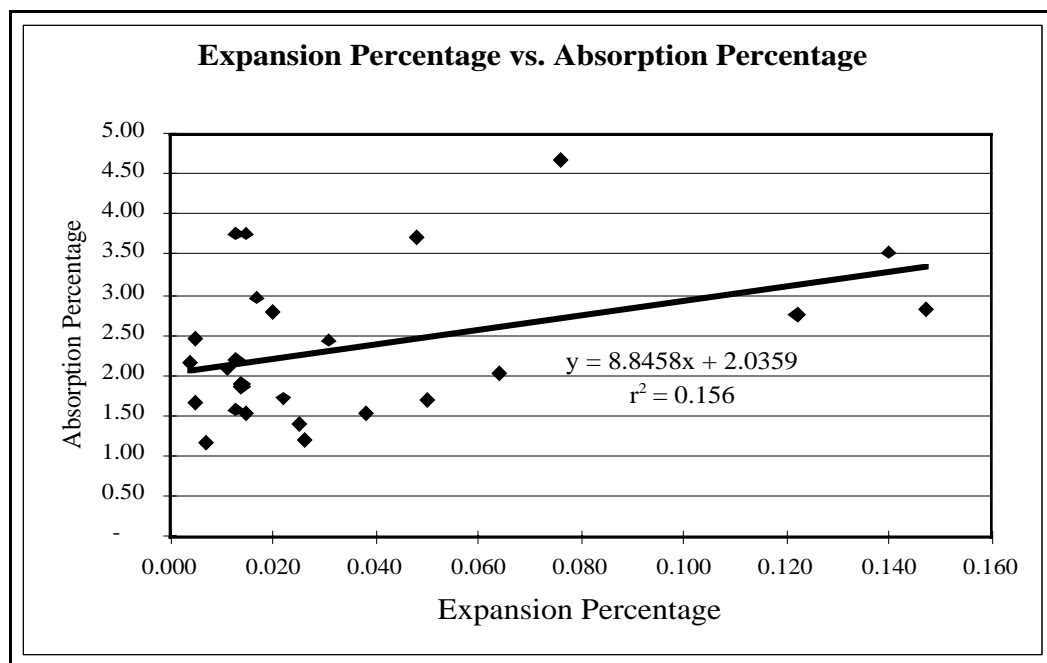

Figure 19. XY plot showing the relationship between expansion percentage and absorption percentage (n = 26).

Of the lithologies examined micrite or microspar matrix-rich lithologies as well as sparry cement-rich lithologies attain class 1 status. Therefore, it seems unlikely that the presence of micrite or microspar matrix in the rocks preferentially produces higher durability aggregates than does the presence of abundant sparry cement. The hypothesis that micrite-rich phylloid-algal lithologies produce durable aggregates seems to be largely supported however. Additionally, other micrite or microspar matrix-rich lithologies such as skeletal wackestone-packstone also commonly produce durable aggregates. Because there are exceptions to these trends and because cement-rich lithologies such as oolite also produce durable aggregates, textural classification cannot be used to confidently predict aggregate durability.

The effect of coarse spar on durability is difficult to establish based on the data collected for this study. The correlation between bulk spar percentage and durability suggests that the more coarse spar present the higher the durability. Alternatively, the correlation between average crystal size and durability suggests that finer average crystal sizes yield higher durability aggregates. Because the correlations are weak for this data set, it is impossible to conclude with certainty that the amount or coarseness of spar present in the rocks has any impact, positive or negative.

In their report on aggregate durability, Wallace and Hamilton (1982) determined that the insoluble residue percentage was significant in predicting aggregate durability. For this reason they included percent insoluble residue value in the Pavement Vulnerability Factor (PVF) calculation that they used to initially identify durable aggregates until physical testing was completed. The correlations between durability factor and percent insoluble residue in my study show no strong correlation. The weak trend suggests that the lower the percent insoluble residue the higher the durability factor and the lower the expansion percentage. Therefore, the hypothesis that a high amount of insoluble residue in the rocks has a negative affect is not refuted. Because the correlations are weak and both class 1 and nonclass 1 aggregates contain variable percentage of insoluble residue, however, support for the hypothesis is tenuous at best, and it is clear that variables other than insoluble residue percentage must be involved.

Of the hypotheses examined, those related to the abundance, distribution, and mineralogy of clay in the rocks and insoluble residues produce the strongest correlations. The most accurate indicator of durability seems to be the total percentage of strata that contain diffuse stylocumulates plus disseminated argillaceous material. These occurrences of clay are most likely to become part of the aggregate following crushing and sorting. The relationship observed suggests that those rocks with low percentages of diffuse stylocumulates and disseminated argillaceous material are likely to qualify as class 1 aggregate. Furthermore, those rocks dominated by concentrated stylocumulates and clay beds with little diffuse stylocumulates and disseminated argillaceous material are also likely to produce durable aggregates. Therefore, the

hypotheses regarding the presence of concentrated and diffuse stylocumulates as well as disseminated argillaceous material are supported.

As mentioned previously, the main cause of d-cracking is thought to be the expansion and contraction of aggregates caused by freezing and thawing of water entrapped in the aggregate. Given this cause of d-cracking and the information presented regarding clay minerals, it is reasonable to believe that the presence of some clay minerals in the aggregates would negatively impact aggregate durability.

Of the three clay minerals detected in the aggregates examined, smectite is likely to have the most negative impact on aggregate durability. The outstanding characteristic of the smectite group of clays is their capacity to absorb water molecules, thus producing marked expansion of the structure (Klein & Hurlbut, 1993). This characteristic explains why those aggregates that contain larger amounts of smectite also exhibit the greatest expansion percentages (Table 3). Similarly, because expansion is so closely related to the durability factor (Figure 6), the presence of smectite is likely to cause a reduction in durability. Clearly smectite must be present in the aggregates in enough abundance to impact negatively durability. Determining the exact threshold for the amount of smectite that negatively impacts durability will require further work.

Conclusions

All limestone textural classifications may produce class one aggregate and the presence of abundant micrite or microspar matrix or abundant sparry cement has no apparent impact on durability. Micrite or microspar matrix-rich lithologies such as phylloid algal wackestones and packstones and skeletal wackestones and packstones, however, are commonly good sources of durable aggregates.

Other geologic properties such as bulk spar percentage, spar size, insoluble residue percentage and grain size produce suggestive trends when related to durability and expansion. These factors do not, however, seem to be reliable indicators of durability.

Of the geologic parameters examined in this study, those related to the abundance, distribution, and mineralogy of clay seem to be the most significant. The strongest correlations between geologic properties and physical test results are related to the total clay percentage, clay distribution, and composition of insoluble residues. The more clay observed in outcrops (total percentage of clay-rich strata) the lower the durability and the higher the expansion percentage. Limestones that contain clay only in concentrated stylocumulates or shale beds are likely to produce class 1 aggregate because the clays and shales are crushed too finely to become part of the aggregate. Limestones with diffuse stylocumulates and disseminated clay are less likely to produce class 1 aggregates.

A further indicator of durability is the composition of the insoluble residues. If the residues contain three clay minerals (illite, kaolinite, and smectite) the durability is likely to decrease. Limestones without detectable clay minerals are likely to produce durable aggregates. Furthermore, if even a small amount of smectite is present in the residues, there is a higher likelihood of failure due to the expansive properties of this group of clay minerals.

Assuming significant correlations between clay content and aggregate durability, we propose use of spectral gamma ray analysis of quarry faces as the method most likely to show a rapid "first cut" indication of degradation in aggregate quality from change in clay content. The apparatus is inexpensive and can be used in the field. If changes in clay content, deleterious to aggregate quality, can be identified during lateral production, then quarrying can be halted, or can proceed in another direction while physical tests are run. Such a procedure could prevent use of substandard concrete in highway construction projects, and is likely to reduce problems with D-cracking in portland cement concrete pavements.

References Cited

Best, C.H., 1974, D-cracking in PCC pavements—cause and prevention: Manhattan, KS: Department of Applied Mechanics, Kansas State University: Report No. KSU-EES-2472.

Biggs, D.L., 1966, Composition of Dolomites in Carbonate Rocks used as Concrete Aggregates: In: Symposium on Geology of Cement Raw Materials - Proceedings of the Forum on Geology of Industrial Minerals, 2nd, p. 101-110.

Bliss, J.D., Quantitative Models for Aggregate; some Types and Examples from Oklahoma Carbonate Rocks: In: Proceedings of the 34th Forum on the Geology of Industrial Minerals, Oklahoma Geological Survey Circular, v. 102, p. 37-45.

Bukovatz, J.E., Crumpton, C.F., Worley, H.E., 1973, Study of d-cracking in Portland cement concrete pavements: Report 1, Field Phase: Topeka, KS: State Highway Commission of Kansas, Planning and Development Department, Research Division.

Bukovatz, J.E., and Crumpton, C.F., 1981, Study of d-cracking in Portland cement concrete pavements: V. 2- Laboratory Phase: Topeka, KS: Kansas Department of Transportation, Planning and Development Department, Research, Development and Implementation Section: Report No. FHWA-KS 81-2.

Chyi, L.L., Pandit, H.L., and Liang, R.L., 1999, Engineering Implications of Carbonate Aggregate Mineralogy: Geological Society of America, North Central Section Abstracts with Programs, 31; 5, p. 9.

Crumpton, C.F., Wojakowski, J., Wallace, H., and Hamilton, L.D., 1994, Study of d-cracking in Portland cement concrete pavement: V. 4—Petrographic phase and final report: Topeka, KS: Kansas Department of Transportation, Division of Operations, Bureau of Materials and Research: Report No. FHWA-KS-94/3.

Dunham, R.J., 1962, Classification of carbonate rocks according to depositional texture *in* Classification of Carbonate Rocks- A Symposium: American Association of Petroleum Geologists, Memoir, no. 1, p. 108-121.

Folk, R.L., 1965, Some aspects of recrystallization in ancient limestones *in* Pray, L.C., and Murray, R.C., eds., Dolomitization and Limestone Diagenesis: A Symposium: Society of Economic Paleontologists and Mineralogists, Special Publication, No. 13, p. 14-48.

Fountain, K.B., McClellan, G.H., Eades, J.L., and Oyen, C.W., 1996, A multiple parameter approach to soundness evaluation of Florida limestone aggregates: Geological Society Annual Meeting Program with Abstracts, 28; 7, p. 408.

Hilltrop, C.L. and Lemish, J., 1960, Relationship of Pore-size distribution and other Rock Properties to Serviceability and of some Carbonate Aggregates: National. Academy of Science-National. Research Council Highway Research Board Bulletin 239, p. 1-23.

Kansas Department of Transportation, 1990, Standard Specifications for State Road and Bridge Construction. Topeka, Kansas.

Klein, C., and Hurlbut, C.S., 1993, Manual of Mineralogy, 21st Edition, John Wiley & Sons: New York, 681 p.

Lasemi, Z. and Smith, D.W., 1999, Dolomite of the Upper Warsaw Formation; a New Source of High Quality Construction Aggregates in West Central Illinois and Southeastern Iowa: Geological Society of America, North Central Section Abstracts with Programs, 31; 5, p. 30.

McKirahan, J. R., 1998, Sequence Stratigraphy of the Lane-Island Creek Shales and the Farley Limestone in Northeastern Kansas and Geologic Factors Affecting the Quality of Limestone Aggregates: University of Kansas Unpublished Master's Thesis, 244 pp.

McKirahan, J, R., Goldstein, R.H., and Franseen, E.K., 2000, Sequence Stratigraphy of the Lane Island Creek Shales and the Farley Limestone in Northeastern Kansas and Geologic Factors Affecting the Quality of Limestone Aggregates: K-TRAN Report KU-97-1, 236 pp.

Oyen, C.W., McClellan, G, and Fountain, K.B., 2001, Concrete Aggregate Analysis via Thin-section Petrography: A Supplementary Method Aiding Evaluation of Carbonate Aggregate Soundness: Geological Society Annual Meeting Program with Abstracts, 33; 6, p. 130.

Shaffer, N.R., Remmes, K., Wenning, A.L., and West, T.R., 2004, Petrology of Carbonate Rocks that Show Marginal Performance as Concrete Aggregate: 40th Forum on the Geology of Industrial Minerals, Program with Abstracts, Bloomington, Indiana, p. 63-64.

Shakoor, A., West, T.R., and Scholer, C.F., 1982, Physical Characteristics of some Indiana Argillaceous Carbonates Regarding their Freeze-thaw Resistance in Concrete: Bulletin of the Association of Engineering Geologists, v. 19, p. 371-384.

Wallace, H.E., and Hamilton, L.D., 1982, An Investigation of Kansas Limestones as they Pertain to the "D-Cracking" Phenomena: Unpublished paper presented to D-Cracking Workshop, Overland Park Kansas, February 17 & 18: Kansas Department of Transportation, 19 p.

West T.R., 1998, Rock Texture, Porosimetry and Durability in Aggregates for Highway Pavements in Indiana: Geological Society of America Annual Meeting Abstracts with Programs, 30; 7, p. 78.

.

MORFH RS: A ROCKCUT RATING SYSTEM FOR MISSOURI HIGHWAYS

NORBERT H. MAERZ

AHMED YOUSSEF

University of Missouri-Rolla, 1006 Kingshighway, Rolla, MO, 65409-0660.

ROBERT LAUER

Missouri Department of Transportation, 1590 Woodlake Drive, Chesterfield, MO, 63017-5712

The Missouri Rock Fall Hazard Rating System (MORFH RS), a risk/consequence based classification system has recently been completed. The system was specially developed for Missouri, which tends to have low but highly weathered cuts, with special problems from highly weathered karst features such as filled sinkholes.

MORFH RS utilizes mobile video imaging for primary screening of rock cuts. Rock cuts identified as potentially problematic are assigned for further evaluation. Images of the rock cut, taken from the video, are used to make measurements of rock cut parameters such as slope height, slope angle, ditch width, ditch depth, potential rock fall quantity, and shoulder width, and other parameters required for the rating. Other properties such as face looseness, instability, weathering, strength, block size need to be assessed by field inspection, for the problematic cuts only. Location information is obtained from a GPS receiver. Rock cut locations, attributes, hazard ratings, digital photographs, GPS coordinates, and other data are presented in a single page report.

MORPH RS then calculates a risk and a consequence rating, based on the measured and assessed parameters. Separating risk and consequence of failure is important because sometimes high risk and low consequence can be tolerated more than low risk and high consequence. In addition, some parameters such as block size are used in both the risk and consequence ratings: Larger block size decreases the risk of failure, but increases the consequence.

MORPH RS, during development, has been used to analyze over 500 Missouri rock cuts. Over 300 cuts were analyzed in detail and are ranked according to risk and consequence. These results can be used by the Department of Transport to prioritize remediation. A simulation has been conducted that shows the relative merits of various forms of remediation treatments.

1. INTRODUCTION

The Missouri Rock Fall Hazard Rating System (MORFH RS) has been developed for Missouri Highways. Missouri Highway rock cuts tend to be relatively low in most cases, often old and/or highly weathered. There are special problems associated with the many weathered karst features, such as filled sinkholes. For this reason and others, existing rock hazard systems were inadequate for Missouri needs. The MORFH RS system was first described in Maerz et al (2003), and is more fully described in Maerz et al. (2004).

Because roads and highways cover hundreds of thousands of miles of highly variable geological terrain, maintaining rock cuts presents a special challenge to geologists and geotechnical engineers. It would be a prohibitive task to do a routing assessment on all the rock cuts. Consequently State Departments of Transports (DOT's) have in the past been reactive to rock cut problems rather than proactive.

More recently several rock fall hazard rating systems have been proposed and implemented by several DOT's in the USA (Youssef et. al., 2003). MORFH RS is a response to the needs of the DOT's and an improvement to existing rating systems.

MORFH RS provides three components, which makes it highly effective:

1. Highway rock cuts are pre-screened to determine which ones need closer examination, by examining video highway logs.
2. The rating system is based on a risk of failure / consequence of failure calculation, which allows for a more informed decision making process.
3. Many of the parameters needed for the rating systems and can be measured on the video images.

2. MORPH RS

2.1 Mobile video screening

MORFH RS is based on mobile highway video technology, which means that highway rock cuts can be routinely imaged (video logged) at highway speeds by technicians, and the video can be replayed at the office where engineers or geologists can rapidly screen the cuts and determine which need more detailed assessment. Video screening can be done using a sophisticated fully instrumented vehicle such as RoadWare's ARAN (Figure 1) (Maerz and McKenna, 1999) or as simple as a video camera mounted in a car or truck (Figure 2) (Maerz et al., 2003).

Figure 1. An example of an Automatic Road Analyzer (ARAN) made by RoadWare Corporation.

Figure 2. Simple video setup.

2.2 Risk-Consequence scheme

The new Missouri rating system is predicated on separating risk (of failure) from consequence (of failure) (Figures 3, 4). While other rating systems may consider both risk of failure and consequence of failure factors, they tend to lump them together. This is incorrect, as some parameters affect risk and consequence in different ways. For instance, the larger the block size, the lower the risk of failure but the higher the consequence of failure. Or, a 90° slope would present the highest risk of failure, while perhaps a 30° slope would present the highest consequence for large rolling blocks and 85° from small bouncing blocks.

In any case, separating risk and consequence seems useful, because it may be possible to concern ourselves only with high risk, high consequence rock cuts. Low risk rock cuts need not worry us because there is small chance of failure, and low consequence cuts need not worry us because the fallen rock is not likely to reach and affect the highway traffic.

2.1.1 MORFH rating system in a nutshell

The MORFH rating system includes 23 factors, including 9 factors for risk, 10 factors for consequence, 3 adjustment factors (including 1 internally calculated value). These factors have been organized into risk (of failure) and consequence (of failure) categories, and identified based on how the factors are evaluated:

1. Parameters such as slope height, slope angle, ditch width, ditch depth, shoulder width, block size, ditch capacity, and expected rock fall quantity can often be measured on computer scaled video images of rock cuts in the office.
2. Parameters such as weathering, face irregularities, face looseness, strength of rock face, water on the face, and design sight distance which are descriptive, and may need field evaluation.
3. Parameters such as average daily traffic, number of lanes, and average vehicle risk which are obtained from the MODOT records or calculated for each section of road.
4. Conditional parameters such as adversely oriented discontinuities, karst features, ditch capacity exceedence, and the effect of bad benches, which are reflected in a conditional ditch shape parameter.

For each parameter, the input value is one of:

1. An actual measurement for all quantifiable parameters, either a number or a measurement in feet or degrees, where measured, estimated, or derived from a database.
2. A class number for all parameters that are not quantifiable. This is on a scale of 0 to 4. The values 0, 1, 2, 3, and 4 correspond to descriptions for each parameter in the charts below, however half ratings (e.g. 2.5) are allowed.

MORFH RS uses the above number to generate a rating value for each factor, typically between 0 and 12 as described below. The system is further described by (Maerz et al., 2004) and in Appendix 1.

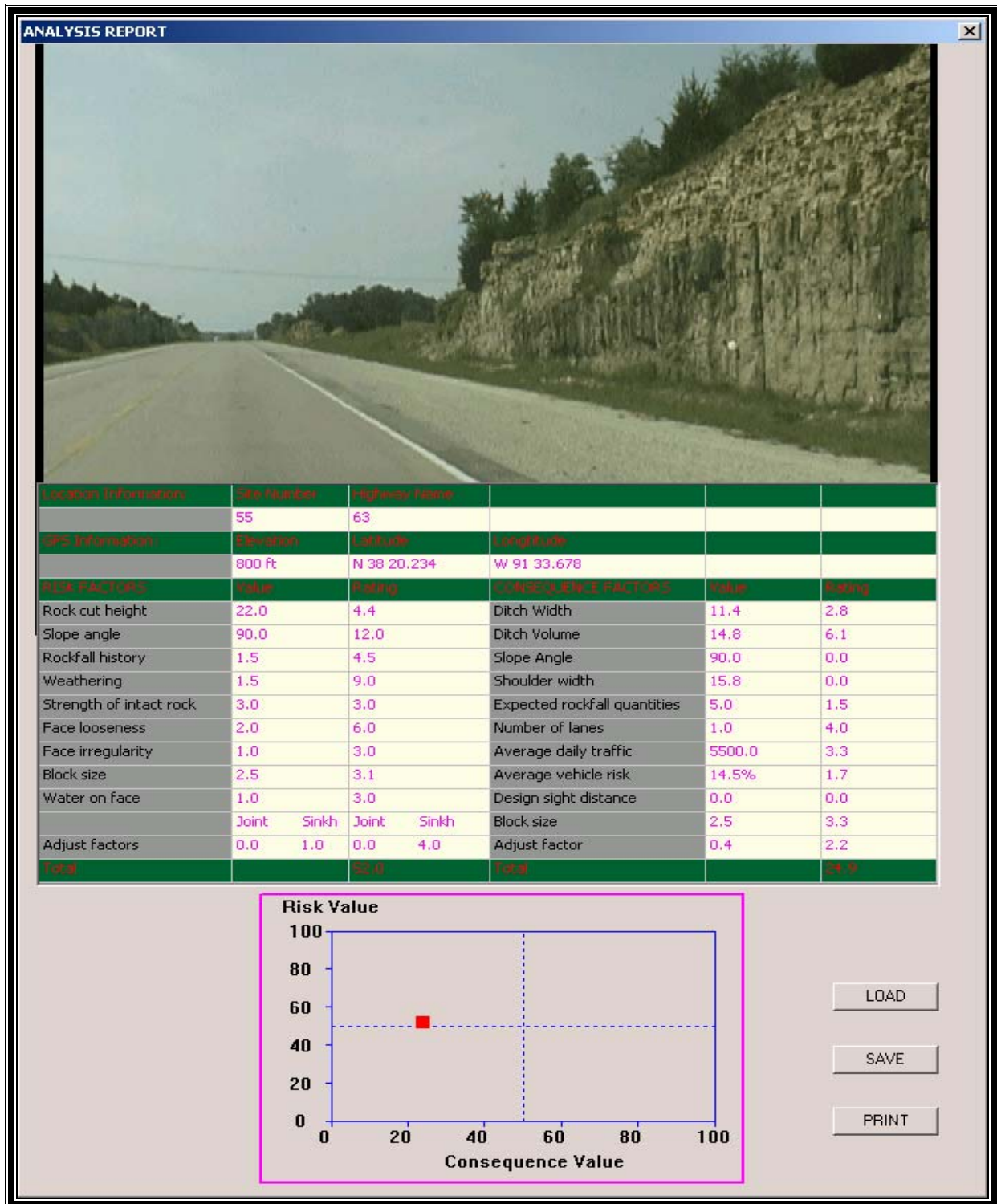| Location Information:	Site Number	Highway Name			
	55	63			
GPS Information:	Elevation	Latitude	Longitude		
	800 ft	N 38 20.234	W 91 33.678		
RISK FACTORS	Value	Rating	CONSEQUENCE FACTORS	Value	Rating
Rock cut height	22.0	4.4	Ditch Width	11.4	2.8
Slope angle	90.0	12.0	Ditch Volume	14.8	6.1
Rockfall history	1.5	4.5	Slope Angle	90.0	0.0
Weathering	1.5	9.0	Shoulder width	15.8	0.0
Strength of intact rock	3.0	3.0	Expected rockfall quantities	5.0	1.5
Face looseness	2.0	6.0	Number of lanes	1.0	4.0
Face irregularity	1.0	3.0	Average daily traffic	5500.0	3.3
Block size	2.5	3.1	Average vehicle risk	14.5%	1.7
Water on face	1.0	3.0	Design sight distance	0.0	0.0
	Joint Sinkh	Joint Sinkh	Block size	2.5	3.3
Adjust factors	0.0 1.0	0.0 4.0	Adjust factor	0.4	2.2
Total		52.0	Total		24.9

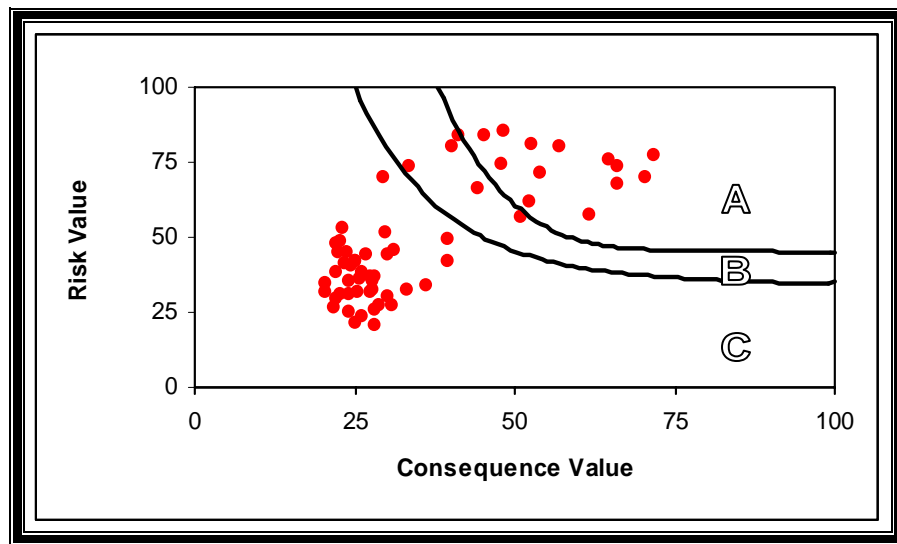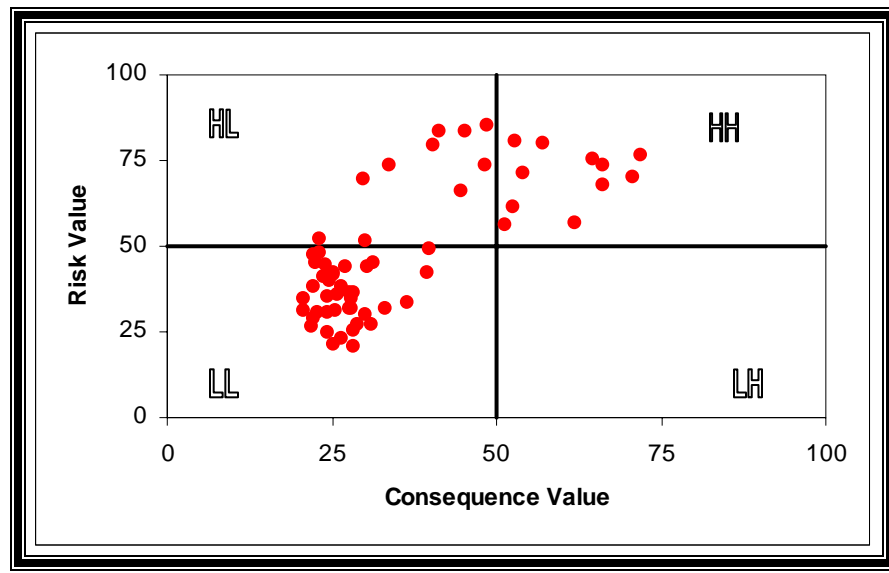Figure 3: Single page report shows the results of evaluation.

Figure 4. An example of a Risk – Consequence diagram for rock cuts from a section of highway 65 in Missouri. Top: diagram for the risk/quadrant data. LL = Low Risk Low Consequence, HL = High Risk Low Consequence, HH = High Risk, High Consequence, and LH = Low Risk High Consequence. Bottom: diagram for the zoned data. A= High Hazard Zone, B = Moderate Hazard Zone, and C = Low Hazard Zone.

2.3. Video scaled measurements

The same images that can be used for video logging and previewing can also be used to measure some of the parameters required for the rating system (Maerz et al., 2003; Youssef et al., 2004). Measurements can be made on single images without extensive vehicle instrumentation and modifications. Although not as accurate as manual measurements in the field, the measurements are sufficiently accurate to provide input data for a rock hazard rating system.

The simple video camera setup used for video logging is set up at an angle of 10º to the right of the direction of travel, and tilted and zoomed so as to give coverage to the top of moderately high rock cuts, and the traveling lane of the highway.

The simplest way to use the system is to use a known length as a scaling object. Figure 5 shows the land width (12' in Missouri) used to set the scale. The horizontal and vertical construct lines in Figure 5 define a plane in which linear measurements are valid. The inclined dotted line is a "ditch reference line", and is used to mark the top/edge of the ditch (at road level) and the foot of the rock cut. The user uses one line to trace the face of the slope and another line to define the vertical extent of the slope. RockSee then automatically calculates the slope height and angle, and presents it in the window.

Similar calculations can be made for shoulder widths, ditch dimensions (and volumes based on a geometric model of the ditch, rectangle, triangle, or trapezoid), and potential rock fall quantities based on measuring the area of loose rock on the face, requiring an assumption of the depth of the loose rock. Other linear measures are possible as long as they are contained in the plane as defined above.

Tests were conducted to determine the accuracy of the RockSee measurements, by comparing to manual measurements. Results showed the average errors were less than 10% which is accurate enough for input into MORFH RS. The following shows the accuracy of all measurements:

Ditch Width	6.0%
Ditch Depth	8.6%
Slope Length	4.2%
Slope Angle	2.7%
Cliff Height	3.9%
Shoulder Width	7.6%
Road Width	2.7%
Rock Cut Length	4.6%

The RockSee program automatically enters the results of the measurements are into a database as described below.
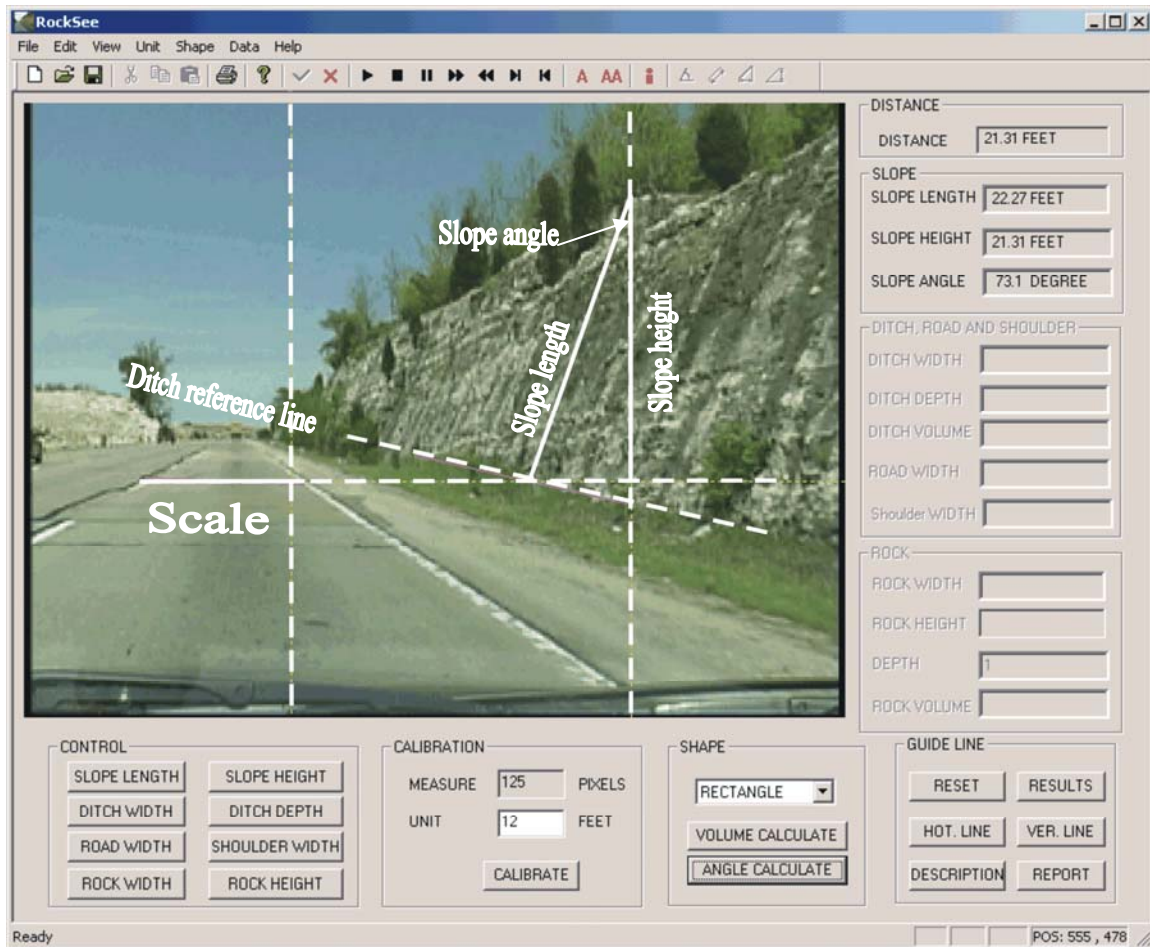
Figure 5. An example of the RockSee measurement of slope height and angle. Dotted lines are constructs, solid lines are measurements.

2.4 Field data collection

As Missouri's roads are long and numerous the use of field data sheets became tedious. A digital data collection system for the field parameters was developed as well as a GIS database management system. For the sites that needed detailed rating, a Pocket PC (Compaq IPAQ with ArcPad®) (Figure 6) was used to edit the site locations, and add the field rated parameters. The IPAQ includes an optional Navman GPS receiver to automatically record the site locations.

Communication (synchronization) with the desktop PC is handled by ActiveSync® software using USB connectivity. (ArcPad runs on desktop PC's as well as mobile computing devices).

Figure 6. Compaq IPAQ PC with ArcPad software for field data collection.

2.4 GIS implementation

ArcGIS® is the database management system that is used for the MORFG RS system. Figure 7 shows the outline of the GIS. In addition to the layer generated for rock cut sites, sorted by highway numbers (63, 44, 65, 55, 54, 70), there are layers that show the road network, the county outlines, geological map, topographic map, shaded relief, and a digital elevation model.

The attribute data is input from both the IPAQ mobile computer (rated parameter values) and from the office computer (RockSee measured parameters).

Figure 8 shows an example of data that can be retrieved from the database. Rock cut sites can be sorted, by county, by highway, by rating or other criteria. Clicking on any individual site will bring up all the attribute data, rating, and stored image if available. Other data such as maintenance records could easily be incorporated into the database.
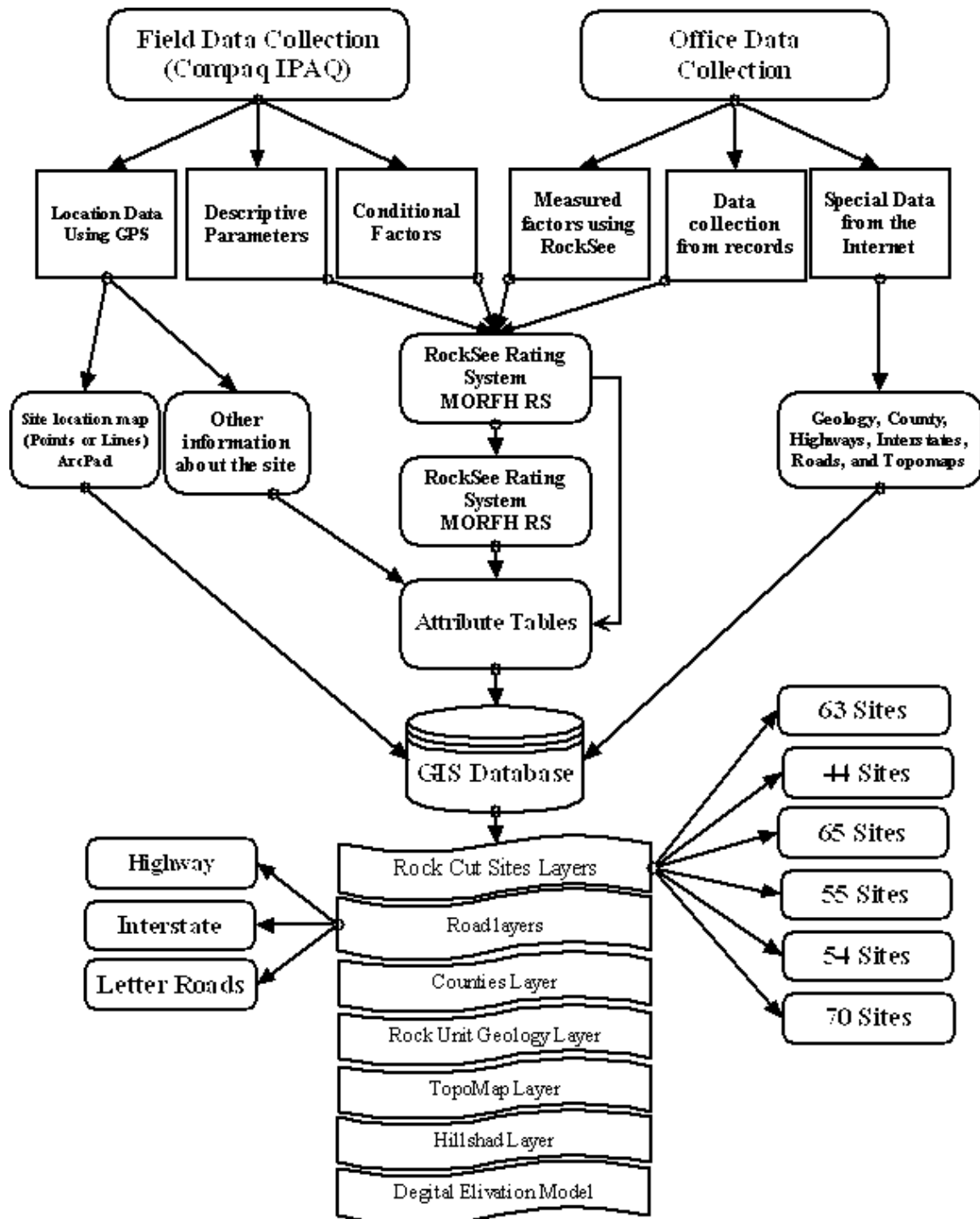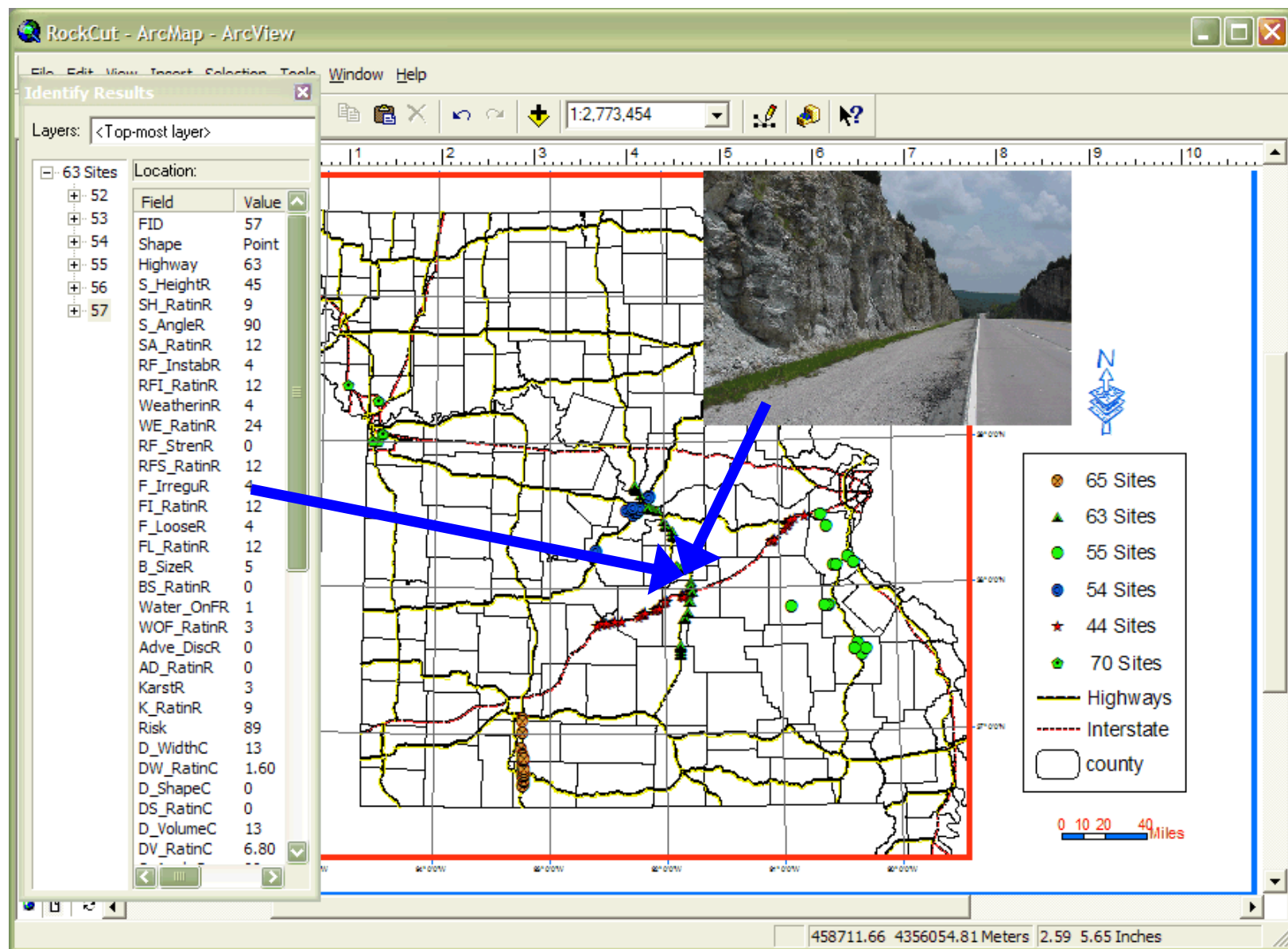
Figure 7. Database management system.

Fig. 8. Example of a GIS implementation. Map shows highways, counties, and sites. Clicking on any site brings ups an attribute table as well as an image from the database.

3. RESULTS OF INVESTIGATIONS

3.1 Missouri ratings

During the development of the systems, over 500 rock cuts in Missouri were evaluated; over 300 were given detailed ratings. Figure 9 shows some typical analysis results for four Missouri highways. Typical Missouri highways contain older rock cuts in carbonate rock with some filled sinks and sandstone rock with large block sizes, highly weathered in some areas. The distribution of the data shows that the data fall in three zones: high risk-high consequence, high risk-low consequence, and low risk-low consequence. Significantly there are many in the high risk-high consequence section for all of the rock cuts. Notably for the highway 65 results, there are a substantial number of low risk-low consequence cuts. These are the new cuts that have been constructed in the last few years.
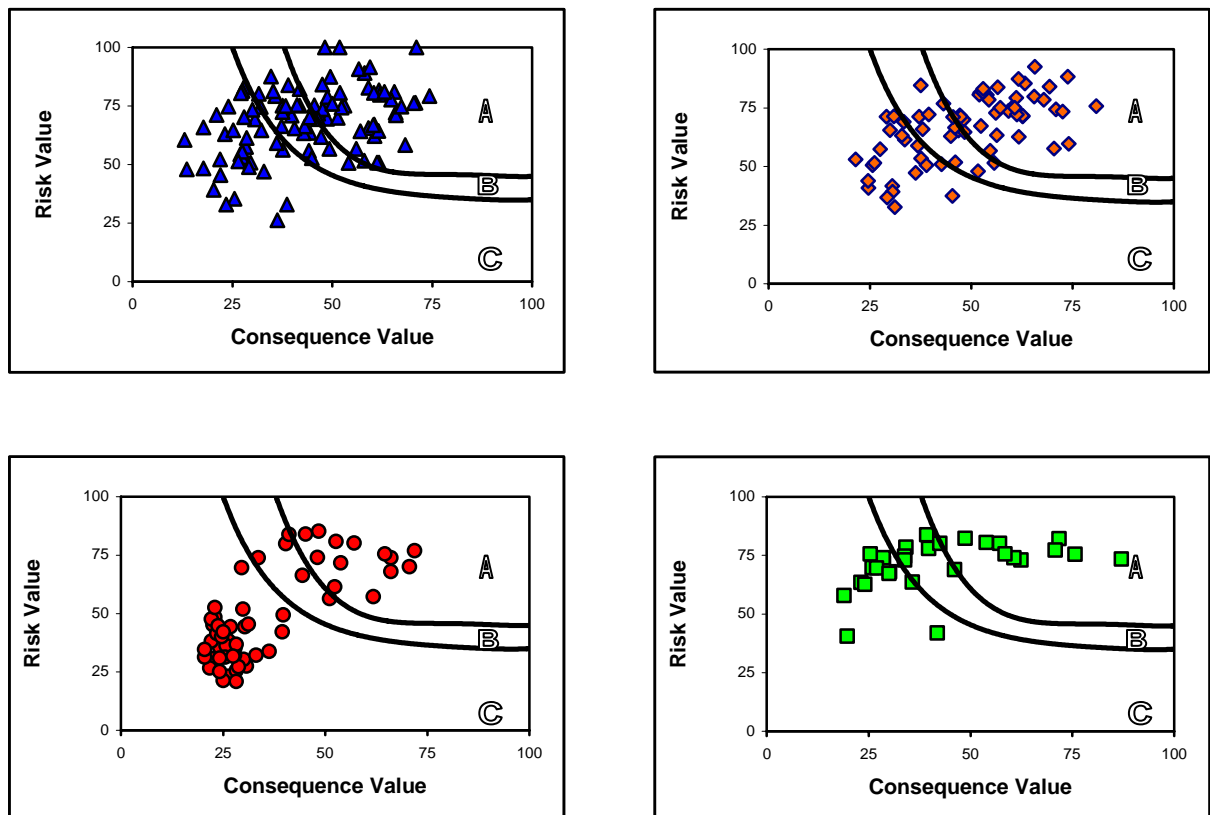

Figure 9. Results of analyses: Top left: Highway 63. Top right: Highway 44. Bottom left: Highway 65. Bottom right: Highway 54 (A= High Hazard Zone, B = Moderate Hazard Zone, and C = Low Hazard Zone).

3.2 Remediation simulations

To demonstrate the effectiveness of remediation techniques, simulations were conducted whereby the effects of scaling, ditch enhancement and trim blasting were simulated by changing the ratings of individual parameters to what they might be if the particular remedial measure was implemented. Figure 10 shows the results of the simulations.

For instance scaling decreases face instability, face looseness, face irregularity, rock fall quantity and increased ditch capacity (ditch cleaning is assumed). As a result the risk rating decreases dramatically while the consequence rating decrease slightly (Figure 10). It is noteworthy that while scaling is the least expensive solution, it is usually a short term solution.

Making ditch improvements (deepening and widening) increases the ditch width, volume, shape and effectiveness. As a result the consequence rating is dramatically reduced (Figure 10). It is however not always possible to increase the size of the ditch without removing some of the rock face.

Cutting back (trim blasting) the slope face decreases face instability, face looseness, face irregularity, rock fall quantity and can often decrease the weathering rating as new rock is exposed. At the same time it is possible and recommended to make ditch improvements increasing ditch capacity, ditch width, volume, shape and effectiveness. As a result there is a dramatic decrease in risk and consequence rating (Figure 10). This is the most costly solution, but also the most permanent, with the possible exception of the return of weathering after a number of years.

4. SUMMARY AND CONCLUSIONS

The Missouri Rock Fall Hazard Rating System (MORFH RS), a risk/consequence based classification system has recently been completed. Although designed for Missouri highways, the system can be adjusted for other jurisdictions by changing out some of the parameters, and perhaps changing the ratings for some of the parameters. In the Missouri system the emphasis has been on evaluating relatively low but highly weathered cuts, with special problems from highly weathered karst features such as filled sinkholes. In other jurisdictions there may be more of an emphasis on adversely oriented structure or other factors.

MORPH RS is very cost effective. Prescreening of video logs immediately reduces the problem of a large highway network with thousands of miles of highways to a more manageable number of rock cuts. Measurements on video images of many of the parameters needed for the rating reduces the amount of effort that must be expended in the field. Mobile computing devices link to GPS and entered into a GIS database make data transfer seamless.

The risk consequence nature of MORPH RS is a dramatic improvement in analysis, because in some cases higher risk may be tolerated while in others higher consequences. More importantly, values of parameters such as block size and slope angle have opposite effects on the risk and on the consequence rating. MORPH RS can be used to prioritize remediation, and the s effect of scaling, ditch modification, and trim blasting has been demonstrated.
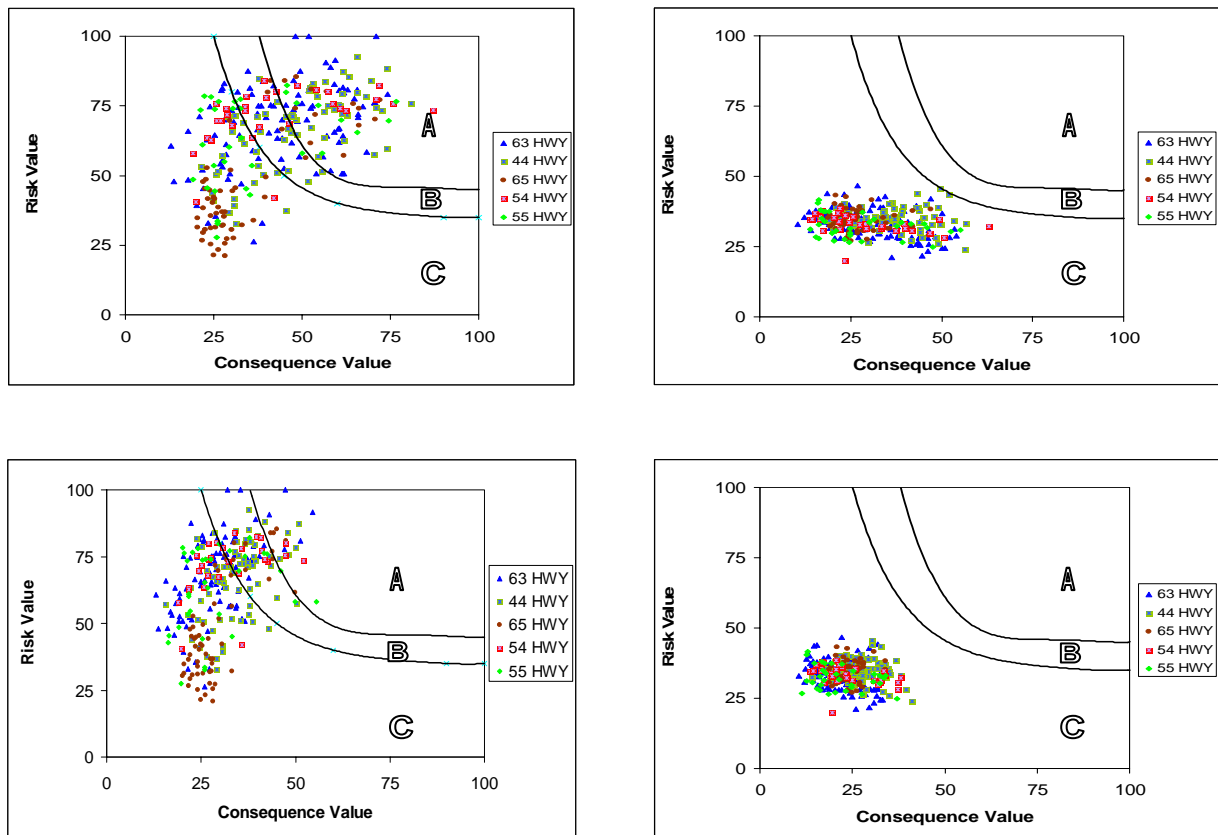
Figure 10. Results of remediation simulations: Top left: All data. Top right: Scaling. Bottom left: Ditch enhancement. Bottom right: Trim blasting. (A= High Hazard Zone, B = Moderate Hazard Zone, and C = Low Hazard Zone).

5. ACKNOWLEDGEMENTS

6. REFERENCES

Maerz, N. H., and McKenna, S., 1999. Mobile highway inventory and measurement system. Transportation Research Record no. 1690, pp. 135-142.

Maerz, N. H., Youssef, A., and Xiang, Q., 2003. Digital imaging for screening and making measurements of features on highway rock cuts. Transportation Research Board, 82nd Annual Meeting, Washington, D.C., Jan. 12-16, 2003, 20 pp.

Maerz, N. H., Youssef, A., and Fennessey, T., 2004. New risk-consequence rock fall hazard rating system for Missouri highways using digital image analysis. Submitted to Environment and Engineering GeoScience, July, 2004.

Youssef, A., Maerz, N. H., and, Fritz, M. A., 2003. A risk-consequence rockfall hazard rating system for Missouri highways. 54th Highway Geology Symposium, Burlington, Vermont, Sep. 24-26, 2003, pp 175-195.

Youssef, A., Maerz, N. H., and Xiang, Q., 2004. RockSee: video image measurements of physical features to aid in highway rock cut characterization. Computers and Geosciences, Aug. 2004.

APPENDIX 1: MORFH RS

SH (Slope height)	10'	20'	30'	40'	50'	60'
(Risk) Rating	2	4	6	8	10	12

SA (Slope angle)	30°	40°	50°	60°	70°	80°	90°
(Risk) Rating	0	2	4	6	8	10	12

for risk side. **AND** for consequence side:

SA (Slope angle	20°	30°	40°	50°	60°	70°	80°	85°	90°
(Consequence) Rating	0	12	10	6	3	2	4	12	0

RI (Rockfall instability)	Class No.	Description	(Risk) Rating
Completely unstable	4	Rocks often fall in this area and there is considerable evidence for that in the ditch and from maintenance records; this will be in sites where severe rock fall events are common	12
Unstable	3	Rocks fall from time to time; the rock falls will occur frequently during certain times of the year, but will not be a significant problem during other times; this also is used where significant rock falls have occurred in the past	9
Partially stable	2	Rocks fall occasionally; rock falls can be expected several times per year, usually during storms.	6
Stable	1	Very few blocks fall during a the year and only during a severe storms	3
Completely stable	0	No rock falls; no historical and physical evidence for any rock fall in the area	0

WF (Weathering factor)	Class No.	Description	(Risk) Rating
High	4	Major erosion features are present, there are many overhanging areas along the rock cut, differential erosion is evident along the rock cut	24
Moderate	3	Some erosion features are present, differential erosion features are large and numerous throughout the rock cut	18
Low	2	Minor differential erosion features appear widely distributed throughout the area, the differential erosion rate is limited	12
Slightly	1	Few differential erosion features, and the erosion rate is very low	6
Fresh	0	No evidence for weathering and the walls are smooth and planar	0

SOIR (Strength of intact rock)	Class No.	Description	(Risk) Rating
Very strong rock	4	> 14504 psi, many blows by the hammer needed to fracture the rock	0
Strong rock	3	7252 – 14504 psi, several blows to fracture the rock	3
Moderately strong rock	2	3626 – 7252 psi, A firm blow needed to fracture the rock	6
Weak rock	1	725 – 3626 psi, can indent the rock with a pick	9
Very weak rock	0	145 - 725 psi, can crumble by hand	12

FI (Face irregularity)	Class No.	Description	(Risk) Rating
Very high irregular face	4	There are many joints and overhanging features, irregular features everywhere throughout the site, the face is stepped everywhere	12
Highly irregular face	3	Much of the face is irregular and there are many joints and stepped faces	9
Moderately irregular face	2	There are many irregular areas in the face	6
Slightly irregular face	1	There are some irregular areas along the face	3
Smooth face	0	Very smooth face	0

FL (Face looseness)	Class No.	Description	(Risk) Rating
Very highly loose material	4	The face is completely covered by loose blocks	12
Highly loose material	3	Much of the face is covered by loose blocks	9
Moderately loose material	2	Some of the face is covered by loose blocks	6
Low loose material	1	Little of the face is covered by loose blocks	3
No loose material	0	There are no loose blocks on the face	0

BS (Block Size)	5'	2.5'	1'	0.5'
(Risk) Rating	0	4	8	12

for risk side. **AND** for consequence side:

BS (Block Size)	0.5'	1'	2.5'	5'
(Consequence) Rating	0	4	8	12

WOF (Water on face)	Class No.	Description	(Risk) Rating
Flowing	4	Water flows from the face	12
Dripping	3	Water drips from the face	9
Wet	2	There is evidence of significant water on the face	6
Damp	1	There is evidence of water on the face	3
Dry	0	There is no water on the face	0

DW (Ditch width)	15'	10'	5'	0'
(Consequence) Rating	0	4	8	12

AND

DV (Ditch volume)	30 ft^3/ft	25 ft^3/ft	20 ft^3/ft	15 ft^3/ft	10 ft^3/ft	5 ft^3/ft	0 ft^3/ft
(Consequence) Rating	0	2	4	6	8	10	12

for vertical slopes with no bad benches. **OR** for non-vertical slopes and bad bench(es):

(Modified) DW (Ditch width)	30'	20'	10'	0'
(Consequence) Rating	0	4	8	12

AND

DS (Ditch shape)	Large back slope (1V:4H), 14°	Moderate back slope (1V:6H), 9°	Slight back slope (1V:8H), 7°	Flat 0°
(Consequence) Rating	0	4	8	12

ERFQ (Expected rock fall quantities)	0 ft^3/ft	10 ft^3/ft	20 ft^3/ft	30 ft^3/ft	40 ft^3/ft
(Consequence)Rating	0	3	6	9	12

SW (Shoulder Width)	12'	9'	6'	3'	0'
(Consequence)Rating	0	3	6	9	12

NOL (number of lanes)	Four lanes	Three lanes	Two lanes	One lane
(Consequence) Rating	0	3	6	12

ADT (Average daily traffic)	5000 Cars / day	10000 Cars / day	15000 Cars / day	20000 Cars / day
(Consequence) Rating	3	6	9	12

AVR (Average vehicle risk)	25% (time a vehicle is in rock cut zone)	50% (time a vehicle is in rock cut zone)	75% (time a vehicle is in rock cut zone)	100% (time a vehicle is in rock cut zone)
(Consequence) Rating	3	6	9	12

DSD (Decision sight distance)	Class No.	Description	(Consequence) Rating
Very limited	3	Distance is very small and there are many vertical and horizontal curves on the roads, vegetation obscures falling rock	12
Limited	2	There are some curves and obstacles on the road not giving the driver enough time to perceive that there are falling rocks on the road	8
Moderate	1	There are few curves and obstacles and the driver can control the vehicle easily because he sees falling or fallen rocks	4
Adequate	0	The road is completely straight with out any obstacles or curves and the driver can see the entire rock face and road at any time	0

Adjustment factor **IF** applicable

AOD (Adversely oriented discontinuities)	< 20º, 90º	20 - 45º	45 - 65º	65- 90º
(Consequence) Rating	0	4	8	12

Adjustment factor **IF** applicable

KE (Karst effect)	Class No.	Description	(Consequence) Rating
Large	4	Karst features that appear on the rock cut face, width is 150', filled by boulders and cobbles with weak materials	12
Medium	3	Karst features that appear on the rock cut face, width is 100', filled by boulders and cobbles with weak materials	9
Small	2	Karst features that appear on the rock cut face, width is 50', filled by boulders and cobbles or undercut with weak materials	6
Possible	1	Carbonate rocks that could possibly have karst features but are not evident on the rock cut face	3
None	0	Non-carbonate rocks (igneous, sandstone)	0

(The following is internally calculated)

ERFQ/DV (Ditch Capacity Exceedence)	1x	2x	3x	4x
Rating Value	0	5	10	15

Bench present?	Yes	No	(if yes look at the bench and faces above the bench)	
	SCORE	4	2	0
Faces above bench	Weathering	High	Low	Fresh
	Face irregularity	High	Moderate	Smooth
	Face looseness	Large	Moderate	No
Bench characteristics	Bench width	Narrow<5'	Moderate 15'	Wide >20'
	Rock on the bench	Large amount	Moderate	None
	Slope of the bench	Toward road	Horizontal	Back slope
	TOTAL SCORE: _____	(if greater than 12 then bench is considered "bad")		

Screening calculation (from video) to determine if detailed assessment is required

Factor	Detailed assessment triggered **IF**
Weathering / Karst	1. A highly weathered rating on the video image, **OR** 2. Any indication of Karst (voids, filled sinks), **OR** 3. Any significant differential erosion (cut back voids, overhangs), **OR**
Face Irregularity / Face Looseness	1. A highly irregular face or a moderately irregular face high on the cut, **OR** 2. A highly loose face or a moderately loose face high on the cut, **OR**
Fallen rock in the ditch or on the cut	Significant amount of loose rock visible in the ditch, **OR**
Ditch effectiveness	Ditch effectiveness is very low (too small, too narrow), **OR**
Adversely oriented discontinuities	Indication of adversely oriented discontinuities, **OR**
Bench(es)	Presence of bench(es).
	NO Detailed assessment triggered IF
Slope height	1. Slope height less than 10', **OR** 2. The slope height is less than the width of the ditch plus the shoulder.

Drilled Shaft Design, Construction, and Inspection Challenges on the Kentucky Lock Project

Charles Hunley, PE, SE[1]
Kurt Schaefer, PE[2]

Abstract

The relocation of US 62/641 and the P&L Railway to new bridges with lengths over 3,100 feet in the tailwater immediately below Kentucky Dam is part of a $650 million Corps of Engineers project to add an additional lock chamber at KY Dam, near Paducah, Kentucky. The bridges will be founded on 72-inch and 84-inch diameter marine drilled shafts in a severe tailwater environment and extreme karst topography. Geotechnical issues included deep alluvial, lacustrine and fluvio-lacustrine soils overlying Mississippian Age limestone formations. These limestone formations were found to exhibit unconfined compressive strengths of up to 40,000 pounds per square inch, and consist of up to 35 percent chert nodules and bands. However, the formations also presented moderate to extreme karst conditions in the form of vertical and horizontal solution features which potentially threatened traditional drilled shaft foundation installations. The site geology, site seismicity, and severe tailwater surface fluctuations and velocities have required unique solutions during design, construction, and inspection of the drilled shafts and the bridges. Construction techniques include kerf-cutting drilling and new German drilling technology. Inspection techniques utilized on the project include Crosshole Sonic Logging (CSL) Testing, Sonar Callipering, and downhole shaft inspection devices to identify karst features and their remediation, shaft verticality, and shaft integrity. This paper will discuss the significant design, construction, and inspection challenges associated with the construction of the drilled shafts for the US 62/641 Bridge over the Tennessee River.

[1]Deputy Structural Engineering Manager, American Consulting Engineers, PLC, Lexington, KY
[2]Associate, Fuller, Mossbarger, Scott, and May Engineers, Inc. (FMSM), Lexington, Ky

Introduction

The Kentucky Lock Addition project is a $650 million US Army Corps of Engineers project to add an additional, longer lock chamber at Kentucky Dam, near Paducah, Kentucky. As part of this project, the existing highway and railway that cross the dam and bridge over the existing lock are being relocated downstream of the Dam. This relocation has resulted in two new approximately 3,100-feet long high-level bridges. These bridges cross the tailwater area below the Dam Spillway, the Powerhouse Island, and span the Lock approach channel. The estimated cost of the two structures is $40.7 million (railroad bridge) and $33.3 million (highway bridge). A rendering of the bridges is illustrated in Figure 1. Figure 2 shows a layout drawing of the highway bridge.
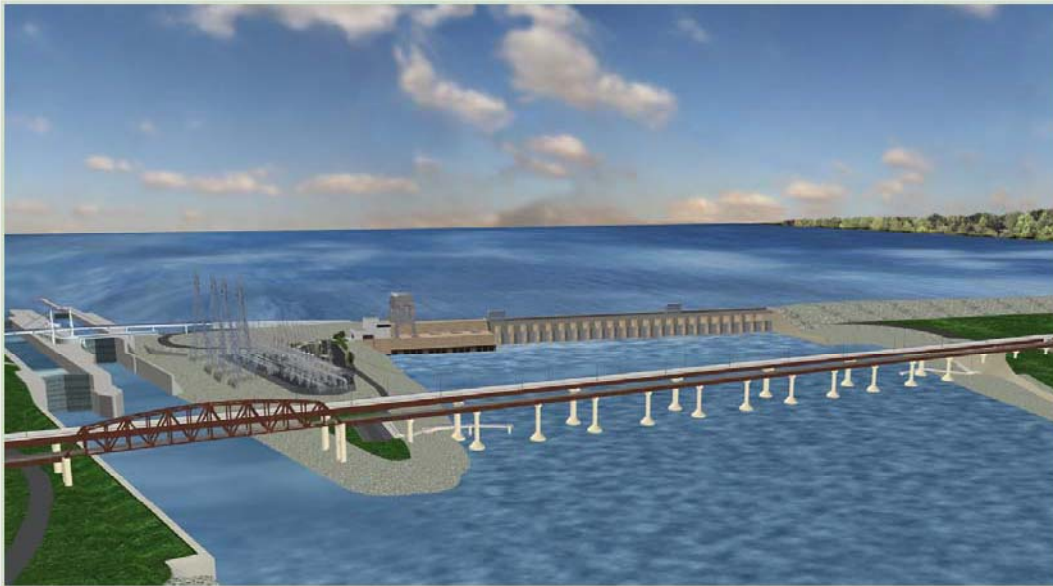
Figure 1: Overall Project Rendering

The construction of the two bridges has been separated into two construction contracts. The Substructure Contract includes the construction of all of the abutments and piers for the two bridges. This contract was awarded in August 2001 to CJ Mahan Construction Company for approximately $36,588,000, with drilled shaft costs totaling 44.7% of the project. The drilled shaft subcontractor is a joint venture between Richard Goettle, Inc. and Case Foundation Company. The project includes 90 individual drilled shafts totaling over 7,730 linear feet with diameters of 48-inches, 72-inches, and 84-inches. The original bid price for the drilled shafts was broken down as follows: $15,088,500 for excavation and placement, $747,700 for testing, and $516,000 for karst bedrock remediation measures.

This paper provides a cursory overview of the drilled shaft aspects of the highway bridge, as space limitations would not allow an extensive discussion of all of the various design/construction aspects and scenarios considered prior to reaching the final design for both bridges.
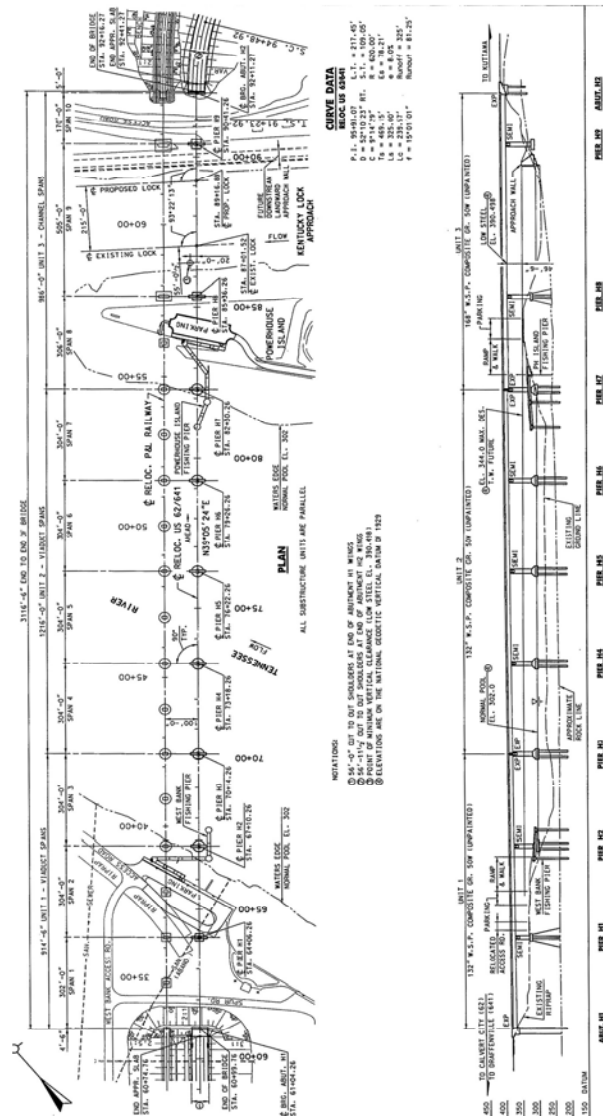
Figure 2: Highway Bridge Layout Drawing

Geologic/Geotechnical Background

To address the geologic and geotechnical issues of the US 62/641 Bridge over the Tennessee River, the question of what conditions were present at the site had to first be answered. The structure site is located in Western Kentucky within the Mississippi Embayment and the Mississippian Plateaus physiographic regions. The Tennessee River separates these two regions, with the Mississippi Embayment being located west of the river and the Mississippian Plateaus being positioned east of the river. As a result, subsurface conditions present to the west of the Tennessee River are substantially different from those identified to the east.

Geologic mapping (USGS Geologic Map of the Calvert City Quadrangle, Livingston and Marshall Counties, Kentucky, 1968) indicates areas of the Kentucky Lock project site pertaining to the US 62/641 bridge over the Tennessee River is underlain by alluvial and

fluvio-lacustrine deposits on the order of 100 feet thick on the west bank of the river, and hydraulic fill which comprises Powerhouse Island near the east bank of the river. The materials underlying the river at the crossing are not specifically identified by the mapping; however, a geologic section developed at a location 3.9 miles downstream of this structure indicates alluvial deposits on the order of 30 feet in thickness underlie the river. After crossing the Tennessee River, the east abutment (Abutment 2) of the US 62/641 Bridge over the Tennessee River will be positioned on the top of a small hill. The referenced mapping indicates this abutment location is underlain by the western extent of soils of the Tuscaloosa Formation. The Tuscaloosa Formation was deposited during the Cretaceous geologic age and is composed of gravel with chert, sand and silt. This formation is reported by the geologic mapping to occur in thicknesses of up to 180 feet. The geologic mapping also indicates that soils within the western area of the mapped Tuscaloosa soils could consist of a mixture of the Tuscaloosa and McNairy Formations. The McNairy Formation was also deposited during the Cretaceous geologic age and is comprised of interbedded sands, clays and gravels.

Bedrock underlying the soils along the alignment of the structure is noted by the referenced mapping to be Mississippian-age units of the Warsaw Limestone and Fort Payne Formations, in descending order. The Warsaw Limestone Formation is described as light gray, thick bedded, coarse grained and bioclastic, with some chert lenses and thin shale laminae. The limestone in this zone varies from light to dark gray, finely- to coarsely crystalline-grained, and is bioclastic to argillaceous. The referenced chert is gray to dark gray, and occurs in irregular beds and discontinuous layers. Underlying the Warsaw Limestone is the Fort Payne Formation. This bedrock unit is comprised of limestone and chert interlayered in beds from one inch to two feet thick. The limestone is described as dark gray, dense to finely crystalline-grained, siliceous, argillaceous, with the upper parts of some zones being shaley. The chert composes approximately 10 to 35 percent of this unit, and occurs in beds and lenticular masses. It is dark gray with a dull luster and weathers to a light gray. The contact between the Warsaw Limestone and the Fort Payne formations was established to be near elevation 270 feet.

Significant karst bedrock features such as solution zones, voids, caves, crevices, and clay-filled zones within the bedrock are known to exist in this region of the state. Previous geotechnical explorations for the existing Kentucky Lock facility, as well as for the proposed lock addition and appurtenances, have encountered karst features in both the Warsaw Limestone and Fort Payne Formations. Occurrences of voids and cavities on the order of one to three feet are common. Typically, the Warsaw Formation contains a higher number and larger sizes of such karst features. An example of the magnitude karst features can display in this region was noted in "Foundation Treatment of Karstic Features under TVA Dams" (Soderberg, 1988).

How these conditions could cause problems for the drilled shafts of the bridge was next addressed. Deep alluvial and fluvio lacustrine deposits are commonly dealt with in drilled shaft installations, therefore the soil conditions at the site were not considered to be a critical design issue. In fact, because of the aggressive tailwater environment, all shafts were designed considering all foundation soils completely removed by scour. The karst features in the bedrock underlying the site, however, were immediately identified as the condition which could pose the greatest threat to shaft installation and performance. Vertical features at the bedrock surface as well as features encountered within the shaft socket below the top of rock could allow concrete loss during placement and /or soil intrusion during concrete placement. Features within the bedrock can also cause a loss of lateral support for the shafts. This loss of lateral support was of significant concern on this bridge because of the foundation design being based on the rock socket of the drilled shaft providing all lateral load resistance. Lastly, because the shafts were designed to be supported by the bedrock in end-bearing only, a void or feature immediately beneath the bearing surface could collapse when loaded, and fail the shaft axially.

A geotechnical exploration was performed prior to final design of the foundation systems for the bridge to determine the bedrock characteristics of the bridge crossing, possibly determine if karst features were present at the substructure element locations, and determine probable bearing elevations for drilled shaft foundation alternates of the bridge. A total of 34 borings were drilled at 11 substructure element locations. Each boring was advanced to the bedrock surface by augering and then into bedrock by rock coring techniques. Because of the anticipated drilled shaft foundations, the rock cores were taken significant lengths into bedrock to search for karst features both within and below the probable socket length. The bedrock encountered correlated well with the geologic mapping and represented both the Warsaw Limestone and the Fort Payne Formation. A total of 56 samples of rock core were tested for unconfined compressive strength and returned values varying from 5,458 pounds per square inch (psi) to 40,777 psi with the majority of samples tested returning strengths of over 20,000 psi. Intact bedrock was therefore found to be stronger than the concrete to be specified for shaft construction. A contradiction to the very strong rock was the presence of karst features within the bedrock. These features were typically found to consist of clay filled seams, voids and solution channels. Drilling for the West Abutment and all the pier locations encountered only horizontal features which were typically less than three feet in vertical dimension. Drilling for the East Abutment to the bridge encountered both horizontal and vertical features. Because of the characteristics of the encountered features, additional borings were advanced and it was determined that both a significant vertical feature (the top of bedrock varied by approximately 61 feet over a horizontal distance of approximately five feet) and significant voids in the bedrock (two over 20-feet in vertical dimension) were present at this location. A portion of the borings drilled at the abutment location are presented in Figure 3 to illustrate the number and magnitude of features encountered. These features caused the redesign of the abutment from a five shaft configuration to a four shaft configuration.
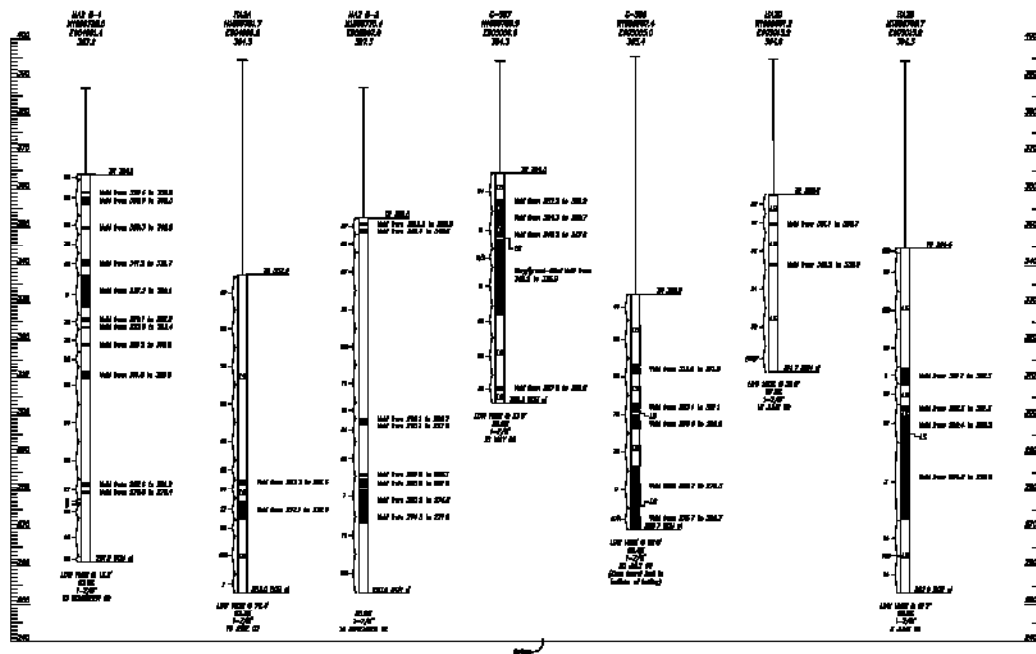
Figure 3: Abutment H2 Boring Logs

Proactive Approach to Conditions Encountered

A preconstruction rock core boring was specified at all drilled shaft locations because of the features encountered during this geotechnical exploration, during construction of the existing Kentucky Lake Lock and Dam, and the fact that the geotechnical exploration for the bridge had been performed prior to the determination of final shaft locations, orientations, and sizes. These preconstruction core holes were positioned at the approximate center of the drilled shaft location and were used to identify features encountered, and establish a maximum bearing elevation for each specific shaft. A total of 34 preconstruction holes were drilled for the US62/641 Bridge over the Tennessee River. It should be noted that Piers 1 and 8 were designed to be supported by point bearing steel piles, and Pier 9 of the bridge was designed as a spread footing bearing on limestone bedrock; therefore no preconstruction borings were advanced at these locations.

Although no vertical features were encountered directly in any of the borings (excluding those for the east abutment) it was still firmly believed that such features would be encountered during actual shaft construction. After all, an exploratory hole with a diameter of roughly three inches could not possibly represent the entire rock surface of a six or seven foot diameter drilled shaft in an area noted for prevalent karst conditions. Therefore, the design team specified that at a minimum, the top five feet of rock socket for every drilled shaft be excavated using a kerf cutting core barrel and the resulting rock core retrieved for observation regarding vertical features within that interval. If a vertical feature was encountered, and maintained a width of six inches or greater at the bottom of the kerf cut, the kerf cut was extended another five feet. If at the bottom

of the second kerf cutting interval the feature remained greater than six inches in width, the contractor was instructed to remediate the feature to provide lateral capacity of the shaft within the rock socket. To reduce construction delays and possible change orders, the design team developed and provided a vertical crevice remediation in the contract documents and drawings, and included vertical crevice remediation as a bid item. The remediation consisted of overdrilling the shaft location to a diameter of ten feet for a depth of ten feet into rock, placing a reinforcing cage inside this excavation, and filling to the bedrock surface with concrete. The original shaft location was then redrilled at design dimensions through the concrete plug after the concrete had been allowed to set. This 10 feet diameter plug was designed to act as a lateral thrust block and was sized to span the typical vertical features exposed during the original dam construction. If the initial kerf cut interval showed no vertical features greater than six inches in width at the bottom surface of the core, the contractor was allowed to advance the shaft by approved drilling methods to the final bearing elevation.

Horizontal features encountered during shaft excavation would also have to be addressed to prevent concrete loss or soil intrusion into the shaft. The locations of these features were noted in the preconstruction cores of each shaft location. If a horizontal feature was greater than six inches in vertical height it was recommended that the feature be remediated prior to advancing the shaft excavation to final bearing elevation. The recommended procedure for remediating a cavity was to drill to a depth of 1.5 feet below the cavity (or group of cavities) and fill the excavation with lean concrete to a height of 1.5 feet above the topmost cavity. After allowing the concrete to cure for one day the concrete was drilled out and the shaft advanced to bearing elevation leaving a 'plug' in the wall of the shaft excavation. Again, to reduce construction delays and costly change orders, the contract documents and drawings included minimum sizes of features to be remediated, suggested remediation techniques, and a bid item for plugging these features. The contractor was also required to submit a remediation technique for approval in conjunction with the excavation plan for the drilled shafts on the project.

In order to assess whether a feature remediation had been successful, and whether or not additional features (not encountered in the preconstruction drilling program) had been exposed by shaft construction, the design team specified that Sonar Caliper Testing be performed in every drilled shaft excavation prior to placement of the steel reinforcing cage. This testing method allowed real time viewing of the sidewalls and bottom of the shaft excavation, as well as hardcopy prints of the wireframe plots. An example of the wireframe plot for a sonar caliper test is presented in Figure 4. This figure shows the same drilled shaft socket before and after remediation. The Sonar Caliper testing was also used to check the verticality of each drilled shaft excavation and verify the plumbness of the shaft met design specifications.

Upon acceptance of a shaft for concrete placement, the question of how to monitor the placement and verify the integrity of the concrete within the shaft had to be addressed. The design team therefore specified Crosshole Sonic Logging (CSL) be performed on each shaft. For shafts greater than five feet in diameter, six CSL tubes were required, and for shafts less than four feet in diameter, four tubes were required. As hoped, the vast majority of shafts tested showed good

quality concrete. However, as described later in this paper, anomalies were noted in one shaft location.
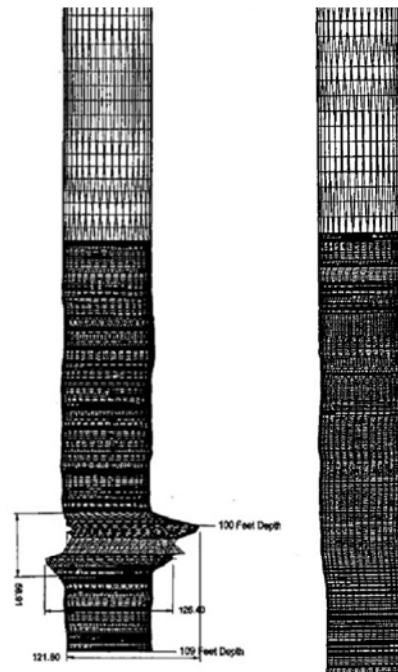

Figure 4: Sonar Caliper Testing (Before and After Cavity Remediation)

Pier and Drilled Shaft Design Issues

In the viaduct portion of the bridges, the tailwater area below the Dam Spillway, the highway piers are founded on four 72-inch diameter marine drilled shafts each. Figure 5 shows a typical highway bridge pier configuration. The drilled shafts extend through approximately 28 feet of water, 31 feet of overburden, and 19 feet (minimum) into karst bedrock. The site geology, site seismicity, severe tailwater surface elevation fluctuations, and flows up to 7 feet per second created significant design challenges on the project.

One design issue was the stream flow forces that the pier must withstand. Due to the proximity of the bridges to the spillway of the Kentucky Dam and the configuration of the hydroelectric turbines, the typical inverse triangular streamflow pressure diagram is not valid for these bridges. During normal to moderately high flows, including when the dam is not spilling at all, the water coming through the turbines is being released at the bottom of the river. During extremely high flows, the water is being dumped through the spillway. Therefore, the streamflow pressure diagram was taken as a uniform pressure throughout the water table and equal to the maximum streamflow pressure as defined in the AASHTO design specifications. With velocities of 7 feet per second and a 100-year flood depth of over 86 feet, this resulted in a significant design issue.

Figure 5: Typical Pier Configuration

Another issue that had a significant impact on the design of the drilled shafts was scour. A scour analysis of the structure was performed, taking into account the proximity of the railroad bridge piers. From the analysis, scour depths at the highway piers were calculated at nearly the depth of the overburden. Given the extent of the potential scour, and the transient nature of the river bottom due to spillway flows, the design of the drilled shafts was performed assuming no lateral support from the overburden materials. Therefore, from a design standpoint, the drilled shafts have an unsupported length of between 45 feet and 65 feet with all of the lateral support being provided by the rock sockets. During design, the rock socket depth was iterated to determine the minimum acceptable rock socket length for lateral capacity. A value of three shaft diameters, or 18 feet for the highway bridge, was verified as the minimum rock socket length acceptable in competent bedrock.

Site seismicity was another key factor in the design of the drilled shafts. The bridge is located in a moderately high seismic region near the New Madrid Fault, with a peak ground acceleration coefficient of 0.15. Also, because of the scour potential, two seismic analyses were performed. One with lateral support from the overburden, and another with the shafts unsupported to the top

of competent rock. This moderate seismic design loading, along with the magnitude of the bridge, proved to be the critical loading and controlled the design of the drilled shafts.

Another key design issue was the potential for vertical crevices at the top of rock. Coupled with the scour potential of the site, this became a significant issue to the design team and the client. The main concern was that, if a significant vertical crevice was discovered during construction, the client wanted a solution which would not create significant delays during construction while the shaft design was investigated and a new shaft design performed for the greater unsupported length. From all of the historical data available, it appeared that most of the vertical crevices uncovered during the dam construction were widest at the top of rock and generally tapered out in the top ten feet of bedrock. Therefore, the design team chose to design the drilled shafts for the possibility that the top of rock would be 10 feet lower than the elevations determined by the geotechnical investigation. This would accommodate any vertical crevices that tapered out in the top 10 feet of bedrock. For crevices deeper than 10-feet, the lateral thrust block concept described previously was suggested for remediating vertical crevices without having to redesign the shaft during construction and potentially increasing the shaft diameter because of a large vertical crevice.

Drilled Shaft Installation Techniques

Due to the water velocities and depths encountered, the Contractor is utilizing a shield casing method to accurately position and stabilize the drilled shaft permanent casings during construction. With the shield casing method, a larger diameter temporary casing is installed to rock and the overburden is augered from the casing, see Figure 6. The kerf cutting drill is then used to perform the first five to ten feet of rock socket excavation as per the vertical crevice remediation requirements. Once the kerf cutting is accepted, concrete is placed in the kerf hole. Before the concrete sets, the permanent casing is twisted through the concrete and into rock. This allows the permanent casing to be set accurately both horizontally and within verticality tolerances in an "open" hole. Once the concrete has set, the permanent casing becomes fixed at the bottom. This provides lateral support for the permanent casing. Then sand is placed in the annulus between the permanent and temporary shield casings to help stabilize the permanent casing within the shield casing. The height of sand placed was determined by lateral analysis to ensure that the shielded permanent casing would not be driven out of deflection tolerances by movement of the shield casing due to stream flow. Then a reverse-circulation drill is used to drill through the concrete inside the permanent casing and down to the shaft tip elevation. After sonar caliper testing and performing any necessary horizontal cavity remediation techniques, the shaft reinforcement cage is lifted into place and the shaft concreted. The drilled shaft concrete design consisted of 4,000psi tremie placed concrete. Finally, once the CSL testing was performed and the shaft reached the specified compressive strength, additional sand was placed in the annulus between the permanent and shield casings to the mudline and the temporary shield casing was removed. Barge-mounted cranes and work barges are used to perform the drilled shaft construction are presented in Figure 7.

Figure 6: Shield Casing Setup

Figure 7: Marine Plant

As discussed earlier, the limestone bedrock in this area is extremely hard. During the first season of construction, the Contractor used a conventional reverse-circulation drill rig for rock socket excavation. However, due to the hardness of the limestone and the presence of significantly harder chert bands within the bedrock, production rates were as low as six inches per hour. In an effort to increase rock socket excavation production and catch up with the project schedule, the Contractor chose to purchase a German-made "WIRTH" pile-top drill rig, see Figure 8. A WIRTH drill is essentially a hydraulic drill rig that attaches to the top of the permanent casing, and pulls on the casing as it advances the drill head into the rock using the reverse circulation drilling system. This decision by the Contractor has proven to be very successful. Using the WIRTH drill, rock socket excavation production rates as high as two to three feet per hour were achieved.

Figure 8: WIRTH Pile-Top Drill

Rock Socket Construction Challenges

Production rates were not the only obstacle during rock socket construction. As mentioned earlier, the karst topography and potential presence of vertical cavities in the rock were also a challenge. The purpose for the specification of kerf cutting the first five (5) plus feet of rock socket was to be able to visually inspect the retrieved rock core for vertical features or poor quality rock near the rock line. However, due to the fractured, karst nature of the limestone and its strength, recovery of the kerf cores was difficult. In one early core retrieval attempt, the hydraulic jacks of the retriever failed while trying to break the kerf core plug free for removal. Also, when the top of the rock was highly fractured, or contained numerous small horizontal cavities, or an open vertical feature split within the kerf core, retrieval of the kerf core proved quite difficult.

With the difficulties associated with the kerf cutting requirements and the success of the WIRTH drill, the Contractor submitted a value engineering proposal to replace the kerf cutting and retrieval process with down-hole shaft inspection using a Shaft Inspection Device (mini-SID) manufactured by GPE, Inc. of Gainesville, Florida. The mini-SID consists of an open bottom "diving bell" that operates on the principal of a camera looking through a volume of gas, contained by water pressure, which has been dropped to the bottom of the shaft. The bottom of the "bell" rests on the rock surface and the gas pressure is equalized to force all water out of the bell. This has the advantage of the camera lens looking through a clear gas as opposed to possibly turbid water in the shaft excavation. In addition, the device is fitted with a video camera to record the inspection, and a water jet to "move" fine debris from the view area of the bell. The mini-SID was used at the five feet and ten feet depths into rock to inspect the entire shaft bottom for the presence of any vertical crevices. These inspection plateaus, as well as the

sonar callipering testing, were used to determine the presence and extent of any vertical crevices that may require remediation. This technique has been used successfully since its introduction, and credited with identifying a vertical crevice/feature in one of the drilled shafts at Pier 2 of the highway bridge.

Problems During Construction

The extensive testing program used during drilled shaft construction has been successful in uncovering several problems during construction. Early detection has allowed the Corps of Engineers and the design team the ability to correct any problems when they happen, protect the quality of the drilled shafts on these bridges, and avoid construction delays.

One concern during the design of the bridges was the presence of horizontal cavities in the bedrock. Sonar Calipering has successfully identified the size and extent of horizontal features in the bedrock during shaft construction and has provided reassurance that the plugging of any horizontal cavities was successful. Another benefit to the use of sonar callipering is that the verticality of a shaft can be verified. On this project, the allowable limits on verticality were set at 1% out of plumb overall and 2% out of plumb in the rock socket. On one shaft, the sonar callipering found that the rock socket excavation was 4.6% out of plumb. The total lean of the rock socket was 12.12 inches in 22 feet. The final decision regarding this shaft was that the drill bit was deflected off center as it advanced through various extremely hard chert layers in the rock socket. The problem with this much lean in the drilled shaft is that the reinforcement cage spacers are not strong enough to force the stiff reinforcement cage over as it is inserted into the drilled shaft. In this case, the original shaft designer came up with a "beam" composed of four steel rolled sections welded together. This "beam" was placed in the center of the hole and extended out of the rock socket and into the permanent casing. The "beam" was designed to resist the maximum bending moment in the shaft.

The significance of the historical data and preliminary data from the initial geotechnical investigations, along with the unique design and large scale of the bridges, were the primary reason that so much effort was put into the drilled shaft testing program on this project. The historical data, namely open-excavation mapping from the construction of the Kentucky Dam Spillway, illustrated the potential for significant and numerous vertical crevices in the bedrock. The design team also discovered early in the project that there was no reasonable design approach to mitigate the presence of a large vertical crevice during the design phase. To the joy of the design team, however, a reasonably significant vertical crevice was found in only one shaft of the 71 shafts located downstream of the spillway. During the initial rock socket excavation and mini-SID inspections at Pier H2 of the highway bridge, it was obvious that these four drilled shafts were located in an area that was karst near the top of rock. At three of the drilled shafts, it was determined that only significant horizontal features were present in the top five to ten feet of the rock socket. Therefore, the original design mitigation technique of analyzing the shaft with the top of rock ten feet lower than the elevation determined during the geotechnical investigation was successful in keeping these shafts from having to be redesigned during construction. However, at one of the piers the combination of the mini-SID inspections

and sonar callipering testing suggested that the shaft was slicing into the side of a vertical crevice. Figure 9 shows the initial sonar callipering results at this shaft. The initial response was to fill the entire rock socket with concrete and then go outside of the drilled shaft in the direction of the anomaly and drill additional core holes into the bedrock to characterize the extent of the vertical crevice. With this additional testing, the design team could make the decision of whether a remediation technique could be used or if the drilled shaft would require redesign. The concrete was placed before the core holes because there was some belief that the feature was narrow and the backside of the feature may have been cleaned out during rock socket excavation. The results of the additional core holes supported this assumption as all of the core holes showed sound rock and concrete. These results led the design team to accept the remediation believing that the vertical feature was narrow and the concrete filled across it. After acceptance, the drilled shaft socket was redrilled through the lean concrete to bearing elevation with a zero tolerance bit to allow for reinforcing cage installation.
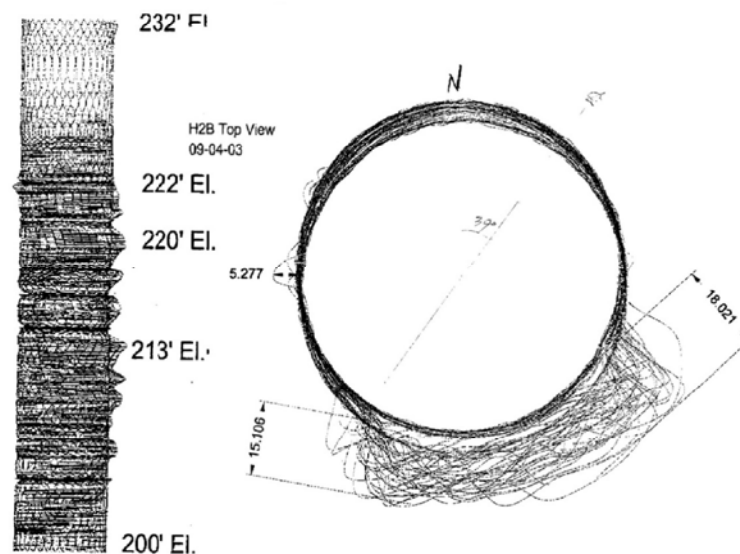
Figure 9: Shaft H2B Sonar Caliper (Before Remediation)

As previously stated, Crosshole Sonic Logging (CSL) testing was used on this project to verify the integrity of the concrete placement in each shaft. This technique was utilized because of the large diameter and length of the shafts, as well as the concern with horizontal cavities caving into the shaft excavation after reinforcing steel placement. The first evidence of an anomaly in the concrete placement was found with the CSL testing at one of the 148-feet long drilled shafts at Abutment H1 of the highway bridge. The CSL testing showed two suspect regions at 95-feet and 112-feet below the shaft top, see Figure 10. These anomalies were located such that they were both above the rock socket and critical in terms of the strength of the shaft. In order to determine if these were regions of poor concrete quality, the Contractor was required to drill three core holes in strategic locations based on the CSL results. The core holes revealed regions of concrete/aggregate separation and communication between the core holes, which the Contractor determined was the result of a tremie pipe that had become loose during that

placement and had allowed the concrete to become segregated. The anomalous zones were basically comprised of aggregate with very little cement. The Contractor was then required to submit a remediation plan to ensure that the areas would not be detrimental to the shaft's long-term integrity. The approved remediation plan included 6,000 psi high-pressure water jetting of the anomalies to remove/dislodge poor quality concrete, and jet grouting with a non-shrink cement grout. After the remediation had been performed and the grout cured, CSL testing was used to verify that the anomalies had been filled with grout. The new CSL test results confirmed that the remediation was successful.
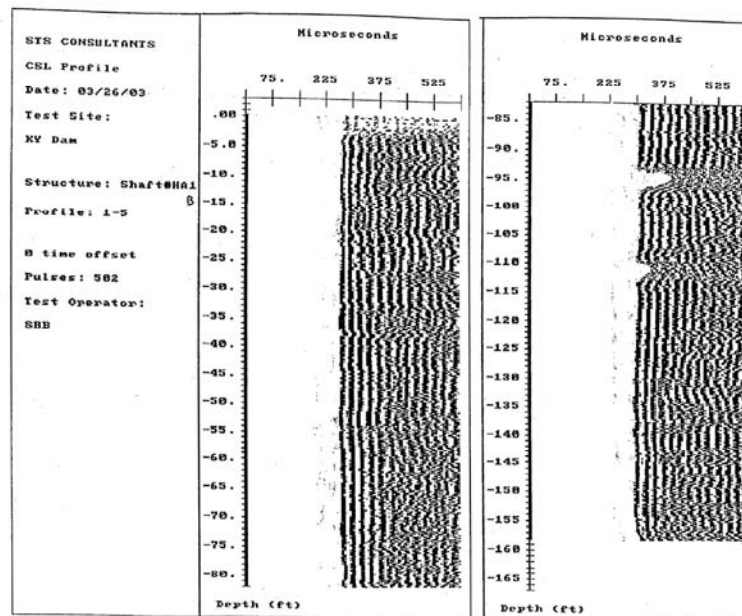
Figure 10: CSL Testing (Showing Two Suspect Regions)

Summary and Conclusions

The highway and railway bridge relocations associated with the Kentucky Lock Addition project are tremendous structures. Drilled shafts proved to be the only viable foundation type for the bridge piers located in the severe tailwater environment below the Kentucky Dam Spillway. The decision, during the design phase of the project, to develop remediation scenarios for anticipated problems and present them in the plans and specifications prevented significant construction delays and costly change orders. Due to the scale, design and construction challenges, and cost of the two bridges, an extensive and proactive construction monitoring and inspection system has been performed. The tools utilized cover nearly the full breadth of proven and acceptable drilled shaft testing techniques. Not only because of the problems found and addressed during construction, but also because of the piece of mind and assurance of the quality of these foundations, this project has been a success. This project has proven that even in an extremely karst and severe environments, a proactive approach during design and construction can lead to the successful use of drilled shafts in the most challenging environments without significant delays or contract modifications.

Acknowledgements

The authors would like to acknowledge the full design team for the highway and railway relocation portions of the Kentucky Lock Addition project:

References

"Design Memorandum No. 4", Highway relocation design team, Kentucky Lock Addition Project, February 2002.

Soderberg II, A.D. (May 1988), "Foundation Treatment of Karstic Features under TVA Dams" ASCE National Convention.

Analysis and Assessment of the Slope Stability in a Copper Mine

Lijun Zhang   Duowen Ding

(Department of civil engineering, Morgan State University)

(lzhang@eng.morgan.edu   dding@eng.morgan.edu)

Abstract

The Rough-Breaking Station Slope in a Copper Mine is a man-made slope. It is located at northeast of the Rough-Breaking Station. The slope height is 120m, the strike is 335^0, the dip direction is 245^0, and the dip angle for initial design is 39^0. The bottom of the slope is 140m in width.

This paper analyzes the stability of the slope and assesses the failure probability of the slope respect to different slope angle by using Monte Carlo Simulation. In this paper, by means of the preferred plane theory, a safe and economical designed slope angle is obtained from comparison of different designs. Furthermore, the slope reliability and real preferred plane are determined by using the method of probability analysis for geological preferred plane and statistical preferred plane.

Key Words: slope, preferred plane, failure probability, stability assessment

Hydrogeological and Engineering Geological Features Associated with Slope Stability

The man-made slope is located at northeast of Rough-Breaking Station in a Copper Mine. The top elevation and the bottom elevation of the slope are 291m and 171m, respectively. The strike of the slope is 335^0 (position direction), the dip direction is 245^0 (position direction), and initial design dip is 39^0. The bottom of the slope is 140m in width.

(1) Strata: The strata that comprised the slope body are the Eozoic metamorphic rock group. The major rock is mica-schist. In this area, the intrusive rock is the neuter-acid intrusive rock of Yanshan mountain orogeny period in where the major rocks are fine-grain amphibolites and quartz-amphibolites. At the top of the slope, there is outcrop of weathered granitiform-amphibolites-porphyry. Engineering Geological map is shown in the Figure 1-1, the section diagram is shown in the Figure 1-2. [1]
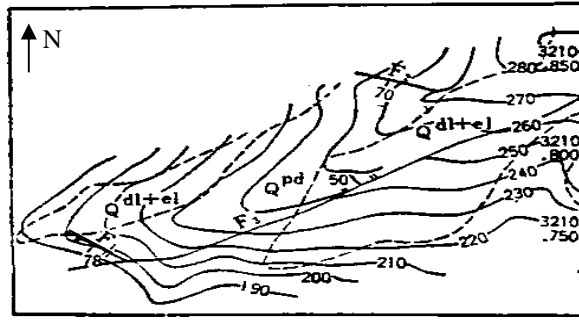
1

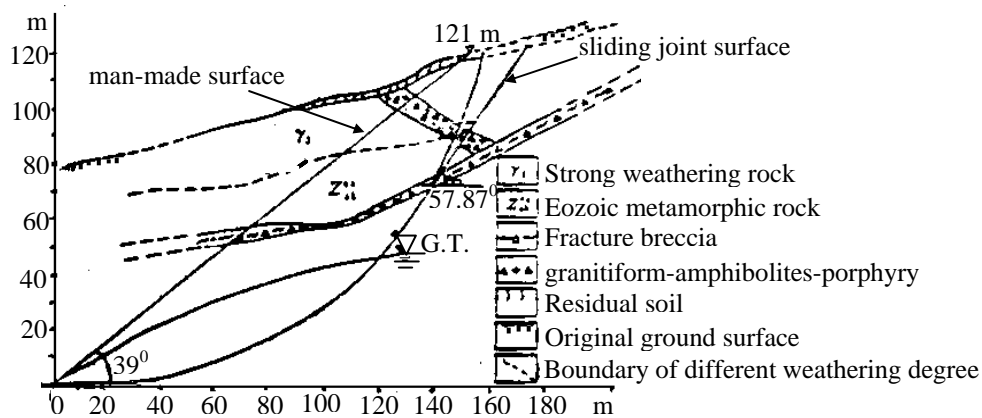Figure 1-1 Engineering Geology Contour Map
(not in scale)

Figure 1-2 The section diagram for computational model (not in scale)

(2) Geologic structure features: This area is located border of southern mine band and southern wing of the syncline. The axis of this syncline is EW (east-west). The structural features of the strata are complex because of the magmata activity frequently in this area. The features of the structures are mainly fractures of faults. [1]

- Fault: There are three faults that go through the Rough-Breaking Station Slope area. Their numbers are F_1, F_2, and F_3 (See Figure 1). F_1 with an elevation of 170m is located at the slope toe and the part above F_1 is removed, so F_1 does not affect the stability of the man-made slope. The geometrical data of the faults are as follows: F_1: $225^0 \angle 78^0$, F_2: $245^0 \angle 70^0$, the fracture zone is about 1-2m in width

and 120m in length within the site. F_3: 295^0-$320^0 \angle 40^0$- 50^0, the length of F_3 is 300m within the site.

- Joint: There are four sets of joints in the area that are close and numerous as well as some of them filled with mud and Fe_2O_3. The characteristics and some data are shown in the following table 1 [1].

Table 1 Preferred planes Characteristics

Number	Geometric Parameters (dip direction$\angle$dip)	Accounting for Proportion of Total Joint's Number	Characteristics
J_1	$245.06^0 \angle 57.87^0$	9%	Well developed, Well linked up
J_2	$118^0 \angle 24^0$	6%	bad linked up
J_3	$45^0 \angle 82^0$	5%	bad linked up
J_4	$335^0 \angle 72^0$	2%	Joint plane contains mud

- Hydrogeological features: The groundwater is the fissure water type in this area. The groundwater table is at a depth of 22.31-50.55m below the groundsurface. The groundwater is mostly recharged from raining. The rock has a good permeability and also this area has a good drainage condition. The influence of the water has to be considered in the slope stability assessment. In this paper, the analysis and computation for considering the influence of the groundwater are based on the groundwater level that was measured during exploration period.

Preferred Plane and Slope Failure Model

The fault F_2 is grouped into the J_1 group to be considered in the slope stability analysis because the dip and dip direction of the fault F_2 is close to the dip and dip

direction of the J_1. Geological preferred plane (Guoyu Luo, 1984) is the fault F_3. The statistical preferred plane includes the J_1, J_2, J_3, J_4 and the slabbing joint with the dip direction of 30^0-126^0 and dip angle of 18^0-31^0. The data of all preferred planes in the slope body are plotted and analyzed on a piece of tracing paper, which is located over the center of the stereonet (Computer drawn by Dr. C. M. St John of the Royal School of Mines, Imperial College, London) by means of a center pin. The equatorial projections of the preferred planes are shown in the figure 2. The figure 2 shows that the intersection lines of most structural planes are oblique toward inside the slope body so that they build up a stable slop body. Eliminating the structural body comprised by the stable structural preferred planes, there are two kinds of slope failure models. They are as follows:

(1) The strike of the joint J_4 is close to the strike of the fault F_3. In addition, the joint J_4 does not play an principal role in controlling slope stability. Due to a relative large intersection angle (average intersection angle =62.5^0) existing between the dip directions of the fault F_3 and the slope, the joint J_4 is grouped into the fault F_3 to be considered. The slope body controlled by the fault F_3 has to cut off another lateral plane and overcomes the sliding resistance force on this lateral plane to slide. According to the principle of minimum shearing plane being orthogonal to the stratum and being also vertical, we can obtain the minimum shearing plane with the strike direction between 295^0 and 320^0. It is shown in figure 3. From figure 3, we know that the minimum shearing plane and the fault F_3 comprise a stable wedge body. Furthermore, we can get a stable slope angle of 56^0. This illustrates that the slope is stable when the dip angle of the slope is less than 56^0. The following

computation will not consider this model until the designed slope angle is changed and larger than 56^0.
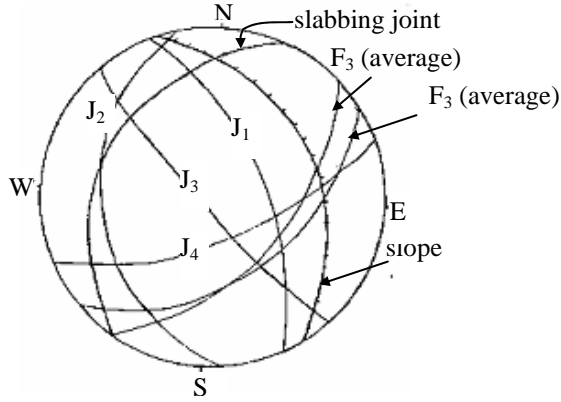

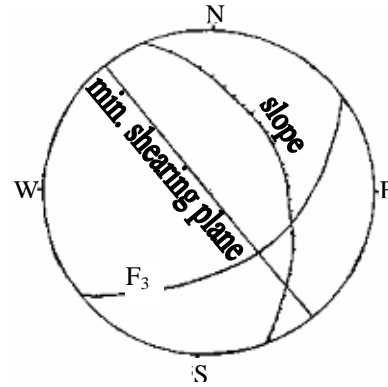Figure 2 The equatorial projections of the preferred planes and slope

Figure 3 The equatorial projections of the minimum shearing plane and slope

(2) The slope body slides along with a zigzag line. Some sliding planes track the preferred plane J_1 (or F_2) and slabbing joint. The middle part between the slabbing joint plane and the slope plane is considered as a circular sliding plane (shown in figure 4). Generalizing the above analysis and discussion, this paper uses the sliding model that the slope body slides along with a circular sliding plane and the tension cracks in upper slope surface extend along with the preferred plane J_1. (Shown in the figure 5).
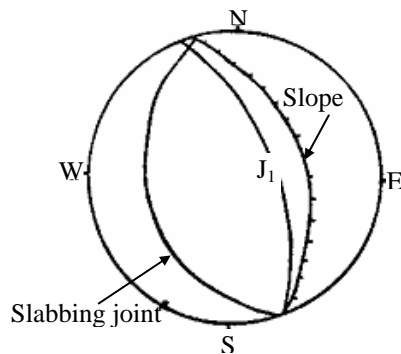
Figure 4 The equatorial projections of slabbing joint, J_1 and slope
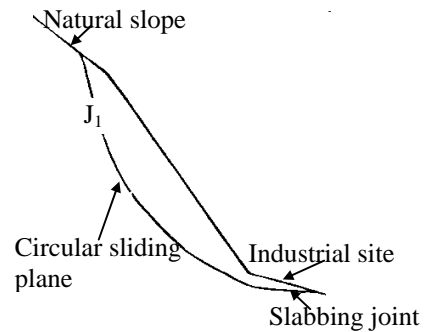

Figure 5 The computational model diagram

Analysis and assessment on the slope stability

Analysis and assessment on the rock slope controlled by preferred planes emphasize the certainty and probability theories. The two models are analyzed and computed. The probability analysis method is stressed. Now, we define the failure probability as follows [3]:

$$P\{Y<Y_L\}=F\{Y_L\} \tag{1}$$

In the equation (1), $Y_L=1$ (Y_L is the factor of safety for limit equilibrium state), Y is a random variable which is the factor of safety in the slope stability analysis. P is the probability when $Y < 1$, it expresses the failure probability of the slope. $F(Y_L)$ is the probability that the slope fails. In other words, $F(Y_L)$ is the failure distribution function. If the distribution of the random variable Y has a density function $f(y)$ [4], then

$$F(Y_L)=\int_0^{Y_L} f(y)dy \tag{1.1}$$

There are two kinds of methods to compute the failure probability of the slope. They are as follows:

(1) Y is assumed to obey normal distribution. Based on the statistical analysis theory, the failure probability of the slope $P\{Y<Y_L)$ is computed.

(2) By using probability statistical simulation method — Monte Carlo method [10], the failure probability of the slope is simulated. In this paper, the key idea of Monte Carlo method is kind of numerical computational method through randomly sampling testing. That is, in N times randomly sampling, times N_A that the factor of safety is less than 1 can be expressed as

$$P\{Y_L\}=N_A/N \tag{2}$$

♦ Determining random variable Y distribution function

The distribution of a random variable is the collection of possible outcomes along with their probabilities. We take a series of observation values (samples) by testing and investigating random variable parameters that belong to Y. These observation values can be conducted for statistical analysis as long as the amount of these observation values is large enough and their determination are random. By drawing empirical graphic or chart, the distribution type and density function type can be obtained. Therefore, compute the mean (u) and variance (σ^2) of the samples. Variance of random variables are non-negative numbers which give an idea of how widely spread the values of the random variable are likely to be; the larger the variance, the more scattered the observations on average. Taking the square root of the variance gives the standard deviation (σ). The variance and standard deviation of a random variable are always non-negative. According to the parameter estimation principles, the distribution of the density function can be determined.

For the mechanical parameters of rock mass, it has been demonstrated that they obey normal distribution [3], [4]. Normal distribution is one of the most frequent and most important distributions in probability theory and in technical calculations. The normal distribution may be described by the following density function [3, 4]:

$$f(\chi)=\frac{1}{\sigma\sqrt{2\pi}}e^{-\frac{1}{2}(\frac{\chi-u}{\sigma})^2} \tag{3}$$

Thus, the mechanical parameters of rock mass can be estimated in sub-sample at n < 50.

♦ Determining fake random parameters of normal distribution

From central limit theorem of probability [3], [4], [12], we know that the distribution of probability of the summation of N independent random variables Ri (mean = ui, variance = σ^2i, i = 1 …. N) with the same distributions is approximate to normal distribution when N is large enough. Their mean (u) and variance (σ^2) are as follows:

$$u = \sum_{i=1}^{N} ui \tag{4}$$

$$\sigma^2 = \sum_{i=1}^{N} \sigma^2 i \tag{5}$$

This is the theory of forming fake random parameter [11] for arbitrary normal distribution. To form a normal random variable z that has arbitrary expected value υ and arbitrary variance σ^2, namely, z~N (υ, σ^2), the formula used is as follows [3], [4]:

$$Y = \upsilon + \sigma(\sum_{i=1}^{N} Ri - \frac{N}{2})\sqrt{N/12} \tag{6}$$

In the equation (6), Ri (i = 1, …N) obey the evenly distribution between [0, 1]. This formula is available when N is large enough. Here, we take N = 12, which is satisfied for required accuracy. Hence, from equation (6), one has

$$Y = \upsilon + \sigma(\sum_{i=1}^{N} R_i - 6) \tag{7}$$

Equation (7) is the formula that gives the random parameters of normal distribution.

8

♦ Determining Y function

In this paper, the assumption of a circular sliding plane (Swedish method) [9] is used to determine Y function.

$$Y = k_s = \frac{\sum c_i l_i + \sum b_i (\gamma h_{1i} + \gamma_m h_{2i} - \gamma_w \frac{h_{wi}}{\cos^2 \alpha_i}) \cos \alpha_i \tan \varphi_i}{\sum b_i (\gamma h_{1i} + \gamma_m h_{2i}) \sin \alpha_i} \qquad (8)$$

where c_i = cohesion on the sliding plane l_i; $\quad \varphi_i$ = frictional angle on the sliding plane l_i;

γ = dry unit weight of the rock; $\quad \gamma_m$ = moisture unit weight of the rock;

γ_w = unit weight of the water; $\quad$ the other parameters are shown in the Figure 6.

Based on the above principles, the computational results are as follows:

• Rigid Body Limit Equilibrium Computational Results [1], [2], [7]

By try-calculation to the same slope angle, the radius of the circular sliding plane and the coordinates of the circular center can be obtained. And then compute by using model (2). The computational formula that is used to run model (2) is equation (8). The parameters used in the computation are shown in the figure 6. The computational result of k_s is shown in the figure 7.
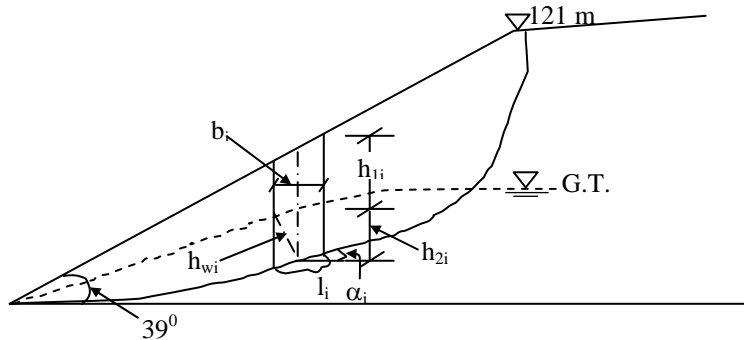

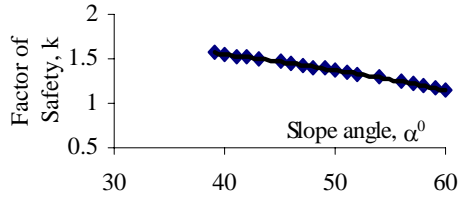
Figure 6 The computational model diagram for equation (8)

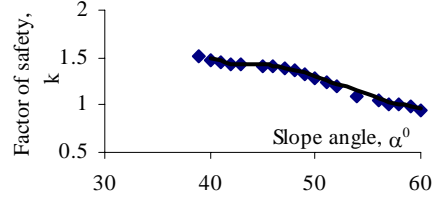Figure 7-1 The relation of k vs. α
without consideration of joint J$_2$

Figure 7-2 The relation of k vs. α
with consideration of joint J$_2$

- Results on Failure Probability Analysis Method [1], [2], [7]

The dip and dip direction of the joint group J$_2$ is used to make an empirical frequency curve. Furthermore, theoretic frequency curve of dip of the J$_2$ is established according to the empirical frequency curve [2], [8] as follows:

$$f(\chi) = \frac{1}{\sqrt{2\pi}\sigma} e^{-\frac{1}{2}(\frac{\chi-u}{\sigma})^2}$$ (9)

where, $\sigma^2 = \hat{\sigma}^2 = 285.25$ \qquad $u = \hat{u} = 57.87^0$

According to the data of mechanical strength characteristics, the strength frequency curve of the joint J$_2$ can be obtained. They are as follows:

$$\text{Cohesion C: } f(x) = \frac{1}{\sqrt{2\pi}\,4.633} xe^{-\frac{1}{2}(\frac{x-4.087}{4.633})^2}$$ (10)

$$\text{Friction angle } \varphi: f(x) = \frac{1}{\sqrt{2\pi}\,7.561} xe^{-\frac{1}{2}(\frac{x-28.818}{7.561})^2}$$ (11)

The failure probability is analyzed and computed using "computation slope failure probability program by Monte Carlo method"[10], [11]. The assumptions of this program are as follows:

The geometry condition and strength parameters in the lower part where the circular sliding plane cuts through are assumed as non-random variables. This is because lower part is determined by minimum principle for the factor of safety as well as the mechanical parameters of rock mass are substituted in strength parameters of rock mass. So, it is assumed that they are not random; but in the upper part, the dip and dip direction of the joint J_2 as well as its strength parameters are considered as random-variable model. The computational result of the failure probability is shown in Figure 8.

• Assessment on the Slope Stability

According to the above analyses, one can be concluded that there is a steep rise in failure probability at the factor of safety (k) = 1.2. Therefore, k_J = 1.2 is considered as the limit stable criteria of slope stability. The slope stability decreases when k is less than 1.2 and the slope will fail when k is less than 1. Figure 8 shows that the slope angle $\alpha < 50^0$, p = 0. Figure 9 shows that k = 1.3, failure probability p = 0. These illustrate that the slope has a good stability at k = 1.3 with $\alpha < 50^0$. Therefore, k_c = 1.3 is used as a criteria for assessing slope stability in this paper. When $\alpha = 39^0$, p = 0, k = 1.504 >> 1.3, it illustrates that the factor of safety is too large which means it costs more money. The slope angle α = 48^0 is selected as design slope angle when k = 1.365 > 1.3, p = 0. There are two advantages for selecting $\alpha = 48^0$ as design angle of the slope: one can fully utilize the stability of nature slope; another one reduces the amount of removal rock mass. This not

only ensures the stability of the man-made slope but also saves big money (about million dollars).
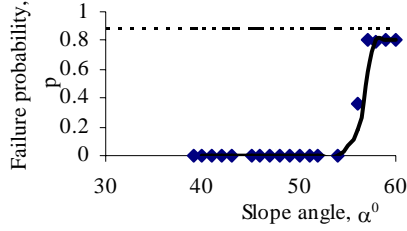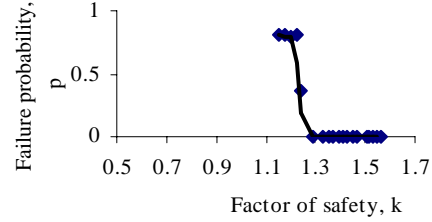

Figure 8 The relation of p vs. α

Figure 9 The relation of p vs. k

Conclusion

(1) This paper uses preferred plane theory to analyze the characteristics of the preferred plane for Rough-Breaking Station slope by in a Copper Mine. Two types of models are established for the analysis of the rock slope stability.

(2) The relationships for the factors of safety of the slope stability vs. slope angle, failure probability of the slope vs. slope angle, and failure probability of the slope vs. the factors of safety are obtained. They are shown in the figure 7, figure 8 and Figure 9. The data has been provided to the designers to design the slope.

(3) According to the value of the failure probability, the standard value of the factor of safety is determined to be used in rigid body limit equilibrium analysis.

(4) The slope stability at Rough-Breaking Station in a Copper Mine is analyzed and assessed by using preferred plane theory. One is recognized that initial design slope angle tends to be small. Therefore, the slope angle $= 48^0$ is selected as design slope angle. It makes that the safety and reasonable investment become uniform in the slope design.

Reference

[1] D. Ding, L. Zhang, 1987, The project Report on the Rough-Breaking Station in DX
     Copper Mine

[2] L. Zhang, 1984, The problem on Mechanic Model for Rock Mass Structure,
     Hydrology and Engineering Geology, Vol. 3, No. 3

[3] Probability, 1979, China Fudan University, Advanced Education Publication
     Company

[4] Probability and Statistics for Engineers and Scientists, Ronald E. Walpole, Raymond
     H. Myers

[5] Xiangong Zhang, 1983, Engineering Geology, Geological Publication Company

[6] Muller. L, 1974, Rock Mechanics

[7] Guoyu Luo, 1990, The Theory and Method of Preferred Plane Analysis on the
     Stability of the Rock Slope, Chinese Journal of Hydrology and Engineering Geology,
     No. 2

[8] D. Ding, 1995, Preferred Plane of Controlling Slope and Its Assessment and
     Anchoring Principles, Chinese Journal of Geotechnical Engineering, No. 6

[9] Lee W. Abramson, Thomas S. Lee, Sunil Sharma, Glenn M. Boyce, Slope Stability
     and Stabilization Methods, A Wiley-Interscience Publication, John Wiley & Sons.
     INC.

[10] Introduction to Monte Carlo Method, http://csep1.phy.ornl.gov/mc/node1

[11] The Analysis of Slope Stability,
      heep://www.geocities.com/collegePark/Quad/2435/links.html

[12] Probability Density Function (pdf), http://ccs.uky.edu/csep/MC/NODE13.html